

**Coumarin-appended Amino Acids and Azaheterocycles:
Design, Synthesis, Photophysical Studies and Sensing
Applications of Selected Compounds**

THESIS

Submitted in partial fulfillment
of the requirements for the degree of

DOCTOR OF PHILOSOPHY

by

SANTOSH KUMARI

ID. NO. 2012PHXF0411P

Under the supervision of

Dr. RAJEEV SAKHUJA



BITS Pilani
Pilani | Dubai | Goa | Hyderabad

**DEPARTMENT OF CHEMISTRY
BIRLA INSTITUTE OF TECHNOLOGY AND SCIENCE
PILANI (RAJASTHAN) INDIA**

2018

**BIRLA INSTITUTE OF TECHNOLOGY AND SCIENCE
PILANI (RAJASTHAN)**

CERTIFICATE

This is to certify that the thesis entitled “**Coumarin-appended Amino Acids and Azaheterocycles: Design, Synthesis, Photophysical Studies and Sensing Applications of Selected Compounds**” submitted by **SANTOSH KUMARI**, ID No. **2012PHXF0411P** for the award of Ph.D. Degree of the Institute embodies the original work done by her under my supervision.

Signature in full of the Supervisor

Name in capital block letters: **Dr. RAJEEV SAKHUJA**
Designation: Associate Professor, Birla Institute of
Technology and Science Pilani, Pilani Campus, Rajasthan
India.

Date:

*Dedicated to
My Husband,
Son and
Parents*

ACKNOWLEDGEMENT

First of all, I would like to submit myself to the creator of the whole thing, my God, who has bestowed upon me loads of blessings, enabling me to make a material part in the field of research. Next, I want to express my sincere thanks and deepest gratitude to my supervisor, Dr. Rajeev Sakhuja, for his suggestions, criticism, infrastructural support, moral support, and constant encouragement. I sincerely thank him for the splendid guidance, inspiration and personal independence given to me during my research period. His endless enthusiasm and receptive feelings will always remain a source of inspiration for me. Without his support, guidance, and help, this thesis would be unfeasible. I hope that my supervisor is in the prime of his health forever and create milestones in the chemical research field.

I am immensely thankful to Prof. Souvik Bhattacharyya (Vice-Chancellor), Prof. Ashoke Kumar sarkar (Director), Mr. Ernest Samuel Ratnakumar J (Registrar), Prof. S. Krishnaswamy (Dean Admin.) Prof. S. Krishnaswamy (Dean, A-GSR), Prof. Jitendra Panwar (Assoc. Dean, A-GSR) and Dr. Hemant R. Jadhav (Ex. Assoc. Dean, A-GSR), Birla Institute of Technology & Science, Pilani (BITS, Pilani) for giving me the opportunity to pursue my doctoral studies by providing necessary facilities. I am additionally appreciative to the office staff of A-GSR, whose accounting assistance helped me in submitting the various estimate documents in time.

I might want to offer my earnest thanks to Prof. S. C. Sivasubramanian and Prof. Anil Kumar (DAC members), for their support, critical review and suggestions during the review my draft thesis and proposal. Likewise, I might want to offer my genuine thanks to faculty members from the Department of Chemistry, BITS Pilani, for their constant guidance. I owe my sincere thanks to Prof. I. R. Laskar (Convener, DRC), and previous DRC conveners Prof. R. K. Roy, Prof. Ajay Sah and Prof. Saumi Ray along with other members of DRC. I would like to acknowledge Head, department of chemistry during my Ph.D work, Prof. S. K. Sah, Prof. Anil Kumar, Prof. Bharti Khungar and Prof. Saumi Ray for providing me an appropriate research facility. Thanks are also due to all the office staff of the department for their help during my work. I specially thank Ms. Pusplata Ji for her kind support. I acknowledge BITS Pilani for providing infrastructure. Also, DST-FIST is also deeply acknowledged for providing instrumentation facilities in the department. I acknowledge UGC-NET JRF for providing me fellowship during the tenure of my Ph.D.

I also would like to express sincere appreciation for my senior Dr. S.M. Abdul Shakoor, for the useful training he gave me in the initial phase of my research. I might want to extraordinarily thank my dear companion Dr. Sunita Joshi for their wonderful helping attitude, who was willing to support me at all times. I would also like to sincerely acknowledge Dr. Kiran Bajaj, who

always gave me the right suggestions, and making my doctorate life more enjoyable and sorted out. I might want to express my gratefulness towards my labmates Mr. Devesh, Mr. Mahesha and Ms. Karishma for their friendship and motivation. Finally, I would like to express my genuine gratefulness to Prof. Dalip Kumar, as his silent support had been my driving force to go forward bravely.

I deeply acknowledge the exceptional special person, my beloved husband Mr. Pradeep Choudhary has supported me throughout my career with lots of tolerance without knowing what I am doing. I am indeed very grateful to him as it is his constant love, care, support and encouragement that has been the main force and motivation of my progress so far and will continue to be so in the days to come. Words and this limited space do not seem adequate to enough to express my indebtedness to my venerable husband.

Next, with humble capitulation and deep wisdom of gratitude, I wish to extend my sincere thanks to my beloved grandmother-in-law Mrs. Chankori Devi and grandparents Mr. Kisan Ji and Mrs. Lali Devi for their continuous love, support, and confidence in me. A special thanks to my grandparents Mr. Syopal, Mr. Mularam and Mrs. Soni Devi for their countless blessings. May the supreme grant peace to their dead souls and provide them a special place in heaven.

Last but absolutely not the least I would like to non-stop my deepest gratitude to my family, especially my parents Mr. Vidhadhar and Mrs. Taramani Devi, my brothers Mr. Vijay and Mr. Dharmendra, my sisters Ms. Nirmala and Ms. Rajani, Ms. Manoj, and my in-laws Mr. Dharmeer Manth and Mrs. Vimla Devi and Mr. Jitendra Manth and Mrs. Suman Devi, and Mr. Mahaveer and Mrs. Kavita Devi, my brother-in-law Sandeep, Kuldeep, Pawan, sister-in-law Bantu and Priyanka for their kind friendship, motivation, supports, encouragements, patience, and the most importantly their endless love.

I deeply acknowledge the particular person and love of my life, whose recent entry into this universe marks the beginning of a long journey, my beloved son Jeeshan Choudhary. Completion of this thesis in the anticipated time would have been difficult for me without his support.

I extend my honest thanks to my friends Mr. Hitesh, Priyanka, Nasrin, Shaheen, Dr. Mukund, Dr. Meenakshi, Mr. Reddy, Mr. Santosh, Mr. Manish, Mr. Shiv, Mr. Nitesh, Mr. Vishal, Mr. Vimal, Pallavi, Khima, Saroj, Vaishali, Sonam, Sushila, Moyna, Sunita. Urmilla. Ranjeeta Arora and all research scholars from the chemistry department and other departments for their continuous support and attractive company during my entire thesis work.

Finally, there are many more relatives, friends, and well-wishers whose faith, support, and even moral support has donated in a vast mode in the end of this work. I express my sincere and special thanks to all of them.

SANTOSH KUMARI

TABLE OF CONTENTS

Certificate

Acknowledgements

Abstract

List of Tables

List of Figures

List of Abbreviations and Symbols

Chapter 1A. Copper-catalyzed C-N/C-O Coupling in Water: A Facile Access to Coumaryl-tagged and Coumaryl-labelled Amino Acids

1A.1	Background	2
1A.2	Introduction	15
1A.3	Results and discussion	19
1A.4	Experimental section	29
1A.5	References	40

Chapter 1B. Copper-catalyzed [3+2] Cycloaddition: A Facile Access to Triazolyl Linked Coumarin-amino acid/Peptide Hybrids

1B.1	Introduction	48
1B.2	Results and discussion	58
1B.3	Experimental section	68
1B.4	References	80

Chapter 2A. Coumarin-derived Selective Hg²⁺ & Li⁺ Chemosensors: Synthesis, Experimental and Theoretical Investigations

2A.1	Introduction	86
2A.2	Results and discussion	98
2A.3	Experimental section	108
2A.4	References	111

Chapter 2B. Coumarin-derived Sensors for Picric Acid Detection: Synthesis, Experimental and Theoretical Investigations

2B.1	Introduction	121
2B.2	Results and discussion	127
2B.3	Experimental section	140
2B.4	References	146

Chapter 3. Copper-catalyzed Cross-Dehydrogenative C(*sp*³)-N Bond Coupling: An Unprecedented Tandem Synthesis of Coumarin-fused Pyrimidines

3.1	Introduction	153
3.2	Results and discussion	163
3.3	Experimental section	176
3.4	X-ray crystallography studies of 54a	187
3.5	References	188

Chapter 4. NH₄OAc-promoted C(*sp*²)-H bond activation and C-N bond formation: an aberrant cascade synthesis of coumarin-fused quinolinones

4.1	Introduction	193
4.2	Results and discussion	202
4.3	Experimental section	215
4.4	X-ray Crystallography Studies of 15ba	224
4.5	References	225

Chapter 5. Conclusions of the thesis

5.1	General conclusions	231
5.2	Specific conclusions	232
5.3	Future scope	238

Appendices

List of publications	A-1
List of presentations in conferences	A-2
Brief bibliography of the candidate	A-3
Brief bibliography of the supervisor	A-4

ABSTRACT

Coumarin moiety has played a center-stage role in designing a good number of fluorescent and fascinating heterocyclic architectures. Coumaryl-labelled/tagged amino acids have received special interest due to their sensitivity to pH and solvent polarity that makes them excellent fluorescent molecules to investigate numerous biological processes in living organisms. Coequally, coumarin-appended and coumarin-fused heterocycles are considered as valuable targets in synthetic chemistry because of their broad range of applications in the field of material and medicinal chemistry. The work disclosed in the present thesis entitled “**Coumarin-appended Amino Acids and Azaheterocycles: Design, Synthesis, Photophysical Studies and Sensing Applications of Selected Compounds**” was successfully executed in due diligence of sustainable chemistry, and the thesis has been divided into five chapters

The **first chapter** of thesis is divided into two parts. **Chapter 1A** of the thesis presents a straightforward Cu-catalyzed microwave-assisted protocol for the synthesis of *N*-coumaryl amino acids by coupling 4-chlorocoumarin and α -L-amino acids in water. Interestingly, various α -amino acids possessing polar and non-polar side chains showcased good reactivity, affording their corresponding *N*-coumaryl amino acids in excellent yields. Absorption and fluorescence spectra of all synthesized compounds were recorded, and quantum yields were computed. The chemical applicability of the synthesized *N*-coumaryl amino acids as a fluorescent probe was illustrated by coupling a representative *N*-coumaryl amino acid with a *N*-terminus dipeptide under coupling conditions to afford *N*-coumaryl tripeptide in high yield. The methodology was further extended to synthesize coumaryl-labelled lysine and tyrosine motifs under Cu-catalyzed microwave-assisted conditions in water.

Chapter 1B of the thesis describes the application of click chemistry for synthesizing triazolyl linked coumarin-amino acid hybrids using two strategies. Following first strategy, Cu-catalyzed azide–alkyne cycloaddition (CuAAC) reaction between clickable protected amino acyl *O*-propargyl esters and 4-azido-2*H*-chromen-2-one (or 7-hydroxy-4-azidomethyl-2*H*-chromen-2-one) comfortably afforded 4-triazolyl (or 4-triazolylmethyl) linked coumarin-amino acid/peptide hybrids in good-to-excellent yields. While following the second strategy, Cu-catalyzed [3+2] cycloaddition reaction between clickable 4-methyl-7-(prop-2-ynyloxy)-2*H*-chromen-2-one (or 4-(prop-2-ynyloxy)-2*H*-chromen-2-one) and α -azido esters furnished two series of 7-*O*-triazolylmethyl and 4-*O*-triazolylmethyl coumarin-amino acid hybrids in 82–90% yields. The

synthesized compounds exhibited good fluorescence properties, and their chemical applicability as fluorescent labels was successfully exemplified by coupling them with appropriate C- or N-terminus amino acids, furnishing corresponding triazolyl linked coumarin-peptide hybrids in high yields.

The **second chapter** of thesis is also divided into two parts. **Chapter 2A** of the thesis discloses the synthesis of two coumarin-derived indole-based probes, which were identified as efficient sensors for selective detection of Hg^{2+} and Li^+ in organo-aqueous media. Among these, *N*-((7-hydroxy-2-oxo-2*H*-chromen-4-yl)methyl)-2-(1*H*-indol-3-yl)acetamide displayed remarkable selectivity towards Hg^{2+} sensing in H_2O -DMF mixture as a turn-off fluorescence response, whereas *N*-((7-hydroxy-2-oxo-2*H*-chromen-4-yl)methyl)-1*H*-indole-2-carboxamide showed remarkable selectivity towards Li^+ sensing in H_2O - CH_3CN as a turn-on fluorescence response. The most probable binding site of complexing Hg^{2+} and Li^+ to the respective probes was explained on the basis of detailed UV-Vis spectroscopic studies, Benesi-Hildebrand plots, ^1H NMR titrations and DFT calculations.

Chapter 2B of the thesis discloses the synthesis of two coumarin-derived imidazolium salts and one benzimidazolium salt, which were identified as efficient sensors for selective detection of picric acid in aqueous medium. The detection limits of the probes for picric acid sensing were calculated to be 107 nM, 87 nM and 208 nM, respectively. Based on the UV-Vis studies, and time resolved fluorescence results, the formation of ground-state charge-transfer complex formation appears to be predominant mechanism in solution, which also got support from DFT calculations.

The **third chapter** of thesis discloses an efficient, one-pot Cu-catalyzed tandem protocol for the synthesis of fluorescent 3-benzyl-2-phenyl-2,3-dihydro-5*H*-chromeno[4,3-*d*]pyrimidin-5-ones from 4-chloro-3-formylcoumarin and benzylamines by *in situ* intramolecular cross-dehydrogenative $\text{C}(\text{sp}^3)\text{-N}$ bond formation under ligand-free ambient conditions. This synthesis was easily scalable, and an array of benzylamines delivered coumarin-fused pyrimidine in moderate-to-good yields. Detailed investigations were performed to propose the mechanism of this unprecedented reaction. The synthesized coumarin-fused pyrimidines exhibited interesting photophysical properties and high quantum yields, and would be potential candidates for facilitating suitable studies in medicinal chemistry and material science.

The **fourth chapter** of thesis discloses a concise cascade strategy for the synthesis of 6*H*-chromeno[4,3-*b*]quinolin-6-ones from 4-hydroxycoumarins and arylhydrazine hydrochlorides in DMSO. The synthetic strategy relies on dual role of ammonium acetate in generating 4-(aminophenyl)coumarin from 4-hydroxycoumarin and arylhydrazine *via* aryl radical formation, and C(*sp*²)-H formylation of coumarin using DMSO as a methine source. The strategy was scalable, and an array of arylhydrazine hydrochlorides delivered chromene-fused quinolinones in good-to-excellent yields. A detailed mechanistic investigation was performed to understand the mechanism of this unique process. All the synthesized coumarin-fused quinolinones exhibited interesting photophysical properties.

Finally, in the **fifth chapter** of the thesis, a summary of the work conducted is presented along with future scope of the research work.

LIST OF TABLES

Table No.	Title	Page No.
1A.3.1	Selected optimization of reaction conditions ^a for the synthesis of 89a	20
1A.3.2	Absorption and fluorescence data of <i>N</i> -coumaryl amino acids (89a-m) ^a	26
1A.3.3	Absorption and fluorescence data of coumaryl-labelled lysine and tyrosine ^a	28
1B.2.1	Synthesis of protected amino acyl <i>O</i> -propargyl esters (33 & 35)	59
1B.2.2	Synthesis of 7-hydroxy-4-triazolylmethyl coumarin-amino acids/peptide hybrids (36 & 37)	60
1B.2.3	Synthesis of 4-triazolyl linked coumarin-amino acid/peptide hybrids (38 & 39)	61
1B.2.4	Synthesis of α -azido esters 43	62
1B.2.5	Synthesis of 7- <i>O</i> -triazolylmethyl and 4- <i>O</i> -triazolylmethyl coumarin-amino acid hybrids 44	63
1B.2.6	Photophysical studies ^a of 36 , 37 , 38 , 39 & 44	66
1B.2.7	Photophysical studies ^a of 4-triazolyl and 7- <i>O</i> -triazolylmethyl coumarin-amino acid hybrid with <i>C</i> -terminus amino acid and <i>N</i> -terminus amino acid 38g , 46 , 44a , 48	67
2A.1.1	Selective examples of coumarin-derived chemosensors for Hg ²⁺ ion detection	93
2A.1.2	Coumarin-derived chemosensors for Li ⁺ ion detection	95
2A.1.3	Selective examples of indole-based chemosensors for Hg ²⁺ ion detection	96
2B.1.1	Selective examples of chemosensors used for picric acid sensing	122
2B.1.2	Reported imidazolium-based sensors for picric acid sensing	125
2B.1.3	Reported benzimidazole/benzimidazolium-based sensors for picric acid sensing	126
3.2.1	Selected optimization of reaction conditions ^a for the synthesis of 54a	164
3.2.2	Absorption and fluorescence data of coumarin-fused pyrimidines (54a-y) ^a	175
4.2.1	Selected optimization of reaction conditions ^a for the synthesis of 15aa	203
4.2.2	Absorption and fluorescence data of coumarin-fused quinolinones (15aa-ci) ^a	214

LIST OF FIGURES

Figure No.	Caption	Page No.
1A.1.1	Selective examples of peptide based drugs	2
1A.1.2	Existing labelling methods for tracking biomolecules	3
1A.1.3	Selective examples of fluorophores used in labelling studies	4
1A.1.4	Applications of coumaryl-labelled amino acids in biochemical research	5
1A.3.1	HPLC analysis of 89a	23
1A.3.2	HPLC analysis of 89a + 89a'	23
1A.3.3	¹ H NMR spectrum of 89a in DMSO- <i>d</i> ₆	23
1A.3.4	¹³ C NMR spectrum of 89a in DMSO- <i>d</i> ₆	24
1A.3.5	UV absorption spectra of 89a-h (a) and 89i-m (c), and emission spectra of 89a-h (b) and 89i-m (d) in MeOH (5x10 ⁻⁵ M) at 25 °C	26
1A.3.6	UV absorption spectra of 94 , 95 , 97a-b and 98a-b (a) and emission spectra of 94 , 95 , 97a-b and 98a-b (b) in MeOH (5x10 ⁻⁵ M) at 25 °C	28
1B.1.1	Representative examples of peptidomimetics modified peptides used for mimicking peptides	48
1B.1.2	Representative examples of peptidomimetics used as renin inhibitors	49
1B.1.3	Structural comparison of <i>trans</i> -amide and <i>cis</i> -amide with 1,4- and 1,5-disubstituted 1,2,3-triazoles, respectively	50
1B.1.4	Selective examples of biological active triazole-modified peptidomimetics	51
1B.1.5	Generalized representation of fluorogenic CuAAC	53
1B.1.6	Selective examples of bioactive triazolyl linked coumarin-alkyl/aryl/heteroaryl hybrids	55
1B.2.1	¹ H NMR spectrum of 36c in DMSO- <i>d</i> ₆	64
1B.2.2	¹³ C NMR spectrum of 36c in DMSO- <i>d</i> ₆	64
1B.2.3	UV absorption spectra of 36a-f , 37a-b (a), 38a-d , 38g , 39a (c) and 44a-f (e) and emission spectra of 36a-f , 37a-b (b), 38a-d , 38g , 39a (d)	67

	and 44a-f (f) in THF (5×10^{-5} M) at 25 °C	
2A.1.1	Schematic diagram for the sensor action	86
2A.1.2	A graphical representation of various chemical and biological analytes	86
2A.1.3	Schematic diagram of the fluorescent sensor action	87
2A.1.4	Intramolecular charge transfer (ICT) phenomena in coumarin	89
2A.1.5	Qualitative comparison of photophysical properties of coumarin derivatives	89
2A.1.6	Selective examples of functionalized coumarins used for detection of various analytes	90
2A.1.7	Amide functionalized coumarins used as chemosensors for metal ion sensing	91
2A.2.1	UV–Vis spectra of probes: 7 (a) (10^{-4} M) upon addition of 5 equiv of Hg^{2+} and other metal ions and 8 (b) (10^{-4} M) upon addition of 5 equiv of Li^+ and other metal ions	99
2A.2.2	Fluorescence spectra of compounds 7 (a) (10^{-4} M) upon addition of metal ions: in $\text{H}_2\text{O} : \text{DMF}$ (7:3, v/v); and 8 (b) (10^{-4} M) upon addition of metal ions: in $\text{H}_2\text{O} : \text{CH}_3\text{CN}$ (7:3, v/v) at $\lambda_{\text{Ex}} = 340$ nm	100
2A.2.3	Column diagrams of the fluorescence intensity of compounds 7 (a; 7 + metal ions) at 465 nm. Grey bars represent the addition of various metal ions to the blank solution and blue bars represent the subsequent addition of Hg^{2+} (5 equiv) to the above solutions (compound + M^{n+} + Hg^{2+}) and 8 (b; 8 + metal ions) at 465 nm. navy blue bars represent the addition of various metal ions to the blank solution and dark cyan bars represent the subsequent addition of Li^+ (5 equiv) to the above solutions (compound + M^{n+} + Li^+)	101
2A.2.4	UV–Vis titration studies of probes 7 (a) and 8 (b) (10^{-4} M) upon gradual increase in the concentration of Hg^{2+} and Li^+ ions, respectively	102
2A.2.5	Fluorescence titration studies of probes 7 (a) and 8 (b) (10^{-4} M) upon gradual increase in the concentration of Hg^{2+} and Li^+ respectively at λ_{Ex}	103

	= 340 nm	
2A.2.6	Stern–Volmer plot of sensors 7 (a) and 8 (b) in response to Hg ²⁺ and Li ⁺ ions. Inset: Stern-Volmer plot obtained at lower concentration of Hg ²⁺ in linear range	103
2A.2.7	Bensei–Hildebrand plot of probes 7 (a) and 8 (b) in response to Hg ²⁺ and Li ⁺ ions	104
2A.2.8	¹ H NMR spectra of 7 (a; top) and 7 + its complex (a; bottom) in DMSO– <i>d</i> ₆ , 8 (b; bottom) and in the presence of (b; 0.5-2 equiv) of Li ⁺ in DMSO– <i>d</i> ₆	105
2A.2.9	Optimize structures of the complex (a; 7 + Hg ²⁺) and (b; 8 + Li ⁺) at most probable Hg and Li binding sites, and their corresponding binding energy values calculated at B3LYP/6-31+G(d,p): Lanl2Dz (for Hg ²⁺ and Li ⁺) level. The binding energy values are computed as *BE = E _{complex} – (E _{compound} + E _{Hg})/ E _{complex} – (E _{compound} + E _{Li})	107
2A.2.10	Proposed binding site for compounds (a; 7 + Hg ²⁺) and (b; 8 + Li ⁺)	107
2B.1.1	Selective examples of nitro-aromatic compounds (NACs)	121
2B.2.1	Fluorescence spectra of 6a (a; left), 6b (c; left) & 7 (e; left) with c = 10 ⁻⁴ M (in water) upon the addition of (5 equiv) different aromatic/non-aromatic analytes; Column diagrams of the relative fluorescence intensity of 6a (b; right), 6b (d; right) & 7 (f; right) with different analytes at λ _{Ex} = 340 nm for 6a and 6b and λ _{Ex} = 300 nm for 7	130
2B.2.2	UV–Vis titration studies of compounds 6a (a), 6b (b) & 7 (c) (10 ⁻⁴ M) with different amounts of picric acid in aqueous medium	131
2B.2.3	Fluorescence titration studies of compounds 6a (a), 6b (b) & 7 (c) (10 ⁻⁴ M) with different amounts of picric acid in an aqueous medium	132
2B.2.4	Stern–Volmer plot in response to picric acid for sensors 6a (a), 6b (b) and 7 (c). Inset: Stern-Volmer plot obtained at lower concentration of picric acid in linear range	133
2B.2.5	Benesi–Hildebrand plot for compounds 6a (a), 6b (b) and 7 (c), at	133

	various concentration of picric acid	
2B.2.6	¹ H NMR spectra of 6a (a; left-top), 6a ≡PA (a; right-top), 6b (b; left-middle), 6b ≡PA (b; right-middle) and 7 (c; left- bottom), 7 ≡PA (c; right-bottom) in DMSO- <i>d</i> ₆	134
2B.2.7	Lifetime decay profile of compounds 6a (a) 6b (b) and 7 (c) respectively) with picric acid ($\lambda_{\text{Ex}} = 370$ nm and monitored at $\lambda_{\text{Em}} = 480$ nm (for 6a) and 410 nm (for 6b) and ($\lambda_{\text{Ex}} = 370$ nm and monitored at $\lambda_{\text{Em}} = 480$ nm) (for 7)	135
2B.2.8	Pictorial representation of the electron transfer phenomenon in the ground state which occurs from the HOMO of picrate anion to the LUMO of 6a (a) and 6b (b)	136
2B.2.9	Absorption spectra of different aromatic analytes and emission spectra of the sensors 6a (a; top-left), 6b (b; top-right) and 7 (c; bottom) in aqueous solution. Inset: the spectral overlap between the emission of the compounds (6a , 6b and 7) with the absorption of picric acid	137
2B.2.10	Visual detection (under 365 nm UV lamp) of compounds 6a (i; a), 6b (ii; a) and 7 (iii; a) adsorbed on TLC plate and with a spot of picric acid solution on compounds 6a (i; b), 6b (ii; b) and 7 (iii; b)	138
2B.2.11	Fluorescence response of compounds 6a (a) and 6b (b) (10^{-4} M) towards picric acid (5 equiv) sensing in real samples	139
2B.2.12	Column diagrams of the fluorescence intensity of compound (10^{-4} M) + Metal ions (5 equiv) at 480 nm and 410 nm for 6a (a) and 6b (b) in aqueous medium. Cyan bars represent the addition of various metal ions to the blank solution and purple bars represent the subsequent addition of picric acid (5 equiv) to the above solutions (compound + M ⁿ⁺ + picric acid)	139
2B.2.13	Photostability test: Fluorescence spectra of 6a (a) and 6b (b) in the presence of 100 μ M of picric acid in aqueous media at different time scale. The spectra are almost same for about 210 min	140

3.1.1	A generalized demonstration of CDC strategy	153
3.1.2	A brief overview of aerobic Cu-catalyzed CDC methodologies	154
3.1.3	Selective examples of biologically active coumarin-fused heterocycles	160
3.2.1	¹ H NMR spectrum of 54a in CDCl ₃	165
3.2.2	¹³ C NMR spectrum of 54a in DMSO- <i>d</i> ₆	165
3.2.3	2D-COSY spectrum of 54a	166
3.2.4	2D-HETCOR spectrum of 54a	166
3.2.5	ORTEP diagrams of 54a (a) <i>S</i> stereoisomer and (b) <i>R</i> stereoisomer	169
3.2.6	Mass analysis of crude product 54z , 54a & 54d using two different benzylamines (23a & 23d)	171
3.2.7	¹ H NMR spectrum of a mixture of 54z & 54z' in CDCl ₃	171
3.2.8	UV absorption spectra of 54a-j , 54w-54y (a), 54k-p (c), 54q-x (e), and emission spectra of 54a-j , 54w-54y (b), 54k-p (d), 54q-x (f) in MeOH (1x10 ⁻⁵ M) at 25 °C; Inset: solution phase (A) and solid state emission (B) of 54f (b), blue), 54o (d), green) and 54t (f), blue) under UV light at room temperature	174
4.1.1	Overview of metal-free strategies reported for the synthesis of quinoline-fused heterocycles	193
4.1.2	Selective examples of reported chromene-fused quinolines	195
4.2.1	¹ H NMR spectrum of 15aa in CDCl ₃	204
4.2.2	¹³ C NMR spectrum of 15aa in CDCl ₃	204
4.2.3	ORTEP diagram of 15ba	208
4.2.4	ESI-HRMS of the crude reaction mixture (15aa) after 1 h	211
4.2.5	UV absorption spectra of 15aa-15aj (a), 15ba-bl (c) and 15ca , 15ce , 15ch & 15ci (d), and emission spectra of 15aa-15aj (b), 15ba-bl (d) and 15ca , 15ce , 15ch & 15ci (f) in THF (5x10 ⁻⁵ M) & (8x10 ⁻⁶ M) at 25 °C	213

LIST OF ABBREVIATIONS AND SYMBOLS

Abbreviation/symbol	Description
%	Percentage
&	And
$(\bar{\nu}_a - \bar{\nu}_f)$	Stokes shift
(SuO) ₂ CO	<i>N,N'</i> -disuccinimidyl carbonate
°C	Degree centigrade
1,10-Phen	1,10-Phenanthroline
¹³ C	Carbon-13
1-Cl-2,4-DNB	1-Chloro-2,4-dinitrobenzene
2,4-DNP	2,4-Dinitrophenol
2-D	Two-dimensional
3,4-DNT/DNT	3,4-Dinitrotoluene
3,5-DNBA	3,5-Dinitrobenzoic acid
3,5-DNSA	3,5-Dinitrosalicylic acid
4-NBA	4-Nitrobenzoic acid
4-NP	4-Nitrophenol
4-NT/NT	4-Nitrotoluene
5-LO	5-Lipoxygenase
Å	Angstrom
AcOH	Acetic acid
Adp	2-Amino-3-(6,7-dimethoxy-4-coumaryl)-propionic acid
Ala	Alanine
AMPA	α -Amino-3-hydroxy-5-methyl-4-isoxazolepropionic acid
Aq.	Aqueous
Ar or Ar	Argon or Aryl
Arg	Arginine
Asn	Asparagine
Asp	Aspartate

atm	Atmosphere
BA	Benzoic acid
BE	Binding energy
BINAP	2,2'-bis(diphenylphosphino)-1,1'-binaphthyl
BLYP	Becke exchange and Lee-Yang-Parr correlation functional
Bn	Benzyl
Boc	<i>tert</i> -butyloxycarbonyl
BODIPY	Boron-dipyrromethene
BSA	Bovin serum albumin
Cat.	Catalytic
Cbz	Carboxybenzyl
CCD	Charge coupled device
CDC	Cross-Dehydrogenative coupling
CNS	Central nervous system
Conc.	Concentrated
COSY	Correlation spectroscopy
CT	Charge transfer
CuAAC	Copper-catalyzed azide-alkyne cycloaddition
Cys	Cysteine
<i>d</i>	Doublet
D	dexer
DABCO	1,4-Diazabicyclo[2.2.2]octane
DABSO	1,4-Diazabicyclo[2.2.2]octane bis(sulfur dioxide)
DAST	Diethylaminosulfur trifluoride
DBU	1,8-Diazabicyclo[5.4.0]undec-7-ene
DBU	1,8-Diazabicyclo[5.4.0]undec-7-ene
DCC	<i>N, N'</i> -Dicyclohexylcarbodiimide
DCE	1,2-Dichloroethane
DCM	Dichloromethane
DCM	Dichloromethane
DCP	Dicumyl peroxide

<i>dd</i>	Doublet of doublet
DEAM	Diethyl acetamidomalonate
DEDA	7,7-Dimethyleicosadienoic acid
DFT	Density functional theory
DIAD	Diisopropylazodicarboxylate
DIEA	Diisopropylethylamine
DIPEA	<i>N,N</i> -Diisopropylethylamine
DL	Detection limit
DLP	Dilauroylperoxide
DMA	<i>N,N</i> -Dimethylacetamide
DMA	Dimethylacetamide
DMAc	Dimethylacetamide
DMAP	4-Dimethylaminopyridine
Dmca	(6,7-dimethoxy-4-coumaryl) alanine
DME	Dimethoxyethane
DME	Dimethoxyethane
DMF	<i>N,N</i> -Dimethylformamide
DMSO	Dimethylsulfoxide
DMSO- <i>d</i> ₆	Deuterated dimethylsulfoxide
DNA	Deoxyribonucleic acid
DNA	Deoxyribonucleic acid
DNA	Deoxyribonucleic acid
DTC	Dithiocarbamate
E	Energy
ECP	Effective core potential
EDC·HCl	1-(3-Dimethylaminopropyl)-3-ethylcarbodiimidehydrochloride
EDGs	Electron-donating groups
EDT	Ethanedithiol
EI	Electron ionization
equiv	Equivalent

ESI	Electron spray ionization (MS)
ESIPT	Excited state intramolecular proton transfer
ESPT	Excited state proton transfer
E _T	Energy transfer efficiency
EtOAc	Ethyl acetate
EtOH	Ethanol
EWGs	Electron-withdrawing groups
Fmoc	Fluorenylmethoxycarbonyl
FmocNHS	9-Fluorenylmethoxycarbonyl- <i>N</i> -hydroxysuccinimide
FRET	Fluorescence resonance energy transfer
g	Gram
GABA	γ -aminobutyric acid
Gln	Glutamine
Glu	Glutamate
Gly	Glycine
h	Hours
Het-Ar	Heteroaryl
HETCOR	Heteronuclear correlation
His	Histidine
HMTA	Hexamethylenetetramine
HOBt	Hydroxybenzotriazole
HOMO	Highest occupied molecular orbital
HPLC	High-performance liquid chromatography
HRMS	High-resolution mass spectra
Hz	Hertz
IBX	2-Iodoxybenzoic acid
IC	Internal conversion
ICT	Internal charge transfer
IEF-PCM	Integral Equation Formalism- Polarizable Continuum Model

Ile	Isoleucine
<i>i</i> -PrOH	Isopropyl alcohol
IR	Infra-red
ISC	Intersystem crossing
<i>J</i>	Coupling constant
K	Kelvin
K_a	Association constant
K_q	Quenching rate constant
K_{sv}	Stern -Volmer quenching constant
L	Laevo
LE	Locally excited
LED	Light emitting diode
Leu	Leucine
Lit.	Literature
LUMO	Lowest unoccupied molecular orbital
Lys	Lysine
M	Molar
<i>m</i>	Multiplet
MCA	Multichannel analyzer
<i>m</i> -CPBA	<i>meta</i> -Chloroperoxybenzoic acid
Met	Methionine
mg	Milligram
MHz	Mega hertz
min	Minutes
mmol	Millimole
MOMCl	Chloromethyl methyl ether
mp	Melting point
MSA	Methanesulfonic acid
MW	Microwave
N	Normality
NACs	Nitro-aromatic compounds
NB	Nitrobenzoic acid

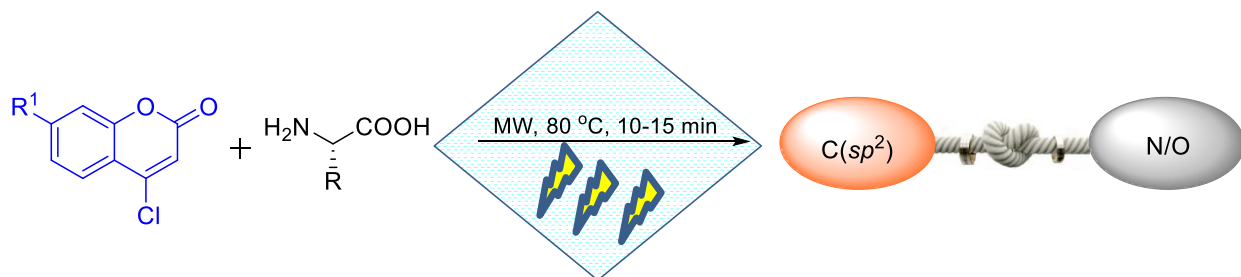
NBS	<i>N</i> -Bromosuccinimide
NCS	<i>N</i> -Chlorosuccinimide
NHC	<i>N</i> -heterocyclic carbene
NIR	Near InfraRed
nm	Nanometer
nM	Nanomolar
NM	Nitromethane
NMM	3- <i>N</i> -methyl morpholine
NMP	<i>N</i> -Methyl-2-pyrrolidone
NMR	Nuclear magnetic resonance
Nu	Nucleophile
<i>o</i>	Ortho
<i>o</i> -DCB	1,2-Dichlorobenzene
ORTEP	Oak ridge thermal ellipsoid plot
-OTf	Trifluoromethanesulfonate
PA	picric acid
PET	Photo-induced electron transfer
Pg	Protecting group
PIDA	Phenyl iodonium diacetate
PivOH	Pivalic acid
ppb	Parts per billion
ppm	Parts per million
psi	Pounds per square inch
<i>p</i> -TSA or <i>p</i> -TsOH	<i>p</i> -Toluenesulfonic acid
Py	Pyridine
R	Rectus
r.t.	Room temperature
RNA	Ribonucleic acid
s	Singlet
S	Sinister
SCRf	Self-consistent reaction field
SDS	Sodium dodecyl sulfate

Ser	Serine
SET	Single electron transfer
S_N	Nucleophilic substitution
S-V	Stern-Volmer
t	Triplet
T	Temperature
TAC	Time to amplitude convertor
TBAB	Tetrabutylammonium bromide
TBABr	Tetra- <i>n</i> -butylammonium bromide
TBHP	<i>tert</i> -Butyl hydroperoxide
TBPB	<i>tert</i> -Butyl peroxybenzoate
TCEP	<i>tris</i> -Carboxyethylphosphine
TCEP	Tris(2-carboxyethyl)phosphine
TCSPC	Time correlated single photon counting
TEA	Triethyl amine
TEMPO	2,2,6,6-tetramethylpiperidine-1-oxyl
TES	Triethylsilane
TFA	Trifluoroacetic acid
TFAA	Trifluoroacetic anhydride
THF	Tetrahydrofuran
Thr	Threonine
TICT	Twisted intramolecular charge transfer
TIS	Triisopropylsilane
TLC	Thin layer chromatography
TMEDA	Tetramethylethylenediamine
TMS	Tetramethylsilane
TMSCl	Trimethylsilyl chloride
TNT	2,4,6-trinitrotoluene
TOF	Quadrupole time-of-flight
TosMIC	<i>p</i> -Toluenesulfonylmethylisocyanide
UV	Ultra Violet
UV-Vis	Ultraviolet-Visible

v/v	Volume per volume
Val	Valine
W	Watt
Xphos	XPhos [2-Dicyclohexylphosphino-2',4',6'-triisopropylbiphenyl]
α	Alpha
β	Beta
γ	Gamma
Δ	Delta
δ	Parts per million
E	Dielectric constant
η	Refractive index
λ_{Em}	Emission Wavelength
λ_{Ex}	Excitation Wavelength
μl	microliter
μM	micromolar
π	Pi
T	Lifetime
Φ	Quantum yield
χ^2	Chi-square
Γ	Emissive rate of fluorophore

Chapter 1A

Copper-catalyzed C-N/C-O Coupling in Water: A Facile Access to Coumaryl-tagged and Coumaryl-labelled Amino Acids



1A.1 Background

Biomolecular recognition is the central event of each signaling step in biology. Amino acids and peptides, the integral fragments of proteins, stand-alone hormones, cytokines, toxins, and antimicrobials are the effectors of most signal transduction processes.¹⁻² Among these, synthetic peptides regulate almost all receptor responses. Also, amino acids, peptides, and proteins are ubiquitous molecules that play key roles in modulating structure, and functioning of living cells.³⁻⁴ However, impairing of amino acid metabolism in the body may lead to various disease conditions (*e.g.* phenylketonuria). To counter this, several peptide based drugs have been developed, and successfully applied in treating certain human diseases.⁵⁻⁶ Some selective examples of peptide based drugs include: (i) Goserelin (marketed as Zoladex) used for treating breast and prostate cancers,⁷ (ii) Glatiramer acetate (marketed as Copaxone) used for multiple sclerosis,⁸ (iii) Epiibatide (marketed as Integrilin) used for acute coronary syndrome and unstable angina,⁹ and (iv) Octreotide (marketed as Sandostatin) used for the treatment of cancer¹⁰ (Figure 1A.1.1).

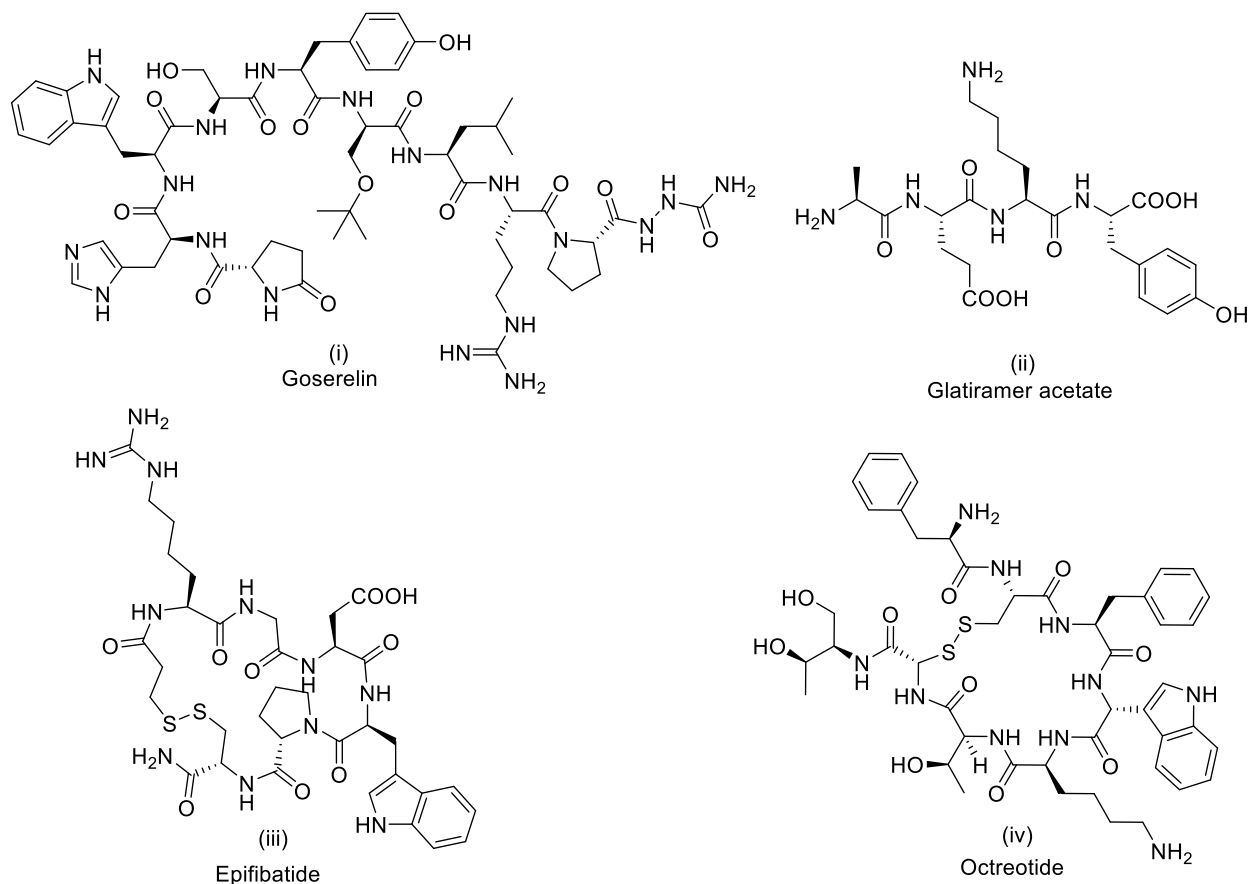


Figure 1A.1.1: Selective examples of peptide based drugs

At present, the approved peptide based drugs are generating reasonable revenues in commercial sector, and the peptide drug market is growing twice as fast in the worldwide drug market. Currently, 60-70 peptide drugs are approved in the global market, and about 100-200 are in clinical trials. Moreover, several peptide-based pharmaceuticals have been developed as useful therapeutic agents that possess high potency, selectivity and accumulate in lower concentration in tissues.¹¹⁻¹⁴ Thus, investigating and understanding biologically relevant interactions and processes, such as receptor–ligand binding, protein structures, protein folding, protein–protein interactions, and enzyme activity relationship using labelling techniques has become an established exercise in biochemical research.¹⁵ In other words, biologically active peptides serve as an interesting starting point in drug discovery processes.^{6,16-17}

In the past, several labelling methods¹⁸ for tracking biomolecules using isotope markers,¹⁹ colorimetric biosensors,²⁰ photochromic compounds,²¹ biomaterials,²² electrochemical sensors,²³ fluorogen²⁴ and fluorescent labels²⁵ have been explored (Figure 1A.1.2).

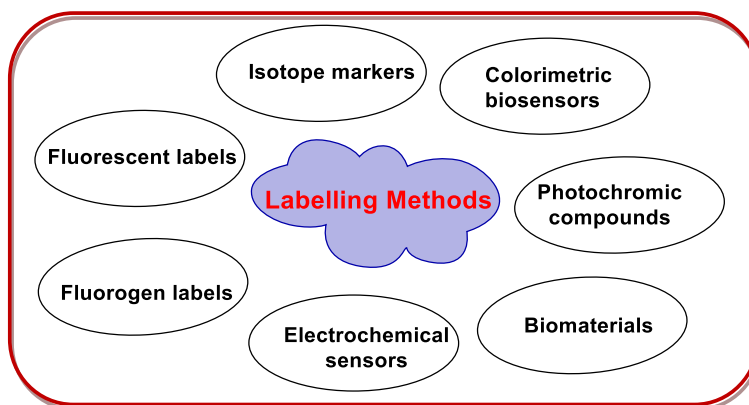


Figure 1A.1.2: Existing labelling methods for tracking biomolecules

Among these, labelling by a fluorescent probe is at the forefront due to its high selectivity, easy-handling and non-destructive nature. Over the years, “a fluorescent tag” also known as a “label” or “probe” has been broadly explored in molecular biology and biotechnology for tracking amino acids *via* chemical attachment.²⁶ Fluorescent labelling is generally accomplished by using a reactive derivative of the fluorophore that selectively binds to a functional group present in the target molecule. Though certain amino acids such as tryptophan, phenylalanine and tyrosine have intrinsic fluorescence, yet extrinsic labels provide far greater advantages for observing biological processes.²⁷⁻²⁸ Ideally, a fluorescent labelled amino acid/peptide can be visualized or counted through photobleaching.

In recent years, much advancement has been made in the area of amino acid/peptide labelling²⁹ at the expense of a variety of fluorophores including fluorescein,³⁰ rhodamine,³¹ coumarin,³² cyanine,³³ Alexa Fluor 405 dyes,³⁴ BODIPY dyes,³⁵ green fluorescent protein,³⁶ and inorganic particles such as quantum dots³⁷ (Figure 1A.1.3). However, some of these are associated with the drawbacks, such as (i) relatively long, flexible linkers between the probe and protein, which questions whether the probe motions faithfully with the motion of the residue to which it is attached, and (ii) multiple charges and relatively large surface areas that can perturb the local structure or motion, and inhibits labelling at certain positions.³⁸⁻⁴⁴

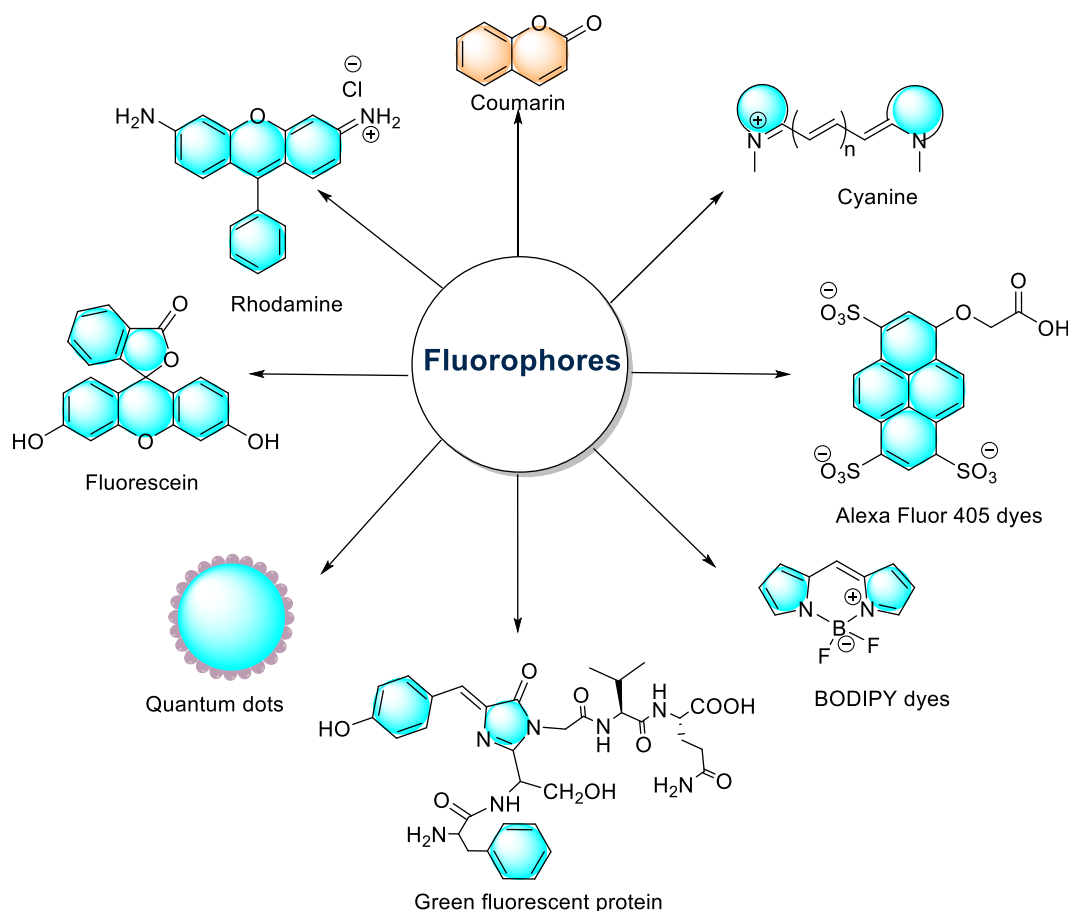


Figure 1A.1.3: Selective examples of fluorophores used in labelling studies

Among these, coumarin is an excellent example of a fluorescent label, providing the most commercially acceptable fluorescent derivatives with the advantages of an extended spectral range, high emission quantum yield, photostability and good solubility in many solvents. Coumarin has two six-membered rings fused together, with one of the ring being a benzene ring, and the other containing alkene functionality and an ester functional group (Figure 1A.1.3). It was

first isolated from Tonka beans in 1820s, and synthetically prepared in 1868 by William Henry Perkin.⁴⁵ Due to ample availability in nature, it permits the basic process of life such as metabolism, transmission of nerve impulses, and identification of biochemical reactions.⁴⁶ Numerous fluorescent coumarin derivatives have been reported, underlying photophysical mechanisms for the observed fluorescence properties. The extensive use of coumarin as covalently attached fluorescent label in biochemical processes has been progressively explored due to dependence of its fluorescence behavior on various properties such as polarity,⁴⁷ polarizability,⁴⁸ microviscosity,⁴⁹ hydrogen bonding potential⁵⁰ and pH.⁵¹ In addition, coumarins are ideal fluorescent guests to probe the nature and binding capacity of host molecules. The polarity and the conformation greatly affects the formation of twisted intramolecular charge transfer (TICT) states, and the polarity changes the relative energy levels; all of which result insignificant and easily measurable changes in the coumarin probe fluorescence.⁵²

In particular, coumaryl-labelled amino acids have received special interest due to their sensitivity to pH and solvent polarity that makes them excellent fluorescent molecules to investigate numerous biological processes in living organisms (Figure 1A.1.4).⁵³⁻⁵⁶

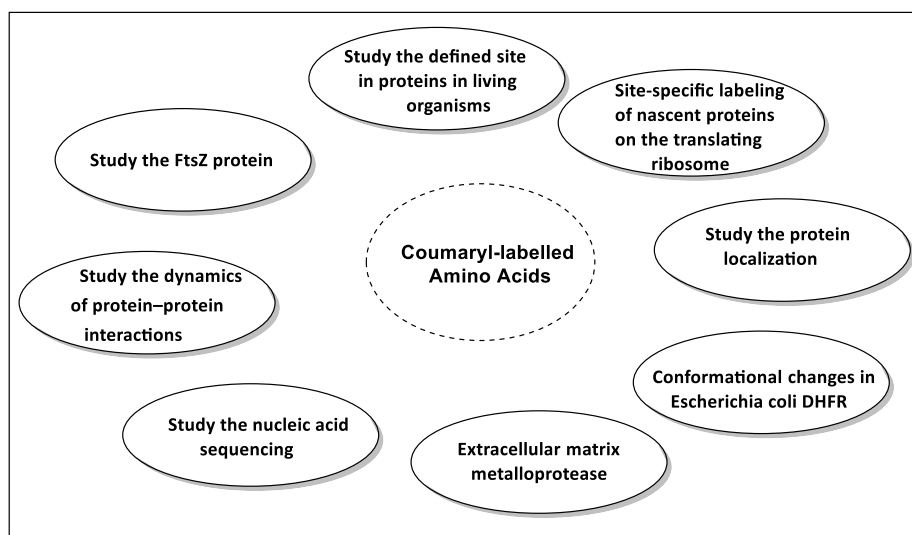
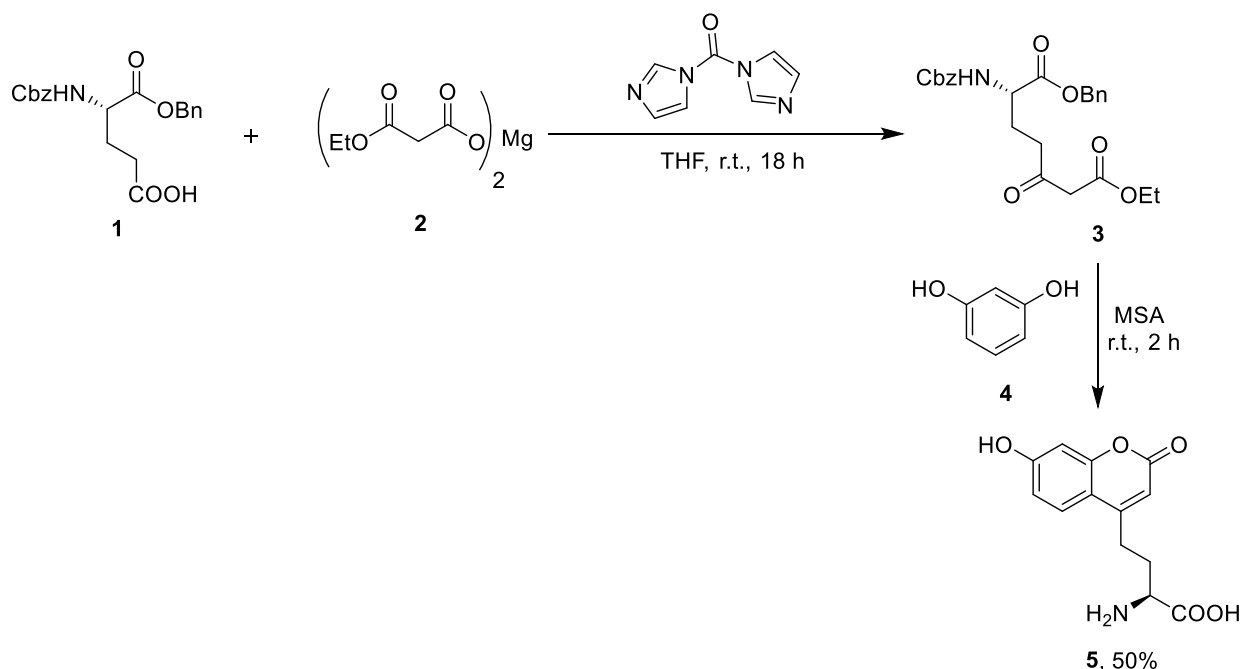


Figure 1A.1.4: Applications of coumaryl-labelled amino acids in biochemical research

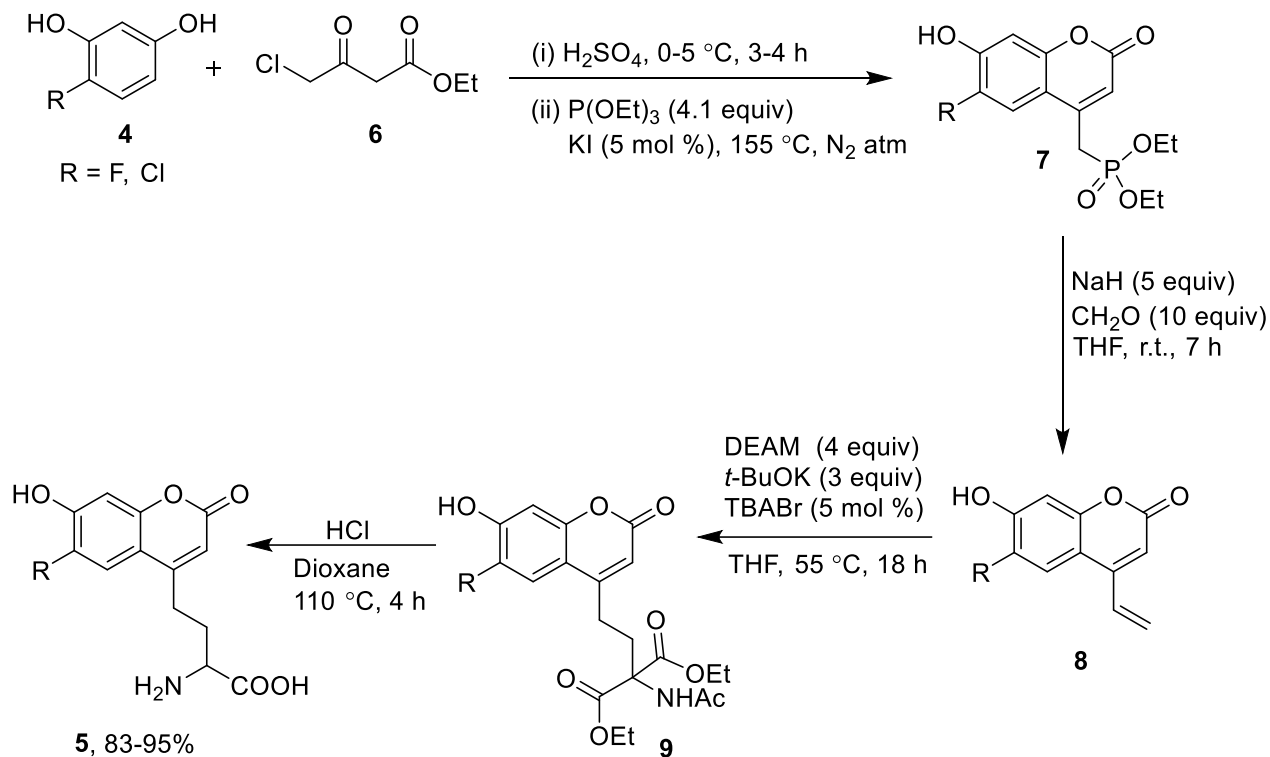
In view of the above importance, immense progress has been witnessed towards the synthesis and application of coumaryl-labelled amino acids and peptides.⁵⁷⁻⁶⁹ A comprehensive summary on the existing strategies used to synthesize different coumaryl-labelled and coumaryl-tagged amino acids and peptides is as follows:

Wang *et al.* reported an excellent protocol for the preparation of α -L-(2-(7-hydroxycoumarin-4-yl)ethyl)glycine (**5**), that was genetically incorporated at the defined site in proteins of living organisms. In this approach, *N*- α -Cbz-*L*-glutamic acid α -benzyl ester (**1**) was first reacted with ethyl magnesium malonate (**2**) to obtain a β -keto ester (**3**), which on reaction with resorcinol (**4**) in presence of methanesulfonic acid (MSA) afforded α -L-(2-(7-hydroxycoumarin-4-yl)ethyl)glycine (**5**) in 50% yield (Scheme 1A.1.1).⁷⁰



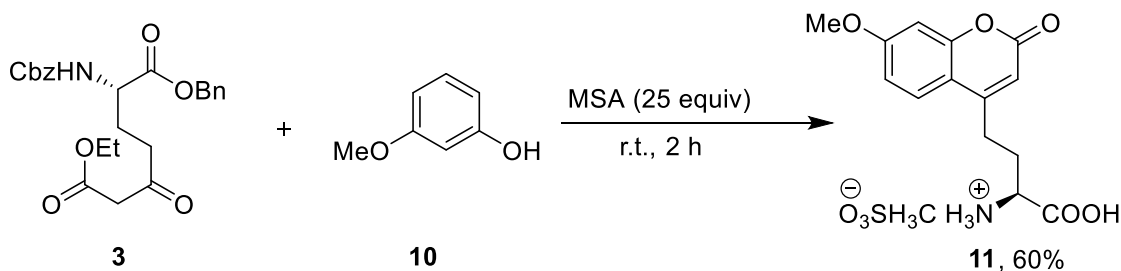
Scheme 1A.1.1: Synthesis of α -L-(2-(7-hydroxycoumarin-4-yl)ethyl)glycine (**5**)

Xu *et al.* followed a five-step protocol to prepare various coumaryl-labelled non-natural amino acids derivatives (**5**), and explored their fluorescence properties (Scheme 1A.1.2). The strategy was initiated by the synthesis of diethyl ((7-hydroxy-2-oxo-2*H*-chromen-4-yl)methyl)phosphonate (**7**) from substituted resorcinols (**4**) and ethyl chloroacetoacetate (**6**) *via* formation of 4-chloromethyl-7-hydroxy-2-oxo-2*H*-chromene, followed by phosphorylation using $\text{P}(\text{OEt})_3$ using catalytic KI. Thereafter, **7** upon Horner-Wadsworth-Emmons reaction with formaldehyde in presence of NaH afforded 4-vinyl-7-hydroxy-2-oxo-2*H*-chromene (**8**), which on reaction with diethyl acetamidomalonate (DEAM) yielded malonate derivative (**9**). Finally, acid-mediated hydrolysis, decarboxylation and deprotection of **9** afforded racemic (2-(7-hydroxycoumarin-4-yl)ethyl)glycine (**5**) (Scheme 1A.1.2).⁶⁵



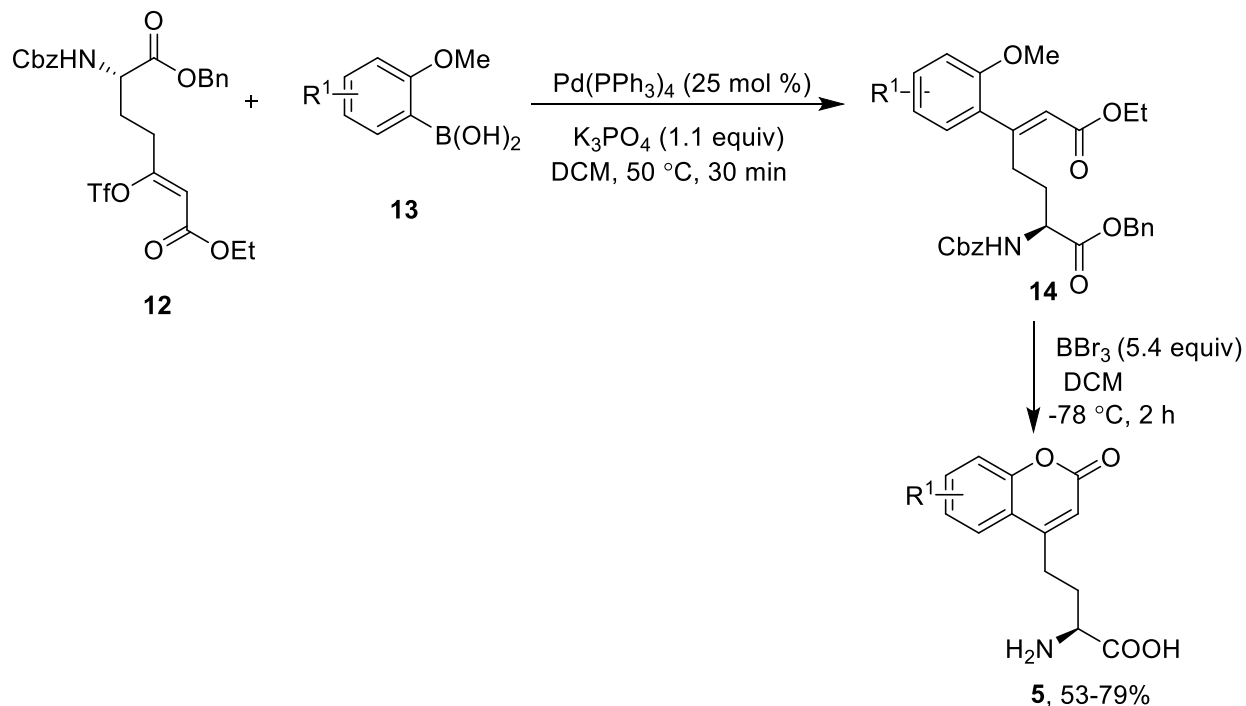
Scheme 1A.1.2: Multistep synthesis of racemic (2-(7-hydroxycoumarin-4-yl)ethyl)glycine (**5**)

Brun *et al.* reported the coupling between 1-benzyl 7-ethyl (*S*)-2-((benzyloxy)carbonyl)amino)-5-oxoheptanedioate (**3**) with 3-methoxyphenol (**10**) using MSA at room temperature to afford enantiomerically pure α -L-(2-(7-methoxycoumarin-4-yl)ethyl)glycine methane sulfonic acid (**11**) in 60% yield (Scheme 1A.1.3).⁷¹



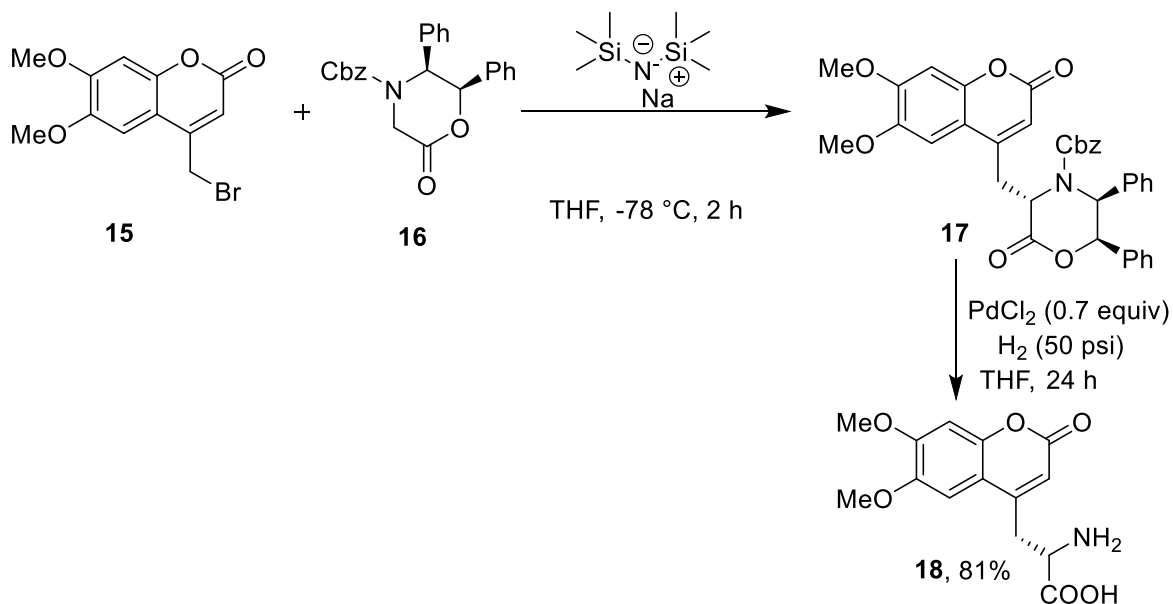
Scheme 1A.1.3: Synthesis of enantiomerically pure α -L-(2-(7-methoxycoumarin-4-yl)ethyl)glycine methane sulfonic acid (**11**)

Moodie *et al.* documented a Pd-catalyzed strategy for coupling *o*-methoxyboronic acids (**13**) and a glutamic acid derived (*Z*)-vinyl triflate (**12**) to afford the cross-coupled product **14**, which upon deprotection and intramolecular cyclization using BBr_3 in DCM resulted in the formation of α -L-(2-(7-substituted coumarin-4-yl)ethyl)glycine (**5**) derivatives (Scheme 1A.1.4).⁷²



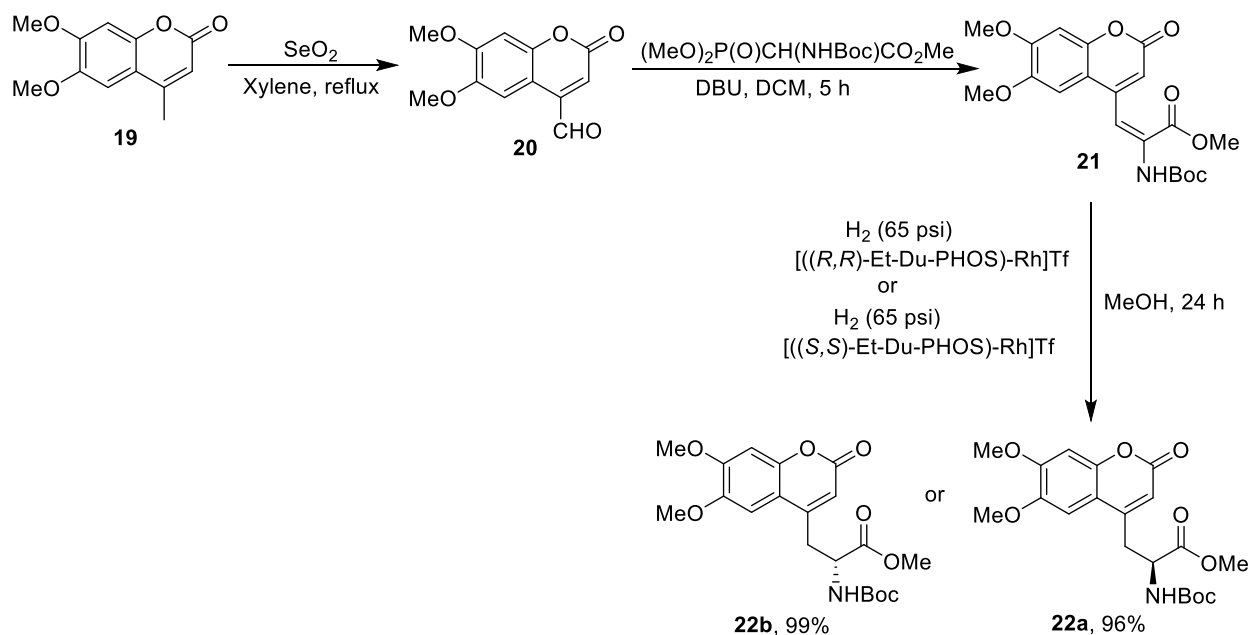
Scheme 1A.1.4: Pd-catalyzed synthesis of α -L-(2-(7-hydroxycoumarin-4-yl)ethyl)glycines (**5**)

Sui *et al.* developed a two-step approach for the synthesis of chiral L-2-amino-3-(6,7-dimethoxy-4-coumaryl)propionic acid (L-Adp) (**18**) in high stereoselectivity (>99.5%) by coupling 4-bromomethyl-6,7-dimethoxycoumarin (**15**) with benzyl (2*R*,3*S*)-6-oxo-2,3-diphenylmorpholine-4-carboxylate (**16**), followed Pd(II) catalyzed reduction of the coupled product **17** (Scheme 1A.1.5). The authors studied the use of L-Adp as fluorophore quencher pair for peptide assays.⁷³



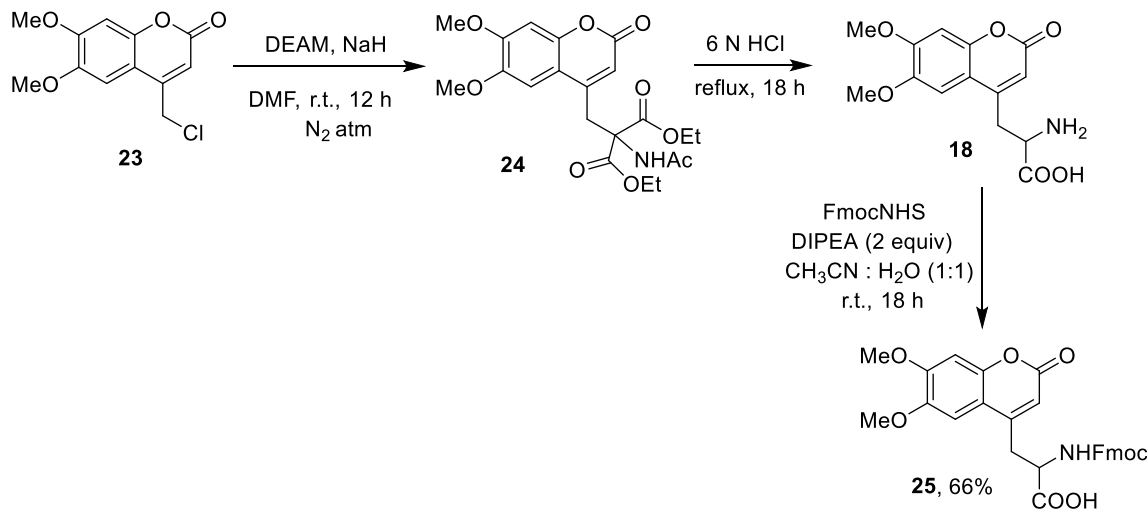
Scheme 1A.1.5: Synthesis of L-2-amino-3-(6,7-dimethoxy-4-coumaryl)propionic acid (**18**)

Wang *et al.* described an asymmetric multistep approach for the synthesis of Boc protected 6,7-dimethoxy coumaryl-labelled alanine (Dmca) starting from commercially available 6,7-dimethoxy-4-methylcoumarin (**19**). The strategy initiated with the oxidation of **19** using selenium dioxide to yield 6,7-dimethoxy-2-oxo-2*H*-chromene-4-carbaldehyde (**20**), which on Horner-Emmons olefination with $(\text{MeO})_2\text{P}(\text{O})\text{CH}(\text{NHBoc})\text{CO}_2\text{Me}$ under basic conditions afforded dehydro amino acid methyl ester (**21**). Asymmetric hydrogenation of **21** using rhodium based chiral catalysts afforded enantiomerically pure Dmca (**22a** & **22b**) in appreciable yields (Scheme 1A.1.6).⁶⁶



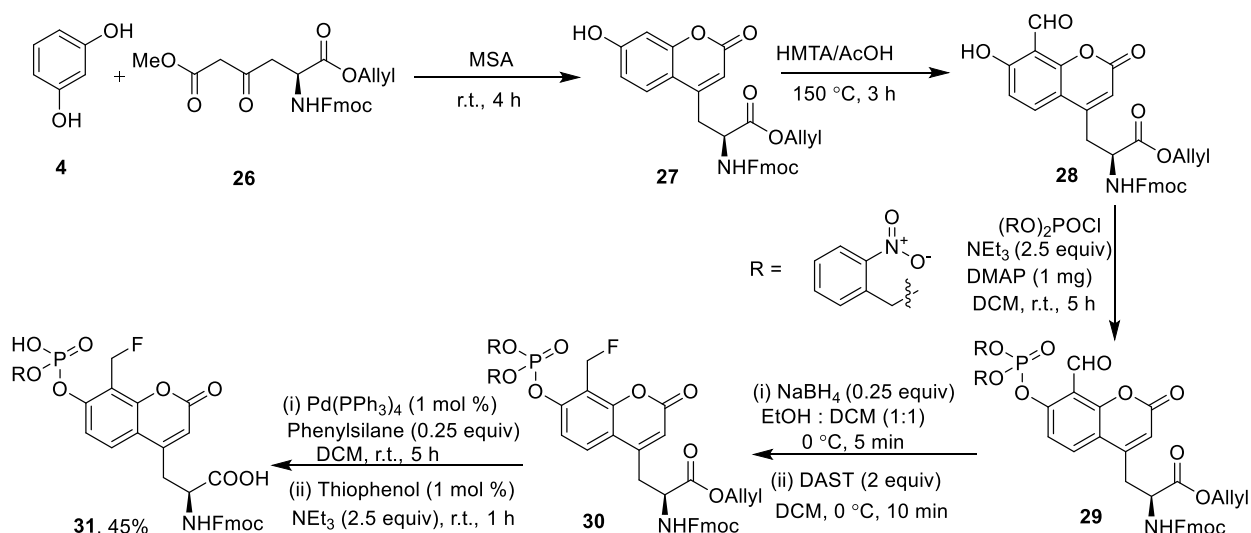
Scheme 1A.1.6: Enantioselective synthesis of Boc protected coumaryl-labelled alanine (Dmca) (**22a-b**)

Bennett *et al.* reported a multistep synthesis of racemic Fmoc protected (6,7-dimethoxy-4-coumaryl)alanine (**25**), and used it for quantitative detection of synthetic peptides in HPLC, and in minimal essential media (MEM). The strategy initiated with coupling of 4-chloromethyl-6,7-dimethoxycoumarin (**23**) with diethyl acetamidomalonate (DEAM) using NaH to produce malonate derivative (**24**), which on acid-mediated hydrolysis, decarboxylation, deprotection and subsequent coupling with 9-fluorenylmethoxycarbonyl-*N*-hydroxysuccinimide (FmocNHS) afforded racemic Fmoc protected (6,7-dimethoxy-4-coumaryl)alanine (**25**) (Scheme 1A.1.7).⁴⁴



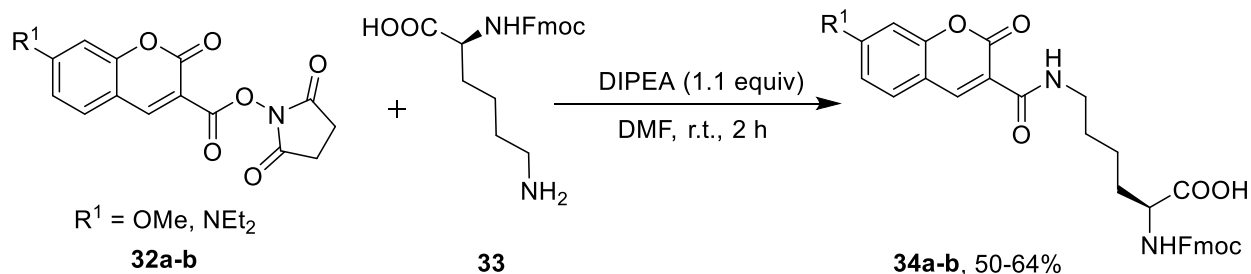
Scheme 1A.1.7: Synthesis of racemic Fmoc protected (6,7-dimethoxy-4-coumaryl)alanine (**25**)

Yao *et al.* reported the synthesis of self-immobilizing and fluorogenic phosphotyrosine (pTyr) mimic, coumaryl-labelled alanine (**31**), which found applications in bioimaging and fluorescence-activated cell sorting. The synthesis was initiated by the coupling of (*S*)-1-allyl 6-methyl 2-(((9*H*-fluoren-9-yl)methoxy)carbonylamino)-4-oxohexanedioate (**26**) with resorcinol (**4**) under acidic conditions to yield 7-hydroxy Fmoc-protected coumaryl-labelled alanine allyl ester (**27**). Further, a four-step methodology involving, a) formylation using Duff reaction, b) phosphorylation using di(2-nitrobenzyl) chlorophosphate [(RO)₂POCl], c) aldehyde reduction, and fluorination using diethylaminosulfur trifluoride (DAST) were performed to afford **30**. Finally, pd-catalyzed allyl deprotection of **30**, followed by benzyl deprotection using triethyl amine and catalytic thiophenol afforded the desired product **31** in 45% yield (Scheme 1A.1.8).⁷⁴



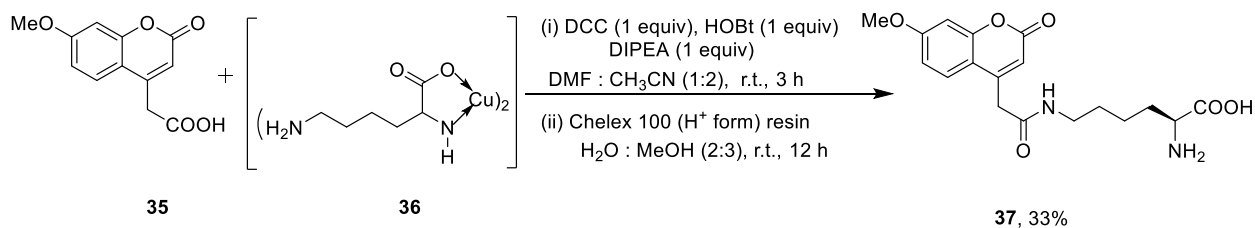
Scheme 1A.1.8: Synthesis of phosphotyrosine (pTyr) mimic, coumaryl-labelled alanine (**31**)

Katritzky group synthesized N^{ϵ} -(7-substituted coumarin-3-carboxyl)-L-Fmoc lysine (Fmoc-Lys(MC)-OH) (**34a-b**) by coupling commercially available N^{α} -Fmoc-L-lysine (**33**) with prior activated 2,5-dioxopyrrolidin-1-yl 7-substituted 2-oxo-2*H*-chromene-3-carboxylate (**32a-b**) in DMF at room temperature (Scheme 1A.1.9). The synthesized derivatives were used as potential tools for cell imaging.⁷⁵



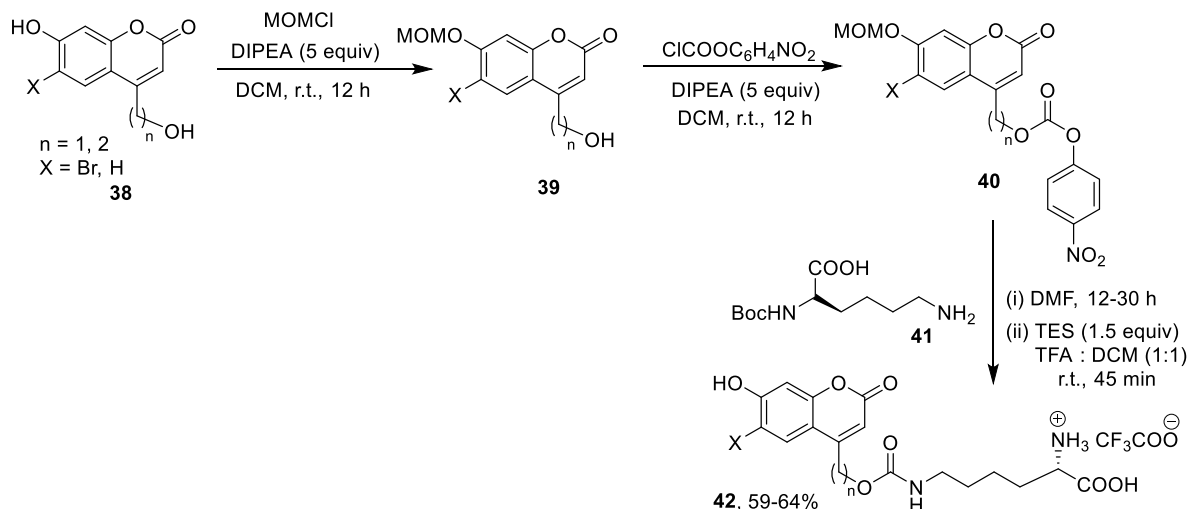
Scheme 1A.1.9: Synthesis of N^{ϵ} -(7-substituted coumarin-3-carboxyl)-L-Fmoc lysine (**34**)

Malkar *et al.* synthesized N^{ϵ} -[(7-methoxycoumarin-4-yl)acetyl]-L-lysine (**37**) by coupling 7-methoxycoumarin-4-ylacetic acid (**35**), with copper chelated L-lysine (**36**) using coupling reagent DCC followed by washing with Chelex 100 (H^+) resin (Scheme 1A.1.10).⁷⁶



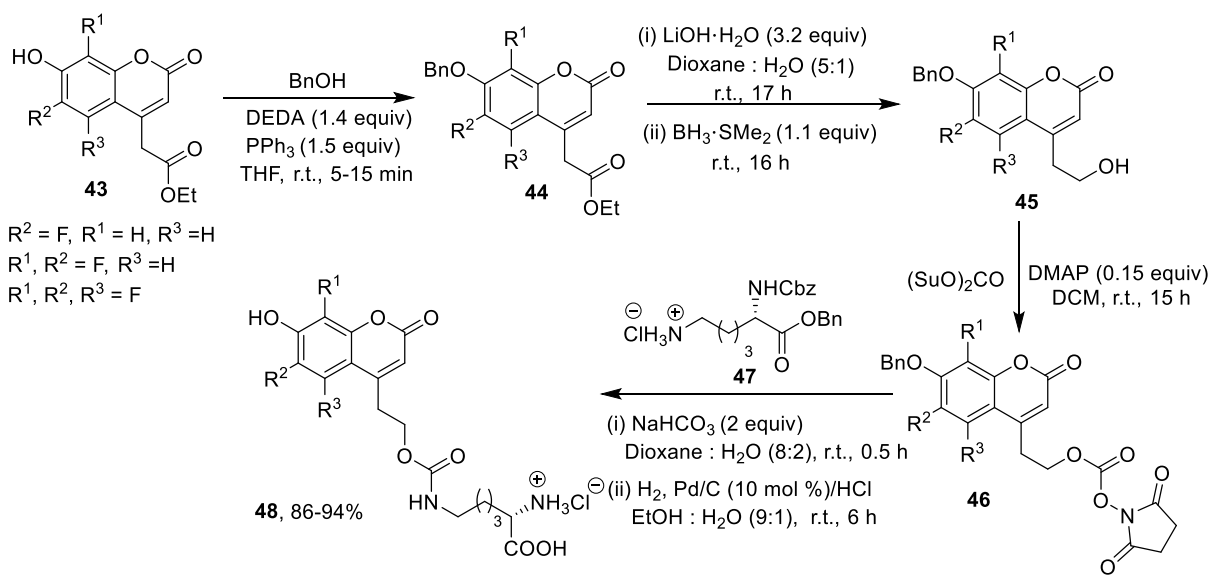
Scheme 1A.1.10: Synthesis of N^{ϵ} -[(7-methoxycoumarin-4-yl)acetyl]-L-lysine (**37**)

Luo *et al.* documented a three-step protocol for synthesizing coumaryl-labelled lysine conjugates that found applications in protein localization, and optical activation of protein function. The multistep synthesis was initiated by the protection of 7-hydroxy coumarin alcohol (**38**) with chloromethyl methyl ether (MOMCl) in the presence of DIPEA to yield protected coumarin alcohol (**39**) derivative, which upon activation using nitrophenylchloroformate furnished coumarin carbonate (**40**) derivative. Finally, **40** on coupling with Boc-Lysine (**41**) in DMF, followed by deprotection using TFA in the presence of triethylsilane (TES) as a cation scavenger afforded coumarin lysine trifluoroacetic acid salts (**42**) (Scheme 1A.1.11).⁷⁷



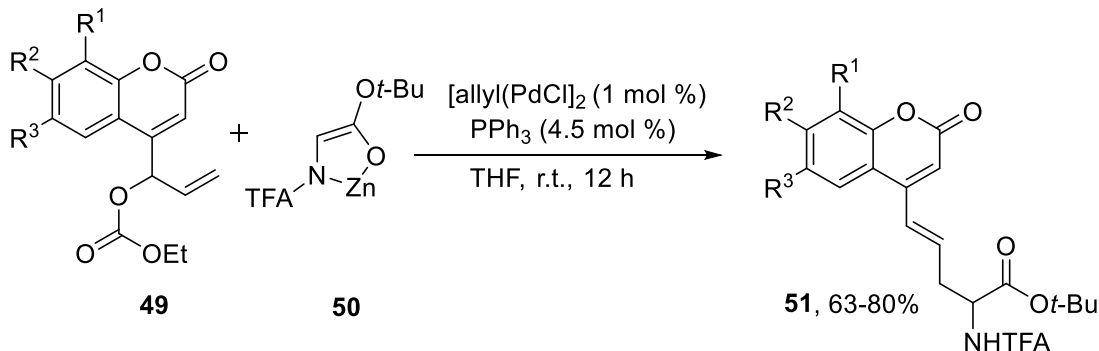
Scheme 1A.1.11: Synthesis of coumaryl-labelled lysine trifluoroacetate salts (**42**)

Very recently, Shukla *et al.* documented a multistep synthesis of fluorinated coumaryl-labelled lysine derivatives, and studied their photophysical properties.⁷⁸ The synthesis was initiated by the protection of phenolic hydroxyl group of ethyl 2-(7-hydroxy-2-oxo-2*H*-chromen-4-yl)acetates with benzyl alcohol (**43**) under Mitsunobu conditions to yield benzylated coumaryl esters (**44**), which on lithium hydroxide-mediated hydrolysis and subsequent reduction with BH₃·SMe₂ produced coumaryl alcohols (**45**). **45** on further activation with *N,N'*-disuccinimidyl carbonate ((SuO)₂CO) afforded OSu-carbonates (**46**), which on coupling with Cbz-protected lysine benzyl ester (**47**), followed by benzyl and Cbz deprotection using (H₂- Pd/C) and aq. HCl furnished the desired products (**48**) in 86-94% yields (Scheme 1A.1.12).⁷⁸



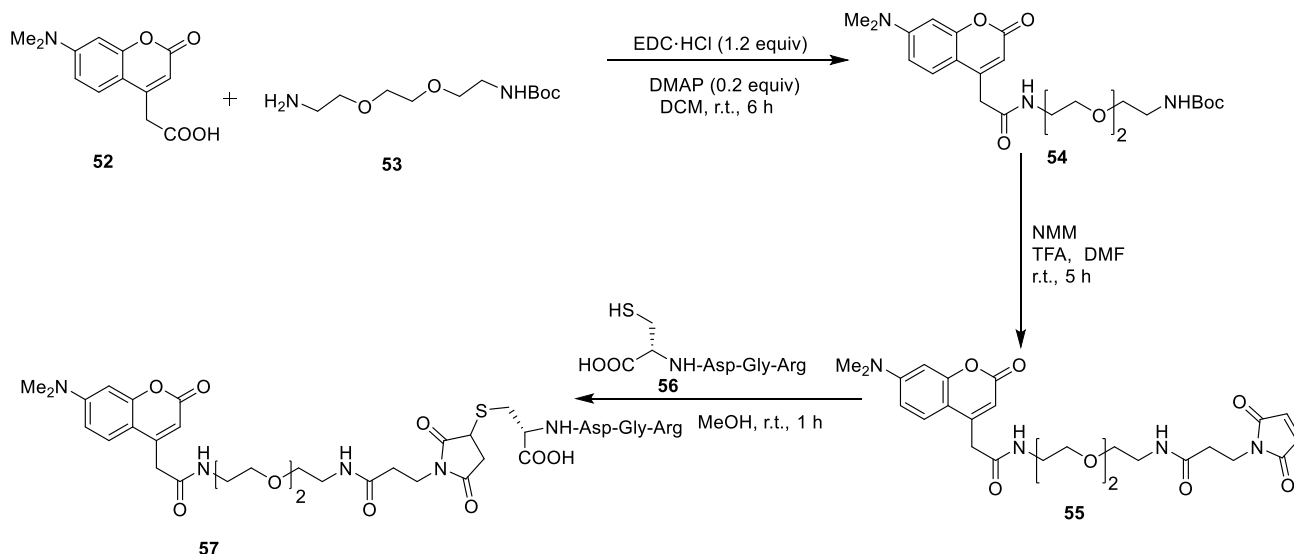
Scheme 1A.1.12: Synthesis of fluorinated coumaryl-labelled lysine (**48**) derivatives

Schmidt *et al.* documented a Pd-catalyzed allylic alkylation reaction of coumaryl activated allylic carbonates (**49**) with zinc chelated glycine-enolate (**50**) to afford novel coumaryl-labelled α -amino acids (**51**) in 63-80% yields (Scheme 1A.1.13).⁷⁹



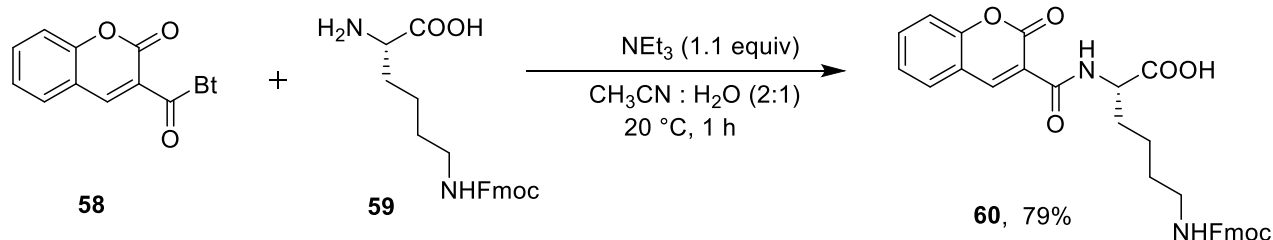
Scheme 1A.1.13: Pd-catalyzed synthesis of coumaryl-labelled α -amino acids (**51**)

Song *et al.* reported the synthesis of coumaryl-labelled Arg-Gly-Asp-Cys conjugate, in three-steps by first coupling of 7-dimethylaminocoumarin-4-acetic acid (**52**) with *N*-Boc-1,8-diamino 3,6-dioxaoctane (**53**) to yield Boc-coumarin-carbamate (**54**). Thereafter, coupling of **54** with 3-*N*-methyl morpholine (NMM) in DMF using TFA afforded coumarin 3-(maleimido)propionamide (**55**), which was finally used for the labelling of Arg-Gly-Asp-Cys-SH (RGD-C) (**56**) in MeOH at room temperature to give coumaryl-labelled Arg-Gly-Asp-Cys conjugate (**57**) (Scheme 1A.1.14).⁶³



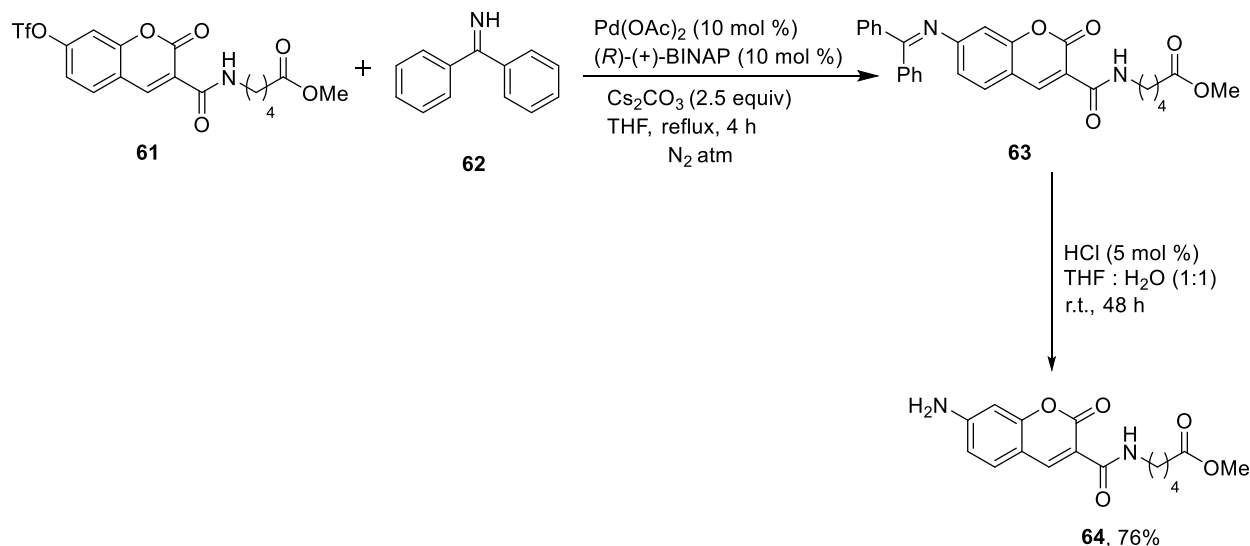
Scheme 1A.1.14: Synthesis of coumaryl-labelled Arg-Gly-Asp-Cys conjugate (**57**)

Apart from these reports, a few more coumaryl-appended amino acids has been synthesized. For example, Katritzky *et al.* documented the synthesis of *N^ε*-coumaryl-labelled *N^γ*-Fmoc-L-lysine (**60**) by coupling coumarinoyl benzotriazole (**58**) with *N^γ*-Fmoc-L-lysine (**59**) in aqueous CH₃CN at 20 °C, (Scheme 1A.1.15).⁸⁰



Scheme 1A.1.15: Synthesis of *N^ε*-coumaryl-labelled *N^γ*-Fmoc-L-lysine (**60**)

Jin *et al.* disclosed a convergent synthesis of 7-aminocoumaryl-appended unnatural amino acid (**64**) by Pd-catalyzed Buchwald–Hartwig cross-coupling of its corresponding 7-*O*-triflate derivative (**61**) with benzophenone imine (**62**), followed by acidic hydrolysis (Scheme. 1A.1.16). The authors used the amino functionalized coumaryl-appended product (**64**) for specific protein labelling in living cells.⁵⁴



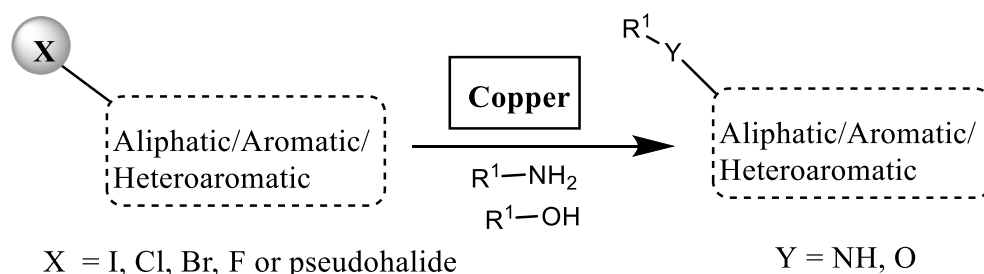
Scheme 1A.1.16: Synthesis of the 7-aminocoumaryl-appended unnatural amino acid (**64**)

Though numerous synthetic strategies are known for coumaryl-labelled and coumaryl-appended amino acids, yet most of the synthetic strategies developed in past involves multistep synthesis with many protection/deprotection steps, provide moderate yields, uses expensive reagents, and also requires tedious purification procedures either by preparative TLC/HPLC or by column chromatography. Thus, developing alternate strategies for the synthesis of coumaryl-

tagged/coumaryl-labelled amino acids is highly desirable. Inspired by the fascinating applications of coumaryl-labelled amino acids/peptides, we anticipated to synthesize novel coumaryl-tagged and coumaryl-labelled amino acids/peptides under Cu-catalyzed conditions.

1A.2 Introduction

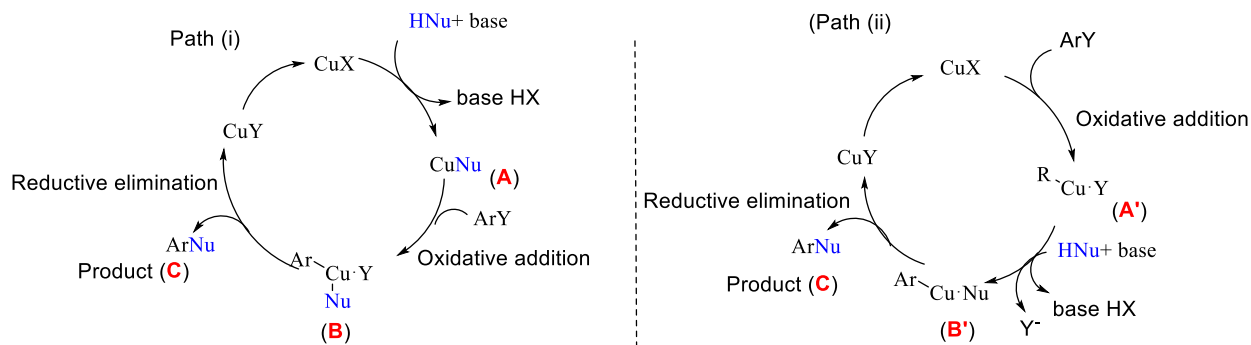
More than half basket of the present chemical inventory consists of molecules with carbon-heteroatom (C-N/C-O/C-S) bonds in their structural periphery. The construction of the C–N/C–O bond is of significant importance, as it opens new avenues for numerous pharmaceuticals, agrochemicals and biologically active compounds. Diverse compounds such as alkaloids,⁸¹ antibiotics,⁸² essential amino acids,⁸³ vitamins,⁸⁴ haemoglobin,⁸⁵ porphyrins,⁸⁶ hormones,⁸⁷ and different oligomers⁸⁸ (nucleic acids, proteins)⁸⁹ contain C-N/C-O bonds in their skeleton.⁹⁰⁻⁹³ Despite significant advancements in the existing C-N/C-O bond forming strategies, the construction of the C–N/C–O bond still remains a major challenge for organic chemists, due to harsh reaction conditions or the use of expensive Pd catalysts.⁹⁴⁻⁹⁶ In this regard, noticeable progress has been made through the employment of different Cu-catalysts, effectively replacing the traditional approaches (Scheme 1A.2.1).⁹⁷⁻¹⁰²



Scheme 1A.2.1: A general representation of Cu-catalyzed C–N/C–O coupling reactions

The utility of copper salts towards the formation of C-N bonds was explored in early 1900 century by Fritz Ullmann and Irma Goldberg. The coupling reaction between aromatic halides and nucleophiles (amines and phenols) in presence of copper has been referred as an Ullmann coupling reaction. To date, this reaction has shown pivotal applications in organic synthesis.¹⁰³⁻¹⁰⁴ Since the first mechanistic hypothesis began to come into view, several mechanisms between 1960 and 1990 were proposed.¹⁰⁵⁻¹⁰⁹ Whereas it was generally agreed that the reaction mechanism of the Ullmann reaction is extensively deliberate and supposed to proceed through two probable catalytic pathways, path (i) & path (ii) (Scheme 1A.2.2).¹⁰⁶ Path (i) initiated with the coordination of the nucleophile to the Cu-catalyst to produce more reactive complex (A), which on oxidative addition

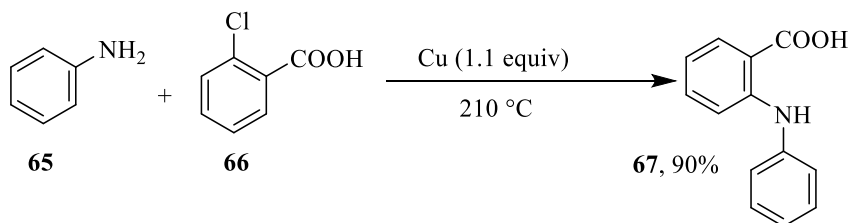
of aryl halide affords **B**. Finally, **B** on reductive elimination yields the aminated product. In path (ii), copper first coordinates to the aromatic ring of the aryl halide *via* oxidative addition to give more electrophilic intermediate (**A'**), which eventually reacts with nucleophile in presence of base to generate intermediate **B'**. **B'** eventually affords the final product **C** upon reductive elimination (Scheme 1A.2.2, Path (i) & (ii)).¹⁰⁷



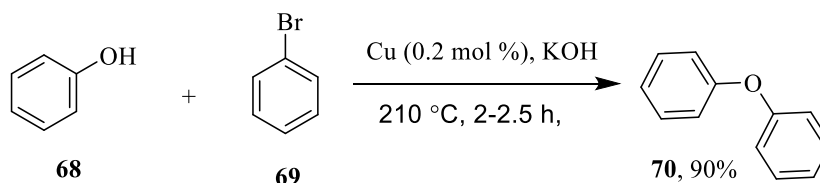
Scheme 1A.2.2: Acceptable mechanistic pathways for Ullmann cross-coupling reaction

As described, Ullmann initially documented an amination reaction between aniline (**65**) and 2-chlorobenzoic acid (**66**) using stoichiometric amount of Cu powder under reflux condition to afford 2-phenylaminobenzoic acid (**67**) (Scheme 1A.2.3 (i)). In 1905, the author further presented a Cu-catalyzed reaction between phenol (**68**) and 2-bromobenzene (**69**) at 210 °C to furnish oxydibenzene (**70**) in 90 % yield (Scheme 1A.2.3 (ii)).¹⁰⁸⁻¹¹⁰

(i) Ullmann, 1903



(ii) Ullmann, 1905

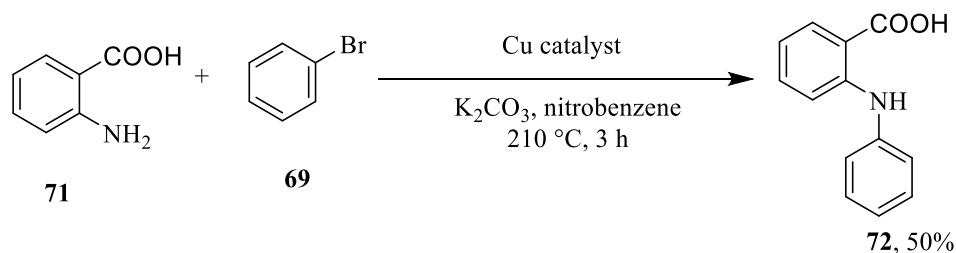


Scheme 1A.2.3: Cu-catalyzed Ullmann C-N/C-O coupling reactions

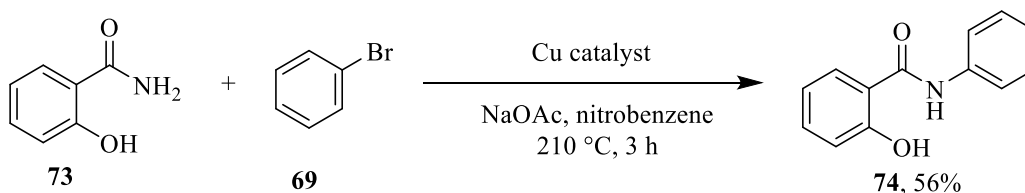
Thereafter, Goldberg reported the direct amination and amidation of 2-aminobenzoic acid (**71**) and 2-hydroxybenzamide (**73**) with bromobenzene (**69**) to obtain **72** and **74**, respectively using copper

catalyst in nitrobenzene at 210 °C (Scheme 1A.2.4).¹¹¹⁻¹¹²

(i) Goldberg, 1906



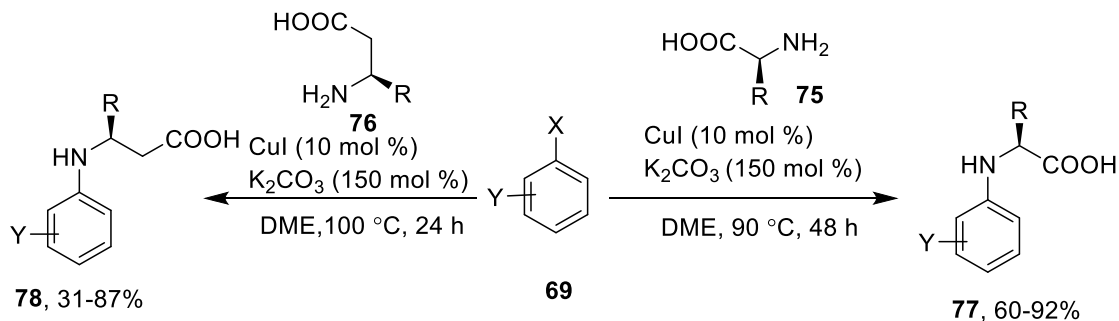
(ii) Goldberg, 1906



Scheme 1A.2.4: Examples of Cu-catalyzed amination and amidation reactions

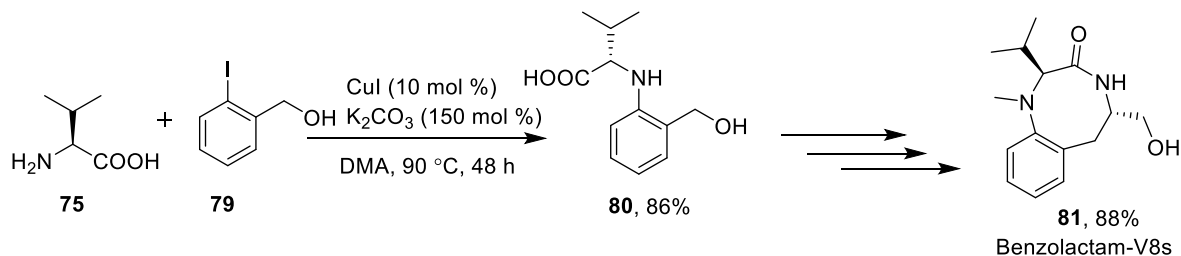
Incidentally, up to early 20th century Cu-catalyzed Ullmann coupling reaction has not been fully explored in organic synthesis due to certain allied drawbacks, including high reaction temperatures (normally above 150 °C), necessity of stoichiometric amount of copper, and limited reaction scope.¹¹³⁻¹¹⁴

However, with the rise in the understanding of the mechanism and introduction of different novel ligands, modified catalytic systems foster the expansion of Ullmann cross-coupling reactions to different substrates with excellent functional group tolerance. In the last decade, pioneer efforts have been devoted by Ma and other scientists to resolve the problem associated with Cu-catalyzed Ullmann coupling by using special ligands under milder reaction condition. In this realm, α -amino acids such as L-proline and *N,N*-dimethylglycine, have been exponentially used to facilitate the rate of most typical Cu-catalyzed Ullmann reactions at comparatively lower temperature with broader substrate tolerance.¹¹⁵⁻¹¹⁶ In addition, Ma group has beautifully exemplified a C-N bond forming protocol for preparing enantiomerically pure *N*-aryl-amino acids (**77** & **78**) in moderate-to-good yields by coupling different α -amino acids (**75**) and β -amino acids (**76**) with substituted aryl halides (**69**) under Cu-catalyzed conditions (Scheme 1A.2.5). The use of comparatively lower reaction temperature was attributed to the chelation assistance provided by amino acid via the formation of chelated copper ions and amino acids complex.¹¹⁷⁻¹¹⁸



Scheme 1A.2.5: Cu-catalyzed reaction of aryl halides (**69**) with α -amino acids (**75**) and β -amino acids (**76**)

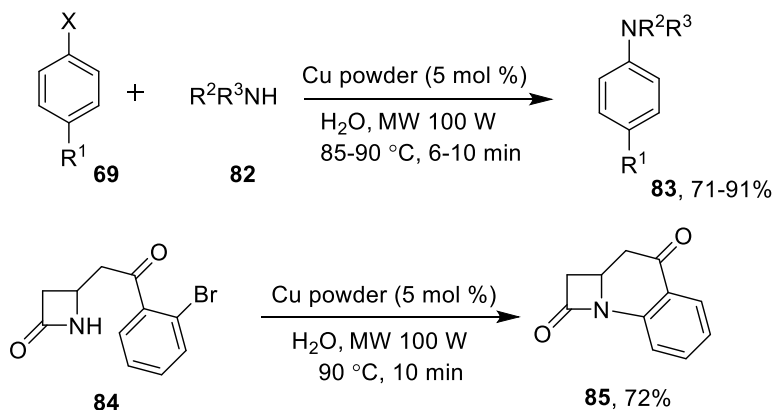
In conjunction to this, the same authors further explored a similar C-N bond forming strategy between 2-iodophenylmethanol (**79**) and L-valine (**75**) to produce *N*-arylated-L-valine derivative (**80**), which is an essential intermediate for the multistep synthesis of benzolactam-V8s scaffold (**81**) (protein kinase activators) (Scheme 1A.2.6).¹¹⁸



Scheme 1A.2.6: Application of Cu-catalyzed strategy to prepare intermediate **80** required to synthesize benzolactam-V8s (**81**)

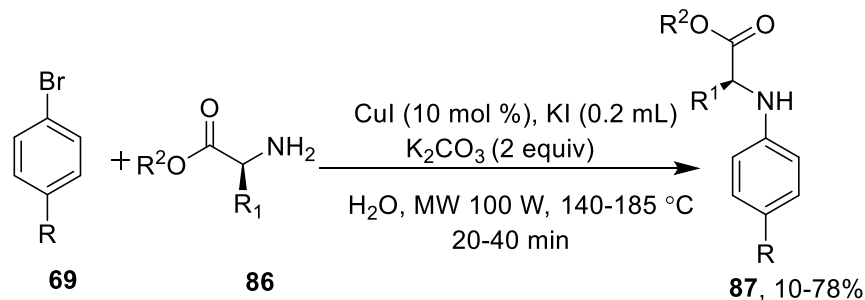
In recent years, microwave heating in combination with water has become an ally of choice for a swifter rate of cross-coupling reactions, for constructing C-N and C-O bonds in a clean and greener way.¹¹⁹⁻¹²⁰ Interestingly, different Cu-catalyzed arylation reactions have been explored in water and acknowledged due to ample availability, non-toxic and, non-flammable nature of water.¹²¹

In this realm, Yadav *et al.* reported a convergent intermolecular Cu-catalyzed base-free C-N coupling reaction for the synthesis of *N*-arylated products **83** from aryl halides (**69**) and amines/amides/imides (**82**) and β -lactams (**84**) in H₂O under microwave irradiation at 85-90 °C (Scheme 1A.2.7). A similar intramolecular strategy was applied to derivatives β -lactam (**84**) in H₂O to obtain cyclic amide (**85**) in 72% yield.¹²²



Scheme 1A.2.7: Cu-catalyzed aqueous MW protocol for inter- and intramolecular *N*-arylation of aryl halides (**69** and **84**)

Notably, Larhed *et al.* presented a Cu-catalyzed protocol for the *N*-arylation of free and protected amino acids (**86**) with a broad range of substituted aryl bromides (**69**) under aqueous microwave conditions in short reaction time, with fairly good yields (Scheme 1A.2.8).¹²³



Scheme 1A.2.8: Cu-catalyzed aqueous MW-assisted protocol for *N*-arylation of amino acids (**86**)

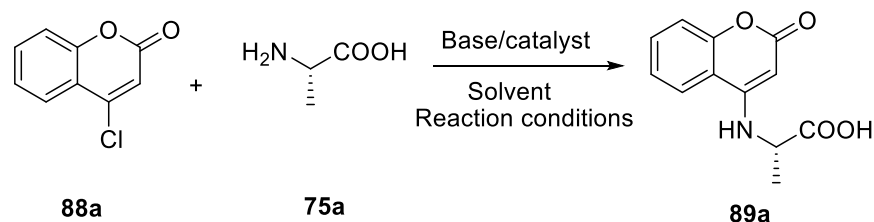
Interestingly, the direct C-N bond forming strategies for the coupling of coumarin moiety and α -amino acids remain unexplored to date. Thus, we envisioned to develop a mild, efficient and greener protocol for the synthesis of *N*-coumaryl amino acids through Cu-catalyzed C-N coupling in water, and extend the methodology towards the synthesis of coumaryl-labelled amino acids.

1A.3 Results and Discussion

Our investigation commenced with optimizing the reaction conditions for coupling 4-chlorocoumarin (**88a**) and L-alanine (**75a**) as model substrates (Table 1A.3.1). Usually, the formation of a C-N bond at 4th position of coumarin proceeds by substitution of chloro/methoxy group by appropriate *N*-nucleophiles in methanol/DMF in presence or absence of a base.¹²⁴ However, under base-free and catalyst-free conditions, no product formation was observed for the reaction between 4-chlorocoumarin (**88a**) and L-alanine (**75a**) in a variety of solvents, such as

DMSO, H₂O, DMF, EtOH (Table 1A.3.1, entry 1). Employment of K₂CO₃ (2 equiv) resulted in the formation of 30% isolated yield of **89a** in DMSO at 100 °C after 16 h, while comparatively lesser yields were obtained in other solvents (Table 1A.3.1, entries 2-5). Interestingly, the use of copper sulfate (5 mol %) resulted in the formation of the desired product **89a** in 42% yield in DMSO after 14 h at 100 °C (Table 1A.3.1, entry 6). No further amelioration in the yield of **89a** was noticed by increasing the reaction time up to 24 h (Table 1A.3.1, entry 7).

Table 1A.3.1: Selected optimization of reaction conditions^a for the synthesis of **89a**



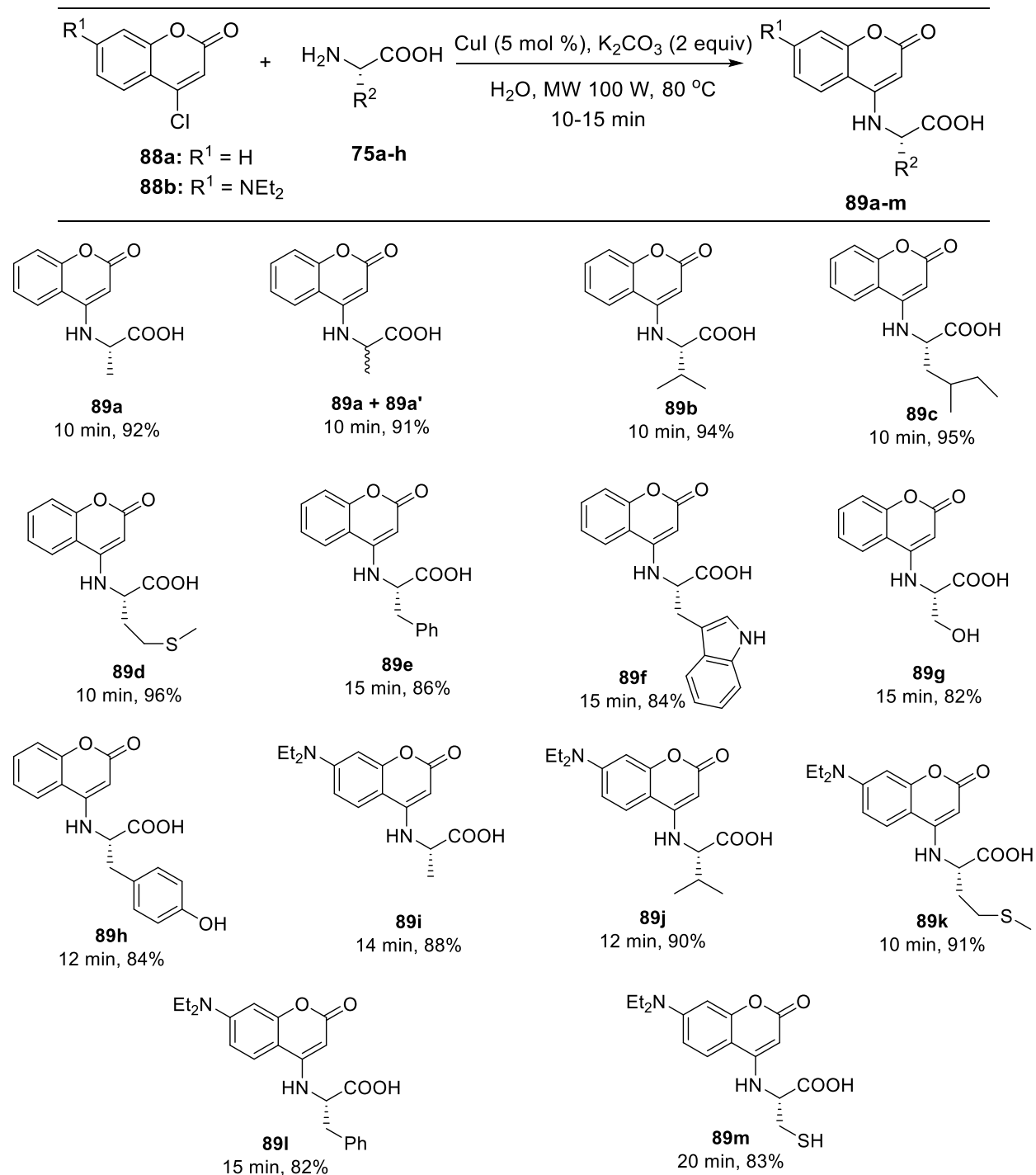
Entry	Base	Catalyst/ ligand	Solvent	T (°C)	Time	Yield ^b (%)
1.	-	-	DMSO/H ₂ O/ DMF/ EtOH	80 to 100	16 h	-
2.	K ₂ CO ₃	-	DMSO	100	16 h	30
3.	K ₂ CO ₃	-	H ₂ O	90	16 h	20
4.	K ₂ CO ₃	-	DMF	100	16 h	15
5.	K ₂ CO ₃	-	EtOH	80	16 h	trace
6.	K ₂ CO ₃	CuSO ₄ ·5H ₂ O	DMSO	100	14 h	42
7.	K ₂ CO ₃	CuSO ₄ ·5H ₂ O	DMSO	100	24 h	43
8.	K ₂ CO ₃	CuBr	DMSO	100	20 h	55
9.	K ₂ CO ₃	CuCl	DMSO	100	20 h	44
10.	K ₂ CO ₃	CuCl ₂	DMSO	100	20 h	40
11.	K ₂ CO ₃	Cu(OAc) ₂	DMSO	100	20 h	56
12.	K ₂ CO ₃	CuI	DMSO	100	14 h	60
13.	K ₂ CO ₃	CuI	H ₂ O	90	12 h	74
14.	K ₂ CO ₃	-	H ₂ O	80 (MW)	20 min	25
15.	K₂CO₃	CuI	H₂O	80 (MW)	10 min	92
16.	Na ₂ CO ₃	CuI	H ₂ O	80 (MW)	10 min	72
17.	CS ₂ CO ₃	CuI	H ₂ O	80 (MW)	10 min	78
18. ^c	K ₂ CO ₃	CuI	H ₂ O	80 (MW)	10 min	64
19. ^d	K ₂ CO ₃	CuI/L-proline	H ₂ O	80 (MW)	10 min	60
20. ^d	K ₂ CO ₃	CuI/ethylene glycol	H ₂ O	80 (MW)	10 min	45
21. ^d	K ₂ CO ₃	CuI/1,10- phenanthroline	H ₂ O	80 (MW)	10 min	60

^a Reaction conditions: **88a** (0.55 mmol), **75a** (0.66 mmol), base (2 equiv of base), catalyst (5 mol %), Solvent (1.5 mL); ^b Isolated yield; ^c (1 equiv of base); ^d Use of ligands (5 mol %), gave extra spots on TLC; MW: Microwave radiations at 100 W.

Next, the use of various copper catalysts including CuBr, CuCl, CuCl₂, Cu(OAc)₂, CuI were investigated (Table 1A.3.1, entries 8-12); of them CuI was found to be most efficient under described conditions, affording **89a** in 60% yield in DMSO after 14 h at 100 °C. Gratifyingly replacing DMSO with water using CuI (5 mol %) at 90 °C yielded 74% of **89a** in 12 h (Table 1A.3.1, entry 13). To expedite the methodology, the same reaction when performed under microwave irradiation resulted in the formation of **89a** in 92% yield, using the CuI/K₂CO₃ in 10 min at 80 °C (Table 1A.3.1, entry 15). However, the absence of CuI from the reaction mixture leads to isolation of only 25% of **89a** in water under microwave irradiation (Table 1A.3.1, entry 14). Replacement of K₂CO₃ with Na₂CO₃ and Cs₂CO₃ produced discouraging results (Table 1A.3.1, entries 16-17). While the use of 1 equiv of base reduces the yield of **89a** to 64% under similar microwave-assisted conditions in water (Table 1A.3.1, entry 18). Surprisingly, the usage of additional ligand did not added any amelioration in the yield of **89a** (Table 1A.3.1, entries 19-21), rather the isolated yields of **89a** decreased as multiple spots were observed on the TLC.

With the optimized conditions in hand, the generality of the developed strategy was studied with a variety of variety of α -L-amino acids. The reaction of 4-chlorocoumarin (**88a**) with **75a-h** under optimized conditions comfortably afforded *N*-coumaryl amino acids (**89a-h**) in 82-96% yields. These include α -amino acids with polar and non-polar side chain such as L-Ala, L-Val, L-Ile, L-Met, L-Trp, L-Ser, L-Phe and L-Tyr. It is noteworthy that amino acids with aliphatic side chain (L-Met, L-Ala, L-Val, and L-Ile) showed higher reactivity than the aromatic amino acids (L-Phe, L-Trp and L-Tyr). We next applied this Cu-catalyzed protocol for the coupling of α -amino acids (**75**) with 4-chloro-7-diethylaminocoumarin (**88b**) under optimized conditions to afford *N*-(7-diethylaminocoumaryl) amino acids (**89i-m**) in 82-91% yields. A small variation in the reactivity of **88b** was observed as compared to **88a**. Interestingly, **89i-m** displayed greater fluorescent behavior as compared to **89a-h**, when visualized on TLC under UV lamp (Scheme 1A.3.1). The coupling of **88a** was also performed with racemic alanine under optimized condition to afford corresponding racemic product **89a** + **89a'**. The normal-phase HPLC-UV chromatography of compound **89a** was carried using *i*-PrOH/hexanes as eluents on a Chiralcel OD-H column. Compound **89a** showed one major peak with retention time (16.9 min), which was nearly the same as the retention time for one of the two peaks revealed by the racemic mixture **89a** + **89a'** (16.2 and 19.5 min) (Figure 1A.3.1 & 1A.3.2). Clearly, the peak at 16.2 min is for the L-isomer **89a**, and

the peak at 19.5 min is for the D-isomer **89a'**. The above analysis confirmed that chiral integrity of the amino acid is retained during this microwave assisted Cu-catalyzed C-N coupling process.



Scheme 1A.3.1: Substrate scope of amino acids (**75a-h**) and 4-chloro coumarin (**88a-b**) for the *N*-coumarinyl amino acids (**89a-m**)

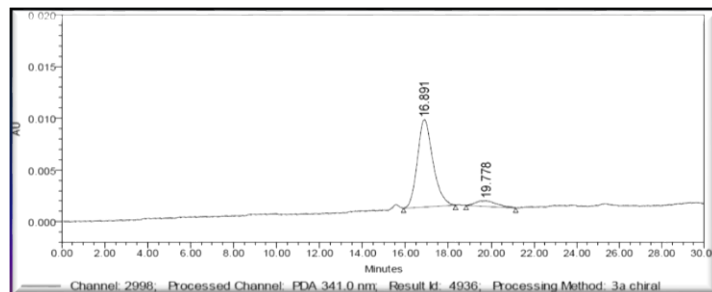


Figure 1A.3.1: HPLC analysis of **89a**

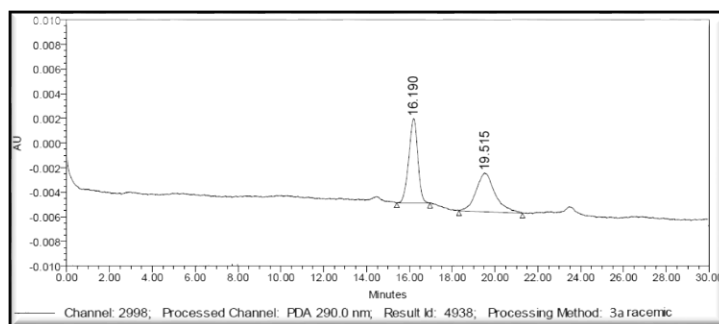


Figure 1A.3.2: HPLC analysis of **89a** + **89a'**

All the synthesized compounds were purified by recrystallization from ethanol, and characterized by detailed spectroscopic analysis. The ^1H NMR spectrum of **89a** showed two characteristic singlets, for one proton each at δ 12.95 and 5.03 for the COOH, and C-3 *H* respectively, along with other expected signals, evidencing the coupling of alanine at the 4-position of coumarin nucleus.

The ^1H and ^{13}C NMR spectra of **89a** are depicted in Figure 1A.3.3 and Figure 1A.3.4, respectively.

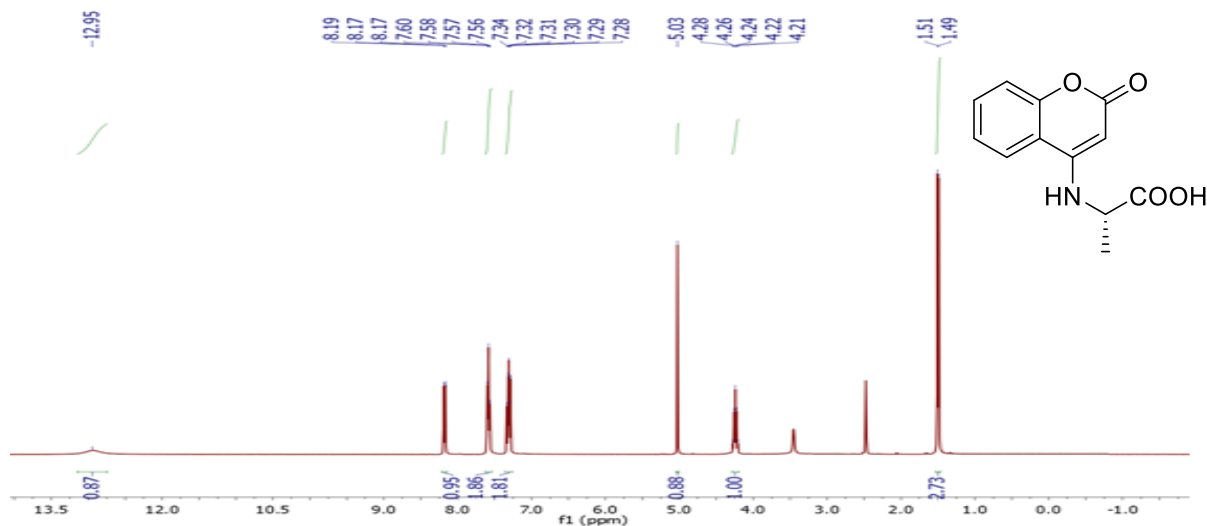


Figure 1A.3.3: ^1H NMR spectrum of **89a** in $\text{DMSO}-d_6$

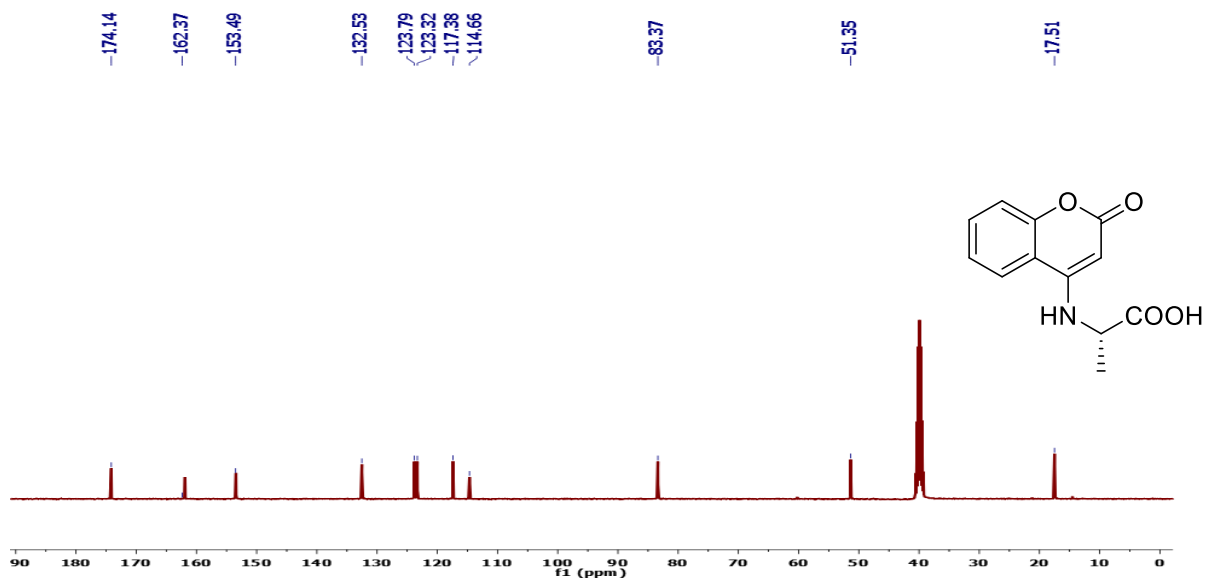
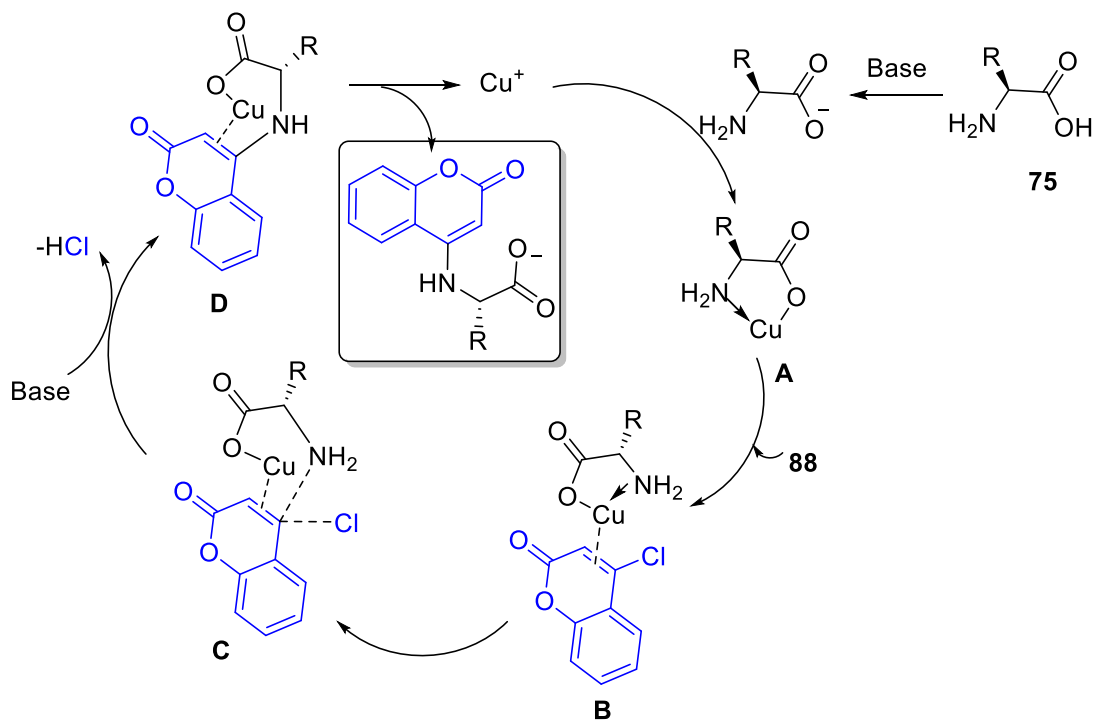


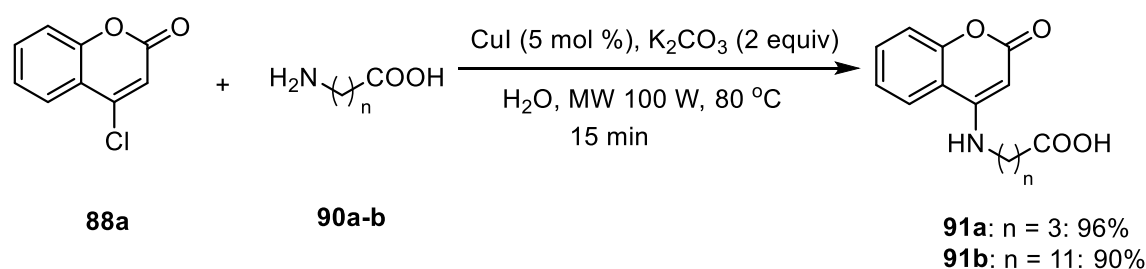
Figure 1A.3.4: ^{13}C NMR spectrum of **89a** in $\text{DMSO}-d_6$

Based on the proposed mechanism of Cu(I)-catalyzed coupling of aryl halides with α -amino acids,¹¹⁸ this reaction is believed to proceed through the chelation of a cuprous ion with α -amino acid (**75**) salt to form chelate **A**, which upon coordination with 4-chlorocoumarin (**88**) yielded the π -complex **B**. Thereafter, base-assisted intramolecular nucleophilic substitution at the 4th position of the coumaryl moiety in **B** gives the product *via* the formation of **C** & **D** (Scheme 1A.3.2).



Scheme 1A.3.2: Plausible mechanism

Furthermore, the developed strategy was employed to couple γ -aminobutyric acid (GABA), a chief inhibitory neurotransmitter in mammalian CNS that plays a vital role in embryonic development and adult neurogenesis.¹²⁶ Neurological disorders such as epilepsy, anxiety disorders, and schizophrenia are caused due to disturbance in GABAergic inhibition.¹²⁷ The robust participation of γ -aminobutyric acid (GABA) in the physiological functioning makes it important to tag it to synthetic fluorophores for understanding the mechanism of its action. Delightfully, the reaction of 4-chlorocoumarin (**88a**) with γ -aminobutyric acid (**90a**) under similar microwave-assisted Cu-catalyzed conditions in water at 80 °C gave *N*-coumaryl γ -aminobutyric acid (**91a**) in 96% yield (Scheme 1A.3.3). Similarly, 12-aminolauryl acid (**90b**), an interesting fatty acid derivative that plays a crucial role in the formation of membranes, lipoproteins and other lipid based molecular assemblies. Pleasingly, the reaction of **90b** with 4-chlorocoumarin (**88a**) under similar conditions afforded *N*-coumaryl 12-aminolauryl acid (**91b**) in 90% yield (Scheme 1A.3.3).



Scheme 1A.3.3: Synthesis of *N*-coumaryl γ -aminobutyric acid & 12-aminolauryl acid via C-N bond coupling in water

To evaluate the potential use of *N*-coumaryl amino acids (**89**) as fluorescent probes, absorption and fluorescence spectra of the synthesized compounds were recorded in MeOH. The wavelengths of the absorption maxima (λ_{Abs}) and fluorescence emission maxima (λ_{Em}), together with their quantum yield for compounds **89i-m**, were measured in MeOH and tabulated in Table 1A.3.2. Overall, **89a-h** showed absorption maxima in the wavelength region of 287-293 nm, while **89i-m** showed absorption maxima in the wavelength region of 348-351 nm. As expected, electron-donating group (NEt_2) at the 7-position in the coumarin nucleus strongly modulated the fluorescence by affecting the energy of the molecule's two lowest excited states,¹²⁵ and thus compounds **89i-m** showed higher quantum yields, and a bathochromic shift of fluorescence maxima (Figure 1A.3.5; c & d) as compared to **89a-h** (Figure 1A.3.5; a & b).

Table 1A.3.2: Absorption and fluorescence data of *N*-coumaryl amino acids (**89a-m**)^a

Compound	λ_{Abs} (nm)	λ_{Em} (nm)	Quantum Yield (Φ) ^d
89a	289	360 ^b	0.012
89b	292	380 ^b	0.059
89c	293	378 ^b	0.066
89d	291	382 ^b	0.111
89e	291	364 ^b	0.141
89f	291	462 ^b	0.030
89g	291	411 ^b	0.087
89h	287	404 ^b	0.220
89i	348	416 ^c	0.480
89j	350	416 ^c	0.410
89k	351	417 ^c	0.300
89l	351	417 ^c	0.510
89m	351	418 ^c	0.200

^aMeasured in MeOH (5×10^{-5} M) at 25 °C; ^bExcited at 320 nm; ^cExcited at 360 nm; ^dMeasured with quinine sulfate in 0.1 N H₂SO₄ as standard.

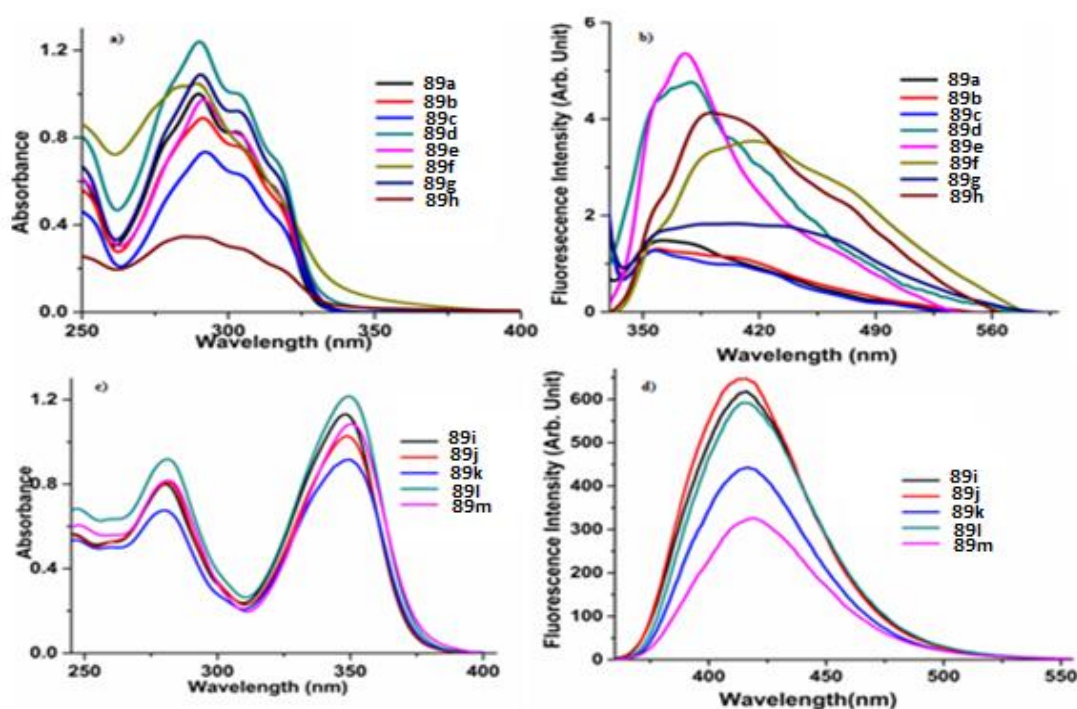
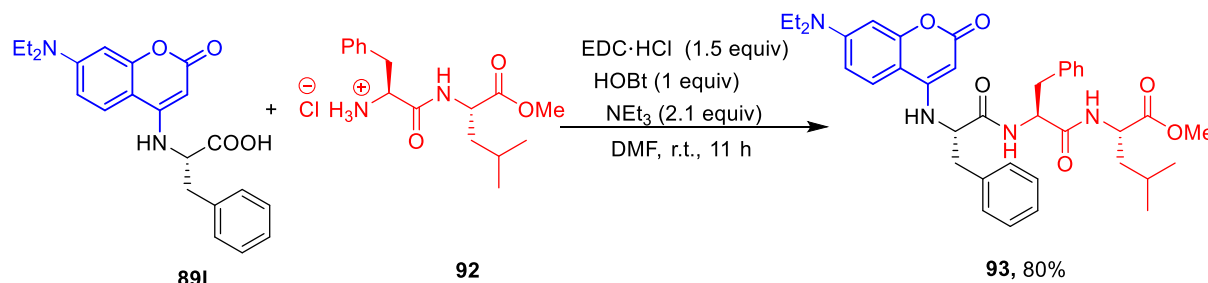


Figure 1A.3.5: UV absorption spectra of **89a-h** (a) and **89i-m** (c), and emission spectra of **89a-h** (b) and **89i-m** (d) in MeOH (5×10^{-5} M) at 25 °C

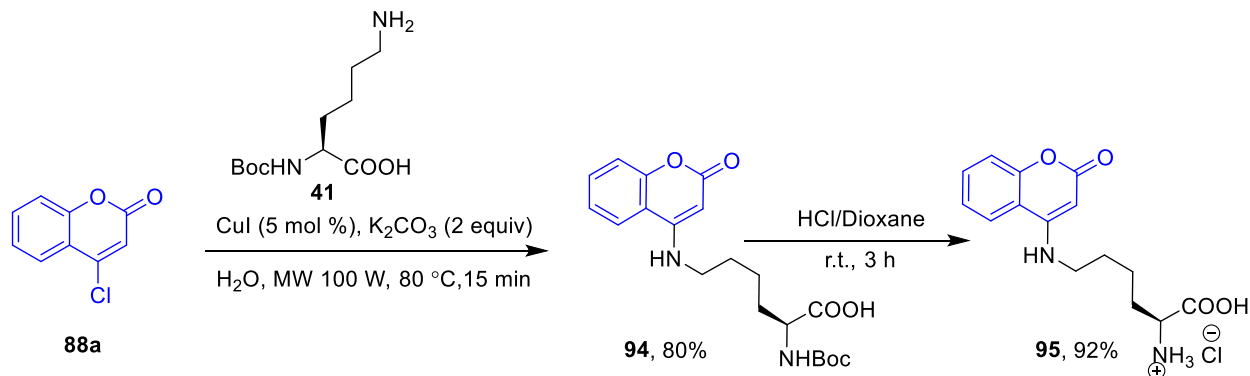
Further, the chemical applicability of *N*-coumaryl amino acids as fluorescent probe was illustrated by reacting **89l** with *N*-terminus dipeptide, HCl·NH₂-L-Phe-L-Leu-OMe (**92**) using

EDC·HCl/HOBt in DMF to afford *N*-coumaryl tripeptide **93** in 80% yield (Scheme 1A.3.4). The above transformation illustrated the capability of *N*-coumaryl amino acids to be used as ideal probes for site-specific labelling for investigating in vitro and in vivo biologically relevant processes.



Scheme 1A.3.4: Coupling of *N*-coumaryl amino acid (**891**) with *N*-terminus dipeptide (**92**)

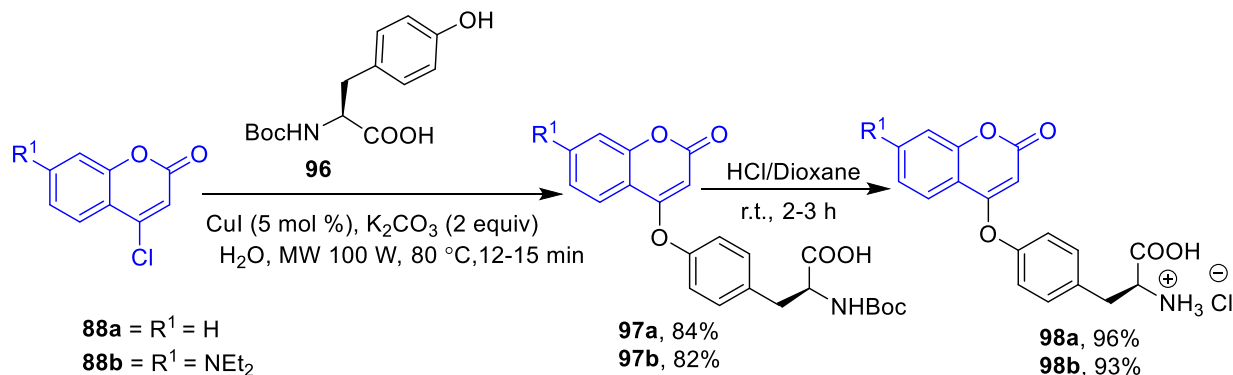
Since the inclusion of a fluorescent labelled amino acid at definite site in proteins is an important strategy for understanding the mechanism of biologically relevant processes,¹²⁸ we envisaged to synthesize two fluorescent labelled amino acids, tyrosine and lysine using our optimized protocol. The endeavour to employ our strategy to a basic-amino acid, urge us to carry the reaction of Boc-protected α -*N*-lysine (**41**) with **88a** under optimized Cu-catalyzed microwave-assisted conditions in water. Interestingly in 15 min, the corresponding Boc protected coumaryl labelled lysine (**94**) was obtained in 80% yield, which on Boc deprotection with HCl/dioxane yielded coumaryl-labelled lysine as a hydrochloride salt (**95**) in 92% yield (Scheme 1A.3.5).



Scheme 1A.3.5: Cu-catalyzed synthesis of coumaryl-labelled lysine (**95**) in water

Selective modification of tyrosine residue is predominantly attractive because surface accessible tyrosine is rather scarce in natural proteins,¹²⁹⁻¹³⁰ and thus selective tagging of tyrosine can lead to site-specific labelling.^{32,131} Thus, the optimized protocol was extended towards the C-O coupling between Boc-protected α -*N*-tyrosine (**96**) and **88a-b** under described conditions to afford **97a-b**

in 82-84% yield, which on Boc deprotection with HCl/dioxane yielded coumaryl-labelled tyrosine conjugates (**98a-b**) as a hydrochloride salts in 93-96% yields (Scheme 1A.3.6).



Scheme 1A.3.6: Cu-catalyzed synthesis of coumaryl-labelled tyrosine (**98**) in water

Absorption and fluorescence studies on coumaryl-labelled lysine (**94** & **95**) and tyrosine conjugates (**97a-b** & **98a-b**) were performed, and the results are summarized in Table 1A.3.3 and Figure 1A.3.6; a & b.

Table 1A.3.3: Absorption and fluorescence data of coumaryl-labelled lysine and tyrosine^a

Compound	λ_{Abs} (nm)	λ_{Em} (nm)	Quantum Yield (Φ) ^d
94	289	398 ^b	0.0051
95	290	394 ^b	0.0054
97a	266	384 ^b	0.0021
98a	277	406 ^b	0.0023
97b	362	446 ^c	0.42
98b	362	448 ^c	0.43

^aMeasured in MeOH (5×10^{-5} M) at 25 °C; ^bExcited at 320 nm; ^cExcited at 360 nm; ^dMeasured with quinine sulfate in 0.1 N H₂SO₄ as standard.

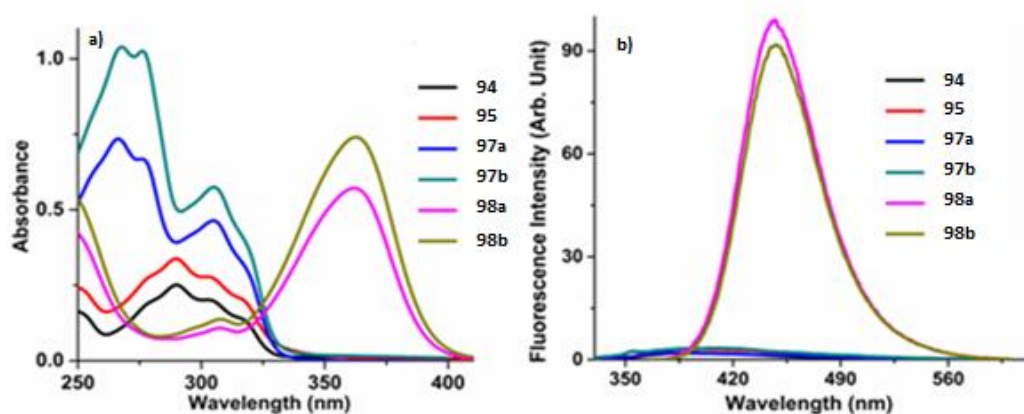
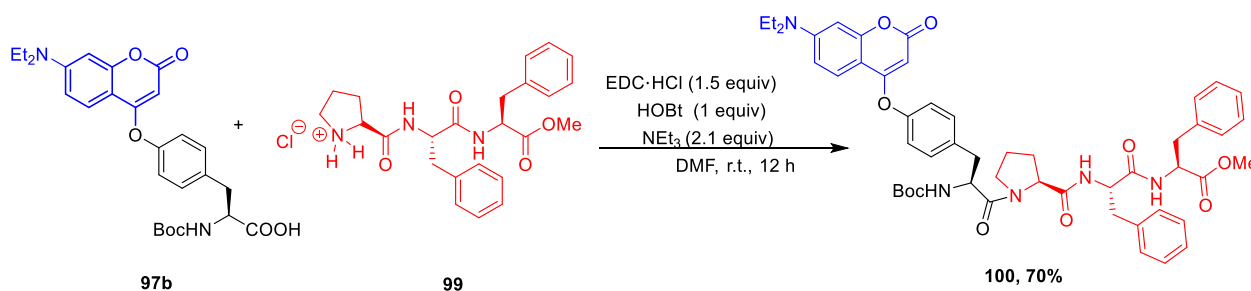


Figure 1A.3.6: UV absorption spectra of **94**, **95**, **97a-b** and **98a-b** (a) and emission spectra of **94**, **95**, **97a-b** and **98a-b** (b) in MeOH (5×10^{-5} M) at 25 °C

Finally, to illustrate a practical application of these coumaryl-labelled amino acids as potential fluorescent labels, we planned to synthesize a fluorescent labelled synthetic derivative of opioid tetrapeptide, Endomorphin-2. Endomorphin-2 is an endogenous selective agonist of the μ -opioid receptor (Tyr-Pro-Phe-Phe-NH₂) found naturally in the spinal cord of many animals.¹³² The agonist action of Endomorphin-2 at the μ -opioid receptors plays pivotal role in physiological functioning in human and many animals.¹³³ The peptide bond reaction of *C*-terminus coumaryl labelled tyrosine (**97b**) with *N*-terminus tripeptide, HCl·NH₂-L-Pro-L-Phe-L-Phe-OMe (**99**) proceeded comfortably in presence of EDC·HCl/HOBt in DMF to afford coumaryl-labelled Endomorphin-2 derivative (**100**) in 70% yield (Scheme 1A.3.7).



Scheme 1A.3.7: Chemical applicability of coumaryl-labelled tyrosine towards the synthesis of coumaryl-labelled Endomorphin-2 derivative (**100**)

In summary, we have developed a mild, efficient, and environmentally benign protocol for the synthesis of *N*-coumaryl amino acids *via* microwave-assisted Cu-catalyzed Ullmann-type coupling between 4-chlorocoumarin and *N*-terminus unprotected amino acids in water. The methodology afforded good-to-excellent yields of a series of *N*-coumaryl amino acids that exhibited excellent photophysical properties. The synthesized *N*-coumaryl amino acids could be used as fluorescent probes for coupling any *N*-terminus peptide of choice to yield fluorescent labelled peptides. Further, C-O and C-N coupling of 4-chlorocoumarin under similar Cu-catalyzed conditions in water afforded coumaryl-labelled tyrosine and lysine motifs. In addition, the chemical applicability of coumaryl-labelled tyrosine was explored to synthesize a derivative of coumaryl-labelled Endomorphin-2 derivative.

1A.4 Experimental Section

General materials and methods

All chemicals were obtained from commercial suppliers and used without further purification. Nuclear Magnetic Resonance spectra were recorded on Bruker 400 spectrometer. All ¹H NMR

experiments were recorded in DMSO- d_6 with TMS as a standard in δ units, parts per million (ppm), and were measured relative to residual DMSO (2.5 ppm) in the deuterated solvent. All ^{13}C NMR spectra were reported in ppm relative to ppm [d_6] DMSO (39.5 ppm). All coupling constants J were reported in Hz. The following abbreviations were used to describe peak splitting patterns when appropriate: s = singlet, d = doublet, t = triplet, dd = doublet of doublet, m = multiplet and brs = broad singlet. High-resolution mass spectrometry (HRMS) was performed with an Agilent 6210 instrument using time-of-flight (TOF-MS) with electro spray ionization (ESI). Melting points were determined on a capillary point apparatus equipped with a digital thermometer and are uncorrected. Microwave reactions were carried in a CEM Discover BenchMate reactor in 10 mL pressure vials at 80 W. Absorption spectra were recorded using dual beam Thermo Evolution 201 UV/Vis/NIR spectrophotometer and fluorescence spectra were recorded using a Shimadzu RF-5301PC spectrofluorometer. The data were analyzed using related software. The concentration of compound in all the solutions was 5×10^{-5} M. Fluorescence quantum yield (ϕ) values were obtained by the following equation. The fluorescence quantum yields were calculated by comparing the total fluorescence intensity (F) under the whole spectrum range by taking standard compound quinine sulfate (prepared as 0.1 N H_2SO_4 solution, $\phi_s = 0.55$).

$$\phi_i = \phi_s \frac{F_i Ab_s \eta_s^2}{F_s Ab_i \eta_i^2}$$

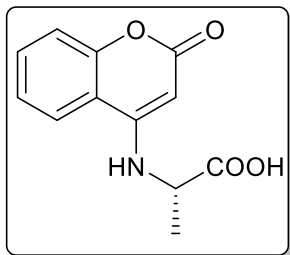
Where, Ab , Absorbance at a particular wavelength; F , fluorescence spectrum area; and η , refraction index. The subscripts in the symbols refer to the standard (s) and to the sample (i). HPLC analysis was performed on Water-2998 Instrument by using stationary phase chiral column chiralcel OD-H and *i*-PrOH/hexanes as solvent system. Specific rotation was measured through RUDOLPH Polarimeter.

General procedure for the synthesis of *N*-coumaryl amino acids

Unprotected α -amino acid (**75**) (1.32 mmol/0.94 mmol, 1.2 equiv) or unnatural amino acid (**90**) (1.32 mmol, 1.2 equiv) dissolved in water (1 mL) was added to a mixture of 4-chlorocoumarin/4-chloro-7-diethylaminocoumarin (**88a-b**) (1.1 mmol/0.79 mmol, 1 equiv), K_2CO_3 (2.2 mmol/1.58 mmol) and CuI (0.05 mmol/0.03 mmol) in a microwave vial containing water (3 mL). The reaction mixture was heated at 80 °C for 10-15 min under microwave irradiation till the disappearance of the starting material (TLC). The reaction mixture was added dropwise to an ice-bath, and concentrated HCl was then added to adjust the pH to 2-3 under cooling conditions to precipitate a

solid. The precipitate was filtered, washed with cold water (3 x 10 mL), and recrystallized from ethanol to afford pure *N*-coumaryl amino acids (**89a-m**, **91a-b**).

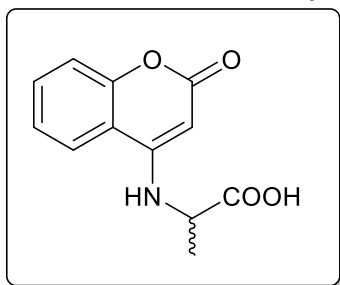
(2-Oxo-2*H*-chromen-4-yl)-L-alanine (89a): White solid; yield: 236 mg (92%); mp: 244–245 °C;



$[\alpha]_D^{25} = -37$ ($c = 1.0$, MeOH); $^1\text{H NMR}$ (400 MHz, DMSO- d_6) δ 12.95 (s, 1H), 8.21 – 8.14 (m, 1H), 7.58 (dd, $J = 9.9, 3.9$ Hz, 2H), 7.35 – 7.26 (m, 2H), 5.03 (s, 1H), 4.24 (q, $J = 7.1$ Hz, 1H), 1.50 (d, $J = 7.1$ Hz, 3H); $^{13}\text{C NMR}$ (100 MHz, DMSO- d_6) δ 174.1, 161.9, 153.5, 153.4, 132.5, 123.8, 123.3, 117.4, 114.7, 83.4, 51.3, 17.5; HRMS (ESI-TOF) (m/z)

calculated $\text{C}_{12}\text{H}_{12}\text{NO}_4^+$: 234.0766; found 234.0762 $[\text{M}+\text{H}]^+$.

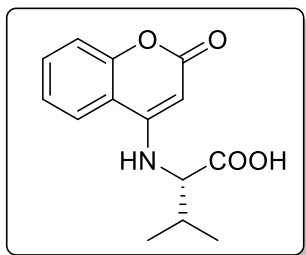
(2-Oxo-2*H*-chromen-4-yl)alanine (89a + 89a'): White solid; yield: 232 mg (91%); mp: 256–258



°C; $[\alpha]_D^{25} = 0$ ($c = 1.0$, MeOH); $^1\text{H NMR}$ (400 MHz, DMSO- d_6) δ 12.95 (s, 1H), 8.21 – 8.14 (m, 1H), 7.58 (dd, $J = 9.9, 3.9$ Hz, 2H), 7.35 – 7.26 (m, 2H), 5.03 (s, 1H), 4.24 (p, $J = 7.1$ Hz, 1H), 1.50 (d, $J = 7.1$ Hz, 3H); $^{13}\text{C NMR}$ (100 MHz, DMSO- d_6) δ 174.0, 161.8, 153.5, 153.4, 132.5, 123.7, 123.3, 117.4, 114.7, 83.4, 51.3, 17.5; HRMS (ESI-TOF) (m/z) calculated $\text{C}_{12}\text{H}_{12}\text{NO}_4^+$: 234.0766; found

234.0759 $[\text{M}+\text{H}]^+$.

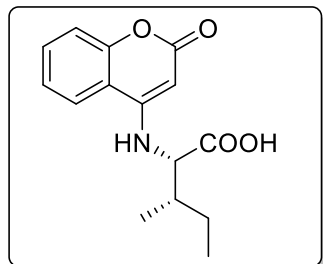
(2-Oxo-2*H*-chromen-4-yl)-L-valine (89b): White solid; yield: 269 mg (94%); mp: 260–261 °C;



$[\alpha]_D^{25} = -117$ ($c = 1.0$, MeOH); $^1\text{H NMR}$ (400 MHz, DMSO- d_6) δ 12.97 (s, 1H), 8.28 (dd, $J = 8.1, 1.2$ Hz, 1H), 7.62 – 7.55 (m, 1H), 7.39 (d, $J = 7.8$ Hz, 1H), 7.35 – 7.27 (m, 2H), 5.12 (s, 1H), 3.78 (t, $J = 8.1$ Hz, 1H), 2.31 – 2.24 (m, 1H), 1.03 – 0.96 (m, 6H); $^{13}\text{C NMR}$ (100 MHz, DMSO- d_6) δ 173.2, 161.8, 153.8, 153.5, 132.53, 123.8, 123.4,

117.3, 114.7, 83.6, 62.7, 29.9, 19.5; HRMS (ESI-TOF) (m/z) calculated $\text{C}_{14}\text{H}_{16}\text{NO}_4^+$: 262.1079; found 262.1064 $[\text{M}+\text{H}]^+$.

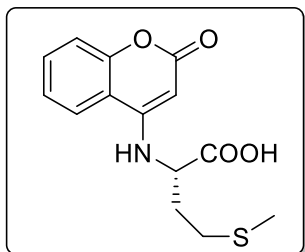
(2-Oxo-2*H*-chromen-4-yl)-L-isoleucine (89c): White solid; yield: 287 mg (95%); mp: 236–238



°C; $[\alpha]_D^{25} = -94$ ($c = 1.0$, MeOH); $^1\text{H NMR}$ (400 MHz, DMSO- d_6) δ 13.00 (s, 1H), 8.28 (dd, $J = 8.1, 1.3$ Hz, 1H), 7.61 – 7.43 (m, 1H), 7.42 (d, $J = 7.8$ Hz, 1H), 7.34 – 7.28 (m, 2H), 5.10 (s, 1H), 3.81 (t, $J = 8.1$ Hz, 1H), 2.13 – 2.06 (m, 1H), 1.63 – 1.55 (m, 1H), 1.33 – 1.23 (m, 1H), 0.95 (d, $J = 6.8$ Hz, 3H), 0.85 (t, $J = 7.4$ Hz, 3H); $^{13}\text{C NMR}$ (100

MHz, DMSO- d_6) δ 173.2, 161.8, 153.7, 153.5, 132.6, 123.8, 123.4, 117.3, 114.6, 83.5, 61.2, 35.7, 25.8, 15.7, 11.1; HRMS (ESI-TOF) (m/z) calculated $C_{16}H_{20}NO_4^+$: 290.1392; found 290.1378 [M+H] $^+$.

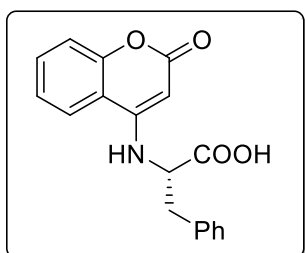
(2-Oxo-2H-chromen-4-yl)-L-methionine (89d): White solid; yield: 309 mg (96%); mp: 215–



217 °C; $[\alpha]^{25}_D = -36$ ($c = 1.0$, MeOH); 1H NMR (400 MHz, DMSO- d_6) δ 13.15 (s, 1H), 8.25 – 8.11 (m, 1H), 7.70 (d, $J = 7.5$ Hz, 1H), 7.65 – 7.56 (m, 1H), 7.32 (dd, $J = 11.0, 8.1$ Hz, 2H), 5.10 (s, 1H), 4.41 – 4.23 (m, 1H), 3.01 – 2.89 (m, 1H), 2.85 – 2.74 (m, 1H), 2.56 (s, 3H), 2.32 (d, $J = 8.4$ Hz, 2H); ^{13}C NMR (100 MHz, DMSO- d_6) δ 172.9,

161.9, 153.8, 153.48, 132.7, 123.9, 123.3, 117.4, 114.8, 83.6, 50.1, 30.5, 25.0, 15.0; HRMS (ESI-TOF) (m/z) calculated $C_{14}H_{16}NO_4S^+$: 294.0800; found 294.0789 [M+H] $^+$.

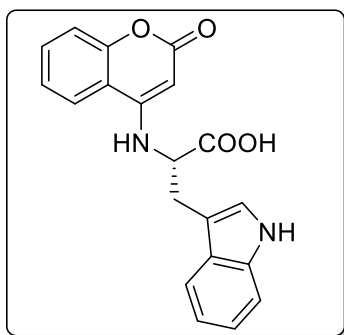
(2-Oxo-2H-chromen-4-yl)-L-phenylalanine (89e): White solid; yield: 292 mg (86%); mp: 236–



238 °C; $[\alpha]^{25}_D = -2$ ($c = 1.0$, MeOH); 1H NMR (400 MHz, DMSO- d_6) δ 8.14 (d, $J = 7.7$ Hz, 1H), 7.67 (d, $J = 7.8$ Hz, 1H), 7.60 (t, $J = 7.4$ Hz, 1H), 7.38 – 7.30 (m, 3H), 7.29 – 7.24 (m, 3H), 7.20 – 7.14 (m, 1H), 5.12 (s, 1H), 4.51 – 4.40 (m, 1H), 3.25 (d, $J = 8.7$ Hz, 2H); ^{13}C NMR

(100 MHz, DMSO- d_6) δ 173.1, 161.8, 153.7, 153.4, 138.1, 132.6, 129.5, 128.7, 127.0, 123.9, 123.1, 117.4, 114.6, 83.5, 57.4, 36.8; HRMS (ESI-TOF) (m/z) calculated $C_{18}H_{16}NO_4^+$: 310.1079; found 310.1062 [M+H] $^+$.

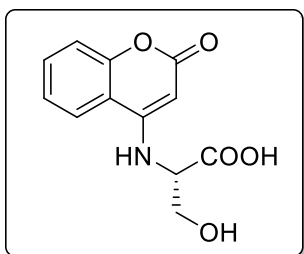
(2-Oxo-2H-chromen-4-yl)-L-tryptophan (89f): White solid; yield: 321 mg (84%); mp: 220–



221 °C; $[\alpha]^{25}_D = -132$ ($c = 1.0$, MeOH); 1H NMR (400 MHz, DMSO- d_6) δ 10.77 (s, 1H), 8.05 (d, $J = 7.1$ Hz, 1H), 7.64 (s, 1H), 7.59 (d, $J = 7.2$ Hz, 1H), 7.55 – 7.48 (m, 1H), 7.29 – 7.21 (m, 4H), 7.05 – 6.96 (m, 1H), 6.94 – 6.85 (m, 1H), 5.05 (s, 1H), 4.23 – 4.16 (m, 1H), 3.41 (d, $J = 15.0$ Hz, 2H); ^{13}C NMR (100 MHz, DMSO- d_6) δ 172.9, 161.9, 153.5, 153.3, 136.5, 132.2, 127.8, 127.1, 124.2, 123.6, 122.9, 121.2, 118.7, 117.3, 114.9, 111.8, 111.2, 82.6, 58.0,

27.4; HRMS (ESI-TOF) (m/z) calculated $C_{20}H_{17}N_2O_4^+$: 349.1188; found 349.1167 [M+H] $^+$.

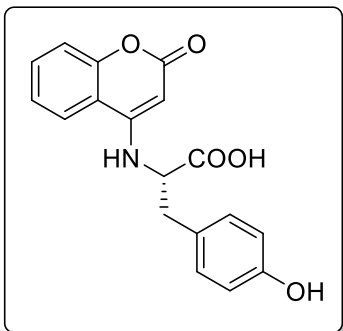
(2-Oxo-2H-chromen-4-yl)-L-serine (89g): White solid; yield: 224 mg (82%); mp: 225–226 °C;



$[\alpha]_D^{25} = -28$ ($c = 1.0$, MeOH); $^1\text{H NMR}$ (400 MHz, DMSO- d_6) δ 8.13 (d, $J = 8.0$ Hz, 1H), 7.60 (t, $J = 7.7$ Hz, 1H), 7.37 – 7.28 (m, 3H), 5.09 (s, 1H), 4.28 – 4.21 (m, 1H), 3.89 (d, $J = 5.2$ Hz, 2H); $^{13}\text{C NMR}$ (100 MHz, DMSO- d_6) δ 171.7, 161.8, 153.5, 153.5, 132.6, 123.8, 123.0, 117.4, 114.7, 83.4, 61.4, 58.7; HRMS (ESI-TOF) (m/z) calculated

$\text{C}_{12}\text{H}_{12}\text{NO}_5^+$: 250.0715; found 250.0703 $[\text{M}+\text{H}]^+$.

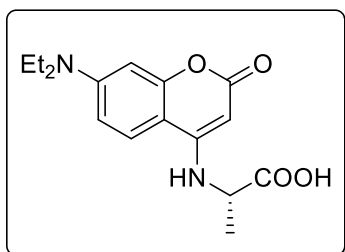
(2-Oxo-2H-chromen-4-yl)-L-tyrosine (89h): White solid; yield: 300 mg (84%); mp: 246–248



°C; $[\alpha]_D^{25} = -12$ ($c = 1.0$, MeOH); $^1\text{H NMR}$ (400 MHz, DMSO- d_6) δ 13.03 (s, 1H), 9.22 (s, 1H), 8.15 (d, $J = 8.2$ Hz, 1H), 7.65 – 7.53 (m, 2H), 7.35 – 7.24 (m, 2H), 7.13 (d, $J = 7.3$ Hz, 2H), 6.62 (d, $J = 7.6$ Hz, 2H), 5.05 (s, 1H), 4.35 – 4.27 (m, 1H), 3.11 (d, $J = 5.9$ Hz, 2H); $^{13}\text{C NMR}$ (100 MHz, DMSO- d_6) δ 173.1, 161.7, 156.4, 153.6, 153.4, 132.5, 130.4, 128.0, 123.8, 123.2, 117.3, 115.5, 114.7, 83.4,

57.9, 36.1; HRMS (ESI-TOF) (m/z) calculated $\text{C}_{18}\text{H}_{16}\text{NO}_5^+$: 326.1028; found 326.1007 $[\text{M}+\text{H}]^+$.

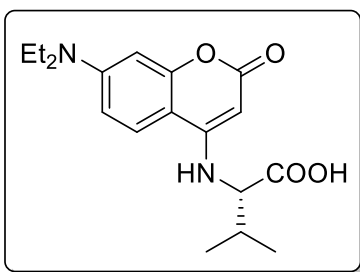
(7-(Diethylamino)-2-oxo-2H-chromen-4-yl)-L-alanine (89i): White solid; yield: 211 mg (88%);



mp: 215–217 °C; $[\alpha]_D^{25} = +28$ ($c = 1.0$, MeOH); $^1\text{H NMR}$ (400 MHz, DMSO- d_6) δ 12.83 (s, 1H), 7.87 (d, $J = 9.1$ Hz, 1H), 7.26 (d, $J = 7.3$ Hz, 1H), 6.62 (dd, $J = 9.1, 2.5$ Hz, 1H), 6.37 (d, $J = 2.5$ Hz, 1H), 4.73 (s, 1H), 4.14 (quin., $J = 7.0$ Hz, 1H), 3.38 (q, $J = 7.0$ Hz, 4H), 1.47 (d, $J = 7.1$ Hz, 3H), 1.09 (t, $J = 7.0$ Hz, 6H); $^{13}\text{C NMR}$

(100 MHz, DMSO- d_6) δ 179.1, 167.4, 160.6, 159.0, 155.4, 129.0, 112.8, 107.3, 102.1, 84.4, 55.9, 49.0, 22.4, 17.5; HRMS (ESI-TOF) (m/z) calculated $\text{C}_{16}\text{H}_{21}\text{N}_2\text{O}_4^+$: 305.1496; found 305.1510 $[\text{M}+\text{H}]^+$.

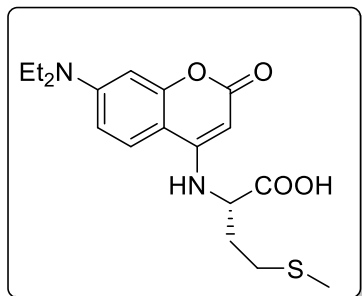
(7-(Diethylamino)-2-oxo-2H-chromen-4-yl)-L-valine (89j): White solid; yield: 201 mg (90%);



mp: 216–218 °C; $[\alpha]_D^{25} = -18$ ($c = 1.0$, MeOH); $^1\text{H NMR}$ (400 MHz, DMSO- d_6) δ 13.04 (s, 1H), 7.96 (d, $J = 9.1$ Hz, 1H), 7.12 (d, $J = 7.7$ Hz, 1H), 6.65 – 6.58 (m, 1H), 6.37 (d, $J = 2.1$ Hz, 1H), 4.83 (s, 1H), 3.67 (t, $J = 8.0$ Hz, 1H), 3.38 (q, $J = 6.8$ Hz, 4H), 2.24 (dd, $J = 14.0, 6.9$ Hz, 1H), 1.09 (t, $J = 6.9$ Hz, 6H), 1.00 – 0.95 (m, 6H); $^{13}\text{C NMR}$ (100 MHz, DMSO- d_6) δ 173.5, 162.6,

155.8, 154.5, 150.7, 124.3, 108.1, 102.6, 97.4, 79.7, 62.6, 44.3, 30.0, 20.0, 19.5, 12.8; HRMS (ESI-TOF) (m/z) calculated $C_{18}H_{25}N_2O_4^+$: 333.1814; found 333.1843 $[M+H]^+$.

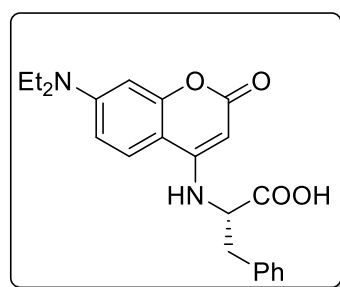
(7-(Diethylamino)-2-oxo-2H-chromen-4-yl)-L-methionine (89k): White solid; yield: 261 mg



(91%); mp: 186–188 °C; $[\alpha]_D^{25} = -13$ (c = 1.0, MeOH); 1H NMR (400 MHz, DMSO- d_6) δ 7.87 (d, $J = 9.1$ Hz, 1H), 7.28 (d, $J = 7.8$ Hz, 1H), 6.63 (dd, $J = 9.1, 2.0$ Hz, 1H), 6.37 (d, $J = 2.1$ Hz, 1H), 4.76 (s, 1H), 4.22 – 4.10 (m, 1H), 3.38 (q, $J = 6.8$ Hz, 4H), 2.65 – 2.51 (m, 2H), 2.22 – 2.07 (m, 2H), 2.03 (s, 3 H), 1.09 (t, $J = 6.9$ Hz, 6H); ^{13}C NMR (100 MHz, DMSO- d_6) δ 173.6, 162.6, 155.8,

154.6, 150.7, 124.2, 108.1, 102.6, 97.4, 79.6, 54.9, 44.3, 31.0, 30.5, 15.0, 12.8; HRMS (ESI-TOF) (m/z) calculated $C_{18}H_{25}N_2O_4S^+$: 365.1528; found 365.1536 $[M+H]^+$.

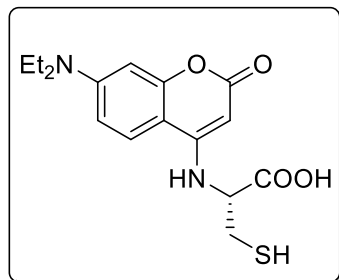
(7-(Diethylamino)-2-oxo-2H-chromen-4-yl)-L-phenylalanine (89l): White solid; yield: 246 mg



(82%); mp: 208–211 °C; $[\alpha]_D^{25} = -12$ (c = 1.0, MeOH); 1H NMR (400 MHz, DMSO- d_6) δ 7.82 (d, $J = 9.2$ Hz, 1H), 7.38 – 7.31 (m, 3H), 7.26 – 7.19 (m, 2H), 7.17 – 7.10 (m, 1H), 6.62 (dd, $J = 9.1, 2.4$ Hz, 1H), 6.33 (d, $J = 2.4$ Hz, 1H), 4.78 (s, 1H), 4.28 (dd, $J = 14.2, 8.0$ Hz, 1H), 3.36 (q, $J = 6.9$ Hz, 4H), 3.22 – 3.16 (m, 2H), 1.07 (t, $J = 6.9$ Hz, 6H); ^{13}C NMR (100 MHz, DMSO- d_6) δ 173.4, 162.6,

155.8, 154.3, 150.7, 138.3, 129.5, 128.6, 126.8, 124.1, 108.1, 102.5, 97.4, 79.6, 57.60, 44.3, 37.0, 12.8; HRMS (ESI-TOF) (m/z) calculated $C_{22}H_{25}N_2O_4^+$: 381.1807; found 381.1821 $[M+H]^+$.

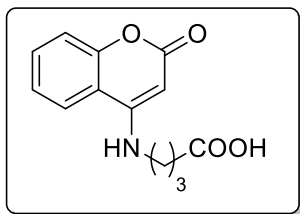
(7-(Diethylamino)-2-oxo-2H-chromen-4-yl)-L-cysteine (89m): White solid; yield: 220 mg



(83%); mp: 196–199 °C; $[\alpha]_D^{25} = +56$ (c = 1.0, MeOH); 1H NMR (400 MHz, DMSO- d_6) δ 7.77 (d, $J = 9.1$ Hz, 1H), 7.43 (d, $J = 7.7$ Hz, 1H), 6.61 (d, $J = 8.8$ Hz, 1H), 6.32 (s, 1H), 4.83 (s, 1H), 4.39 (dd, $J = 12.5, 8.0$ Hz, 1H), 3.37 (q, $J = 6.8$ Hz, 4H), 3.32 – 3.28 (m, 1H), 3.26 – 3.21 (m, 1H), 1.09 (t, $J = 6.7$ Hz, 6H); ^{13}C NMR (100 MHz, DMSO- d_6) δ 172.3, 162.7, 155.7, 154.4, 150.6, 124.1, 108.1,

102.3, 97.2, 79.7, 54.8, 44.3, 38.8, 12.8; HRMS (ESI-TOF) (m/z) calculated $C_{16}H_{21}N_2O_4S^+$: 337.1212; found 337.1230 $[M+H]^+$.

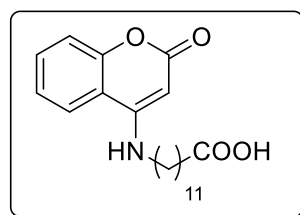
4-((2-Oxo-2H-chromen-4-yl)amino)butanoic acid (91a): White solid; yield: 244 mg (96%);



mp: 201–205 °C; $^1\text{H NMR}$ (400 MHz, $\text{DMSO-}d_6$) δ 12.13 (s, 1H), 8.02 (d, $J = 7.9$ Hz, 1H), 7.65 (t, $J = 5.1$ Hz, 1H), 7.59 – 7.52 (m, 1H), 7.28 (t, $J = 7.8$ Hz, 2H), 5.16 (s, 1H), 3.24 (dd, $J = 13.1, 6.6$ Hz, 2H), 2.33 (t, $J = 7.2$ Hz, 2H), 1.87 – 1.77 (m, 2H); $^{13}\text{C NMR}$ (100 MHz, $\text{DMSO-}d_6$) δ 174.6, 162.0, 153.6, 153.6, 132.3, 123.7, 122.9, 117.4, 114.9, 81.8,

42.1, 31.4, 23.3; HRMS (ESI-TOF) (m/z) calculated $\text{C}_{13}\text{H}_{14}\text{NO}_4^+$: 248.0922; found 248.0913 $[\text{M}+\text{H}]^+$.

12-((2-Oxo-2H-chromen-4-yl)amino)dodecanoic acid (91b): White solid; yield: 355 mg (90%);



mp: 163–166 °C; $^1\text{H NMR}$ (400 MHz, $\text{DMSO-}d_6$) δ 11.66 (s, 1H), 8.04 (d, $J = 10.3$ Hz, 1H), 7.70 – 7.51 (m, 2H), 7.28 (d, $J = 8.2$ Hz, 2H), 5.10 (s, 1H), 3.27 – 3.14 (m, 2H), 2.24 – 2.02 (m, 2H), 1.63–1.58 (m, 2H), 1.51 – 1.43 (m, 2H), 1.21 – 1.08 (m, 14H); $^{13}\text{C NMR}$ (100 MHz, $\text{DMSO-}d_6$) δ 175.0, 162.0, 153.5, 152.3, 132.2, 123.7, 122.9, 117.4,

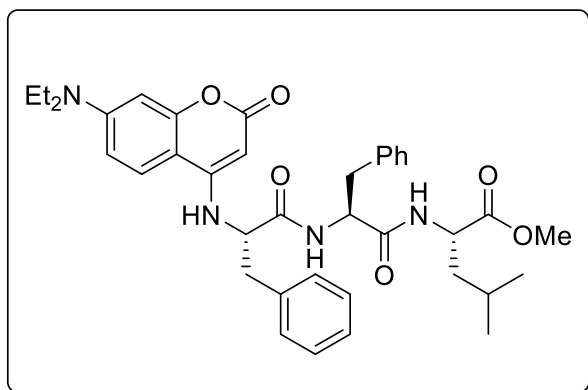
115.0, 81.6, 42.8, 38.8, 35.9, 34.2, 29.4, 29.2, 29.1, 27.9, 27.0, 25.8, 25.0; HRMS (ESI-TOF) (m/z) calculated $\text{C}_{21}\text{H}_{30}\text{NO}_4^+$: 360.2174; found 360.2163 $[\text{M}+\text{H}]^+$.

General procedure for the linear elongation of C-terminus N-coumaryl amino acids:

Synthesis of N-coumaryl tripeptide

To a stirred solution of **891** (0.132 g, 0.36 mmol) in DMF, triethyl amine (0.1 mL, 0.75 mmol) was added at 0 °C, and subsequently EDC·HCl (0.85 g, 0.45 mmol), HOBt (0.48 g, 0.36 mmol) and was added. The reaction mixture was stirred for 15 min at 0 °C. Later $\text{HCl}\cdot\text{NH}_2\text{-L-Phe-L-Leu-OMe}$ (**92**) (0.100 g, 0.30 mmol) was added, and the reaction mixture was stirred at room temperature for 11 h. The completion of the reaction was monitored by TLC. After the completion of the reaction, crushed-ice was added that resulted in the precipitation of the product, which was filtrated, washed with cold water and recrystallized from ethanol to give pure **93**.

Methyl (7-(diethylamino)-2-oxo-2H-chromen-4-yl)-L-phenylalanyl-L-phenylalanyl-L-



leucinate (93): White solid; yield: 156 mg (80%); mp: 163–166 °C; ^1H NMR (400 MHz, $\text{DMSO-}d_6$) δ 8.54 (d, $J = 7.9$ Hz, 1H), 8.45 (d, $J = 7.9$ Hz, 1H), 7.80 (d, $J = 8.7$ Hz, 1H), 7.31 (d, $J = 7.1$ Hz, 1H), 7.25 – 7.07 (m, 10H), 6.59 (d, $J = 8.6$ Hz, 1H), 6.30 (s, 1H), 4.77 (s, 1H), 4.60 – 4.52 (m, 1H), 4.33 – 4.24 (m, 2H), 3.59 (s, 3H), 3.40 (m, overlapped by moisture of DMSO, 4H),

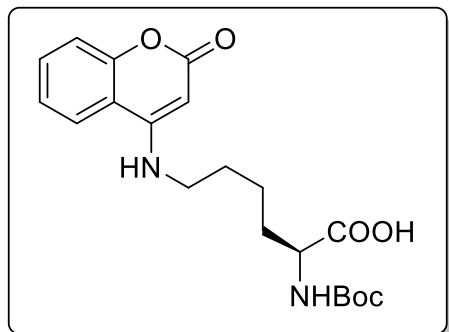
2.97 – 2.88 (m, 2H), 2.82 – 2.72 (m, 2H), 1.55 – 1.50 (m, 2H), 1.33 (d, $J = 7.3$ Hz, 1H), 1.06 (t, $J = 5.8$ Hz, 6H), 0.85 – 0.78 (m, 6H); ^{13}C NMR (100 MHz, $\text{DMSO-}d_6$) δ 173.2, 171.5, 171.4, 162.7, 155.7, 154.1, 150.6, 138.6, 137.9, 137.8, 129.7, 129.6, 129.5, 128.6, 126.7, 124.3, 108.1, 102.4, 97.2, 79.6, 57.7, 54.1, 52.4, 50.7, 44.3, 37.7, 24.7, 23.2, 22.1, 21.7, 12.7; HRMS (ESI-TOF) (m/z) calculated $\text{C}_{37}\text{H}_{43}\text{N}_4\text{O}_6^+$: 639.3182; found 639.3193 [M-CH_3] $^+$.

Typical procedure for the synthesis of coumaryl-labelled lysine

Boc α -N-lysine (**41**) (1.32 mmol) dissolved in water (1 mL) was added to a mixture of 4-chlorocoumarin (**88a**) (1.1 mmol), K_2CO_3 (2.2 mmol) and CuI (0.05 mmol) in water (3 mL). The reaction mixture was heated at 80 °C for 15 min under microwave irradiation till the disappearance of the starting material. The reaction mixture was added dropwise to an ice-bath, and concentrated HCl was then added to adjust the pH to 2-3 under cooling conditions to precipitate a solid. The precipitate was filtered, washed with cold-water (3 x 10 mL) and recrystallized from ethanol to give pure coumaryl-labelled Boc-protected lysine (**94**).

A solution of dioxane-HCl was added dropwise to **94** (0.150 g) dissolved in dioxane at 0 °C. The reaction was stirred at room temperature for 3 h, and monitored *via* TLC. After the completion, the reaction mixture was completely concentrated, washed with diethyl ether and filtered-off to yield **95** as pure product.

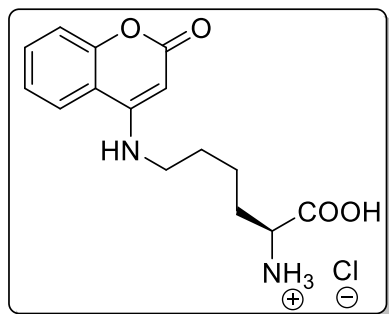
***N*²-(*tert*-Butoxycarbonyl)-*N*⁶-(2-oxo-2*H*-chromen-4-yl)-*L*-lysine (**94**):** White solid; yield: 343



mg (80%); mp: 270–272 °C; $[\alpha]_D^{25} = +58$ ($c = 1.0$, MeOH); ¹H NMR (400 MHz, DMSO-*d*₆) δ 8.22 (brs, 1H), 7.61–7.33 (m, 4H), 6.78 (s, 1H), 5.04 (s, 1H), 4.21–4.02 (m, 1H), 2.96–2.84 (m, 2H), 1.99–1.83 (m, 2H), 1.48–1.21 (m, 13H); ¹³C NMR (100 MHz, DMSO-*d*₆) δ 172.0, 162.0, 156.1, 154.0, 153.5, 132.6, 123.9, 123.4, 117.4, 114.7, 83.2, 77.9, 56.6, 39.3, 30.9, 29.5, 28.7, 23.7; HRMS (ESI-TOF) (m/z)

calculated C₂₀H₂₇N₂O₆⁺: 391.1869; found 391.1822 [M+H]⁺.

(*S*)-1-carboxy-5-((2-oxo-2*H*-chromen-4-yl)amino)pentan-1-aminium chloride (95**):** White



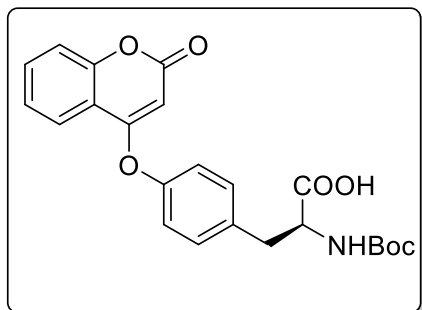
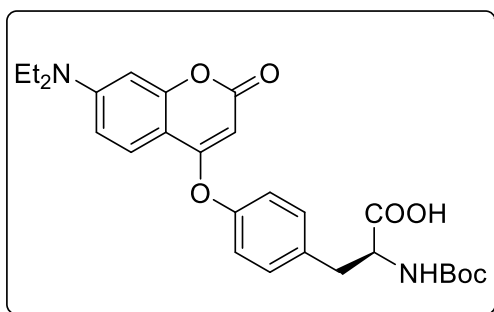
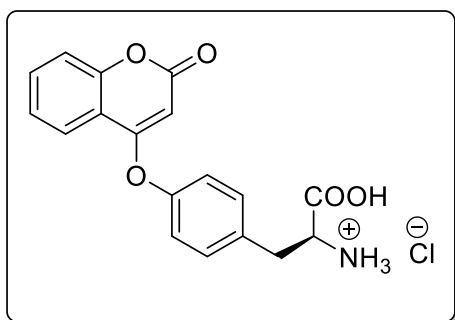
solid; yield: 115 mg (92%); mp: 210–212 °C; ¹H NMR (400 MHz, DMSO-*d*₆) δ 8.30 (d, $J = 7.8$ Hz, 1H), 7.96 (brs, 3H), 7.64 (d, $J = 7.5$ Hz, 1H), 7.58 (t, $J = 7.5$ Hz, 1H), 7.38–7.24 (m, 2H), 5.03 (s, 1H), 4.12–4.06 (m, 1H), 2.80–2.74 (m, 2H), 2.03–1.93 (m, 1H), 1.90–1.77 (m, 1H), 1.66–1.52 (m, 2H), 1.48–1.31 (m, 2H); ¹³C NMR (100 MHz, DMSO-*d*₆) δ 173.5, 162.0, 154.0,

153.4, 132.6, 123.9, 123.7, 117.4, 114.7, 83.2, 56.3, 38.8, 30.5, 26.9, 23.3; HRMS (ESI-TOF) (m/z) calculated C₁₅H₂₀ClN₂O₄⁺: 327.1111; found 327.1161 [M+H]⁺.

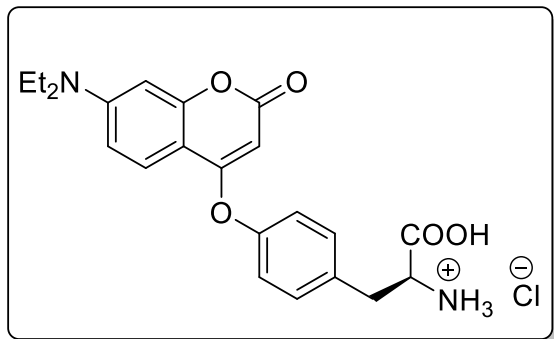
Typical procedure for the synthesis of coumaryl-labelled tyrosine

Boc *N*-tyrosine (**96**) (1.3 mmol/0.94 mmol) dissolved in water (1 mL) was added to a mixture of **88a-b** (1.1 mmol/0.79 mmol), K₂CO₃ (2.2 mmol/1.58 mmol) and CuI (0.05 mmol/0.03 mmol) in water (3 mL). The reaction mixture was heated at 80 °C for 12–15 min under microwave irradiation till the disappearance of the starting material. The reaction mixture was then added dropwise to an ice-bath, and concentrated HCl was then added to adjust the pH to 2–3 under cooling conditions to precipitate a solid. The precipitate was filtered, and washed with cold-water (3 x 10 mL), and recrystallized from ethanol to give pure coumaryl-labelled Boc-protected tyrosine (**97a-b**).

A solution of dioxane-HCl was added dropwise to **97a-b** (0.150 g) dissolved in dioxane at 0 °C. The reaction was stirred at room temperature for 2–3 h and monitored *via* TLC. After the completion, the reaction mixture was completely concentrated, washed with diethyl ether and filtered-off to yield **98a-b** as pure product.

(S)-2-((*tert*-Butoxycarbonyl)amino)-3-(4-((2-oxo-2*H*-chromen-4-yl)oxy)phenyl)propanoic acid (97a):White solid; yield: 392 mg (84%); mp: 180–183 °C; $[\alpha]_D^{25} = -4$ ($c = 1.0$, MeOH); ^1H NMR (400 MHz, DMSO- d_6) δ 8.02 (d, $J = 7.0$ Hz, 1H), 7.80 – 7.69 (m, 1H), 7.47 – 7.40 (m, 4H), 7.25 (d, $J = 5.4$ Hz, 2H), 6.89 (d, $J = 4.4$ Hz, 1H), 5.14 (s, 1H), 4.18 – 4.09 (m, 1H), 3.14 – 3.09 (m, 1H), 2.95 – 2.85 (m, 1H), 1.32 (s, 9H); ^{13}C NMR (100 MHz, DMSO- d_6) δ 166.4, 161.6, 155.7, 153.5, 151.0, 137.6, 133.9, 131.8, 130.5, 125.0, 123.4, 121.2, 117.1, 115.3, 93.1, 78.3, 55.80, 36.9, 28.6; HRMS (ESI-TOF) (m/z) calculated $\text{C}_{23}\text{H}_{24}\text{NO}_7^+$: 426.1552; found 426.1568 $[\text{M}+\text{H}]^+$.**(S)-2-((*tert*-Butoxycarbonyl)amino)-3-(4-((7-(diethylamino)-2-oxo-2*H*-chromen-4-yl)oxy)phenyl)propanoic acid (97b):** White solid; yield: 321 mg (82%); mp: 233–235 °C; $[\alpha]_D^{25}$  $= -128$ ($c = 1.0$, MeOH); ^1H NMR (400 MHz, DMSO- d_6) δ 7.72 (d, $J = 9.0$ Hz, 1H), 7.36 (d, $J = 7.1$ Hz, 2H), 7.19 (d, $J = 7.7$ Hz, 2H), 7.01 (d, $J = 7.9$ Hz, 1H), 6.95 – 6.82 (m, 1H), 6.56 (s, 1H), 4.75 (s, 1H), 4.13 – 4.04 (m, 1H), 3.40 (m, overlapped by moisture of DMSO, 4H), 3.12 – 3.08 (m, 1H), 2.89 – 2.83 (m, 1H), 1.32 (s,9H), 1.13 (t, $J = 6.7$ Hz, 6H); ^{13}C NMR (100 MHz, DMSO- d_6) δ 174.1, 167.3, 162.6, 156.2, 155.7, 151.7, 151.2, 137.2, 131.6, 121.3, 115.3, 109.2, 102.8, 96.9, 87.6, 78.4, 52.5, 44.6, 36.8, 28.6, 12.7; HRMS (ESI-TOF) (m/z) calculated $\text{C}_{27}\text{H}_{33}\text{N}_2\text{O}_7^+$: 497.2280; found 497.2296 $[\text{M}+\text{H}]^+$.**(S)-2-Amino-3-(4-((2-oxo-2*H*-chromen-4-yl)oxy)phenyl)propanoic acid hydrochloride (98a):**White solid; yield: 121 mg (96%); mp: 226–228 °C; $[\alpha]_D^{25} = +10$ ($c = 1.0$, MeOH); ^1H NMR (400MHz, DMSO- d_6) δ 8.39 (brs, 3H), 8.04 (d, $J = 7.2$ Hz, 1H), 7.76 (t, $J = 7.7$ Hz, 1H), 7.48 – 7.43 (m, 4H), 7.33 (d, $J = 8.3$ Hz, 2H), 5.34 (s, 1H), 4.17 (t, $J = 5.9$ Hz, 1H), 3.27 (dd, $J = 14.0, 5.3$ Hz, 1H), 3.15 (dd, $J = 14.0, 7.3$ Hz, 1H); ^{13}C NMR (100 MHz, DMSO- d_6) δ 170.9, 166.5, 161.8, 153.5, 151.7, 134.7, 133.9, 132.2, 125.0, 123.4, 121.9, 117.0, 115.2, 93.4, 54.2, 35.6; HRMS (ESI-TOF) (m/z) calculated $\text{C}_{18}\text{H}_{16}\text{NO}_5^+$: 326.1028; found 326.1096 $[\text{M}-\text{Cl}]^+$.

(S)-2-Amino-3-(4-((7-(diethylamino)-2-oxo-2H-chromen-4-yl)oxy)phenyl)propanoic acid hydrochloride (98b): White solid; yield: 121 mg (93%); mp: 191–193 °C; $[\alpha]_D^{25} = +238$ (c = 1.0,



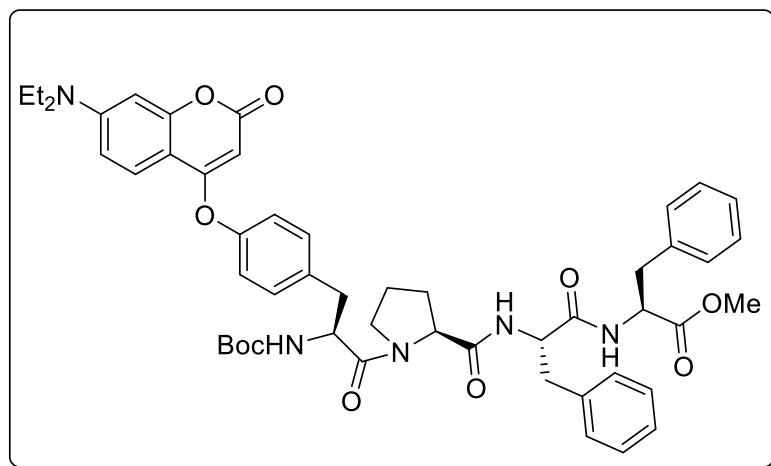
MeOH); $^1\text{H NMR}$ (400 MHz, $\text{DMSO}-d_6$) δ 8.43 (brs, 3H), 7.74 (d, $J = 9.0$ Hz, 1H), 7.44 (d, $J = 8.4$ Hz, 2H), 7.28 (d, $J = 8.4$ Hz, 2H), 6.77 (d, $J = 11.0$ Hz, 1H), 6.57 (s, 1H), 4.93 (s, 1H), 4.29 – 4.20 (m, 1H), 3.45 (q, $J = 6.9$ Hz, 4H), 3.25 – 3.20 (m, 1H), 3.17 – 3.12 (m, 1H), 1.13 (t, $J = 6.9$ Hz, 6H); $^{13}\text{C NMR}$ (100 MHz, $\text{DMSO}-d_6$) δ 170.8, 167.3, 162.8,

156.2, 152.0, 151.7, 133.7, 132.0, 122.0, 115.8, 109.3, 102.7, 96.9, 87.8, 53.6, 44.6, 35.4, 12.7; HRMS (ESI-TOF) (m/z) calculated $\text{C}_{22}\text{H}_{25}\text{N}_2\text{O}_5^+$: 397.1763; found 397.1742 $[\text{M}-\text{Cl}]^+$.

Typical procedure for the synthesis of coumaryl-labelled Endomorphin-2 derivative

Compound **100** was synthesized by coupling **97b** (0.129 g, 0.26 mmol) with $\text{HCl}\cdot\text{NH}_2\text{-L-Pro-L-Phe-L-Phe-OMe}$ (**99**)¹³³ (0.100 g, 0.21 mmol) following the procedure employed earlier for the synthesis of **93**.

Methyl ((S)-2-((tert-butoxycarbonyl)amino)-3-(4-((7-(diethylamino)-2-oxo-2H-chromen-4-yl)oxy)phenyl)propanoyl)-L-prolyl-L-phenylalanyl-L-phenylalaninate (100): White solid;



yield: 132 mg (70%); mp: 150–152 °C; $^1\text{H NMR}$ (400 MHz, $\text{DMSO}-d_6$) δ 8.40 (d, $J = 7.4$ Hz, 1H), 7.72 (d, $J = 9.0$ Hz, 1H), 7.40 (dd, $J = 19.8, 8.4$ Hz, 2H), 7.29 – 7.12 (m, 14H), 6.76 (d, $J = 10.0$ Hz, 1H), 6.56 (s, 1H), 4.77 (s, 1H), 4.51 – 4.46 (m, 2H), 4.43 – 4.28 (m, 2H), 3.56 (s, 3H), 3.45 (d, $J =$

6.7 Hz, 4H), 3.10 – 2.89 (m, 5H), 2.81 – 2.76 (m, 3H), 1.86 – 1.82 (m, 1H), 1.87 – 1.77 (m, 2H), 1.74 – 1.65 (m, 1H), 1.29 (s, 9H), 1.14 (t, $J = 6.9$ Hz, 6H); $^{13}\text{C NMR}$ (100 MHz, $\text{DMSO}-d_6$) δ 172.1, 171.6, 171.4, 170.8, 167.3, 162.6, 156.3, 155.7, 151.7, 151.2, 138.0, 137.5, 136.9, 131.9, 131.8, 129.7, 129.5, 129.5, 128.7, 128.5, 127.0, 126.7, 124.3, 121.4, 109.2, 102.8, 97.0, 87.7, 78.5,

60.0, 55.4, 54.1, 54.0, 52.3, 47.2, 44.6, 37.8, 37.1, 36.5, 28.6, 12.7; HRMS (ESI-TOF) (m/z) calculated $C_{51}H_{60}N_5O_{10}^+$: 902.4340; found 902.4325 $[M+H]^+$.

1A.5 References

- (1) Law, B.; Weissleder, R.; Tung, C. H. *Biomacromolecules* **2006**, *7*, 1261-1265.
- (2) Navo, C. D.; Asin, A.; Gomez Orte, E.; Gutierrez Jimenez, M. I.; Companon, I.; Ezcurra, B.; Avenoza, A.; Busto, J. H.; Corzana, F.; Zurbano, M. M. *Chemistry—A European Journal* **2018**, *24*, 7991-8000.
- (3) Jung, G.; Beck Sickinger, A. G. *Angewandte Chemie International Edition* **1992**, *31*, 367-383.
- (4) Toniolo, C.; Crisma, M.; Formaggio, F.; Valle, C.; Cavicchioni, G.; Precigoux, G.; Aubry, A.; Kamphuis, J. *Biopolymers: Original Research on Biomolecules* **1993**, *33*, 1061-1072.
- (5) Craik, D. J.; Fairlie, D. P.; Liras, S.; Price, D. *Chemical Biology & Drug Design* **2013**, *81*, 136-147.
- (6) Fosgerau, K.; Hoffmann, T. *Drug Discovery Today* **2015**, *20*, 122-128.
- (7) Wells, A.; Souto, J. C. S.; Solava, J.; Kassis, J.; Bailey, K. J.; Turner, T. *Clinical Cancer Research* **2002**, *8*, 1251-1257.
- (8) Duda, P. W.; Schmied, M. C.; Cook, S. L.; Krieger, J. I.; Hafler, D. A. *The Journal of Clinical Investigation* **2000**, *105*, 967-976.
- (9) Dunn, A.; Chow, M. S. S. *Formulary* **1998**, *33*, 632.
- (10) Ajani, J. A. *Oncology* **2002**, *16*, 89-96.
- (11) Bruckdorfer, T.; Marder, O.; Albericio, F. *Current Pharmaceutical Biotechnology* **2004**, *5*, 29-43.
- (12) Sun, L. *Modern Chemistry and Applications* **2013**, *1*, 1-2.
- (13) Mulder, K.; Lima, L. A.; Miranda, V.; Dias, S. C.; Franco, O. L. *Frontiers in Microbiology* **2013**, *4*, 321.
- (14) Baral, A.; Roy, S.; Dehsorkhi, A.; Hamley, I. W.; Mohapatra, S.; Ghosh, S.; Banerjee, A. *Langmuir* **2014**, *30*, 929-936.
- (15) Dillingham, M. S.; Wallace, M. I. *Organic & Biomolecular Chemistry* **2008**, *6*, 3031-3037.
- (16) Kaspar, A. A.; Reichert, J. M. *Drug Discovery Today* **2013**, *18*, 807-817.
- (17) Hughes, J. P.; Rees, S.; Kalindjian, S. B.; Philpott, K. L. *British Journal of Pharmacology* **2011**, *162*, 1239-1249.

- (18) Sahoo, H. *RSC Advances* **2012**, *2*, 7017-7029.
- (19) Ong, S. E.; Mann, M. *Nature Protocols* **2006**, *1*, 2650-2660.
- (20) Li, H.; Rothberg, L. *Proceedings of the National Academy of Sciences* **2004**, *101*, 14036-14039.
- (21) Soh, N.; Yoshida, K.; Nakajima, H.; Nakano, K.; Imato, T.; Fukaminato, T.; Irie, M. *Chemical Communications* **2007**, 5206-5208.
- (22) Harris, L. G.; Foster, S. J.; Richards, R. G. *Eur Cell Mater* **2002**, *4*, 39-60.
- (23) Cagnin, S.; Caraballo, M.; Guiducci, C.; Martini, P.; Ross, M.; SantaAna, M.; Danley, D.; West, T.; Lanfranchi, G. *Sensors* **2009**, *9*, 3122-3148.
- (24) Chen, Y.; Tsao, K.; Keillor, J. W. *Canadian Journal of Chemistry* **2014**, *93*, 389-398.
- (25) Modesti, M. In *Single Molecule Analysis*; Springer: **2011**, p 101-120.
- (26) Lukinavicius, G.; Reymond, L.; Umezawa, K.; Sallin, O.; D'Este, E.; Göttfert, F.; Ta, H.; Hell, S. W.; Urano, Y.; Johnsson, K. *Journal of the American Chemical Society* **2016**, *138*, 9365-9368.
- (27) Carmel, A.; Kessler, E.; Yaron, A. *European Journal of Biochemistry* **1977**, *73*, 617-625.
- (28) Bandyopadhyay, P.; Saha, K. *Chemical Physics Letters* **2008**, *457*, 227-231.
- (29) Haugland, R. P. *The Handbook: A Guide to Fluorescent Probes and Labeling Technologies*; Life Technologies, **2005**.
- (30) Pabst, R.; Miyasaka, M.; Dudler, L. *Immunology* **1986**, *59*, 217-222.
- (31) Hug, H.; Los, M.; Hirt, W.; Debatin, K. M. *Biochemistry* **1999**, *38*, 13906-13911.
- (32) Katritzky, A. R.; Narindoshvili, T. *Organic & Biomolecular Chemistry* **2009**, *7*, 627-634.
- (33) Kostenko, O. M.; Dmitrieva, S. Y.; Tolmachev, O. I.; Yarmoluk, S. M. *Journal of Fluorescence* **2002**, *12*, 173-175.
- (34) Hnedzko, D.; McGee, D. W.; Rozners, E. *Bioorganic & Medicinal Chemistry* **2016**, *24*, 4199-4205.
- (35) Mendive Tapia, L.; Subiros Funosas, R.; Zhao, C.; Albericio, F.; Read, N. D.; Lavilla, R.; Vendrell, M. *Nature Protocols* **2017**, *12*, 1588-1619.
- (36) Remington, S. J. *Protein Science* **2011**, *20*, 1509-1519.
- (37) He, X.; Gao, L.; Ma, N. *Scientific Reports* **2013**, *3*, 2825.

- (38) Cohen, B. E.; Pralle, A.; Yao, X.; Swaminath, G.; Gandhi, C. S.; Jan, Y. N.; Kobilka, B. K.; Isacoff, E. Y.; Jan, L. Y. *Proceedings of the National Academy of Sciences* **2005**, *102*, 965-970.
- (39) De Filippis, V.; De Boni, S.; De Dea, E.; Dalzoppo, D.; Grandi, C.; Fontana, A. *Protein Science* **2004**, *13*, 1489-1502.
- (40) Cohen, B. E.; McAnaney, T. B.; Park, E. S.; Jan, Y. N.; Boxer, S. G.; Jan, L. Y. *Science* **2002**, *296*, 1700-1703.
- (41) Faure, M. P.; Gaudreau, P.; Shaw, I.; Cashman, N. R.; Beaudet, A. *Journal of Histochemistry & Cytochemistry* **1994**, *42*, 755-763.
- (42) Fernandez Carneado, J.; Kogan, M. J.; Castel, S.; Giralt, E. *Angewandte Chemie International Edition* **2004**, *43*, 1811-1814.
- (43) Lohse, J.; Nielsen, P. E.; Harrit, N.; Dahl, O. *Bioconjugate Chemistry* **1997**, *8*, 503-509.
- (44) Bennett, F. A.; Barlow, D. J.; Dodoo, A. N.; Hider, R. C.; Lansley, A. B.; Lawrence, M. J.; Marriott, C.; Bansal, S. S. *Analytical Biochemistry* **1999**, *270*, 15-23.
- (45) Perkin, W. H. *Journal of the Chemical Society* **1868**, *21*, 53-63.
- (46) Smith, A. D.; Datta, S. P.; Smith, G. H. *Oxford Dictionary of Biochemistry and Molecular Biology*; Oxford University, **1997**.
- (47) Jones II, G.; Jackson, W. R.; Kanoktanaporn, S.; Halpern, A. M. *Optics Communications* **1980**, *33*, 315-320.
- (48) Barooah, N.; Pemberton, B. C.; Johnson, A. C.; Sivaguru, J. *Photochemical & Photobiological Sciences* **2008**, *7*, 1473-1479.
- (49) Steege, K. E.; Wang, J.; Uhrich, K. E.; Castner, E. W. *Macromolecules* **2007**, *40*, 3739-3748.
- (50) Lopez Arbeloa, T.; Lopez Arbeloa, F.; Tapia, M. J.; Lopez Arbeloa, I. *The Journal of Physical Chemistry* **1993**, *97*, 4704-4707.
- (51) Patalakha, N.; Yufit, D.; Kirpichenok, M.; Gordeeva, N.; Struchkov, Y. T.; Grandberg, I. *Chemistry of Heterocyclic Compounds* **1991**, *27*, 32-37.
- (52) Wagner, B. D. *Molecules* **2009**, *14*, 210-237.
- (53) Lauer Fields, J. L.; Broder, T.; Sritharan, T.; Chung, L.; Nagase, H.; Fields, G. B. *Biochemistry* **2001**, *40*, 5795-5803.
- (54) Jin, X.; Uttamapinant, C.; Ting, A. Y. *ChemBioChem* **2011**, *12*, 65-70.

- (55) Lang, K.; Chin, J. W. *Chemical Reviews* **2014**, *114*, 4764-4806.
- (56) Uttamapinant, C.; White, K. A.; Baruah, H.; Thompson, S.; Fernandez Suarez, M.; Puthenveetil, S.; Ting, A. Y. *Proceedings of the National Academy of Sciences* **2010**, *107*, 10914-10919.
- (57) Takaoka, Y.; Ojida, A.; Hamachi, I. *Angewandte Chemie International Edition* **2013**, *52*, 4088-4106.
- (58) Pashkova, A.; Moskovets, E.; Karger, B. L. *Analytical Chemistry* **2004**, *76*, 4550-4557.
- (59) Goncalves, M. S. T. *Chemical Reviews* **2008**, *109*, 190-212.
- (60) Wombacher, R.; Cornish, V. W. *Journal of Biophotonics* **2011**, *4*, 391-402.
- (61) Ngo, J. T.; Tirrell, D. A. *Accounts of Chemical Research* **2011**, *44*, 677-685.
- (62) Knight, C. G.; Willenbrock, F.; Murphy, G. *FEBS letters* **1992**, *296*, 263-266.
- (63) Song, H. Y.; Ngai, M. H.; Song, Z. Y.; MacAry, P. A.; Hobley, J.; Lear, M. J. *Organic & Biomolecular Chemistry* **2009**, *7*, 3400-3406.
- (64) Bennett, F. A.; Barlow, D. J.; Dodoo, A. N.; Hider, R. C.; Lansley, A. B.; Lawrence, M. J.; Marriott, C.; Bansal, S. S. *Tetrahedron Letters* **1997**, *38*, 7449-7452.
- (65) Xu, X.; Hu, X.; Wang, J. *Beilstein Journal of Organic Chemistry* **2013**, *9*, 254.
- (66) Wang, W.; Li, H. *Tetrahedron Letters* **2004**, *45*, 8479-8481.
- (67) Kele, P.; Sui, G.; Huo, Q.; Leblanc, R. M. *Tetrahedron: Asymmetry* **2000**, *11*, 4959-4963.
- (68) Knight, C. G. *Biochemical Journal* **1991**, *274*, 45-48.
- (69) Murakami, H.; Hoshika, T.; Ashizuka, Y.; Hashimoto, K.; Sisido, M. *Biomacromolecules* **2000**, *1*, 118-125.
- (70) Wang, J.; Xie, J.; Schultz, P. G. *Journal of the American Chemical Society* **2006**, *128*, 8738-8739.
- (71) Brun, M. P.; Bischoff, L.; Garbay, C. *Angewandte Chemie International Edition* **2004**, *43*, 3432-3436.
- (72) Moodie, L. W. K.; Chammaa, S.; Kindahl, T.; Hedberg, C. *Organic Letters* **2017**, *19*, 2797-2800.
- (73) Sui, G.; Kele, P.; Orbulescu, J.; Huo, Q.; Leblanc, R. M. *Letters in Peptide Science* **2001**, *8*, 47-51.
- (74) Ge, J.; Li, L.; Yao, S. Q. *Chemical Communications* **2011**, *47*, 10939-10941.
- (75) Katritzky, A. R.; Narindoshvili, T.; Angrish, P. *Synthesis* **2008**, *2008*, 2013-2022.

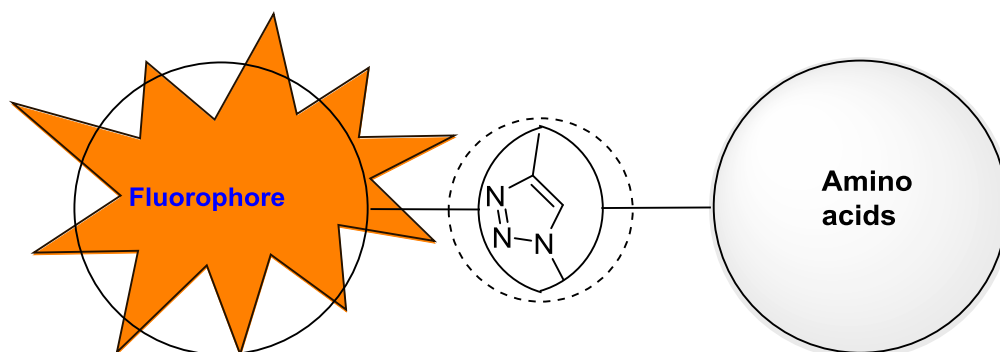
- (76) Malkar, N. B.; Fields, G. B. *Letters in Peptide Science* **2000**, 7, 263-267.
- (77) Luo, J.; Uprety, R.; Naro, Y.; Chou, C.; Nguyen, D. P.; Chin, J. W.; Deiters, A. *Journal of the American Chemical Society* **2014**, 136, 15551-15558.
- (78) Shukla, L.; Moodie, L. W.; Kindahl, T.; Hedberg, C. *The Journal of Organic Chemistry* **2018**, 83, 4792-4799.
- (79) Schmidt, L.; Doroshenko, T.; Barbie, P.; Grüter, A.; Jung, G.; Kazmaier, U. *Synthesis* **2016**, 48, 3077-3086.
- (80) Katritzky, A. R.; Yoshioka, M.; Narindoshvili, T.; Chung, A.; Johnson, J. V. *Organic & Biomolecular Chemistry* **2008**, 6, 4582-4586.
- (81) Pelletier, S. W. *Alkaloids: Chemical and Biological Perspectives*; Springer, **1999**.
- (82) Suhadolnik, R. J. *Nucleoside Antibiotics*; John Wiley & Sons, **1970**.
- (83) Volpi, E.; Kobayashi, H.; Sheffield Moore, M.; Mittendorfer, B.; Wolfe, R. R. *The American Journal of Clinical Nutrition* **2003**, 78, 250-258.
- (84) Brown, B. G.; Zhao, X. Q.; Chait, A.; Fisher, L. D.; Cheung, M. C.; Morse, J. S.; Dowdy, A. A.; Marino, E. K.; Bolson, E. L.; Alaupovic, P. *New England Journal of Medicine* **2001**, 345, 1583-1592.
- (85) Perutz, M. F. *Nature* **1970**, 228, 726-734.
- (86) Hovhannisyanyan, G.; Haroutiunian, S.; Margaryan, K.; Ghazaryan, R.; Aroutiounian, R. *Environmental Biology* **2005**, 23, 379-382.
- (87) Hormones, E.; Group, P. C. C. *Journal of the National Cancer Institute* **2008**, 100, 170-183.
- (88) Tsao, T.-S.; Tomas, E.; Murrey, H. E.; Hug, C.; Lee, D. H.; Ruderman, N. B.; Heuser, J. E.; Lodish, H. F. *Journal of Biological Chemistry* **2003**, 278, 50810-50817.
- (89) Hemmingsen, S. M.; Woolford, C.; Van Der Vies, S. M.; Tilly, K.; Dennis, D. T.; Georgopoulos, C. P.; Hendrix, R. W.; Ellis, R. J. *Nature* **1988**, 333, 330-334.
- (90) Bariwal, J.; Van der Eycken, E. *Chemical Society Reviews* **2013**, 42, 9283-9303.
- (91) Evano, G.; Blanchard, N.; Toumi, M. *Chemical Reviews* **2008**, 108, 3054-3131.
- (92) Hili, R.; Yudin, A. K. *Nature Chemical Biology* **2006**, 2, 284-287.
- (93) Samanta, S.; Beharry, A. A.; Sadowski, O.; McCormick, T. M.; Babalhavaeji, A.; Tropepe, V.; Woolley, G. A. *Journal of the American Chemical Society* **2013**, 135, 9777-9784.

- (94) Yamaguchi, J.; Yamaguchi, A. D.; Itami, K. *Angewandte Chemie International Edition* **2012**, *51*, 8960-9009.
- (95) Nakamura, I.; Yamamoto, Y. *Chemical Reviews* **2004**, *104*, 2127-2198.
- (96) Cho, S. H.; Kim, J. Y.; Kwak, J.; Chang, S. *Chemical Society Reviews* **2011**, *40*, 5068-5083.
- (97) Shi, Z.; Zhang, C.; Tang, C.; Jiao, N. *Chemical Society Reviews* **2012**, *41*, 3381-3430.
- (98) Brasche, G.; Buchwald, S. L. *Angewandte Chemie International Edition* **2008**, *47*, 1932-1934.
- (99) Wang, X.; Jin, Y.; Zhao, Y.; Zhu, L.; Fu, H. *Organic Letters* **2011**, *14*, 452-455.
- (100) Zhao, J.; Wang, Y.; He, Y.; Liu, L.; Zhu, Q. *Organic Letters* **2012**, *14*, 1078-1081.
- (101) Liu, Q.; Wu, P.; Yang, Y.; Zeng, Z.; Liu, J.; Yi, H.; Lei, A. *Angewandte Chemie International Edition* **2012**, *51*, 4666-4670.
- (102) Li, L.; Yu, P.; Cheng, J.; Chen, F.; Pan, C. *Chemistry Letters* **2012**, *41*, 600-602.
- (103) Nishino, M.; Hirano, K.; Satoh, T.; Miura, M. *Angewandte Chemie International Edition* **2012**, *51*, 6993-6997.
- (104) Zhang, G.; Miao, J.; Zhao, Y.; Ge, H. *Angewandte Chemie* **2012**, *124*, 8443-8446.
- (105) Kunz, K.; Scholz, U.; Ganzer, D. *Synlett* **2003**, *2003*, 2428-2439.
- (106) Sambiagio, C.; Marsden, S. P.; Blacker, A. J.; McGowan, P. C. *Chemical Society Reviews* **2014**, *43*, 3525-3550.
- (107) Beletskaya, I. P.; Cheprakov, A. V. *Coordination Chemistry Reviews* **2004**, *248*, 2337-2364.
- (108) Ullmann, F. *Reports of the German Chemical Society* **1903**, *36*, 2382-2384.
- (109) Ullmann, F.; Mauthner, F. *Reports of the German Chemical Society* **1903**, *36*, 4026-4034.
- (110) Ullmann, F.; Sponagel, P. *Reports of the German Chemical Society* **1906**, *350*, 83-107.
- (111) Goldberg, I. *Reports of the German Chemical Society* **1906**, *39*, 1691-1692.
- (112) Surry, D. S.; Buchwald, S. L. *Chemical Science* **2011**, *2*, 27-50.
- (113) Baig, R. B. N.; Varma, R. S. *Chemical Society Reviews* **2012**, *41*, 1559-1584.
- (114) Polshettiwar, V.; Varma, R. S. *Accounts of Chemical Research* **2008**, *41*, 629-639.
- (115) Allen, S. E.; Walvoord, R. R.; Padilla Salinas, R.; Kozlowski, M. C. *Chemical Reviews* **2013**, *113*, 6234-6458.
- (116) Polshettiwar, V.; Varma, R. S. *Chemical Society Reviews* **2008**, *37*, 1546-1557.

- (117) Ma, D.; Xia, C. *Organic Letters* **2001**, *3*, 2583-2586.
- (118) Ma, D.; Zhang, Y.; Yao, J.; Wu, S.; Tao, F. *Journal of the American Chemical Society* **1998**, *120*, 12459-12467.
- (119) Li, B.; Dixneuf, P. H. *Chemical Society Reviews* **2013**, *42*, 5744-5767.
- (120) Dallinger, D.; Kappe, C. O. *Chemical Reviews* **2007**, *107*, 2563-2591.
- (121) Gronnow, M. J.; White, R. J.; Clark, J. H.; Macquarrie, D. J. *Organic Process Research & Development* **2005**, *9*, 516-518.
- (122) Yadav, L. D. S.; Yadav, B. S.; Rai, V. K. *Synthesis* **2006**, *2006*, 1868-1872.
- (123) Rottger, S.; Sjoberg, P. J. R.; Larhed, M. *Journal of Combinatorial Chemistry* **2007**, *9*, 204-209.
- (124) Stunic, Z.; Trkovnik, M.; Lacan, M.; Jankovic, R. *Journal of Heterocyclic Chemistry* **1981**, *18*, 511-513.
- (125) Stoyanov, E. V.; Ivanov, I. C. *Molecules* **2004**, *9*, 627-631.
- (126) Owens, D. F.; Kriegstein, A. R. *Nature Reviews Neuroscience* **2002**, *3*, 715-727.
- (127) Paredes, R. G.; Agmo, A. *Neuroscience & Biobehavioral Reviews* **1992**, *16*, 145-170.
- (128) Kuo, P. Y.; Yang, D. Y. *The Journal of Organic Chemistry* **2008**, *73*, 6455-6458.
- (129) Zhou, Z.; Fahrni, C. J. *Journal of the American Chemical Society* **2004**, *126*, 8862-8863.
- (130) Seixas de Melo, J. S.; Becker, R. S.; Macanita, A. L. *The Journal of Physical Chemistry* **1994**, *98*, 6054-6058.
- (131) Cserep, G. B.; Herner, A.; Wolfbeis, O. S.; Kele, P. *Bioorganic & Medicinal Chemistry Letters* **2013**, *23*, 5776-5778.
- (132) Le Merrer, J.; Becker, J. A. J.; Befort, K.; Kieffer, B. L. *Physiological Reviews* **2009**, *89*, 1379-1412.
- (133) Mollica, A.; Costante, R.; Stefanucci, A.; Pinnen, F.; Luisi, G.; Pieretti, S.; Borsodi, A.; Bojnik, E.; Benyhe, S. *European Journal of Medicinal Chemistry* **2013**, *68*, 167-177.

Chapter 1B

Copper-catalyzed [3+2] Cycloaddition: A Facile Access to Triazolyl Linked Coumarin-amino acid/ Peptide Hybrids



1B.1 Introduction

Amino acids and peptides display various physiological actions in living cells, and thus act as hormones, enzyme inhibitors and neurotransmitters. However their clinical applications are limited due to their rapid hydrolysis by peptidase enzymes. To overcome this, peptides have been replaced by peptidomimetics that are small peptide-like molecules possessing esters, thioesters, thioamides, hydrazides, ureas, or a variety of heterocycles including tetrazoles, imidazoles, oxazoles and triazoles as substitute of amide bond (Figure. 1B.1.1).¹⁻⁴

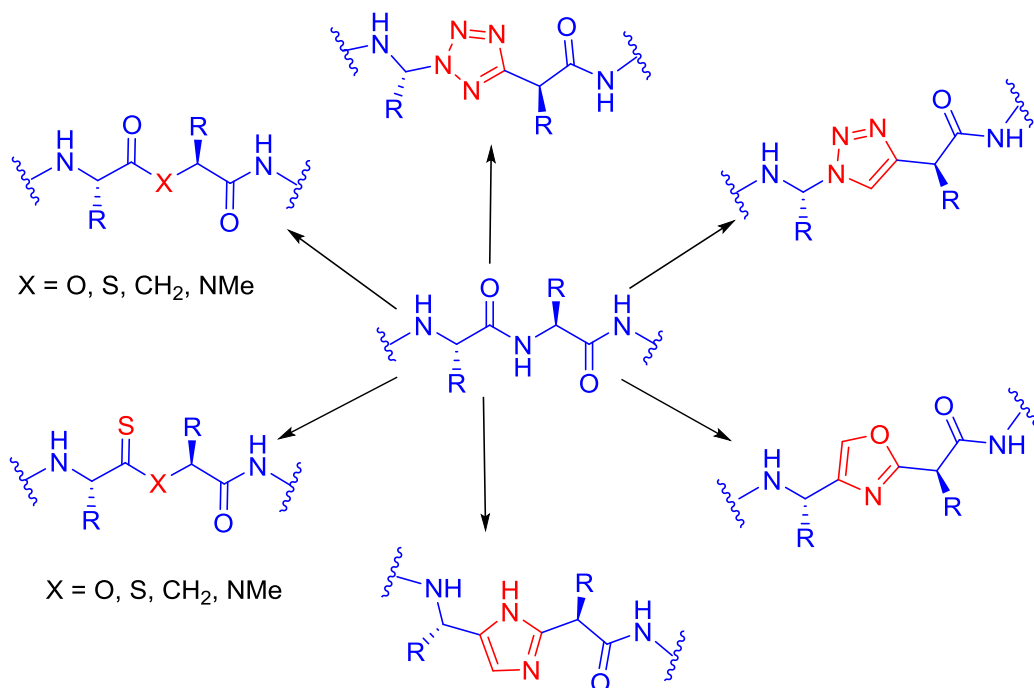


Figure 1B.1.1: Representative examples of peptidomimetics modified peptides used for mimicking peptides

The demand for modified peptides obtained by bioisosteric replacement of an amide bond by such functionalities is driving extensive research effort in the field of drug discovery due to their improved stability profiles and pharmacokinetic properties. Many structural modifications of peptides guided by rational design and molecular modeling have been proposed to develop novel synthetic approaches for their synthesis. In addition, several key synthetic strategies such as solid-phase synthesis of non-peptide libraries extended the range of chemical space covered with peptidomimetics. For *e.g.*, Pepstatin, the first synthetic renin inhibitor (*N*-acyl-pentapeptide, isovaleryl-L-valyl-L-valyl-statyl-L-alanyl-statine)⁵ was replaced by first-generation peptide analogs (*e.g.* H-142)⁶ due to their low potency and poor solubility. Due to poor bioavailability,

short duration of action, and low potencies, none of the first-generation analogs completed clinical investigations, and thus were replaced by second-generation renin inhibitors (e.g. Remikiren)⁷ that resisted degradation by peptidases, and exhibited great efficacy *in vivo* towards hypertension and inhibitors for liver enzyme renin. However, due to short half-life on oral delivery, it has been recently replaced by Aliskiren,⁸⁻¹³ which is a third-generation orally active renin inhibitor that is currently marketed (Figure 1B.1.2).

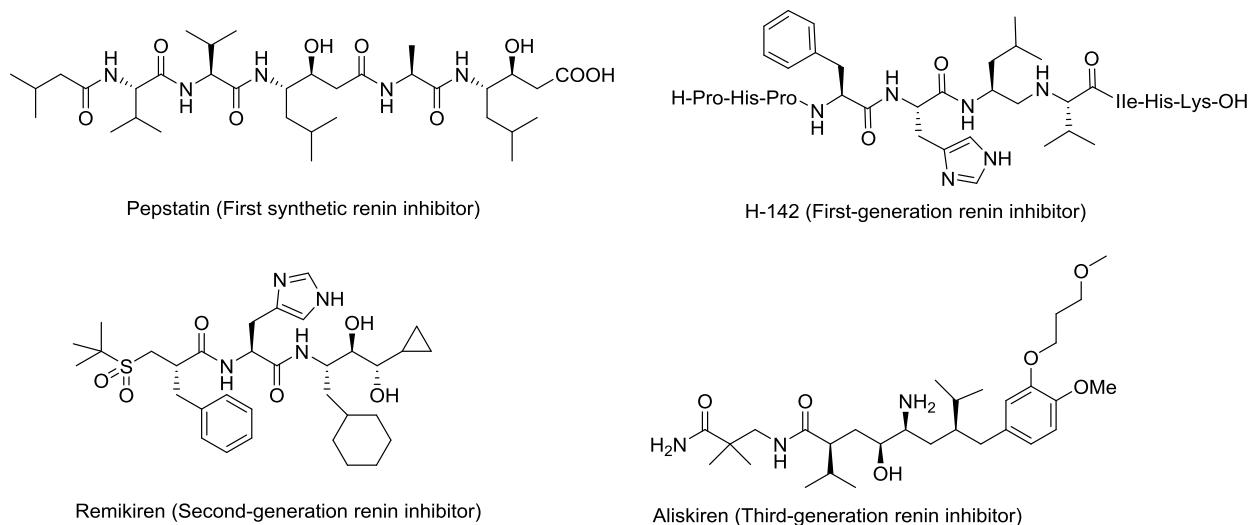


Figure 1B.1.2: Representative examples of peptidomimetics used as renin inhibitors

Strikingly, a triazole ring has been considered as a non-classical bioisostere of the peptide bond. Its functions to act as a helical component,¹⁴ a β -turn unit,¹⁵ and a *cis* or *trans*-prolyl ratio modifier in linear peptidomimetics¹² have been studied by few researchers. Further, triazole-based peptidomimetics have received considerable interest due to similarity of their electronic and structural characteristics with that of an amide bond (Figure 1B.1.3). Contentedly, both 1,2,3-triazole and amide bond are planar, of similar size, possess a high dipolar moment, and feature similar H-bonding capabilities.^{16,17} In contrast to amide bond, the 1,2,3-triazole moiety is resistant to be cleaved by proteases. All these characteristics ascertain 1,2,3-triazole to be an attractive amide-bond surrogate for peptide backbone engineering with increased hydrolytic stability. Moreover, inclusion of 1,4- and 1,5-disubstituted 1,2,3-triazoles into peptide backbone provides a direct access to “linear” and “bent” peptide surrogates, respectively. However, there are some significant structural discrepancies between *trans*-amide bond and 1,4-disubstituted triazole, or *cis*-amide bond and 1,5-disubstituted 1,2,3-triazole surrogates in peptides, most notably an increased distance between the amino acid side chains of approximately 25%.

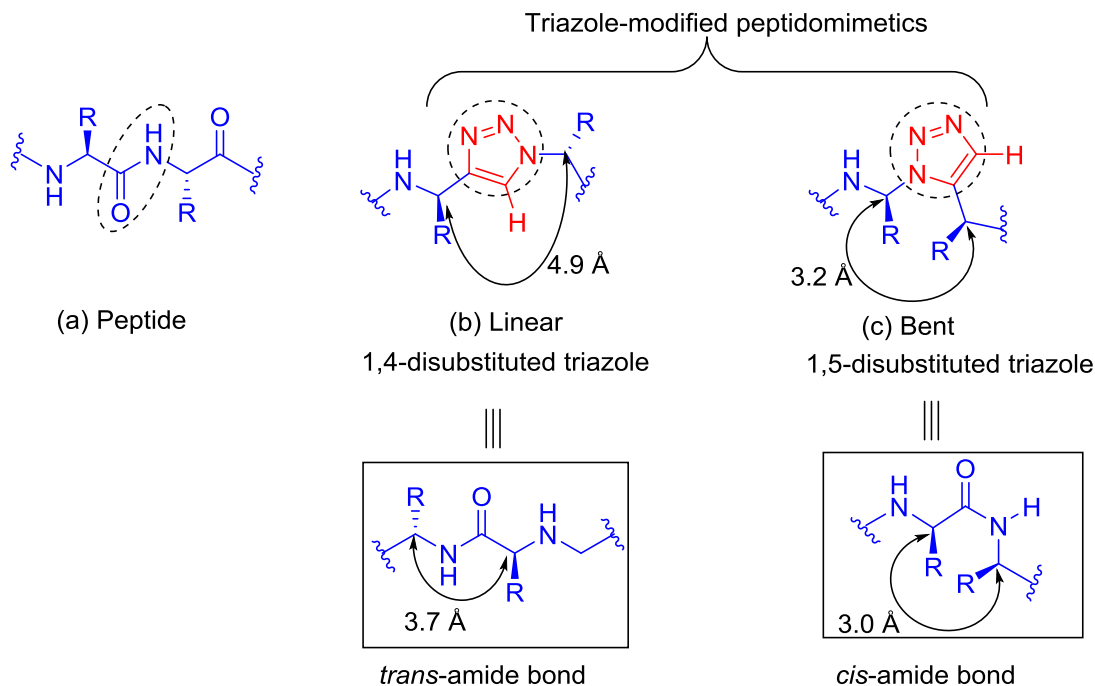


Figure 1B.1.3: Structural comparison of *trans*-amide and *cis*-amide with 1,4- and 1,5-disubstituted 1,2,3-triazoles, respectively

Thus, 1,2,3-triazole-modified peptidomimetics are attractive non-natural molecules for drug discovery because of their versatile pharmacological profile.^{15,18-21} For example, triazole-modified peptidomimetics have been used as tyrosinase inhibitor,¹⁹ anticancer agents,²¹ PDZ domain inhibitor,²⁰ β -turn inducer¹⁵ and AMPA receptor ligand²² (Figure 1B.1.4). Moreover, they have been an integral component of protein-like oligomers and non-peptidic protein mimetic foldamers.^{23,24} In addition, stable analogues of glycoamino acids and glycopeptides in which the non-sugar acetal-heteroatom has been replaced by a triazole moiety, are reported with exceptional medical and nutritional applications.^{13,25-27} Consequently, triazole nucleus has been recognized in many natural products, and exhibited numerous pharmaceutical activities, including antiseptic, analgesic, anticonvulsant, antibiotic, antiallergic, antiinflammatory, diuretic, fungicidal, insecticidal, herbicidal, antibacterial, antiviral, antidepressant, antimicrobial, antitumor, antihypertensive and antimigraine.²⁸⁻³⁰

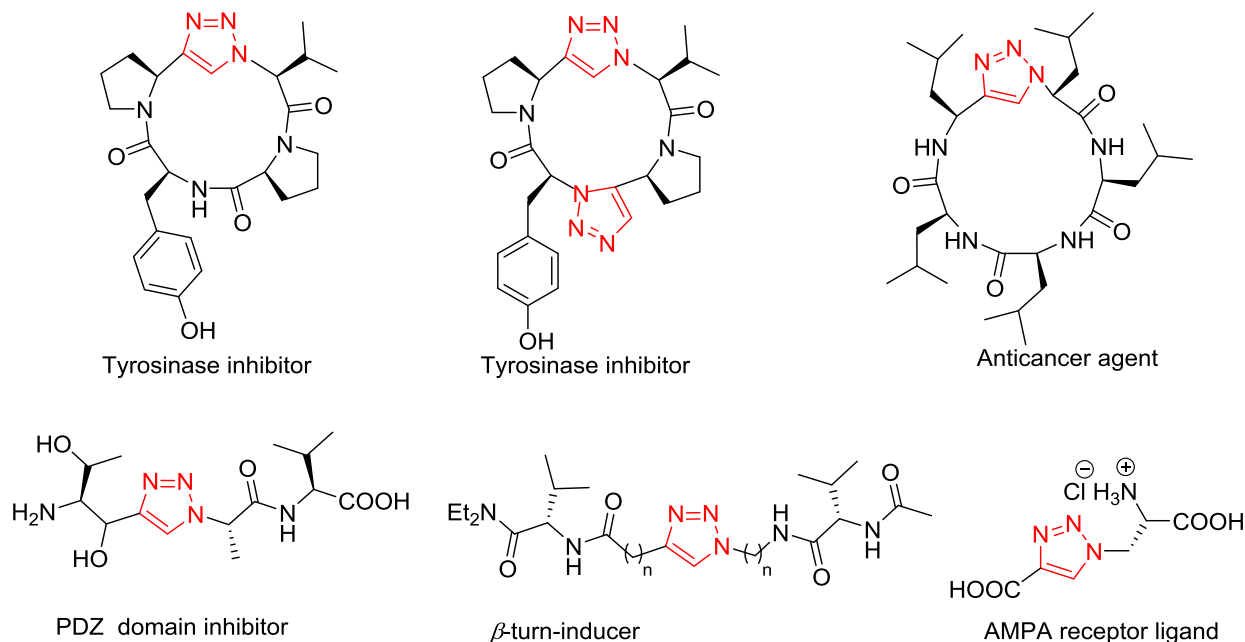
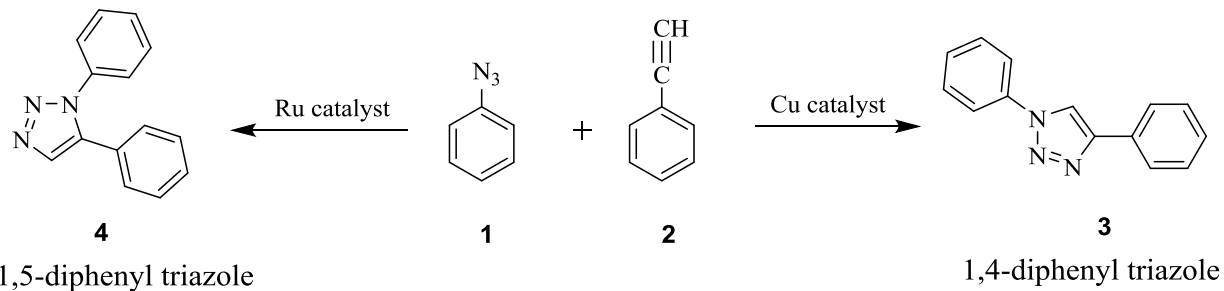


Figure 1B.1.4: Selective examples of biological active triazole-modified peptidomimetics

Due to diverse applications of triazoles, much attention has been devoted towards their construction by various research groups. In this realm, the cycloaddition reaction between an organic azide and alkyne that was discovered in early 20th century, proved to be a backbone for constructing triazolyl-linked dendrimers, DNA-cleaving agents, and structural components of highly branched polymers, especially in liquid crystals and so on.³¹⁻³⁶ Surprisingly, the cycloaddition reaction didn't gain much attention until 1960s when Huisgen and coworkers explored this reaction, and carried out a comprehensive study to unveil the mechanism of the reaction.³⁷⁻³⁹ Interestingly, in 2001 Sharpless introduced the term 'click chemistry' for the reactions that are easy to perform, yield no byproducts, remain unaffected by the nature of groups being connected, and able to performed under mild conditions and in water as a solvent of choice.⁴⁰ In broader sense, click chemistry reactions are considered as a "state of art" for chemists because of valuable features, including shorter reaction time, and excellent selectivity.⁴¹ Additionally, it can be conducted over a pH range from 3 to 12, with high atom-economy, large thermodynamic driving force (>84 kJ/mol) to favor a single reaction product.⁴² In mid-90s, it was reported that thermal cycloaddition of an alkyne and azide leads to the formation of a mixture of regioisomers. Later, it was established that copper and ruthenium catalysis⁴³ display high regioselective behavior for the [3+2] cycloaddition between phenyl azide (1) and phenyl

acetylene (**2**) to exclusively afford 1,4- and 1,5-diphenyl triazoles (**3** & **4**), respectively (Scheme 1B.1.1).⁴³

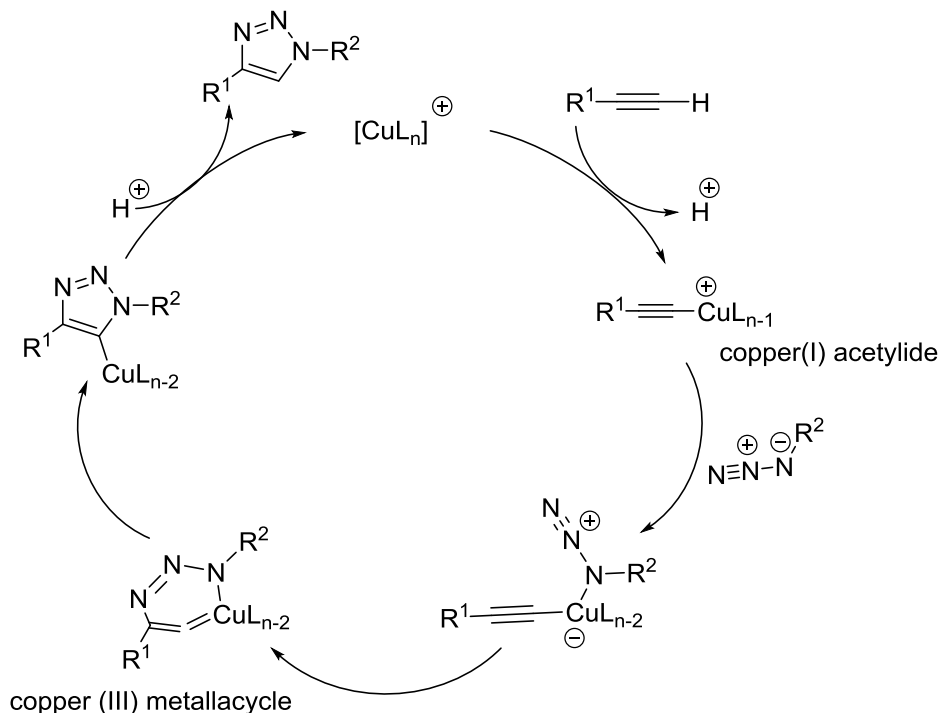


Scheme 1B.1.1: Metal catalyzed [3+2] cycloaddition for the synthesis 1,4- and 1,5-diphenyl 1,2,3-triazoles

Among these strategies, Cu-catalyzed azide-alkyne cycloaddition (CuAAC) is a premier example of click chemistry⁴⁴ that has been explored for building covalent connections between complex molecular architectures.⁴² More than 1000 research articles have been published on CuAAC since the Meldal and Fokin–Sharpless publications of 2002, which described the most favorable reaction conditions.⁴⁵ CuAAC remains unaffected by a variety of functional groups, and can be achieved using a variety of Cu(I) catalysts and solvents, including aqueous medium. Some of the examples of commonly used pre-catalysts for CuAAC are: (i) a Cu(II) salt together with a reducing agent, (ii) a Cu(I) salt together with a base or amine ligand and a reducing agent in order to inhibit aerobic oxidation to Cu(II), (iii) a Cu(0) (wire, turnings, powder, or nanoparticles), the surface of which forms the required Cu(I) species, (iv) cupric salts or complexes such as Cu(OAc)₂ in absence of a reductant.^{46,47} Although ligands are usually not necessary to carry out the CuAAC reaction, they have reported to enhance the reaction rate.

In spite of its simple outlook, its mechanism remains debatable, and has been proposed on the basis of density functional theory (DFT) calculations and kinetic studies (Scheme 1B.1.2).⁴⁸⁻⁵⁰ Initially, a bimetallic mechanism was proposed in which the alkynyl was coordinated to one Cu center to form copper-acetylide coordination complex, whereas the azide attacked a second one. After reinvestigation, another related mechanism was suggested which was believed to be initiated by the generation of active Cu(I) catalyst from Cu(I) salts or Cu(II) salts using sodium ascorbate as the reducing agent. DFT calculations have shown that nitrogen-based ligands can stabilize the Cu(I) oxidation state under aerobic, aqueous conditions, and promote the desired transformation (Scheme 1B.1.2).^{50,51} In 2013, Worrell *et al.* showed that two Cu(I) atoms of the

catalytic complex become equivalent and can hike, however the way of binding of the azide to the Cu(I) π -complexes has not been established experimentally.⁵²



Scheme 1B.1.2: Generalized mechanism for CuAAC reaction

Strikingly, 1,4-disubstituted 1,2,3-triazoles possess interesting chemical properties such as tolerance to acidic, basic, oxidative, and reductive conditions, which have been explored for preparing calixarenes, rotaxanes, dendrimers, polymers, carbohydrate clusters, and studying carbohydrate conjugation by triazole ligation.^{16,42,53,54} Interestingly, the diverse fluorescence properties of the triazolyl linked conjugates resulted by CuAAC between aryl/heteroaryl acetylenes and azides have immensely contributed to the success of CuAAC (Figure 1B.1.5).³⁵ This is due to increased emission intensity and variation in emission wavelength properties of the conjugates, desirable to act as fluorogenic probes for bioimaging.

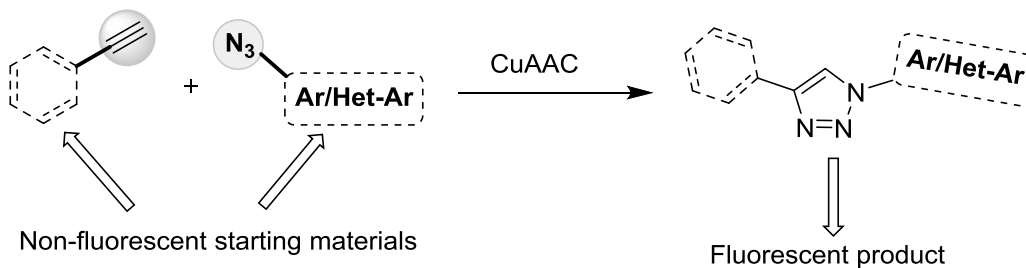
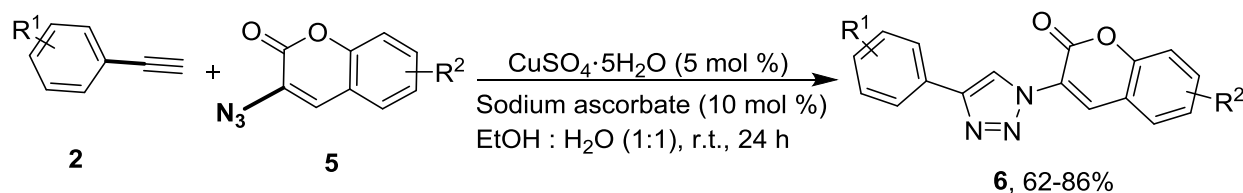


Figure 1B.1.5: Generalized representation of fluorogenic CuAAC

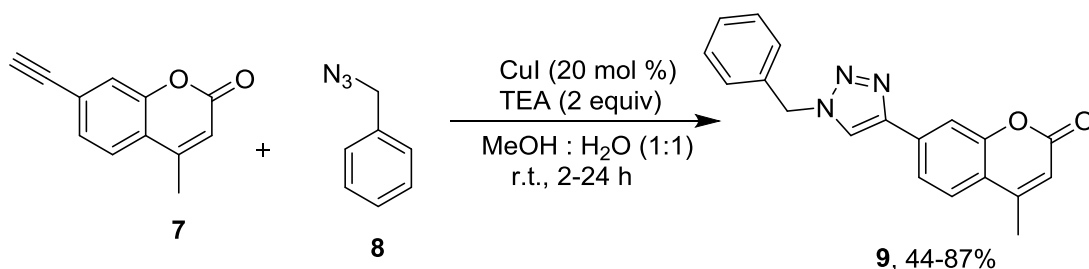
Under this domain, coumarins have exhibited interesting fluorescence properties, and a high degree of sensitivity to their local environment, including polarity and viscosity. This sensitivity has led to their widespread application as sensitive fluorescent probes for a wide range of homogeneous and heterogeneous materials.

In 2004, Sivakumar *et al.* synthesized triazolyl linked coumarin-aryl hybrids (**6**) by CuAAC between non-fluorescent 3-azidocoumarins (**5**) and aryl acetylenes (**2**) in a mixture of water and ethanol at room temperature (Scheme 1B.1.3).⁵⁵



Scheme 1B.1.3: Synthesis of triazolyl linked coumarin-aryl hybrids (**6**)

Similarly, Key *et al.* reported the synthesis of 7-(1-benzyl-1*H*-1,2,3-triazol-4-yl)-4-methyl-2*H*-chromen-2-one (**9**) by CuACC between 7-alkynyl-4-methyl coumarin (**7**) and benzyl azide (**8**) in water and methanol (1:1) using triethylamine and CuI (Scheme 1B.1.4). The authors also studied the photophysical properties of the synthesized compounds and inferred that triazole formation enhances the fluorescence and induce shifts in emission wavelength.⁵⁶



Scheme 1B.1.4: Synthesis of 7-(1-benzyl-1*H*-1,2,3-triazol-4-yl)-4-methyl-2*H*-chromen-2-one (**9**)

Thereafter, the scope of CuAAC reaction has been explored for the synthesis of numerous 1,2-3-triazolyl linked coumarin-alkyl/aryl/heteroaryl hybrids that have exhibited versatile biological activities including, antitumor, antitubercular, antiinflammatory, anticancer, and antifungal activities. For example, compound (i) is a potent 5-lipoxygenase (5-LO) inhibitor,⁵⁷ coumarin-triazole-dithiocarbamate hybrid (ii) is a LSD1 inhibitor,⁵⁸ coumarin-triazole-thiophene hybrid (iii) is a non-peptidic protease inhibitor,⁵⁹ coumarin-triazole-coumarin hybrid (iv) is an

antitubercular & antimicrobial agent,⁶⁰ coumarin-triazole-chalcone hybrid (v) is an anticancer agent,⁶¹ and coumarin-triazole-aryl hybrid is an antiinflammatory agent⁶² (Figure 1B.1.6).

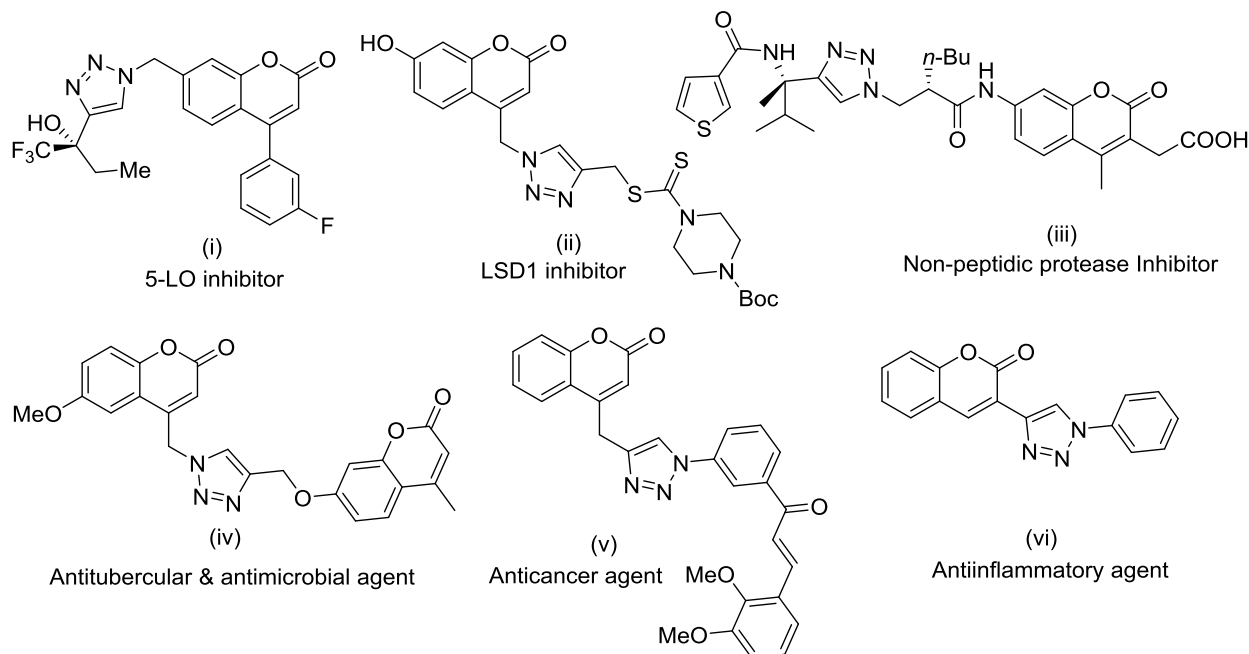
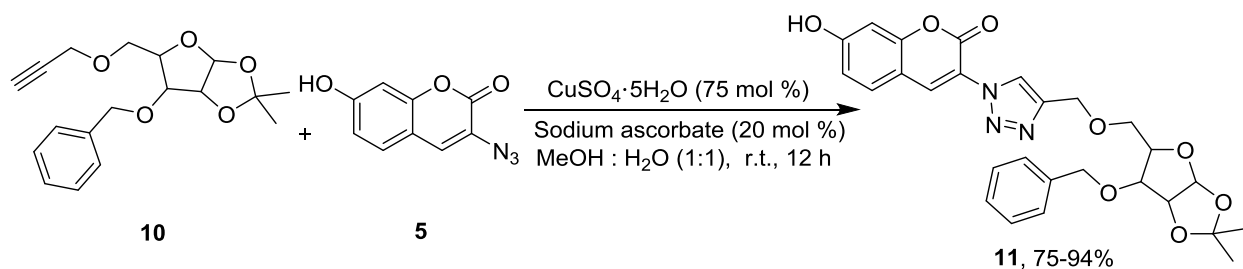


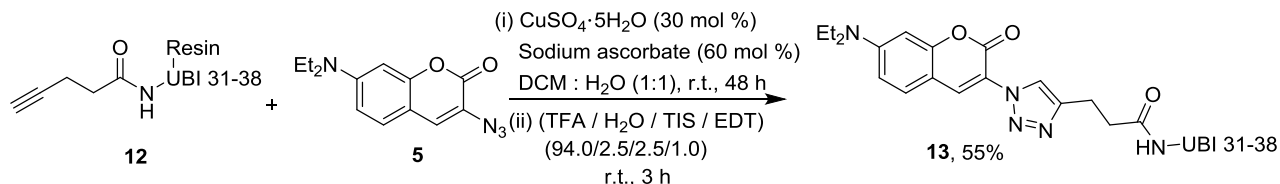
Figure 1B.1.6: Selective examples of bioactive triazolyl linked coumarin-alkyl/aryl/heteroaryl hybrids

Also, CuAAC has also been explored to prepare coumarin-appended bioconjugates, to label various biomolecules in cells^{63,64} and even animals⁶⁵ by linking them with functionalized coumarins *via* triazole ring. As a result, the synthesis of coumarin-appended carbohydrates, nucleosides,^{66,67} proteins,⁶⁸ peptides^{69,70} and amino acids^{71,72} have received eye-catching interest. For example, Pai *et al.* synthesized triazolyl linked coumarin-glyco conjugate (**11**) from alkynyl functionalized glycosaccharide (**10**) and 7-hydroxy-3-azidocoumarin (**5**) in water and methanol (1:1), using sodium ascorbate and $\text{CuSO}_4 \cdot 5\text{H}_2\text{O}$ at room temperature. The synthesized conjugate was studied for their antibacterial activities against a series of gram +ve, gram -ve bacteria. (Scheme 1B.1.5).⁷³



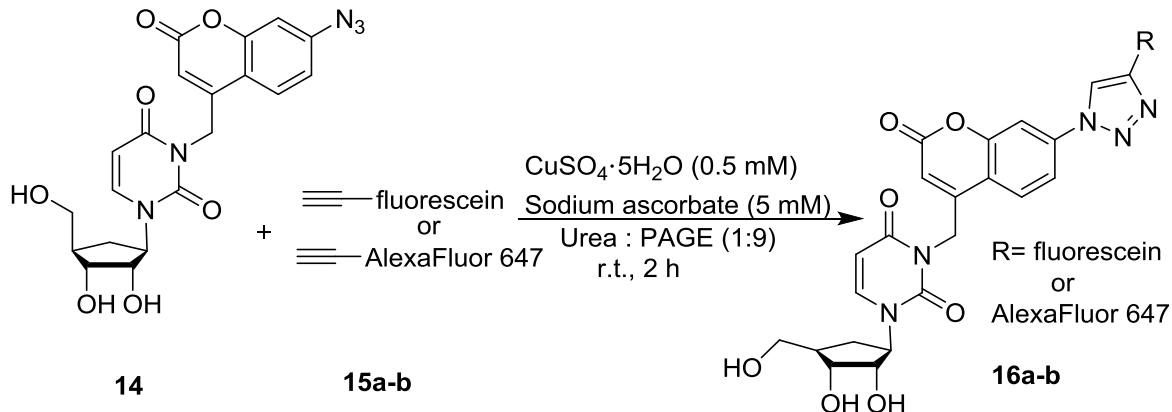
Scheme 1B.1.5: Synthesis of triazolyl linked coumarin-glyco conjugate (**11**)

Ferreira *et al.* prepared a peptide-coumarin conjugate (**13**) via Cu-catalyzed azide-alkyne cycloaddition (CuACC) between resin bounded alkynyl functionalized UBI31-38 peptide (**12**) and 3-azidocoumarin derivative (**5**). The conjugate (**13**) was assayed for *in vitro* cytotoxicity and antifungal activity against *Cryptococcus gattii* and *Cryptococcus neoformans*. The conjugate exhibited increased antifungal efficacy when compared with the individual peptide, coumarin, or triazole moieties (Scheme 1B.1.6).⁷⁴



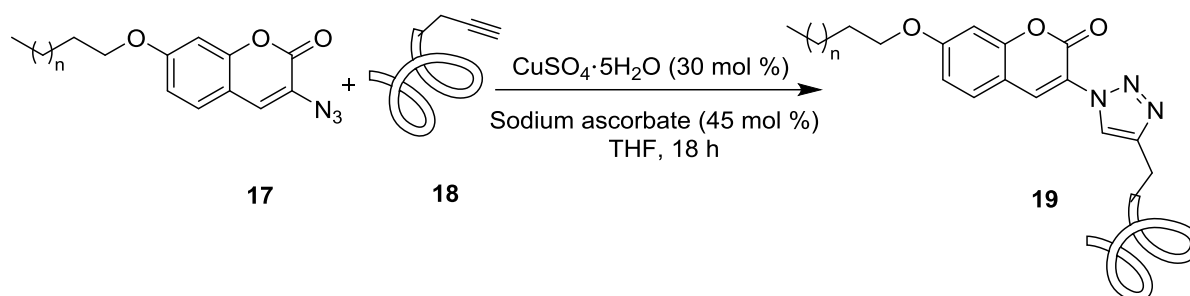
Scheme 1B.1.6: Synthesis of triazolyl linked coumarin-peptide conjugate (**13**)

Kellner *et al.* documented the synthesis of triazolyl linked coumarin-appended alexafluor 647 and fluorescein conjugates (**16a-b**) by CuAAC between azido-functionalized coumarin-appended uridine (UN3C) (**14**) and alkynyl functionalized alexafluor 647 and fluorescein (**15a-b**), respectively. The conjugates were synthesized in moderate-to-good yields, and were used to monitor *t*-RNA configuration (Scheme 1B.1.7).⁷⁵



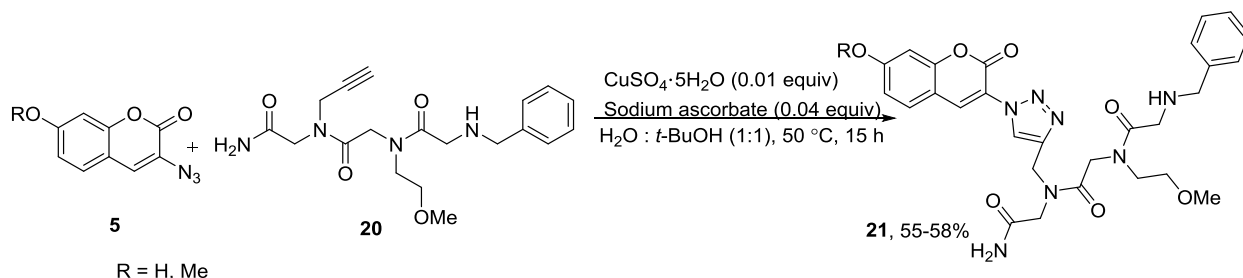
Scheme 1B.1.7: Synthesis of triazolyl linked coumarin-alexfluor 647 and fluorescein (**16a-b**) conjugates

Dirks *et al.* documented the coupling of 3-azidocoumarin (**17**) with alkynyl-functionalized bovin serum albumin (BSA) (**18**) under click reaction conditions to afford a highly fluorescent coumarin-labelled bovin serum albumin (**19**), which exemplified an excellent example of protein-polymer conjugation (Scheme 1B.1.8).⁷⁶



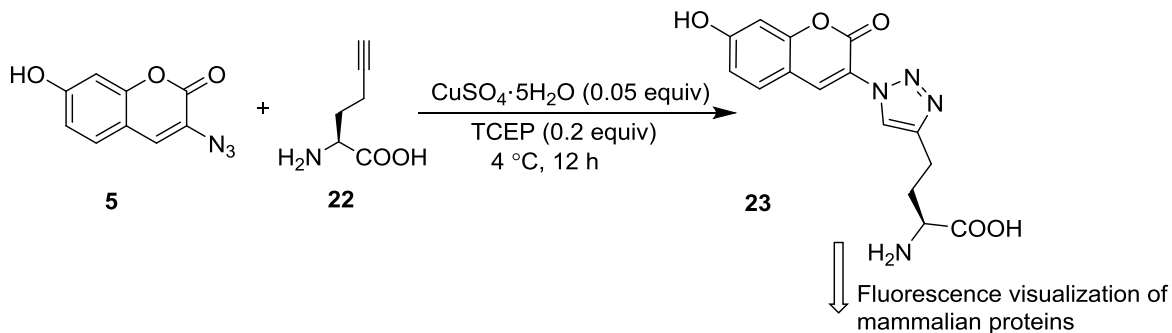
Scheme 1B.1.8: Labelling of alkyne-functionalized BSA (**18**) with azidocoumarin (**17**)

Lim *et al.* described the synthesis and application of triazolyl linked coumarin-labelled peptides towards selective detection of Cu^{2+} and CN^- ion in DMF. Two triazolyl linked coumarin-labelled fluorescent probes (**21**) were synthesized in 55-58% yields by clicking 3-azidocoumarin (**5**) with alkyne-functionalized peptide (**20**) using $\text{CuSO}_4 \cdot 5\text{H}_2\text{O}$ and sodium ascorbate in *tert*-butyl alcohol and water solution (v/v = 1:1) at 50 °C (Scheme 1B.1.9).⁷⁷



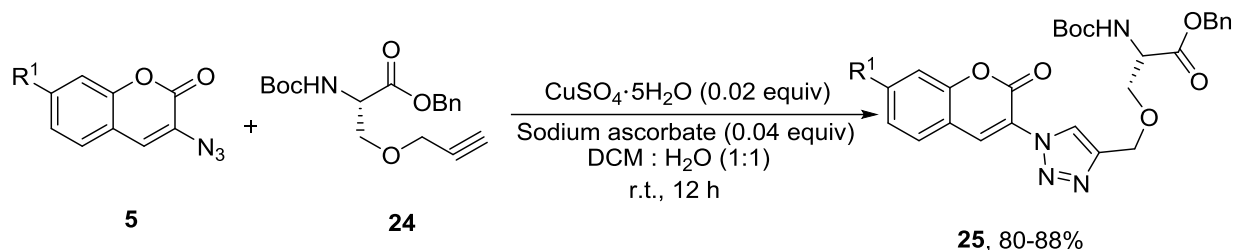
Scheme 1B.1.9: Labelling of peptide (**20**) with substituted 3-azidocoumarin (**5**)

Beatty *et al.* documented the bio-orthogonal labelling of unnatural amino acid, homopropargylglycine (Hpg) (**22**) with non-fluorescent 3-azido-7-hydroxycoumarin (**5**) using $\text{CuSO}_4 \cdot 5\text{H}_2\text{O}$ at 4 °C in presence of tris(carboxyethyl)phosphine (TCEP) to afford triazolyl linked coumarin-labelled amino acid (**23**), which was used for fluorescence visualization of mammalian proteins (Scheme 1B.1.10).⁷⁸



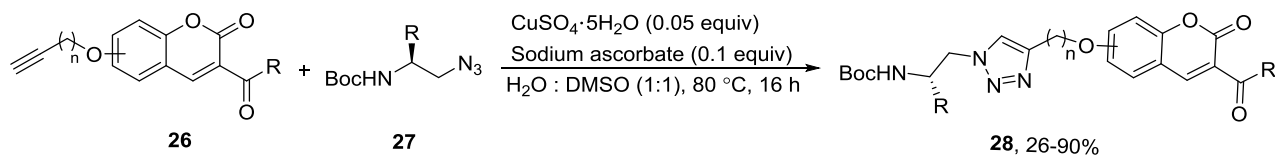
Scheme 1B.1.10: Labelling of unnatural amino acid (Hpg) (**22**) with 3-azido-7-hydroxycoumarin (**5**)

Li *et al.* reported the reaction of 3-azidocoumarin (**5**) with benzyl *N*-(*tert*-butoxycarbonyl)-*O*-(prop-2-yn-1-yl)-L-serinate (**24**) under Cu-catalyzed conditions to afford triazolyl linked coumarin-serine conjugates (**25**) in 80-88% yield (Scheme 1B.1.11). The photophysical properties of the synthesized derivatives were studied.⁷⁹



Scheme 1B.1.11: Labelling of serine derivative (**24**) with substituted 3-azidocoumarin (**5**)

Mertens *et al.* reported the synthesis of triazolyl linked coumarin-labelled modified amino acids (**28**) by clicking azido-functionalized modified amino acids (**27**) with 7-*O*-alkynyl-functionalized coumarin (**26**) under Cu-catalyzed conditions in a mixture of water and DMSO at 80 °C (Scheme 1B.1.12). The authors also studied the absorption and fluorescence properties of synthesized compounds in MeOH.⁸⁰



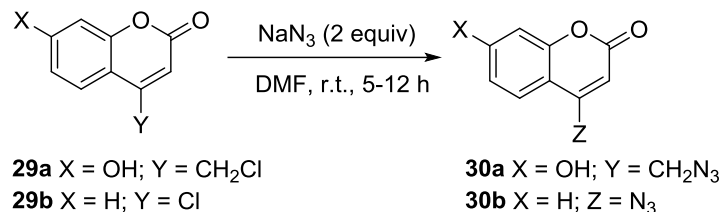
Scheme 1B.1.12: Synthesis of triazolyl linked coumarin-labelled amino acids (**28**)

In view of the above discussion, we envisioned that augmenting triazole moiety between coumarin-amino acids will yield triazolyl linked coumarin-amino acid hybrids with interesting fluorescence properties that may be used for studying various biological interactions in labelling studies.

1B.2 Results and Discussion

We envisioned exploring the application of click chemistry for synthesizing the targeted molecules following two strategies. The first strategy aimed to click alkynyl-functionalized amino acid with azido-functionalized coumarin, while, the second strategy aimed to click azido-functionalized amino acid with alkynyl-functionalized coumarin. The work commenced with the synthesis of azido-functionalized coumarins, 7-hydroxy-4-azidomethyl-2*H*-chromen-2-one (**30a**) and 4-azido-2*H*-chromen-2-one (**30b**) which were synthesized by the reaction of NaN₃ with 7-

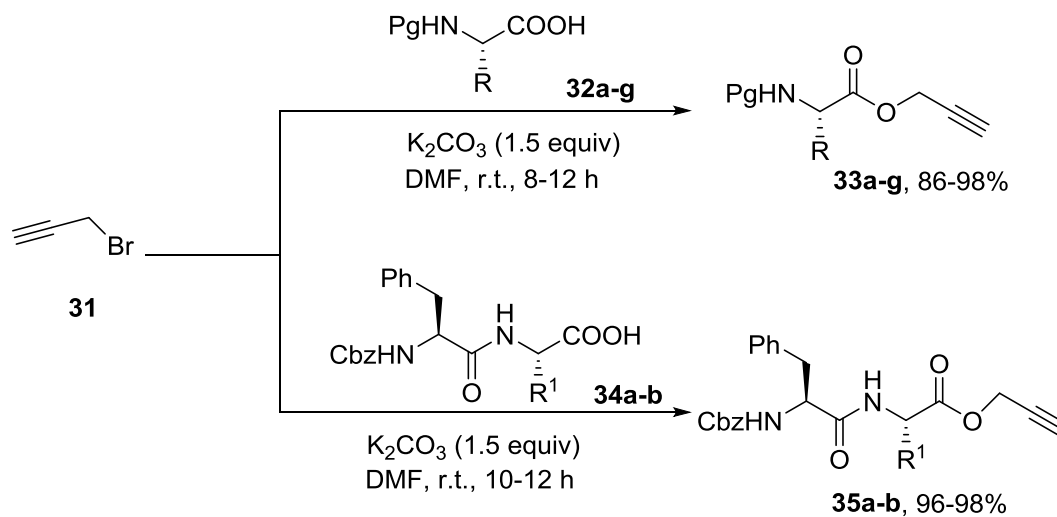
hydroxy-4-chloromethyl-2*H*-chromen-2-one (**29a**) and 4-chloro-2*H*-chromen-2-one (**29b**), respectively, following literature procedures (Scheme 1B.2.1).^{81,82}



Scheme 1B.2.1: Synthesis of azido-functionalized coumarins (**30a-b**)

In order to employ the first strategy, esterification of different protected amino acids (**32a-g**) was carried with propargyl bromide (**31**) using K₂CO₃ in DMF at room temperature to yield protected amino acyl *O*-propargyl esters (**33a-g**) (Table 1B.1.1). In addition, two novel dipeptidoyl *O*-propargyl esters (**35a**) and (**35b**) were also synthesized by the esterification of *Z*-protected peptides (**34a**) and (**34b**), with propargyl bromide (**31**) respectively (Table 1B.2.1).⁸³⁻⁸⁵

Table 1B.2.1: Synthesis of protected amino acyl *O*-propargyl esters (**33** & **35**)

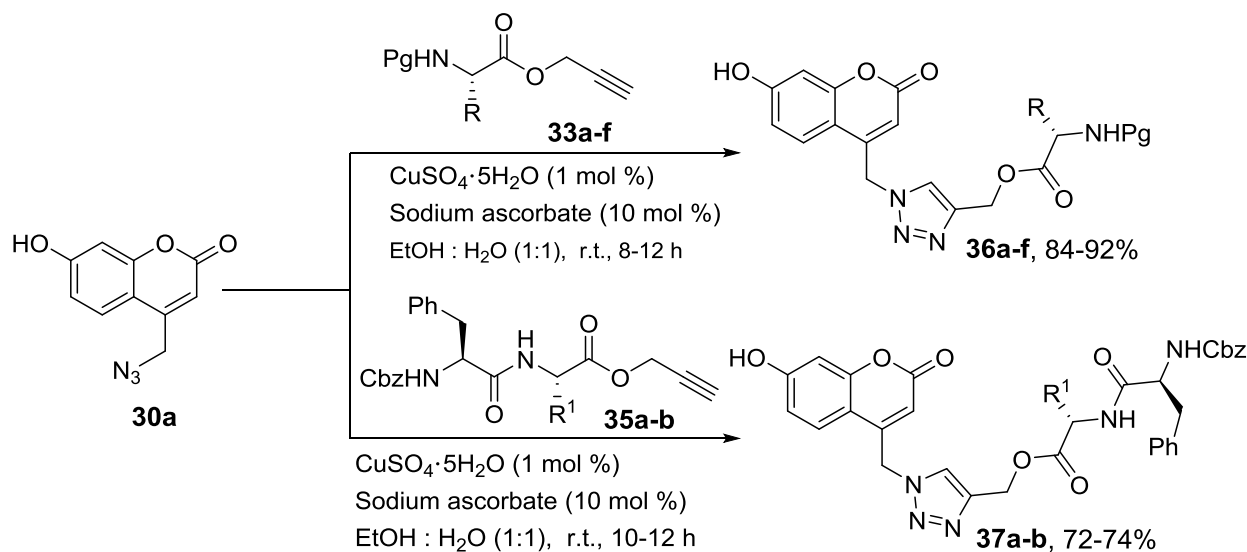


S. No.	Protected Amino acids/peptides	Product	Yield ^a (%)	mp (°C)
1.	Boc-L-Phe-OH (32a)	33a	90	Oil
2.	Cbz-L-Ala-OH (32b)	33b	86	58-60
3.	Cbz-L-Phe-OH (32c)	33c	88	64-66
4.	Fmoc-L-Phe-OH (32d)	33d	96	90-92
5.	Fmoc-L-Leu-OH (32e)	33e	98	96-97
6.	Fmoc-L-Ile-OH (32f)	33f	97	102-103
7.	Boc-L-Ala-OH (32g)	33g	87	Oil
8.	Cbz-L-Phe-L-Trp-OH (34a)	35a	98	120-122
9.	Cbz-L-Phe-L-Ala-OH (34b)	35b	96	126-128

^aIsolated yield

We next attempted the Cu-catalyzed azide–alkyne cycloaddition (CuAAC) reaction between clickable alkynyl-functionalized amino acids/peptides and azido-functionalized coumarins. Gratifyingly, 7-hydroxy-4-azidomethyl-2*H*-chromen-2-one (**30a**) on cycloaddition with different protected *α*-amino acyl *O*-propargyl esters **33a–f**, using CuSO₄·5H₂O and sodium ascorbate at room temperature, yielded their corresponding triazolyl linked coumarin-amino acids hybrids **36a–f** in 84–92% yield in 8–12 h (Table 2B.2.2). Furthermore, 7-hydroxy-4-azidomethyl-2*H*-chromen-2-one (**30a**) on cycloaddition with dipeptidoyl *O*-propargyl ester (**35a**) or (**35b**) under similar reaction conditions yielded 7-hydroxy-4-triazolylmethyl coumarin-peptide hybrids in 72–74% yields (**37a–b**) (Table 1B.2.2).

Table 1B.2.2: Synthesis of 7-hydroxy-4-triazolylmethyl coumarin-amino acid/peptide hybrids (**36** & **37**)



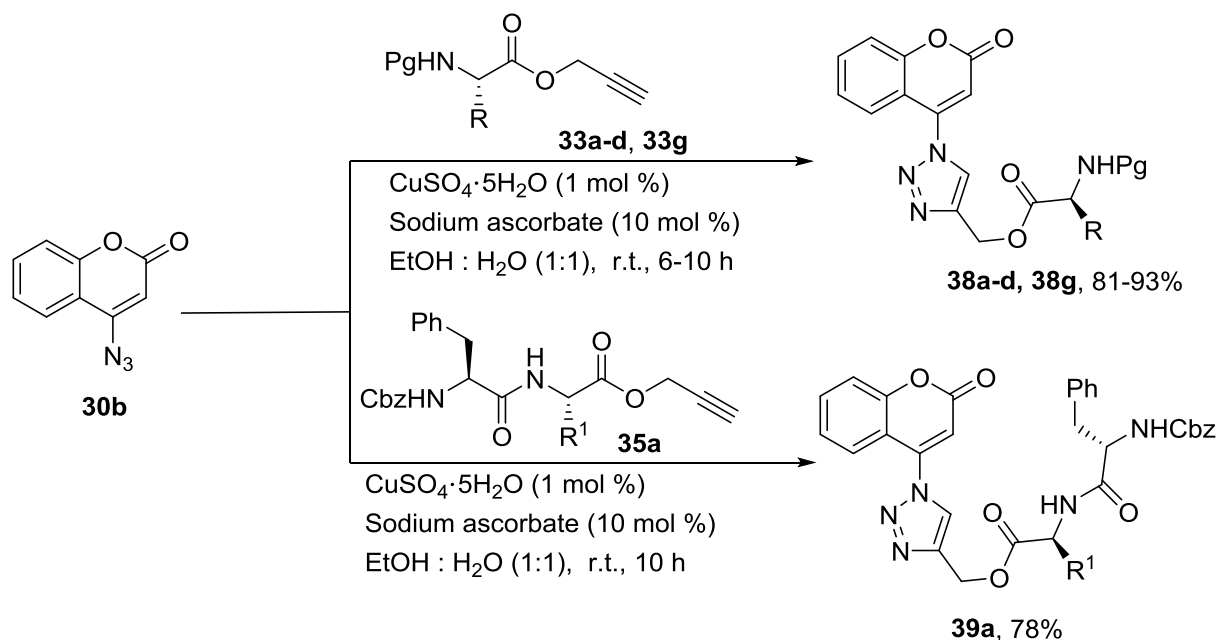
S. No.	Protected amino acyl <i>O</i> -propargyl esters	Product	Yield ^a (%)	mp (°C)
1.	Boc-L-Phe-OCH ₂ C≡CH (33a)	36a	85	143–145
2.	Cbz-L-Ala-OCH ₂ C≡CH (33b)	36b	92	147–149
3.	Cbz-L-Phe-OCH ₂ C≡CH (33c)	36c	87	150–152
4.	Fmoc-L-Phe-OCH ₂ C≡CH (33d)	36d	86	148–150
5.	Fmoc-L-Leu-OCH ₂ C≡CH (33e)	36e	84	146–148
6.	Fmoc-L-Ile-OCH ₂ C≡CH (33f)	36f	85	143–146
7.	Cbz-L-Phe-L-Trp-OCH ₂ C≡CH (35a)	37a	72	155–158
8.	Cbz-L-Phe-L-Ala-OCH ₂ C≡CH (35b)	37b	74	153–155

^aIsolated yield

We next extended the methodology for synthesizing few triazolyl derivatives of **30b**. The cycloaddition of 4-azido-2*H*-chromen-2-one (**30b**) with protected amino acyl *O*-propargyl esters,

33a–d and **33g**, using $\text{CuSO}_4 \cdot 5\text{H}_2\text{O}$ and sodium ascorbate yielded the corresponding 4-triazolyl coumarin-amino acid hybrids (**38a–d** & **38g**), in 81–93% yields (Table 1B.2.3). Similarly, 4-azido-2*H*-chromen-2-one (**30b**) on cycloaddition with dipeptidoyl *O*-propargyl ester (**35a**) under similar reaction conditions yielded 4-triazolyl coumarin-dipeptide hybrids (**39a**) in 78% yield (Table 1B.2.3).

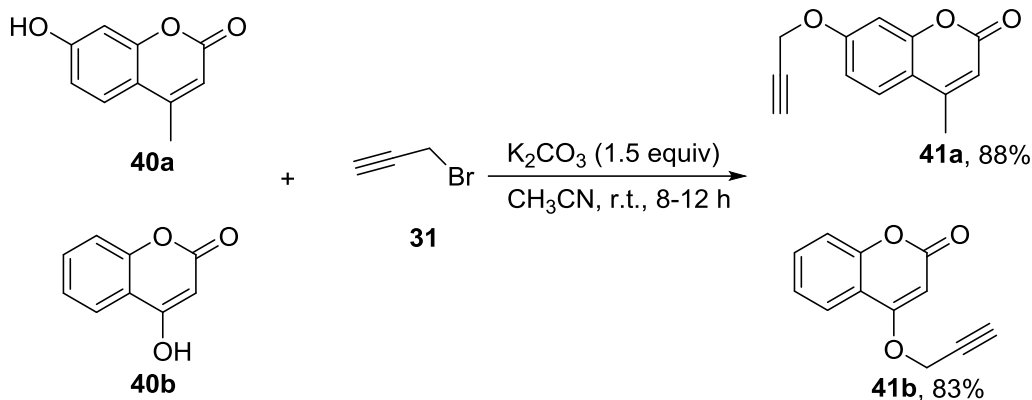
Table 1B.2.3: Synthesis of 4-triazolyl linked coumarin-amino acid/peptide hybrids (**38** & **39**)



S. No.	Protected amino acyl <i>O</i> -propargyl esters	Product	Yield ^a (%)	mp (°C)
1.	Boc-L-Phe-OCH ₂ C≡CH (33a)	38a	85	138-140
2.	Cbz-L-Ala-OCH ₂ C≡CH (33b)	38b	91	139-142
3.	Cbz-L-Phe-OCH ₂ C≡CH (33c)	38c	93	143-145
4.	Fmoc-L-Phe-OCH ₂ C≡CH (33d)	38d	89	134-136
5.	Boc-L-Ala-OCH ₂ C≡CH (33g)	38g	81	133-135
6.	Cbz-L-Phe-L-Trp-OCH ₂ C≡CH (35a)	39a	78	150-152

^aIsolated yield

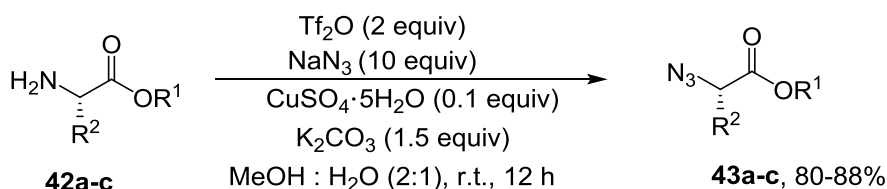
For exemplifying the second strategy, two alkynyl-functionalized coumarins namely, 4-methyl-7-(prop-2-ynyloxy)-2*H*-chromen-2-one (**41a**) and 4-(prop-2-ynyloxy)-2*H*-chromen-2-one (**41b**) were prepared by *O*-alkylation of 4-methyl-7-hydroxy-2*H*-chromen-2-one (**40a**) and 4-hydroxy-2*H*-chromene-2-one (**40b**), respectively, with propargyl bromide (**31**) using K_2CO_3 in CH_3CN at room temperature following literature procedures.⁸⁶



Scheme 1B.2.2: Synthesis of alkyne-functionalized coumarins (**41a-b**)

In addition, α -azido esters (**43a-c**) were synthesized by the reaction of triflic azide (prepared *in situ*) with α -amino esters (**42a-c**), following literature procedures (Table 1B.2.4).^{22,87}

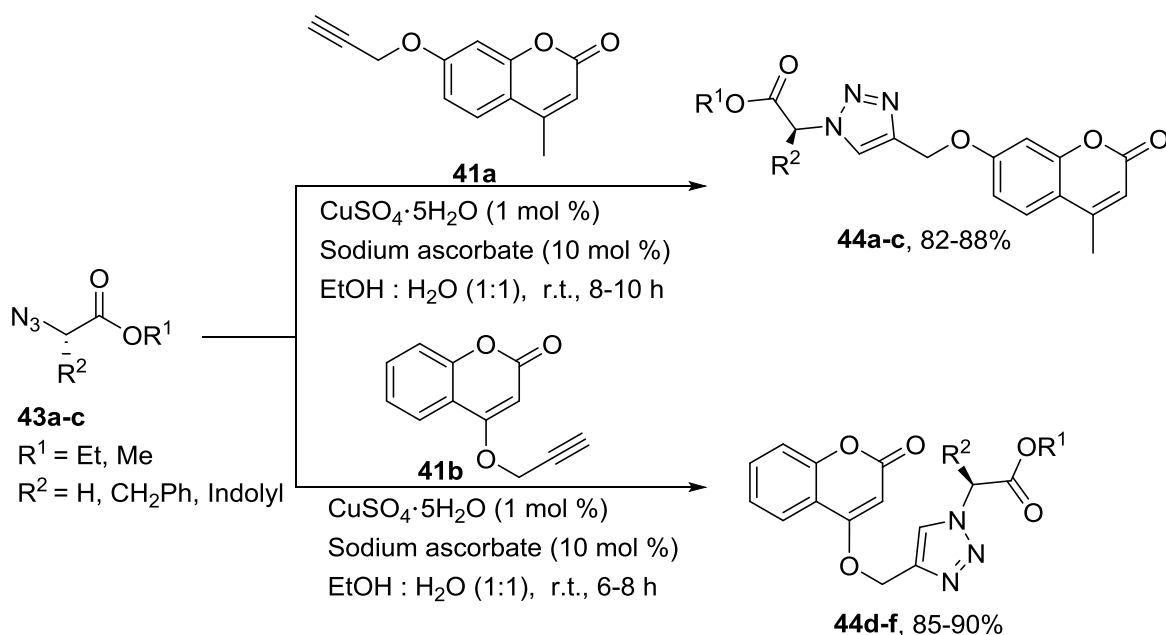
Table 1B.2.4: Synthesis of α -azido esters **43**



S. No.	α -Amino esters (42a-c)	Product	Yield ^a (%)	mp (°C)
1.	L-Gly-OEt (42a)	43a	88	Oil
2.	L-Phe-OMe (42b)	43b	84	Oil
3.	L-Trp-OMe (42c)	43c	80	Oil

^aIsolated yield

Thereafter, Cu-catalyzed cycloaddition reaction was carried between clickable alkyne-functionalized coumarins and α -azido esters. Pleasingly, the reaction of 4-methyl-7-(prop-2-ynyloxy)-2H-chromen-2-one (**41a**) and 4-(prop-2-ynyloxy)-2H-chromen-2-one (**41b**) with clickable α -azido esters **43a-c** using $\text{CuSO}_4 \cdot 5\text{H}_2\text{O}$ and sodium ascorbate yielded 7-O-triazolylmethyl and 4-O-triazolylmethyl coumarin-amino acid hybrids, **44a-f** in 82–90% yields (Table 1B.2.5).

Table 1B.2.5: Synthesis of 7-*O*-triazolylmethyl and 4-*O*-triazolylmethyl coumarin-amino acid hybrids **44**

S. No.	α -Azido ester (Reactant 1)	Reactant 2	Product	Yield ^a (%)	mp (°C)
1.	N ₃ -L-Gly-OEt (43a)	41a	44a	88	129-132
2.	N ₃ -L-Phe-OMe (43b)	41a	44b	85	133-135
3.	N ₃ -L-Trp-OMe (43c)	41a	44c	82	138-140
4.	N ₃ -L-Gly-OEt (43a)	41b	44d	90	128-130
5.	N ₃ -L-Phe-OMe (43b)	41b	44e	87	130-132
6.	N ₃ -L-Trp-OMe (43c)	41b	44f	85	134-136

^a Isolated yield

All the products were characterized by their detailed spectral studies (¹H NMR, ¹³C NMR, and high-resolution mass spectrometry (HRMS)). The absence of any minor or duplicate signals in the ¹H NMR spectra of triazolyl linked coumarin-dipeptide hybrids (**37a-b**, **39a**), and their univocal correspondence to the expected structures showed them not to be a mixture of any possible diastereoisomers (that might have resulted due to two chiral centres of dipeptide).

As a representative example, the ¹H and ¹³C NMR spectra of **36c** is depicted in Figure 1B.2.1 and Figure 1B.2.2, respectively.

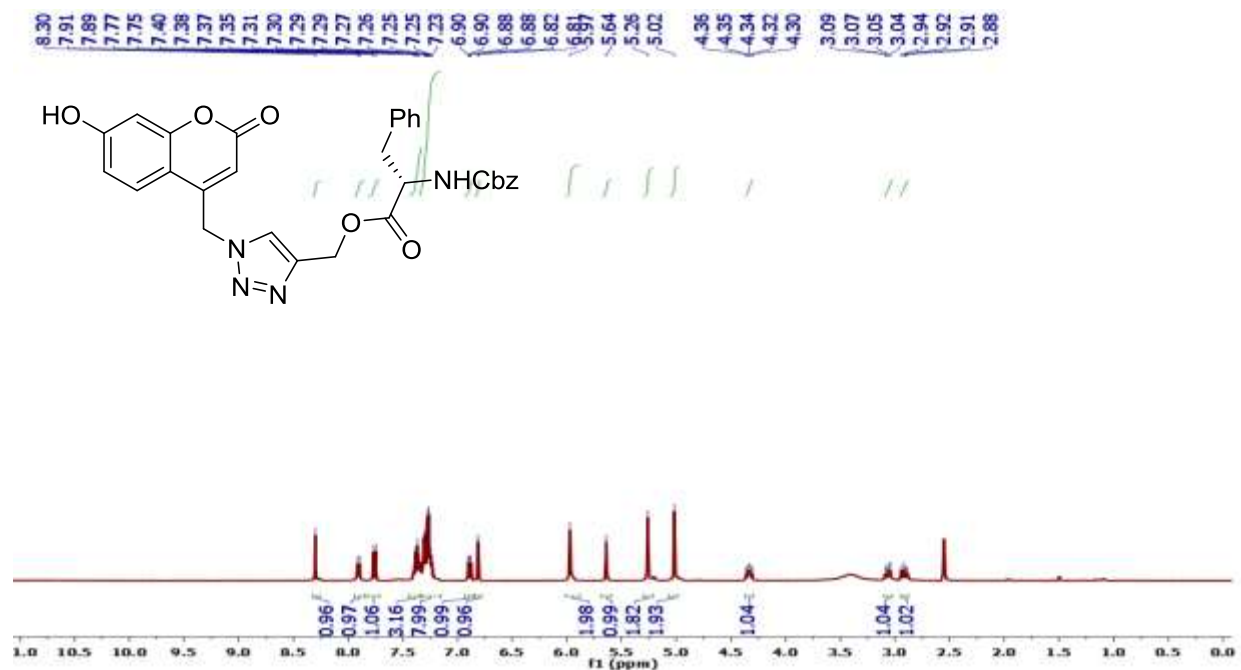


Figure 1B.2.1: ^1H NMR spectrum of **36c** in $\text{DMSO-}d_6$

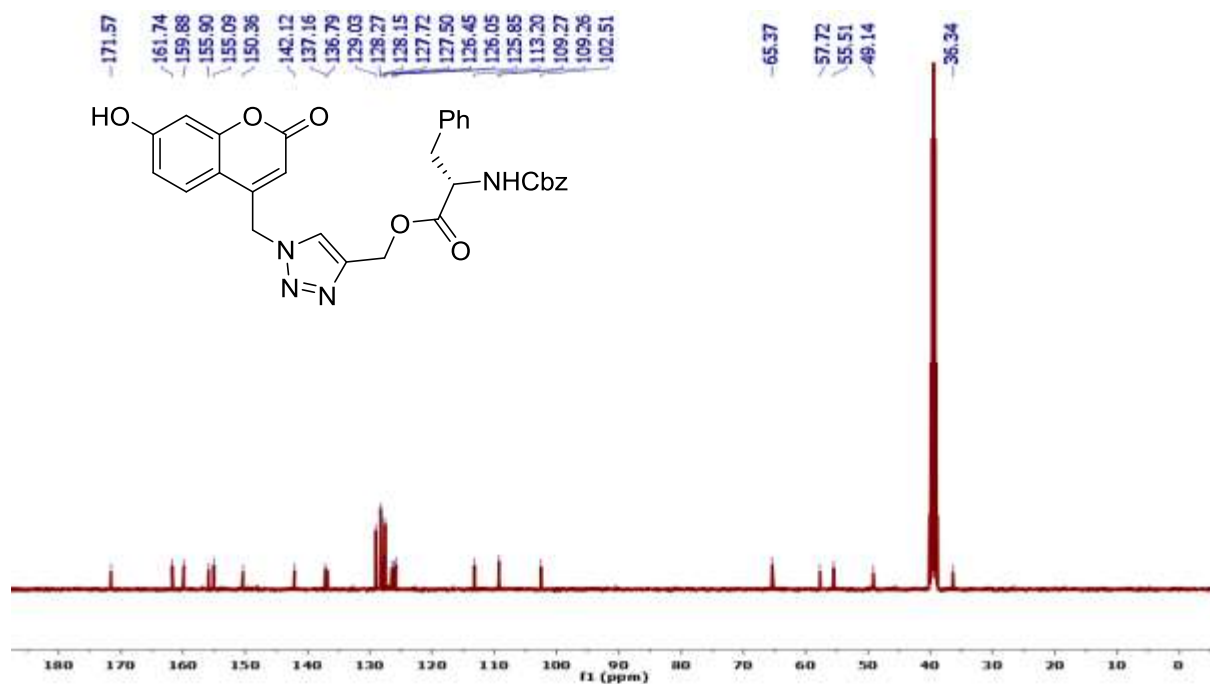
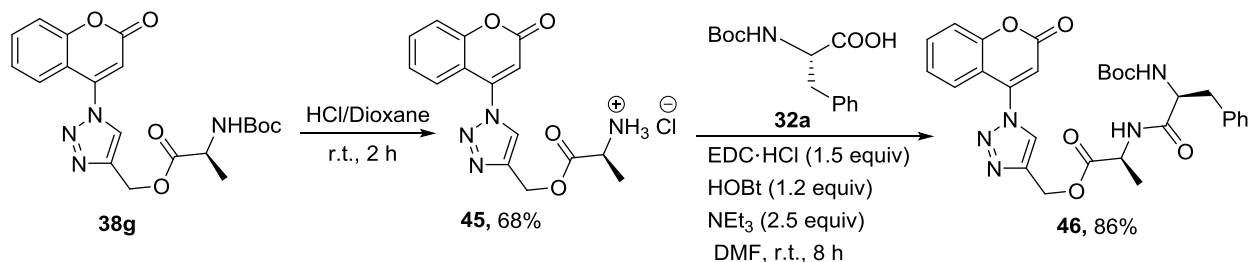


Figure 1B.2.2: ^{13}C NMR spectrum of **36c** in $\text{DMSO-}d_6$

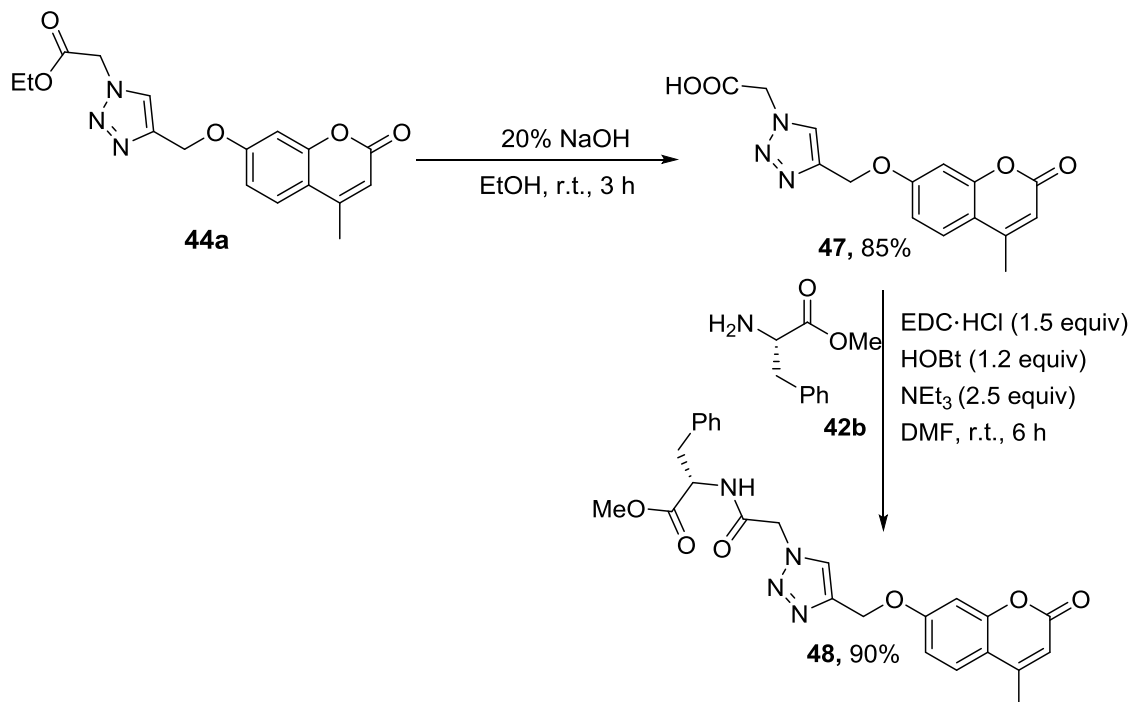
To further demonstrate the chemical utility of the synthesized triazolyl linked coumarin-amino acid hybrids as fluorescent labels, their linear elongation by coupling them with appropriate C- or N-terminus amino acid in solution phase was attempted. As a model example, **38g** on reaction with dioxane/HCl yielded unprotected 4-triazolyl linked coumarin-amino acid as a hydrochloride

salt (**45**) in 68%, which on further reaction with Boc-L-phenylalanine (**32a**) using EDC·HCl/HOBt in DMF afforded **46** in 86% yield (Scheme 1B.2.3). The absence of any minor or duplicate signals in the ^1H NMR spectrum of **46**, and their univocal correspondence to the expected structure revealed the absence of any possible diastereoisomers or epimers mixtures.



Scheme 1B.2.3: Coupling of 4-triazolyl linked coumarin-amino acid hybrid (**38g**) with C-terminus amino acid (**32a**)

Similar chemical applicability of 7-*O*-triazolylmethyl coumarin-amino acid hybrids as fluorescent label was demonstrated using one of its derivatives *viz.* **44a**. Hydrolysis of **44a** with 20% NaOH solution in ethanol followed by acidic workup gave **47** in 85% yield, which on reaction with L-phenylalanine methyl ester (**42b**) using EDC·HCl/HOBt in DMF afforded **48** in 90% yield (Scheme 1B.2.4).



Scheme 1B.2.4: Coupling of 7-*O*-triazolylmethyl linked coumarin-amino acid hybrids (**44a**) with *N*-terminus amino acid (**42b**)

The steady-state absorption and emission parameters of newly synthesized derivatives of coumarin were studied in tetrahydrofuran (THF) solvent. In addition, we were also studied UV-Visible absorption and fluorescence spectra of few representative conjugates in polar protic methanol (MeOH) solvent. The absorption maxima (λ_{Abs}), emission maxima (λ_{Em}), Stokes shift ($\bar{\nu}_a - \bar{\nu}_f$), extinction coefficient (ϵ) and quantum yields (Φ) of compounds **36a-f**, **37a-b**, **38a-d**, **38g**, **39a** and **44a-f** in THF and MeOH solvents are listed in Table 1B.2.6 (Figure 1B.2.3; a-f).

Table 1B.2.6: Photophysical studies^a of **36**, **37**, **38**, **39** & **44**

Compound	Solvent	λ_{Abs} (nm)	λ_{Em}^b (nm)	$\bar{\nu}_a - \bar{\nu}_f$ (cm^{-1})	ϵ ($\text{M}^{-1} \text{cm}^{-1}$)	Quantum Yield ^c (Φ)
36a	THF	323	388	5186.6	7860	0.136
36b	THF	323	388	5199.9	18500	0.140
36c	THF	323	387	5120.0	9120	0.162
36d	THF	266	389	5252.8	16460	0.184
	MeOH	265	411	6250.1	13840	0.220
36e	THF	266	388	5119.9	20860	0.150
36f	THF	266	387	5119.9	19700	0.143
37a	THF	324	388	5120.0	4960	0.190
37b	THF	275	388	5186.6	13780	0.161
38a	THF	280	383	5003.3	27580	0.018
38b	THF	280	383	5071.9	9620	0.025
38c	THF	280	383	5101.2	26900	0.048
38d	THF	267	381	5042.9	12860	0.091
	MeOH	265	411	6343.1	5820	0.140
38g	THF	280	413	7036.9	17640	0.009
39a	THF	281	383	5476.8	9400	0.096
44a	THF	318	380	4992.7	6360	0.201
44b	THF	318	380	5061.3	17500	0.240
	MeOH	316	392	6134.8	23600	0.302
44c	THF	280	381	5336.8	32000	0.280
44d	THF	275	382	5090.7	31200	0.038
44e	THF	275	382	5535.9	11600	0.082
	MeOH	265	401	6004.5	5640	0.120
44f	THF	275	382	5535.9	32400	0.096

^aMeasured in THF (or MeOH) (5×10^{-5} M) at 25 °C; ^bExcited at 325 nm; ^cMeasured with quinine sulfate in 0.1 N H_2SO_4 as standard.

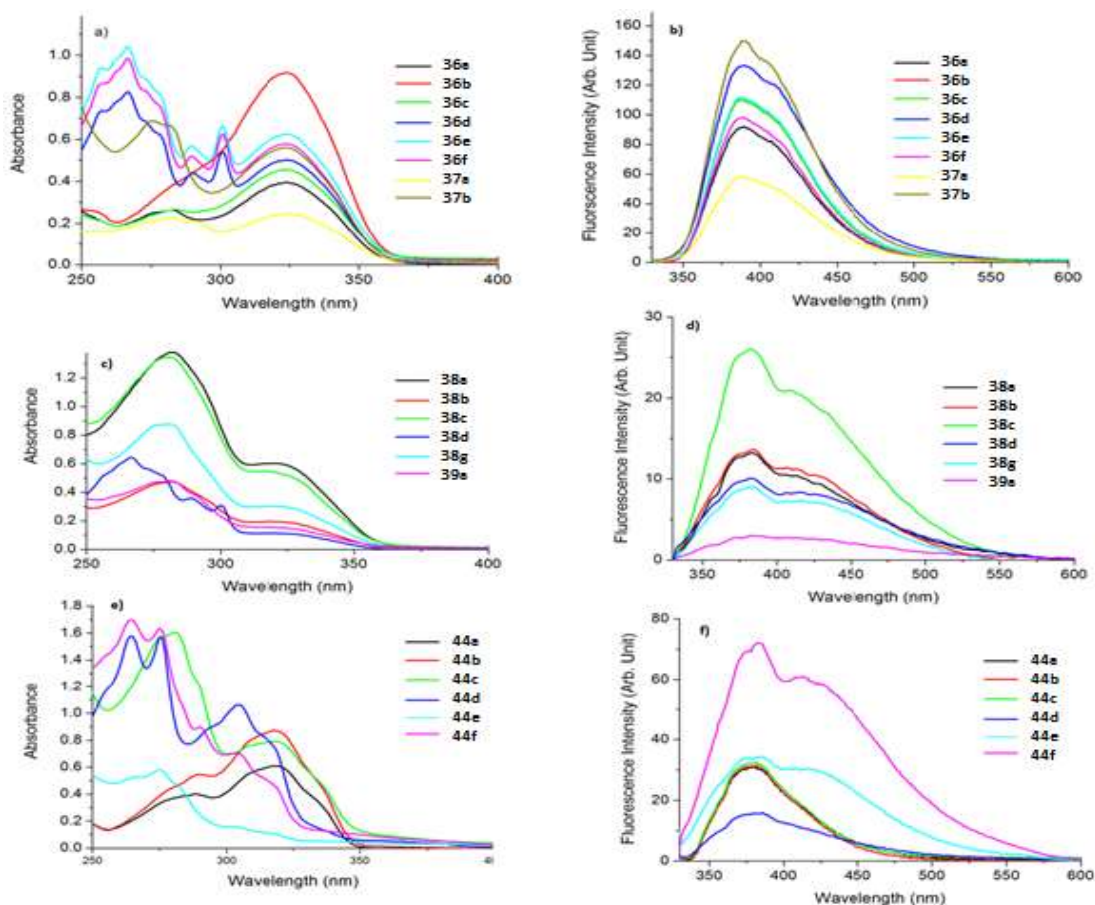


Figure 1B.2.3: UV absorption spectra of **36a-f**, **37a-b** (a), **38a-d**, **38g**, **39a** (c) and **44a-f** (e) and emission spectra of **36a-f**, **37a-b** (b), **38a-d**, **38g**, **39a** (d) and **44a-f** (f) in THF (5×10^{-5} M) at 25 °C

Finally, the absorption and emission spectra of **46** and **48** was recorded in THF in order to compare and contrast different spectroscopic data with the **38g** and **44a**, and the related spectroscopic data are summarized in Table 1B.2.7.

Table 1B.2.7: Photophysical studies^a of 4-triazolyl and 7-*O*-triazolylmethyl coumarin-amino acid hybrid with *C*-terminus amino acid and *N*-terminus amino acid **38g**, **46**, **44a**, **48**

Compound	Solvent	λ_{Abs} (nm)	$\lambda_{\text{Em}}^{\text{b}}$ (nm)	$\bar{\nu}_a - \bar{\nu}_f$ (cm^{-1})	ϵ ($\text{M}^{-1} \text{cm}^{-1}$)	Quantum Yield ^c (Φ)
38g	THF	280	384	7036.9	17640	0.009
46	THF	281	381	5071.9	10800	0.110
44a	THF	318	380	4962.7	6360	0.201
48	THF	265	382	5306.3	19500	0.340

^aMeasured in THF (5×10^{-5} M) at 25 °C; ^bExcited at 325 nm; ^cMeasured with quinine sulfate in 0.1 N H_2SO_4 as standard.

In summary, we have synthesized a library of triazolyl linked coumarin-amino acid and peptide hybrids in good-to-excellent yields. The synthesized compounds exhibited good fluorescence properties. The design further allows the linear elongation of triazolyl based hybrids to fluorescent tagged peptides or peptidomimetics by coupling them with appropriate C- or N-terminus amino acids. Compounds with an electron-donating group at C-7 position of coumarin showed high quantum yields (0.009–0.34) that could be suitable for use in peptide assays. The potential applications of these molecules include wide range of investigating cellular processes and other aspects of biological mechanism and function.

1B.3 Experimental Section

General materials and methods

All chemicals were obtained from commercial suppliers, and used without further purification. Melting points were determined in open capillary tubes on a MPA120-automated melting point apparatus, and are uncorrected. Reactions were monitored using thin layer chromatography (TLC) on 0.2 mm silica gel F254 plates (Merck). The chemical structures of final products and intermediates were characterized by nuclear magnetic resonance spectra (^1H NMR, ^{13}C NMR) determined on a Bruker NMR spectrometer 300 or 400 MHz, 75 (or 100 MHz). ^{13}C NMR spectra are fully decoupled. Chemical shifts were reported in parts per million (ppm) using deuterated solvent peak or tetramethylsilane as internal standard. HRMS was performed on an Agilent 6210 instrument using time-of-flight mass spectrometry (TOF-MS) with electrospray ionization (ESI). Electronic absorption spectra were taken using dual beam Thermo Evolution 201 UV/Vis/NIR spectrophotometer and fluorescence spectra were recorded using Shimadzu RF-5301PC spectrofluorometer. The data were analyzed using the related software. The concentration of the coumarin derivatives in all the solutions prepared in solvents THF and MeOH was 5×10^{-5} M. Fluorescence quantum yield (ϕ) values were obtained by the following equation. The fluorescence quantum yields were calculated by comparing the total fluorescence intensity (F) under the whole spectrum range by taking standard compound quinine sulfate (prepared as 0.1 N H_2SO_4 solution, $\phi_s = 0.55$).

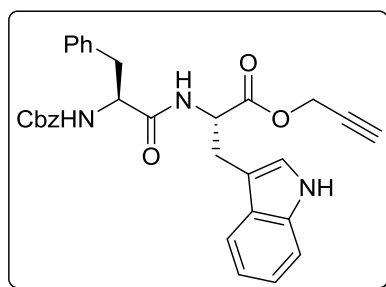
$$\phi_i = \phi_s \frac{F_i Ab_s \eta_s^2}{F_s Ab_i \eta_i^2}$$

Where, Ab , Absorbance at a particular wavelength; F , fluorescence spectrum area; and η , refraction index. The subscripts in the symbols refer to the standard (s) and to the sample (i).

Synthesis of protected amino acyl or dipeptidoyl *O*-propargyl esters

N-Protected amino acid or dipeptide (**32a–g** or **34a–b**) (0.100g, 1 equiv) was dissolved in anhydrous DMF (10 mL) and the solution was cooled to $-10\text{ }^{\circ}\text{C}$. Anhydrous K_2CO_3 (1.5 equiv) was added to the solution, and the stirring continued until a syrup-like solution formed. Propargyl bromide (**31**) (2 equiv, 80% solution in toluene) was added dropwise to the reaction mixture, and the stirring continued at $-10\text{ }^{\circ}\text{C}$ for 1 h. The reaction mixture was then stirred at room temperature for 8–12 h and monitored *via* TLC, until the disappearance of the starting material. The reaction mixture was then added dropwise in an ice-bath, and the precipitated white solid was collected by filtration and washed with cold water ($3 \times 20\text{ mL}$) to yield pure **33** or **35**. Compounds **33a–g** was characterized by comparison of their physical & spectroscopic data with that reported in literature.^{83–85}

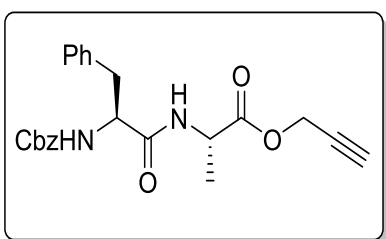
Prop-2-yn-1-yl ((benzyloxy)carbonyl)-L-phenylalanyl-L-tryptophanate (35a): White solid;



yield: 0.110 g (98%); mp: $120\text{--}122\text{ }^{\circ}\text{C}$; ^1H NMR (400 MHz, $\text{DMSO-}d_6 + \text{CDCl}_3$) δ 10.84 (s, 1H), 8.44 (brs, 1H), 7.52 (s, 1H), 7.41 – 7.12 (m, 13H), 7.11 – 6.95 (m, 2H), 5.02 – 4.85 (m, 2H), 4.75 – 4.58 (m, 3H), 4.34 (brs, 1H), 3.38 (brs, 1H), 3.18 (d, $J = 20.1\text{ Hz}$, 2H), 3.01 (d, $J = 11.9\text{ Hz}$, 1H), 2.74 (s, 1H); ^{13}C NMR (100 MHz, $\text{DMSO-}d_6 + \text{CDCl}_3$) δ 171.7, 170.8, 155.7,

137.9, 136.8, 136.0, 129.1, 128.1, 127.8, 127.5, 127.4, 127.0, 126.1, 123.7, 120.9, 118.4, 117.9, 111.3, 108.9, 77.7, 77.5, 65.3, 55.8, 52.9, 52.2, 37.5, 26.8.

Prop-2-yn-1-yl ((benzyloxy)carbonyl)-L-phenylalanyl-L-alaninate (35b): White solid; yield:



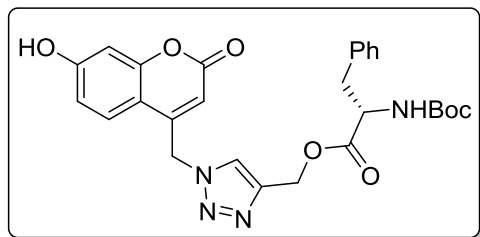
0.105 g (96%); mp: $126\text{--}128\text{ }^{\circ}\text{C}$; ^1H NMR (300 MHz, $\text{DMSO-}d_6$) δ 8.54 (d, $J = 6.0\text{ Hz}$, 1H), 7.48 (d, $J = 8.1\text{ Hz}$, 1H), 7.37 – 7.09 (m, 10H), 4.90 (s, 2H), 4.70 (s, 2H), 4.30 (dd, $J = 13.1, 6.8\text{ Hz}$, 2H), 3.55 (s, 1H), 3.00 (d, $J = 13.2\text{ Hz}$, 1H), 2.71 (t, $J = 12.1\text{ Hz}$, 1H), 1.31 (d, $J = 6.5\text{ Hz}$, 3H); ^{13}C NMR (75

MHz, $\text{DMSO-}d_6$) δ 172.3, 156.4, 138.7, 137.5, 129.7, 128.8, 128.6, 128.2, 128.0, 126.8, 78.7, 78.5, 65.7, 56.4, 52.9, 48.1, 37.9, 17.2.

General procedure for the synthesis of 7-hydroxy-4-triazolylmethyl or 4-triazolyl linked coumarin-amino acid/peptide hybrids

To a solution of 4-azidomethyl-7-hydroxycoumarin (**30a**) or 4-azidocoumarin (**30b**) (1 equiv) in EtOH : H₂O (1:1), protected amino acyl/dipeptidoyl *O*-propargyl ester (**33** or **35**), (1 equiv) was added followed by addition of CuSO₄·5H₂O (0.01 equiv) and sodium ascorbate (0.1 equiv). The reaction mixture was stirred at room temperature for 6–12 h and monitored *via* TLC. After completion of the reaction, the reaction mixture was concentrated, diluted with water and ammonium hydroxide (2–3 mL), and extracted into dichloromethane (3 × 20 mL). Organic layer was separated, dried over anhydrous sodium sulfate and concentrated to evaporate the volatiles. The crude compound was recrystallized from ethanol to yield pure **36a–f**, **37a–b**, **38a–d**, **38g**, or **39a**.

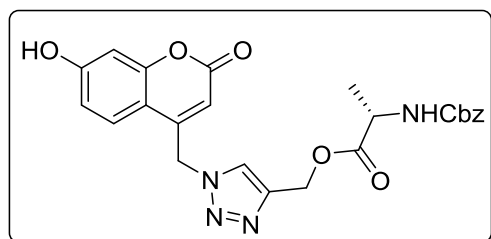
(1-((7-Hydroxy-2-oxo-2*H*-chromen-4-yl)methyl)-1*H*-1,2,3-triazol-4-yl)methyl (tert-butoxycarbonyl)-L-phenylalaninate (36a**):** White solid; yield: 0.201 g (85%);



mp: 143–145 °C; ¹H NMR (400 MHz, DMSO-*d*₆) δ 10.65 (s, 1H), 8.21 (s, 1H), 7.71 (d, *J* = 8.7 Hz, 1H), 7.27 – 7.16 (m, 6H), 6.83 (dd, *J* = 8.7, 7.1 Hz, 1H), 6.76 (s, 1H), 5.90 (s, 2H), 5.62 (brs, 1H), 5.25 – 5.12 (m, 2H), 4.24 – 4.14 (m, 1H), 2.98 (dd, *J* = 13.8, 5.0 Hz, 1H),

2.86 (dd, *J* = 13.5, 5.01 Hz, 1H), 1.29 (s, 9H); ¹³C NMR (100 MHz, DMSO-*d*₆ + CDCl₃) δ 171.8, 161.6, 159.8, 155.3, 155.1, 150.2, 142.1, 137.3, 129.0, 128.0, 126.3, 125.9, 125.7, 113.1, 109.4, 109.3, 102.5, 78.2, 57.6, 55.2, 49.1, 36.3, 28.0; HRMS (ESI-TOF) *m/z* calculated C₂₇H₂₈N₄O₇Na⁺: 543.1837; found 543.1850 [M+Na]⁺.

(1-((7-Hydroxy-2-oxo-2*H*-chromen-4-yl)methyl)-1*H*-1,2,3-triazol-4-yl)methyl ((benzyloxy)carbonyl)-L-alaninate (36b**):** White solid; yield: 0.200 g (92%);

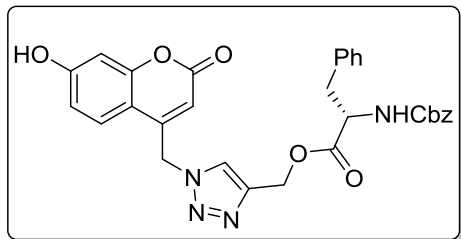


mp: 147–149 °C; ¹H NMR (400 MHz, DMSO-*d*₆) δ 7.77 (s, 1H), 7.30 (d, *J* = 7.5 Hz, 1H), 7.22 – 7.14 (m, 6H), 6.70 (d, *J* = 7.6 Hz, 1H), 6.61 (s, 1H), 5.62 – 5.55 (m, 2H), 5.51 (s, 2H), 5.20 – 5.13 (m, 1H), 5.01 – 4.90 (m, 2H), 4.27 – 4.17 (m, 1H), 1.26 (d, *J* = 6.5 Hz, 3H);

¹³C NMR (100 MHz, CDCl₃) δ 173.0, 161.5, 161.18, 156.1, 155.2, 148.9, 143.1, 136.0, 128.6, 128.3, 128.0, 125.5, 125.0, 114.0, 110.5, 109.7, 103.5, 67.1, 58.1, 50.3, 49.8, 18.0; HRMS (ESI-

TOF) m/z calculated $C_{24}H_{24}N_4O_7Na^+$: 501.1390; found 501.1381 $[M+Na]^+$.

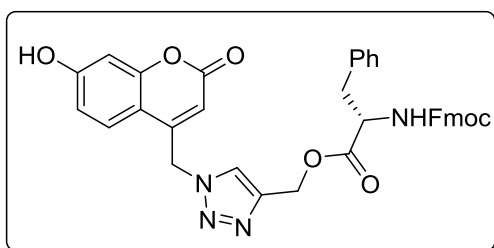
(1-((7-Hydroxy-2-oxo-2H-chromen-4-yl)methyl)-1H-1,2,3-triazol-4-yl)methyl ((benzyloxy)carbonyl)-L-phenylalaninate (36c): White solid; yield: 0.220 g (87%); mp:



150–152 °C; 1H NMR (400 MHz, $DMSO-d_6$) δ 8.30 (s, 1H), 7.90 (d, $J = 8.1$ Hz, 1H), 7.76 (d, $J = 8.8$ Hz, 1H), 7.36 – 7.29 (m, 3H), 7.28 – 7.21 (m, 8H), 6.89 (dd, $J = 8.7, 2.3$ Hz, 1H), 6.81 (s, 1H), 5.97 (s, 2H), 5.64 (brs, 1H), 5.26 (s, 2H), 5.02 (s, 2H), 4.37 – 4.29 (m, 1H), 3.04 (dd, J

= 13.8, 5.1 Hz, 1H), 2.88 (dd, $J = 13.7, 5.01$ Hz, 1H); ^{13}C NMR (100 MHz, $DMSO-d_6$) δ 171.6, 161.7, 159.9, 155.9, 155.1, 150.4, 142.1, 137.2, 136.8, 129.0, 128.3, 128.2, 127.7, 127.5, 126.5, 126.1, 125.9, 113.2, 109.3, 109.3, 102.5, 65.4, 57.7, 55.5, 49.1, 36.3; HRMS (ESI-TOF) m/z calculated $C_{30}H_{26}N_4O_7Na^+$: 577.1693; found 577.1694 $[M+Na]^+$.

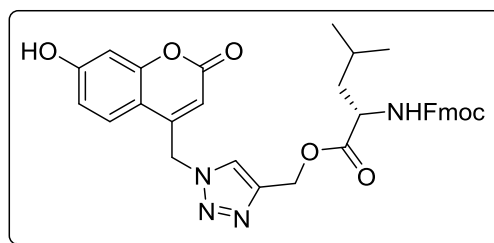
(1-((7-Hydroxy-2-oxo-2H-chromen-4-yl)methyl)-1H-1,2,3-triazol-4-yl)methyl ((9H-fluoren-9-yl)methoxy)carbonyl)-L-phenylalaninate (36d): White solid; yield: 0.252 g



(86%); mp: 148–150 °C; 1H NMR (300 MHz, $CDCl_3$) δ 7.72 (d, $J = 7.5$ Hz, 2H), 7.61 (s, 1H), 7.53 – 7.47 (m, 3H), 7.41 – 7.33 (m, 4H), 7.31 – 7.27 (m, 2H), 7.22 – 7.16 (m, 3H), 7.04 (s, 1H), 6.83 (d, $J = 8.5$ Hz, 1H), 6.76 (s, 1H), 5.77 (brs, 1H), 5.60 – 5.38 (m, 2H),

5.32 – 5.17 (m, 2H), 4.61 (dd, $J = 13.7, 7.6$ Hz, 1H), 4.31 – 4.24 (m, 2H), 4.13 (t, $J = 6.7$ Hz, 1H), 3.15 – 3.00 (m, 2H); ^{13}C NMR (75 MHz, $CDCl_3$) δ 171.4, 162.0, 161.5, 160.8, 156.1, 155.8, 155.6, 148.3, 148.0, 143.6, 143.1, 141.3, 135.5, 129.3, 128.7, 127.8, 127.2, 120.0, 114.0, 111.5, 109.8, 103.9, 67.2, 58.2, 55.0, 47.1, 38.0, 29.8; HRMS (ESI-TOF) m/z calculated $C_{37}H_{30}N_4O_7Na^+$: 665.2021; found 665.2007 $[M+Na]^+$.

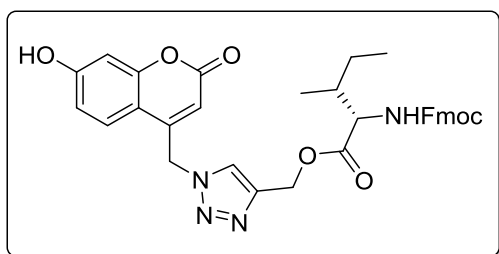
(1-((7-Hydroxy-2-oxo-2H-chromen-4-yl)methyl)-1H-1,2,3-triazol-4-yl)methyl ((9H-fluoren-9-yl)methoxy)carbonyl)-L-leucinate (36e): White solid; yield: 0.233 g (84%);



mp: 146–148 °C; 1H NMR (400 MHz, $DMSO-d_6$) δ 8.30 (s, 1H), 7.90 (d, $J = 7.4$ Hz, 2H), 7.85 (t, $J = 8.7$ Hz, 1H), 7.74 – 7.67 (m, 2H), 7.43 (t, $J = 7.2$ Hz, 2H), 7.38 – 7.30 (m, 2H), 6.84 (d, $J = 8.5$ Hz, 1H), 6.77 (s, 1H), 6.29 (s, 1H), 5.92 (d, $J = 10.5$ Hz, 2H), 5.53 –

5.51 (m, 1H), 5.28 – 5.18 (m, 2H), 4.36 – 4.19 (m, 2H), 4.12 – 4.01 (m, 1H), 3.39 (q, $J = 6.8$ Hz, 1H), 1.66 – 1.38 (m, 2H), 1.12 – 1.08 (m, 1H), 0.85 (2d, $J = 5.5$ Hz each, 6H); ^{13}C NMR (100 MHz, DMSO- d_6) δ 172.6, 162.1, 159.9, 156.1, 155.1, 150.4, 143.8, 142.5, 142.2, 139.6, 126.0, 125.2, 121.3, 113.3, 109.7, 109.1, 108.9, 102.5, 65.6, 64.9, 57.5, 52.2, 49.1, 46.6, 24.1, 22.7, 21.1; HRMS (ESI-TOF) m/z calculated $\text{C}_{34}\text{H}_{32}\text{N}_4\text{O}_7\text{Na}^+$: 631.2189; found 631.2163 $[\text{M}+\text{Na}]^+$.

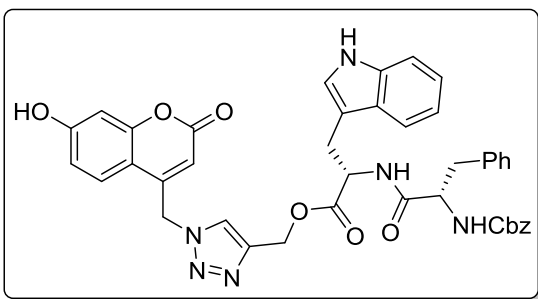
(1-((7-Hydroxy-2-oxo-2H-chromen-4-yl)methyl)-1H-1,2,3-triazol-4-yl)methyl ((9H-fluoren-9-yl)methoxy)carbonyl)-L-isoleucinate (36f): White solid; yield: 0.235 g



(85%); mp: 143–146 °C; ^1H NMR (400 MHz, DMSO- d_6 + CDCl_3) δ 10.58 (s, 1H), 8.26 (s, 1H), 7.84 (d, $J = 7.5$ Hz, 2H), 7.76 – 7.69 (m, 3H), 7.66 (d, $J = 8.8$ Hz, 1H), 7.40 (t, $J = 7.4$ Hz, 2H), 7.31 (t, $J = 6.6$ Hz, 2H), 6.81 (dd, $J = 8.7$ Hz, 1H), 6.74 (d, $J = 2.3$ Hz,

1H), 5.87 (s, 2H), 5.55 (brs, 1H), 5.26 – 5.21 (m, 2H), 4.30 – 4.26 (m, 2H), 4.24 – 4.18 (m, 1H), 4.04 – 3.99 (m, 1H), 1.84 – 1.75 (m, 1H), 1.42 – 1.33 (m, 1H), 1.24 (brs, 1H), 0.83 – 0.73 (m, 6H); ^{13}C NMR (100 MHz, DMSO- d_6 + CDCl_3) δ 171.5, 161.6, 159.8, 156.2, 155.1, 150.1, 143.7, 143.6, 142.2, 140.7, 127.5, 126.9, 125.8, 125.7, 125.2, 119.9, 113.1, 109.2, 109.2, 102.5, 65.7, 58.5, 57.2, 49.1, 46.6, 36.1, 24.8, 15.3, 10.9; HRMS (ESI-TOF) m/z calculated $\text{C}_{34}\text{H}_{32}\text{N}_4\text{O}_7\text{Na}^+$: 631.2164; found 631.2164 $[\text{M}+\text{Na}]^+$.

(1-((7-Hydroxy-2-oxo-2H-chromen-4-yl)methyl)-1H-1,2,3-triazol-4-yl)methyl ((benzyloxy)carbonyl)-L-phenylalanyl-L-tryptophanate (37a): Yellow solid; yield: 0.243 g

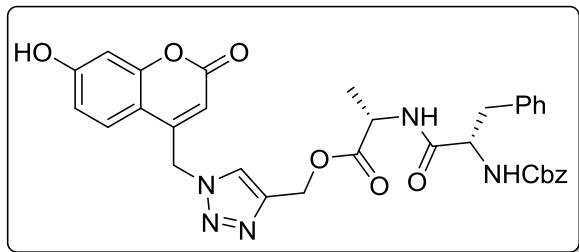


(72%); mp: 155–158 °C; ^1H NMR (300 MHz, DMSO- d_6) δ 10.88 (s, 1H), 8.51 (d, $J = 7.0$ Hz, 1H), 8.14 (s, 1H), 7.69 (d, $J = 8.6$ Hz, 1H), 7.48 – 7.44 (m, 2H), 7.34 – 7.17 (m, 13H), 7.10 – 6.95 (m, 2H), 6.84 (d, $J = 8.6$ Hz, 1H), 6.77 (s, 1H), 5.88 (s, 2H), 5.54 (brs, 1H), 5.21 – 5.11 (m, 2H),

4.98 – 4.86 (m, 2H), 4.57 (dd, $J = 12.4, 6.0$ Hz, 1H), 4.32 (t, $J = 7.4$ Hz, 1H), 3.22 – 3.09 (m, 2H), 2.94 (d, $J = 14.1$ Hz, 1H), 2.67 (d, $J = 14.0$ Hz, 1H); ^{13}C NMR (75 MHz, DMSO- d_6) δ 172.4, 171.9, 162.3, 160.5, 156.3, 155.9, 155.6, 155.3, 151.3, 150.9, 142.7, 138.6, 137.5, 136.6, 129.7, 128.8, 128.5, 128.2, 128.0, 127.6, 126.7, 126.6, 126.3, 124.3, 121.5, 119.0, 118.5, 113.8, 112.0, 109.7, 103.10, 65.8, 58.3, 56.4, 53.7, 49.7, 38.0, 27.4; HRMS (ESI-TOF) m/z calculated

$C_{41}H_{36}N_6O_8Na^+$: 763.2480; found 763.2487 $[M+Na]^+$.

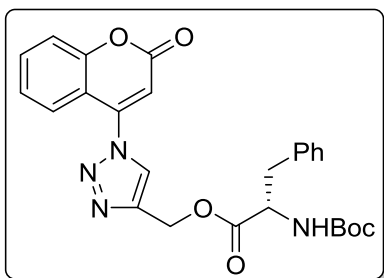
(1-((7-Hydroxy-2-oxo-2H-chromen-4-yl)methyl)-1H-1,2,3-triazol-4-yl)methyl ((benzyloxy)carbonyl)-L-phenylalanyl-L-alaninate (37b): Yellow solid; yield: 0.211 g



(74%); mp: 153–155 °C; 1H NMR (400 MHz, $DMSO-d_6$) δ 10.79 (s, 1H), 8.57 (s, 1H), 8.32 (s, 1H), 7.70 (d, $J = 8.3$ Hz, 1H), 7.48 (d, $J = 7.9$ Hz, 1H), 7.38 – 7.17 (m, 10H), 6.85 (d, $J = 8.2$ Hz, 1H), 6.78 (s, 1H), 5.91 (s, 2H), 5.55 (brs,

1H), 5.28 – 5.17 (m, 2H), 4.94 (s, 2H), 4.34 – 4.28 (m, 2H), 2.99 (d, $J = 13.6$ Hz, 1H), 2.69 (t, $J = 13.8$ Hz, 1H), 1.31 (brs, 3H); ^{13}C NMR (100 MHz, $DMSO-d_6$) δ 172.2, 171.7, 161.8, 159.9, 155.8, 155.1, 150.4, 142.3, 138.1, 137.0, 129.2, 128.2, 128.0, 127.6, 127.4, 127.0, 127.0, 126.2, 126.0, 125.9, 113.2, 109.3, 109.1, 102.5, 65.1, 57.6, 55.7, 49.1, 47.6, 37.3, 16.7. HRMS (ESI-TOF) m/z calculated $C_{33}H_{31}N_5O_8Na^+$: 648.2085; found 648.2065 $[M+Na]^+$.

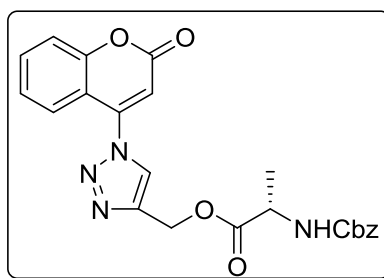
(1-(2-Oxo-2H-chromen-4-yl)-1H-1,2,3-triazol-4-yl)methyl (tert-butoxycarbonyl)-L-phenylalaninate (38a): White solid; yield: 0.222 g (85%); mp: 138–140 °C; 1H NMR (300



MHz, $CDCl_3$) δ 8.05 (s, 1H), 7.93 (d, $J = 7.6$ Hz, 1H), 7.77 (t, $J = 7.7$ Hz, 1H), 7.56 (d, $J = 8.3$ Hz, 1H), 7.45 (t, $J = 7.5$ Hz, 1H), 7.36 – 7.27 (m, 3H), 7.19 (d, $J = 6.8$ Hz, 2H), 6.62 (s, 1H), 5.47 (s, 2H), 5.08 (d, $J = 6.5$ Hz, 1H), 4.68 (d, $J = 6.0$ Hz, 1H), 3.18 (d, $J = 6.8$ Hz, 2H), 1.47 (s, 9H); ^{13}C NMR (75 MHz, $CDCl_3$) δ 172.0, 159.6, 155.3, 154.4, 146.7, 135.8, 133.8, 129.4, 128.7,

127.3, 125.6, 125.2, 117.7, 114.3, 110.2, 80.4, 58.1, 54.7, 38.1, 28.4; HRMS (ESI-TOF) m/z calculated $C_{26}H_{26}N_4O_6Na^+$: 513.1751; found 513.1745 $[M+Na]^+$.

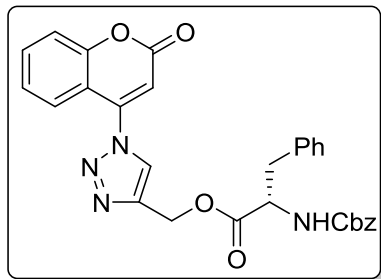
(1-(2-Oxo-2H-chromen-4-yl)-1H-1,2,3-triazol-4-yl)methyl(benzyloxy)carbonyl)-L-alaninate (38b): White solid; yield: 0.218 g (91%); mp: 139–142 °C; 1H NMR (300 MHz, $CDCl_3$)



δ 7.97 (s, 1H), 7.78 – 7.63 (m, 1H), 7.59 – 7.46 (m, 1H), 7.38 – 7.27 (m, 1H), 7.23 – 7.03 (m, 6H), 6.43 (s, 1H), 5.39 – 5.02 (m, 3H), 4.94 (s, 2H), 4.24 (d, $J = 3.5$ Hz, 1H), 1.29 (brs, 3H); ^{13}C NMR (75 MHz, $CDCl_3$) δ 173.1, 159.6, 156.4, 155.8, 154.4, 146.6, 136.5, 136.2, 133.7, 128.6, 128.2, 128.0, 125.6, 125.1, 117.7, 114.3, 110.2, 67.1, 58.2, 49.9, 18.2; HRMS (ESI-TOF)

m/z calculated $C_{23}H_{20}N_4O_6Na^+$: 471.1282; found 471.1275 $[M+Na]^+$.

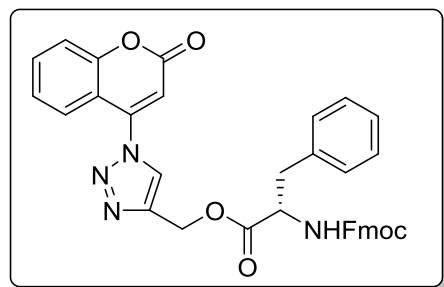
(1-(2-Oxo-2H-chromen-4-yl)-1H-1,2,3-triazol-4-yl)methyl((benzyloxy)carbonyl)-L-phenylalaninate (38c): White solid; yield: 0.260 g (93%); mp: 143–145 °C; 1H NMR (300



MHz, $CDCl_3$) δ 7.84 (s, 1H), 7.76 (d, J = 7.9 Hz, 1H), 7.61 (t, J = 7.7 Hz, 1H), 7.40 (d, J = 8.4 Hz, 1H), 7.34 – 7.26 (m, 4H), 7.19 – 7.16 (m, 2H), 7.17 – 7.10 (m, 3H), 7.01 (d, J = 6.7 Hz, 2H), 6.46 (s, 1H), 5.34 (brs, 2H), 5.20 (d, J = 7.9 Hz, 1H), 5.01 (s, 2H), 4.61 (dd, J = 12.8, 6.2 Hz, 1H), 3.06 (d, J = 5.4 Hz, 2H); ^{13}C NMR (75 MHz, $CDCl_3$) δ 171.6, 159.7, 159.4, 155.8, 154.4,

146.6, 143.4, 136.1, 135.4, 133.8, 129.4, 128.7, 128.3, 128.1, 127.4, 125.6, 125.2, 121.5, 117.7, 114.2, 110.2, 67.3, 58.2, 55.0, 38.1; HRMS (ESI-TOF) m/z calculated $C_{29}H_{24}N_4O_6Na^+$: 547.1599; found 547.1588 $[M+Na]^+$.

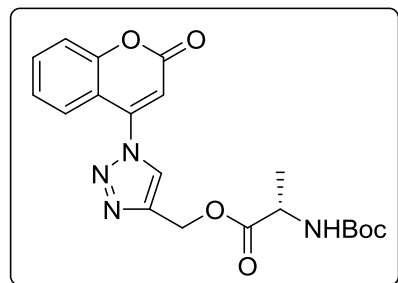
(1-(2-Oxo-2H-chromen-4-yl)-1H-1,2,3-triazol-4-yl)methyl (((9H-fluoren-9-yl)methoxy)carbonyl)-L-phenylalaninate (38d): White solid; yield: 0.291 g (89%);



mp: 134–136 °C; 1H NMR (300 MHz, $CDCl_3$) δ 7.90 (s, 1H), 7.76 (m, 4H), 7.63 (t, J = 7.5 Hz, 1H), 7.53 (d, J = 7.0 Hz, 2H), 7.43 – 7.38 (m, 4H), 7.33 – 7.27 (m, 3H), 7.24 – 7.17 (m, 2H), 7.14 – 7.04 (m, 1H), 6.50 (s, 1H), 5.50 – 5.35 (m, 2H), 5.34 – 5.25 (m, 1H), 4.71 (t, J = 6.1 Hz, 1H), 4.42 – 4.37 (m, 2H), 4.18 (d, J = 6.1 Hz, 1H), 3.15 (d, J = 6.2

Hz, 2H); ^{13}C NMR (75 MHz, $CDCl_3$) δ 171.5, 159.5, 155.6, 154.2, 146.4, 143.6, 141.3, 135.4, 134.7, 133.8, 133.6, 129.3, 128.8, 128.6, 127.7, 127.3, 127.1, 125.4, 124.9, 120.0, 117.6, 114.1, 110.1, 67.0, 58.2, 54.9, 47.1, 37.9; HRMS (ESI-TOF) m/z calculated $C_{36}H_{28}N_4O_6Na^+$: 635.1919; found 635.1901 $[M+Na]^+$.

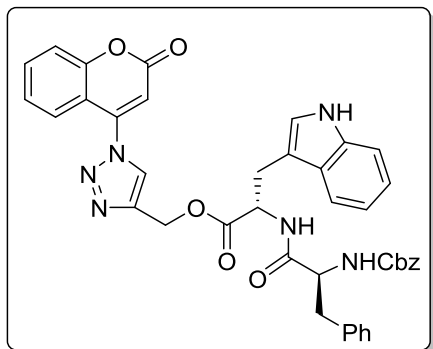
(1-(2-Oxo-2H-chromen-4-yl)-1H-1,2,3-triazol-4-yl)methyl (tert-butoxycarbonyl)-L-alaninate (38g): White solid; yield: 0.179 g (81%); mp: 133–135 °C; 1H NMR (300 MHz,



$CDCl_3$) δ 8.16 (s, 1H), 7.87 (d, J = 7.8 Hz, 1H), 7.67 (t, J = 7.8 Hz, 1H), 7.46 (d, J = 8.1 Hz, 1H), 7.36 (t, J = 7.8 Hz, 1H), 6.58 (s, 1H), 5.43 (q, J = 13.0 Hz, 2H), 5.01 (d, J = 4.8 Hz, 1H), 4.30 (t, J = 6.6 Hz, 1H), 1.42 (brs, 3H), 1.39 (s, 9H); ^{13}C NMR (75 MHz, $CDCl_3$) δ 173.5, 159.6, 155.3, 154.4, 146.7,

143.9, 133.7, 125.6, 125.2, 125.0, 117.7, 114.3, 110.2, 80.3, 58.1, 49.5, 28.4, 18.2; HRMS (ESI-TOF) m/z calculated $C_{20}H_{22}N_4O_6Na^+$: 437.1441; found 437.1432 $[M+Na]^+$.

(1-(2-Oxo-2H-chromen-4-yl)-1H-1,2,3-triazol-4-yl)methyl ((benzyloxy)carbonyl)-L-phenylalanyl-L-tryptophanate (39a): Yellow solid; yield: 0.296 g (78%); mp: 150–152 °C;



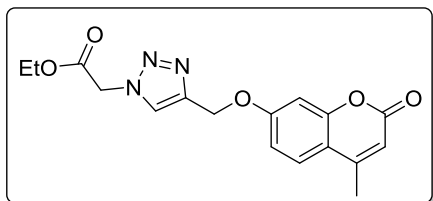
1H NMR (400 MHz, $DMSO-d_6$) δ 11.1 (s, 1H), 8.79 (brs, 2H), 7.94 (brs, 2H), 7.80 – 7.62 (m, 4H), 7.49 – 7.33 (m, 12H), 7.25 – 7.12 (m, 2H), 7.04 (s, 1H), 5.46 (s, 2H), 5.09 (s, 2H), 4.87 – 4.76 (m, 1H), 4.53 – 4.44 (m, 1H), 3.42 – 3.27 (m, 2H), 3.13 – 3.04 (m, 1H), 2.86 – 2.75 (m, 1H); ^{13}C NMR (100 MHz, $DMSO-d_6$) δ 171.9, 171.3, 159.4, 155.8, 153.6, 145.7, 142.6, 138.0, 136.9, 136.0, 133.5, 129.1,

128.2, 127.9, 127.6, 127.4, 127.0, 126.3, 125.4, 125.0, 123.8, 123.7, 121.0, 118.4, 118.0, 117.1, 114.20, 111.4, 110.6, 109.1, 65.2, 57.3, 55.8, 53.1, 37.3, 26.8; HRMS (ESI-TOF) m/z calculated $C_{40}H_{34}N_6O_7Na^+$: 733.2369; found 733.2381 $[M+Na]^+$.

General procedure for the synthesis of 7-*o*- or 4-*o*-triazolyl methyl coumarin-amino acid hybrids

To a solution of 4-methyl-7-(prop-2-ynyloxy)-coumarin (**41a**) or 4-(prop-2-ynyloxy)-coumarin (**41b**) (0.100 g, 1 equiv), was added α -azidoester [**43a–c**, (1 equiv)] in EtOH : H_2O (1:1). This was followed by addition of $CuSO_4 \cdot 5H_2O$ (0.01 equiv) and sodium ascorbate (0.1 equiv). The reaction mixture was stirred at room temperature for 6–10 h and monitored *via* TLC. After completion of the reaction, the reaction mixture was concentrated and the residue was diluted with water and ammonium hydroxide (2–3 mL). Thereafter, the mixture was extracted into dichloromethane (3×20 mL). Organic layer was separated, dried over anhydrous sodium sulfate and concentrated to yield product which was recrystallized from ethanol to yield pure **44a–f**.

Ethyl 2-(4-(((4-methyl-2-oxo-2H-chromen-7-yl)oxy)methyl)-1H-1,2,3-triazol-1-yl)acetate (44a): White solid; yield: 0.141 g (88%); mp: 129–132 °C; 1H NMR (300 MHz, $CDCl_3$) δ

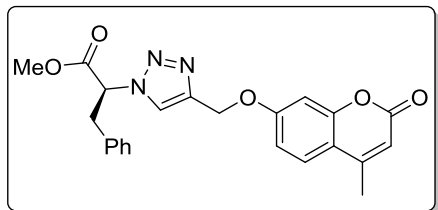


7.82 (s, 1H), 7.50 (d, $J = 8.6$ Hz, 1H), 6.98 – 6.89 (m, 2H), 6.14 (s, 1H), 5.28 (s, 2H), 5.18 (s, 2H), 4.27 (q, $J = 7.1$ Hz, 2H), 2.39 (s, 3H), 1.30 (t, $J = 7.1$ Hz, 3H); ^{13}C NMR (75 MHz, $CDCl_3$) δ 161.2, 155.2, 152.6, 143.6, 126.0, 125.8,

124.5, 114.2, 112.5, 112.4, 102.2, 62.7, 62.3, 51.0, 18.8, 14.2; HRMS (ESI-TOF) m/z calculated

$C_{17}H_{17}N_3O_5Na^+$: 366.1056; found 366.1060 $[M+Na]^+$.

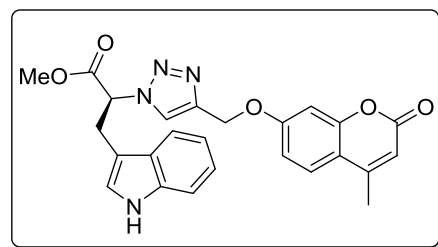
Methyl (S)-2-(4-(((4-methyl-2-oxo-2H-chromen-7-yl)oxy)methyl)-1H-1,2,3-triazol-1-yl)-3-phenylpropanoate (44b): White solid; yield: 0.166 g (85%); mp: 133–135 °C; 1H NMR (300



MHz, $CDCl_3$) δ 7.69 (s, 1H), 7.48 (d, $J = 6.6$ Hz, 1H), 7.21 – 7.09 (m, 3H), 7.02 – 6.81 (m, 4H), 6.12 (s, 1H), 5.62 – 5.52 (m, 1H), 5.20 (s, 2H), 3.74 (s, 3H), 3.52 – 3.38 (m, 2H), 2.37 (s, 3H); ^{13}C NMR (75 MHz, $CDCl_3$) δ 168.6, 161.3, 161.2, 155.2, 152.5, 143.4, 143.1, 134.5, 128.9, 127.7, 125.8, 123.3,

114.1, 112.6, 112.4, 102.2, 64.2, 62.4, 53.3, 39.1, 18.9; HRMS (ESI-TOF) m/z calculated $C_{23}H_{21}N_3O_5Na^+$: 442.1385; found 442.1373 $[M+Na]^+$.

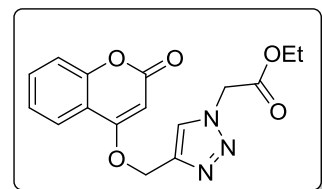
Methyl (S)-3-(1H-indol-3-yl)-2-(4-(((4-methyl-2-oxo-2H-chromen-7-yl)oxy)methyl)-1H-1,2,3-triazol-1-yl)propanoate (44c): White solid; yield: 0.175 g (82%); mp: 138–140 °C; 1H NMR



(300 MHz, $DMSO-d_6$) δ 10.85 (s, 1H), 8.44 (s, 1H), 7.70 (d, $J = 8.8$ Hz, 1H), 7.51 (d, $J = 7.8$ Hz, 1H), 7.32 (d, $J = 8.0$ Hz, 1H), 7.14 (s, 1H), 7.10 – 6.94 (m, 4H), 6.24 (s, 1H), 5.87 (t, $J = 7.6$ Hz, 1H), 5.24 (s, 2H), 3.73 (s, 3H), 3.71 – 3.67 (m, 2H), 2.42 (s, 3H); ^{13}C NMR (75 MHz, $DMSO-d_6$)

δ 169.6, 161.6, 160.7, 155.2, 154.0, 142.3, 136.5, 127.2, 127.0, 125.7, 124.3, 121.7, 119.1, 118.5, 114.0, 113.1, 112.0, 108.6, 102.1, 63.3, 62.2, 53.5, 27.8, 18.7; HRMS (ESI-TOF) m/z calculated $C_{25}H_{22}N_4O_5Na^+$: 481.1496; found 481.1482 $[M+Na]^+$.

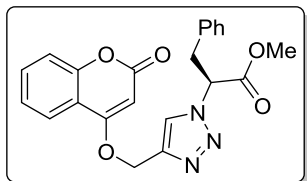
Ethyl 2-(4-(((2-oxo-2H-chromen-4-yl)oxy)methyl)-1H-1,2,3-triazol-1-yl)acetate (44d): White



solid; yield: 0.148 g (90%); mp: 128–130 °C; 1H NMR (300 MHz, $CDCl_3$) δ 7.87 (s, 1H), 7.72 (d, $J = 7.8$ Hz, 1H), 7.48 (t, $J = 7.7$ Hz, 1H), 7.24 – 7.14 (m, 2H), 5.81 (s, 1H), 5.32 (s, 2H), 5.18 (s, 2H), 4.24 (q, $J = 7.0$ Hz, 2H), 1.27 (t, $J = 7.1$ Hz, 3H); ^{13}C NMR (75

MHz, $CDCl_3$) δ 166.1, 165.0, 162.7, 153.4, 142.0, 132.6, 125.0, 124.0, 123.2, 116.8, 115.5, 91.3, 62.7, 51.1, 14.2. HRMS (ESI-TOF) m/z calculated $C_{16}H_{15}N_3O_5Na^+$: 352.0911; found 352.0904 $[M+Na]^+$.

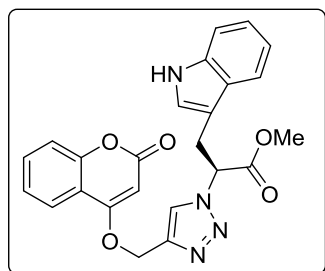
Methyl (S)-2-(4-(((2-oxo-2H-chromen-4-yl)oxy)methyl)-1H-1,2,3-triazol-1-yl)-3-phenylpropanoate (44e): White solid; yield: 0.176 g (87%); mp: 130–132 °C; ¹H NMR (300



MHz, CDCl₃) δ 7.80 (s, 1H), 7.69 (d, *J* = 7.3 Hz, 1H), 7.48 (t, *J* = 7.7 Hz, 1H), 7.27 – 7.09 (m, 5H), 6.93 (d, *J* = 3.2 Hz, 2H), 5.75 (s, 1H), 5.65 – 5.56 (m, 1H), 5.23 (s, 2H), 3.73 – 3.68 (m, 3H), 3.51 – 3.38 (m, 2H); ¹³C NMR (75 MHz, CDCl₃) δ 168.5, 164.9, 162.6, 153.4, 134.4,

132.6, 128.9, 127.8, 124.0, 123.2, 116.8, 115.5, 91.2, 64.4, 62.7, 53.3, 39.1; HRMS (ESI-TOF) *m/z* calculated C₂₂H₁₉N₃O₅Na⁺: 428.1226; found 428.1217 [M+Na]⁺.

Methyl (S)-3-(1H-indol-3-yl)-2-(4-(((2-oxo-2H-chromen-4-yl)oxy)methyl)-1H-1,2,3-triazol-1-yl)propanoate (44f): White solid; yield: 0.188 g (85%); mp: 134–136 °C; ¹H NMR (300



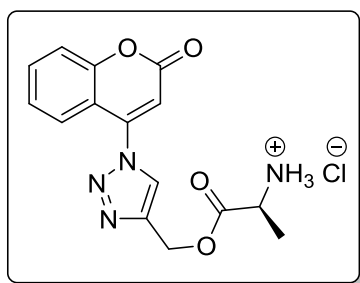
MHz, DMSO-*d*₆) δ 10.88 (s, 1H), 8.52 (s, 1H), 7.71 – 7.65 (m, 2H), 7.50 – 7.29 (m, 5H), 7.06 – 7.00 (m, 1H), 6.95 (t, *J* = 7.4 Hz, 1H), 6.14 (s, 1H), 5.90 (t, *J* = 7.6 Hz, 1H), 5.39 (s, 2H), 3.75 (s, 3H), 3.72 – 3.68 (m, 2H); ¹³C NMR (75 MHz, DMSO-*d*₆) δ 169.5, 164.8,

162.1, 153.3, 141.3, 136.4, 133.4, 127.3, 126.0, 124.8, 124.4, 123.4, 121.6, 119.1, 118.4, 117.0, 115.6, 112.0, 108.6, 91.9, 63.5, 63.3, 53.7, 27.8; HRMS (ESI-TOF) *m/z* calculated C₂₄H₂₀N₄O₅Na⁺: 462.1776; found 462.1772 [M+Na]⁺.

Synthesis of (1-(2-oxo-2H-chromen-4-yl)-1H-1,2,3-triazol-4-yl)methyl-L-alaninate hydrochloride (45)

A solution of dioxane/HCl was added dropwise to **38g** (0.150 g, 1 equiv) that was initially dissolved in dioxane at 0 °C. The reaction was stirred at room temperature for 2 h and monitored *via* TLC. After reaction completion, the reaction mixture was completely concentrated, washed with diethyl ether, and filtered-off to give **45**.

(1-(2-Oxo-2H-chromen-4-yl)-1H-1,2,3-triazol-4-yl)methyl-L-alaninate hydrochloride (45):



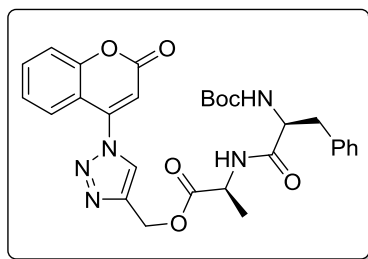
White solid; yield: 0.082 g (68%); mp: 160–162 °C; ¹H NMR (300 MHz, DMSO-*d*₆) δ 8.99 (s, 1H), 7.87 (d, *J* = 8.1 Hz, 1H), 7.78 (t, *J* = 7.6 Hz, 1H), 7.57 (s, 1H), 7.45 (t, *J* = 7.4 Hz, 1H), 6.95 (s, 1H), 5.47 (s, 2H), 4.15 (dd, *J* = 13.4, 6.5 Hz, 1H), 3.39 (brs (merged with moisture of DMSO), 3H), 1.50 (d, *J* = 6.8 Hz, 3H); ¹³C NMR (100 MHz, DMSO-*d*₆ + CDCl₃) δ 169.6, 159.3,

153.6, 145.7, 142.2, 133.4, 126.6, 125.5, 124.9, 117.1, 114.1, 110.4, 58.2, 47.9, 15.6.

Synthesis of (1-(2-oxo-2H-chromen-4-yl)-1H-1,2,3-triazol-4-yl)methyl(*tert*-butoxycarbonyl)-L-phenylalanyl-L-alaninate (46)

To a stirred solution of **45** (0.050 g, 1 equiv) in DMF, triethyl amine (2.5 equiv) was added at 0 °C and subsequently EDC·HCl (1.5 equiv) and HOBT (1.2 equiv) were added. The reaction mixture was stirred for 15 min at 0 °C. And then, Boc-L-phenylalanine (**32a**) (0.038 g, 1 equiv) was added. The reaction was stirred at room temperature for 8 h, and the completion of the reaction was monitored by TLC. After the completion of the reaction, crushed-ice was added that resulted in the precipitation of the product which was filtrated, washed with cold-water, and recrystallized from ethanol to afford **46**.

(1-(2-Oxo-2H-chromen-4-yl)-1H-1,2,3-triazol-4-yl)methyl(*tert*-butoxycarbonyl)-L-phenylalanyl-L-alaninate (46): White solid; yield: 0.070 g (86%); mp: 145–147 °C; ¹H NMR (400 MHz,

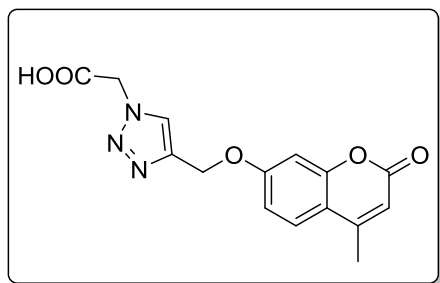


DMSO-*d*₆ + CDCl₃) δ 8.81 (s, 1H), 8.42 (s, 1H), 7.83 (d, *J* = 8.4 Hz, 1H), 7.75 (s, 1H), 7.54 (d, *J* = 8.1 Hz, 1H), 7.40 (d, *J* = 8.0 Hz, 1H), 7.27 – 7.10 (m, 5H), 6.90 – 6.83 (m, 1H), 6.71 (d, *J* = 7.7 Hz, 1H), 5.34 (s, 2H), 4.45 – 4.34 (m, 1H), 4.25 – 4.18 (m, 1H), 2.95 (d, *J* = 13.8 Hz, 1H), 2.68 (d, *J* = 12.0 Hz, 1H), 1.37 (brs, 3H), 1.29 (s, 9H); ¹³C NMR (100 MHz, DMSO-*d*₆ +

CDCl₃) δ 172.1, 171.8, 159.2, 155.1, 153.6, 145.7, 142.7, 137.9, 133.3, 129.1, 127.8, 126.2, 126.0, 125.5, 124.8, 117.0, 114.1, 110.3, 77.9, 57.3, 55.2, 47.6, 37.4, 28.1, 16.8.

Synthesis of 2-(4-(((4-methyl-2-oxo-2H-chromen-7-yl)oxy)methyl) 1H-1,2,3-triazol-1-yl)acetic Acid (47)

To a solution of **44a** (0.100 g, 1 equiv) in ethanol cooled to 0 °C, a solution of 20% NaOH in water (5 mL) was added dropwise. The reaction was stirred at room temperature for 3 h, and monitored *via* TLC. After the completion of the reaction, ethanol was completely removed under reduced pressure to give the corresponding salt of the acid, which was acidified using 4 N HCl at 0 °C, and the aqueous layer was extracted with dichloromethane and concentrated to afford pure **47**.

2-(4-(((4-Methyl-2-oxo-2H-chromen-7-yl)oxy)methyl)-1H-1,2,3-triazol-1-yl)acetic acid (47):

White solid; yield: 0.078 g (85%); mp: 110–112 °C; ^1H NMR (400 MHz, $\text{DMSO}-d_6 + \text{CDCl}_3$) δ 8.23 (s, 1H), 7.66 (d, $J = 8.8$ Hz, 1H), 7.12 (s, 1H), 7.03 (d, $J = 8.8$ Hz, 1H), 6.17 (s, 1H), 5.29 (s, 2H), 5.26 (s, 2H), 2.41 (s, 3H); ^{13}C NMR (100 MHz, $\text{DMSO}-d_6 + \text{CDCl}_3$) δ 168.3, 161.0, 160.0, 154.7, 152.9, 141.8, 126.2, 126.0, 113.3, 112.5,

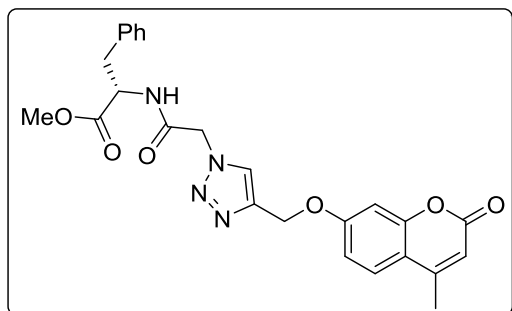
111.3, 101.5, 61.6, 50.6, 18.1.

Synthesis of methyl (2-(4-(((4-methyl-2-oxo-2H-chromen-7-yl)oxy)methyl)-1H-1,2,3-triazol-1-yl)acetyl)-L-phenylalaninate (48)

To the stirred solution of **47** (0.050 g, 1 equiv) in DMF, triethyl amine (2.5 equiv) was added at 0 °C and subsequently EDC.HCl (1.5 equiv) and HOBT (1.2 equiv) were added. The reaction mixture was stirred for 15 min at 0 °C. Later L-phenylalanine methyl ester (**42b**) (0.029 g, 1 equiv) was added, and the reaction was stirred at room temperature for 6 h. The completion of the reaction was monitored by TLC. After the completion of the reaction, crushed-ice was added that resulted in the precipitation of the product, which was filtrated, washed with cold-water, and recrystallized from ethanol to afford **48**.

Methyl (2-(4-(((4-methyl-2-oxo-2H-chromen-7-yl)oxy)methyl)-1H-1,2,3-triazol-1-yl)acetyl)-L-phenylalaninate (48):

White solid; yield: 0.068 g (90%); mp: 135–137 °C; ^1H NMR (400 MHz, $\text{DMSO}-d_6 + \text{CDCl}_3$) δ 8.89 (d, $J = 7.7$ Hz, 1H), 8.09 (s, 1H), 7.64 (d, $J = 8.8$ Hz, 1H), 7.31 – 7.25 (m, 2H), 7.24 – 7.18 (m, 3H), 7.10 (d, $J = 2.2$ Hz, 1H), 7.01 (dd, $J = 8.8, 2.2$ Hz, 1H), 6.16 (s, 1H), 5.26 (s, 2H), 5.14 (q, $J = 16.2$ Hz, 2H), 4.57 (dd, $J = 13.7, 8.1$ Hz, 1H), 3.64 (s, 3H), 3.08 (dd, $J = 13.8, 5.5$ Hz, 1H), 2.95 (dd, $J = 13.8, 5.7$ Hz, 1H), 2.40 (s, 3H); ^{13}C NMR (100 MHz, $\text{DMSO}-d_6 + \text{CDCl}_3$) δ 171.3, 165.3, 161.0, 160.0, 154.7, 152.9, 141.6, 136.5, 129.0, 128.2, 126.5, 126.1, 126.0, 113.3, 112.4, 111.3, 101.4, 61.5, 53.6, 51.8, 51.3, 36.8, 18.1.



1B.4 References

- (1) Choudhary, A.; Raines, R. T. *ChemBioChem* **2011**, *12*, 1801-1807.
- (2) Valverde, I. E.; Mindt, T. L. *CHIMIA International Journal for Chemistry* **2013**, *67*, 262-266.
- (3) Meanwell, N. A. *Journal of Medicinal Chemistry* **2011**, *54*, 2529-2591.
- (4) Vagner, J.; Qu, H.; Hruba, V. J. *Current Opinion in Chemical Biology* **2008**, *12*, 292-296.
- (5) Marciniszyn, J.; Hartsuck, J. A.; Tang, J. *Journal of Biological Chemistry* **1976**, *251*, 7088-7094.
- (6) Cumin, F.; Evin, G.; Fehrentz, J.-A.; Seyer, R.; Castro, B.; Menard, J.; Corvol, P. *Journal of Biological Chemistry* **1985**, *260*, 9154-9157.
- (7) Rahuel, J.; Rasetti, V.; Maibaum, J.; Rueger, H.; Gösche, R.; Cohen, N.; Stutz, S.; Cumin, F.; Fuhrer, W.; Wood, J. *Chemistry & Biology* **2000**, *7*, 493-504.
- (8) Allikmets, K. *Vascular Health and Risk Management* **2007**, *3*, 809-815.
- (9) Borg, S.; Estenne-Bouhtou, G.; Luthman, K.; Csoeregh, I.; Hesselink, W.; Hacksell, U. *The Journal of Organic Chemistry* **1995**, *60*, 3112-3120.
- (10) Boeglin, D.; Cantel, S.; Heitz, A.; Martinez, J.; Fehrentz, J.-A. *Organic Letters* **2003**, *5*, 4465-4468.
- (11) Holub, J. M.; Kirshenbaum, K. *Chemical Society Reviews* **2010**, *39*, 1325-1337.
- (12) Tam, A.; Arnold, U.; Soellner, M. B.; Raines, R. T. *Journal of the American Chemical Society* **2007**, *129*, 12670-12671.
- (13) Coffey, S. B.; Aspnes, G.; Londregan, A. T. *ACS Combinatorial Science* **2015**, *17*, 706-709.
- (14) Horne, W. S.; Yadav, M. K.; Stout, C. D.; Ghadiri, M. R. *Journal of the American Chemical Society* **2004**, *126*, 15366-15367.
- (15) Oh, K.; Guan, Z. *Chemical Communications* **2006**, *0*, 3069-3071.
- (16) Hua, Y.; Flood, A. H. *Chemical Society Reviews* **2010**, *39*, 1262-1271.
- (17) Pedersen, D. S.; Abell, A. *European Journal of Organic Chemistry* **2011**, *2011*, 2399-2411.
- (18) Angell, Y. L.; Burgess, K. *Chemical Society Reviews* **2007**, *36*, 1674-1689.
- (19) Bock, V. D.; Speijer, D.; Hiemstra, H.; van Maarseveen, J. H. *Organic & Biomolecular Chemistry* **2007**, *5*, 971-975.

- (20) Bach, A.; Pedersen, T. B.; Strømgaard, K. *MedChemComm* **2016**, *7*, 531-536.
- (21) Davis, M. R.; Singh, E. K.; Wahyudi, H.; Alexander, L. D.; Kunicki, J. B.; Nazarova, L. A.; Fairweather, K. A.; Giltrap, A. M.; Jolliffe, K. A.; McAlpine, S. R. *Tetrahedron* **2012**, *68*, 1029-1051.
- (22) Stanley, N. J.; Pedersen, D. S.; Nielsen, B.; Kvist, T.; Mathiesen, J. M.; Bräuner-Osborne, H.; Taylor, D. K.; Abell, A. D. *Bioorganic & Medicinal Chemistry Letters* **2010**, *20*, 7512-7515.
- (23) Angelo, N. G.; Arora, P. S. *The Journal of Organic Chemistry* **2007**, *72*, 7963-7967.
- (24) Marion, A.; Góra, J.; Kracker, O.; Fröhr, T.; Latajka, R.; Sewald, N.; Antes, I. *Journal of Chemical Information and Modeling* **2017**, *58*, 90-110.
- (25) Kuijpers, B. H.; Groothuys, S.; Hawner, C.; Dam, J. t.; Quaedflieg, P. J.; Schoemaker, H. E.; Delft, F. L. v.; Rutjes, F. P. *Organic Process Research & Development* **2008**, *12*, 503-511.
- (26) Van Dijk, M.; Rijkers, D. T.; Liskamp, R. M.; van Nostrum, C. F.; Hennink, W. E. *Bioconjugate Chemistry* **2009**, *20*, 2001-2016.
- (27) Bock, V. D.; Hiemstra, H.; Van Maarseveen, J. H. *European Journal of Organic Chemistry* **2006**, *2006*, 51-68.
- (28) Thirumurugan, P.; Matosiuk, D.; Jozwiak, K. *Chemical Reviews* **2013**, *113*, 4905-4979.
- (29) Nwe, K.; Brechbiel, M. W. *Cancer Biotherapy and Radiopharmaceuticals* **2009**, *24*, 289-302.
- (30) Gehringer, M.; Laufer, S. A. *Angewandte Chemie International Edition* **2017**, *56*, 15504-15505.
- (31) Breinbauer, R.; Köhn, M. *ChemBioChem* **2003**, *4*, 1147-1149.
- (32) Malke, M.; Barqawi, H.; Binder, W. H. *ACS Macro Letters* **2014**, *3*, 393-397.
- (33) Arseneault, M.; Wafer, C.; Morin, J.-F. *Molecules* **2015**, *20*, 9263-9294.
- (34) El-Sagheer, A. H.; Brown, T. *Accounts of Chemical Research* **2012**, *45*, 1258-1267.
- (35) Jaffry, U.; Muñoz-Bonilla, A.; Herrasti, P. *Polymer science: research advances, practical applications and educational aspects*, Edited by A. Méndez-Vilas A. Solano **2016**, 139-149.
- (36) Qin, A.; Lam, J. W.; Tang, B. Z. *Macromolecules* **2010**, *43*, 8693-8702.
- (37) Huisgen, R. *Angewandte Chemie International Edition in English* **1963**, *2*, 633-645.

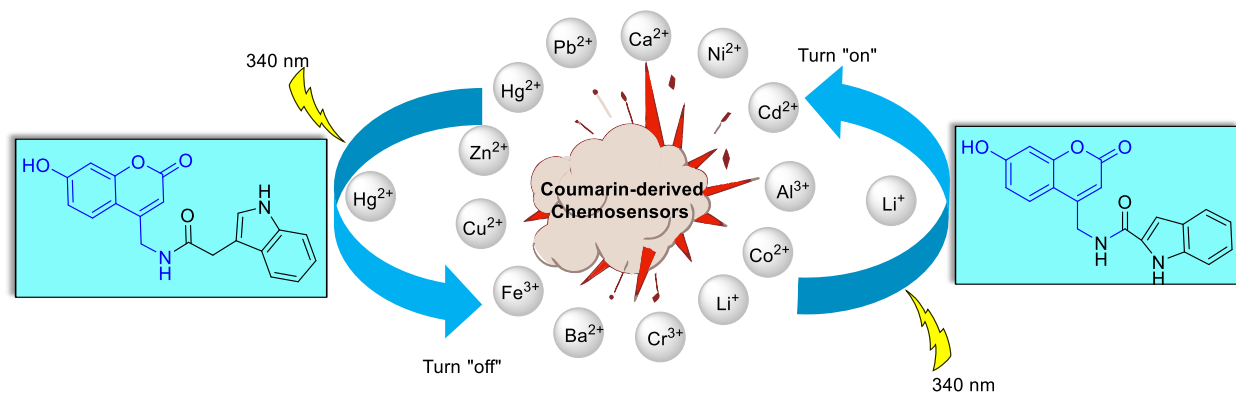
- (38) Huisgen, R. *Pure and Applied Chemistry* **1989**, *61*, 613-628.
- (39) Huisgen, R.; Szeimies, G.; Möbius, L. *Chemische Berichte* **1967**, *100*, 2494-2507.
- (40) Uhlig, N.; Li, C.-J. *Chemical Science* **2011**, *2*, 1241-1249.
- (41) Amblard, F.; Cho, J. H.; Schinazi, R. F. *Chemical Reviews* **2009**, *109*, 4207-4220.
- (42) Meldal, M.; Tornøe, C. W. *Chemical Reviews* **2008**, *108*, 2952-3015.
- (43) Johansson, J. R.; Beke-Somfai, T.; Said Stålsmeden, A.; Kann, N. *Chemical Reviews* **2016**, *116*, 14726-14768.
- (44) Moses, J. E.; Moorhouse, A. D. *Chemical Society Reviews* **2007**, *36*, 1249-1262.
- (45) Kislukhin, A. A.; Hong, V. P.; Breitenkamp, K. E.; Finn, M. *Bioconjugate Chemistry* **2013**, *24*, 684-689.
- (46) Hein, J. E.; Fokin, V. V. *Chemical Society Reviews* **2010**, *39*, 1302-1315.
- (47) Gerard, B.; Ryan, J.; Beeler, A. B.; Porco Jr, J. A. *Tetrahedron* **2006**, *62*, 6405-6411.
- (48) Barsoum, D. N.; Okashah, N.; Zhang, X.; Zhu, L. *The Journal of Organic Chemistry* **2015**, *80*, 9542-9551.
- (49) Yamada, Y. M.; Sarkar, S. M.; Uozumi, Y. *Journal of the American Chemical Society* **2012**, *134*, 9285-9290.
- (50) Shao, C.; Wang, X.; Zhang, Q.; Luo, S.; Zhao, J.; Hu, Y. *The Journal of Organic Chemistry* **2011**, *76*, 6832-6836.
- (51) Hein, J. E.; Tripp, J. C.; Krasnova, L. B.; Sharpless, K. B.; Fokin, V. V. *Angewandte Chemie International Edition* **2009**, *48*, 8018-8021.
- (52) Worrell, B.; Malik, J.; Fokin, V. V. *Science* **2013**, *340*, 457-460.
- (53) Kolb, H. C.; Sharpless, K. B. *Drug Discovery Today* **2003**, *8*, 1128-1137.
- (54) Chouhan, G.; James, K. *Organic Letters* **2011**, *13*, 2754-2757.
- (55) Sivakumar, K.; Xie, F.; Cash, B. M.; Long, S.; Barnhill, H. N.; Wang, Q. *Organic Letters* **2004**, *6*, 4603-4606.
- (56) Key, J. A.; Koh, S.; Timerghazin, Q. K.; Brown, A.; Cairo, C. W. *Dyes and Pigments* **2009**, *82*, 196-203.
- (57) Shaabani, S.; Shaabani, A.; Ng, S. W. *ACS Combinatorial Science* **2014**, *16*, 176-183.
- (58) Ye, X.-W.; Zheng, Y.-C.; Duan, Y.-C.; Wang, M.-M.; Yu, B.; Ren, J.-L.; Ma, J.-L.; Zhang, E.; Liu, H.-M. *MedChemComm* **2014**, *5*, 650-654.

- (59) Wood, W. J.; Patterson, A. W.; Tsuruoka, H.; Jain, R. K.; Ellman, J. A. *Journal of the American Chemical Society* **2005**, *127*, 15521-15527.
- (60) Sandhu, S.; Bansal, Y.; Silakari, O.; Bansal, G. *Bioorganic & Medicinal Chemistry* **2014**, *22*, 3806-3814.
- (61) Pingaew, R.; Saekee, A.; Mandi, P.; Nantasenamat, C.; Prachayasittikul, S.; Ruchirawat, S.; Prachayasittikul, V. *European Journal of Medicinal Chemistry* **2014**, *85*, 65-76.
- (62) Stefani, H. A.; Gueogjan, K.; Manarin, F.; Farsky, S. H.; Zukerman-Schpector, J.; Caracelli, I.; Rodrigues, S. R. P.; Muscará, M. N.; Teixeira, S. A.; Santin, J. R. *European Journal of Medicinal Chemistry* **2012**, *58*, 117-127.
- (63) Link, A. J.; Tirrell, D. A. *Journal of the American Chemical Society* **2003**, *125*, 11164-11165.
- (64) Kele, P.; Li, X.; Link, M.; Nagy, K.; Herner, A.; Lőrincz, K.; Béni, S.; Wolfbeis, O. S. *Organic & Biomolecular Chemistry* **2009**, *7*, 3486-3490.
- (65) Prescher, J. A.; Bertozzi, C. R. *Nature Chemical Biology* **2005**, *1*, 13-21.
- (66) El-Sagheer, A. H.; Brown, T. *Chemical Society Reviews* **2010**, *39*, 1388-1405.
- (67) Gierlich, J.; Burley, G. A.; Gramlich, P. M.; Hammond, D. M.; Carell, T. *Organic Letters* **2006**, *8*, 3639-3642.
- (68) Baruah, H.; Puthenveetil, S.; Choi, Y. A.; Shah, S.; Ting, A. Y. *Angewandte Chemie International Edition* **2008**, *47*, 7018-7021.
- (69) Brennan, J. L.; Hatzakis, N. S.; Tshikhudo, T. R.; Dirvianskyte, N.; Razumas, V.; Patkar, S.; Vind, J.; Svendsen, A.; Nolte, R. J.; Rowan, A. E. *Bioconjugate Chemistry* **2006**, *17*, 1373-1375.
- (70) Nguyen, D. P.; Lusic, H.; Neumann, H.; Kapadnis, P. B.; Deiters, A.; Chin, J. W. *Journal of the American Chemical Society* **2009**, *131*, 8720-8721.
- (71) Best, M. D. *Biochemistry* **2009**, *48*, 6571-6584.
- (72) Lang, K.; Davis, L.; Torres-Kolbus, J.; Chou, C.; Deiters, A.; Chin, J. W. *Nature Chemistry* **2012**, *4*, 298-304.
- (73) Pai, N.; Vishwasrao, S.; Wankhede, K. *Journal of Chemical and Pharmaceutical Research* **2012**, *4*, 4946-4952.

- (74) Ferreira, S. Z.; Carneiro, H. C.; Lara, H. A.; Alves, R. B.; Resende, J. M.; Oliveira, H. M.; Silva, L. M.; Santos, D. A.; Freitas, R. P. *ACS Medicinal Chemistry Letters* **2015**, *6*, 271-275.
- (75) Kellner, S.; Seidu-Larry, S.; Burhenne, J.; Motorin, Y.; Helm, M. *Nucleic Acids Research* **2011**, *39*, 7348-7360.
- (76) Dirks, A. J.; Cornelissen, J. J.; Nolte, R. J. *Bioconjugate Chemistry* **2009**, *20*, 1129-1138.
- (77) Lim, B.; Lee, J. *Molecules* **2016**, *21*, 339.
- (78) Beatty, K. E.; Liu, J. C.; Xie, F.; Dieterich, D. C.; Schuman, E. M.; Wang, Q.; Tirrell, D. A. *Angewandte Chemie* **2006**, *118*, 7524-7527.
- (79) Li, C.; Henry, E.; Mani, N. K.; Tang, J.; Brochon, J. C.; Deprez, E.; Xie, J. *European Journal of Organic Chemistry* **2010**, *2010*, 2395-2405.
- (80) Mertens, M. D.; Guetschow, M. *Synthesis* **2014**, *46*, 2191-2200.
- (81) Kováč, M.; Sabatié, A.; Floch, L. *Arkivoc* **2001**, (vi), 100-108.
- (82) Lin, W.; Long, L.; Feng, J.; Wang, B.; Guo, C. *European Journal of Organic Chemistry* **2007**, *2007*, 4301-4304.
- (83) Bew, S. P.; Hiatt-Gipson, G. D. *The Journal of Organic Chemistry* **2010**, *75*, 3897-3899.
- (84) Aravinda, T.; Naik, H. B.; Naik, H. P. *International Journal of Peptide Research and Therapeutics* **2009**, *15*, 273-279.
- (85) Gao, G.; Sanda, F.; Masuda, T. *Macromolecules* **2003**, *36*, 3932-3937.
- (86) Anand, N.; Jaiswal, N.; Pandey, S. K.; Srivastava, A.; Tripathi, R. P. *Carbohydrate Research* **2011**, *346*, 16-25.
- (87) Ko, E.; Liu, J.; Perez, L. M.; Lu, G.; Schaefer, A.; Burgess, K. *Journal of the American Chemical Society* **2010**, *133*, 462-477.

Chapter 2A

**Coumarin-derived Selective Hg^{2+} & Li^+ Chemosensors:
Synthesis, Experimental and Theoretical
Investigations**



2A.1 Introduction

The word sensor is derived from a latin word sentio, meaning to feel. It is referred to a device that detects a certain external action, and as a result generates a signal that can be interpreted. A sensor can also be interpreted as a device that responds to a physical stimulus for the detection and measurement of a physical property, and transmits a resulting impulse (Figure 2A.1.1).



Figure 2A.1.1: Schematic diagram for the sensor action

In general, different stimuli such as acoustic, biological, chemical, electric, magnetic, optical, mechanical, radiation and thermal could be introduced in the sensors to receive appropriate outputs.¹⁻⁴ Among these, a chemosensor transduces a chemical entity, while a biosensor integrates a biological recognition element with the physiochemical transducers.⁵ Figure 2A.1.2 depicts a graphical representation of various chemical and biological analytes that could be detected by chemosensors and biosensors.

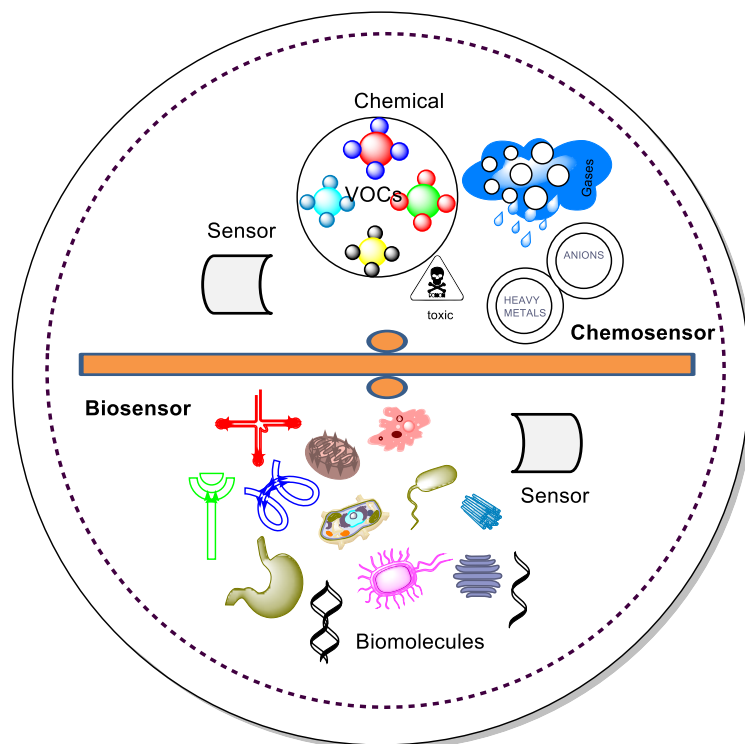


Figure 2A.1.2: A graphical representation of various chemical and biological analytes

In the past, various methods have been applied for the detection of different analytes, including atomic absorption spectrometry, gas chromatography, ion mobility, inductively coupled plasma

mass spectroscopy (ICPMS), and voltammetry.^{6,7} In spite of reasonable advancements, these methods require expensive and sophisticated instrumentation setup, and are not suitable for direct assays.

In striking contrast, fluorescence sensing offers numerous advantages such as accuracy, intrinsic sensitivity, low-cost detection, selectivity, and thus has been successfully employed for the detection of metal ions, anions, gases, explosives, nucleic acid, amino acids and enzymes in organic and aqueous environments.⁸⁻¹⁰ With a rapid response time in the scale of 10^{-8} s and diversity of emission wavelengths, sensing using fluorescent chemical entities provide the real-time monitoring of various analytes. In addition, fluorescence travels without specific physical guide and no reference is required, which enormously simplifies the technical and instrumental requirements and reduces the measurement costs.¹¹ Thus, the fluorescence sensing technology has become a very powerful and indispensable tool for future miniaturized detections and screenings. Fluorescence sensing technology has exhibited widespread applications in clinical diagnostics, environmental monitoring, analytical chemistry, and biomedical science. In some instances, the word fluorescent sensor is used to describe the complete detection system that includes the light source, the molecular probes, the optical components, and the detectors connected to an electronic system used to process the signal. A fluorescent sensor consists of a receptor and a fluorophore constructed by linkage, integration or conjugation. Most commonly, fluorescent sensors/probes bind to the guest (analytes) *via* non-covalent interactions including, hydrogen bonding, hydrophobic interactions, metal coordination, electrostatic interactions, and reversible covalent bond formation. Analyte binding with the sensor alters the electronic and/or molecular structure of the sensor to induce changes in fluorescence properties that can be detected by a fluorescence spectroscopy. In specific, the binding of a sensor (receptor-fluorophore) to the guest (analyte) disturbs the original relationship with respect to electron or charge transfer between the probe and guest in the sensors “excited or ground state”, and leads to change in the emission wavelength or intensity^{12,13} (Figure 2A.1.3).



Figure 2A.1.3: Schematic diagram of the fluorescent sensor action

Two commonly observed mechanisms by which an analyte can modulate the electronic structure, and hence the fluorescence behaviors are energy transfer and electron transfer between the analyte and photo-excited fluorophore. Such processes can give rise to either a “turn-off” or a “turn-on” fluorescence response, due to fluorescence quenching or enhancement, respectively. Förster resonance energy transfer (FRET), internal charge transfer (ICT) and photo-induced electron transfer (PET) phenomenon¹⁴⁻¹⁶ are examples of some output signal mechanisms related to fluorescence sensing. A part from turn-off and turn-on chemosensors, ratiometric fluorescent sensors is another sub-class that relies on analyte-induced changes in the intensity of two or more emission bands (shift in the excitation and/or emission maxima in presence of analytes). Accordingly, a variety of approaches have been used to manipulate these properties for designing appropriate user-friendly platforms for optical detection of analytes.¹⁷⁻¹⁹ Due to diverse applications of chemical sensors in biological, medicinal, environment and industrial fields, and also due to less availability of natural products with intrinsic fluorescence, developing organic fluorophores and related chemosensors with special features is highly desirable.²⁰

Heterocyclic chemistry constitutes the most important subdivision of organic chemistry. More than the 90% drugs contain heterocycles building up a strong interface between chemistry and biology.^{21,22} Functionalized and fused heterocycles derived from several classes of fluorophores including coumarin,²³ fluorescein,²⁴ rhodamine dye,²⁵ 4,4-difluoro-4-bora-3a,4a-diaza-sindacene (BODIPY) dye,²⁶ cyanine dye,²⁷ naphthalimide,²⁸ distyryl ketone,²⁹ 5-aryl-2-pyridyloxazoles³⁰ have served as interesting fluorescent architectures for selective sensing of various analytes.

Among these, coumarin and its derivatives demonstrate satisfactory fluorescence in the visible light region and thus been used in organic light-emitting diodes and laser dyes. Although the tunability of the absorbance and fluorescence of coumarin compounds was observed in the year 1940,^{17,31} yet the molecular origin of their optical properties remains an object of intense investigations for many years. Wheelock's results have showed that the accumulation of electron-donating groups in the 4, 6, or 7 position and/or electron-withdrawing groups in the 3 position shifts the fluorescence band to longer wavelengths.³² The replacement of C=O with a C=S group results in the quenching of fluorescence due to the shifts in the absorbance towards longer wavelength (red shift).¹⁷ In addition, coumarins are classic examples of push-pull dye, in which the intra-molecular charge transfer (ICT) proceeds from benzene ring to pyranone moiety. Typically presence of electron-donating groups (EDGs) at the 7-position (donor) or electron-

withdrawing groups (EWGs) at the 3-position (acceptor),^{33,34} can promote the ICT process, thereby enhancing the fluorescence intensity of coumarin (Figure 2A.1.4).

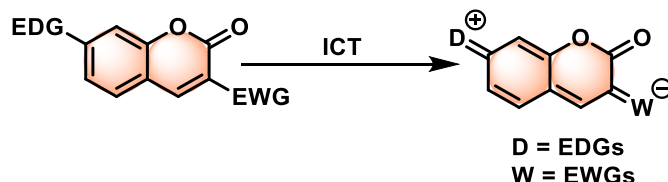


Figure 2A.1.4: Intramolecular charge transfer (ICT) phenomena in coumarin

Jones *et al.* studied the effect of different polar and non-polar solvents (solvent polarity) on the fluorescence spectra of many coumarin derivatives, and found that an increase in the solvent polarity red-shifted the absorbance as well as emission with broadening of emission spectra due to increased hydrogen bonding. In a similar study, Sharma *et al.* estimated the excited-state dipole moment of 4- and 7-substituted coumarin derivatives, and determined the observed shift in both emission and absorption peaks with solvent polarity.³⁵ A qualitative comparison of the photophysical properties of different coumarin derivatives is shown in Figure 2A.1.5.^{17,36}

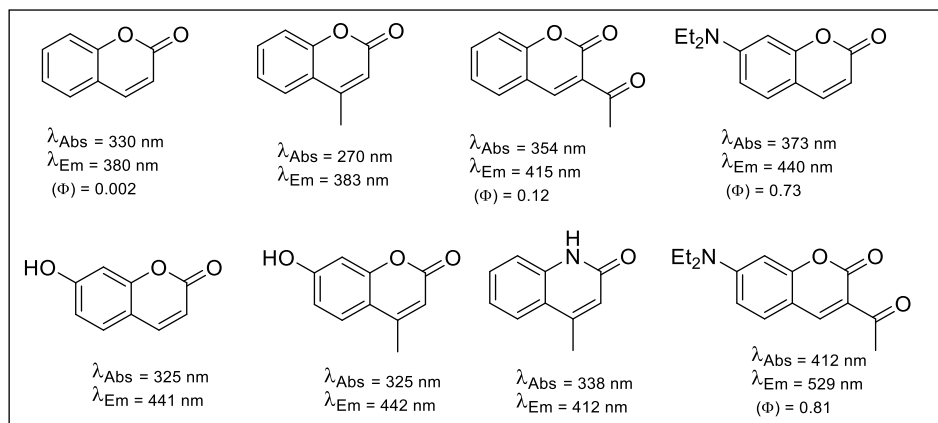


Figure 2A.1.5: Qualitative comparison of photophysical properties of coumarin derivatives

Even though the unsubstituted coumarin does not show noteworthy photoluminescent properties, yet its substituted analogs demonstrate good fluorescence properties, and thus coumarin-derivatives have been used as fluorescent probes of pH, biothiols, enzymes, amines, amino acids, chemical warfare agents, proteins, hydrogen peroxide, hydroxyl radicals, polymeric micelles, DNA and RNA, oxygen, titania, nitric oxide, nitroxide, anions, and metal ions.³⁷

With relevance to the recognition and sensing of biologically and environmentally important metal ions, much attention has been devoted towards developing coumarin-derived chemosensors for cation recognition,²⁰ fluoro- and chromogenic chemodosimeters for heavy metal ion detection in

solution and biospecimens,²¹ and metal-ion-responsive fluorescent probes for two-photon excitation microscopy.²² Some selective examples of functionalized coumarins used for detection of various analytes,³⁸⁻⁵⁵ are represented in Figure 2A.1.6.

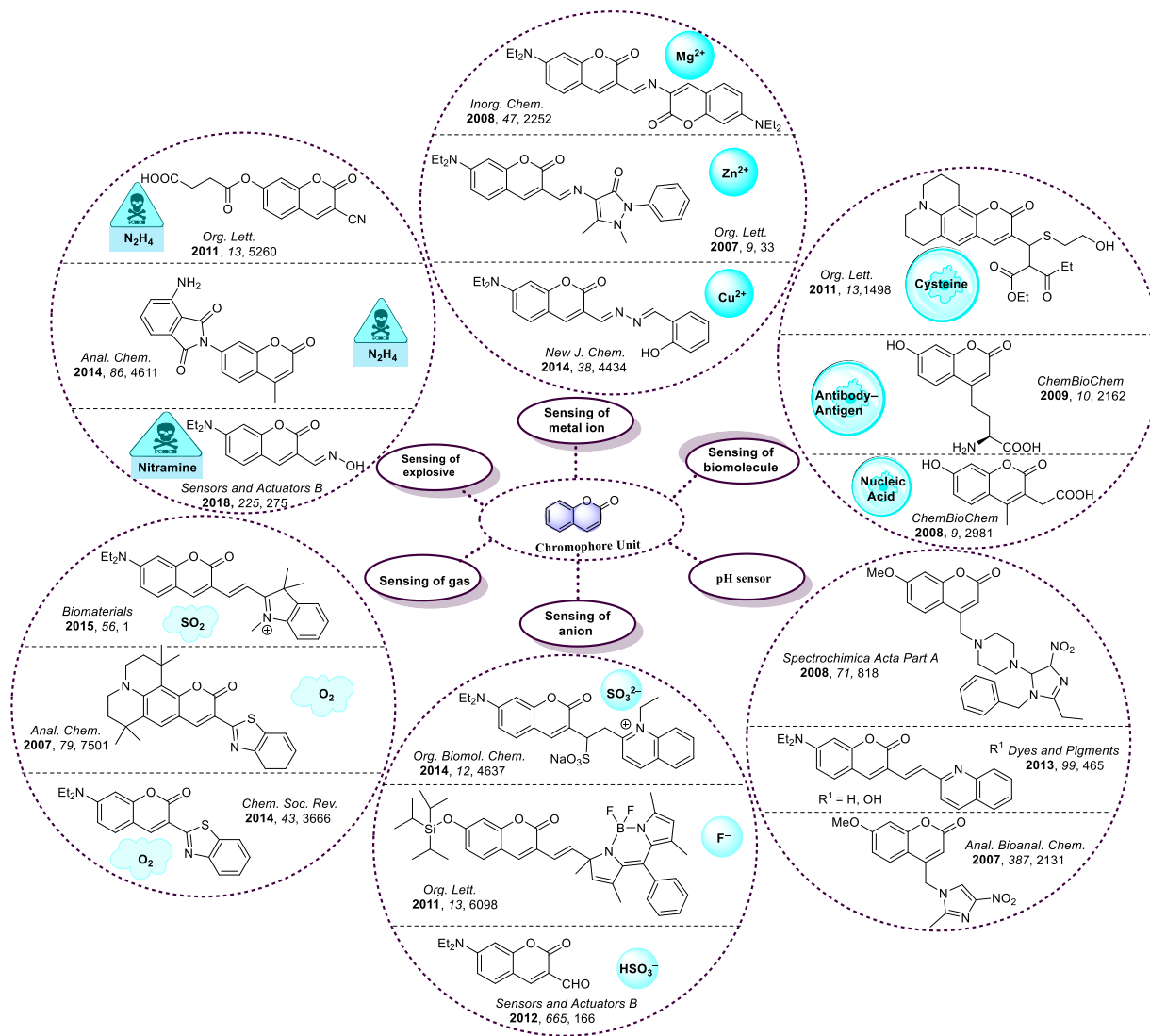


Figure 2A.1.6: Selective examples of functionalized coumarins used for detection of various analytes

Interestingly, coumarin derivatives have served as efficient chemosensors of metal ions comprised of Hg(II), Cu(II), Zn(II), Ni(II), Ca(II), Pb(II), Mg(II), Fe(III), Al(III), Cr(III), and Ag(I).^{17,50,57-58} Several coumarin-derived systems have also exhibited simultaneous sensitivity towards two or more metal ions, *e.g.* Ca(II) and Mg(II), Ni(II) and Co(II), Cu(II) and Hg(II), Na(I) and K(I), Cu(II) and Ni(II), Hg(II) and Ag(I), Cu(II)/Ni(II)/Cd(II), Zn(II)/Cd(II)/Pb(II), or Ni(II)/Pd(II)/Ag(I). In

particular, amide functionalized coumarins have proved their unique potential as efficient and selective metal ion sensors⁵⁶⁻⁶⁷ (Figure 2A.1.7).

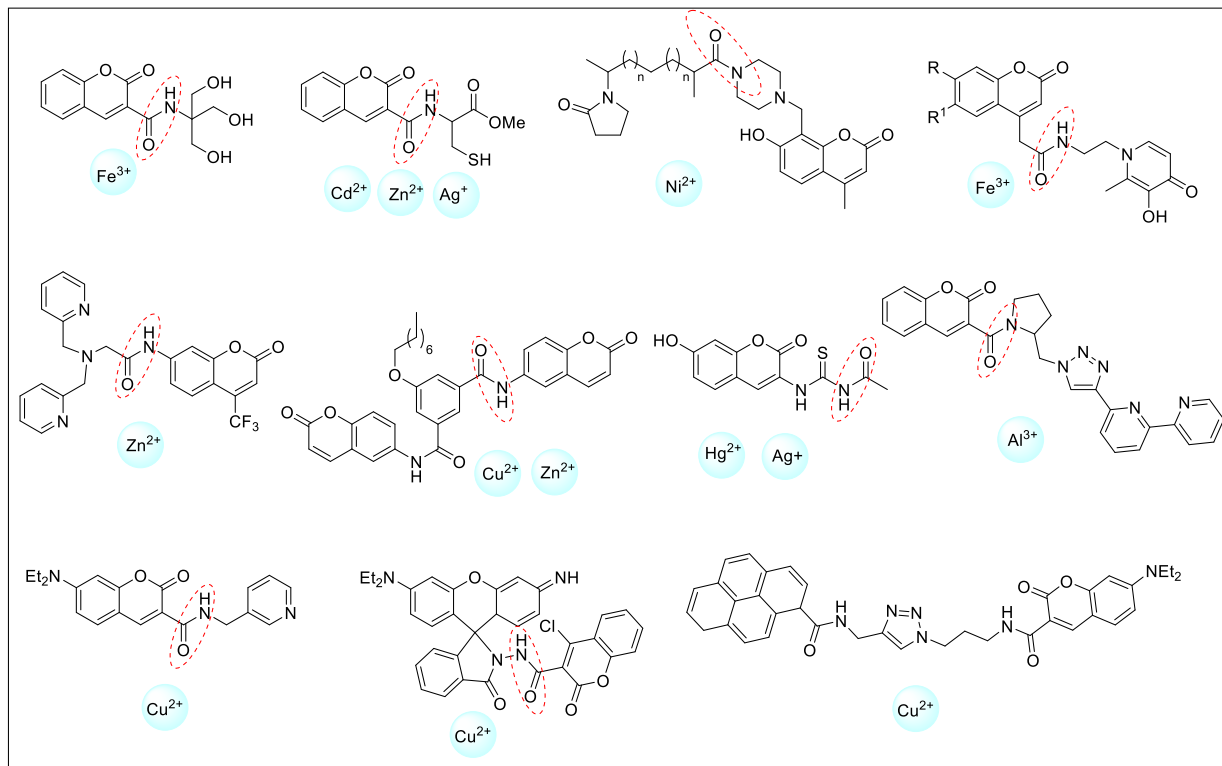
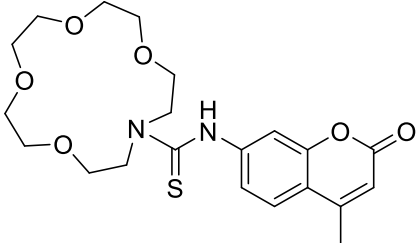
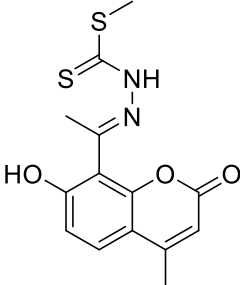
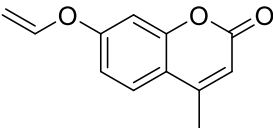
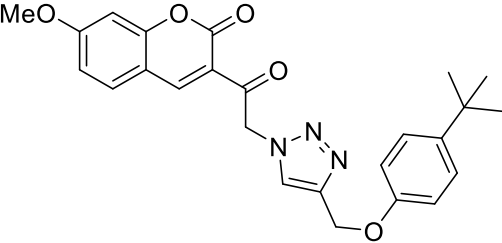
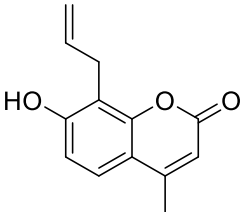
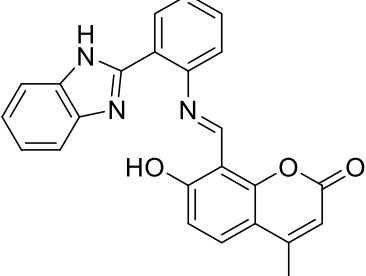
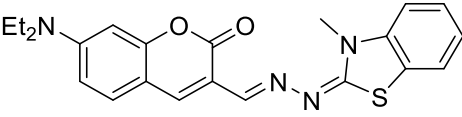
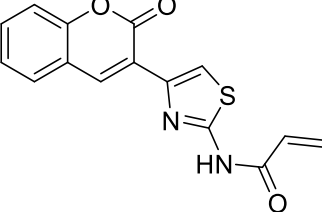


Figure 2A.1.7: Amide functionalized coumarins used as chemosensors for metal ion sensing

Furthermore, the detection of metal ions involved in biological processes (*e.g.*, sodium, potassium, calcium, magnesium), clinical diagnostics (*e.g.*, lithium, aluminum, potassium), or pollution (*e.g.*, lead, mercury, cadmium) have gained special attention in the last two decades.^{12,68-70} Among these metal ions, mercury is a highly hazardous and ubiquitous pollutant of the global environment,⁷¹ and atmospheric mercury eventually generates toxic methylmercury that enters human body through aquatic food chains.⁷² Mercury has high bioaccumulation and persistence character in the environment and living organisms.⁷³ It can easily pass through the skin, respiratory and cell membrane, and has been considered as one of the major cause of human neurological diseases, DNA damage and mitosis impairment.⁷⁴⁻⁷⁶ Its high affinity for thiol groups present in proteins and enzymes has lead to the dysfunction of cells, and consequently caused health problems such as prenatal brain damage, serious cognitive and minamata disease.⁷⁷⁻⁷⁹ Thus, considerable efforts have been made towards designing “turn-on” (enhancement of fluorescence in the presence of Hg^{2+}), “turn-off” (quenching of fluorescence by Hg^{2+}), and ratiometric (shift in the excitation and/or emission maxima in presence of Hg^{2+}) probes based on rhodamine,^{80,81} fluorescein,^{82,83} *N*-

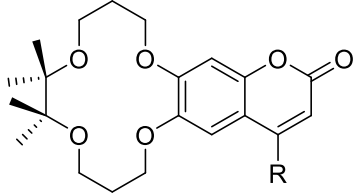
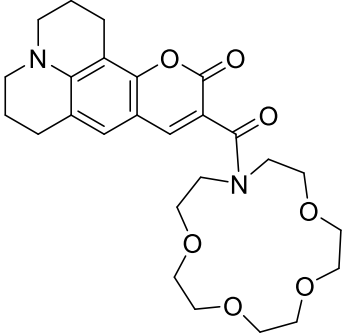
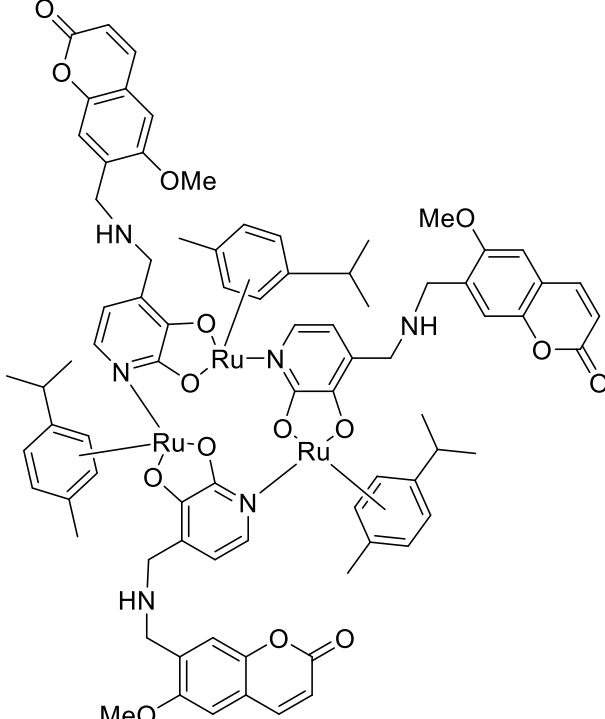
dansylcarboxamide,⁸⁴ naphthalimide,⁸⁵ thiosemicarbazone,⁸⁶ anthrylacetylamide,⁸⁷ crown ethers,⁸⁸ thiocarbamate,⁸⁹ anthraquinone,⁹⁰ porphyrin,⁹¹ benzothiazole,⁹² phenylenediaminetriamide,¹⁹ hydroxyquinoline,⁹³ anthracene,⁹⁴ phenoxazinone⁹⁵ and other complex molecular architectures,^{96,97} for selective detection of mercury ions. Few chemosensors based on coumarin scaffold have been developed for selective sensing of Hg²⁺ in aqueous medium. For example, Voutsadaki *et al.* reported a ratiometric fluorescent ion probe based on a monoaza-15-crown-5 moiety connected to 7-amino-4-methylcoumarin *via* a thiourea linker, which exhibited high selectivity for Hg²⁺ ions in water (Table 2A.1.1, entry 1).⁹⁸ El-Shekheby *et al.* reported a coumarin dithioate based chelation-enhanced selective “off–on” fluorescent probe for sensing trace amounts of Hg²⁺, Ag⁺ and Ag⁻ nanoparticles (Table 2A.1.1, entry 2).⁹⁹ In 2017, Wu *et al.* reported the application of 4-methyl-7-(vinyl-oxo)-2H-chromen-2-one as a fluorescent chemosensor for the selective recognition of Hg²⁺ in 0.12 μM range (Table 2A.1.1, entry 3).¹⁰⁰ Ho *et al.* synthesized fluorescent chemosensor based on triazole moiety connected to coumarin *via* acetyl bridge for selective sensing of Hg²⁺ by 1.8-fold fluorescence enhancement, respectively (Table 2A.1.1, entry 4).¹⁰¹ Gao *et al.* synthesized 7-hydroxy-8-allyl-4-methyl-2H-chromene-2-one and observed that it selectively detects Hg²⁺ ion in aqueous media *via* “turn-on” mechanism (Table 2A.1.1, entry 5).¹⁰² In 2017, Gao *et al.* documented a coumarin-derived benzimidazole system linked *via* imine linker, for simultaneous and selective detection of Hg²⁺ and Cu²⁺ (Table 2A.1.1, entry 6).¹⁰³ In 2017, Jiao *et al.* synthesized coumarin-derived benzothiazolinone hydrazone that exhibited high selectivity towards Hg²⁺ ions (DL = 1 nM) (Table 2A.1.1, entry 7).¹⁰⁴ Very recently, Pankaj *et al.* reported the synthesis of coumaryl-based thiazolyl-acrylamide (OCTAA) as a fluorescent monomer, which upon radical polymerization generates Hg(II)-ion imprinted polymer (IIP) capable for selective nanomolar detection of mercury (Table 2A.1.1, entry 8).¹⁰⁵

Table 2A.1.1: Selective examples of coumarin-derived chemosensors for Hg²⁺ ion detection

<p>Entry 1</p>  <p>Sensing Solvent⁹⁸ = H₂O</p>	<p>Entry 2</p>  <p>Detection Limit⁹⁹ = 0.29 μM Sensing Solvent = H₂O : MeOH (v/v = 1:1)</p>
<p>Entry 3</p>  <p>Detection Limit¹⁰⁰ = 0.12 μM Sensing Solvent = HEPES buffer solution</p>	<p>Entry 4</p>  <p>Detection Limit¹⁰¹ = 12.5 mM Sensing Solvent = MeOH : DCM (v/v = 9:1)</p>
<p>Entry 5</p>  <p>Detection Limit¹⁰² = 0.512 μM Sensing Solvent = CH₃CN : H₂O (v/v = 9:1)</p>	<p>Entry 6</p>  <p>Detection Limit¹⁰³ = 0.1202 μM Sensing Solvent = HEPESbuffer : DMSO</p>
<p>Entry 7</p>  <p>Detection Limit¹⁰⁴ = 1 nM Sensing Solvent = CH₃CN</p>	<p>Entry 8</p>  <p>Detection Limit¹⁰⁵ = 0.020 μM Sensing Solvent = DMSO</p>

On the other hand, lithium is known to demonstrate versatile and significant roles in industrial applications as well as biological and medicinal chemistry.¹⁰⁶ Lithium ions belong to the group of the five biologically most important alkali and alkaline-earth metal cations. Lithium-containing drug preparations are routinely used in medical and clinical applications for the treatment of manic-depressive psychosis.^{107,108} Other uses of lithium include treatment of skin diseases such as dermatitis, autoimmune and immunological diseases, in which patients are required to take the drug over periods of several months or even years. Thus, the concentration of Li^+ ions in blood serum after drug intake varies strongly, and reliable determination of the Li^+ ion concentration levels in blood samples is highly desirable for successful and safe therapeutic applications. This is because too low levels of Li^+ ions show no effect at all, and an overdose can lead to life-threatening toxic effects. In general, Li^+ concentrations in serum during the treatment should be within the narrow range of 0.6 and 1.2 mM.^{109,110} In addition, determination of Li^+ levels in serum must be monitored efficiently in the presence of other cations such as Na^+ , K^+ and Ca^{2+} . Several chemosensors based on diaza-9-crown-3,¹¹¹ *N*-(9-methylanthracene)-25,27-bis(1-propyloxy)-4-*tert*-butylcalix,¹¹² squarylium dye,¹¹³ 1-(9-anthryl)-4-ferrocenyl-2-aza-1,3-butadiene,¹¹⁴ Biginelli-based organic nanoparticle,¹¹⁵ porphyrin¹¹⁶ and polymer based fluoroionophore architectures are reported for Li^+ sensing in different solvent systems. Very recently, one such example was reported by Sakai and Akutagawa, whereby quinoxalinone based fluorescent probe senses the cations ($\text{M}^+ = \text{Li}^+$ and Na^+) and anions ($\text{X}^- = \text{F}^-$, Cl^- , Br^- , and CH_3COO^-) in organic solvent.¹¹⁷ However, very few reports on the development of coumarin-derived fluorescent chemosensors for selective recognition of Li^+ ion in organic solvents have appeared. In this regard, Citterio *et al.* designed and developed pH independent coumarin-based fluorescent probe for selective detection of Li^+ in organo-aqueous solution (DL = 0.6 mM) (Table 2A.1.2, entry 1).¹¹⁸ Taziaux, *et al.* reported coumarin 343 linked to monoaza-crown ethers based fluorescent sensor for selective detection of Li^+ in CH_3CN (Table 2A.1.2, entry 2).¹¹⁹ Hamilton *et al.* reported the water soluble (arene)Ru-based 12-metallacrown-3 complex as a selective “off-on” fluorescent sensor for Li^+ in water (100 mM phosphate buffer, pH 8.0) (Table 2A.1.2, entry 3).^{120,121}

Table 2A.2.2: Coumarin-derived chemosensors for Li⁺ ion detection

<p>Entry 1</p>  <p>Detection Limit¹¹⁸ = 0.6 mM Sensing Solvent = H₂O : MeOH (v/v = 99:1)</p>	<p>Entry 2</p>  <p>Sensing Solvent¹¹⁹ = CH₃CN</p>
<p>Entry 3</p>  <p>Sensing Solvent¹²⁰ = H₂O : MeOH (v/v = 9:1)</p>	

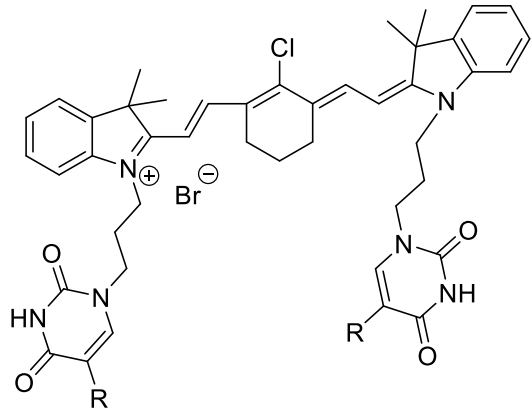
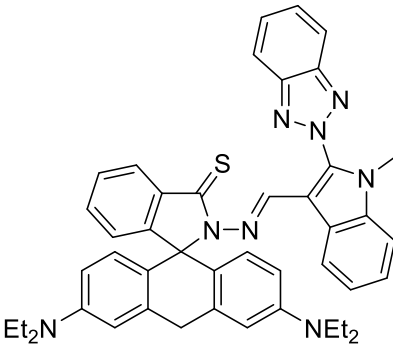
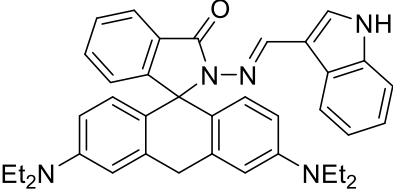
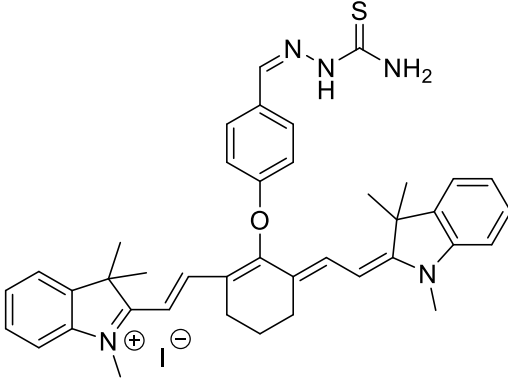
In spite of reasonable detection limits exhibited by most of the above mentioned coumarin-derived Hg²⁺ and Li⁺ chemosensors (Table 2A.1.1 & Table 2A.1.2), designing more effective Hg²⁺ and Li⁺ chemosensors capable of selectively detecting these ions at low concentrations in aqueous medium, and in presence of other ions, remains an appealing and necessary field of research.

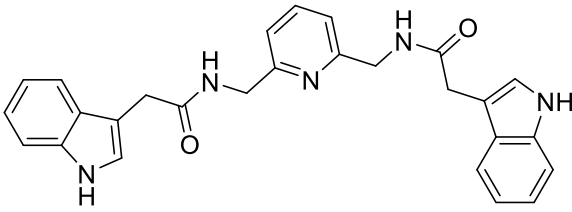
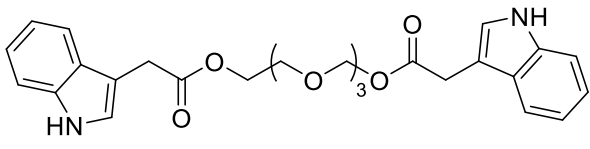
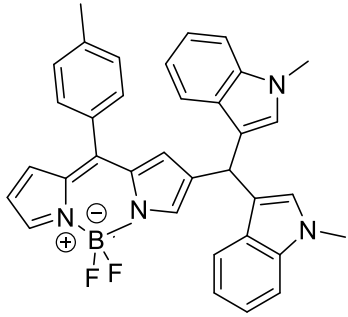
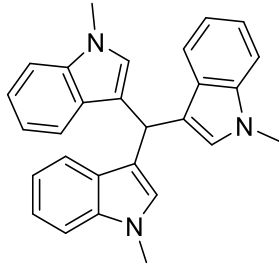
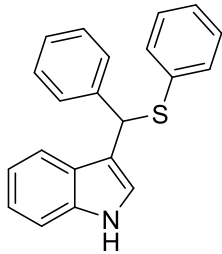
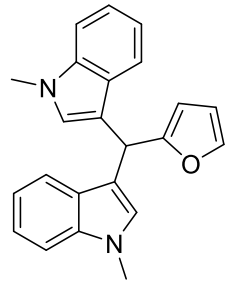
In the present context, indole provides a potential coordination site for different metal ions to bind and provide a sensing platform due to N–H hydrogen bond donor.¹²²⁻¹²⁵ In indole, N–H hydrogen bonding, hydrogen-bond-induced π -electron delocalization, and N–H

deprotonation have accounted for inducing signalling to produce the necessary results.¹²⁶ Considerable efforts have been made by leading scientists towards designing indole-based fluorescent probes for different metal ions sensing.¹²⁷⁻¹³¹

With respect to the prevailing discussion, leading scientist such as Luo, Kaur, Sun, Huang, Liu, Khan and Iyer and others have reported indole-based probes for selective sensing of Hg^{2+} ions (Table 2A.1.3),¹³²⁻¹⁴¹ while the examples of indole-based Li^+ ion chemosensors are untraceable.

Table 2A.1.3: Selective examples of indole-based chemosensors for Hg^{2+} ion detection

<p>Entry 1</p>  <p>Detection Limit¹³² = 10 μM Sensing Solvent = H_2O</p>	<p>Entry 2</p>  <p>Detection Limit¹³³ = 11 nM Sensing Solvent = EtOH : MOPS (v/v = 7:3)</p>
<p>Entry 3</p>  <p>Detection Limit¹³⁴ = 0.05 μM Sensing Solvent = Phosphate buffer : DMSO</p>	<p>Entry 4</p>  <p>Detection Limit¹³⁵ = 0.0193 μM Sensing Solvent = MeOH : H_2O (v/v = 1:9)</p>

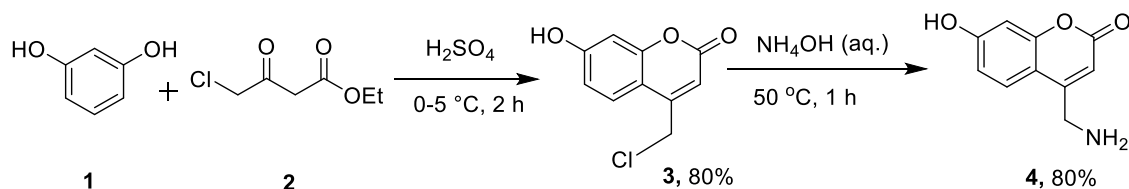
<p>Entry 5</p>  <p>Detection Limit¹³⁶ = 101.6 μM Sensing Solvent = H₂O : DMSO (v/v = 1:1)</p>	<p>Entry 6</p>  <p>Detection Limit¹³⁷ = 6.8 μM Sensing Solvent = H₂O : EtOH (v/v = 1:2)</p>
<p>Entry 7</p>  <p>Detection Limit¹³⁸ = 0.33 μM Sensing Solvent = CH₃CN</p>	<p>Entry 8</p>  <p>Detection Limit¹³⁹ = 1.21 μM Sensing Solvent = CH₃CN</p>
<p>Entry 9</p>  <p>Detection Limit¹⁴⁰ = 30 nM Sensing Solvent = CH₃CN : H₂O (v/v = 9:1)</p>	<p>Entry 10</p>  <p>Detection Limit¹⁴¹ = 7.67 μM Sensing Solvent = CH₃CN</p>

In nut shell, majority of the developed chemosensors for Hg²⁺ and Li⁺ ions are associated with limitations of multisteps involved in their synthesis, low quantum yields, short emission wavelength, fluorescence quenching, and poor selectivity over other metal ions and inability to detect in aqueous medium.

Thus, we envisioned that appropriately affixing indole moiety to a coumarin nucleus *via* amide bond will produce coumarin-derived indole conjugates that might exhibit interesting and selective sensing behaviour towards Hg²⁺ and Li⁺ metal ions.

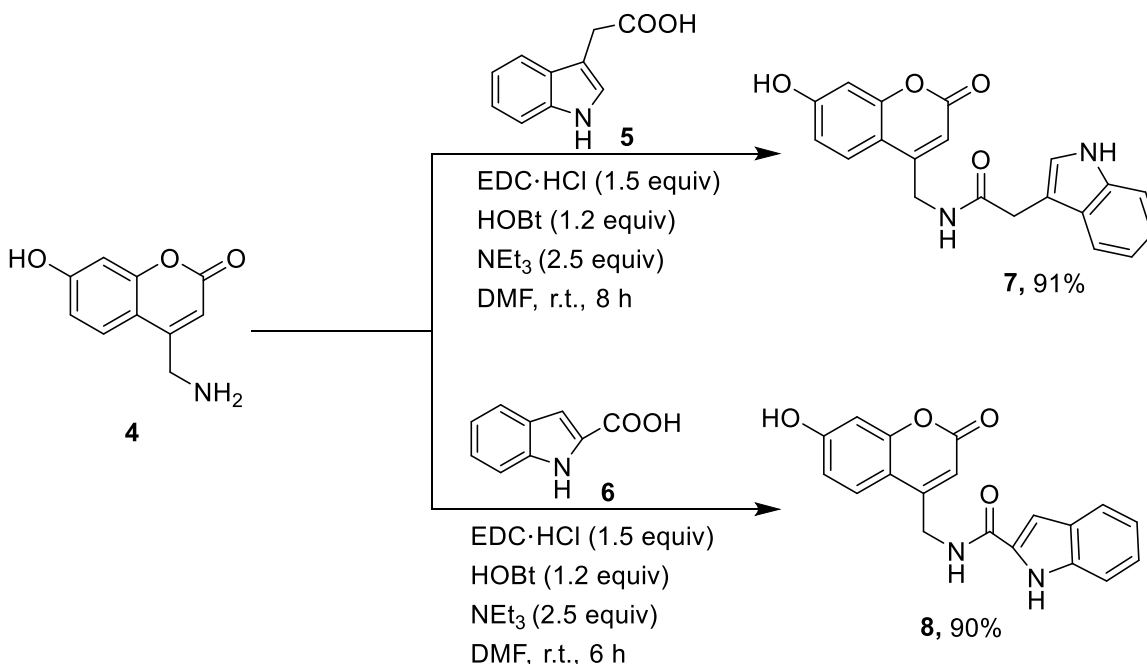
2A.2 Results and Discussion

The desired coumarin indole-based probes were synthesized in straight-forward approach as outlined in schemes 2A.2.1 and 2A.2.2. The synthesis commenced with the reaction of commercially available resorcinol (**1**) with ethyl chloroacetoacetate (**2**) in presence of sulfuric acid at 0–5 °C to afford 4-(chloromethyl)-7-hydroxy-2*H*-chromen-2-one¹⁴² (**3**), which on reaction with 25% ammonium hydroxide at 50 °C for 1 h yielded 7-hydroxy-4-(aminomethyl)coumarin¹⁴³ (**4**) in 80 % yield (Scheme 2A.2.1).



Scheme 2A.2.1: Synthesis of 7-hydroxy-4-(aminomethyl)coumarin (**4**)

Thereafter, the coupling of 7-hydroxy-4-(aminomethyl)coumarin (**4**) with indole-3-acetic acid (**5**) and indole-2-carboxylic acid (**6**) using EDC·HCl/HOBt in DMF at room temperature for 6–8 h yielded indole-based fluorescent probes **7** & **8** in 90–91% yields, respectively (Scheme 2A.2.2).



Scheme 2A.2.2: Synthesis of coumarin-derived indole-based probes (**7** and **8**)

The compounds **7** & **8** were completely characterized by ¹H NMR, ¹³C NMR and high-resolution mass spectrometry.

Spectroscopic measurements (UV–Vis absorption and steady state fluorescence emission) of sensors **7** & **8** were measured in organo-aqueous solution in absence and presence of metal ions at room temperature under ambient conditions. In order to identify an appropriate solvent system, selectivity studies were first performed with a number of solvent systems, including H₂O : CH₃CN, H₂O : THF, H₂O : DMF and H₂O : DMSO. Compound **7** showed good fluorescence efficiency in H₂O : DMF and exhibited a strong absorption band centered at 294 nm, along with a weak hump at 344 nm in H₂O : DMF (7:3, v/v) mixture. On the other hand, compound **8** showed good fluorescence efficiency in H₂O : CH₃CN, and exhibited strong absorption bands centered at 322 nm and 280 nm. On excitation at 340 nm, the probes **7** and **8** gave an emission maxima at 465 nm, with quantum yield of ($\Phi = 0.22$), and ($\Phi = 0.129$) respectively, thereby exhibiting high fluorescence in H₂O : DMF (7:3, v/v) and H₂O : CH₃CN (7:3, v/v) mixture.

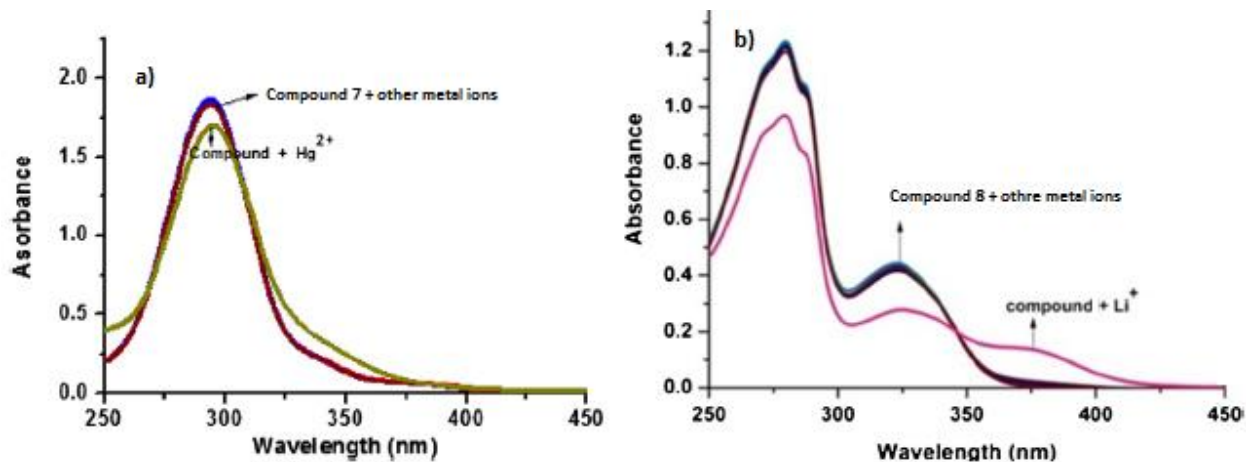


Figure 2A.2.1: UV–Vis spectra of probes: **7** (a) (10^{-4} M) upon addition of 5 equiv of Hg^{2+} and other metal ions and **8** (b) (10^{-4} M) upon addition of 5 equiv of Li^{+} and other metal ions

The binding affinities of the compounds **7** and **8** was next studied towards various metal ions (5 equiv) such as Li^{+} , Ba^{2+} , Al^{3+} , Cd^{2+} , Zn^{2+} , Cr^{3+} , Ni^{2+} , Pb^{2+} , Cu^{2+} , Ca^{2+} , Co^{2+} , Fe^{3+} , Hg^{2+} and K^{+} using UV–Vis absorption measurements. Gratifyingly, a red shift of 3–4 nm was observed in the absorption band of compound **7** at 294 nm along with an attenuation in its intensity upon addition of Hg^{2+} (5 equiv); albeit no change was observed upon addition of other metal ions (Figure 2A.2.1; a). In the UV–Vis spectra of compound **8**, a new red shifted band emerged at 375 nm, when Li^{+} was added (Figure 2A.2.1; b). This could be due to delocalization of electrons on formation of complex between Li^{+} and compound **8**. Moreover, the red-shift could be explained due to the intramolecular charge transfer (ICT) process, and the lowering of the band gap between HOMO

and LUMO on complexation with Li^+ . Importantly, no distinguishable spectral change in the UV–Vis spectrum of compound **8** was observed in the presence of other tested metal ions.

To further explore sensing behavior of probes **7** and **8**, the effect of adding different metal ions (5 equiv) including Li^+ , Ba^{2+} , Al^{3+} , Cd^{2+} , Zn^{2+} , Cr^{3+} , Ni^{2+} , Pb^{2+} , Cu^{2+} , Hg^{2+} , Ca^{2+} , Co^{2+} , Fe^{3+} on the fluorescence spectra of compounds **7** and **8** was investigated. It was observed that the fluorescence spectrum of **7** remains unaffected upon addition of metal ions such as Li^+ , Ba^{2+} , Al^{3+} , Cd^{2+} , Zn^{2+} , Cr^{3+} , Ni^{2+} , Pb^{2+} , Cu^{2+} , Ca^{2+} , Co^{2+} , Fe^{3+} (5 equiv). However, on addition of Hg^{2+} (5 equiv) a dramatic quenching in the fluorescence was observed, which subsequently lead to reduction in quantum yield to 0.05 (Figure 2A.2.2; a). This fluorescence quenching could be due to excitation energy transfer from the probe to the metal d-orbital and/or metal to compound charge transfer. It was worth noticing that the emission intensity of compound **7** was quenched to about ~73% in the presence of Hg^{2+} in $\text{H}_2\text{O} : \text{DMF}$ (7:3, v/v) solvent system. Thus, a clear ‘turn-off’ fluorescence response, with considerably high selectivity towards Hg^{2+} ion in aqueous DMF solution was observed by the indole-based probe **7**. On the other hand, addition of Li^+ (5 equiv) to a solution of probe **8** in $\text{H}_2\text{O} : \text{CH}_3\text{CN}$ showed fluorescence enhancement, and an increase in quantum yield to $\Phi = 0.262$, while addition of metal ions including Ba^{2+} , Pb^{2+} , Ca^{2+} , Ni^{2+} , Cd^{2+} , Cr^{3+} , Al^{3+} , Zn^{2+} , Co^{2+} , Hg^{2+} , Cu^{2+} and Fe^{3+} (5 equiv) did not affect the fluorescence spectra of compound **8** (Figure 2A.2.2; b).

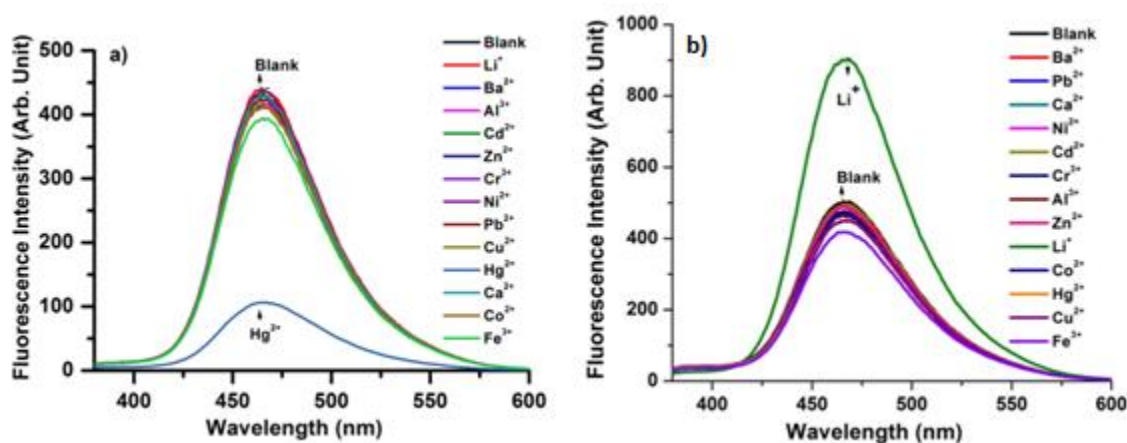


Figure 2A.2.2: Fluorescence spectra of compounds **7** (a) (10^{-4} M) upon addition of metal ions: in $\text{H}_2\text{O} : \text{DMF}$ (7:3, v/v); and **8** (b) (10^{-4} M) upon addition of metal ions: in $\text{H}_2\text{O} : \text{CH}_3\text{CN}$ (7:3, v/v) at $\lambda_{\text{Ex}} = 340$ nm

For an effective sensor, ion-selectivity is a point of concern. To evaluate the selectivity of compounds **7** and **8** toward detecting Hg^{2+} & Li^+ ions over other metal ions respectively, competitive fluorescence experiments were carried out. The fluorescence intensity of solutions containing compound **7** mixed with other common interfering metal ions such as Li^+ , Ba^{2+} , Al^{3+} , Cd^{2+} , Zn^{2+} , Cr^{3+} , Ni^{2+} , Pb^{2+} , Cu^{2+} , Ca^{2+} , Co^{2+} , Fe^{3+} (5 equiv each) in presence and absence of Hg^{2+} (5 equiv) was measured and compared (Figure 2A.2.3; a). The emission intensity of solutions containing different metal ions exhibited high impact in the presence of Hg^{2+} ions (Figure 2A.2.3; a, blue bars), while not much difference in the emission intensity of the solution containing the same metal ion was observed in the absence of Hg^{2+} (Figure 2A.2.3; a, grey bars). Thus, the interference from metal ions was eliminated, and compound **7** displayed high sensitivity to Hg^{2+} . Similarly, to evaluate the selectivity of compound **8** towards Li^+ ions over other metal ions, competitive fluorescence experiments of the Li^+ (5 equiv) solutions mixed with other common interfering metal ions such as Ba^{2+} , Pb^{2+} , Ca^{2+} , Ni^{2+} , Cd^{2+} , Cr^{3+} , Al^{3+} , Zn^{2+} , Co^{2+} , Hg^{2+} , Cu^{2+} , Fe^{3+} , Na^+ and K^+ (5 equiv) were carried out.

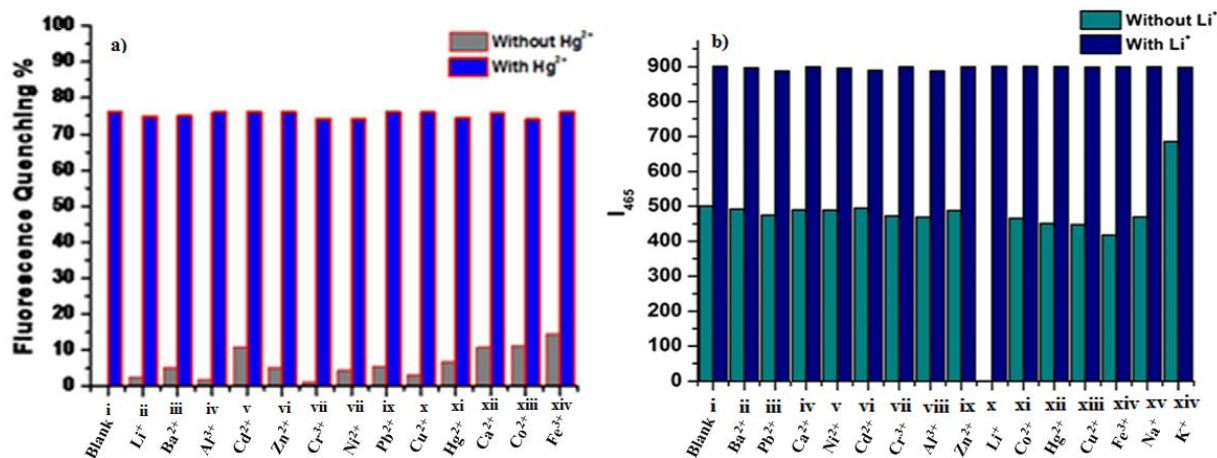


Figure 2A.2.3: Column diagrams of the fluorescence intensity of compounds **7** (a; **7** + metal ions) at 465 nm. Grey bars represent the addition of various metal ions to the blank solution and blue bars represent the subsequent addition of Hg^{2+} (5 equiv) to the above solutions (compound + M^{n+} + Hg^{2+}) and **8** (b; **8** + metal ions) at 465 nm. navy blue bars represent the addition of various metal ions to the blank solution and dark cyan bars represent the subsequent addition of Li^+ (5 equiv) to the above solutions (compound + M^{n+} + Li^+)

In Figure 2A.2.3; b, (navy blue bars), represent the intensity of the emitted radiation in the presence of Li^+ ions in solution together with individual metal ions such as Ba^{2+} , Pb^{2+} , Ca^{2+} , Ni^{2+} , Cd^{2+} , Cr^{3+} , Al^{3+} , Zn^{2+} , Li^+ , Co^{2+} , Hg^{2+} , Cu^{2+} , Fe^{3+} , Na^+ and K^+ that showed high impact on the

emission intensity when compared to the (Figure 2A.2.3; b, dark cyan bars), which corresponds to the emission intensity of a solution of the same metal ion in the absence of Li^+ . The results showed that the fluorescence enhancement of compound **8** was not affected by the competing ions. Therefore compound **8** could be used as highly selective sensor for detection of Li^+ ions in the presence of other common metal ions.

The absorption titration was next performed on compounds **7** and **8** with an incremental addition of Hg^{2+} ions and Li^+ ions, respectively (Figure 2A.2.4). Delightfully, a red shift of 3–4 nm in the absorption band centered at 294 nm, along with attenuation in the intensity of maximum absorption band was observed with a gradual increase of Hg^{2+} ions with compound **7** (Figure 2A.2.4; a). This could be due to intramolecular charge transfer (ICT) effects upon addition of Hg^{2+} and the possibility of complexation between the probe and Hg^{2+} ion. The incremental addition of Li^+ to probe **8** (Figure 2A.2.4; b) lead to a progressive increase in the absorption band around 375 nm in UV–Vis titration spectrum, suggesting that the compound **8** has high sensitivity towards Li^+ ion. The spectral changes with the formation of isosbetic point at 340 nm indicated the formation of single complex species between sensor **8** and Li^+ ion (Figure 2A.2.4; b).

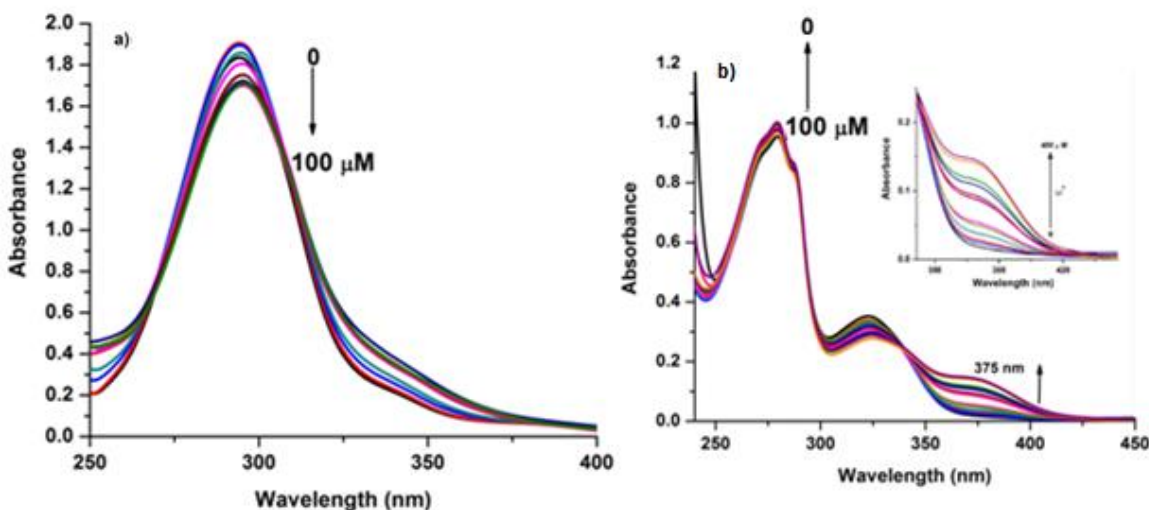


Figure 2A.3.4: UV–Vis titration studies of probes **7** (a) and **8** (b) (10^{-4} M) upon gradual increase in the concentration of Hg^{2+} and Li^+ ions, respectively

The chemosensing properties of compounds **7** and **8** were further investigated by performing fluorescence spectrophotometric titration studies. In fluorescence spectrum, the fluorescence intensity of **7** at $\lambda_{\text{Em}} = 465$ nm was gradually decreased on increasing the concentrations of Hg^{2+}

ion (Figure 2A.2.5; a). While, increasing the concentration of Li^+ leads to a continuous fluorescence enhancement in the fluorescence intensity of **8** around 465 nm (Figure 2A.2.5; b).

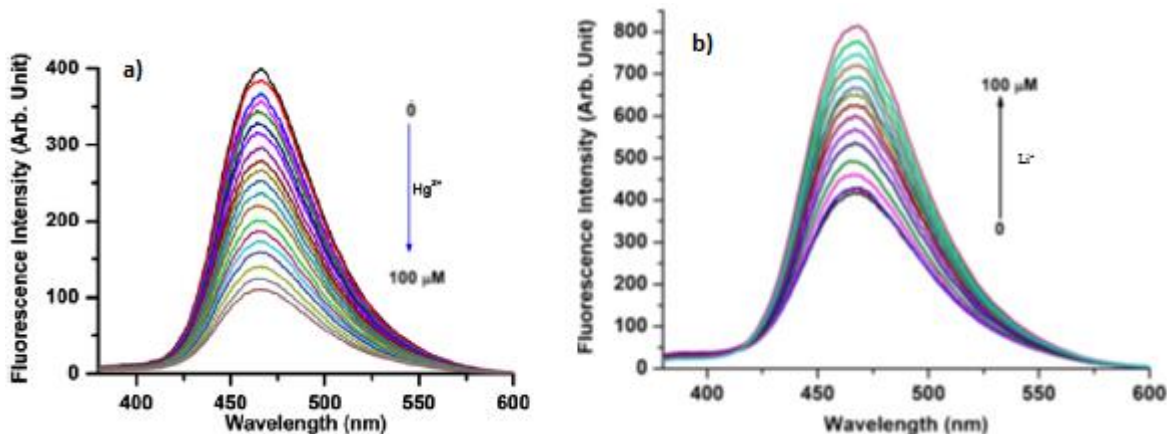


Figure 2A.2.5: Fluorescence titration studies of probes **7** (a) and **8** (b) (10^{-4} M) upon gradual increase in the concentration of Hg^{2+} and Li^+ respectively at $\lambda_{\text{Ex}} = 340$ nm

By using the above fluorescence titration results, the detection limit (DL) was calculated¹⁴⁴⁻¹⁴⁶ to be 143 nM for the compound **7** & 37.1 nM compound **8** for Hg^{2+} and Li^+ ions respectively, based on $3\sigma/m$, where σ corresponds to the standard deviation of the blank measurements, and m is the slope in the plot of the intensity versus the sample concentration (Figure 2A.2.6; a & b).

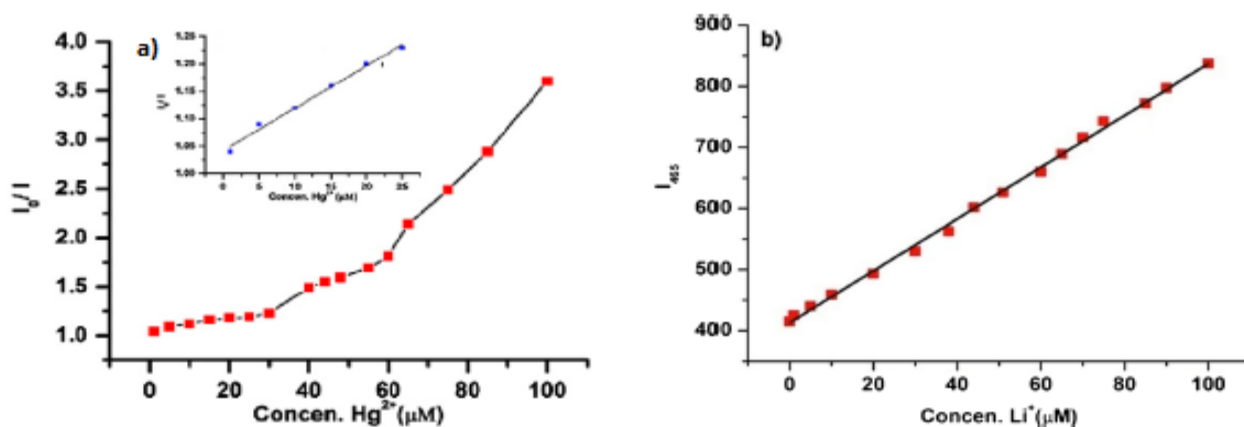


Figure 2A.2.6: Stern–Volmer plot of sensors **7** (a) and **8** (b) in response to Hg^{2+} and Li^+ ions. Inset: Stern–Volmer plot obtained at lower concentration of Hg^{2+} in linear range

Figure 2A.2.6; a & b shows a good linearity between fluorescence intensity at 465 nm emission wavelength and concentrations of Hg^{2+} and Li^+ in the range 0 to 30 μM , for the sensors **7** and **8** respectively. Thus the sensors are capable for nanomolar detection of mercury and lithium ion in organo-aqueous mixtures.

We next constructed the Benesi–Hildebrand plot¹⁴⁷ to investigate the binding stoichiometry and the association constant for the sensors **7** and **8**. The linearity of Benesi–Hildebrand plot (Figure 2A.2.7; a & b) between $1/(F_0 - F_i)$ against $1/[\text{Hg}^{2+}]$ and $1/(F_0 - F_i)$ against $1/[\text{Li}^+]$ indicated 1:1 stoichiometry between sensor **7** and Hg^{2+} ion and **8** and Li^+ ion. The association constant (K_a) was found to be $6.4 \times 10^3 \text{ M}^{-1}$ and $5.5 \times 10^3 \text{ M}^{-1}$ for the probes **7** and **8** respectively, as obtained from Benesi-Hildebrand plot. The high value of association constant (K_a) indicated the formation of a strong complex between Hg^{2+} and **7**, and Li^+ and **8**, respectively.

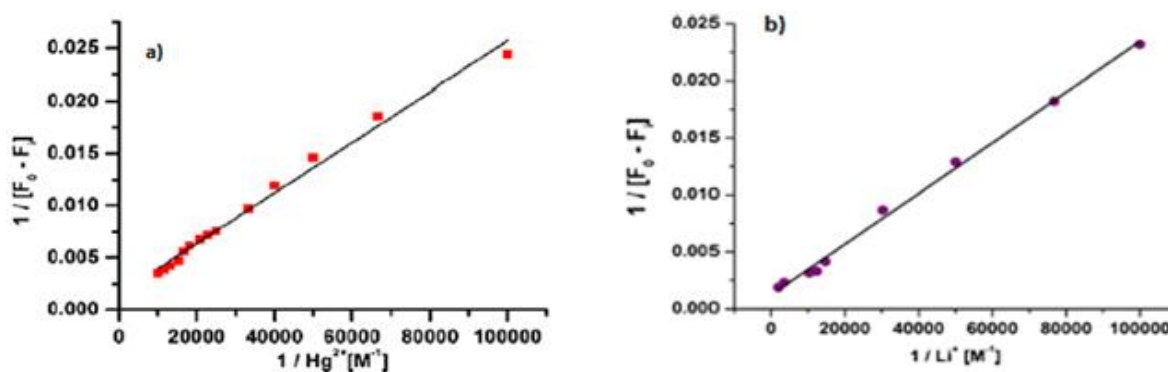


Figure 2A.2.7: Benesi–Hildebrand plot of probes **7** (a) and **8** (b) in response to Hg^{2+} and Li^+ ions

Proposed binding site for metal sensing

Based on spectroscopic measurements, the synthesized coumarin-derived indole-based probes **7** and **8** were found to act as a selective recognition probe for Hg^{2+} and Li^+ ions, respectively. To understand the binding mode of the probes with Hg^{2+} and Li^+ ions, a few other spectroscopic analysis of probes **7** and **8** and its Hg^{2+} -complex and Li^+ -complex were performed. The structural scaffold of the probes provides four binding sites for the metal ions (Hg^{2+} & Li^+) to bind. These includes (a) N-H part of indole ring, (b) N-H group of amidic linkage, (c) C=O unit of the amidic linkage, and (d) C=O of the coumarin moiety. In order to identify the most prominent binding site, ^1H NMR of the synthesized Hg^{2+} -complex (prepared by stirring equimolar quantities of **7** and mercuric chloride under ambient conditions) was compared with that of probe **7** (Figure 2A.2.8; a) An upfield shift in indolic N-H proton by 0.14 ppm and a downfield shift in amidic N-H by 0.33 ppm was observed upon complexation with Hg^{2+} ion, thereby indicating the binding of Hg^{2+} to both indolic and amidic NH, *via* 1:1 stoichiometric ratio. This is also in accordance with Benesi-Hildebrand plot. In addition, slight changes in the chemical shifts of other aromatic protons were also observed, indicating an indirect effect of complexation of Hg^{2+} ion *via* N atoms.^{136,148-}

¹⁵⁰ These findings also indicated that interaction between organic framework and metal ion to be

of non-covalent character.¹³⁶ The selective binding for Hg²⁺ ion to the probe could be a probable outcome of judicious balance between amidic-NH and indolic-NH donor centres, for which Hg²⁺ showed a particular greater affinity¹³⁶ and probably matching of ionic radius of Hg²⁺ with the cavity created between the two nitrogen atoms.

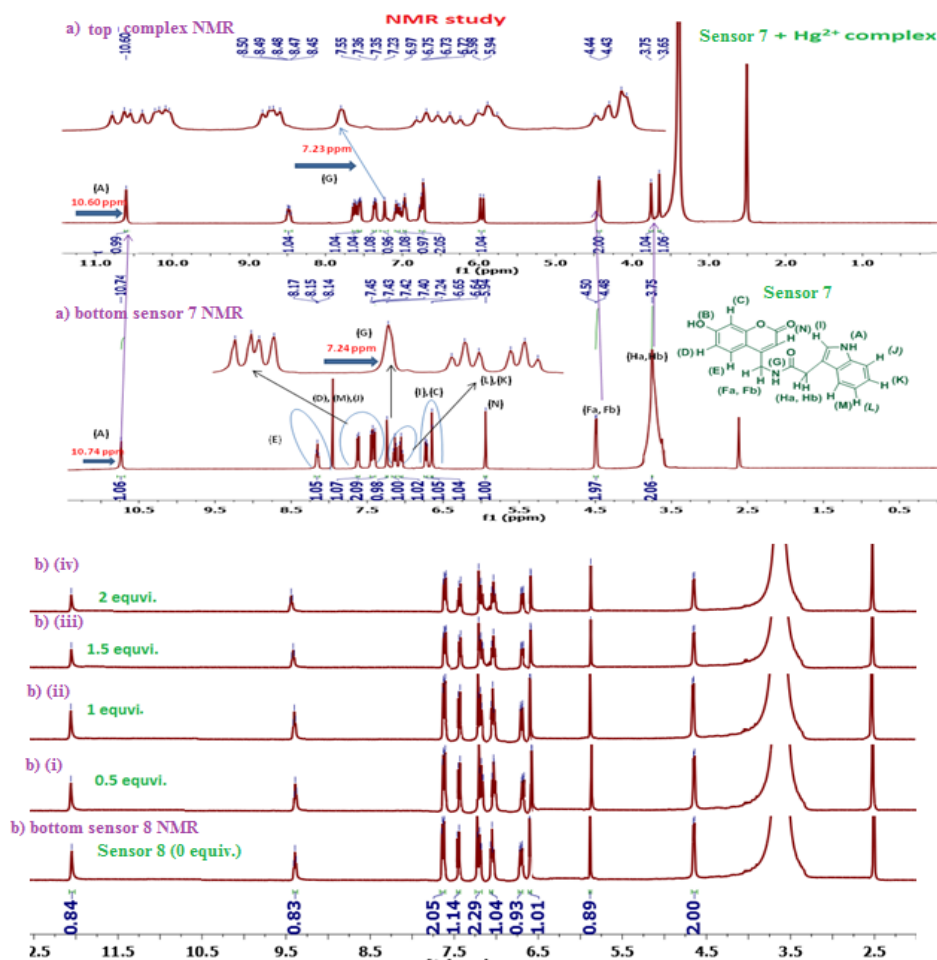


Figure 2A.2.8: ¹H NMR spectra of **7** (a; top) and **7** + its complex (a; bottom) in DMSO-*d*₆, **8** (b; bottom) and in the presence of (b; 0.5-2 equiv) of Li⁺ in DMSO-*d*₆

For compound **8**, ¹H NMR titration experiments were carried out in DMSO-*d*₆ (Figure 2A.2.8; b). The addition of 1 equivalent of lithium salt to the solution of compound **8** in DMSO-*d*₆ led to slight downfield shift in the positions of indolic N-H (0.007 ppm) and amidic NH (0.008 ppm), thereby indicating the possibility of binding Li⁺ to indolic and amidic N-H (Figure 2A.2.8; b). No further change in the ¹H NMR of compound **8** was observed upon adding more than 1 equivalent of Li⁺, thereby confirming 1:1 stoichiometry, as earlier suggested by Benesi-Hildebrand plot. The

results suggested the binding of compound **8** to Li^+ by a rigid conjugation system through interactions with indolic N-H and amide protons.¹³⁶

To further provide a strong support for the proposed binding mechanism, the interaction of Hg^{2+} and Li^+ respectively with the probes **7** and **8** in terms of molecular and electronic level was studied using DFT based modeling technique. Binding energy calculations were performed to determine the most possible binding site of Hg^{2+} and Li^+ in the compounds. The binding energy values corresponding to the binding of Hg^{2+} and Li^+ at the four possible binding sites (mentioned above) were computed. The optimization run for the structure holding Hg^{2+} ion at amide N was not converged after several attempts. So we omitted probable amide N site for Hg^{2+} attachment from our present consideration. It was quite evident from the BE values that the indolic N-atom is the most preferable site for Hg^{2+} ion attachment, followed by coumarin C=O and amide C=O. The calculated binding energy values also suggested a strong interaction between Hg^{2+} ion and probe **7**, and this seems to be a thermodynamically favorable process. Lower electronegativity of nitrogen compared to oxygen could be a possible explanation for higher affinity of Hg^{2+} ion towards the nitrogen site. In addition, it appeared that the binding of Hg^{2+} ion to the compound introduced a large amount of structural strain to the system, and this modulates the physiochemical properties of the probe (Figure 2A.2.9; a). In addition, from the computed BE values (Figure 2A.2.9; b), it became clear that the attachment of Li^+ on the amidic N-H in compound **8** is thermodynamically most preferable (BE = -320.67 kcal/mole). Indeed, the indolic N-H (BE = -220.14 kcal/mole) in compound **8** also appears to be a potential binding site and might be stabilized by some kind of weak interaction (bridging) with the neighboring oxygen of C=O group. However, the computed bond distance values show that the Li is relatively closer to nitrogen compared to the oxygen atom. The Li-N bond length is 1.69 Å⁰ whereas the Li-O is 1.98 Å⁰. So, it can be argued that the bonding between Li-O rather appears to be a weak interaction. It is worth mentioning that the higher binding affinity of Li^+ for amidic N-H is also evident from the experimental spectroscopic data.

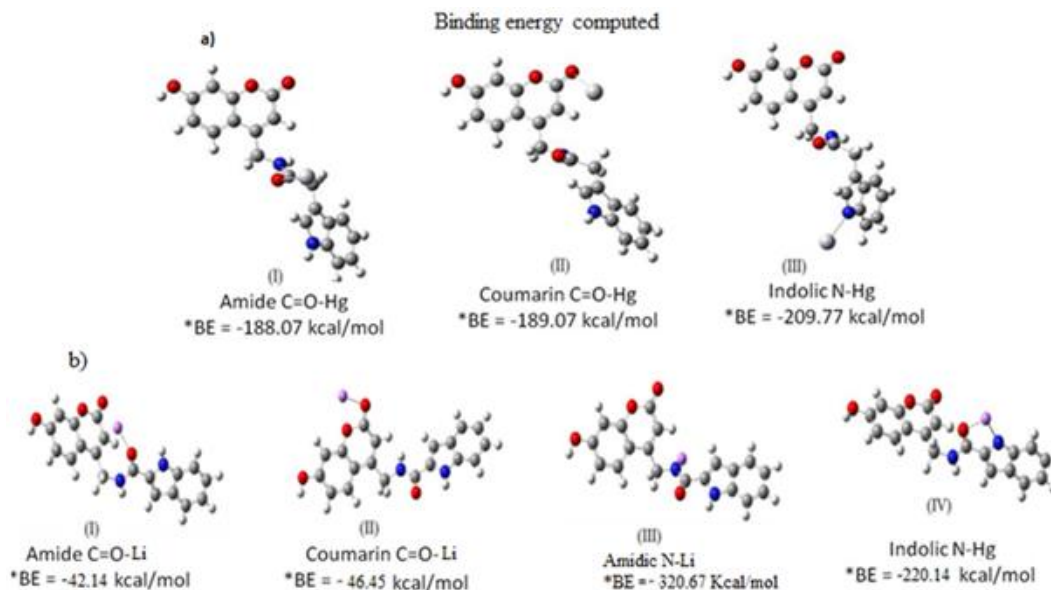


Figure 2A.2.9: Optimize structures of the complex (a; **7** + Hg²⁺) and (b; **8** + Li⁺) at most probable Hg and Li binding sites, and their corresponding binding energy values calculated at B3LYP/6-31+G(d,p): Lan12Dz (for Hg²⁺ and Li⁺) level. The binding energy values are computed as *BE = $E_{\text{complex}} - (E_{\text{compound}} + E_{\text{Hg}})$ / $E_{\text{complex}} - (E_{\text{compound}} + E_{\text{Li}})$

Based on the ¹H NMR studies, Benesi–Hildebrand plots and DFT calculation results, the possible mode of binding for **7** + Hg²⁺ and **8** + Li⁺ is proposed (Figure 2A.2.10; a & b).

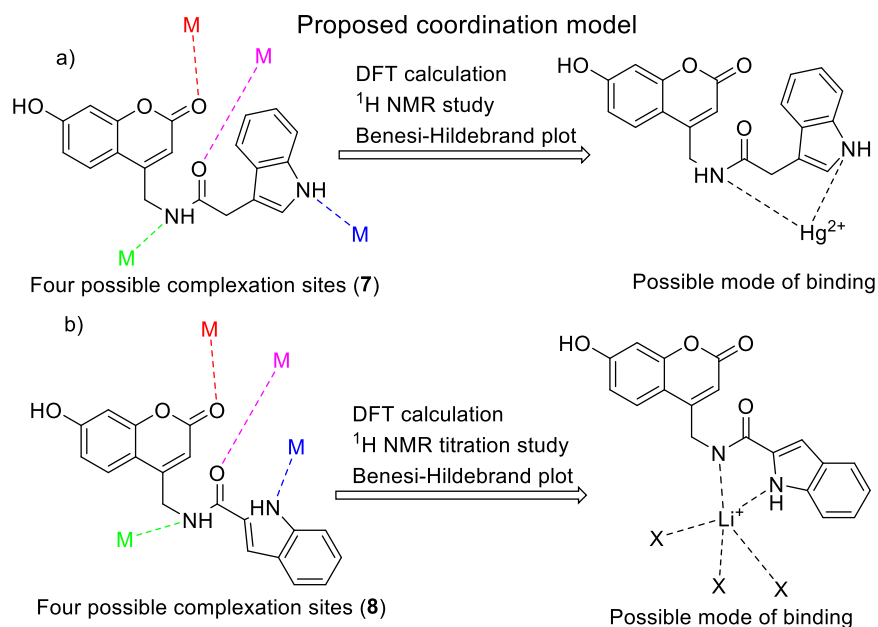


Figure 2A.2.10: Proposed binding site for compounds (a; **7** + Hg²⁺) and (b; **8** + Li⁺)

In summary, two new coumarin-derived indoles-based probes have been synthesized and identified as efficient sensors for selective detection of Hg^{2+} and Li^+ in organo-aqueous media. Detection limit was found to be as low as 143 nM, and 37.1 nM for the sensors **7** and **8** for the Hg^{2+} and Li^+ ions respectively. The most probable binding site of complexing Hg^{2+} and Li^+ was explained on the basis of detailed UV–Vis spectroscopic studies, Benesi–Hildebrand plot, ^1H NMR titration and DFT calculation.

2A.3 Experimental Section

General material and methods

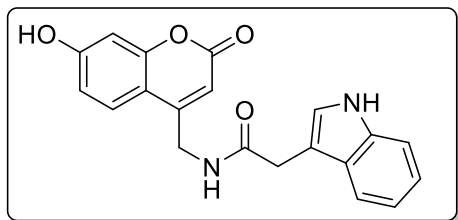
All the chemicals and reagents were purchased from Sigma-Aldrich, Alfa Aesar, and Spectrochem India Pvt. Ltd and used without further purification. Milli-Q water was used in all the experiments. The solvents used were purchased from Merck (India) and were distilled and dried before use. Nuclear Magnetic Resonance (NMR) spectra were recorded on Bruker 400 spectrometer. ^1H NMR spectra were recorded at 25 °C with TMS as the internal reference in δ units, parts per million (ppm), and were measured relative to residual $\text{DMSO}-d_6$ (2.5 ppm) in the deuterated solvent. ^{13}C NMR spectra were reported in ppm relative to ppm [d_6] DMSO (39.5 ppm). All coupling constants J are expressed in Hz. The following abbreviations were used to describe peak splitting patterns when appropriate: s = singlet, d = doublet, t = triplet, dd = doublet of doublet, m = multiplet and brs = broad singlet. High-resolution mass spectrometry (HRMS) was performed with an Agilent 6210 instrument using time-of-flight (TOF-MS) instrument with electro spray ionization (ESI) source. Melting points were determined on a capillary point apparatus equipped with a digital thermometer and are reported uncorrected. Absorption spectra were recorded with the help of dual beam Thermo Evolution 201 UV/Vis/NIR spectrophotometer and fluorescence spectra were recorded with the help of Shimadzu, RF-5301PC Spectrofluorometer. The data were analyzed using related software.

General procedure for the synthesis of coumarin-derived indole-based probes

The starting material, 7-hydroxy-4-(aminomethyl)coumarin (**4**) required for the synthesis was prepared *via* two-step approach according to previously reported procedure (Scheme 2A.2.1).⁸³⁻⁸⁴ To a stirred solution of 7-hydroxy-4-(aminomethyl)coumarin (**4**) (0.300 g, 1.5 mmol, 1 equiv) in DMF, triethyl amine (2.5 equiv) was added dropwise at 0 °C. Thereafter, 2-(1*H*-indol-3-yl)acetic acid (**5**) (0.329 g, 1.8 mmol, 1.2 equiv) or 1*H*-indole-2-carboxylic acid (**6**) (0.303 g, 1.8 mmol, 1.2

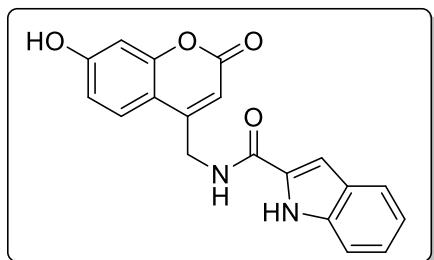
equiv) was added. Subsequently EDC·HCl (0.448 g, 2.3 mmol, 1.5 equiv) and HOBT (0.252 g, 1.8 mmol, 1.2 equiv) were added, and the reaction mixture was stirred under ambient conditions for 6–8 h. The progress of the reaction was monitored by TLC. After the completion of the reaction, crushed ice was added that resulted in the precipitation of the product **7** (or **8**), which was filtrated, washed with cold water and recrystallized from ethanol.

N-((7-Hydroxy-2-oxo-2H-chromen-4-yl)methyl)-2-(1H-indol-3-yl)acetamide (7): Off-white solid; yield: 0.494 g (91%); mp 150–152 °C; ¹H NMR (400 MHz, DMSO-*d*₆) δ 10.74 (s, 1H), 8.15 (t, *J* = 5.6 Hz, 1H), 7.62 (d, *J* = 7.8 Hz, 1H), 7.42 (dd, *J* = 12.9, 8.5 Hz, 2H), 7.24 (s, 1H), 7.13 (t, *J* = 7.5 Hz, 1H), 7.05 (t, *J* = 7.4 Hz, 1H), 6.72 (dd, *J* = 8.8, 2.0 Hz, 1H), 6.65 (d, *J* = 2.1 Hz, 1H),



5.94 (s, 1H), 4.49 (d, *J* = 5.5 Hz, 2H), 3.75 (s, 2H); ¹³C NMR (100 MHz, DMSO-*d*₆) δ 175.5, 171.7, 168.4, 161.6, 156.4, 154.4, 136.6, 127.7, 125.6, 124.4, 121.4, 119.1, 118.8, 115.8, 111.8, 109.0, 104.7, 103.1, 60.3, 33.0; HRMS (ESI-MS) (*m/z*) calculated C₂₀H₁₇N₂O₄⁺: 349.1188; found 349.1196 [M+H]⁺.

N-((7-Hydroxy-2-oxo-2H-chromen-4-yl)methyl)-1H-indole-2-carboxamide (8): White solid; yield: 0.235 g (90%); mp: 232–234 °C; ¹H NMR (400 MHz, DMSO-*d*₆) δ 12.11 (s, 1H), 9.47 (t, *J* = 5.6 Hz, 1H), 7.65 (t, *J* = 8.2 Hz, 2H), 7.47 (d, *J* = 8.2 Hz, 1H), 7.25 (s, 1H), 7.23 – 7.18 (m, 1H), 7.05 (s, 1H), 6.77 (dd, *J* = 8.8, 2.2 Hz, 1H), 6.68 (d, *J* = 2.2 Hz, 1H), 5.93 (s, 1H), 4.67 (d, *J* = 5.3 Hz, 2H); ¹³C



NMR (100 MHz DMSO-*d*₆) δ 166.0, 161.9, 161.4, 156.1, 154.4, 137.2, 131.7, 127.5, 125.8, 124.0, 122.1, 120.3, 115.0, 112.9, 108.4, 106.0, 104.0, 103.1, 56.0; HRMS (ESI-MS) (*m/z*) calculated C₁₉H₁₅N₂O₄⁺: 335.1024; found 335.1039 [M+H]⁺.

General procedure for UV/fluorescence measurements

General procedure for UV/fluorescence measurements

UV/Fluorescence measurements were carried in H₂O : DMF (7:3; v/v) and H₂O: CH₃CN (7:3; v/v) with different metal ions (5 equiv), keeping the concentration of compounds **7** and **8** at 10⁻⁴ M. UV/Fluorescence titrations were carried in H₂O : DMF (7:3; v/v) and H₂O : CH₃CN (7:3; v/v) with gradual increase in the concentration of Hg²⁺ (0 to 100 μM) and Li⁺ (0 to 100 μM) in a micro quartz cuvette. For each addition, at least three

UV/fluorescence spectrums were recorded at 298 K to obtain concordant value. The λ_{Ex} was chosen 340 nm for the compounds, with 3 nm slit width.

Procedure for calculation of quantum yield

The fluorescence quantum yield was determined by using quinine sulphate in 0.1 N sulfuric acid ($\Phi = 0.55$) as the standard reference.¹⁵¹ The quantum yield is calculated using the following equation:¹⁵²

$$\phi_s = \phi_r \frac{F_s A_r \eta_s^2}{F_r A_s \eta_r^2}$$

where A_r and A_s are the absorbance of the 'reference standard' and 'sample' respectively at the excitation wavelength, F_r and F_s are the relative integrated fluorescent intensities (area under the fluorescence curve, peak area) of the reference and samples respectively. η_r and η_s are respectively the refractive indices of the solvents in which the reference standard and samples are prepared.

Computational details

A comprehensive theoretical simulation using sophisticated DFT^{153,154} based method has been performed to understand the relative stability, electronic environment and the photophysical behaviour of the complexes. The DFT based calculations are efficient and reliable computational tools that can provide some useful insights to the experimental findings. In the present work, DFT based calculations were performed using Gaussian09¹⁵⁵ package at B3LYP^{156,157} level (using 6-31+G(d,p) basis sets for (Hg²⁺ & Li⁺) all atoms except Hg). The Hg is defined at effective core potential (ECP) based LanL2DZ basis.^{158,159} In addition, geometry of the sensor **7** (or **8**) along with its different analogues (after attachment of Hg²⁺ & Li⁺) are fully optimized at B3LYP/6-31G(d,p) level.^{160,161} Implicit solvent environment for water has been taken into account under self-consistent reaction field (SCRF)¹⁶² methodology using IEF-PCM¹⁶³ (Integral Equation Formalism- Polarizable Continuum Model) formalism as implemented in Gaussian09 program suit. All the structures were optimized at B3LYP/6-31+G(d,p) level followed by corresponding frequency calculations. Absence of any negative frequencies indicates the global minima for the optimized geometry on potential energy surface. The visual graphics related to the calculations were created using GaussView¹⁶⁴ and Avogadro visualization programs.

2A.4 References

- (1) Pohanka, M.; Pavliš, O.; Skládal, P. *Sensors* **2007**, *7*, 341-353.
- (2) Shamsipur, M.; Asgari, M.; Maragheh, M. G.; Matt, D. *Sensors and Actuators B: Chemical* **2015**, *209*, 9-14.
- (3) Akyildiz, I. F.; Su, W.; Sankarasubramaniam, Y.; Cayirci, E. *IEEE Communications Magazine* **2002**, *40*, 102-114.
- (4) Akyildiz, I. F.; Su, W.; Sankarasubramaniam, Y.; Cayirci, E. *Computer Networks* **2002**, *38*, 393-422.
- (5) Anand, T.; Sivaraman, G.; Chellappa, D. *Journal of Photochemistry and Photobiology A: Chemistry* **2014**, *281*, 47-52.
- (6) Kim, H. N.; Lee, M. H.; Kim, H. J.; Kim, J. S.; Yoon, J. *Chemical Society Reviews* **2008**, *37*, 1465-1472.
- (7) Demchenko, A. P. *Introduction to fluorescence sensing*; Springer Science & Business Media, **2008**.
- (8) Kim, J. S.; Quang, D. T. *Chemical Reviews* **2007**, *107*, 3780-3799.
- (9) Bell, T. W.; Hext, N. M. *Chemical Society Reviews* **2004**, *33*, 589-598.
- (10) Lippincott-Schwartz, J. *Annual Review of Biochemistry* **2011**, *80*, 327-332.
- (11) Mohr, G. J. *Analytical and Bioanalytical Chemistry* **2006**, *386*, 1201-1214.
- (12) De Silva, A. P.; Gunaratne, H. N.; Gunnlaugsson, T.; Huxley, A. J.; McCoy, C. P.; Rademacher, J. T.; Rice, T. E. *Chemical Reviews* **1997**, *97*, 1515-1566.
- (13) Wu, J.; Liu, W.; Ge, J.; Zhang, H.; Wang, P. *Chemical Society Reviews* **2011**, *40*, 3483-3495.
- (14) Xu, Z.; Baek, K.-H.; Kim, H. N.; Cui, J.; Qian, X.; Spring, D. R.; Shin, I.; Yoon, J. *Journal of the American Chemical Society* **2009**, *132*, 601-610.
- (15) Bell, T. W.; Hext, N. M. In *Optical Biosensors*; Elsevier: **2002**, p 331-368.
- (16) Sreenath, K.; Allen, J. R.; Davidson, M. W.; Zhu, L. *Chemical Communications* **2011**, *47*, 11730-11732.
- (17) Trenor, S. R.; Shultz, A. R.; Love, B. J.; Long, T. E. *Chemical Reviews* **2004**, *104*, 3059-3078.
- (18) De Melo, J. S.; Fernandes, P. *Journal of Molecular Structure* **2001**, *565*, 69-78.
- (19) Wang, J.; Qian, X.; Cui, J. *The Journal of Organic Chemistry* **2006**, *71*, 4308-4311.

-
- (20) Valeur, B.; Leray, I. *Coordination Chemistry Reviews* **2000**, *205*, 3-40.
- (21) Quang, D. T.; Kim, J. S. *Chemical Reviews* **2010**, *110*, 6280-6301.
- (22) Sumalekshmy, S.; Fahrni, C. J. *Chemistry of Materials* **2010**, *23*, 483-500.
- (23) Zhao, Y.; Zheng, Q.; Dakin, K.; Xu, K.; Martinez, M. L.; Li, W.-H. *Journal of the American Chemical Society* **2004**, *126*, 4653-4663.
- (24) Felbeck, T.; Hoffmann, K.; Lezhnina, M. M.; Kynast, U. H.; Resch-Genger, U. *The Journal of Physical Chemistry C* **2015**, *119*, 12978-12987.
- (25) Chen, J.; Liu, W.; Zhou, B.; Niu, G.; Zhang, H.; Wu, J.; Wang, Y.; Ju, W.; Wang, P. *The Journal of Organic Chemistry* **2013**, *78*, 6121-6130.
- (26) Chen, J.; Burghart, A.; Derecskei-Kovacs, A.; Burgess, K. *The Journal of Organic Chemistry* **2000**, *65*, 2900-2906.
- (27) Shindy, H. *Dyes and Pigments* **2017**, *145*, 505-513.
- (28) Georgiev, N. I.; Bojinov, V. B.; Nikolov, P. S. *Dyes and Pigments* **2011**, *88*, 350-357.
- (29) Xu, X. T.; Zhang, K.; Du, Z. Y.; Lu, Y. J.; Zhang, R. R.; Zhu, H. In *Advanced Materials Research*; Trans Tech Publ: **2011**; Vol. 236, p 1143-1146.
- (30) Herbert Hall, J.; Chien, J. Y.; Kauffman, J. M.; Litak, P. T.; Adams, J. K.; Henry, R. A.; Hollins, R. A. *Journal of Heterocyclic Chemistry* **1992**, *29*, 1245-1273.
- (31) Kovač, B.; Novak, I. *Spectrochimica Acta Part A: Molecular and Biomolecular Spectroscopy* **2002**, *58*, 1483-1488.
- (32) Wheelock, C. E. *Journal of the American Chemical Society* **1959**, *81*, 1348-1352.
- (33) Upadhyay, K.; Mishra, R. K.; Kumar, V.; Chowdhury, P. R. *Talanta* **2010**, *82*, 312-318.
- (34) Barooah, N.; Mohanty, J.; Pal, H.; Bhasikuttan, A. C. *Organic & Biomolecular Chemistry* **2012**, *10*, 5055-5062.
- (35) Jones, G.; Jackson, W. R.; Choi, C. Y.; Bergmark, W. R. *The Journal of Physical Chemistry* **1985**, *89*, 294-300.
- (36) Jung, Y.; Jung, J.; Huh, Y.; Kim, D. *Journal of Analytical Methods in Chemistry* **2018**, *2018*, 1.
- (37) Brown, M. E.; Gallagher, P. K. *Handbook of thermal analysis and calorimetry: recent advances, techniques and applications*; Elsevier, **2011**; Vol. 5, 1-756.
- (38) Ray, D.; Bharadwaj, P. *Inorganic Chemistry* **2008**, *47*, 2252-2254.

- (39) Wu, J.-S.; Liu, W.-M.; Zhuang, X.-Q.; Wang, F.; Wang, P.-F.; Tao, S.-L.; Zhang, X.-H.; Wu, S.-K.; Lee, S.-T. *Organic Letters* **2007**, *9*, 33-36.
- (40) Yeh, J.-T.; Chen, W.-C.; Liu, S.-R.; Wu, S.-P. *New Journal of Chemistry* **2014**, *38*, 4434-4439.
- (41) Jung, H. S.; Ko, K. C.; Kim, G.-H.; Lee, A.-R.; Na, Y.-C.; Kang, C.; Lee, J. Y.; Kim, J. S. *Organic Letters* **2011**, *13*, 1498-1501.
- (42) Mills, J. H.; Lee, H. S.; Liu, C. C.; Wang, J.; Schultz, P. G. *ChemBioChem* **2009**, *10*, 2162-2164.
- (43) Franzini, R. M.; Kool, E. T. *ChemBioChem* **2008**, *9*, 2981-2988.
- (44) Vasylevska, A. S.; Karasyov, A. A.; Borisov, S. M.; Krause, C. *Analytical and Bioanalytical Chemistry* **2007**, *387*, 2131-2141.
- (45) Saleh, N. i.; Al-Soud, Y. A.; Nau, W. M. *Spectrochimica Acta Part A: Molecular and Biomolecular Spectroscopy* **2008**, *71*, 818-822.
- (46) Zhu, S.; Lin, W.; Yuan, L. *Dyes and Pigments* **2013**, *99*, 465-471.
- (47) Tan, L.; Lin, W.; Zhu, S.; Yuan, L.; Zheng, K. *Organic & Biomolecular Chemistry* **2014**, *12*, 4637-4643.
- (48) Cao, X.; Lin, W.; Yu, Q.; Wang, J. *Organic Letters* **2011**, *13*, 6098-6101.
- (49) Yang, Y.; Huo, F.; Zhang, J.; Xie, Z.; Chao, J.; Yin, C.; Tong, H.; Liu, D.; Jin, S.; Cheng, F. *Sensors and Actuators B: Chemical* **2012**, *166*, 665-670.
- (50) Xu, W.; Teoh, C. L.; Peng, J.; Su, D.; Yuan, L.; Chang, Y.-T. *Biomaterials* **2015**, *56*, 1-9.
- (51) Borisov, S. M.; Klimant, I. *Analytical Chemistry* **2007**, *79*, 7501-7509.
- (52) Wang, X.-d.; Wolfbeis, O. S. *Chemical Society Reviews* **2014**, *43*, 3666-3761.
- (53) Choi, M. G.; Hwang, J.; Moon, J. O.; Sung, J.; Chang, S.-K. *Organic Letters* **2011**, *13*, 5260-5263.
- (54) Cui, L.; Ji, C.; Peng, Z.; Zhong, L.; Zhou, C.; Yan, L.; Qu, S.; Zhang, S.; Huang, C.; Qian, X. *Analytical Chemistry* **2014**, *86*, 4611-4617.
- (55) Chen, J.-B.; Li, B.; Xiong, Y.; Sun, J. *Sensors and Actuators B: Chemical* **2018**, *255*, 275-282.
- (56) Yao, J.; Dou, W.; Qin, W.; Liu, W. *Inorganic Chemistry Communications* **2009**, *12*, 116-118.

- (57) Oliveira, E.; Nunez, C.; Rodríguez-González, B.; Capelo, J. L.; Lodeiro, C. *Inorganic Chemistry* **2011**, *50*, 8797-8807.
- (58) Wang, B.-Y.; Liu, X.-Y.; Ding, S.-L.; Su, Z.-X. *Journal of Polymer Research* **2011**, *18*, 1315-1322.
- (59) Ma, Y.; Luo, W.; Quinn, P. J.; Liu, Z.; Hider, R. C. *Journal of Medicinal Chemistry* **2004**, *47*, 6349-6362.
- (60) Xu, Z.; Liu, X.; Pan, J.; Spring, D. R. *Chemical Communications* **2012**, *48*, 4764-4766.
- (61) Ghosh, K.; Sarkar, T.; Tarafdar, D. *Supramolecular Chemistry* **2012**, *24*, 197-203.
- (62) Tsukamoto, K.; Shinohara, Y.; Iwasaki, S.; Maeda, H. *Chemical Communications* **2011**, *47*, 5073-5075.
- (63) Maity, D.; Govindaraju, T. *Inorganic Chemistry* **2010**, *49*, 7229-7231.
- (64) Jung, H. S.; Kwon, P. S.; Lee, J. W.; Kim, J. I.; Hong, C. S.; Kim, J. W.; Yan, S.; Lee, J. Y.; Lee, J. H.; Joo, T. *Journal of the American Chemical Society* **2009**, *131*, 2008-2012.
- (65) Goswami, S.; Sen, D.; Das, A. K.; Das, N. K.; Aich, K.; Fun, H.-K.; Quah, C. K.; Maity, A. K.; Saha, P. *Sensors and Actuators B: Chemical* **2013**, *183*, 518-525.
- (66) Lau, Y. H.; Rutledge, P. J.; Watkinson, M.; Todd, M. H. *Chemical Society Reviews* **2011**, *40*, 2848-2866.
- (67) Song, Y.; Chen, Z.; Li, H. *Current Organic Chemistry* **2012**, *16*, 2690-2707.
- (68) Silva, A. P.; NimaláGunaratne, H.; MarkáLynch, P.; Glenn, E.; SamankumaraáSandanayake, K. R. A. *Chemical Society Reviews* **1992**, *21*, 187-195.
- (69) White, B. R.; Holcombe, J. A. *Talanta* **2007**, *71*, 2015-2020.
- (70) Prodi, L.; Bolletta, F.; Montalti, M.; Zaccheroni, N. *Coordination Chemistry Reviews* **2000**, *205*, 59-83.
- (71) Pirrone, N.; Cinnirella, S.; Feng, X.; Finkelman, R. B.; Friedli, H. R.; Leaner, J.; Mason, R.; Mukherjee, A. B.; Stracher, G. B.; Streets, D. G. *Atmospheric Chemistry and Physics* **2010**, *10*, 5951-5964.
- (72) Li, Y.; Wu, C.-Y. *Environmental Science & Technology* **2006**, *40*, 6444-6448.
- (73) Girginova, P. I.; Daniel-da-Silva, A. L.; Lopes, C. B.; Figueira, P.; Otero, M.; Amaral, V. S.; Pereira, E.; Trindade, T. *Journal of Colloid and Interface Science* **2010**, *345*, 234-240.
- (74) Gutknecht, J. *The Journal of Membrane Biology* **1981**, *61*, 61-66.

- (75) Tchounwou, P. B.; Ayensu, W. K.; Ninashvili, N.; Sutton, D. *Environmental Toxicology: An International Journal* **2003**, *18*, 149-175.
- (76) Davidson, P. W.; Myers, G. J.; Cox, C.; Shamlaye, C. F.; Marsh, D. O.; Tanner, M. A.; Berlin, M.; Sloane-Reeves, J.; Cernichiari, E.; Choisy, O. *Neurotoxicology* **1995**, *16*, 677-688.
- (77) Clarkson, T. W.; Magos, L. *Critical Reviews in Toxicology* **2006**, *36*, 609-662.
- (78) Harris, H. H.; Pickering, I. J.; George, G. N. *Science* **2003**, *301*, 1203-1203.
- (79) Ferrara, R.; Mazzolai, B.; Lanzillotta, E.; Nucaro, E.; Pirrone, N. *Science of the Total Environment* **2000**, *259*, 115-121.
- (80) Ding, J.; Li, H.; Wang, C.; Yang, J.; Xie, Y.; Peng, Q.; Li, Q.; Li, Z. *ACS Applied Materials & Interfaces* **2015**, *7*, 11369-11376.
- (81) Wang, H.-H.; Xue, L.; Yu, C.-L.; Qian, Y.-Y.; Jiang, H. *Dyes and Pigments* **2011**, *91*, 350-355.
- (82) Nolan, E. M.; Lippard, S. J. *Journal of the American Chemical Society* **2003**, *125*, 14270-14271.
- (83) Wang, J.; Ma, M.; Huang, R.; Wang, L.; Chen, A.; Hu, J. *Analytical Methods* **2015**, *7*, 2295-2299.
- (84) Dhir, A.; Bhalla, V.; Kumar, M. *Organic Letters* **2008**, *10*, 4891-4894.
- (85) Huang, C.-B.; Li, H.-R.; Luo, Y.; Xu, L. *Dalton Transactions* **2014**, *43*, 8102-8108.
- (86) Mahapatra, A. K.; Roy, J.; Sahoo, P.; Mukhopadhyay, S. K.; Chattopadhyay, A. *Organic & Biomolecular Chemistry* **2012**, *10*, 2231-2236.
- (87) Song, K.-C.; Kim, M. H.; Kim, H. J.; Chang, S.-K. *Tetrahedron Letters* **2007**, *48*, 7464-7468.
- (88) Dai, H.; Liu, F.; Gao, Q.; Fu, T.; Kou, X. *Luminescence* **2011**, *26*, 523-530.
- (89) Pal, S.; Hatai, J.; Samanta, M.; Shaurya, A.; Bandyopadhyay, S. *Organic & Biomolecular Chemistry* **2014**, *12*, 1072-1078.
- (90) Liu, R.-L.; Lu, H.-Y.; Li, M.; Hu, S.-Z.; Chen, C.-F. *RSC Advances* **2012**, *2*, 4415-4420.
- (91) Grieshaber, D.; MacKenzie, R.; Voeroes, J.; Reimhult, E. *Sensors* **2008**, *8*, 1400-1458.
- (92) Wagh, Y. B.; Kuwar, A.; Sahoo, S. K.; Gallucci, J.; Dalal, D. S. *RSC Advances* **2015**, *5*, 45528-45534.

- (93) Shi, L.; Song, W.; Li, Y.; Li, D.-W.; Swanick, K. N.; Ding, Z.; Long, Y.-T. *Talanta* **2011**, *84*, 900-904.
- (94) Kaur, N.; Kaur, B. *Spectrochimica Acta Part A: Molecular and Biomolecular Spectroscopy* **2017**, *181*, 60-64.
- (95) Descalzo, A. B.; Martínez-Máñez, R.; Radeaglia, R.; Rurack, K.; Soto, J. *Journal of the American Chemical Society* **2003**, *125*, 3418-3419.
- (96) Shi, B.; Zhang, P.; Wei, T.; Yao, H.; Lin, Q.; Liu, J.; Zhang, Y. *Tetrahedron* **2013**, *69*, 7981-7987.
- (97) Wei, T.; Li, J.; Bai, C.; Lin, Q.; Yao, H.; Xie, Y.; Zhang, Y. *Science China Chemistry* **2013**, *56*, 923-927.
- (98) Voutsadaki, S.; Tsikalas, G. K.; Klontzas, E.; Froudakis, G. E.; Katerinopoulos, H. E. *Chemical Communications* **2010**, *46*, 3292-3294.
- (99) El-Shekheby, H. A.; Mangood, A. H.; Hamza, S. M.; Al-Kady, A. S.; Ebeid, E. Z. M. *Luminescence* **2014**, *29*, 158-167.
- (100) Wu, C.; Wang, J.; Shen, J.; Bi, C.; Zhou, H. *Sensors and Actuators B: Chemical* **2017**, *243*, 678-683.
- (101) Ho, I.-T.; Lai, T.-L.; Wu, R.-T.; Tsai, M.-T.; Wu, C.-M.; Lee, G.-H.; Chung, W.-S. *Analyst* **2012**, *137*, 5770-5776.
- (102) Gao, B.; Gong, W.-T.; Zhang, Q.-L.; Ye, J.-W.; Ning, G.-L. *Sensors and Actuators B: Chemical* **2012**, *162*, 391-395.
- (103) Gao, Y.; Zhang, C.; Peng, S.; Chen, H. *Sensors and Actuators B: Chemical* **2017**, *238*, 455-461.
- (104) Jiao, Y.; Zhou, L.; He, H.; Yin, J.; Duan, C. *Talanta* **2017**, *162*, 403-407.
- (105) Hande, P. E.; Samui, A. B.; Kulkarni, P. S. *Sensors and Actuators B: Chemical* **2017**, *246*, 597-605.
- (106) Bach, R. O. *Lithium, current applications in science, medicine, and technology*; Wiley-Interscience, **1985**, 1-422.
- (107) Yin, J.; Hu, Y.; Yoon, J. *Chemical Society Reviews* **2015**, *44*, 4619-4644.
- (108) Strobel, P.; Thiery, F.; Darie, C.; Proux, O.; Ibarra-Palos, A.; Bacia, M.; Soupart, J. *Journal of Materials Chemistry* **2005**, *15*, 4799-4808.
- (109) Jope, R. *Molecular Psychiatry* **1999**, *4*, 117.

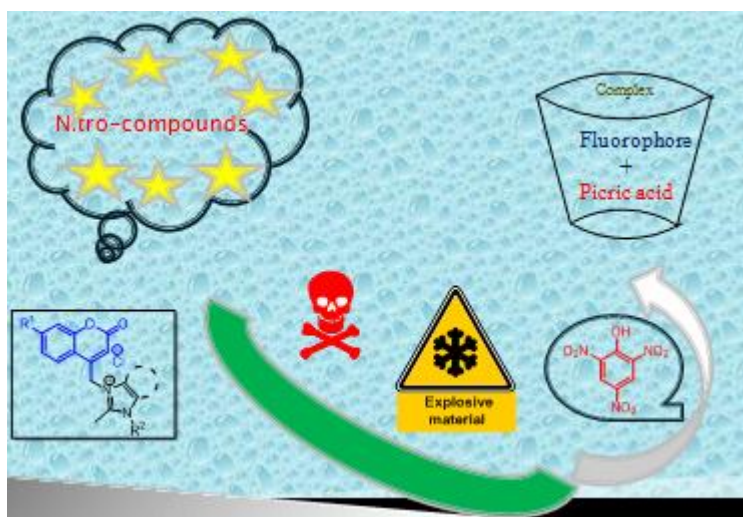
- (110) Manji, H. K.; Potter, W. Z.; Lenox, R. H. *Archives of General Psychiatry* **1995**, *52*, 531-543.
- (111) Gunnlaugsson, T.; Bichell, B.; Nolan, C. *Tetrahedron Letters* **2002**, *43*, 4989-4992.
- (112) Benco, J. S.; Nienaber, H. A.; McGimpsey, W. G. *Journal of Photochemistry and Photobiology A: Chemistry* **2004**, *162*, 289-296.
- (113) Kim, S.-H.; Han, S.-K.; Park, S.-H.; Yoon, C.-M.; Keum, S.-R. *Dyes and Pigments* **1999**, *43*, 21-25.
- (114) Caballero, A.; Tormos, R.; Espinosa, A.; Velasco, M. D.; Tárraga, A.; Miranda, M. A.; Molina, P. *Organic Letters* **2004**, *6*, 4599-4602.
- (115) Kaur, G.; Singh, A.; Venugopalan, P.; Kaur, N.; Singh, N. *RSC Advances* **2016**, *6*, 1792-1799.
- (116) Tabata, M.; Nishimoto, J.; Kusano, T. *Talanta* **1998**, *46*, 703-709.
- (117) Nakane, Y.; Takeda, T.; Hoshino, N.; Sakai, K.-I.; Akutagawa, T. *The Journal of Physical Chemistry A* **2015**, *119*, 6223-6231.
- (118) Citterio, D.; Takeda, J.; Kosugi, M.; Hisamoto, H.; Sasaki, S.-I.; Komatsu, H.; Suzuki, K. *Analytical Chemistry* **2007**, *79*, 1237-1242.
- (119) Taziaux, D.; Soumillion, J.-P.; Jiwan, J.-L. H. *Journal of Photochemistry and Photobiology A: Chemistry* **2004**, *162*, 599-607.
- (120) Hamilton, G. R.; Sahoo, S. K.; Kamila, S.; Singh, N.; Kaur, N.; Hyland, B. W.; Callan, J. F. *Chemical Society Reviews* **2015**, *44*, 4415-4432.
- (121) Rochat, S.; Grote, Z.; Severin, K. *Organic & Biomolecular Chemistry* **2009**, *7*, 1147-1153.
- (122) Kar, C.; Adhikari, M. D.; Ramesh, A.; Das, G. *Inorganic Chemistry* **2013**, *52*, 743-752.
- (123) Ma, L.-J.; Liu, Y.-F.; Wu, Y. *Chemical Communications* **2006**, 2702-2704.
- (124) Rocha, A.; Marques, M. M. B.; Lodeiro, C. *Tetrahedron Letters* **2009**, *50*, 4930-4933.
- (125) Pathak, S.; Das, D.; Kundu, A.; Maity, S.; Guchhait, N.; Pramanik, A. *RSC Advances* **2015**, *5*, 17308-17318.
- (126) Jose, D. A.; Kumar, D. K.; Ganguly, B.; Das, A. *Organic Letters* **2004**, *6*, 3445-3448.
- (127) Bose, P.; Ghosh, P. *Chemical Communications* **2010**, *46*, 2962-2964.
- (128) Vázquez, M.; Fabbrizzi, L.; Taglietti, A.; Pedrido, R. M.; González-Noya, A. M.; Bermejo, M. R. *Angewandte Chemie International Edition* **2004**, *43*, 1962-1965.
- (129) Fabian, J.; Nakazumi, H.; Matsuoka, M. *Chemical Reviews* **1992**, *92*, 1197-1226.

- (130) Wu, P.; Brand, L. *Analytical Biochemistry* **1994**, *218*, 1-13.
- (131) Boiocchi, M.; Del Boca, L.; Gómez, D. E.; Fabbrizzi, L.; Licchelli, M.; Monzani, E. *Journal of the American Chemical Society* **2004**, *126*, 16507-16514.
- (132) Long, L.; Tan, X.; Luo, S.; Shi, C. *New Journal of Chemistry* **2017**, *41*, 8899-8904.
- (133) Liu, H.; Ding, H.; Zhu, L.; Wang, Y.; Chen, Z.; Tian, Z. *Journal of Fluorescence* **2015**, *25*, 1259-1266.
- (134) Tang, Y.; Jiang, G.-F. *Tetrahedron Letters* **2017**, *58*, 2846-2849.
- (135) Gao, X.; Wu, W.; Xi, J.; Zheng, H. *RSC Advances* **2017**, *7*, 32732-32736.
- (136) Sun, Y.-L.; Wu, A.-T. *Journal of Fluorescence* **2013**, *23*, 629-634.
- (137) Huang, H.-J.; Chir, J.-L.; Cheng, H.-J.; Chen, S.-J.; Hu, C.-H.; Wu, A.-T. *Journal of Fluorescence* **2011**, *21*, 1021-1026.
- (138) Kaur, N.; Kaur, P.; Bhatia, G.; Singh, K.; Singh, J. *RSC Advances* **2016**, *6*, 82810-82816.
- (139) Kaur, P.; Kaur, S.; Singh, K.; Sharma, P. R.; Kaur, T. *Dalton Transactions* **2011**, *40*, 10818-10821.
- (140) Dar, A. A.; Dwivedi, A. K.; Iyer, P. K.; Khan, A. T. *Asian Journal of Green Chemistry* **2018**, *2*, 171-180.
- (141) Kaur, P.; Kaur, S.; Singh, K. *Organic & Biomolecular Chemistry* **2012**, *10*, 1497-1501.
- (142) Lin, W.; Long, L.; Feng, J.; Wang, B.; Guo, C. *European Journal of Organic Chemistry* **2007**, *2007*, 4301-4304.
- (143) Onderwater, R. C.; Venhorst, J.; Commandeur, J. N.; Vermeulen, N. P. *Chemical Research in Toxicology* **1999**, *12*, 555-559.
- (144) Neupane, L. N.; Kim, J. M.; Lohani, C. R.; Lee, K.-H. *Journal of Materials Chemistry* **2012**, *22*, 4003-4008.
- (145) Yang, M.-H.; Thirupathi, P.; Lee, K.-H. *Organic Letters* **2011**, *13*, 5028-5031.
- (146) Zhang, F.; Wang, L.; Chang, S.-H.; Huang, K.-L.; Chi, Y.; Hung, W.-Y.; Chen, C.-M.; Lee, G.-H.; Chou, P.-T. *Dalton Transactions* **2013**, *42*, 7111-7119.
- (147) Benesi, H. A.; Hildebrand, J. *Journal of the American Chemical Society* **1949**, *71*, 2703-2707.
- (148) El-Nahass, M. N.; El-Aziz, D. M. A.; Fayed, T. A. *Sensors and Actuators B: Chemical* **2014**, *205*, 377-390.

- (149) Chauhan, K.; Singh, P.; Singhal, R. K. *ACS Applied Materials & Interfaces* **2015**, *7*, 26069-26078.
- (150) Chen, L.; Yang, L.; Li, H.; Gao, Y.; Deng, D.; Wu, Y.; Ma, L.-J. *Inorganic Chemistry* **2011**, *50*, 10028-10032.
- (151) Mishra, H.; Pant, S.; Tripathi, H. B. *Journal of Fluorescence* **2008**, *18*, 17-27.
- (152) Ranjith, C.; Vijayan, K.; Praveen, V. K.; Kumar, N. S. *Spectrochimica Acta Part A: Molecular and Biomolecular Spectroscopy* **2010**, *75*, 1610-1616.
- (153) Parr, R. G.; Yang, W.; Oxford University Press, **1989**, 1-325.
- (154) Kohn, W.; Sham, L. *Physical Review* **1965**, *137*, A1697.
- (155) Frisch, M.; Trucks, G.; Schlegel, H. B.; Scuseria, G. E.; Robb, M. A.; Cheeseman, J. R.; Scalmani, G.; Barone, V.; Mennucci, B.; Petersson, G. *Inc., Wallingford, CT* **2009**, 200.
- (156) Becke, A. D. *The Journal of Chemical Physics* **1993**, *98*, 5648-5652.
- (157) Lee, C.; Yang, W.; Parr, R. G. *Physical Review B* **1988**, *37*, 785-789.
- (158) Frisch, M. J.; Trucks, G.; Schlegel, H. B.; Scuseria, G.; Robb, M.; Cheeseman, J.; Scalmani, G.; Barone, V.; Mennucci, B.; Petersson, G. *Gaussian Inc. Wallingford CT* **2009**, 27, 34.
- (159) Zhao, Y.; Schultz, N. E.; Truhlar, D. G. *Journal of Chemical Theory and Computation* **2006**, *2*, 364-382.
- (160) Zhao, Y.; Truhlar, D. G. *Theoretical Chemistry Accounts* **2008**, *120*, 215-241.
- (161) Schäfer, A.; Huber, C.; Ahlrichs, R. *The Journal of Chemical Physics* **1994**, *100*, 5829-5835.
- (162) Xu, X.; Truhlar, D. G. *Journal of Chemical Theory and Computation* **2011**, *7*, 2766-2779.
- (163) Miertuš, S.; Scrocco, E.; Tomasi, J. *Chemical Physics* **1981**, *55*, 117-129.
- (164) Miertus, S.; Tomasi, J. *Chemical Physics* **1982**, *65*, 239-245.

Chapter 2B

Coumarin-derived Sensors for Picric Acid Detection: Synthesis, Experimental and Theoretical Investigations



2B.1 Introduction

Development of cost-efficient, selective, portable, fast, and sensitive methods for the detection of explosives has attracted great research interest in recent years.¹⁻³ These explosives include nitro-aromatics, nitro-amines, nitrate-esters, and peroxides.⁴ In particular, nitro-aromatic compounds (NACs) are constituents of many unexploded land mines and explosives used for terrorism and criminal activities, and thus a result of exhaustive environmental pollution. Some selective examples of explosive nitro-aromatic compounds are shown in Figure 2B.1.1. Among these nitro-aromatic compounds (NACs), 2,4-dinitrotoluene, 2,4,6-trinitrotoluene, and picric acid (PA), are warfare explosives and toxic pollutants.⁵

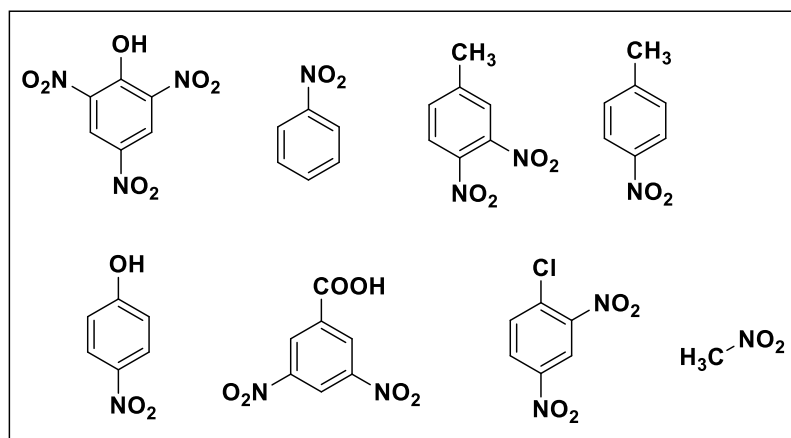


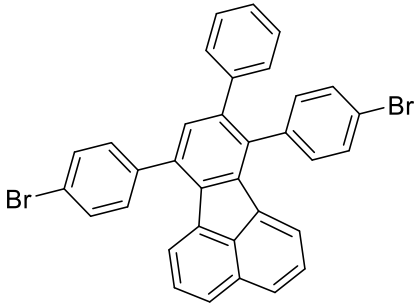
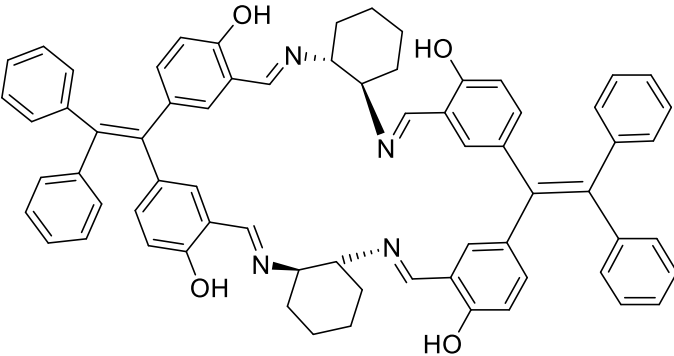
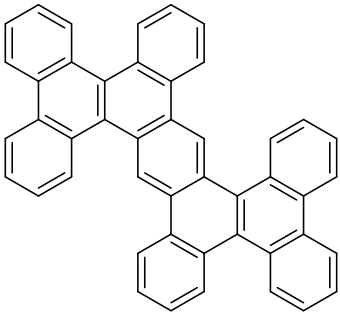
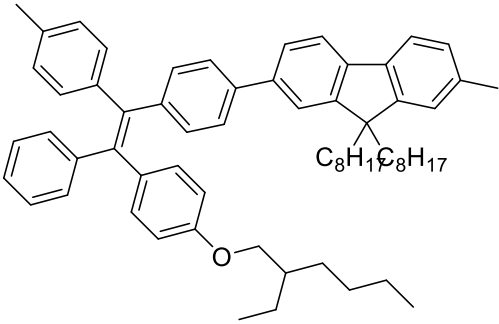
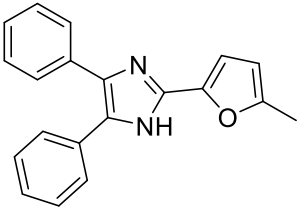
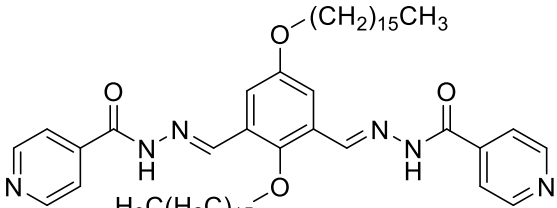
Figure 2B.1.1: Selective examples of nitro-aromatic compounds (NACs)

Among these NACs, picric acid (PA), whose explosive power is even higher than that of TNT, is well-known for its explosive, poisonous and carcinogenic behavior.^{6,7} In spite of these characteristic behavior and high water-solubility, its continued excessive use in pharmaceuticals, leather and dye industries, and in the manufacture of rocket fuel and fireworks and matches has led to an inevitable contamination of soil and ground-water.^{8,9} In addition, picric acid contamination damages the skin, eyes, and cause organ rupturing in the respiratory system of human beings and wildlife.¹⁰⁻¹² Picramic acid, a product obtained during metabolic process of picric acid possess about ten times more mutagenic activity than PA.¹³ Thus, detection of picric acid is of significant concern for national security, battlefield protection, and industrial and environmental safety control.¹⁴

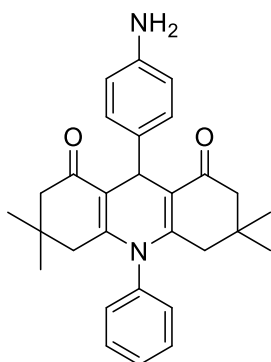
Among various methods employed for picric acid detection, fluorescence sensing is widely employed because of its high sensitivity, quick response, easy sample preparation, *etc.*

Even though versatile π -electron-rich fluorescent organic molecules,¹⁵ polymers,¹⁶⁻¹⁹ metal-organic architectures²⁰⁻²³ self-assemblies,^{24,25} nanoaggregates,²⁶⁻²⁹ *etc.* have been employed to detect the presence of electron-deficient nitro-aromatics, especially picric acid. Some selective examples of fluorescent chemosensors used for detection of picric acid are summarized in Table 2B.1.1.^{19,24,25,29-38}

Table 2B.1.1: Selective examples of chemosensors used for picric acid sensing

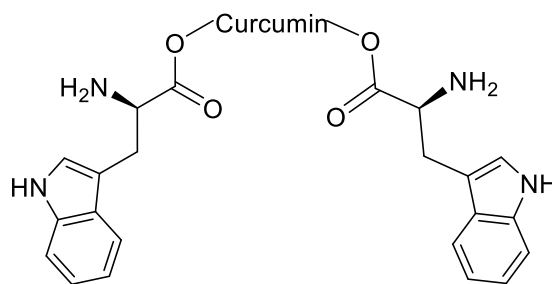
<p>Entry 1</p>  <p>Sensing Solvent³⁰ = EtOH</p>	<p>Entry 2</p>  <p>Detection Limit²⁹ = 5 nM Sensing Solvent = H₂O : THF (v/v = 9:1)</p>
<p>Entry 3</p>  <p>Detection Limit²⁵ = 300 ppb Sensing Solvent = H₂O : THF (v/v = 9:1)</p>	<p>Entry 4</p>  <p>Detection Limit¹⁹ = 2 ppb Sensing Solvent = H₂O</p>
<p>Entry 5</p>  <p>Detection Limit³¹ = 684 ppb Sensing Solvent = DMSO</p>	<p>Entry 6</p>  <p>Detection Limit³² = 11 nM Sensing Solvent = H₂O</p>

Entry 7



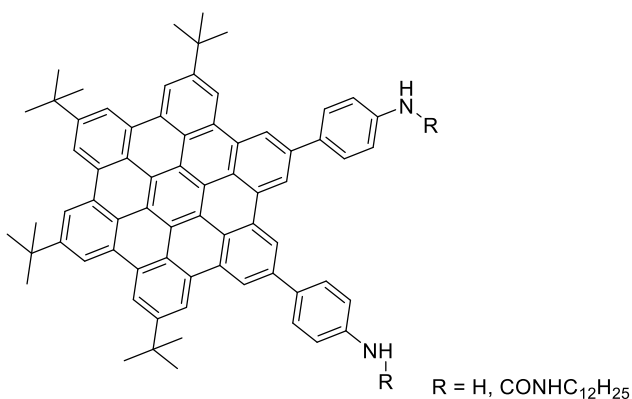
Detection Limit³³ = 2.4 μ M
Sensing Solvent = MeOH

Entry 8



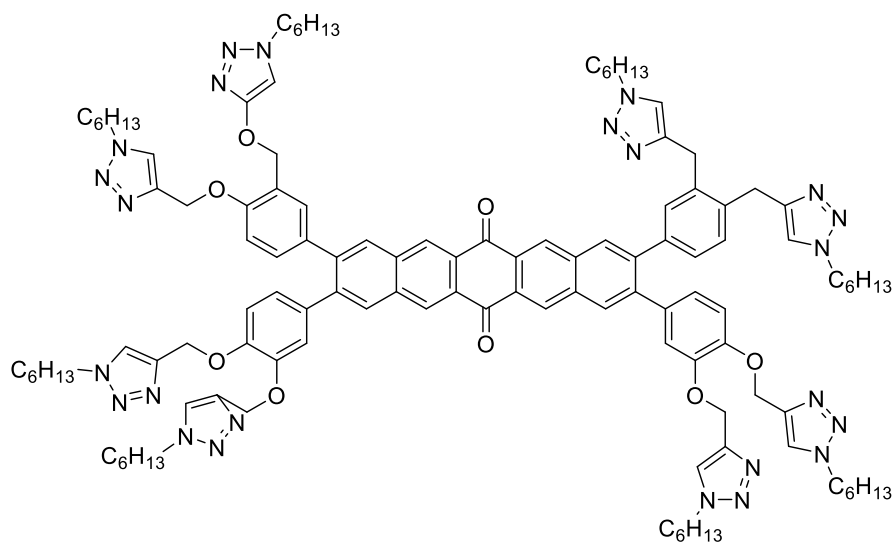
Detection Limit³⁴ = 13.51 nM
Sensing Solvent = H₂O

Entry 9

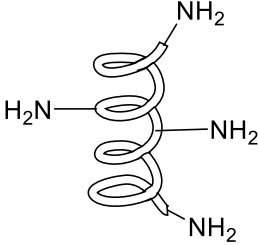
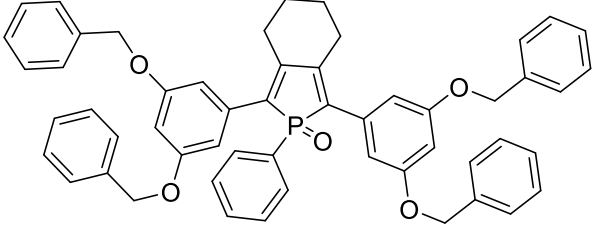


Detection Limit³⁵ = 4 nM & 9 nM
Sensing Solvent = H₂O : THF (v/v = 4:6)

Entry 10



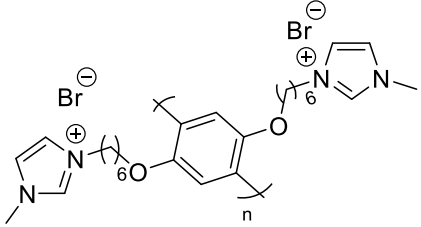
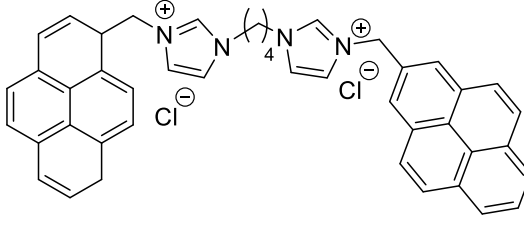
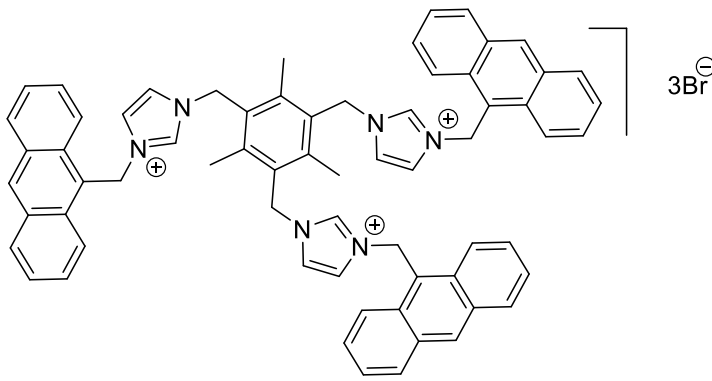
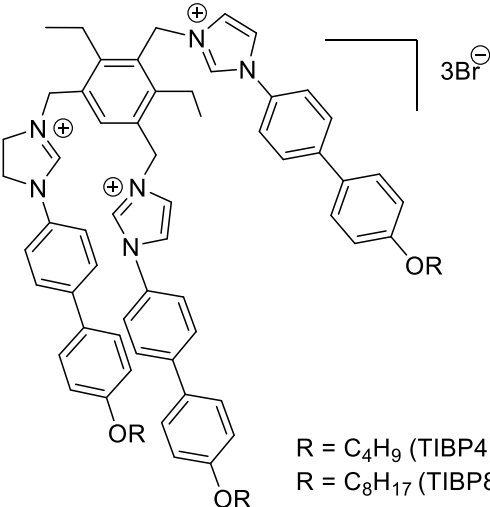
Detection Limit³⁶ = 350 nM
Sensing Solvent = Toluene : DCM (v/v = 8:2)

<p>Entry 11</p>  <p>Bovine serum albumin (BSA)</p> <p>Detection Limit³⁷ = 17.2 nM</p> <p>Sensing Solvent = H₂O</p>	<p>Entry 12</p>  <p>Detection Limit³⁸ = 2.03 mM</p> <p>Sensing Solvent = THF : H₂O (v/v = 9:1)</p>
---	--

In spite of much progress, most of the reported chemosensors suffer from the drawbacks associated by the interference from other nitro-aromatic compounds such as nitrotoluene (NT), dinitrotoluene (DNT), and nitrobenzene (NB). Also, most of the reported sensors detect explosives in organic solvents, and their sensing performance gets degraded when applied to aqueous medium. This is highly desirable as sensing of picric acid and other nitro-aromatic explosives in soil/groundwater is essential for locating unexploded material in buried landmines/underwater mines, and for determining ground-water contamination at war sites and military bases.³⁹ Thus, detection of picric acid at very low concentrations in aqueous medium by suitable water-soluble chemosensors in high selectivity is highly desirable.

Among various heterocyclic architectures, imidazolium salts have been extensively studied as ionic liquids, soluble supports, scavengers, *N*-heterocyclic carbene (NHC) precursors, fluorescent protein tags⁴⁰⁻⁴⁴ and chemosensors for anions and biomolecules detection.^{45,46} However, very few imidazolium-based sensors have been explored towards selective sensing of picric acid and other nitro-explosives.⁴⁷⁻⁴⁹ One such example was reported by Hussain *et al.* wherein, fluorescence-amplified detection of picric acid was achieved in aqueous media using an imidazolium-based cationic conjugated polyelectrolyte (Table 2B.1.2, entry 1)²⁶. Ding *et al.* studied the effect of surfactant micelles on the photophysical behaviour of a cationic bispyrene fluorophore. The author, found that the studied sensor exhibits an on-off response to multiple explosives with the highest sensitivity to picric acid (PA) in the anionic SDS micelles (Table 2B.1.2, entry 2).⁴⁸ Roy *et al.* reported an anthracene-functionalized fluorescent tris-imidazolium salt that selectively detected picric acid in DMSO and DMSO-H₂O system (Table 2B.1.2, entry 3).⁵⁰ Sandhu *et al.* synthesized tripods (TIBP4 and TIBP8), and selectively detected picric acid in H₂O-DMSO (Table 2B.1.2, entry 4).⁵¹

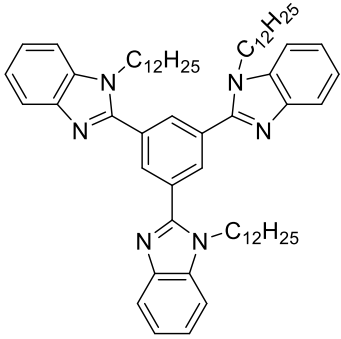
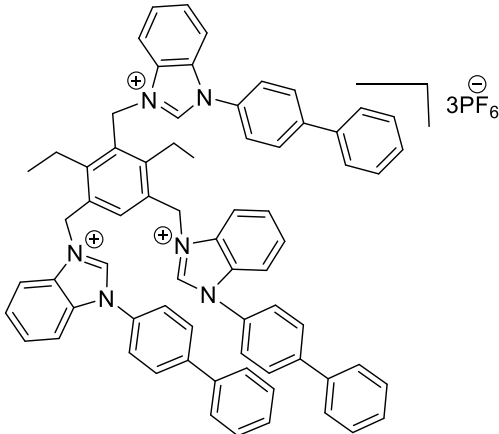
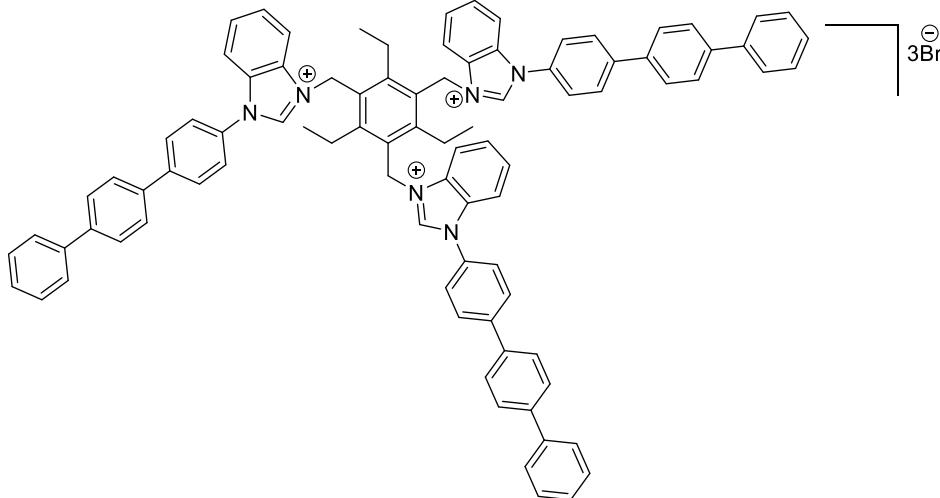
Table 2B.1.2: Reported imidazolium-based sensors for picric acid sensing

<p>Entry 1</p>  <p>Detection Limit²⁶ = 56.11×10^{-2} nM Sensing Solvent = H₂O</p>	<p>Entry 2</p>  <p>Detection Limit⁴⁸ = 1 μM Sensing Solvent = H₂O</p>
<p>Entry 3</p>  <p>Detection Limit⁵⁰ = 467 nM Sensing Solvent = DMSO</p>	
<p>Entry 4</p>  <p>R = C₄H₉ (TIBP4) R = C₈H₁₇ (TIBP8)</p> <p>Detection Limit⁵¹ = 25 nM & 10⁻⁵ nM Sensing Solvent = H₂O : DMSO (v/v = 98:2)</p>	

Similarly, benzimidazole derivatives have also been widely used for numerous applications in biomedicine,⁵²⁻⁵⁵ liquid materials,⁵⁶⁻⁵⁸ flame retardants,⁵⁹ supramolecular chemistry,⁶⁰ and coordination chemistry.⁶¹ Some of its derivatives have been applied for sensing CO₂.⁶² As far as

picric acid sensing is concerned, few benzimidazole derivatives are reported for selective sensing of picric acid. For example, Xiong *et al.* reported the application of 1,3,5-tri(1*H*-benzimidazol-2-yl)benzene derivatives for the selective detection of picric acid in picogram level in THF (Table 2B.1.3, entry 1).⁶³ In 2014, Kumar *et al.* reported the use of benzimidazolium tripod probe for the selective sensing of picric acid in H₂O-DMSO mixture (Table 2B.1.3, entry 2).⁶⁴ Recently, Sandhu *et al.* also reported the use of 1-(*p*-terphenyl)-benzimidazolium-based probe (TRIPOD-TP), for aggregation/disaggregation-modulated detection of picric acid (PA) in a mixture of H₂O-DMSO (Table 2B.1.3, entry 3).⁶⁵

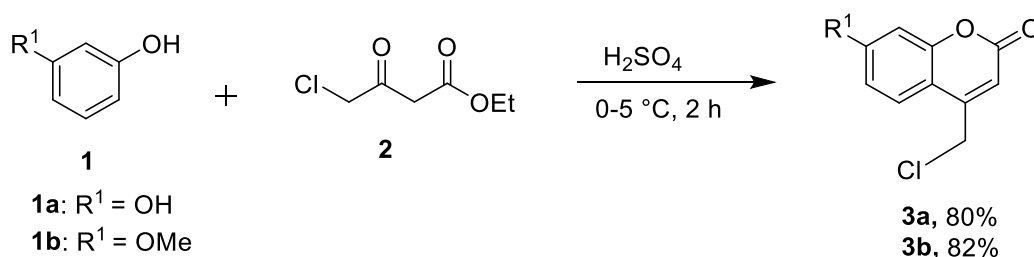
Table 2B.1.3: Reported benzimidazole/benzimidazolium-based sensors for picric acid sensing

<p>Entry 1</p>  <p>Detection Limit⁶³ = 50 ppb Sensing Solvent = THF</p>	<p>Entry 2</p>  <p>Detection Limit⁶⁴ = 1 nM Sensing Solvent = H₂O : DMSO (v/v = 98:2)</p>
<p>Entry 3</p>  <p>Detection Limit⁶⁵ = 5×10^{-4} nM Sensing Solvent = H₂O : DMSO (v/v = 98:2)</p>	

As already discussed, coumarin derivatives have been used as fluorescent chemosensors due to their low toxicity and ease to be modified for sensing of different analytes.⁶⁶ Few coumarin-derived imidazole and benzimidazole derivatives are known, and have been studied as biologically active compounds in medicinal chemistry,^{67,68} while a few have reported as selective chemosensors for different metal ions.^{69,70} However, to the best of our knowledge, coumarin-derived imidazole/benzimidazole remains unexplored towards the detection of picric acid. Thus, we envisioned that coumarin-derived imidazolium and benzimidazolium salts might selectively detect picric acid in aqueous media.

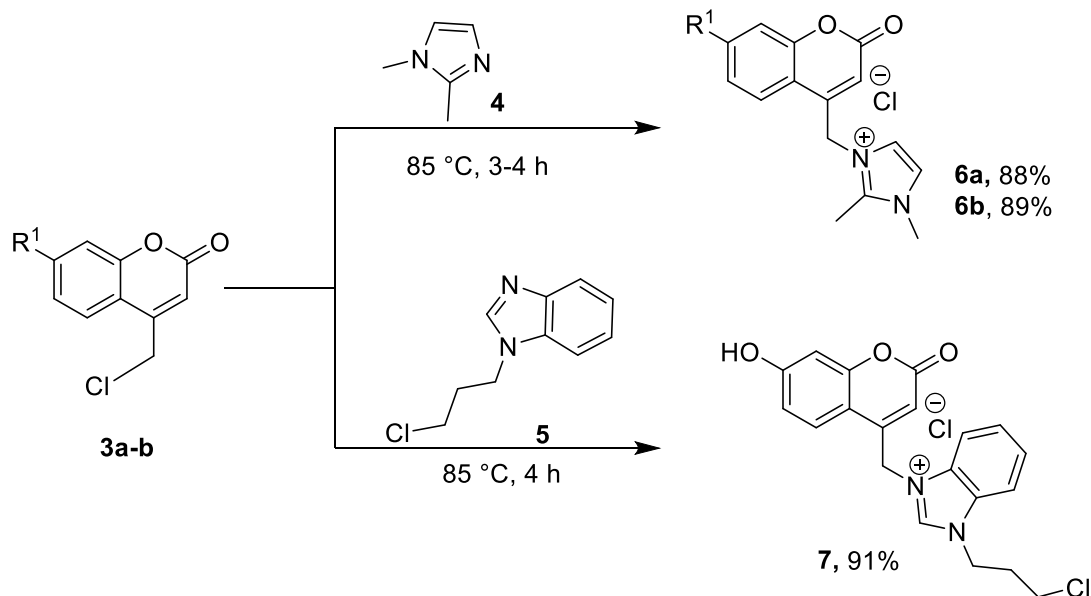
2B.2 Results and Discussion

With an aim to synthesize coumarin-derived imidazolium and benzimidazolium based water-soluble fluorophores, we initiated their synthesis starting from 4-(chloromethyl)-7-hydroxy-2*H*-chromen-2-one (**3a**) [or 4-(chloromethyl)-7-methoxy-2*H*-chromen-2-one (**3b**)],⁷¹ which were prepared in a straight-forward approach by coupling resorcinol (**1a**) [or *m*-methoxyphenol (**1b**)] with ethyl chloroacetoacetate in presence of sulfuric acid at 0–5 °C (Scheme 2B.2.1).



Scheme 2B.2.1: Synthesis of substituted 4-chloromethyl coumarin (**3a** and **3b**)

Thereafter, the reaction of **3a** (or **3b**) with 1,2-dimethylimidazole (**4**) at 85 °C for 3–4 h yielded **6a** (or **6b**) in excellent yields (Scheme 2B.2.2). Similarly, the reaction of **3a** with 1-(3-chloropropyl)benzimidazole at 85 °C for 4 h yielded **7** in 91% yield (Scheme 2B.2.2).



Scheme 2B.2.2: Synthesis of coumarin-derived imidazolium/benzimidazolium chloride (**6a-b** & **7**)

The compounds were well characterized by ¹H NMR, ¹³C NMR and high resolution mass spectrometry. Spectroscopic measurements (UV–Vis absorption and steady state fluorescence emission) of the compounds **6a**, **6b** and **7** were measured in aqueous solution in absence and presence of several aromatic/non-aromatic compounds as analytes. The compounds **6a** and **6b** exhibited excellent fluorescence in absence of aromatic/non-aromatic analytes in water. Addition of aromatic/non-aromatic analytes, such as 4-NBA, 1-Cl-2,4-DNB, 3,4-DNT, BA, 4-NT, NB, mesitylene, *p*-cresol, NM, 3,5-DNBA, 4-NP and 2,4-DNP (5 equiv each) did not produce any change in the fluorescence spectra of compounds **6a** and **6b**. However, addition of picric acid (5 equiv) produced a significant change in the fluorescence spectra, and resulted in quenching of fluorescence. The fluorescence intensity of compounds **6a** and **6b** decreased like an “on–off” sensing response (Figure. 2B.2.1; a, c). For an excellent sensor, high selectivity is a matter of necessity. Thus, column charts were prepared for selective recognition of aromatic/non-aromatic compounds. The selectivity of compounds **6a** and **6b** towards picric acid was determined by performing competitive experiments of solutions mixed with other common interfering aromatic/non-aromatic analytes such as 4-NBA, 1-Cl-2,4-DNB, 3,4-DNT, BA, 4-NT, NB, mesitylene, *p*-cresol, NM, 3,5-DNBA, 4-NP, 2,4-DNP (Figure 4B.2.1; b, d), respectively. No significant variation was observed in the fluorescence quenching caused by picric acid of compounds **6a** and **6b** in presence of other aromatic/non-aromatic analytes. Thus, compounds **6a**

and **6b** could be used as highly selective sensors for the detection of picric acid in the presence of other aromatic/non-aromatic compounds. Similarly, variation in the fluorescence spectrum of compound **7** was investigated by addition of aromatic/non-aromatic analytes (5 equiv), namely nitrobenzene (NB), 3,4-dinitrotoulene (3,4-DNT), benzoic acid (BA), 4-nitrotoulene (4-NT), mesitylene, *p*-cresol, 3,5-dinitrobenzoic acid (3,5-DNBA), nitromethane (NM), 1-chloro-2,4-dinitrobenzene (1-Cl-2,4-DNB), 3,5-dinitrosalicylic acid (3,5-DNSA) and 2,4-dinitrophenol (2,4-DNP). Interestingly, the fluorescence of the compound **7** remains unaffected, while fluorescence intensity drastically decreases upon addition of picric acid (PA) (5 equiv), resulting in fluorescence quenching (Figure. 2B.2.1; e). The fluorescence intensity of compound **7** decreased like an on-off sensing response. In addition, competitive experiments were performed by mixing (5 equiv) of other common interfering aromatic/non-aromatic compounds such as (i) mesitylene (ii) *p*-cresol (iii) NB (iv) 1-Cl-2,4-DNB (v) 4-NBA (vi) NM (vii) 4-NT (viii) 3,5-DNBA (ix) BA (x) 3,4-DNT (xi) 4-NP (xii) 3,5-DNSA and (xiii) 2,4-DNP (Figure. 2B.2.1; f) respectively, to a solution of compound **7** with and without picric acid. No significant variation in the fluorescence quenching caused by picric acid was observed in the presence of aromatic/non-aromatic compounds. Thus, the compound **7** could also be used as highly selective sensor for detection of picric acid in the presence of aromatic/non-aromatic compounds.

Upon addition of picric acid, the colourless solution of compounds **6a**, **6b** and **7** (in water) changes to pale yellow, indicating the formation of complexes between **6a**, **6b** and **7** and picric acid. Interestingly, the quenching efficiencies of compounds **6a**, **6b** and **7** towards picric acid were found to be 96.8%, 98% and 95.4% respectively, indicating their effectiveness to detect picric acid over other aromatic compounds.

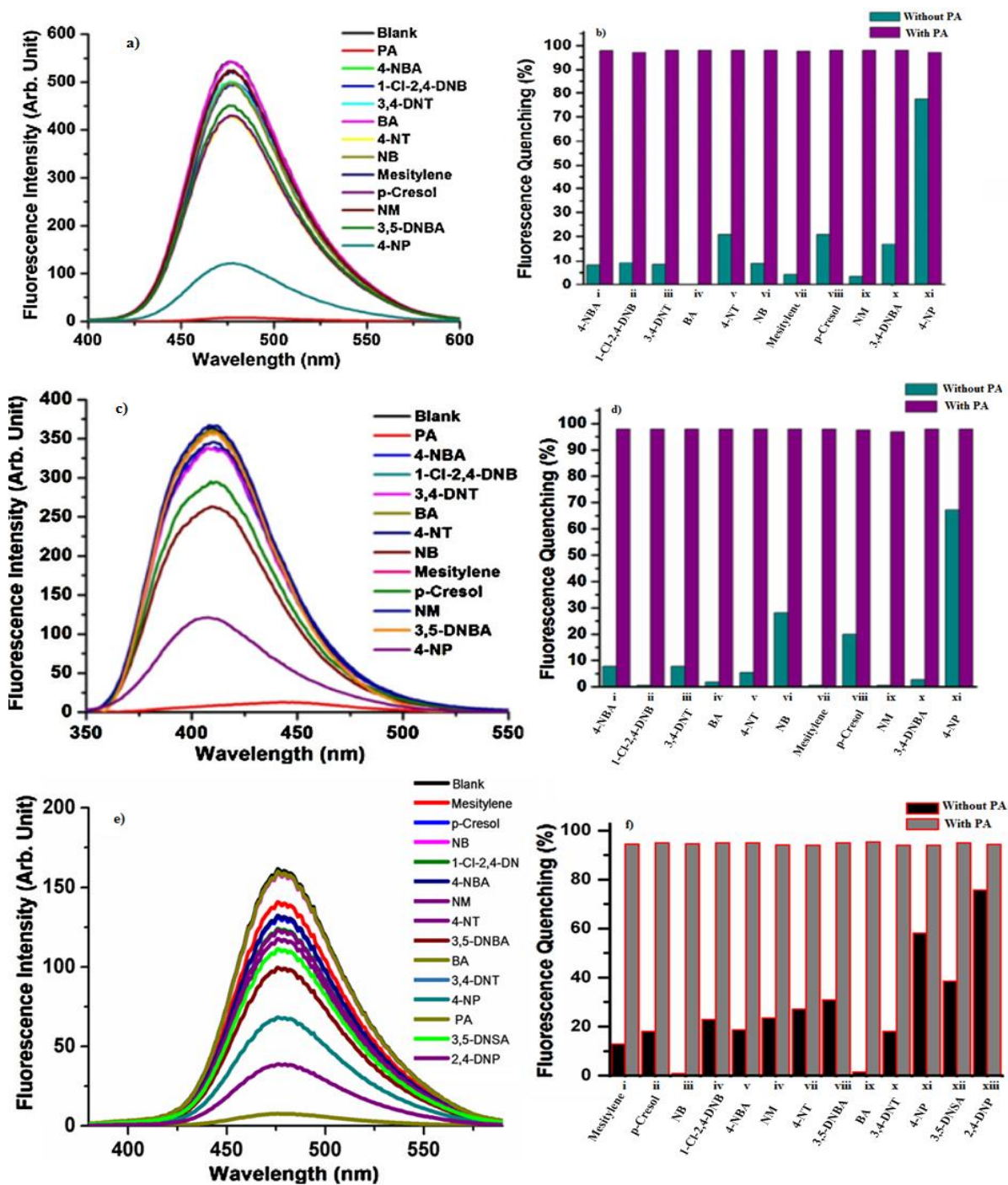


Figure 2B.2.1: Fluorescence spectra of **6a** (a; left), **6b** (c; left) & **7** (e; left) with $c = 10^{-4}$ M (in water) upon the addition of (5 equiv) different aromatic/non-aromatic analytes; Column diagrams of the relative fluorescence intensity of **6a** (b; right), **6b** (d; right) & **7** (f; right) with different analytes at $\lambda_{\text{Ex}} = 340$ nm for **6a** and **6b** and $\lambda_{\text{Ex}} = 300$ nm for **7**

UV–Vis titration study was next performed to revive more information about the interaction between compounds **6a**, **6b** and **7** with picric acid. The effect of sequential addition of picric acid on the electronic absorption spectra of compounds **6a**, **6b** and **7** is shown in Figure (2B.2.2; a, b, c). The UV–Vis absorption spectra in water displayed absorption band characteristic of coumarin with absorption maxima (λ_{max}) around ~ 325 nm for compounds **6a**, **6b** and **7**. For compound **6a** and **6b**, the absorbance slowly increased, and the band at 325 nm red-shifted upon the addition of picric acid. After 85 μM addition of picric acid, the absorbance attained saturation, and further addition of picric acid did not bring any spectral change. Overall, the absorbance maxima red-shifted from 325 nm to 340 nm, with sequential increasing picric acid concentration from 0 to 100 μM (Figure 2B.2.2; a, b). This change in absorbance could be due to complex formation in ground state upon addition of PA.

For compound **7**, upon addition of picric acid, a continuous increase in absorbance was observed along with the appearance of a new band at 406 nm (at 100 μM picric acid concentration) (Figure 2B.2.2; c). This red shift in absorbance and appearance of a new band clearly indicates the formation of a ground state complex with picric acid for the compound **7**.

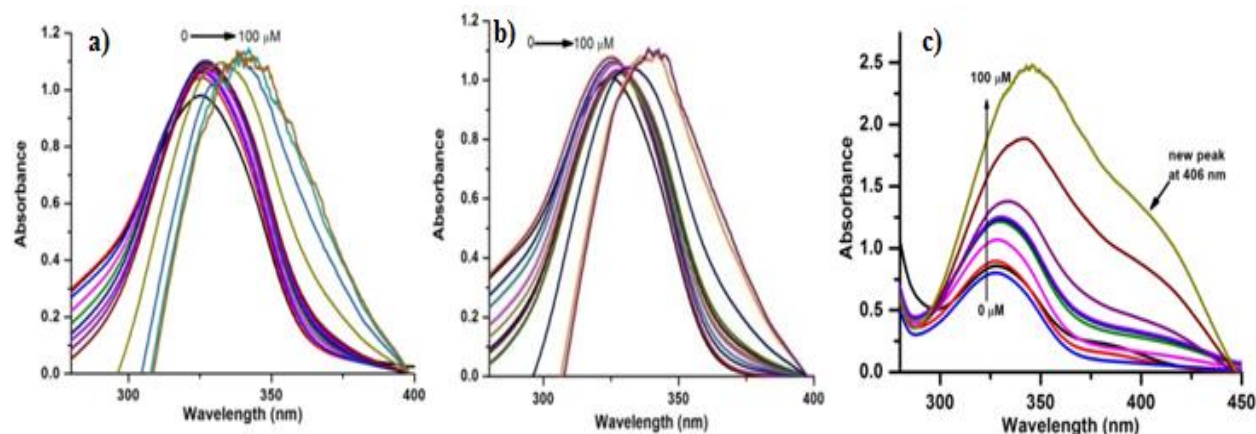


Figure 2B.2.2: UV–Vis titration studies of compounds **6a** (a), **6b** (b) & **7** (c) (10^{-4} M) with different amounts of picric acid in aqueous medium

To observe the effect on the fluorescence properties, the fluorescence titration curve of compounds **6a**, **6b** and **7** with increasing concentration of picric acid were plotted (Figure. 2B.2.3; a, b, c). The fluorescence titration for compounds **6a**, **6b** and **7** revealed that the fluorescence intensity gradually decreased upon addition of picric acid.

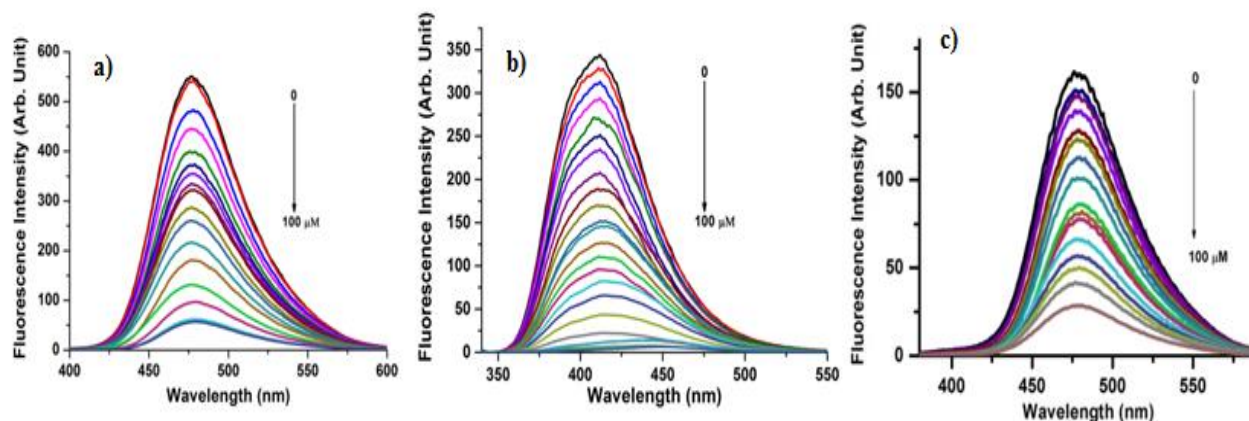


Figure 2B.2.3: Fluorescence titration studies of compounds **6a** (a), **6b** (b) & **7** (c) (10^{-4} M) with different amounts of picric acid in an aqueous medium

Detection limits (DL) were next determined from the fluorescence titration curves. The detection limit were calculated⁷²⁻⁷⁴ to be 107 nM, 87 nM and 208 nM for the compounds **6a**, **6b** and **7** respectively, for picric acid sensing. This was based on $3\sigma/m$, where σ corresponds to the standard deviation of the blank measurements, and m is the slope in the plot of the intensity versus the sample concentration. The quenching behaviour was characterised by the quenching efficiency (I_0/I) and quenching constant (K_{SV}) by using Stern–Volmer equation, $I_0/I = 1 + K_{SV} [Q]$, where I_0 is the initial fluorescence intensity in the absence of analytes, I is the intensity in presence of analytes, $[Q]$ is the molar concentration of analytes and K_{SV} is the quenching constant. The Stern–Volmer quenching constant was calculated from the slope of the Stern–Volmer plot (Figure 2B.2.4; a, b, c). The quenching constant (K_{SV}) for compounds **6a**, **6b** and **7** were calculated, and found to be $2.2 \times 10^4 \text{ M}^{-1}$, $5 \times 10^4 \text{ M}^{-1}$ and $1.58 \times 10^4 \text{ M}^{-1}$ respectively, confirming the high sensitivity of the compounds **6a**, **6b** and **7** towards picric acid sensing. It was evident from Figure (2B.2.4; a, b, c) that at lower picric acid concentrations, the Stern–Volmer plot is close to linear, whereas at higher concentrations it deviates from linearity, and increases nearly exponentially, demonstrating an amplified quenching process. The non-linear nature of the Stern–Volmer plot suggested the possibility of a self-absorption or an additional effective energy transfer mechanism.⁷⁵

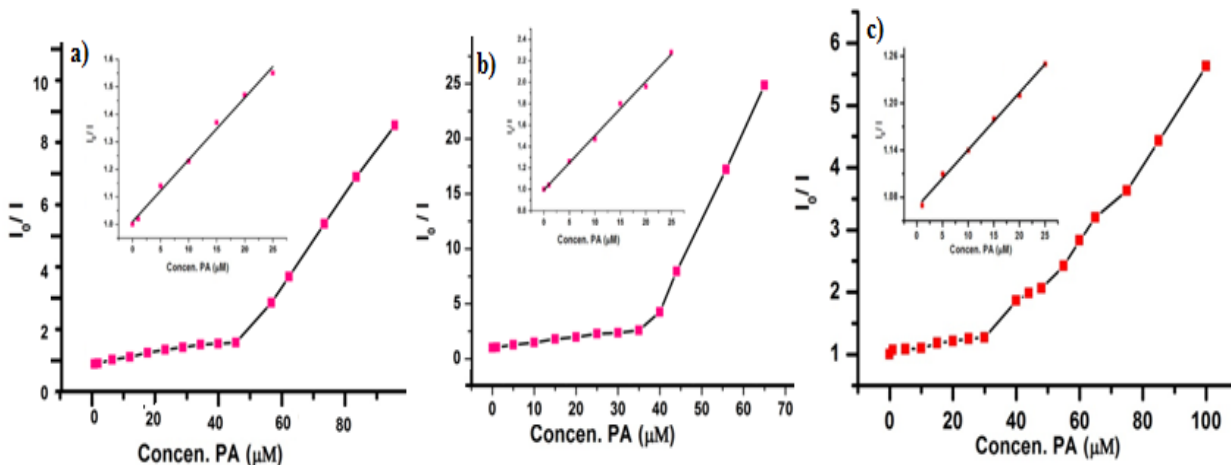


Figure 2B.2.4: Stern–Volmer plot in response to picric acid for sensors **6a** (a), **6b** (b) and **7** (c). Inset: Stern-Volmer plot obtained at lower concentration of picric acid in linear range

The association constants and binding stoichiometry were next determined by the fluorescence spectral changes constructing Benesi–Hildebrand plot analysis as described in literature.⁷⁶⁻⁷⁸ The linearity of Benesi–Hildebrand plot (Figure. 2B.2.5; a, b, c) between $1/(F_0-F_i)$ against $1/[PA]$ indicates the 1:1 stoichiometry between compounds **6a**, **6b** and **7** and picric acid. The association constant was found to be $K_a = 2.5 \times 10^4 \text{ M}^{-1}$, $K_a = 4.1 \times 10^4 \text{ M}^{-1}$ and $K_a = 1.01 \times 10^4 \text{ M}^{-1}$ for the compounds **6a**, **6b** and **7** respectively, as obtained from Benesi–Hildebrand plot. The high value of association constants K_a indicated the possibility of strong complex formation between picric acid and the compounds **6a**, **6b** and **7**.

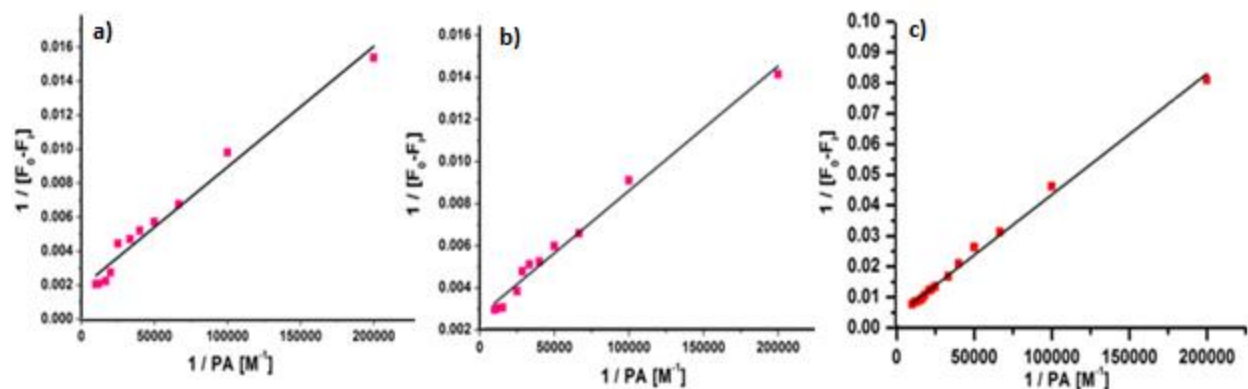


Figure 2B.2.5: Benesi–Hildebrand plot for compounds **6a** (a), **6b** (b) and **7** (c), at various concentration of picric acid

Spectral studies of complexes

To further confirm the stoichiometric ratio between the compounds and picric acid, the yellow complexes were prepared and isolated from ethanolic solution of compounds **6a**, **6b** and **7** and picric acid at room temperature, and were analyzed by spectroscopic studies. The ^1H NMR spectra of **6a**≡PA, **6b**≡PA and **7**≡PA complexes indicated a prominent peak around δ 8.5 in DMSO- d_6 , which corresponds to picrate anion (Figure. 2B.2.6; a, b & c) right-side. The relative integration of picrate anion protons to that of coumarin-derived imidazolium/benzimidazolium systems confirmed the formation of complexation of compounds **6a**, **6b** and **7** with picrate anion in 1:1 molar ratio. In addition to this, slight changes in the chemical shift of imidazole and benzimidazole protons were also observed that further affirmed the complexation of compounds **6a**, **6b** and **7** with picric acid.

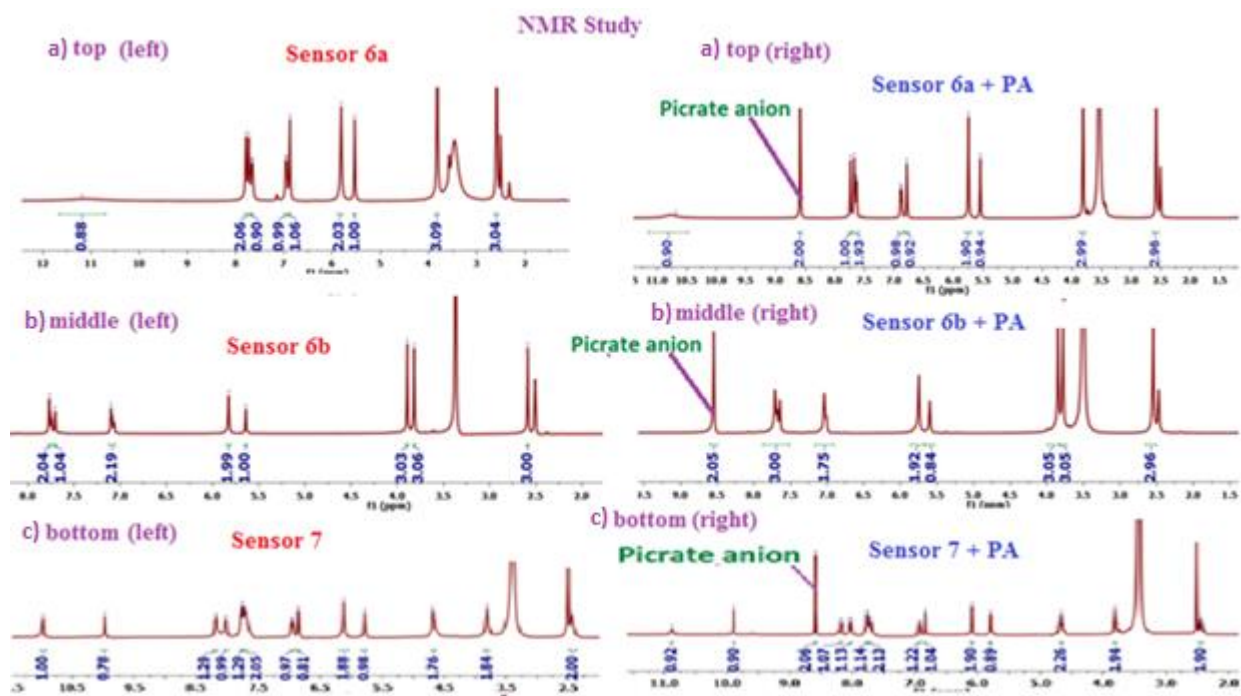


Figure 2B.2.6: ^1H NMR spectra of **6a** (a; left-top), **6a**≡PA (a; right-top), **6b** (b; left-middle), **6b**≡PA (b; right-middle) and **7** (c; left- bottom), **7** ≡PA (c; right-bottom) in DMSO- d_6

Quenching mechanism study

The nature of attenuation of the picric acid to the fluorescence emission of the sensors **6a**, **6b** and **7** was interrogated by steady state measurements, time-resolved measurements and theoretical studies. The UV-Vis spectrum of compounds **6a**, **6b** and **7** displayed a significant red-shift upon gradual addition of picric acid, suggesting the existence of complex formation in the

ground state. To confirm our steady-state measurements, time-resolved fluorescence studies were carried out which revealed ground-state complex formation, and thus indicated the mechanism to be static quenching as no change in the fluorescence lifetime of the compounds were observed in presence of picric acid (Figure 2B.2.7; a, b, c).

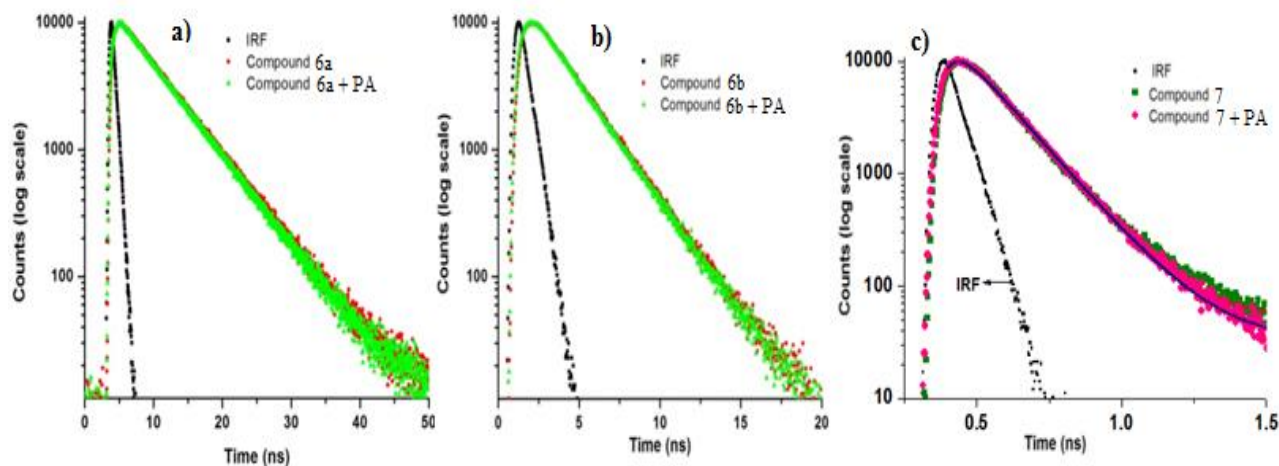


Figure 2B.2.7: Lifetime decay profile of compounds **6a** (a) **6b** (b) & **7** (c) with picric acid ($\lambda_{\text{Ex}} = 370$ nm for **6a-b** & **7** and monitored at $\lambda_{\text{Em}} = 480$ nm (for **6a**), $\lambda_{\text{Em}} = 410$ nm (for **6b**) and for **7** $\lambda_{\text{Em}} = 480$ nm

To further comprehend the mode of interaction between compounds **6a**, **6b** and **7** with picric acid, theoretical studies were performed. Density functional theory (DFT) calculations were carried out with B3LYP/6-311G basis set using Gaussian 09 program in order to understand the fluorescence quenching mechanism of compounds **6a**, **6b** and **7** on addition of picric acid. The DFT studies revealed that the ground state electron transfer from picrate anion to the positively charged compounds **6a**, **6b** and **7** is possible. The energy of highest occupied molecular orbital (HOMO) and lowest occupied molecular orbital (LUMO) of the free compounds **6a** are -0.325 eV and -0.177 eV while that for **6b** are -0.331 eV, -0.179 eV (Figure 4B.2.8; a, b) respectively. On the other hand, the energies of HOMO and LUMO of picrate anion are -0.112 eV and +0.021 eV (Figure 4B.2.8; c) respectively. Hence, the ground-state electronic charge transfer from the HOMO of picrate anion to the LUMO of **6a** (or **6b**) may result in high quenching efficiency.

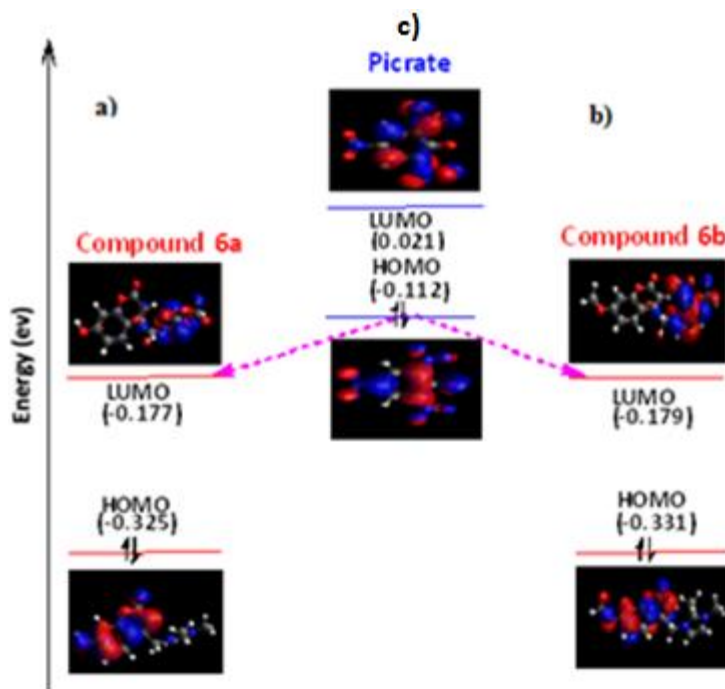


Figure 2B.2.8: Pictorial representation of the electron transfer phenomenon in the ground state which occurs from the HOMO of picrate anion to the LUMO of **6a** (a) and **6b** (b)

Similarly, theoretical results direct towards the possibility of a ground-state electronic charge transfer from the HOMO of picrate anion to the LUMO of the compound **7** that results in high quenching efficiency. However HOMOs of other nitro-explosives were found to have low energy levels than the LUMO of the sensor molecule, thereby discarding the possibility of electron transfer and resulting in low quenching efficiencies.

In striking contrast, the non-linear behavior of the Stern–Volmer plot of compounds **6a**, **6b** and **7** for picric acid suggested the involvement of energy transfer process in the quenching process. To further confirm it, the emission spectra of compounds **6a**, **6b** and **7** were plotted along with the absorption spectra of picric acid and other aromatic/non-aromatic analytes (Figure 2B.2.9). An overlapping of the emission band of compounds with the absorption band of picric acid suggested an efficient energy transfer from the sensors **6a**, **6b** and **7** to picric acid, which results in fluorescence quenching.^{28,79,80} However, the UV–Vis studies and lifetime measurements along with the theoretical studies suggested the electronic charge transfer in ground state to be the predominant mechanism responsible for efficient quenching as the spectral overlap for energy transfer observed for the sensors **6a**, **6b** and **7** is small.

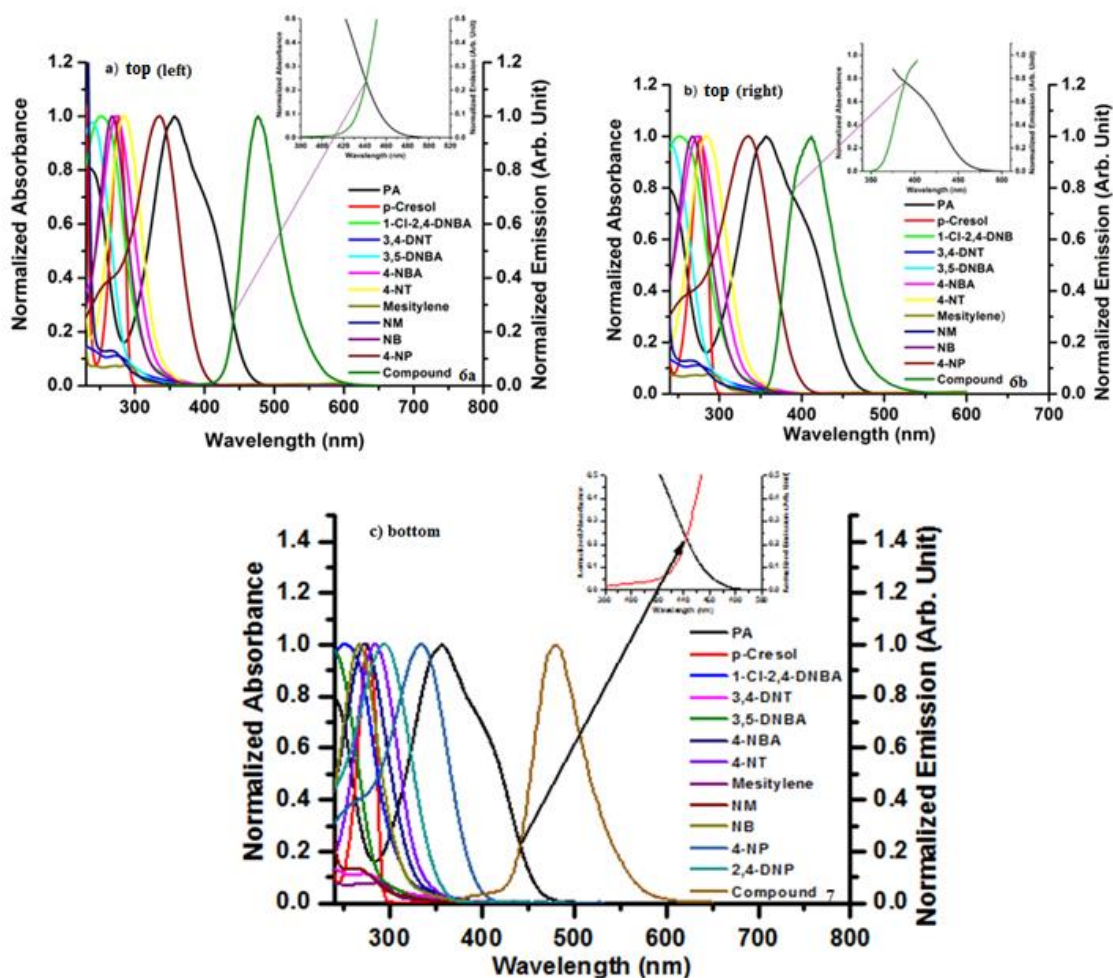


Figure 2B.2.9: Absorption spectra of different aromatic analytes and emission spectra of the sensors **6a** (a; top-left), **6b** (b; top-right) and **7** (c; bottom) in aqueous solution. Inset: the spectral overlap between the emission of the compounds (**6a**, **6b** and **7**) with the absorption of picric acid

Visual detection of picric acid in solid state under UV Light

Visual detection of picric acid is very convenient for security scanning and prompt identification in solid state. Compounds **6a**, **6b** and **7** adsorbed on a thin-layer chromatography (TLC) plate displayed strong emission [Figure 2B.2.10; (i; a), (ii; a), & (iii; a)]. When a spot of picric acid solution is adsorbed on the sensors **6a**, **6b** and **7**, fluorescence quenching was observed by the naked eye [Figure. 4B.2.10; (i; b), (ii; b) & (iii; b)] after illuminating under 365 nm UV lamp.

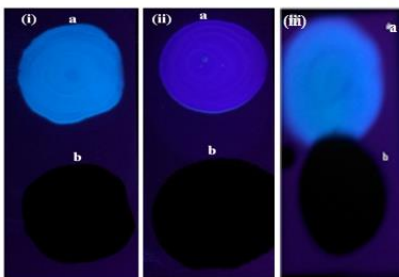


Figure 2B.2.10: Visual detection (under 365 nm UV lamp) of compounds **6a** (i; a), **6b** (ii; a) and **7** (iii; a) adsorbed on TLC plate and with a spot of picric acid solution on compounds **6a** (i; b), **6b** (ii; b) and **7** (iii; b)

Finally, a comparative study to elucidate the unprecedented selectivity of compounds **6a**, **6b** and **7** towards picric acid using three different nitrophenols with varying acidic strength was conducted. These include 4-nitrophenol (NP), 2,4-dinitrophenol (2,4-DNP) and 2,4,6-trinitrophenol (PA). The fluorescence quenching of compounds **6a**, **6b** and **7** was found to be maximum by picric acid, followed by 2,4-DNP and then 4-NP. This is in concordance with the acidic behaviour and water dissociation ability of these nitrophenols that could accelerate the electrostatic interactions between cationic **6a**, **6b** and **7** and picric acid.²⁶ It was also clear that **6a** and **7** resulted in fluorescence quenching after its treatment with picric acid, with detection limit reaching upto 107 and 208 nM (96.8% and 95.4% quenching observed with 5 equiv picric acid), whereas **6b** showed much better results in the detection of picric acid with the detection limit reaching to 87 nM (98% quenching observed with 5 equiv picric acid). Based on these observations, **6b** seems to be best for picric acid sensing among the other two compounds tested in water.

Sensing of picric acid in real samples

To investigate the practical application of synthesized compounds **6a** and **6b**, the fluorescence response of the **6a** and **6b** for picric acid were tested in real samples. Here, the real samples were prepared by using pond water, tap water, and drinking water spiked with picric acid, and the fluorescence activities for these samples were analyzed. It was found that the fluorescence turn-off for these samples follow the same pattern that was observed for the laboratory samples. The fluorescence spectra for real sample analysis of compounds **6a** and **6b** are shown in Figure 2B.2.11.

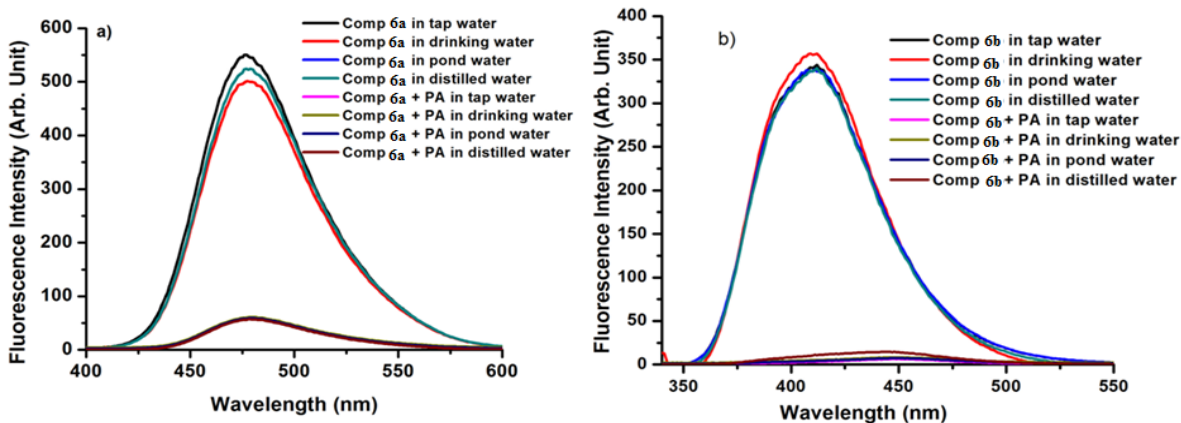


Figure 2B.2.11: Fluorescence response of compounds **6a** (a) and **6b** (b) (10^{-4} M) towards picric acid (5 equiv) sensing in real samples

Again, in environmental samples, there could be impurities due to the presence of different metal ions in low concentrations. Therefore, to further investigate the interference by metal ions on sensing picric acid, we analyzed the fluorescence sensing of compounds **6a** and **6b** for picric acid in presence of different metal ions. Figure 2B.2.12 depicts that neither the compounds showed fluorescence response to such metal ions, nor the presence of such metal ions (5 equiv) alter the sensitivity towards picric acid. This might be due to the absence of proper binding sites at the sensing materials for metal ions which finally helps in selectively sensing picric acid.

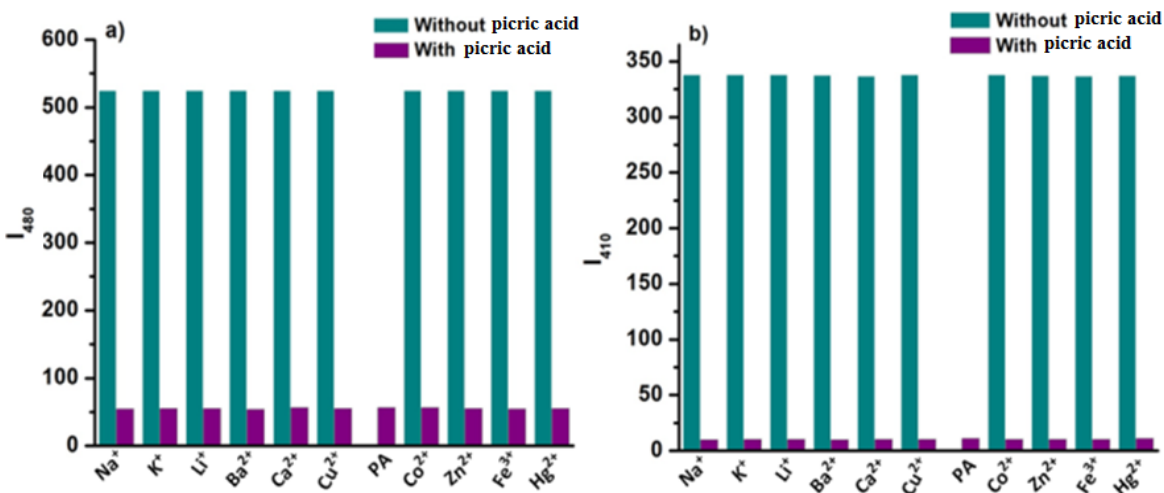


Figure 2B.2.12: Column diagrams of the fluorescence intensity of compound (10^{-4} M) + Metal ions (5 equiv) at 480 nm and 410 nm for **6a** (a) and **6b** (b) in aqueous medium. Cyan bars represent the addition of various metal ions to the blank solution and purple bars represent the subsequent addition of picric acid (5 equiv) to the above solutions (compound + M^{n+} + picric acid)

Photostability studies of the sensors

In addition to the selectivity for picric acid, the photostability and required time for sensing is an important parameter for practical applications. As mentioned earlier, the fluorescence response for picric acid is very instant, and hence applicable for quick detection process. In general, the organic fluorescence is not photostable and their fluorescence activities of compounds **6a** and **6b** change with time. In the present case, the fluorescence intensity do not change with time scale as demonstrated in Figure 2B.2.13.

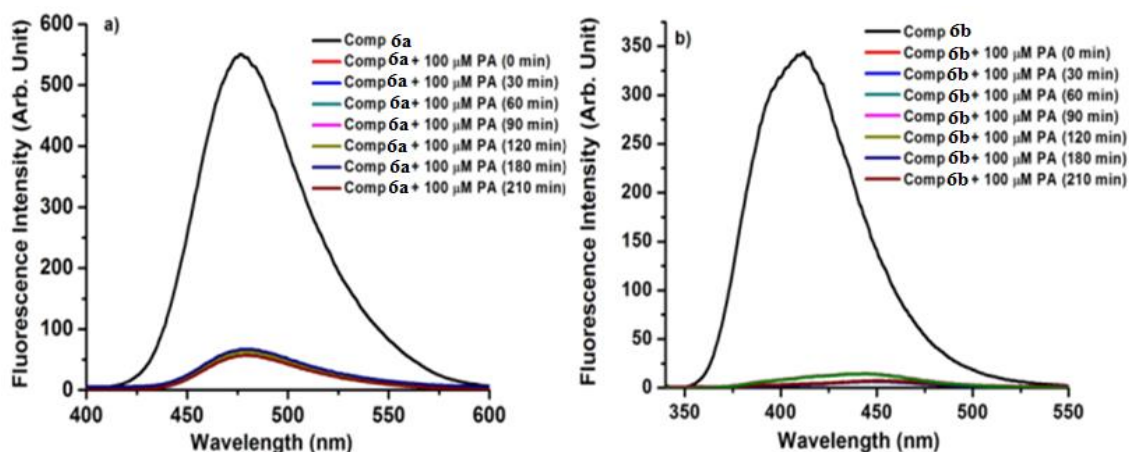


Figure 2B.2.13: Photostability test: Fluorescence spectra of **6a** (a) and **6b** (b) in the presence of 100 μM of picric acid in aqueous media at different time scale. The spectra are almost same for about 210 min

In summary, we have designed and synthesized coumarin-derived imidazolium and benzimidazolium-based chemosensors for selective sensing of picric acid in aqueous medium. The Stern–Volmer quenching constant (K_{SV}) for sensors **6a**, **6b** and **7** were found to be $2.2 \times 10^4 \text{ M}^{-1}$, $5 \times 10^4 \text{ M}^{-1}$ and $1.58 \times 10^4 \text{ M}^{-1}$ with the detection limit for picric acid to be 107 nM, 87 nM and 208 nM, respectively. Based on the UV–Visible studies, and the time resolved fluorescence results, the formation of ground-state charge-transfer complex formation appears to be predominant mechanism in solution, which also got support from DFT calculations.

2B.3 Experimental Section

General materials and methods

All the chemicals were purchased from Sigma-Aldrich, Alfa Aesar, and Spectrochem India Pvt. Ltd and used without further purification. The solvents used were purchased from Merck (India) and were distilled and dried before use. Nuclear Magnetic Resonance

spectra were recorded on Bruker 400 spectrometer. All ^1H NMR experiments were reported with TMS as a standard in δ units, parts per million (ppm), and were measured relative to residual DMSO- d_6 (2.5 ppm) in the deuterated solvent. All ^{13}C NMR spectra were reported in ppm relative to ppm [D $_6$] DMSO (39.5 ppm). All coupling constants J were reported in Hz. The following abbreviations were used to describe peak splitting patterns when appropriate: s = singlet, d = doublet, t = triplet, dd = doublet of doublet, m = multiplet and br s = broad singlet. Melting points were determined on a capillary point apparatus equipped with a digital thermometer and are uncorrected. Mass spectra were recorded on an AB SCIEX TOF/TOF 5800 spectrometer.

Absorption spectra were taken using dual beam Thermo Evolution 201 UV/Vis/NIR spectrophotometer and fluorescence spectra were recorded using a Shimadzu RF-5301PC spectrofluorometer. Milli-Q water was used in all the experiments. The fluorescence lifetimes were measured from time resolved intensity decays by the method of time correlated single photon counting (TCSPC) technique. The light source used was picoseconds diode laser (Nano LED) at 370 nm (Horiba Jobin Yvon, USA). The data were analyzed using related software. The concentration of compound in all the solutions was 10^{-4} M. The structures of the HOMO and LUMO states of the investigated compound were determined using theoretical calculations within the framework of density functional theory (DFT) calculations at the level of B3LYP/6-311G(d,p) as implemented in the Gaussian 09 package of programs.

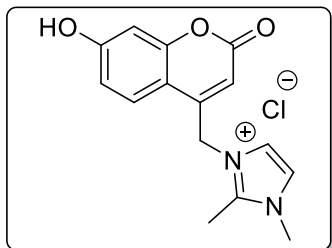
Procedure for the synthesis of coumarin-derived imidazolium/benzimidazolium salts

A mixture of **3a** (0.500 g, 2.3 mmol) (or **3b**; 0.500 g, 2.2 mmol) and 1,2-dimethylimidazole (0.385 g, 4.7 mmol) (or 0.364 g, 4.4 mmol) were taken in a 50 mL round-bottom flask, and heated at 85 °C for 3–4 h. Completion of reaction mixture was monitored by thin layer chromatography, after which the reaction mixture was poured into excess ethyl acetate, and stirred for 2 h to get a precipitate. The process was repeated thrice to remove excess 1,2-dimethylimidazole. The precipitate was then filtered out and dried to obtain pure **6a** or **6b**.

For preparing coumarin-derived benzimidazolium salt (**7**), 1-(3-chloropropyl)benzimidazole (**5**) (0.892 g, 4.6 mmol) was added dropwise to a vigorously stirred solution of **3a** (0.500 g, 2.3 mmol) in a 50 mL round-bottom flask, and the

reaction mixture was heated at 85 °C for 4 h. Thereafter, the above work-up process was repeated to obtain pure **7**.

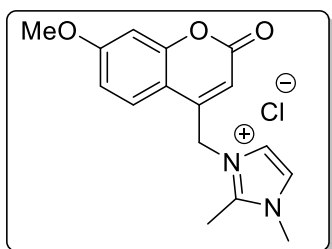
3-((7-Hydroxy-2-oxo-2H-chromen-4-yl)methyl)-1,2-dimethyl-1H-imidazol-3-ium chloride (6a): White Solid; yield: 0.293 g (88%); mp: 280–282 °C; ¹H NMR (400 MHz,



DMSO-*d*₆) δ 11.19 (s, 1H), 7.80 – 7.73 (m, 2H), 7.66 (d, *J* = 7.4 Hz, 1H), 6.95 (d, *J* = 7.2 Hz, 1H), 6.88 (brs, 1H), 5.81 (s, 2H), 5.53 (s, 1H), 3.82 (s, 3H), 2.59 (s, 3H); ¹³C NMR (100 MHz DMSO-*d*₆) δ 162.5, 160.5, 155.3, 150.3, 146.4, 126.4, 123.6, 122.1, 113.7, 109.4, 107.6, 102.9, 47.9, 35.6, 9.8;

HRMS (ESI-MS) (*m/z*) calculated C₁₅H₁₆N₂O₃⁺: 272.1160; found 272.1423 [M–Cl+H]⁺.

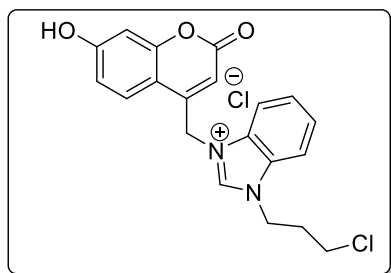
3-((7-Methoxy-2-oxo-2H-chromen-4-yl)methyl)-1,2-dimethyl-1H-imidazol-3-ium chloride (6b): Brown Solid; yield: 0.285 g (89%); mp: 230–231 °C; ¹H NMR (400 MHz,



DMSO-*d*₆) δ 7.76 (d, *J* = 9.0 Hz, 2H), 7.71 (brs, 1H), 7.12 – 7.05 (m, 2H), 5.83 (s, 2H), 5.64 (s, 1H), 3.89 (s, 3H), 3.82 (s, 3H), 2.59 (s, 3H); ¹³C NMR (100 MHz DMSO-*d*₆) δ 163.3, 160.3, 155.3, 150.1, 146.4, 126.4, 123.6, 122.1, 112.9, 110.7, 108.7, 101.4, 56.6, 47.9, 35.6, 9.8; HRMS (ESI-MS) (*m/z*)

calculated C₁₆H₁₈N₂O₃⁺: 286.1317; found 286.1334 [M–Cl+H]⁺.

1-(3-Chloropropyl)-3-((7-hydroxy-2-oxo-2H-chromen-4-yl)methyl)-1H-benzo[d]imidazol-3-ium chloride (7): White Solid; yield: 0.400 g (91%); mp: 236–238 °C; ¹H NMR (400 MHz,



DMSO-*d*₆) δ 10.97 (s, 1H), 9.97 (s, 1H), 8.19 (d, *J* = 7.7 Hz, 1H), 8.03 (d, *J* = 7.8 Hz, 1H), 7.77 (d, *J* = 8.6 Hz, 1H), 7.71 (dd, *J* = 13.8, 6.2 Hz, 2H), 6.95 (d, *J* = 7.3 Hz, 1H), 6.86 (brs, 1H), 6.12 (s, 2H), 5.78 (s, 1H), 4.71 – 4.64 (m, 2H), 3.86 – 3.77 (m, 2H), 2.49 – 2.37 (m, 2H); ¹³C NMR (100 MHz DMSO-*d*₆) δ 162.4, 160.4, 155.5, 149.4, 144.2, 132.0, 131.8, 127.5, 126.5,

114.3, 113.8, 109.5, 108.9, 103.1, 47.0, 45.2, 42.6, 31.5; HRMS: (ESI-MS) (*m/z*) calculated C₂₀H₁₈+N₂O₃⁺: 369.1099; found 369.1004 [M–Cl]⁺.

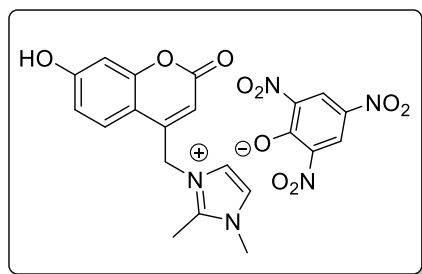
Procedure for fluorescence sensing of picric acid

Fluorescence quenching titrations studies in water were carried out with gradual increase in picric acid concentration (5 μM , 10 μM and so on) in a micro quartz cuvette, keeping the concentration of compounds **6a**, **6b** and **7** at 10^{-4} M. For each addition, at least three fluorescence spectrums were recorded at 298 K to obtain concordant value. The λ_{Ex} was chosen 340 nm for **6a** & **6b** and λ_{Ex} was chosen 300 for the compound **7**, with 3 nm slit width. There was no change in the shape of the emission spectra except gradual quenching of the initial fluorescence emission intensity upon titration with picric acid.

Synthesis of **6a**≡PA complex

To a solution of compound **6a** (0.050 g, 0.163 mmol) in ethanol, was added an ethanolic solution of picric acid (0.186 g, 0.815 mmol) was added dropwise at room temperature. The reaction mixture was stirred for 3 h at 25 °C, and then the yellow solid precipitated was filtered and washed with ethanol.

(7-Hydroxy-2-oxo-2H-chromen-4-yl)methyl)-1,2-dimethyl-1H-imidazol-3-ium 2,4,6-

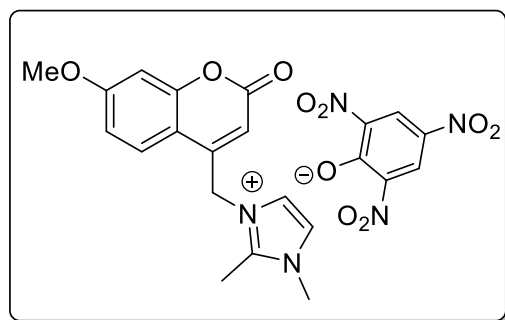


trinitrophenolate (6a≡PA): Yellow Solid; yield: 96% (0.078 g); mp: 238–240 °C; ^1H NMR (400 MHz, $\text{DMSO}-d_6$) δ 10.68 (s, 1H), 8.59 (s, 2H), 7.74 (s, 1H), 7.68 – 7.62 (m, 2H), 6.88 (d, $J = 8.5$ Hz, 1H), 6.79 (s, 1H), 5.75 (s, 2H), 5.55 (s, 1H), 3.81 (s, 3H), 2.58 (s, 3H).

Synthesis of **6b**≡PA complex

Synthesis of **6b**≡PA complex was prepared in similar way by treating **6b** (0.050 g, 0.15 mmol) with picric acid (0.178 g, 0.77 mmol) in ethanol.

3-((7-Methoxy-2-oxo-2H-chromen-4-yl)methyl)-1,2-dimethyl-1H-imidazol-3-ium 2,4,6-



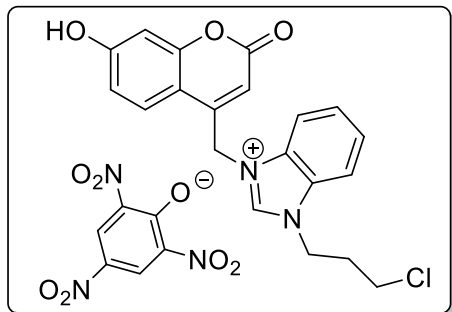
trinitrophenolate (6b≡PA): Yellow Solid; yield: 95% (0.076 g); mp: 180–181 °C; ^1H NMR (400 MHz, $\text{DMSO}-d_6$) δ 8.58 (s, 2H), 7.73 (d, $J = 12.4$ Hz, 2H), 7.68 (s, 1H), 7.11 – 7.01 (m, 2H), 5.78 (s, 2H), 5.63 (s, 1H), 3.88 (s, 3H), 3.81 (s, 3H), 2.58 (s, 3H). 7.76 (d, $J = 9.0$ Hz, 2H), 7.71 (s, 1H), 7.12 – 7.05 (m, 2H), 5.83 (s, 2H), 5.64 (s, 1H), 3.89 (s, 3H), 3.82 (s, 3H), 2.59 (s,

3H).

Synthesis of 7≡PA complex

Synthesis of 7≡PA complex was also prepared in similar way by treating **7** (0.050 g, 0.12 mmol) with picric acid (0.141 g, 0.61 mmol) in ethanol.

1-(3-Chloropropyl)-3-((7-hydroxy-2-oxo-2H-chromen-4-yl)methyl)-1H-benzo[d]imidazol-3-ium 2,4,6-trinitrophenolate (7≡PA): Yellow Solid; yield: (0.068 g, 93%); mp: 141–142 °C; ¹H



NMR (400 MHz, DMSO-*d*₆) δ 10.87 (s, 1H), 9.89 (s, 1H), 8.59 (s, 2H), 8.18 (d, *J* = 8.3 Hz, 1H), 8.02 (d, *J* = 8.0 Hz, 1H), 7.78 (s, 1H), 7.75 – 7.70 (m, 2H), 6.93 (dd, *J* = 8.7, 2.3 Hz, 1H), 6.83 (d, *J* = 2.2 Hz, 1H), 6.10 (s, 2H), 5.79 (s, 1H), 4.68 (t, *J* = 6.9 Hz, 2H), 3.81 (t, *J* = 6.3 Hz, 2H), 2.47 – 2.41 (m, 2H).

Quantum yield of sensors

The fluorescence quantum yield of studied compounds **6a**, **6b** and **7** were determined by using quinine sulfate in 0.1 N H₂SO₄ (Φ = 0.55) as the standard reference.⁸¹ The quantum yield is calculated using the following equation:⁸²

$$\phi_s = \phi_r \frac{F_s A_r \eta_s^2}{F_r A_s \eta_r^2}$$

where *A_r* and *A_s* are the absorbance of the ‘reference standard’ and ‘sample’ respectively at the excitation wavelength, *F_r* and *F_s* are the relative integrated fluorescent intensities (area under the fluorescence curve, peak area) of the reference and samples respectively. *η_r* and *η_s* are respectively the refractive indices of the solvents in which the reference standard and samples are prepared.

Fluorescence quenching (%) measurement

The quenching percentage was calculated using the equation as follows:⁸³⁻⁸⁵

$$\text{Fluorescence quenching \%} = (1 - I/I_0) \times 100\%$$

where *I*₀ is the initial fluorescence intensity in the absence of analyte, *I* is the fluorescence intensity in the presence of corresponding analyte.

Calculation of Stern -Volmer constant

The Stern–Volmer relationship establishes the correlation of intensity changes with the quencher concentration [Q] as follows:⁸³⁻⁸⁵

$$I_0/I = 1 + K_{SV}[Q]$$

where I_0 and I are the intensity, in the absence and presence of picric acid, respectively, K_{SV} is the Stern-Volmer quenching constant and $[Q]$ is the concentration of picric acid.

Method used for detection limit calculation

For the determination of detection limit,^{11,86} various samples of compounds with concentration 10^{-4} M containing different picric acid concentration (5 μ M, 10 μ M and so on) were prepared. The fluorescence spectrum was then recorded for each sample by exciting at 340 nm for **6a** and **6b** and 300 nm for **7**. A calibration curve was plotted between change in the fluorescence intensity and concentration of picric acid to obtain the regression curve equation. The detection limit (LOD) was then calculated using the equation $3\sigma/K$, where σ is the standard deviation (SD) for compounds **6a**, **6b** and **7** solution intensity in the absence of picric acid and K denotes the slope of the curve. To determine the Signal/Noise ratio, the emission intensity of compound in water without picric acid was measured by 10 times and the standard deviation of blank measurements was determined.

Fluorescence quenching titration study in water medium

Fluorescence quenching titration study in water was carried out with gradual increasing picric acid concentration (1 μ M, 5 μ M, 10 μ M and so on). For each addition, at least three fluorescence spectrums were recorded at 298 K to obtain concordant value. The λ_{Ex} was chosen 340 nm, 300 nm for studied compound with 3 nm slit width.

The Stern–Volmer relationship establishes the correlation of intensity changes with the quencher concentration $[Q]$ as follows:

$$I_0/I = 1 + K_{SV}[Q]$$

where I_0 and I are the intensity, in the absence and presence of picric acid, respectively, K_{SV} is the Stern–Volmer quenching constant and $[Q]$ is the concentration of picric acid.

Benesi–Hildebrand equation

where, F_0 is the fluorescence intensity of sensor, F_i the fluorescence intensity obtained with picric acid diff. Concentration, F_{min} the fluorescence intensity obtained with excess amount of picric acid.

Lifetime measurements

Goodness of the fits was evaluated by the χ^2 criterion and the randomness of the residuals of the fitted function to data. Care was taken in data analysis to differentiate between the mono exponential and bi exponential fits by judging the χ^2 values, standard deviation and weighted residuals. For lifetime measurements, fluorescence decays were analyzed by multi-exponential iterative fitting program provided by DAS-6 decay analysis software.

$$F(t) = \sum_i \alpha_i \exp(t / \tau_i)$$

Where, α_i is a pre-exponential factor representing the fractional contribution to the time resolved decay of the component with a lifetime τ_i .

DFT study

The structures of the HOMO and LUMO states of the investigated compounds were determined with the help of theoretical calculations, in the frame-work of density functional theory (DFT) calculations at the level of B3LYP/6-311G (d,p) in a suite of Gaussian 09 programs.

2B.4 References

- (1) Yinon, J.; *Analytical Chemistry* **2003**, *5*, 98-105.
- (2) Rouhi, A. M. *Chemical & Engineering News* **1997**, *75*, 14-14.
- (3) Steinfeld, J. I.; Wormhoudt, J. *Annual Review of Physical Chemistry* **1998**, *49*, 203-232.
- (4) Thomas, S. W.; Joly, G. D.; Swager, T. M. *Chemical Reviews* **2007**, *107*, 1339-1386.
- (5) Chakraborti, D.; Hussam, A.; Alauddin, M. *J. Environmental Science and Health, Part A* **2003**, *38*, 1-305.
- (6) Fainberg, A. *Science* **1992**, *255*, 1531-1537.
- (7) Germain, M. E.; Knapp, M. J. *Journal of the American Chemical Society* **2008**, *130*, 5422-5423.
- (8) Shen, J.; Zhang, J.; Zuo, Y.; Wang, L.; Sun, X.; Li, J.; Han, W.; He, R. *Journal of Hazardous Materials* **2009**, *163*, 1199-1206.
- (9) Peng, Y.; Zhang, A.-J.; Dong, M.; Wang, Y.-W. *Chemical Communications* **2011**, *47*, 4505-4507.
- (10) Dong, M.; Wang, Y. W.; Zhang, A. J.; Peng, Y. *Chemistry—An Asian Journal* **2013**, *8*, 1321-1330.

- (11) Kaur, S.; Bhalla, V.; Vij, V.; Kumar, M. *Journal of Materials Chemistry C* **2014**, *2*, 3936-3941.
- (12) Madhu, S.; Bandela, A.; Ravikanth, M. *RSC Advances* **2014**, *4*, 7120-7123.
- (13) Wollin, K.-M.; Dieter, H. *Archives of Environmental Contamination and Toxicology* **2005**, *49*, 18-26.
- (14) Hong, Y.; Lam, J. W.; Tang, B. Z. *Chemical Society Reviews* **2011**, *40*, 5361-5388.
- (15) Toal, S. J.; Trogler, W. C. *Journal of Materials Chemistry* **2006**, *16*, 2871-2883.
- (16) Kartha, K. K.; Babu, S. S.; Srinivasan, S.; Ajayaghosh, A. *Journal of the American Chemical Society* **2012**, *134*, 4834-4841.
- (17) Dong, W.; Fei, T.; Palma-Cando, A.; Scherf, U. *Polymer Chemistry* **2014**, *5*, 4048-4053.
- (18) Sohn, H.; Sailor, M. J.; Magde, D.; Trogler, W. C. *Journal of the American Chemical Society* **2003**, *125*, 3821-3830.
- (19) Xu, B.; Wu, X.; Li, H.; Tong, H.; Wang, L. *Macromolecules* **2011**, *44*, 5089-5092.
- (20) Nagarkar, S. S.; Joarder, B.; Chaudhari, A. K.; Mukherjee, S.; Ghosh, S. K. *Angewandte Chemie* **2013**, *125*, 2953-2957.
- (21) Lan, A.; Li, K.; Wu, H.; Olson, D. H.; Emge, T. J.; Ki, W.; Hong, M.; Li, J. *Angewandte Chemie* **2009**, *121*, 2370-2374.
- (22) Bhalla, V.; Pramanik, S.; Kumar, M. *Chemical Communications* **2013**, *49*, 895-897.
- (23) Gong, Y.-N.; Jiang, L.; Lu, T.-B. *Chemical Communications* **2013**, *49*, 11113-11115.
- (24) Bhalla, V.; Kaur, S.; Vij, V.; Kumar, M. *Inorganic Chemistry* **2013**, *52*, 4860-4865.
- (25) Ma, J.; Lin, T.; Pan, X.; Wang, W. *Chemistry of Materials* **2014**, *26*, 4221-4229.
- (26) Hussain, S.; Malik, A. H.; Afroz, M. A.; Iyer, P. K. *Chemical Communications* **2015**, *51*, 7207-7210.
- (27) Sk, M. P.; Chattopadhyay, A. *RSC Advances* **2014**, *4*, 31994-31999.
- (28) Hou, X.-G.; Wu, Y.; Cao, H.-T.; Sun, H.-Z.; Li, H.-B.; Shan, G.-G.; Su, Z.-M. *Chemical Communications* **2014**, *50*, 6031-6034.
- (29) Feng, H. T.; Zheng, Y. S. *Chemistry—A European Journal* **2014**, *20*, 195-201.
- (30) Venkatramaiah, N.; Kumar, S.; Patil, S. *Chemical Communications* **2012**, *48*, 5007-5009.
- (31) Rajput, J. K. *Sensors and Actuators B: Chemical* **2018**, *259*, 990-1005.
- (32) Dey, N.; Samanta, S. K.; Bhattacharya, S. *ACS Applied Materials & Interfaces* **2013**, *5*, 8394-8400.

- (33) Chemate, S.; Erande, Y.; Mohbiya, D.; Sekar, N. *RSC Advances* **2016**, *6*, 84319-84325.
- (34) Gogoi, B.; Sen Sarma, N. *ACS Applied Materials & Interfaces* **2015**, *7*, 11195-11202.
- (35) Vij, V.; Bhalla, V.; Kumar, M. *ACS Applied Materials & Interfaces* **2013**, *5*, 5373-5380.
- (36) Bhalla, V.; Gupta, A.; Kumar, M.; Rao, D. S.; Prasad, S. K. *ACS Applied Materials & Interfaces* **2013**, *5*, 672-679.
- (37) Sun, X.; Ma, X.; Kumar, C. V.; Lei, Y. *Analytical Methods* **2014**, *6*, 8464-8468.
- (38) Shiraishi, K.; Sanji, T.; Tanaka, M. *ACS Applied Materials & Interfaces* **2009**, *1*, 1379-1382.
- (39) McQuade, D. T.; Pullen, A. E.; Swager, T. M. *Chemical Reviews* **2000**, *100*, 2537-2574.
- (40) Ruiz, J.; Mesa, A. F.; Sol, D. *Organometallics* **2015**, *34*, 5129-5135.
- (41) He, X.; Chan, T. H. *Organic Letters* **2007**, *9*, 2681-2684.
- (42) Agrigento, P.; Beier, M. J.; Knijnenburg, J. T.; Baiker, A.; Gruttadauria, M. *Journal of Materials Chemistry* **2012**, *22*, 20728-20735.
- (43) Kaur, H.; Zinn, F. K.; Stevens, E. D.; Nolan, S. P. *Organometallics* **2004**, *23*, 1157-1160.
- (44) Boydston, A. J.; Vu, P. D.; Dykhno, O. L.; Chang, V.; Wyatt, A. R.; Stockett, A. S.; Ritschdorff, E. T.; Shear, J. B.; Bielawski, C. W. *Journal of the American Chemical Society* **2008**, *130*, 3143-3156.
- (45) Zheng, Y.; Tan, C.; Drummen, G. P.; Wang, Q. *Spectrochimica Acta Part A: Molecular and Biomolecular Spectroscopy* **2012**, *96*, 387-394.
- (46) Singh, A.; Singh, A.; Singh, N. *Dalton Transactions* **2014**, *43*, 16283-16288.
- (47) Malik, A. H.; Hussain, S.; Kalita, A.; Iyer, P. K. *ACS Applied Materials & Interfaces* **2015**, *7*, 26968-26976.
- (48) Ding, L.; Bai, Y.; Cao, Y.; Ren, G.; Blanchard, G. J.; Fang, Y. *Langmuir* **2014**, *30*, 7645-7653.
- (49) Hussain, S.; Malik, A. H.; Iyer, P. K. *ACS Applied Materials & Interfaces* **2015**, *7*, 3189-3198.
- (50) Roy, B.; Bar, A. K.; Gole, B.; Mukherjee, P. S. *The Journal of Organic Chemistry* **2013**, *78*, 1306-1310.
- (51) Sandhu, S.; Kumar, R.; Singh, P.; Kumar, S. *Journal of Materials Chemistry C* **2016**, *4*, 3209-3216.

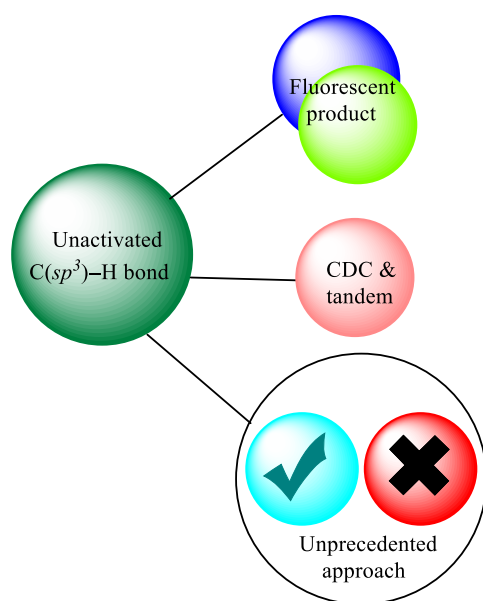
- (52) Mao, Z.; Wang, Z.; Li, J.; Song, X.; Luo, Y. *Synthetic Communications* **2010**, *40*, 1963-1977.
- (53) Frei, R.; Breitbach, A. S.; Blackwell, H. E. *Angewandte Chemie International Edition* **2012**, *51*, 5226-5229.
- (54) Narasimhan, B.; Sharma, D.; Kumar, P. *Medicinal Chemistry Research* **2012**, *21*, 269-283.
- (55) Peng, P.; Xiong, J.-F.; Mo, G.-Z.; Zheng, J.-L.; Chen, R.-H.; Chen, X.-Y.; Wang, Z.-Y. *Amino Acids* **2014**, *46*, 2427-2433.
- (56) Wiggins, K. M.; Kerr, R. L.; Chen, Z.; Bielawski, C. W. *Journal of Materials Chemistry* **2010**, *20*, 5709-5714.
- (57) Muth, M. A.; Carrasco-Orozco, M.; Thelakkat, M. *Advanced Functional Materials* **2011**, *21*, 4510-4518.
- (58) Xiong, J.-F.; Luo, S.-H.; Huo, J.-P.; Liu, J.-Y.; Chen, S.-X.; Wang, Z.-Y. *The Journal of Organic Chemistry* **2014**, *79*, 8366-8373.
- (59) Xiong, J.-F.; Luo, S.-H.; Wang, Q.-F.; Wang, Z.-Y.; Qi, J. *Designed Monomers and Polymers* **2013**, *16*, 389-397.
- (60) Zhu, K.; Vukotic, V. N.; Loeb, S. J. *Angewandte Chemie* **2012**, *124*, 2210-2214.
- (61) He, Q. T.; Li, X. P.; Liu, Y.; Yu, Z. Q.; Wang, W.; Su, C. Y. *Angewandte Chemie* **2009**, *121*, 6272-6275.
- (62) Guo, Z.; Song, N. R.; Moon, J. H.; Kim, M.; Jun, E. J.; Choi, J.; Lee, J. Y.; Bielawski, C. W.; Sessler, J. L.; Yoon, J. *Journal of the American Chemical Society* **2012**, *134*, 17846-17849.
- (63) Xiong, J.-F.; Li, J.-X.; Mo, G.-Z.; Huo, J.-P.; Liu, J.-Y.; Chen, X.-Y.; Wang, Z.-Y. *The Journal of Organic Chemistry* **2014**, *79*, 11619-11630.
- (64) Kumar, R.; Sandhu, S.; Singh, P.; Hundal, G.; Hundal, M. S.; Kumar, S. *Asian Journal of Organic Chemistry* **2014**, *3*, 805-813.
- (65) Sandhu, S.; Kumar, R.; Singh, P.; Mahajan, A.; Kaur, M.; Kumar, S. *ACS Applied Materials & Interfaces* **2015**, *7*, 10491-10500.
- (66) Wang, L.; Li, H.; Cao, D. *Sensors and Actuators B: Chemical* **2013**, *181*, 749-755.

- (67) Holiyachi, M.; Samundeeswari, S.; Chougala, B. M.; Naik, N. S.; Madar, J.; Shastri, L. A.; Joshi, S. D.; Dixit, S. R.; Dodamani, S.; Jalalpure, S. *Monatshefte für Chemie-Chemical Monthly* **2018**, *149*, 595-609.
- (68) Tsay, S.-C.; Lin, S.-Y.; Huang, W.-C.; Hsu, M.-H.; Hwang, K. C.; Lin, C.-C.; Horng, J.-C.; Chen, I.; Hwu, J. R.; Shieh, F.-K. *Molecules* **2016**, *21*, 228-244.
- (69) Saleh, N. i.; Al-Soud, Y. A.; Nau, W. M. *Spectrochimica Acta Part A: Molecular and Biomolecular Spectroscopy* **2008**, *71*, 818-822.
- (70) Zhao, B.; Liu, T.; Fang, Y.; Wang, L.; Song, B.; Deng, Q. *Tetrahedron Letters* **2016**, *57*, 4417-4423.
- (71) Lin, W.; Long, L.; Feng, J.; Wang, B.; Guo, C. *European Journal of Organic Chemistry* **2007**, *2007*, 4301-4304.
- (72) Neupane, L. N.; Kim, J. M.; Lohani, C. R.; Lee, K.-H. *Journal of Materials Chemistry* **2012**, *22*, 4003-4008.
- (73) Yang, M.-H.; Thirupathi, P.; Lee, K.-H. *Organic Letters* **2011**, *13*, 5028-5031.
- (74) Zhang, F.; Wang, L.; Chang, S.-H.; Huang, K.-L.; Chi, Y.; Hung, W.-Y.; Chen, C.-M.; Lee, G.-H.; Chou, P.-T. *Dalton Transactions* **2013**, *42*, 7111-7119.
- (75) Salinas, Y.; Martínez-Mañez, R.; Marcos, M. D.; Sancenón, F.; Costero, A. M.; Parra, M.; Gil, S. *Chemical Society Reviews* **2012**, *41*, 1261-1296.
- (76) Benesi, H. A.; Hildebrand, J. *Journal of the American Chemical Society* **1949**, *71*, 2703-2707.
- (77) Singh, H.; Sindhu, J.; Khurana, J. M. *Sensors and Actuators B: Chemical* **2014**, *192*, 536-542.
- (78) Dhar, P.; Pal, A.; Mohanty, P.; Bag, B. *Sensors and Actuators B: Chemical* **2015**, *219*, 308-314.
- (79) Wang, J.; Mei, J.; Yuan, W.; Lu, P.; Qin, A.; Sun, J.; Ma, Y.; Tang, B. Z. *Journal of Materials Chemistry* **2011**, *21*, 4056-4059.
- (80) Sun, X.; Wang, Y.; Lei, Y. *Chemical Society Reviews* **2015**, *44*, 8019-8061.
- (81) Mishra, H.; Pant, D.; Pant, T.; Tripathi, H. *Journal of Photochemistry and Photobiology A: Chemistry* **2006**, *177*, 197-204.
- (82) Ranjith, C.; Vijayan, K.; Praveen, V. K.; Kumar, N. S. *Spectrochimica Acta Part A: Molecular and Biomolecular Spectroscopy* **2010**, *75*, 1610-1616.

- (83) Xue, Q.; Huang, H.; Wang, L.; Chen, Z.; Wu, M.; Li, Z.; Pan, D. *Nanoscale* **2013**, *5*, 12098-12103.
- (84) Zhou, Y.; Qu, Z.-b.; Zeng, Y.; Zhou, T.; Shi, G. *Biosensors and Bioelectronics* **2014**, *52*, 317-323.
- (85) Fan, L.; Hu, Y.; Wang, X.; Zhang, L.; Li, F.; Han, D.; Li, Z.; Zhang, Q.; Wang, Z.; Niu, L. *Talanta* **2012**, *101*, 192-197.
- (86) En, D.; Guo, Y.; Chen, B.-T.; Dong, B.; Peng, M.-J. *RSC Advances* **2014**, *4*, 248-253.

Chapter 3

Copper-catalyzed Cross-Dehydrogenative C(*sp*³)-N Bond Coupling: An Unprecedented Tandem Synthesis of Coumarin-fused Pyrimidines



3.1 Introduction

Transition-metal-catalyzed C–H bond activation reactions are currently at the forefront of modern organic synthesis.¹ Over the years, the functionalization of activated/unactivated C(*sp*²)–H bonds has witnessed tremendous fame, furnishing a gallery of functionalized heterocyclic architectures.² On the other hand, the construction of C–C and C–X (X = N, O, S, P) bonds using unactivated C(*sp*³)–H bonds have geared up pervasively. Outstanding achievements have been documented by cross-dehydrogenative coupling (CDC) strategies that foster several chemical transformations by generating different libraries of complex molecules much rapidly (Figure 3.1.1).^{3–8}



Figure 3.1.1: A generalized demonstration of CDC strategy

Although, Pd-catalyzed reactions have attributed most successful protocols for the oxidative cross-coupling reactions, yet recent years have noticed several inclinations to replace palladium catalyst⁹ with other cost-effective and less-toxic transition metal-catalytic systems.^{10–12} In this context, copper catalysts have emerged as powerful strikers, furnishing complex organic molecules in limited steps *via* C–H bond activation protocols.^{12–17} Intriguingly, copper can exchange its oxidation state from Cu(0) to Cu(III) through one-electron or two-electron processes.¹⁸ As a result, the radical pathway and the two-electron bond-forming pathway *via* organometallic intermediates are postulated under appropriate conditions. The single-electron transfer (SET) from the electron-rich substrates to Cu(II) species is proposed to initiate an order of steps that eventually affords the oxidative coupled products.^{14,19}

Furthermore, the utility of aerial oxygen as oxidant has been broadly explored in different Cu-catalyzed reactions.²⁰ Pleasingly, the performance of Cu-catalyzed reactions drastically increases in the presence of “oxygen” either by acting as a pool for electrons (oxidase activity) or as a source of oxygen atoms that are incorporated into the product (oxygenase activity), or both.^{21,22} The oxidation of copper with oxygen is a facile process allowing catalytic turnover in net oxidative processes, and ready access to the higher Cu(III) oxidation state that enables a range of powerful transformations, including two-electron reductive elimination to Cu(I).

Thus, the cost-effectiveness, relatively better stability, easy-usability and the accessibility to synthesize complex molecules from simple starting materials in minimum actions have popularized the Cu-catalyzed CDC reactions.¹⁴ In addition, extensive efforts have been made by various research groups towards the constructing nascent C–C and C–X (hetero atom) bonds *via* Cu-catalyzed CDC approach under aerobic condition.^{14,20} A brief overview of Cu-catalyzed aerobic CDC methodologies is depicted in a pictorial representation (Figure 3.1.2).

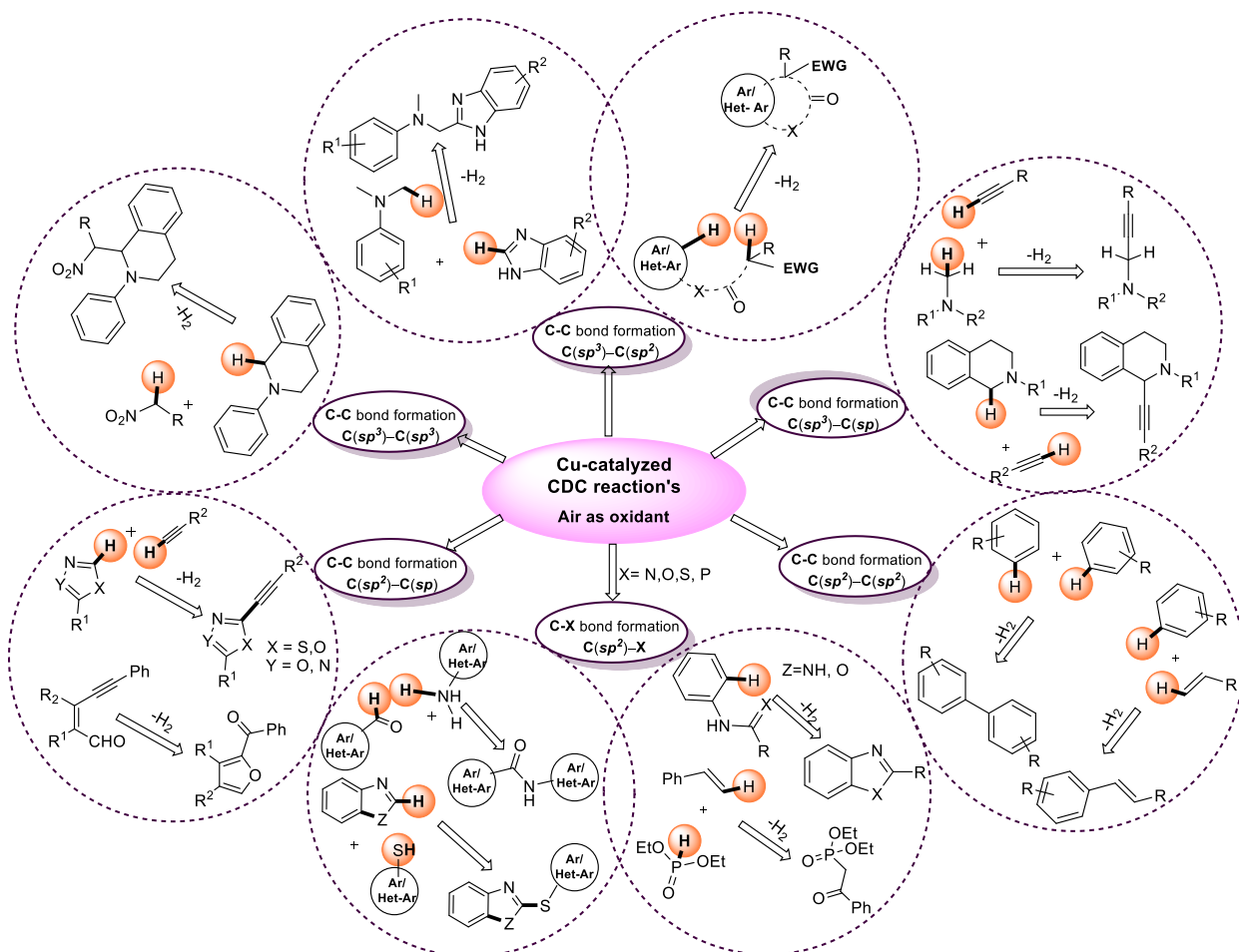


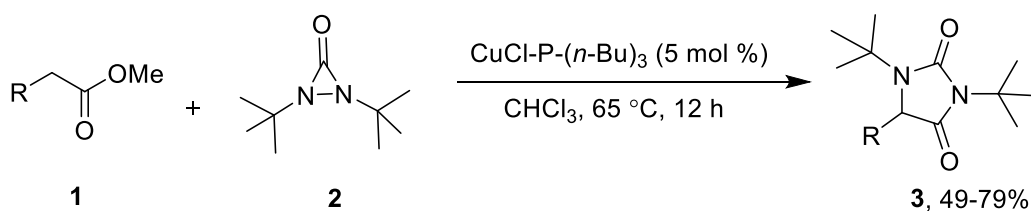
Figure 3.1.2: A brief overview of aerobic Cu-catalyzed CDC methodologies

In particular, Cu-catalyzed intramolecular cyclization reactions have gained significant interest towards the construction of a plethora of heterocycles by functionalizing different C(*sp*)–H, C(*sp*²)–H, and C(*sp*³)–H bonds. Among these, the transformation of unreactive C(*sp*³)–H bond into C–X (X = S, N, O) bond has received noticeable appreciation.^{21,23-25}

In fact, the selective activation/functionalization of alkyl C(*sp*³)–H bonds are considered to be highly challenging and “state of the art” to chemists due to the robust nature of such bonds.²² The

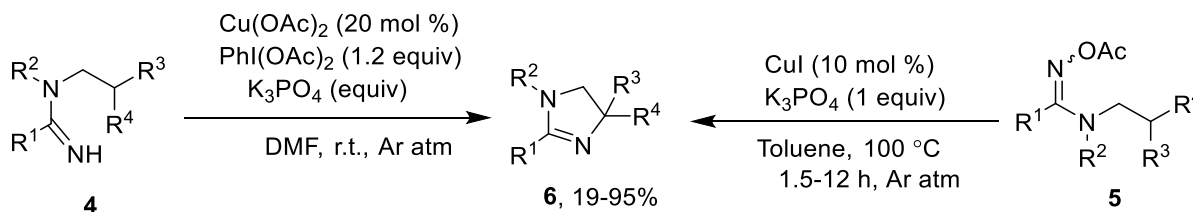
development of strategies to selectively functionalize these abundant bonds has faced tremendous difficulties, which is due to poor reactivity of $C(sp^3)$ -H bonds that is attributable to their high bond energies (typically 90–100 kcal/mol), low acidity (estimated $pK_a = 45$ –60) and unreactive molecular orbital profile.

In spite of these factors, the current era has witnessed unique $C(sp^3)$ -H bond functionalization strategies by mean of different Cu-catalyst.²⁶ Zhao *et al.* presented a path defining $C(sp^3)$ -H amination strategy for the synthesis of various hydantoins (**3**) from methyl aryl acetates (**1**) employing CuCl as catalyst and di-*tert*-butyldiaziridinone (**2**) as nitrogen source (Scheme 3.1.1).²⁷



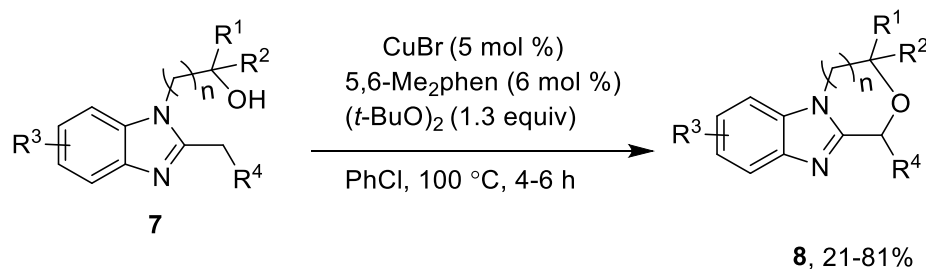
Scheme 3.1.1: Cu-catalyzed $C(sp^3)$ -H amination strategy for the synthesis of hydantoins (**3**)

Chen *et al.* disclosed a convergent and straightforward Cu-catalyzed oxidative protocol for the synthesis of dihydroimidazoles (**6**) by intramolecular aliphatic $C(sp^3)$ -H amination of amidines (**4**) using iodobenzene diacetate (PIDA) as an oxidant in DMF at room temperature.²⁸ Later the authors developed another Cu-catalyzed redox-neutral protocol for the same chemical transformation from amidoximes (**5**) without using PIDA in comparative yields (Scheme 3.1.2)²⁹



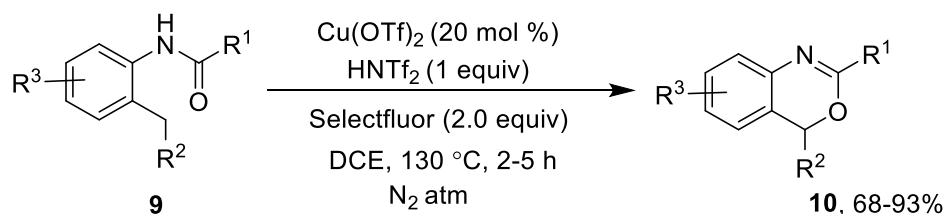
Scheme 3.1.2: Cu-catalyzed intramolecular aliphatic $C(sp^3)$ -H amination strategy towards the synthesis of dihydroimidazoles (**6**)

Takemura *et al.* developed an efficient protocol for the Cu-catalyzed oxidative intramolecular $C(sp^3)$ -H alkoxylation in *N*-(hydroxylalkyl)imidazoles (**7**), to afford differentazole-fused cyclic ethers (**8**) in moderate-to-excellent yields, using 5,6-dimethyl-1,10-phenanthroline in chlorobenzene (Scheme 3.1.3).³⁰



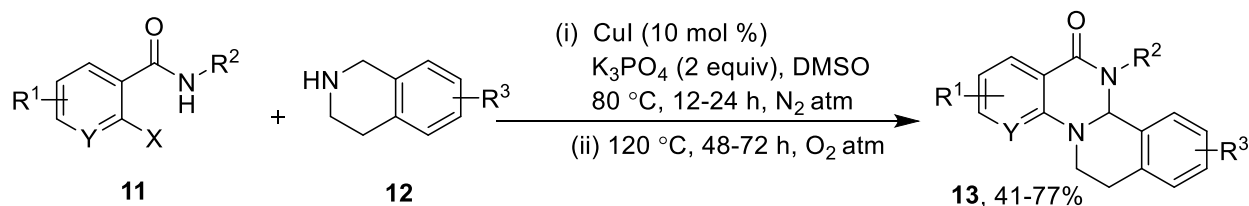
Scheme 3.1.3: Cu-catalyzed intramolecular C(*sp*³)-H alkoxylation strategy towards the synthesis ofazole-fused cyclic ethers (**8**)

Li *et al.* presented a diversified Cu-catalyzed intramolecular benzylic C(*sp*³)-O cyclization in *N*-*o*-tolylbenzamides (**9**) using Selectfluor as an oxidant for synthesizing 4*H*-3,1-benzoxazines (**10**) in moderate-to-excellent yields (Scheme 3.1.4).³¹



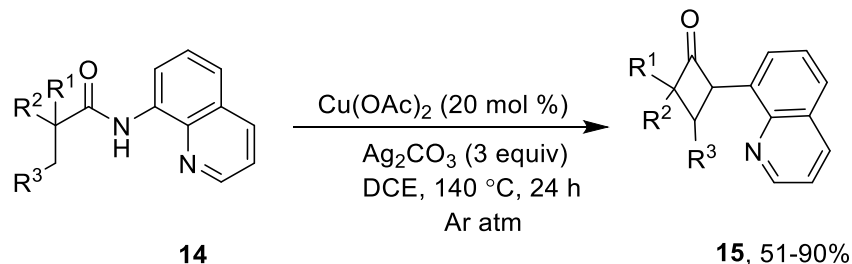
Scheme 3.1.4: Cu-catalyzed intramolecular benzylic C(*sp*³)-O cyclization strategy towards the synthesis of 4*H*-3,1-benzoxazines (**10**)

Tian *et al.* reported a Cu-catalyzed one-pot synthetic protocol for the synthesis of substituted tetrahydroisoquinolino[2,1-*a*]quinazolinone derivatives (**13**) in 41-77% yields by reacting substituted *N*-substituted-2-halobenzamides (**11**) with substituted 1,2,3,4-tetrahydroisoquinolines (**12**) using K₃PO₄ in DMSO *via* C-H activation followed by cyclization (Scheme 3.1.5).³²



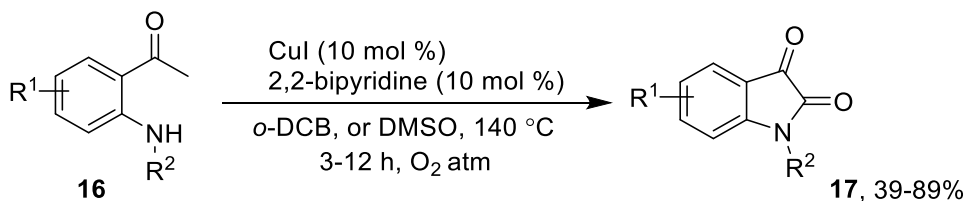
Scheme 3.1.5: Cu-catalyzed CDC strategy towards the synthesis of tetrahydroisoquinolino[2,1-*a*]quinazolinones (**13**)

Wang *et al.* reported a Cu-catalyzed C(*sp*³)-H functionalization reaction for the synthesis of four-membered β -lactam derivatives (**15**) in high yields *via* intramolecular amidation of *N*-(quinolin-8-yl)pivalamide derivatives (**14**), employing CuCl as a catalyst and Ag₂CO₃ as an oxidant under an argon atmosphere (Scheme 3.1.6).³³



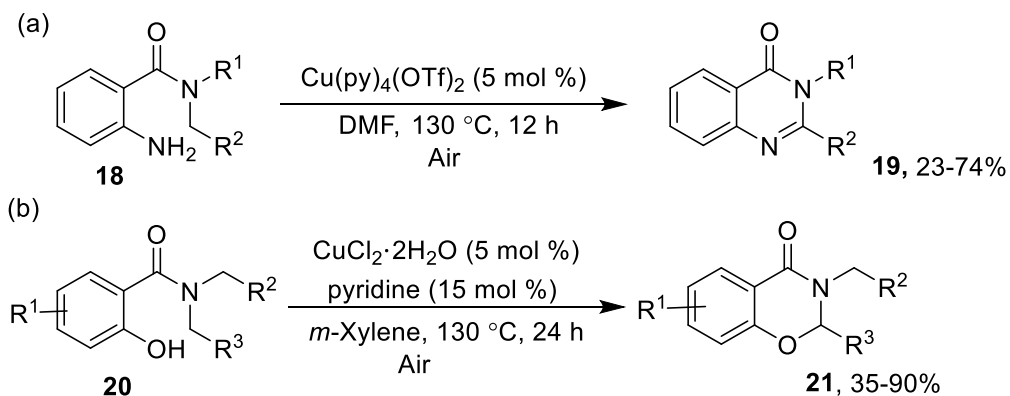
Scheme 3.1.6: Cu-catalyzed intramolecular CDC strategy towards the synthesis of β -lactams (**15**)

Huang *et al.* documented an efficient Cu-catalyzed intramolecular C–H amination protocol for the synthesis of isatins derivatives (**17**) in moderate-to-good yields from 2-aminoacetophenones (**16**) employing CuI as a catalyst and molecular oxygen as the oxidant (Scheme 3.1.7).³⁴



Scheme 3.1.7: Cu-catalyzed intramolecular CDC strategy towards the synthesis of isatins (**17**)

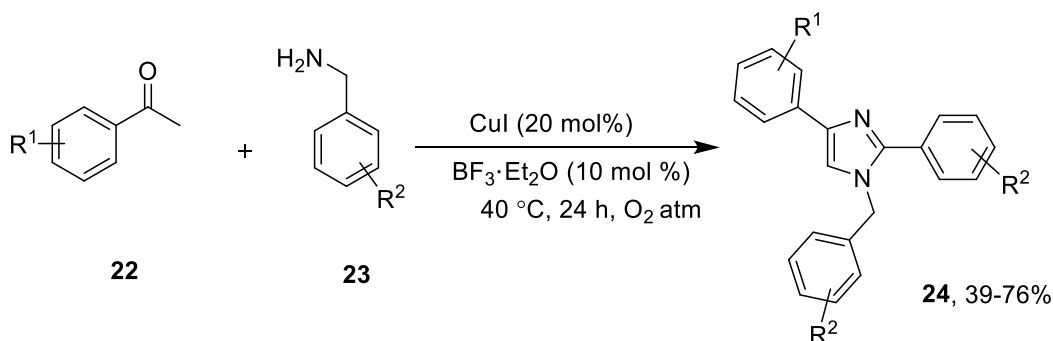
Very recently, Gholap *et al.* disclosed a Cu-catalyzed strategy for intramolecular cyclization of 2-amino-*N,N*-dialkylbenzamides (**18**) to afford 2,3-disubstituted-4(3*H*)-quinazolinones (**19**) via a SET based oxidative coupling, involving an iminium radical cation as a possible intermediate (Scheme 3.1.8a).³⁵ Prior to this report, the authors also reported similar Cu-catalyzed methodology for the synthesis of dihydrooxazinones (**21**) by intramolecular dehydrogenative coupling of salicylamides (**20**) (Scheme 3.1.8b).³⁶



Scheme 3.1.8: Cu-catalyzed intramolecular CDC strategy towards the synthesis of 2,3-disubstituted-4(3*H*)-quinazolinones (**19**) & dihydrooxazinones (**21**)

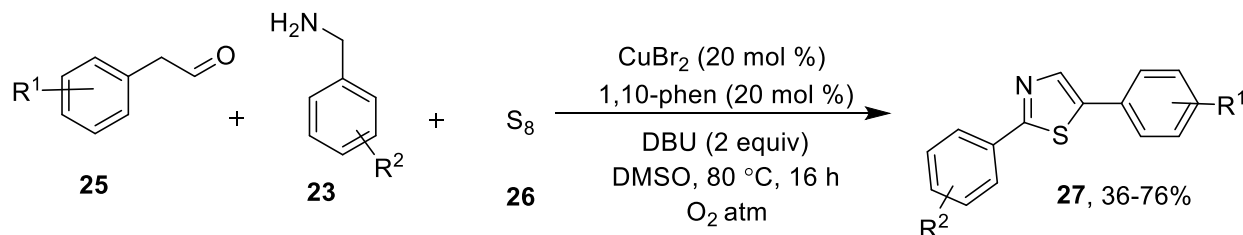
In striking contrast, benzylamines (**23**) are valuable coupling partners used for the synthesis of different natural products, agrochemicals, polymers, and pharmaceuticals. Cu-catalyzed oxidative C(sp^3)-H bond functionalization protocol has been efficiently explored in the construction of aryl/heteroaryl C-N bonds using benzylamines as a precursor.

Cai *et al.* presented a tandem Cu-catalyzed C(sp^3)-H oxidative dehydrogenative protocol for the synthesis of substituted imidazoles (**24**) in moderate-to-good yields from acetophenones (**22**) and benzylamines (**23**) using CuI as the catalyst and molecular oxygen as an oxidant (Scheme 3.1.9).³⁷



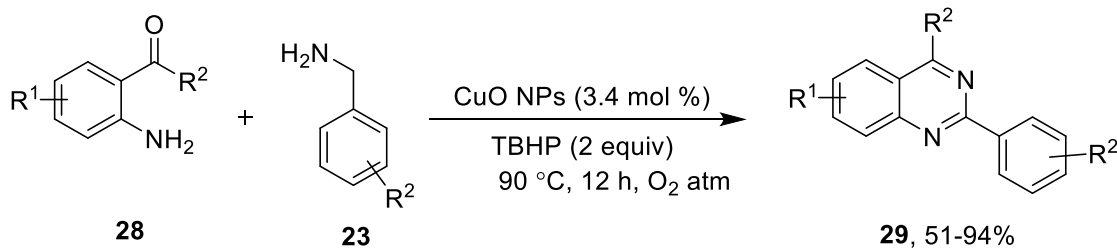
Scheme 3.1.9: Cu-catalyzed C(sp^3)-H CDC strategy towards the synthesis of substituted imidazoles (**24**)

Wang *et al.* developed an efficient and practical approach for the synthesis of thiazoles (**27**) in decent yields from phenyl aceteldehydes (**25**), benzylamines (**23**), and elemental sulfur (**26**) through multiple C(sp^3)-H bond forming processes, using Cu(II) as catalyst and DBU as a base in DMSO (Scheme 3.1.10).³⁸



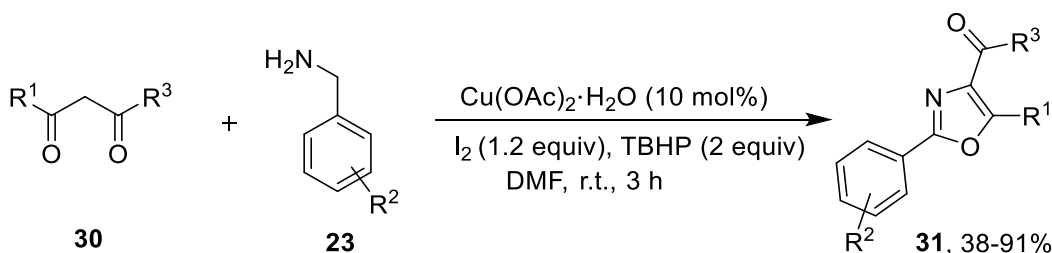
Scheme 3.1.10: Cu-catalyzed CDC strategy towards the tandem synthesis of thiazoles (**27**)

Zhang *et al.* reported the copper oxide nanoparticle-catalyzed oxidative dehydrogenative strategies for synthesis of quinazolines derivatives (**29**) in high yields from 2-aminobenzophenones (**28**) and benzylamines (**23**) using TBHP as the oxidant (Scheme 3.1.11).³⁹



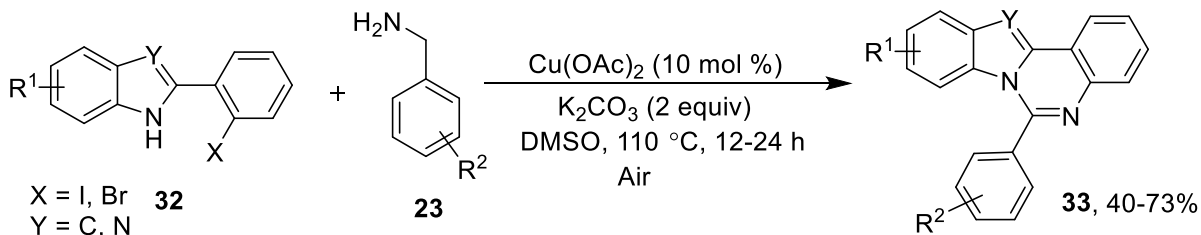
Scheme 3.1.11: Cu-catalyzed CDC strategy towards the synthesis of 2-phenylquinazolines (**29**)

Wan *et al.* reported the synthesis of polysubstituted oxazoles (**31**) in good yields from β -diketones (**30**) and benzylamines (**23**) via Cu-catalyzed tandem oxidative cyclization protocol (Scheme 3.1.12).⁴⁰



Scheme 3.1.12: Cu-catalyzed tandem CDC strategy towards the synthesis of oxazoles (**31**)

Sang *et al.* prepared indolo[1,2-c]quinazolines (**33**) via intermolecular *N*-arylation and intramolecular aerobic oxidative C–H amination from 2-(2-halophenyl)-1*H*-indoles (**32**) and benzylamines (**23**) under Cu-catalyzed conditions using air as an oxidant (Scheme 3.1.13).⁴¹



Scheme 3.1.13: Cu-catalyzed intermolecular *N*-arylation and intramolecular aerobic oxidative C–H amination strategy towards the synthesis of indolo[1,2-c]quinazolines (**33**)

In addition, cross-dehydrogenative coupling (CDC) has been explored towards the tandem synthesis of fused coumarins that are essential structural motifs of many alkaloids, and have exhibited versatile biological activities including anticancer,⁴² antitumor,⁴³ estrogen mimic,⁴⁴ antifungal,⁴⁵ antitubercular,⁴⁶ and progesterone receptor modulator activities⁴⁷ (Figure 3.1.3).

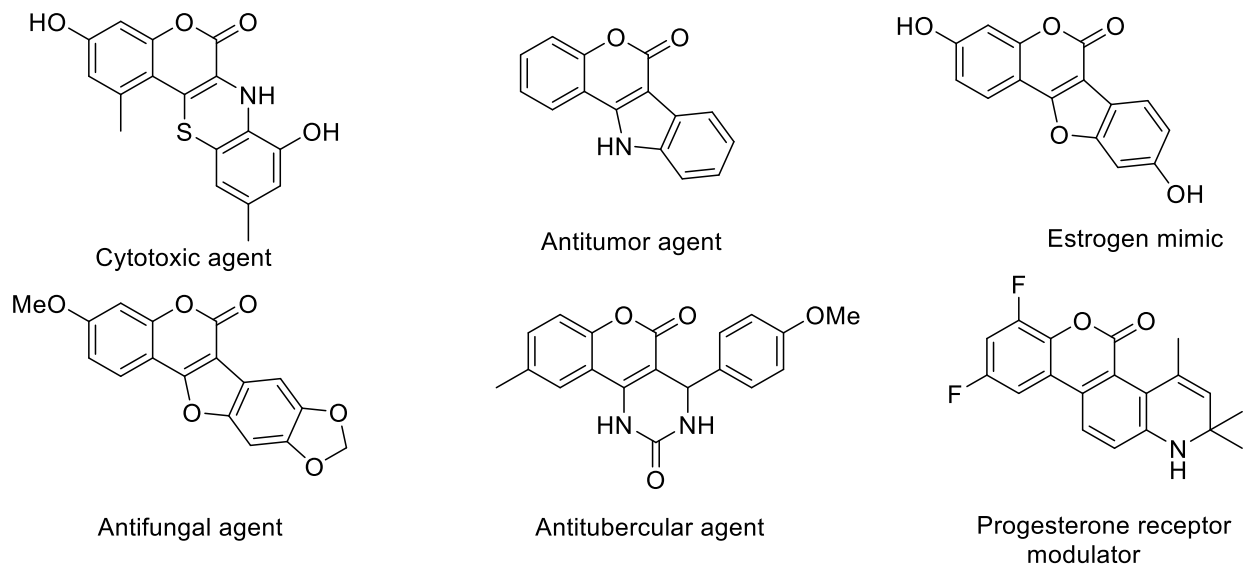
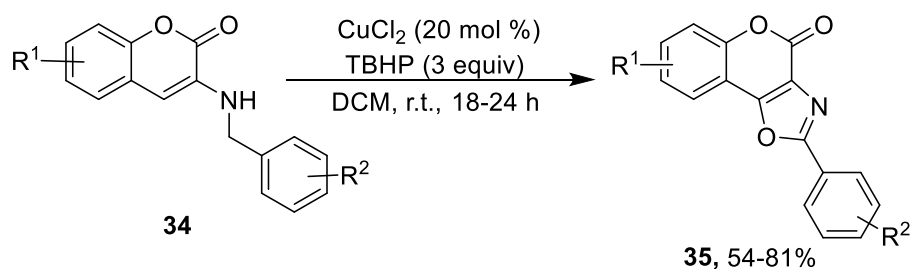


Figure 3.1.3: Selective examples of biologically active coumarin-fused heterocycles

Several fluorescent coumarin-fused hetero-skeletons assembled *via* π -conjugated motifs have been used as optical brightening agents, light-emitting diodes, chemosensors, laser devices, and markers for biomedical imaging.⁴⁸⁻⁵¹

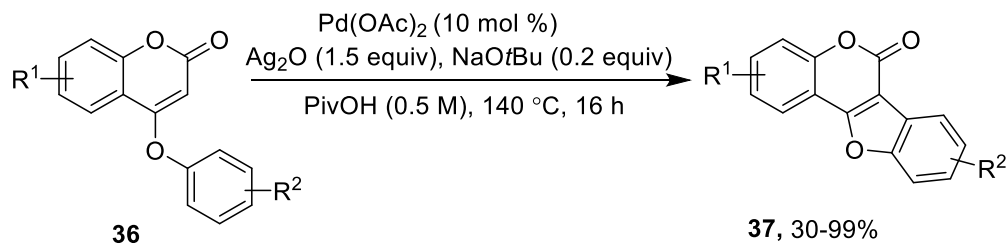
Because of significant applications of coumarin-fused heterocycles as pharmaceuticals and functional materials, researchers have substantially contributed to their synthesis *via* transition-metal-catalyzed CDC strategies.⁵²⁻⁵⁸ In this realm, Belal *et al.* prepared coumarin-fused oxazoles (**35**) *via* oxidative Cu-catalyzed CDC protocol using TBHP as an oxidant in DCM at room temperature (Scheme 3.1.14).⁵²



Scheme 3.1.14: Cu-catalyzed CDC approach towards the synthesis of coumarin-fused oxazoles (**35**)

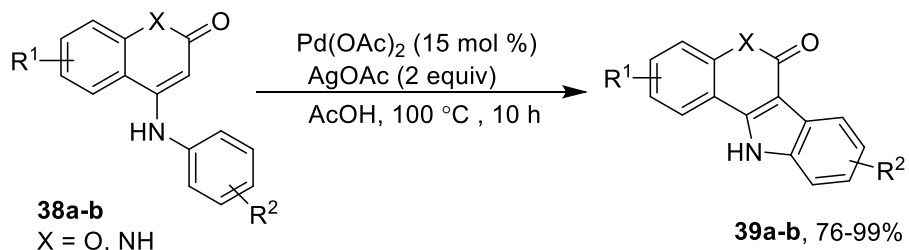
Apart from the Cu-catalyzed strategy, few Pd-catalyzed cross-dehydrogenative coupling approaches have also been developed for preparing coumarin-fused heterocycles.

For example, Mackey *et al.* reported an intramolecular aryl–heteroaryl coupling approach from (**36**) via double C–H activation under Pd-catalyzed conditions, accessing coumarin-fused benzofurans (**37**) in good-to-excellent yields (Scheme 3.1.15).⁵³



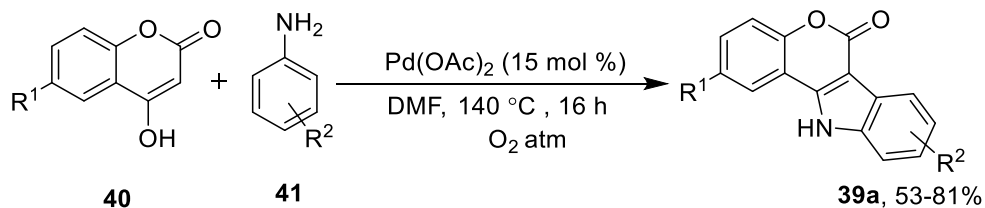
Scheme 3.1.15: Pd-catalyzed CDC approach towards the synthesis of coumarin-fused benzofurans (**37**)

Similarly, Cheng *et al.* documented Pd-catalyzed intramolecular oxidative cross-dehydrogenative coupling in substituted 4-(phenylamino)-2*H*-chromen-2-ones (**38a**) and 4-(phenylamino)-2*H*-quinolin-2-ones (**38b**) in acetic acid, to afford indole-fused polyheterocycles (**39a-b**) in good-to-excellent yields (Scheme 3.1.16).⁵⁴



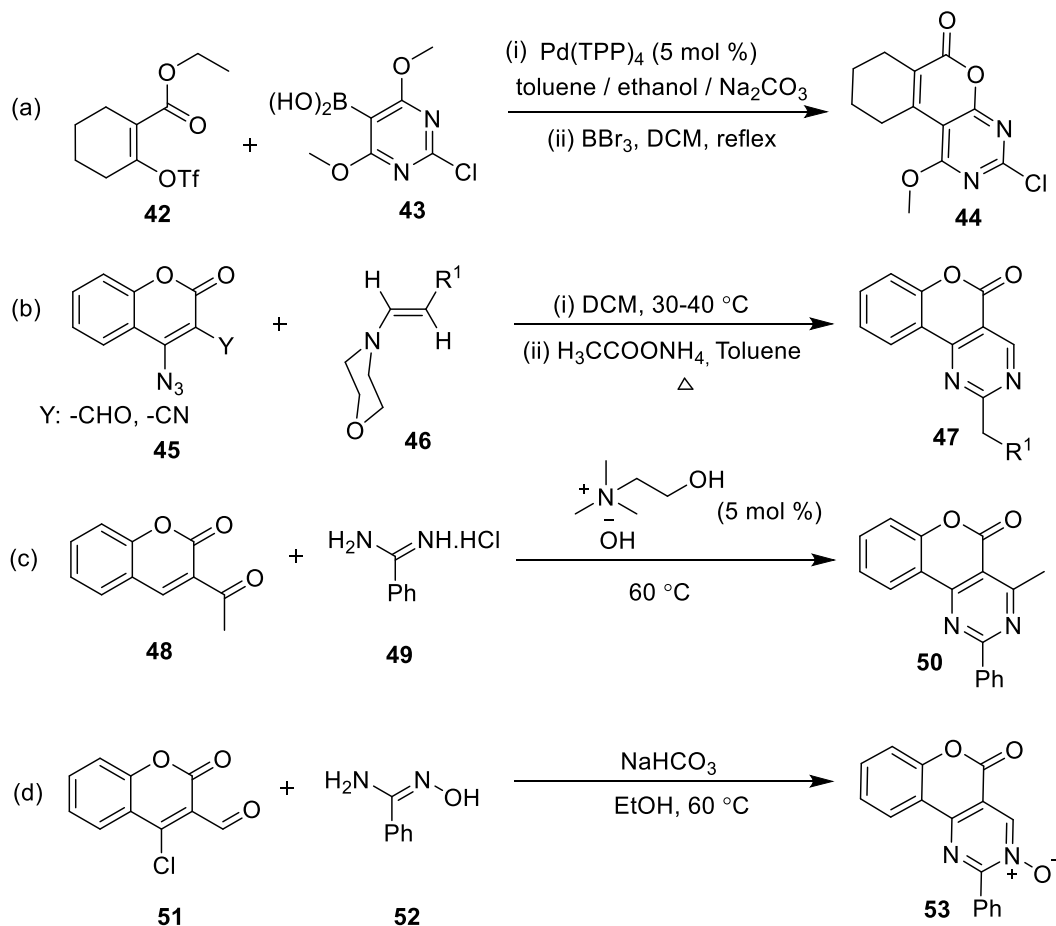
Scheme 3.1.16: Pd-catalyzed CDC approach towards the synthesis of indole-fused polyheterocycles (**39a-b**)

Dey *et al.* documented a Pd-catalyzed strategy for the synthesis of substituted indole-fused coumarins (**39a**) via an oxidative cross-dehydrogenative coupling reaction between 4-hydroxy coumarins (**40**) and anilines (**41**) (Scheme 3.1.17).⁵⁵



Scheme 3.1.17: Pd-catalyzed CDC approach towards the synthesis of indole-fused coumarins (**39a**)

In particular, coumarin-fused pyrimidines have received much attention, and several routes for their synthesis have been documented. Some of these include: (a) a Pd-catalyzed synthesis of tetrahydro-6*H*-isochromeno[3,4-*d*]pyrimidin-6-one from pyrimidinylboronic acid and cyclic enol triflates, followed by BBr₃-mediated cyclization (Scheme 3.1.18a),⁵⁹ (b) base-mediated ring-closure synthesis of benzopyranopyrimidin-5-ones from 3-formyl (or cyano)-coumaryl amidines using ammonium acetate (Scheme 3.1.18b),⁶⁰ (c) choline hydroxide-catalyzed synthesis of 4-methyl-2-phenyl-5*H*-chromeno[4,3-*d*]pyrimidin-5-one *via* tandem oxidative annulation of 3-acetyl coumarin with benzamidiniumhydrochloride (Scheme 3.1.18c),⁶¹ and (d) base-mediated synthesis of chromeno-pyrimidine-*N*-oxide from 4-chloro-3-formylcoumarin and aromatic carboxamide oximes (Scheme 3.1.18d).⁶²



Scheme 3.1.18: Existing synthetic routes to various coumarin-fused pyrimidines

Despite a few advancements, most of the described strategies suffer from one or more drawbacks, including the use of Pd catalyst, pre-activated starting materials, expensive and moisture-sensitive reagents, harsh conditions, and multistep synthetic procedures. Thus, it is highly desirable to

develop an atom-economical and environmentally benign protocol for the synthesis of coumarin-fused pyrimidines.

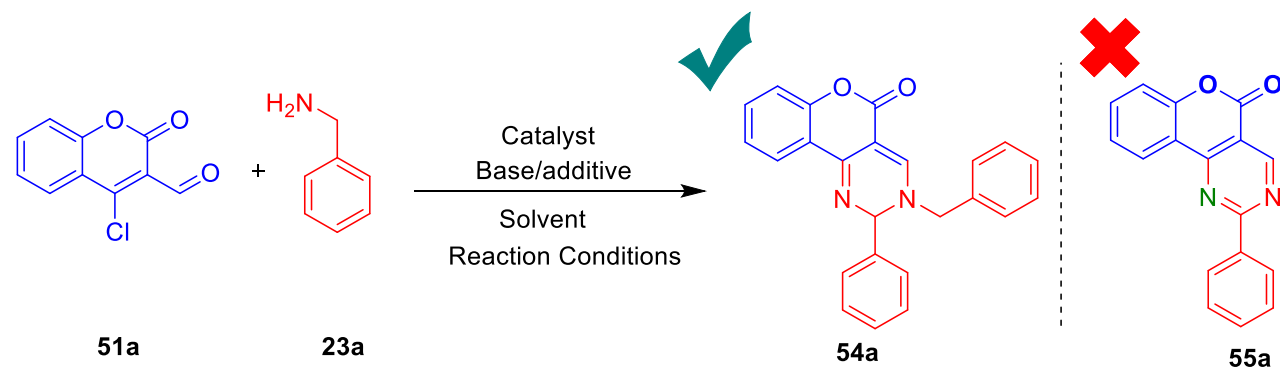
In this chapter, we envisioned the synthesis of coumarin-fused pyrimidines by intramolecular cross-dehydrogenative C(*sp*³)-N bond forming between from 4-chloro-3-formylcoumarin and benzylamines in a tandem fashion.

3.2 Results and Discussion

Our preliminary investigation started by standardizing the model reaction between 4-chloro-3-formylcoumarin (**51a**, 1 equiv) and benzylamine (**23a**, 1 equiv) using potassium carbonate (K₂CO₃) and sodium azide (NaN₃) as a nitrogen source under Cu(I)-catalyzed conditions. To our delight and surprise, 3-benzyl-2-phenyl-2,3-dihydro-5*H*-chromeno[4,3-*d*]pyrimidin-5-one (**54a**) was isolated in 30% yield over the expected product **55a**, when the reaction was carried out in DMSO at 80 °C (Table 3.2.1, entry 1). The structure of **54a** was unambiguously confirmed by ¹H NMR, ¹³C NMR, 2D-NMR experiments and HRMS analysis, indicating the non-participation of sodium azide in this oxidative tandem cyclization. Interestingly, by increasing the number of equivalents of benzylamine to 2 and 3, **54a** was obtained in 42% and 50% isolated yields, respectively in absence of sodium azide (Table 3.2.1, entries 2-3). Solvent screening studies showed that the solvent plays a crucial role in this oxidative cyclization process. The yield of **54a** decreased when DMSO was replaced with solvents such as dioxane, CH₃CN, DCM, and THF (Table 3.2.1, entry 4). However, the yield of **54a** significantly increased to 70% when the model reaction was performed in DMF at 80 °C for 12 h (Table 3.2.1, entry 5). Subsequently, the catalyst screening studies inferred that other Cu catalysts such as CuBr, CuCl, Cu₂O, Cu(OAc)₂, CuBr₂, and CuCl₂ showed less catalytic activity than CuI, affording the desired product **54a** in comparatively lower yields (Table 3.2.1, entries 6–11). Other transition-metal catalysts such as FeCl₃, NiCl₂, and Pd(OAc)₂ failed to produce the desired product under similar reaction conditions (Table 3.2.1, entry 12). To further increase the product yield, the reaction temperature, reaction time, and oxidant were optimized. No appreciable change in the yield of **54a** was observed by increasing the reaction temperature to 100 °C, or by increasing the reaction time to 15 h in two separate experiments (Table 3.2.1, entries 13-14). Further, not much increment in the yield of **54a** was observed by performing the experiment under oxygen atmosphere (Table 3.2.1, entry 15). On the other hand, the use of external oxidants such as TBHP, K₂S₂O₈, PIDA, or CH₃COOH provided unsatisfactory results (Table 3.2.1, entries 16–

19). No appreciable change in the yield of **54a** was observed by using two equivalents of Cs_2CO_3 in place of K_2CO_3 (Table 3.2.1, entry 20).

Table 3.2.1: Selected optimization of reaction conditions^a for the synthesis of **54a**



Entry	Catalyst	Base/(additive)	Solvent	Oxidant	Yield ^b (%)
1. ^c	CuI	K_2CO_3 (NaN_3)	DMSO	Air	30
2. ^d	CuI	K_2CO_3	DMSO	Air	42
3.	CuI	K_2CO_3	DMSO	Air	50
4. ^e	CuI	K_2CO_3	Dioxane/DCM/THF/ CH_3CN	Air	25–45
5.	CuI	K_2CO_3	DMF	Air	70
6.	CuBr	K_2CO_3	DMF	Air	50
7.	CuCl	K_2CO_3	DMF	Air	52
8.	Cu_2O	K_2CO_3	DMF	Air	40
9.	$\text{Cu}(\text{OAc})_2$	K_2CO_3	DMF	Air	55
10.	CuBr_2	K_2CO_3	DMF	Air	53
11.	CuCl_2	K_2CO_3	DMF	Air	52
12.	$\text{FeCl}_3/\text{NiCl}_2/Pd(\text{OAc})_2$	K_2CO_3	DMF	Air	NR
13. ^f	CuI	K_2CO_3	DMF	Air	70
14. ^g	CuI	K_2CO_3	DMF	Air	71
15.	CuI	K_2CO_3	DMF	O_2	73
16. ^h	CuI	K_2CO_3	DMF	TBHP	60
17. ^h	CuI	K_2CO_3	DMF	$\text{K}_2\text{S}_2\text{O}_8$	48
18. ^h	CuI	K_2CO_3	DMF	PIDA	50
19. ^h	CuI	K_2CO_3	DMF	AcOH	NR
20.	CuI	Cs_2CO_3	DMF	Air	68

^aReaction conditions: **51a** (0.25 mmol), **23a** (0.75 mmol), catalyst (10 mol %), K_2CO_3 (0.50 mmol), solvent (5 mL), 80 °C, 12 h; ^bIsolated yield; ^c**23a** (0.25 mmol); ^d**23a** (0.50 mmol); ^eT = reflux for 12 h; ^fT = 100 °C (for 12 h); ^gT = 80 °C (for 15 h); ^hoxidant (0.50 mmol); NR: no reaction.

The ^1H and ^{13}C NMR spectra of **54a** are presented in Figure 3.2.1 and Figure 3.2.2, respectively.

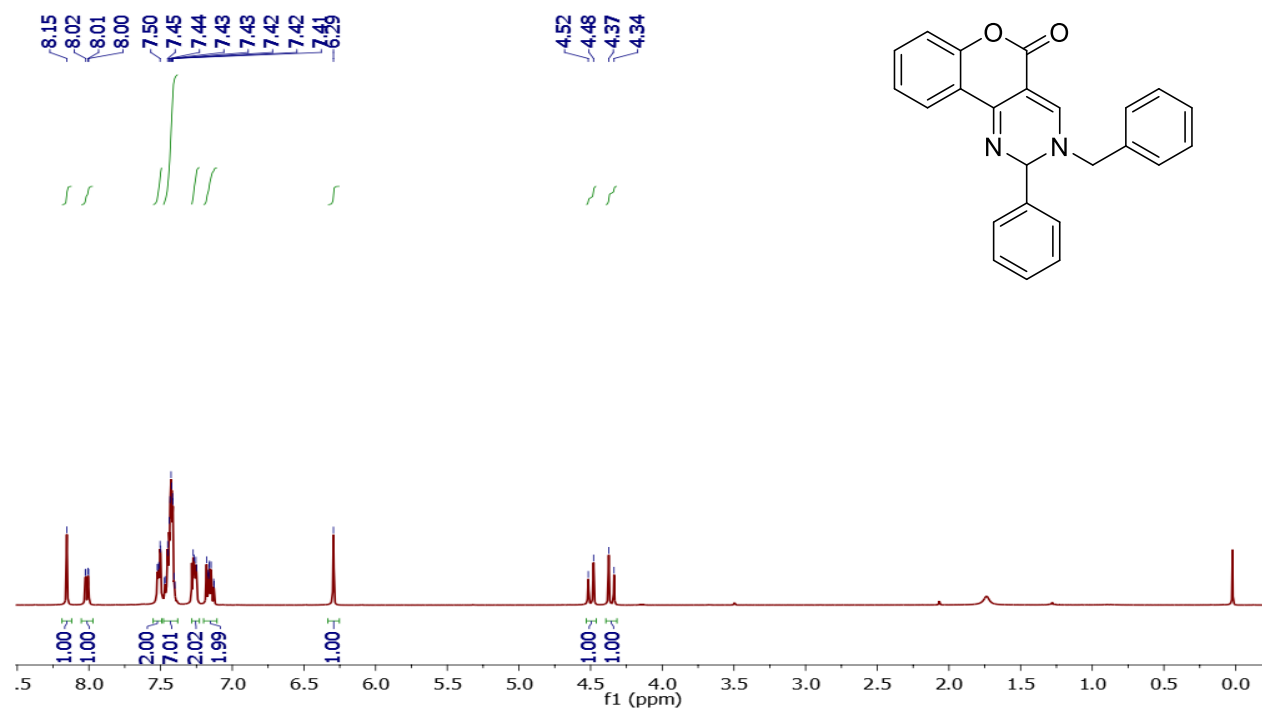


Figure 3.2.1: ^1H NMR spectrum of **54a** in CDCl_3

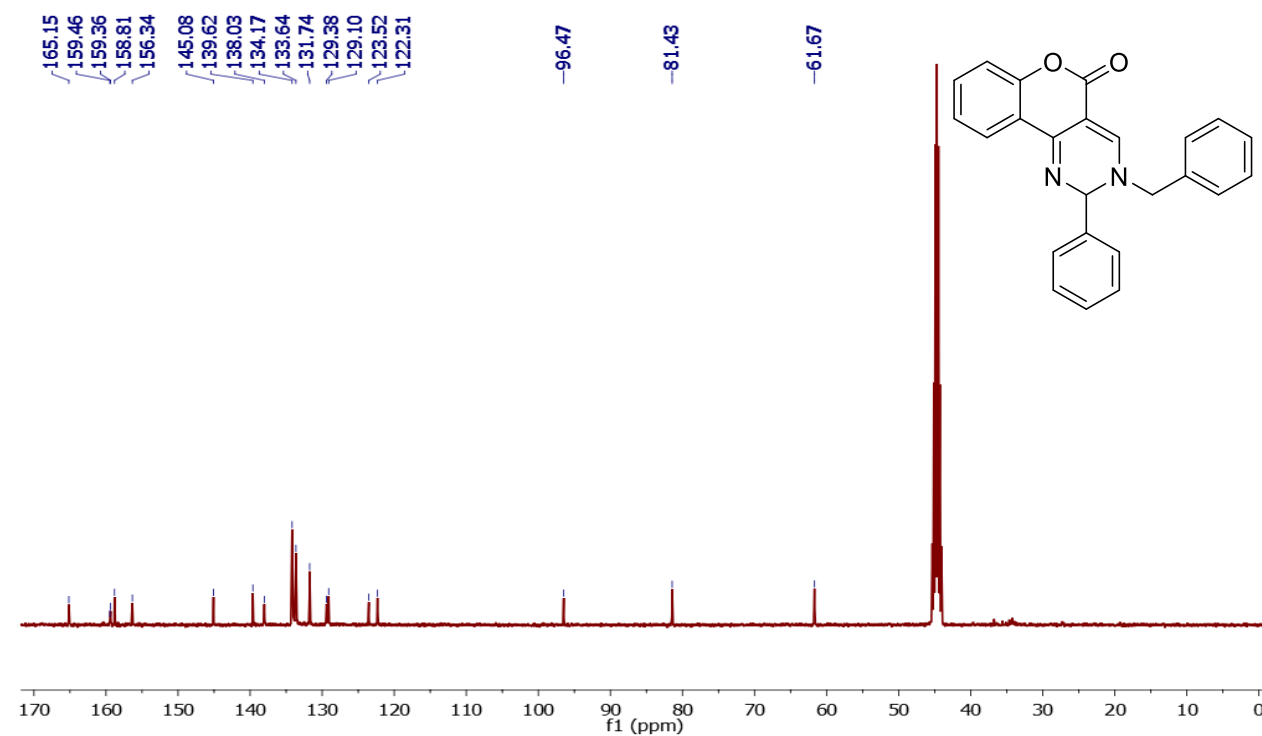


Figure 3.2.2: ^{13}C NMR spectrum of **54a** in $\text{DMSO-}d_6$

The 2D-COSY & HETCOR spectra of **54a** are presented in Figure 3.2.3 and Figure 3.2.4, respectively.

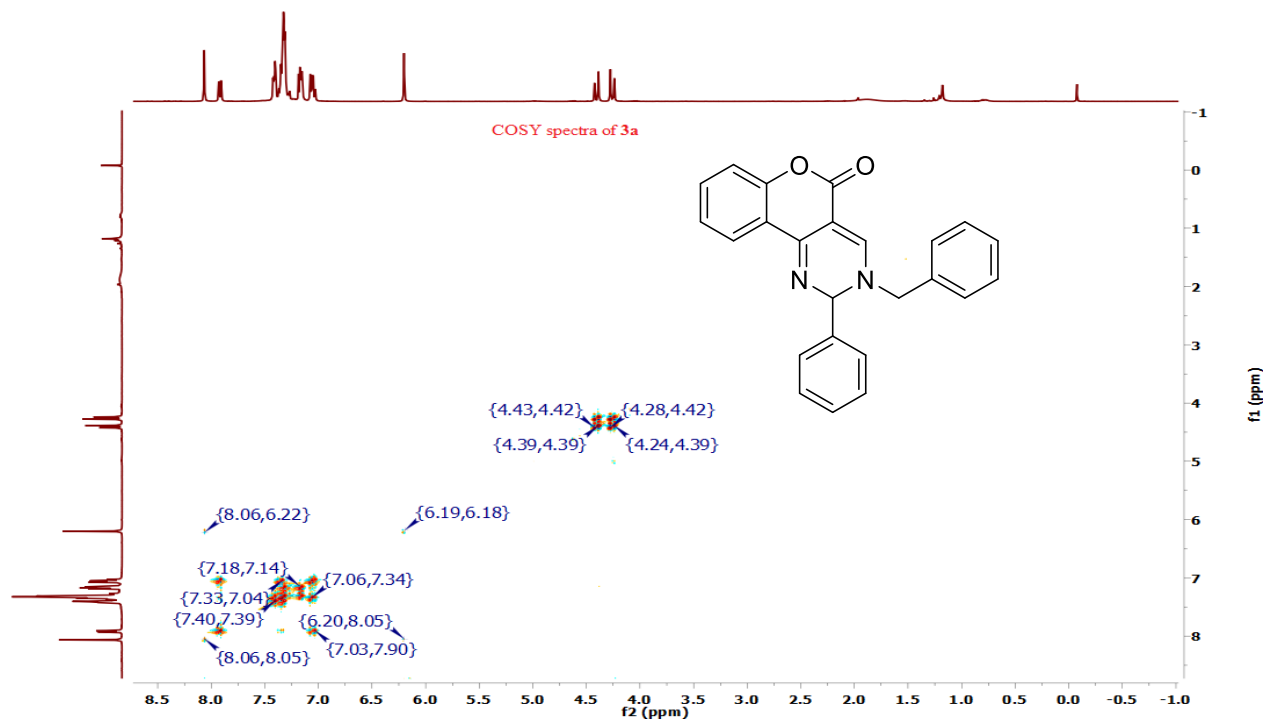


Figure 3.2.3: 2D-COSY spectrum of **54a**

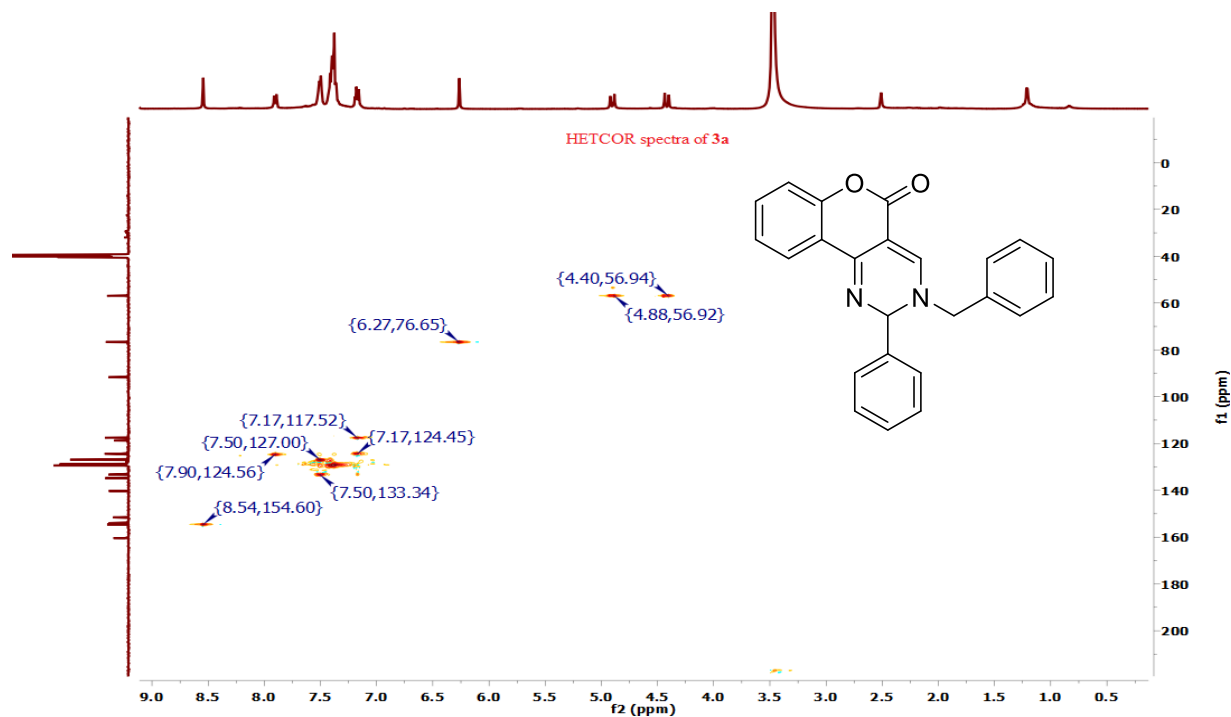
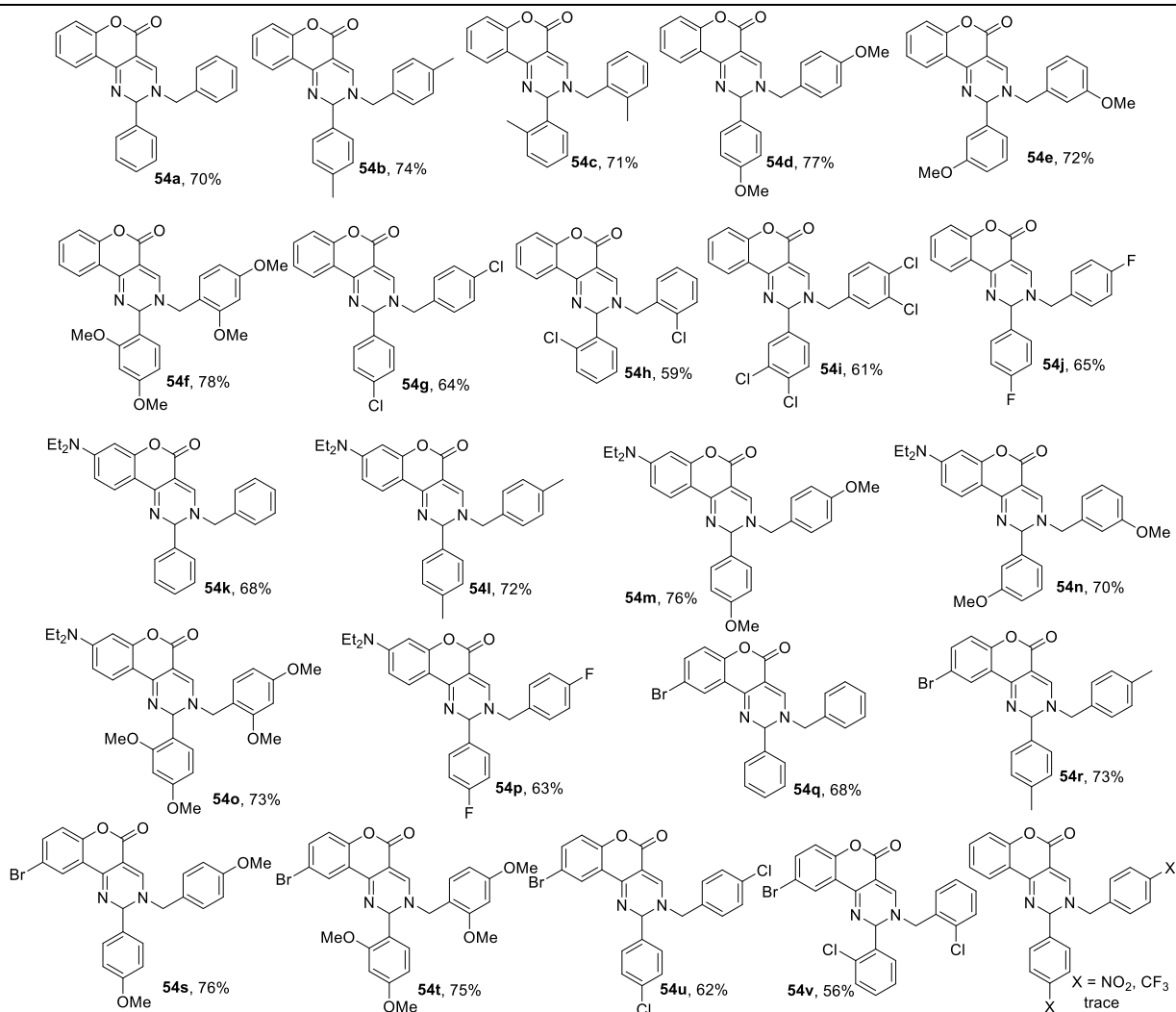
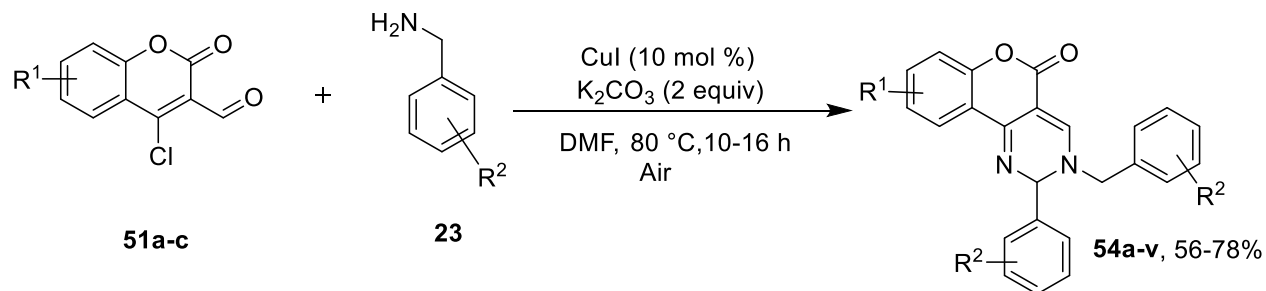


Figure 3.2.4: 2D-HETCOR spectrum of **54a**

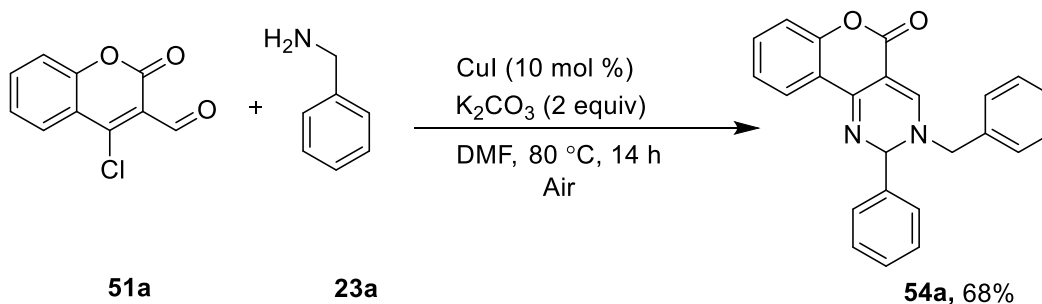
With optimized conditions (Table 3.2.1, entry 5) in hand, diverse benzylamines were used to investigate the generality and scope of this tandem oxidative cyclization (Scheme 3.2.1). Electron-donating benzylamine substrates (**23b–f**) showed better reactivity, affording the corresponding coumarin-fused pyrimidines (**54b–f**) in 71–78% yields. Chloro- and fluoro-substituted benzylamines (**23g–i** & **23j**) afforded the desired products (**54g–i** & **54j**) in comparatively lower yields. A small variation in the reactivity of *ortho*-, *meta*-, and *para*-substituted benzylamines (**23b–j**) was clearly evident from the yields of the corresponding products (**54b–j**).

In addition, the performance of the protocol was also evaluated by the efficient condensation of 4-chloro-7-(diethylamino)-2-oxo-2*H*-chromene-3-carbaldehyde (**51b**) with different substituted benzylamines. In this case, the presence of electron-donating groups (4-Me, 4-OMe, 3-OMe, 2,4-diOMe) and halogens (4-F) on benzylamine exhibited almost similar or slightly lower reactivity, affording the corresponding coumarin-fused pyrimidines (**54k–p**) in 58–76% yields (Scheme 3.2.1). The strategy was further applied to electron-deficient 6-bromo-4-chloro-2-oxo-2*H*-chromene-3-carbaldehyde (**51c**), offering the desired products **54q–v** in 56–76% yield (Scheme 3.2.1). In particular, the presence of electron-rich benzylamines showed faster transformation over the electron-deficient benzylamines. Unfortunately, benzylamines possessing strong electron-withdrawing groups such as CF₃ or NO₂ failed to react under the optimized conditions, yielding trace amount of the corresponding products, which were not isolated. All the synthesized compounds were purified by column chromatography, and characterized by detailed spectroscopic analysis.



Scheme 3.2.1: Substrate scope of benzylamines (**23a-j**) and 4-chloro-3-formylcoumarin (**51a-c**) for the synthesis of coumarin-fused pyrimidines (**54a-v**)

To assess the scalability of this Cu(I)-catalyzed tandem oxidative cyclization, a gram-scale reaction of **51a** with **23a** (3 equiv) was carried under optimized conditions, affording the desired product **54a** in an appreciable yield of 68% (1.19 g) (Scheme 3.2.2).



Scheme 3.2.2: Gram-scale synthesis of **54a**

To further confirm the proposed structure, as a representative example, single crystals of **54a** were grown from a mixture of ethyl acetate and methanol for X-ray diffraction (XRD) studies. Compound **54a** crystallizes in the $C2/c$ group. The ORTEP diagrams of the **54a** (*S* & *R* stereoisomers) (CCDC No. 1575437) are shown in Figure 3.2.5. Although compound **54a** carries a chiral carbon center, it crystallizes in the centro-symmetric space group due to its existence as racemic mixture. The *S* stereoisomer is shown in Figure 3.2.5; a), the ORTEP diagram of the *R* stereoisomer is shown in Figure 3.2.5; b).

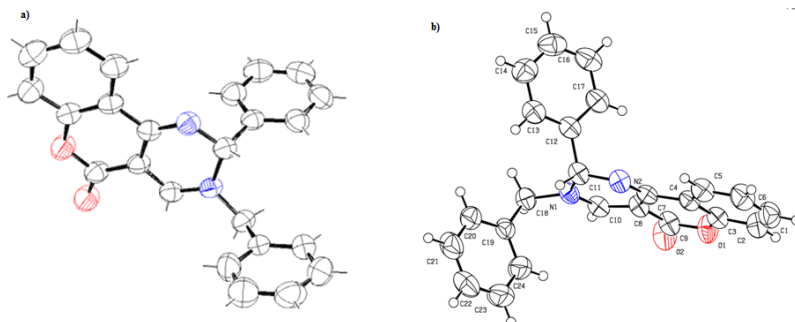
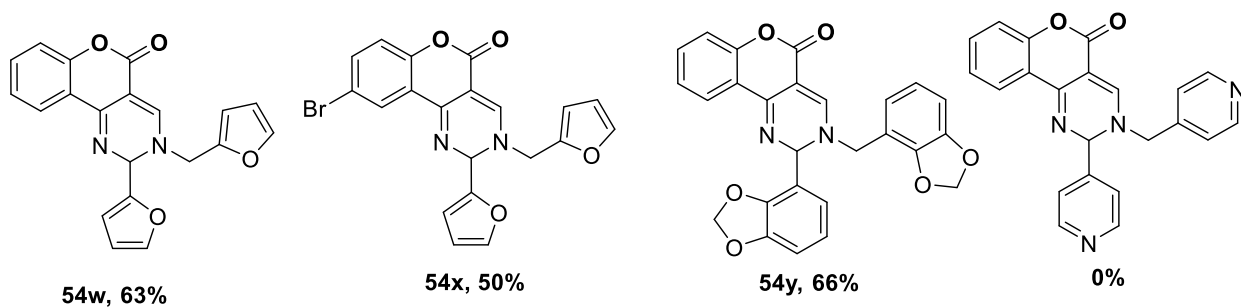
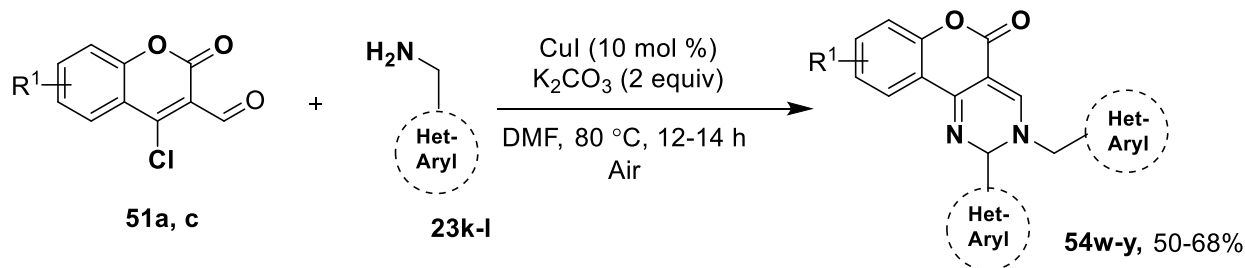


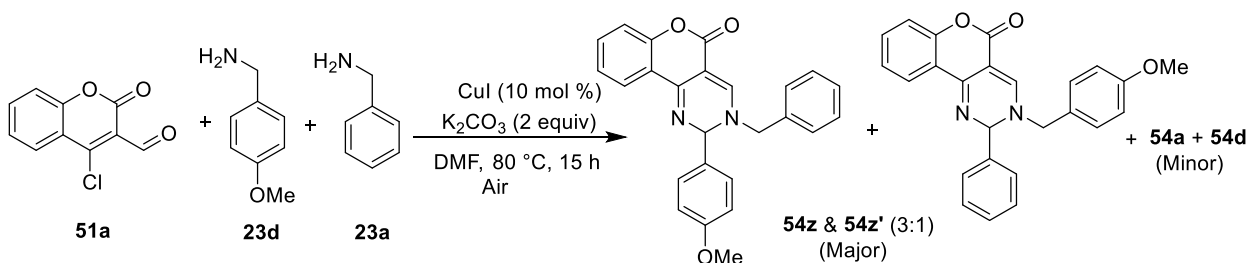
Figure 3.2.5: ORTEP diagrams of **54a** (a) *S* stereoisomer and (b) *R* stereoisomer

The synthetic generality of this tandem CDC protocol was also investigated using heteroarylmethanamines. Furan-2-ylmethanamine and benzo[*d*][1,3]dioxol-4-ylmethanamine showed fairly good reactivity, affording the desired coumarin-fused pyrimidines (**54w-y**) in 50–66% yields (Scheme 3.2.3). Unfortunately, pyridin-4-ylmethanamine failed to react under the optimized conditions, even upon heating at 80 °C in DMF up to 24 h.



Scheme 3.2.3: Substrate scope of heteroarylmethanamines (**23k-l**) and 4-chloro-3-formylcoumarin (**51a, 51c**) for the synthesis of coumarin-fused pyrimidines (**54w-y**)

Next, the synthetic versatility of this tandem reaction was studied using two different benzylamines (**23a** & **23d**). Interestingly, the reaction of **51a** with benzylamines **23d** (1 equiv) and **23a** (1 equiv) (added in a sequential manner) under Cu(I)-catalyzed conditions afforded a mixture of closely visualized product spots on TLC plates; the HRMS of the crude product affirmed the formation of cross-coupled and homo-coupled products (Scheme 3.2.4) (HRMS of the crude product is shown in Figure 3.2.6). Gratifyingly, we were able to separate the major cross-coupled products (**54z** + **54z'**) from homo-coupled products (**54a** & **54d**) using column chromatography. However, the ¹H NMR of the cross-coupled product shown in Figure 3.2.7, indicated it to be mixture of two possible structural isomers **54z** & **54z'**.



Scheme 3.2.4: Synthesis of cross-coupled coumarin-fused pyrimidines (**54z** & **54z'**) using two different benzylamines (**23a** & **23d**)

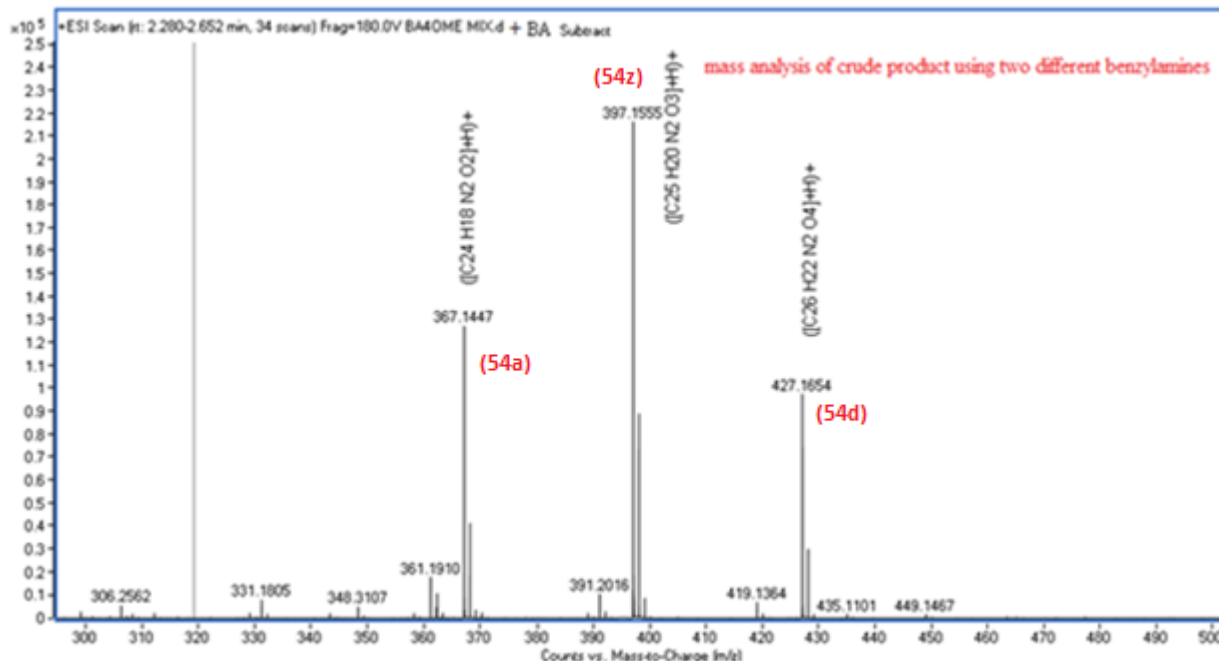


Figure 3.2.6: Mass analysis of crude product **54z**, **54a** & **54d** using two different benzylamines (**23a** & **23d**)

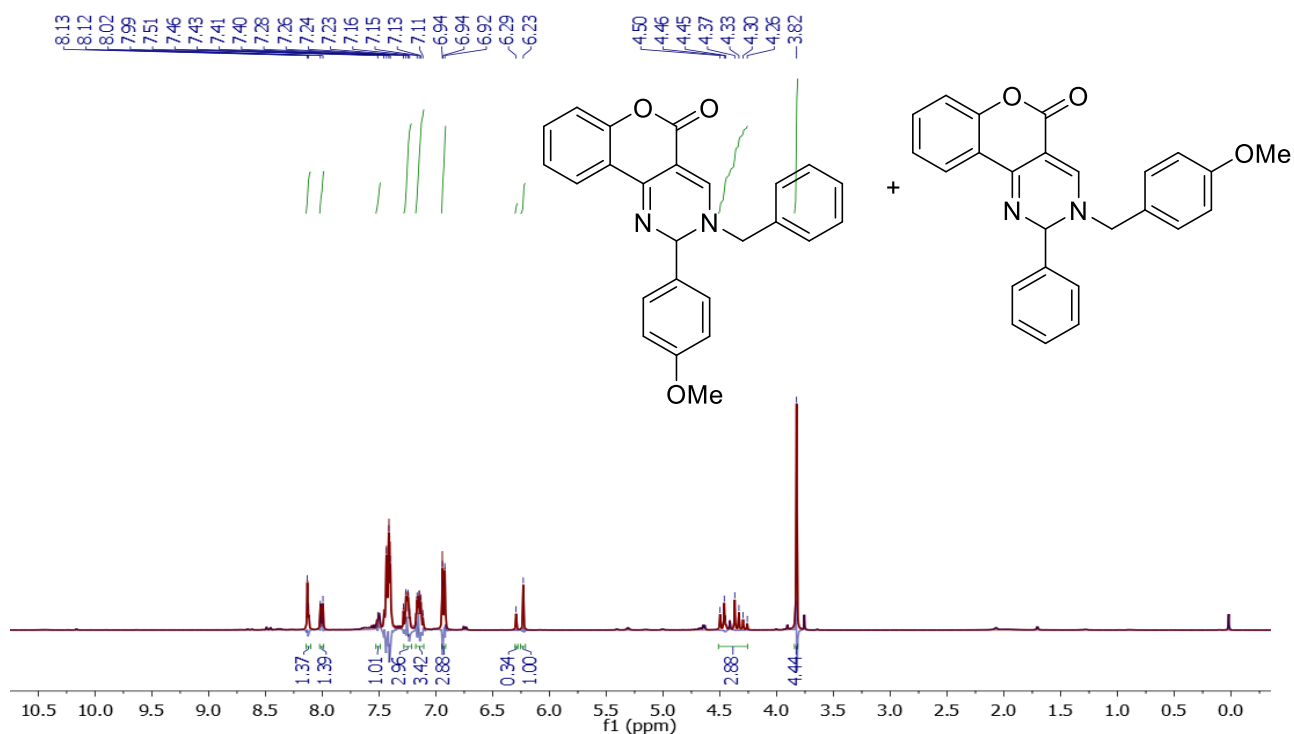
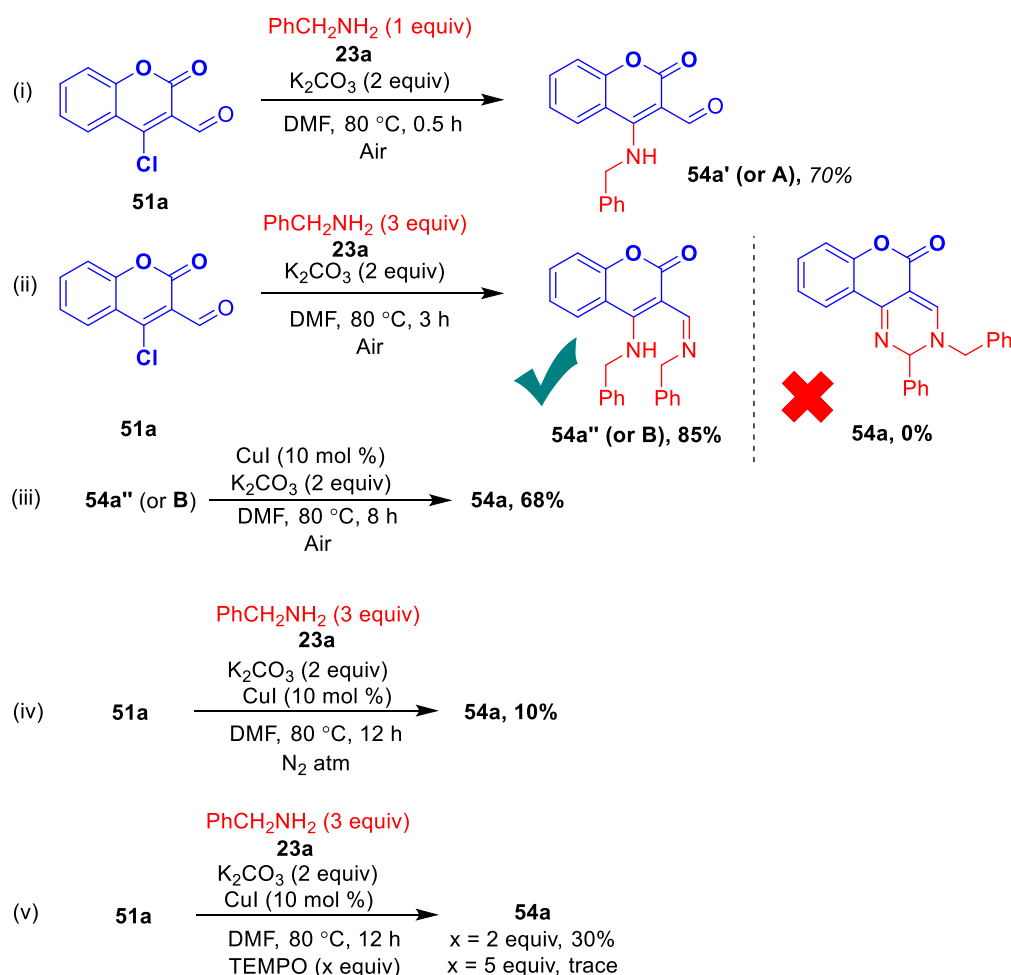


Figure 3.2.7: ¹H NMR spectrum of a mixture of **54z** & **54z'** in CDCl₃

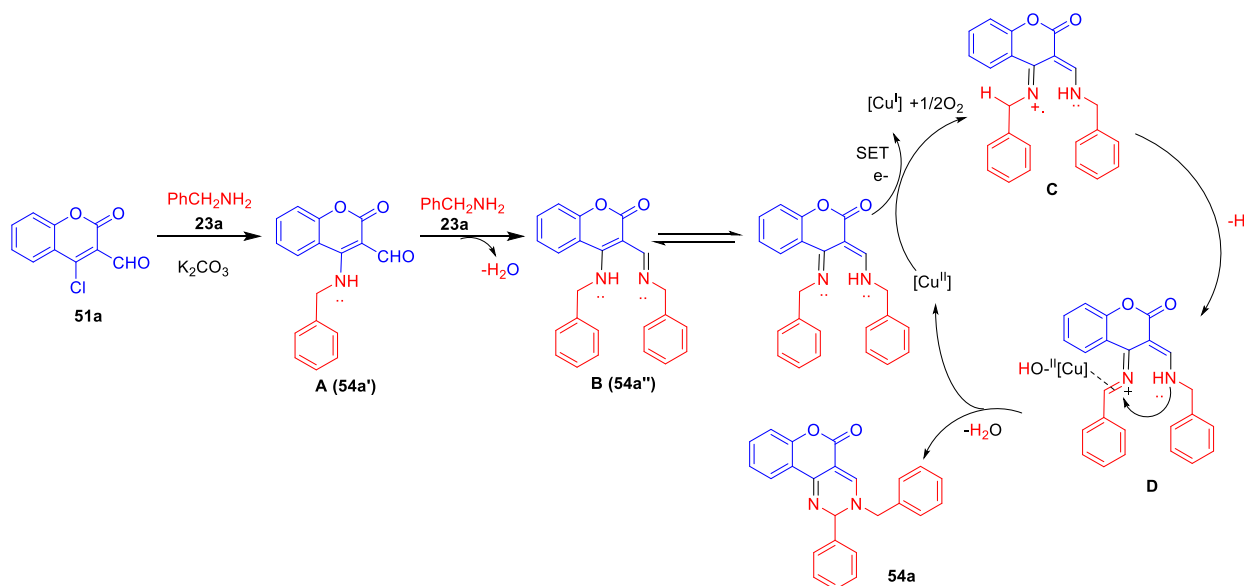
To gain some insights into the reaction mechanism, a few preliminary experiments were performed (Scheme 3.2.5). A stoichiometric reaction between **51a** and **23a** (1 equiv each)

in DMF at 80 °C under catalyst-free conditions furnished **54a'** in 70% yield within 30 min (Scheme 3.2.5i). Subsequently, the reaction between **51a** (1 equiv) and **23a** (3 equiv) under catalyst-free conditions exclusively produced intermediate **54a''** in 3 h (but not **54a**); further heating of **54a''** with CuI (10 mol %) afforded the desired product **54a** in 68% yield (Scheme 3.2.5ii and 3.2.5iii). These experimental findings clearly indicated a vital role of Cu(I) in the oxidative intramolecular cyclization. The reluctance of **51a** to react with **23a** in nitrogen atmosphere under optimized conditions, produced **54a** in very low yields, confirmed the necessity of aerial oxygen in this oxidative transformation (Scheme 3.2.5iv). Interestingly, the yield of **54a** significantly decreased with the increase in the amount of radical quencher TEMPO. This shows the possibility of a dose-dependent free-radical mechanistic pathway for the oxidative cyclization in the presence of a Cu catalyst (Scheme 3.2.5v).



Scheme 3.2.5: Preliminary experiments for investigating the reaction mechanism

Based on these studies and reports in literature,⁶³⁻⁶⁷ a plausible mechanistic pathway is proposed for the tandem oxidative cyclization (Scheme 3.2.6). The reaction is initiated by the aromatic nucleophilic substitution (S_NAr) of chloro with benzylamine, followed by imination with the second molecule of benzylamine, producing intermediate **B** via **A**. Thereafter, an one-electron oxidation of **B** with Cu(I)/O₂ via single-electron transfer (SET) mechanism generates iminium cation radical **C**, which upon subsequent hydrogen radical loss generates cationic-Cu hydroxo species **D**. Finally, nucleophilic attack with a neighboring amine forms the product **54a**.



Scheme 3.2.6: Plausible mechanism

Interestingly, compounds **54a–j** & **54q–v** showed blue fluorescence, whereas **54k–p** showed intense green fluorescence in the solution phase (or solid state) at room temperature under a UV lamp (Figure 3.2.8; a, b, c, d, e & f). The fluorescence emission maxima (λ_{Em}) of all the compounds (**54a–v**) were recorded in MeOH, and their quantum yields were calculated (Figure 3.2.8, Table 3.2.2).

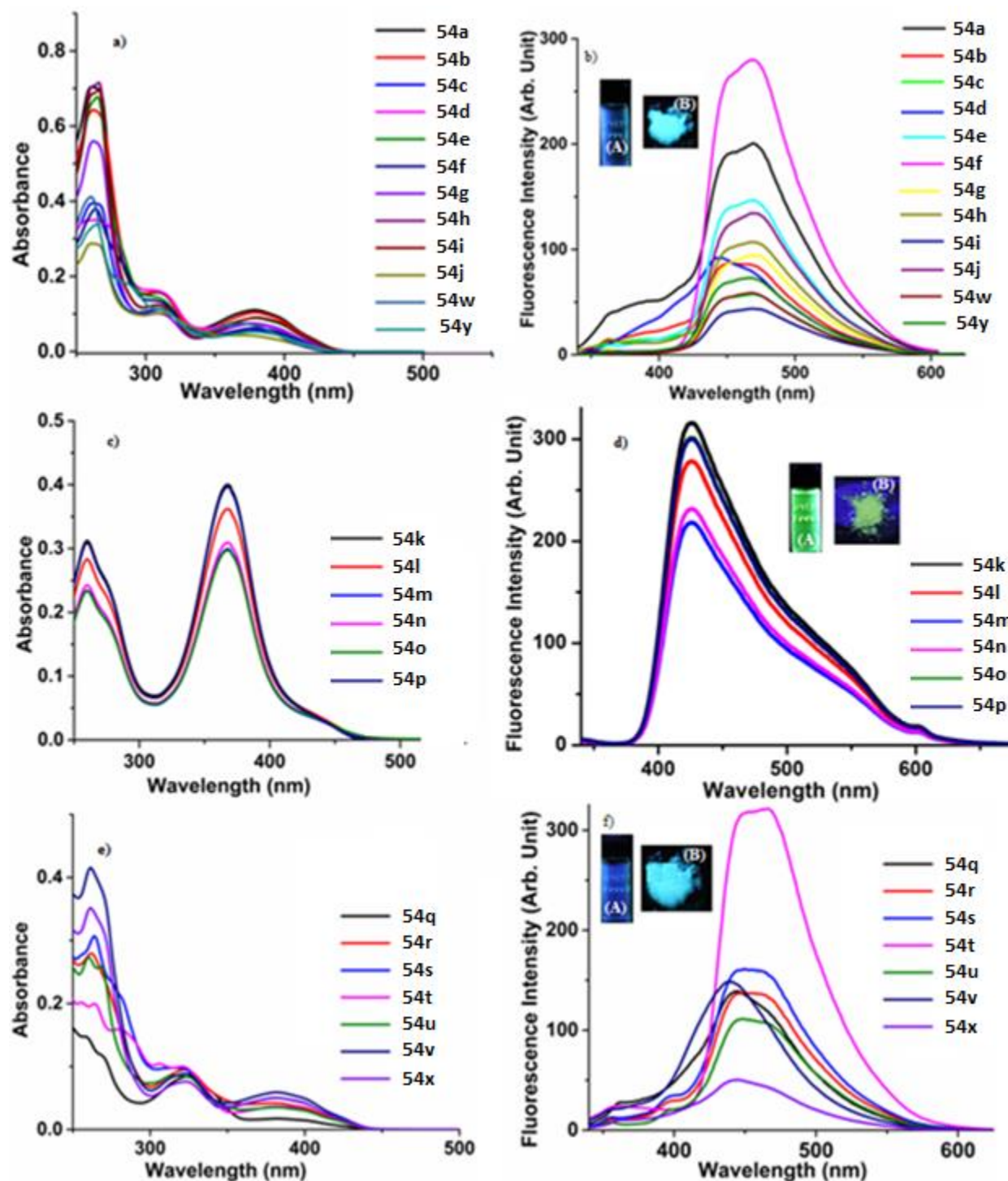


Figure 3.2.8: UV absorption spectra of **54a-j**, **54w-54y** (a), **54k-p** (c), **54q-x** (e), and emission spectra of **54a-j**, **54w-54y** (b), **54k-p** (d), **54q-x** (f) in MeOH (1×10^{-5} M) at 25 °C; Inset: solution phase (A) and solid state emission (B) of **54f** (b), blue), **54o** (d), green) and **54t** (f), blue) under UV light at room temperature

Table 3.2.2: Absorption and fluorescence data of coumarin-fused pyrimidines (**54a-y**)^a

Compound	λ_{Abs} (nm)	$\lambda_{\text{Em}}^{\text{b}}$ (nm)	Quantum Yield (Φ) ^c
54a	379, 310	469	0.064
54b	383, 321	469	0.035
54c	386, 314	470	0.028
54d	379, 307	468	0.032
54e	317, 266	469	0.062
54f	379, 307	472	0.100
54g	386, 314	469	0.046
54h	383, 307	468	0.055
54i	393, 314	468	0.021
54j	383, 310	469	0.052
54k	368, 261	426	0.120
54l	368, 261	426	0.115
54m	368, 261	426	0.111
54n	368, 258	426	0.112
54o	371, 261	426	0.151
54p	368, 262	426	0.122
54q	382, 258	448	0.061
54r	380, 263	453	0.052
54s	381, 264	459	0.058
54t	382, 264	470	0.098
54u	382, 260	453	0.044
54v	382, 261	444	0.055
54w	383, 307	467	0.024
54x	382, 261	448	0.023
54y	379, 317	466	0.030

^aMeasured in MeOH (1×10^{-5} M) at 25 °C; ^bExcited at 325 nm; ^cMeasured with quinine sulfate in 0.1 N H₂SO₄ as standard.

In summary, a Cu(I)-catalyzed tandem aerobic oxidative strategy was developed for the synthesis of substituted 2,3-dihydro-5*H*-chromeno[4,3-*d*]pyrimidin-5-one *via* cross-dehydrogenative C(*sp*³)-N bond coupling. This Cu-catalyzed protocol tolerated diverse substituted benzylamines and heteroarylmethanamines, affording the desired products in moderate-to-good yields. The utility of this protocol was also demonstrated by the synthesis of coumarin-fused pyrimidines in a gram-scale. Interesting photophysical properties and high quantum yields of the products reported in this work will facilitate further studies in medicinal chemistry and material science.

3.3 Experimental Section

General materials and methods

All reagents and chemicals were purchased from commercial source and used as received. Required solvents for reaction were dried by standard procedures prior to use. ^1H NMR spectra were recorded on 400 MHz spectrometer, and the chemical shifts are reported in δ units, parts per million (ppm), and referred to the internal standard TMS set as 0.00 ppm, relative to residual chloroform (7.26 ppm) or DMSO (2.5 ppm) in the deuterated solvent. Data are reported as follows: the following abbreviations were used to describe peak splitting patterns: s = singlet, d = doublet, t = triplet, dd = doublet of doublet and m = multiplet. Coupling constants J were reported in Hz. The ^{13}C NMR spectra were reported in ppm relative to deuteriochloroform (77.0 ppm) or [d_6] DMSO (39.5 ppm). Proton assignments were made using ^1H - ^1H homonuclear correlation spectroscopy (COSY) and ^1H - ^{13}C heteronuclear correlation spectroscopy (HETCOR) at 400 MHz. Melting points were determined on a capillary point apparatus equipped with a digital thermometer, and are uncorrected. High-resolution mass spectra were recorded with a TOF analyzer spectrometer by using electrospray mode. Flash Column chromatography was performed on silica gel, 100–200 mesh. Analytical thin-layer chromatography was carried out on silica gel 60 F-254 plates. Products were visualized using UV and shown blue colour and yellow colour under uv light. Absorption spectra were recorded using dual beam Thermo Evolution 201 UV/Vis/NIR spectrophotometer and fluorescence spectra were recorded using a Shimadzu RF-5301PC spectrofluorometer. The data were analyzed using related software. The concentration of compound in all the solutions was 1×10^{-5} M. Fluorescence quantum yield (ϕ) values were obtained by the following equation. The fluorescence quantum yields were calculated by comparing the total fluorescence intensity (F) under the whole spectrum range by taking standard compound quinine sulfate (prepared as 0.1N H_2SO_4 solution, $\phi_s = 0.55$).

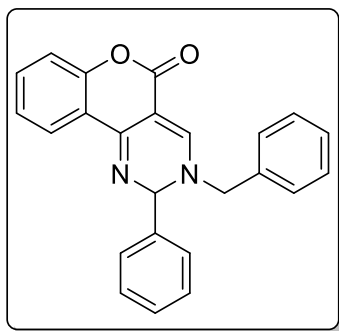
$$\phi_i = \phi_s \frac{F_i Ab_s \eta_s^2}{F_s Ab_i \eta_i^2}$$

Where, Ab : absorbance at a particular wavelength; F : fluorescence spectrum area; and η : refraction index. The subscripts in the symbols refer to the standard (s) and to the sample (i).

General procedure for the synthesis of coumarin-fused pyrimidines

A mixture of **51** (0.47 mmol, 1.0 equiv), benzylamine **23** (1.4 mmol, 3.0 equiv), K_2CO_3 (0.94 mmol, 2 equiv) and CuI (0.047 mmol, 10 mol %) were heated in DMF (8.0 mL) at 80 °C under ambient conditions for 10-16 h. On completion of the reaction as indicated by TLC, the reaction mixture was cooled to room temperature and diluted with ice-water. The mixture was extracted with ethyl acetate (3×20 mL), and the organic layer was separated and dried over Na_2SO_4 . The organic layer was concentrated, and the crude product was subjected to silica gel column chromatography SiO_2 (100-200 mesh), with (hexanes/EtOAc, 8:2) as the eluent to afford the desired product **54a-y**.

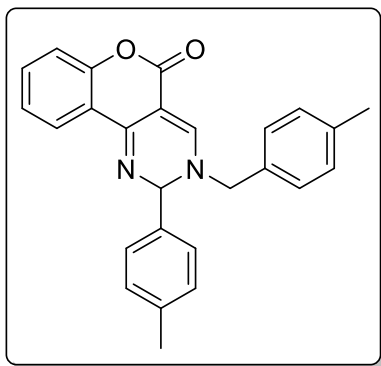
3-Benzyl-2-phenyl-2,3-dihydro-5H-chromeno[4,3-d]pyrimidin-5-one (54a): Off-white solid;



yield: 123 mg (70%); mp: 184–186 °C; 1H NMR (400 MHz, $CDCl_3$) δ 8.15 (s, 1H), 8.01 (dd, $J = 7.9, 1.5$ Hz, 1H), 7.55 – 7.49 (m, 2H), 7.48 – 7.37 (m, 7H), 7.28 – 7.24 (m, 2H), 7.20 – 7.14 (m, 2H), 6.29 (s, 1H), 4.50 (d, $J = 14.8$ Hz, 1H), 4.35 (d, $J = 14.7$ Hz, 1H); ^{13}C NMR (100 MHz, $DMSO-d_6$) δ 165.2, 159.5, 159.4, 158.8, 156.3, 145.1, 139.6, 138.0, 134.2, 133.6, 131.7, 129.4, 129.1, 123.5, 122.3, 96.5, 81.4, 61.7; HRMS (ESI-TOF) (m/z) calculated

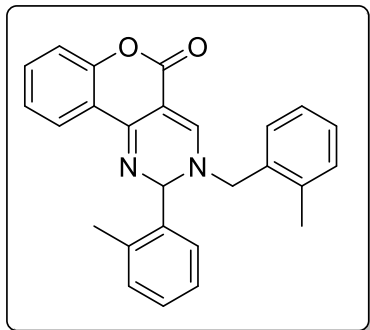
$C_{24}H_{19}N_2O_2^+$: 367.1441; found 367.1447 $[M+H]^+$.

3-(4-Methylbenzyl)-2-(p-tolyl)-2,3-dihydro-5H-chromeno[4,3-d]pyrimidin-5-one (54b): Off-white solid; yield: 138 mg (74%); mp: 170–172 °C; 1H NMR (400 MHz,



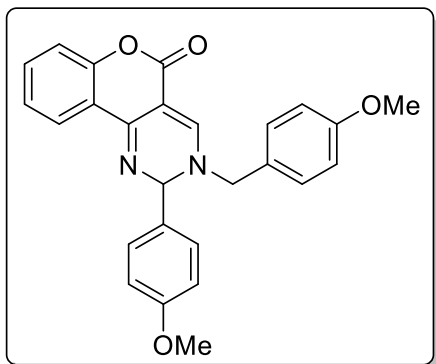
$CDCl_3$) δ 8.12 (s, 1H), 8.00 (dd, $J = 7.9, 1.5$ Hz, 1H), 7.46 – 7.41 (m, 2H), 7.39 (d, $J = 1.7$ Hz, 1H), 7.26 – 7.22 (m, 4H), 7.17 – 7.11 (m, 4H), 6.26 (s, 1H), 4.44 (d, $J = 14.6$ Hz, 1H), 4.30 (d, $J = 14.6$ Hz, 1H), 2.39 (s, 6H); ^{13}C NMR (100 MHz, $CDCl_3$) δ 161.7, 154.1, 153.0, 151.6, 139.5, 139.2, 137.0, 132.6, 130.1, 129.8, 129.3, 128.5, 126.7, 124.6, 123.9, 118.7, 117.4, 91.6, 77.8, 57.6, 21.3, 21.2; HRMS

(ESI-TOF) (m/z) calculated $C_{26}H_{23}N_2O_2^+$: 395.1754; found 395.1760 $[M+H]^+$.

3-(2-Methylbenzyl)-2-(*o*-tolyl)-2,3-dihydro-5*H*-chromeno[4,3-*d*]pyrimidin-5-one (54c):

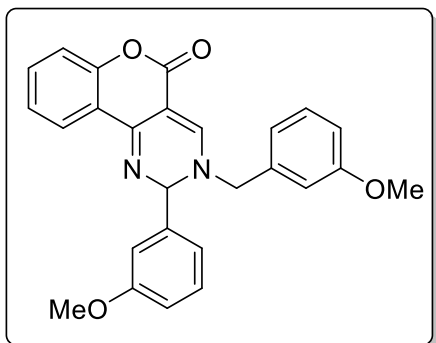
Off-white solid; yield: 133 mg (71%); mp: 178–180 °C; ^1H NMR (400 MHz, CDCl_3) δ 8.10 (s, 1H), 7.98 (dd, $J = 8.3$, 1.7 Hz, 1H), 7.54 – 7.49 (m, 1H), 7.44 – 7.40 (m, 1H), 7.33 – 7.29 (m, 2H), 7.28 – 7.23 (m, 4H), 7.18 – 7.10 (m, 3H), 6.57 (s, 1H), 4.44 (d, $J = 14.8$ Hz, 1H), 4.31 (d, $J = 14.7$ Hz, 1H), 2.49 (s, 3H), 2.23 (s, 3H); ^{13}C NMR (100 MHz, CDCl_3) δ 161.6, 154.0, 153.5, 151.3, 137.5, 137.2, 135.4, 132.5,

131.4, 131.3, 129.9, 129.6, 129.5, 129.0, 126.9, 126.9, 126.3, 124.6, 123.8, 118.8, 117.4, 91.7, 75.7, 55.9, 19.2, 19.1; HRMS (ESI-TOF) (m/z) calculated $\text{C}_{26}\text{H}_{23}\text{N}_2\text{O}_2^+$: 395.1754; found 395.1745 $[\text{M}+\text{H}]^+$.

3-(4-Methoxybenzyl)-2-(4-methoxyphenyl)-2,3-dihydro-5*H*-chromeno[4,3-*d*]pyrimidin-5-one (54d): White solid; yield: 156 mg (77%); mp: 169–171 °C; ^1H NMR (400 MHz, CDCl_3) δ 

8.09 (s, 1H), 8.01 (dd, $J = 7.9$, 1.5 Hz, 1H), 7.47 – 7.41 (m, 3H), 7.19 – 7.12 (m, 4H), 6.96 – 6.91 (m, 4H), 6.24 (s, 1H), 4.41 (d, $J = 14.5$ Hz, 1H), 4.29 (d, $J = 14.5$ Hz, 1H), 3.84 (brs, 3H), 3.84 (brs, 3H); ^{13}C NMR (100 MHz, CDCl_3) δ 161.7, 160.5, 160.2, 154.1, 152.7, 151.6, 132.6, 132.3, 130.0, 128.1, 124.6, 124.1, 123.9, 118.7, 117.4, 114.8, 114.4, 91.4, 77.5, 57.3, 55.4, 55.3;

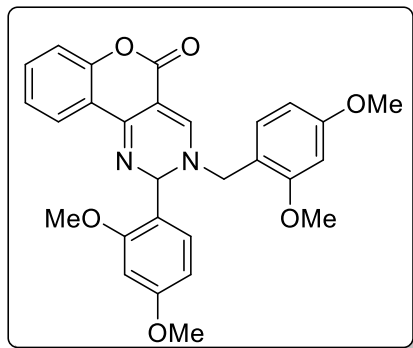
HRMS (ESI-TOF) (m/z) calculated $\text{C}_{26}\text{H}_{23}\text{N}_2\text{O}_4^+$: 427.1652; found 427.1653 $[\text{M}+\text{H}]^+$.

3-(3-Methoxybenzyl)-2-(3-methoxyphenyl)-2,3-dihydro-5*H*-chromeno[4,3-*d*]pyrimidin-5-one (54e): White solid; yield: 146 mg (72%); mp: 170–172 °C; ^1H NMR (400 MHz, CDCl_3) δ 

8.15 (s, 1H), 8.00 (d, $J = 7.4$ Hz, 1H), 7.43 (t, $J = 7.2$ Hz, 1H), 7.36 – 7.31 (m, 2H), 7.15 – 7.09 (m, 3H), 7.03 (s, 1H), 6.92 (t, $J = 7.9$ Hz, 2H), 6.84 (d, $J = 7.1$ Hz, 1H), 6.75 (s, 1H), 6.27 (s, 1H), 4.47 (d, $J = 14.6$ Hz, 1H), 4.31 (d, $J = 14.7$ Hz, 1H), 3.80 (brs, 6H); ^{13}C NMR (100 MHz, CDCl_3) δ 161.6, 160.3, 160.2, 154.1, 153.3, 151.8, 141.2, 134.1, 132.7, 130.5, 130.3, 124.6, 124.0, 120.6, 119.0, 118.6, 117.4,

114.5, 114.3, 114.2, 112.8, 91.7, 77.9, 57.9, 55.4, 55.3; HRMS (ESI-TOF) (m/z) calculated $C_{26}H_{23}N_2O_4^+$: 427.1652; found 427.1660 $[M+H]^+$.

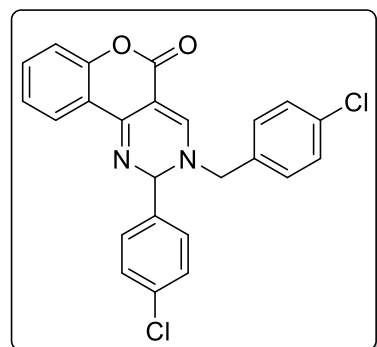
3-(2,4-Dimethoxybenzyl)-2-(2,4-dimethoxyphenyl)-2,3-dihydro-5H-chromeno[4,3-*d*]pyrimidin-5-one (54f): Pale–yellow solid; yield: 182 mg (78%); mp: 174–176 °C; 1H



NMR (400 MHz, $CDCl_3$) δ 8.06 (s, 1H), 8.03 – 7.99 (m, 1H), 7.45 (d, $J = 8.2$ Hz, 1H), 7.43 – 7.38 (m, 1H), 7.15 – 7.06 (m, 3H), 6.73 (s, 1H), 6.51 – 6.44 (m, 4H), 4.35 (d, $J = 14.1$ Hz, 1H), 4.23 (d, $J = 14.1$ Hz, 1H), 3.89 (s, 3H), 3.81 (brs, 6H), 3.78 (s, 3H); ^{13}C NMR (100 MHz, $CDCl_3$) δ 161.9, 161.6, 159.2, 157.0, 154.0, 153.2, 151.9, 132.2, 131.9, 129.9, 124.6, 123.6, 121.8, 119.0, 117.3, 113.3,

105.2, 104.3, 98.9, 98.5, 90.4, 71.4, 55.6, 55.5, 55.5, 55.4, 53.0; HRMS (ESI-TOF) (m/z) calculated $C_{28}H_{27}N_2O_6^+$: 487.1864; found 487.1861 $[M+H]^+$.

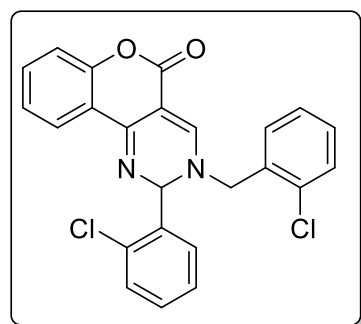
3-(4-Chlorobenzyl)-2-(4-chlorophenyl)-2,3-dihydro-5H-chromeno[4,3-*d*]pyrimidin-5-one (54g): Pale–yellow solid; yield: 132 mg (64%); mp: 162–164 °C; 1H NMR (400



MHz, $CDCl_3$) δ 8.14 (s, 1H), 8.00 – 7.97 (m, 1H), 7.49 – 7.45 (m, 1H), 7.43 – 7.39 (m, 6H), 7.20 – 7.15 (m, 4H), 6.24 (s, 1H), 4.48 (d, $J = 14.9$ Hz, 1H), 4.32 (d, $J = 14.9$ Hz, 1H); ^{13}C NMR (100 MHz, $CDCl_3$) δ 161.4, 154.0, 153.2, 152.0, 138.0, 135.5, 135.3, 133.0, 130.9, 129.7, 129.6, 129.4, 128.0, 124.6, 124.1, 118.4, 117.5, 92.4, 77.2, 57.3; HRMS (ESI-TOF) (m/z) calculated $C_{24}H_{17}Cl_2N_2O_2^+$: 435.0662;

found 435.0652 $[M+H]^+$.

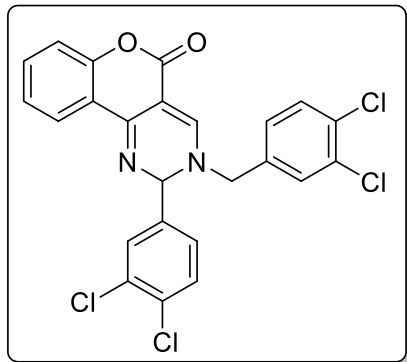
3-(2-Chlorobenzyl)-2-(2-chlorophenyl)-2,3-dihydro-5H-chromeno[4,3-*d*]pyrimidin-5-one (54h): Pale–yellow solid; yield: 123 mg (59%); mp: 170–172 °C; 1H NMR (400



MHz, $CDCl_3$) δ 8.14 (s, 1H), 8.04 – 8.00 (m, 1H), 7.72 – 7.69 (m, 1H), 7.46 – 7.41 (m, 3H), 7.35 – 7.28 (m, 5H), 7.17 – 7.13 (m, 2H), 6.89 (s, 1H), 4.50 (s, 2H); ^{13}C NMR (100 MHz, $CDCl_3$) δ 161.5, 154.0, 153.9, 152.2, 137.3, 134.7, 132.8, 131.5, 130.9, 130.8, 130.6, 130.4, 130.1, 130.0, 128.8, 128.0, 127.6, 124.8, 124.0, 118.6, 117.4, 92.0, 75.2, 55.6; HRMS

(ESI-TOF) (m/z) calculated $C_{24}H_{17}Cl_2N_2O_2^+$: 435.0662; found 435.0644 $[M+H]^+$.

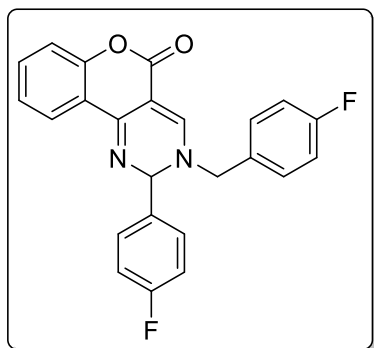
3-(3,4-Dichlorobenzyl)-2-(3,4-dichlorophenyl)-2,3-dihydro-5H-chromeno[4,3-*d*]pyrimidin-5-one (54i): Yellow solid; yield: 146 mg (61%); mp: 160–162 °C; 1H NMR



(400 MHz, $CDCl_3$) δ 8.18 (s, 1H), 8.01 – 7.97 (m, 1H), 7.54 – 7.46 (m, 4H), 7.35 – 7.30 (m, 2H), 7.22 – 7.16 (m, 2H), 7.10 (dd, $J = 8.2, 2.1$ Hz, 1H), 6.23 (s, 1H), 4.50 (d, $J = 15.1$ Hz, 1H), 4.34 (d, $J = 15.1$ Hz, 1H); ^{13}C NMR (100 MHz, $CDCl_3$) δ 161.3, 154.0, 153.3, 152.3, 139.4, 133.9, 133.8, 133.8, 133.6, 133.3, 132.6, 131.5, 131.3, 130.1, 128.6, 127.2, 125.8, 124.7, 124.3, 117.6, 93.1,

76.9, 55.1; HRMS (ESI-TOF) (m/z) calculated $C_{24}H_{15}Cl_4N_2O_2^+$: 502.9882; found 502.9868 $[M+H]^+$.

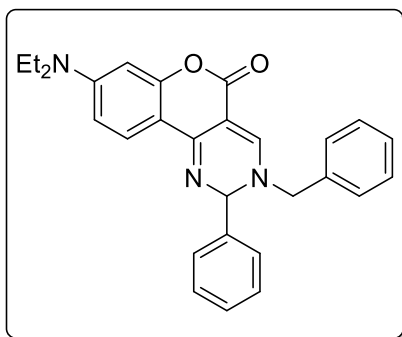
3-(4-Fluorobenzyl)-2-(4-fluorophenyl)-2,3-dihydro-5H-chromeno[4,3-*d*]pyrimidin-5-one (54j): Pale-yellow solid; yield: 124 mg (65%); mp: 173–175 °C; 1H NMR (400



MHz, $CDCl_3$) δ 8.14 (s, 1H), 7.99 (d, $J = 7.1$ Hz, 1H), 7.52 – 7.42 (m, 3H), 7.26 – 7.21 (m, 2H), 7.17 (d, $J = 7.8$ Hz, 2H), 7.15 – 7.08 (m, 4H), 6.26 (s, 1H), 4.47 (d, $J = 14.8$ Hz, 1H), 4.34 (d, $J = 14.8$ Hz, 1H); ^{13}C NMR (100 MHz, $CDCl_3$) δ 164.6, 164.4, 162.1, 161.9, 161.5, 154.1, 153.1, 152.0, 132.9, 130.2, 130.2, 128.6, 128.5, 124.6, 124.1, 118.4, 117.5, 116.7, 116.4, 116.3, 116.1, 92.2, 77.2, 57.3;

HRMS (ESI-TOF) (m/z) calculated $C_{24}H_{17}F_2N_2O_2^+$: 403.1253; found 403.1252 $[M+H]^+$.

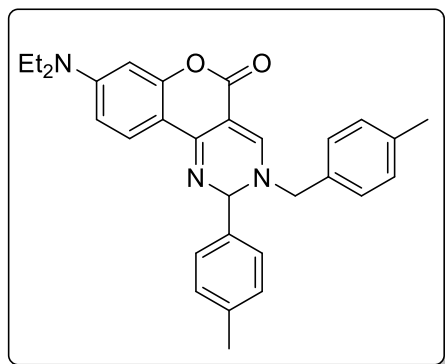
3-Benzyl-8-(diethylamino)-2-phenyl-2,3-dihydro-5H-chromeno[4,3-*d*]pyrimidin-5-one (54k): Yellow solid; yield: 106 mg (68%); mp: 159–161 °C; 1H NMR (400 MHz, $CDCl_3$)



δ 8.09 (s, 1H), 7.80 (d, $J = 9.0$ Hz, 1H), 7.72 (dd, $J = 8.3, 1.1$ Hz, 1H), 7.52 – 7.46 (m, 2H), 7.42 – 7.38 (m, 5H), 7.27 – 7.22 (m, 1H), 7.13 (t, $J = 7.8$ Hz, 1H), 6.46 (dd, $J = 9.0, 2.5$ Hz, 1H), 6.35 (d, $J = 2.5$ Hz, 1H), 6.21 (s, 1H), 4.46 (d, $J = 14.8$ Hz, 1H), 4.35 (d, $J = 14.8$ Hz, 1H), 3.39 (q, $J = 7.1$ Hz, 4H), 1.19 (t, $J = 7.1$ Hz, 6H); ^{13}C NMR (100 MHz, $CDCl_3$) δ 162.5, 155.8, 152.6, 151.6, 151.3,

140.3, 137.5, 132.9, 130.3, 129.3, 129.2, 129.1, 129.0, 128.3, 127.5, 126.8, 125.9, 108.2, 98.0, 77.6, 57.8, 44.7, 12.5; HRMS (ESI-TOF) (m/z) calculated $C_{28}H_{28}N_3O_2^+$: 438.2176; found 438.2179 $[M+H]^+$.

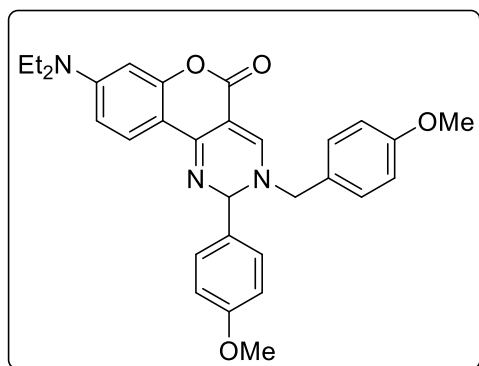
8-(Diethylamino)-3-(4-methylbenzyl)-2-(*p*-tolyl)-2,3-dihydro-5*H*-chromeno[4,3-*d*]pyrimidin-5-one (54l): Yellow solid; yield: 120 mg (72%); mp: 170–171 °C; 1H NMR (400 MHz,



$CDCl_3$) δ 8.04 (s, 1H), 7.80 (d, $J = 9.0$ Hz, 1H), 7.37 (d, $J = 8.0$ Hz, 2H), 7.22 – 7.18 (m, 4H), 7.13 (d, $J = 7.9$ Hz, 2H), 6.45 (dd, $J = 9.0, 2.5$ Hz, 1H), 6.34 (d, $J = 2.5$ Hz, 1H), 6.16 (s, 1H), 4.39 (d, $J = 14.6$ Hz, 1H), 4.29 (d, $J = 14.6$ Hz, 1H), 3.38 (q, $J = 7.1$ Hz, 4H), 2.38 (brs, 6H), 1.18 (t, $J = 7.1$ Hz, 6H); ^{13}C NMR (100 MHz, $CDCl_3$) δ 162.5, 155.8, 152.3, 151.4, 151.3,

139.1, 138.9, 137.6, 130.0, 129.7, 129.6, 128.4, 126.7, 125.9, 108.1, 106.0, 98.0, 91.3, 77.3, 57.5, 44.7, 21.3, 21.2, 12.5; HRMS (ESI-TOF) (m/z) calculated $C_{30}H_{32}N_3O_2^+$: 466.2489; found 466.2493 $[M+H]^+$.

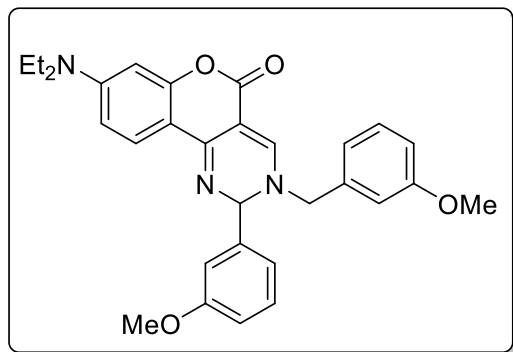
8-(Diethylamino)-3-(4-methoxybenzyl)-2-(4-methoxyphenyl)-2,3-dihydro-5*H*-chromeno[4,3-*d*]pyrimidin-5-one (54m): Yellow solid; yield: 135 mg (76%); mp: 169–



171 °C; 1H NMR (400 MHz, $DMSO-d_6$) δ 8.30 (s, 1H), 7.62 (d, $J = 8.9$ Hz, 1H), 7.37 (d, $J = 8.7$ Hz, 2H), 7.28 (d, $J = 8.6$ Hz, 2H), 6.97 – 6.92 (m, 4H), 6.52 – 6.47 (m, 1H), 6.26 (d, $J = 2.4$ Hz, 1H), 6.06 (s, 1H), 4.72 (d, $J = 14.4$ Hz, 1H), 4.29 (d, $J = 14.5$ Hz, 1H), 3.76 (s, 3H), 3.75 (s, 3H), 3.40 (m, overlapped by moisture of $DMSO$, 4H), 1.08 (t, $J =$

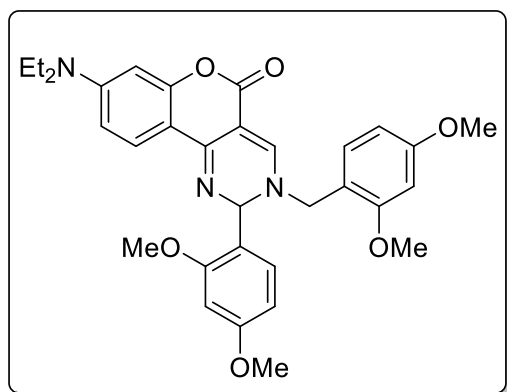
6.9 Hz, 6H); ^{13}C NMR (100 MHz, $CDCl_3 + DMSO-d_6$) δ 160.8, 160.3, 160.1, 159.2, 155.9, 152.1, 151.4, 130.0, 129.7, 129.2, 128.3, 128.1, 114.8, 114.3, 114.2, 108.3, 98.0, 91.2, 77.2, 57.2, 55.4, 44.7, 12.5; HRMS (ESI-TOF) (m/z) calculated $C_{30}H_{32}N_3O_4^+$: 498.2387; found 498.2393 $[M+H]^+$.

8-(Diethylamino)-3-(3-methoxybenzyl)-2-(3-methoxyphenyl)-2,3-dihydro-5H-chromeno[4,3-*d*]pyrimidin-5-one (54n): Yellow solid; yield: 125 mg (70%); mp: 178–



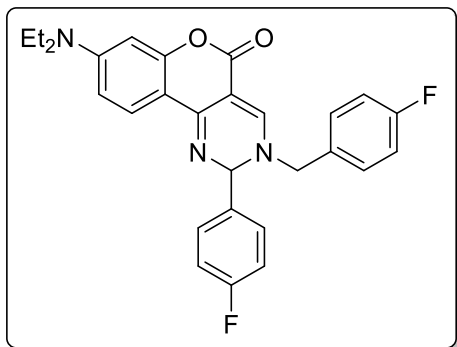
181 °C; ^1H NMR (400 MHz, $\text{DMSO-}d_6$) δ 8.40 (s, 1H), 7.65 (d, $J = 8.9$ Hz, 1H), 7.33 – 7.28 (m, 2H), 7.05 (d, $J = 7.6$ Hz, 1H), 6.97 – 6.90 (m, 5H), 6.51 (dd, $J = 9.0, 2.0$ Hz, 1H), 6.27 (d, $J = 2.1$ Hz, 1H), 6.14 (s, 1H), 4.81 (d, $J = 14.7$ Hz, 1H), 4.38 (d, $J = 14.7$ Hz, 1H), 3.74 (brs, 3H), 3.73 (brs, 3H), 3.37 (q, $J = 7.0$ Hz, 4H), 1.17 (t, $J = 7.0$ Hz, 6H); ^{13}C NMR (100 MHz, $\text{DMSO-}d_6$) δ 161.1, 160.0, 159.9, 155.8, 153.9, 151.4, 151.2, 142.6, 136.8, 130.5, 125.9, 120.8, 119.1, 114.5, 114.1, 112.9, 108.6, 105.7, 97.6, 91.4, 76.4, 56.8, 55.6, 44.4, 12.8; HRMS (ESI-TOF) (m/z) calculated $\text{C}_{30}\text{H}_{32}\text{N}_3\text{O}_4^+$: 498.2387; found 498.2406 $[\text{M}+\text{H}]^+$.

8-(Diethylamino)-3-(2,4-dimethoxybenzyl)-2-(2,4-dimethoxyphenyl)-2,3-dihydro-5H-chromeno[4,3-*d*]pyrimidin-5-one (54o): Yellow solid; yield: 146 mg (73%); mp: 168–



170 °C; ^1H NMR (400 MHz, $\text{DMSO-}d_6$) δ 8.31 (s, 1H), 7.70 (d, $J = 9.0$ Hz, 1H), 7.30 (d, $J = 8.5$ Hz, 1H), 7.17 (d, $J = 8.1$ Hz, 1H), 6.62 (d, $J = 2.2$ Hz, 2H), 6.57 (brs, 1H), 6.54 (brs, 1H), 6.53 (d, $J = 2.2$ Hz, 1H), 6.41 (s, 1H), 6.37 (s, 1H), 4.63 (d, $J = 14.2$ Hz, 1H), 4.35 (d, $J = 14.1$ Hz, 1H), 3.82 (s, 3H), 3.77 (brs, 6H), 3.74 (s, 3H), 3.40 (m, overlapped by moisture of DMSO, 4H), 1.10 (t, $J = 7.0$ Hz, 6H); ^{13}C NMR (100 MHz, $\text{DMSO-}d_6$) δ 162.0, 161.8, 160.3, 159.3, 157.7, 156.6, 154.5, 151.4, 132.0, 129.8, 126.4, 113.7, 109.3, 106.1, 105.4, 99.1, 98.8, 97.6, 89.5, 56.2, 56.1, 55.9, 55.8, 52.9, 44.6, 12.8; HRMS (ESI-TOF) (m/z) calculated $\text{C}_{32}\text{H}_{36}\text{N}_3\text{O}_6^+$: 558.2599; found 558.2615 $[\text{M}+\text{H}]^+$.

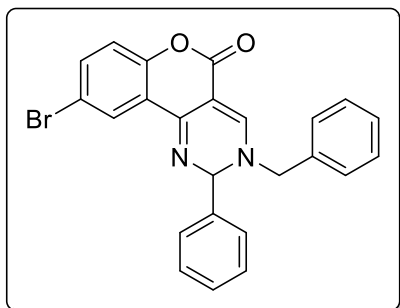
8-(Diethylamino)-3-(4-fluorobenzyl)-2-(4-fluorophenyl)-2,3-dihydro-5H-chromeno[4,3-d]pyrimidin-5-one (54p): Yellow solid; yield: 107 mg (63%); mp: 165–



166 °C; ^1H NMR (400 MHz, $\text{DMSO-}d_6$) δ 9.02 (s, 1H), 8.14 (d, $J = 9.3$ Hz, 1H), 7.63 – 7.59 (m, 2H), 7.53 – 7.49 (m, 2H), 7.26 – 7.20 (m, 4H), 6.81 (d, $J = 8.1$ Hz, 1H), 6.52 (s, 1H), 6.40 (s, 1H), 5.15 (d, $J = 14.5$ Hz, 1H), 4.86 (d, $J = 14.5$ Hz, 1H), 3.40 (m, overlapped by moisture of DMSO, 4H), 1.12 (t, $J = 6.7$ Hz, 6H); ^{13}C NMR (100 MHz, $\text{DMSO-}d_6$) δ

162.1, 161.5, 158.8, 157.9, 157.5, 154.7, 152.2, 133.1, 133.1, 131.8, 131.7, 130.0, 130.0, 129.7, 129.6, 127.9, 116.6, 116.3, 116.3, 116.1, 110.6, 97.6, 91.1, 68.2, 57.8, 45.0, 12.8; HRMS (ESI-TOF) (m/z) calculated $\text{C}_{28}\text{H}_{26}\text{F}_2\text{N}_3\text{O}_2^+$: 474.1988; found 474.1989 $[\text{M}+\text{H}]^+$.

3-Benzyl-9-bromo-2-phenyl-2,3-dihydro-5H-chromeno[4,3-d]pyrimidin-5-one (54q):

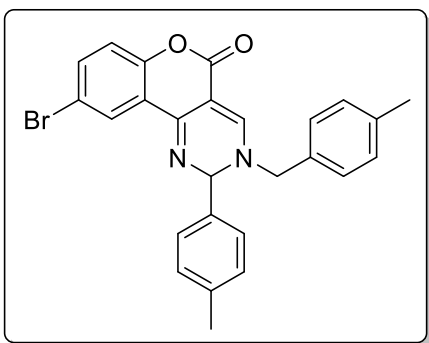


White solid; yield: 105 mg (68%); mp: 154–166 °C; ^1H NMR (400 MHz, $\text{DMSO-}d_6$) δ 8.55 (s, 1H), 7.94 (d, $J = 2.5$ Hz, 1H), 7.69 – 7.64 (m, 1H), 7.52 – 7.48 (m, 2H), 7.42 – 7.37 (m, 8H), 7.16 (d, $J = 8.8$ Hz, 1H), 6.26 (s, 1H), 4.90 (d, $J = 14.7$ Hz, 1H), 4.42 (d, $J = 14.6$ Hz, 1H); ^{13}C NMR (100 MHz, $\text{DMSO-}d_6$) δ 164.6, 159.6, 158.0, 155.9,

144.8, 140.5, 139.5, 134.3, 134.2, 134.0, 133.7, 133.7, 133.3, 131.8, 131.4, 125.5, 124.9, 121.0, 96.0, 81.5, 61.7; HRMS (ESI-TOF) (m/z) calculated $\text{C}_{24}\text{H}_{18}\text{BrN}_2\text{O}_2^+$: 445.0551; found 445.0546 $[\text{M}+\text{H}]^+$.

9-Bromo-3-(4-methylbenzyl)-2-(*p*-tolyl)-2,3-dihydro-5H-chromeno[4,3-d]pyrimidin-

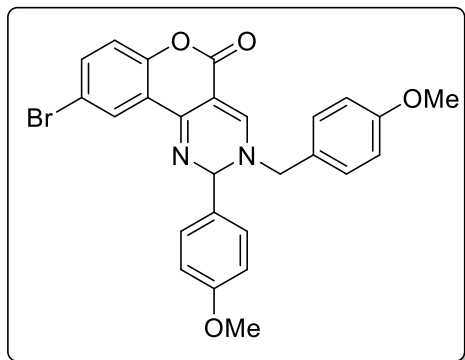
5-one (54r): White solid; yield: 120 mg (73%); mp: 169–170 °C; ^1H NMR (400 MHz,



CDCl_3) δ 8.13 (d, $J = 2.5$ Hz, 1H), 8.10 (s, 1H), 7.53 – 7.49 (m, 1H), 7.39 (d, $J = 8.0$ Hz, 2H), 7.26 – 7.22 (m, 4H), 7.13 (d, $J = 8.0$ Hz, 2H), 7.04 (d, $J = 8.8$ Hz, 1H), 6.24 (s, 1H), 4.43 (d, $J = 14.6$ Hz, 1H), 4.29 (d, $J = 14.6$ Hz, 1H), 2.40 (s, 3H), 2.39 (s, 3H); ^{13}C NMR (100 MHz, CDCl_3) δ 161.1, 153.1, 153.0, 150.6, 139.7, 139.3, 136.8, 135.3, 130.1, 130.0, 129.0, 128.5, 127.3,

126.6, 120.5, 119.2, 116.8, 91.1, 77.9, 57.7, 21.3, 21.2; HRMS (ESI-TOF) (m/z) calculated $C_{26}H_{22}BrN_2O_2^+$: 473.0859; found 473.0868 $[M+H]^+$.

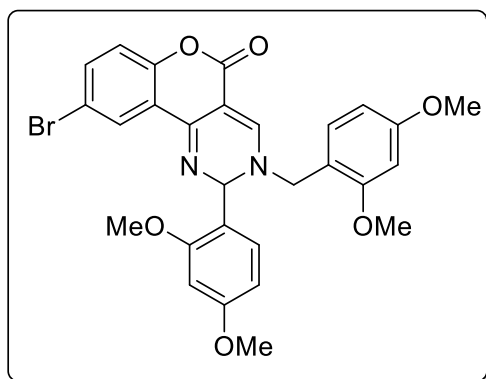
9-Bromo-3-(4-methoxybenzyl)-2-(4-methoxyphenyl)-2,3-dihydro-5H-chromeno[4,3-*d*]pyrimidin-5-one (54s): White solid; yield: 133 mg (76%); mp: 139–141 °C; 1H NMR



(400 MHz, $DMSO-d_6$) δ 8.44 (s, 1H), 7.96 – 7.92 (s, 1H), 7.69 – 7.66 (m, 1H), 7.45 – 7.41 (m, 2H), 7.30 (d, $J = 8.5$ Hz, 2H), 7.16 (d, $J = 8.8$ Hz, 1H), 6.96 (d, $J = 8.0$ Hz, 4H), 6.20 (s, 1H), 4.77 (d, $J = 14.4$ Hz, 1H), 4.33 (d, $J = 14.4$ Hz, 1H), 3.76 (brs, 6H); ^{13}C NMR (100 MHz, $DMSO-d_6$) δ 160.3, 159.9, 159.8, 154.2, 153.2, 150.3, 135.6, 132.6, 130.6, 128.4,

126.6, 126.3, 120.9, 120.1, 116.2, 114.8, 114.7, 90.7, 76.2, 56.3, 55.7, 55.6; HRMS (ESI-TOF) (m/z) calculated $C_{26}H_{22}BrN_2O_4^+$: 505.0757; found 505.0762 $[M+H]^+$.

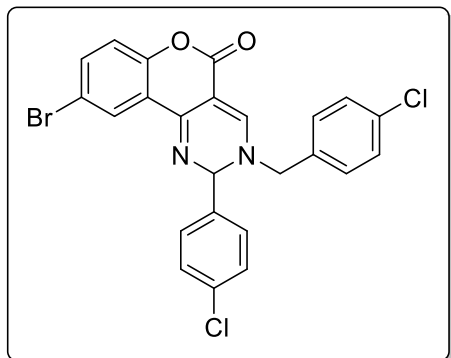
9-Bromo-3-(2,4-dimethoxybenzyl)-2-(2,4-dimethoxyphenyl)-2,3-dihydro-5H-chromeno[4,3-*d*]pyrimidin-5-one (54t): White solid; yield: 147 mg (75%); mp: 158–160 °C; 1H NMR



(400 MHz, $DMSO-d_6$) δ 8.22 (s, 1H), 7.89 – 7.86 (m, 1H), 7.66 – 7.62 (m, 1H), 7.32 (d, $J = 8.5$ Hz, 1H), 7.17 – 7.12 (m, 2H), 6.63 – 6.59 (m, 1H), 6.56 – 6.51 (m, 4H), 4.55 (d, $J = 14.2$ Hz, 1H), 4.26 (d, $J = 14.2$ Hz, 1H), 3.83 (s, 3H), 3.76 (brs, 6H), 3.74 (s, 3H); ^{13}C NMR (100 MHz, $DMSO-d_6$) δ 166.5, 166.4, 164.6, 164.0, 162.0, 157.9, 157.3, 155.0, 142.4, 140.4, 136.7, 134.3, 131.4, 126.3, 125.0,

124.8, 121.6, 120.9, 120.5, 119.6, 118.7, 110.9, 110.1, 103.9, 103.5, 94.3, 75.9, 60.9, 60.8, 60.6, 60.5, 57.2; HRMS (ESI-TOF) (m/z) calculated $C_{28}H_{26}BrN_2O_6^+$: 565.0969; found 565.0990 $[M+H]^+$.

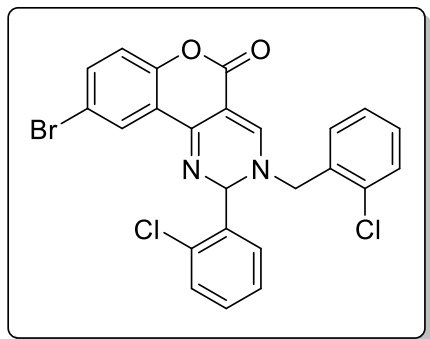
9-Bromo-3-(4-chlorobenzyl)-2-(4-chlorophenyl)-2,3-dihydro-5H-chromeno[4,3-*d*]pyrimidin-5-one (54u): White solid; yield: 111 mg (62%); mp: 148–150 °C; ^1H NMR



(400 MHz, $\text{DMSO-}d_6$) δ 8.58 (s, 1H), 7.94 (d, $J = 2.5$ Hz, 1H), 7.68 – 7.64 (m, 1H), 7.53 – 7.49 (m, 2H), 7.46 – 7.38 (m, 6H), 7.17 (d, $J = 8.8$ Hz, 1H), 6.30 (s, 1H), 4.87 (d, $J = 14.8$ Hz, 1H), 4.49 (d, $J = 14.8$ Hz, 1H); ^{13}C NMR (100 MHz, $\text{DMSO-}d_6$) δ 164.5, 159.9, 159.8, 158.0, 155.7, 143.7, 140.5, 138.8, 138.7, 138.4, 135.6, 134.0, 133.7, 131.4, 131.4, 125.4, 124.9, 121.0,

96.4, 80.8, 61.1; HRMS (ESI-TOF) (m/z) calculated $\text{C}_{24}\text{H}_{16}\text{BrCl}_2\text{N}_2\text{O}_2^+$: 512.9767; found 512.9775 $[\text{M}+\text{H}]^+$.

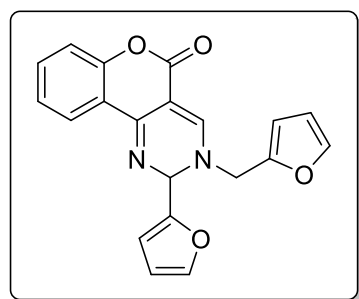
9-Bromo-3-(2-chlorobenzyl)-2-(2-chlorophenyl)-2,3-dihydro-5H-chromeno[4,3-*d*]pyrimidin-5-one (54v): White solid; yield: 100 mg (56%); mp: 146–148 °C; ^1H NMR



(400 MHz, $\text{DMSO-}d_6$) δ 8.60 (s, 1H), 7.88 (d, $J = 2.5$ Hz, 1H), 7.68 – 7.64 (m, 1H), 7.59 – 7.57 (m, 1H), 7.52 (s, 1H), 7.44 (d, $J = 5.6$ Hz, 3H), 7.38 – 7.35 (m, 3H), 7.18 – 7.15 (m, 1H), 6.69 (s, 1H), 4.91 (d, $J = 15.1$ Hz, 1H), 4.61 (d, $J = 15.1$ Hz, 1H); ^{13}C NMR (100 MHz, $\text{DMSO-}d_6$) δ 166.9, 159.7, 156.3, 153.2, 150.6, 137.2, 135.9, 133.9, 132.2, 131.4, 131.4, 131.1, 131.1, 131.0,

130.3, 130.2, 130.2, 130.0, 129.3, 129.0, 128.5, 128.2, 127.7, 126.6, 120.6, 120.2, 116.3, 90.4, 74.7, 55.2; HRMS (ESI-TOF) (m/z) calculated $\text{C}_{24}\text{H}_{16}\text{BrCl}_2\text{N}_2\text{O}_2^+$: 512.9767; found 512.9775 $[\text{M}+\text{H}]^+$.

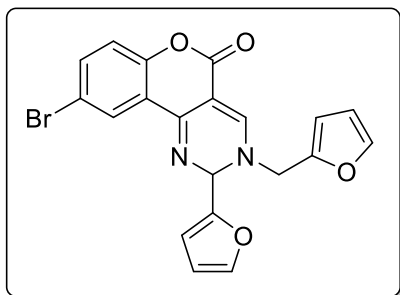
2-(Furan-2-yl)-3-(furan-2-ylmethyl)-2,3-dihydro-5H-chromeno[4,3-*d*]pyrimidin-5-one (54w): Pale–yellow solid; yield: 105 mg (63%); mp: 174–176 °C; ^1H NMR (400



MHz, CDCl_3) δ 8.10 (dd, $J = 8.1, 1.5$ Hz, 1H), 8.00 (s, 1H), 7.51 – 7.44 (m, 3H), 7.22 – 7.16 (m, 2H), 6.45 (t, $J = 2.2$ Hz, 2H), 6.42 – 6.38 (m, 1H), 6.38 – 6.36 (m, 2H), 4.64 (d, $J = 15.4$ Hz, 1H), 4.54 (d, $J = 15.4$ Hz, 1H); ^{13}C NMR (100 MHz, CDCl_3) δ 161.5, 154.1, 154.1, 152.2, 151.4, 146.0, 144.3, 143.4, 132.9, 124.6, 124.0, 118.5, 117.5, 111.4, 110.9, 110.6,

109.2, 93.4, 70.8, 50.5; HRMS (ESI-TOF) (m/z) calculated $C_{20}H_{15}N_2O_4^+$: 347.1026; found 347.1038 $[M+H]^+$.

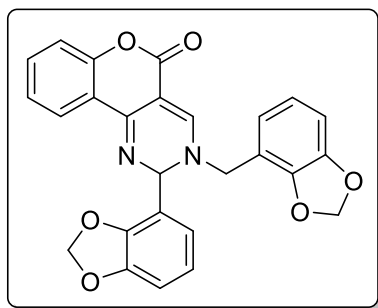
9-Bromo-2-(furan-2-yl)-3-(furan-2-ylmethyl)-2,3-dihydro-5H-chromeno[4,3-*d*]pyrimidin-5-one (54x): White solid; yield: 74 mg (50%); mp: 164–166 °C; 1H NMR



(400 MHz, $CDCl_3$) δ 8.22 (d, $J = 2.4$ Hz, 1H), 8.00 (s, 1H), 7.53 – 7.48 (m, 1H), 7.49 – 7.42 (m, 2H), 7.06 (d, $J = 8.7$ Hz, 1H), 6.49 – 6.43 (m, 2H), 6.43 – 6.34 (m, 3H), 4.62 (d, $J = 15.4$ Hz, 1H), 4.53 (d, $J = 15.4$ Hz, 1H); ^{13}C NMR (100 MHz, $CDCl_3$) δ 160.9, 153.0, 152.5, 151.1, 145.8, 144.3, 143.5, 135.6, 127.3, 125.0, 120.2, 119.3,

117.0, 111.5, 110.9, 110.6, 109.3, 92.8, 70.9, 50.5; HRMS (ESI-TOF) (m/z) calculated $C_{20}H_{14}BrN_2O_4^+$: 425.0131; found 425.0130 $[M+H]^+$.

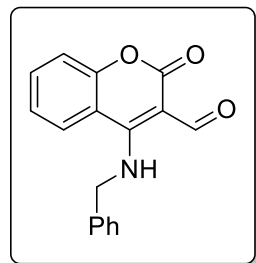
2-(Benzo[*d*][1,3]dioxol-4-yl)-3-(benzo[*d*][1,3]dioxol-4-ylmethyl)-2,3-dihydro-5H-chromeno[4,3-*d*]pyrimidin-5-one (54y): White solid; yield: 143 mg (66%); mp: 178–



179 °C; 1H NMR (400 MHz, $CDCl_3$) δ 8.09 (s, 1H), 8.00 (d, $J = 6.9$ Hz, 1H), 7.43 (t, $J = 7.4$ Hz, 1H), 7.13 (t, $J = 8.0$ Hz, 2H), 7.00 (d, $J = 1.6$ Hz, 1H), 6.94 – 6.88 (m, 1H), 6.81 (d, $J = 7.9$ Hz, 2H), 6.74 – 6.68 (m, 2H), 6.19 (s, 1H), 6.01 – 5.96 (m, 4H), 4.38 (d, $J = 14.6$ Hz, 1H), 4.25 (d, $J = 14.6$ Hz, 1H); ^{13}C NMR (100 MHz, $CDCl_3$) δ 161.6, 154.1, 152.8,

151.7, 148.6, 148.6, 148.6, 148.4, 134.0, 132.7, 125.8, 124.6, 123.9, 122.5, 120.3, 118.6, 117.4, 108.8, 108.5, 108.4, 107.2, 101.6, 101.5, 91.5, 77.6, 57.6; HRMS (ESI-TOF) (m/z) calculated $C_{26}H_{19}N_2O_6^+$: 455.1238; found 455.1253 $[M+H]^+$.

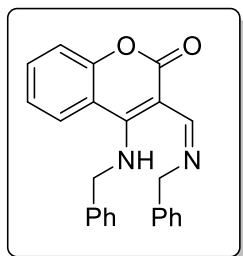
4-(Benzylamino)-2-oxo-2H-chromene-3-carbaldehyde (54a'): Yellow solid; yield: 92



mg (70%); mp: 198–200 °C; 1H NMR (400 MHz, $CDCl_3$) δ 12.32 (s, 1H), 10.17 (s, 1H), 8.01 (dd, $J = 8.3, 1.1$ Hz, 1H), 7.66 – 7.62 (m, 1H), 7.47 – 7.36 (m, 6H), 7.26 – 7.22 (m, 1H), 5.09 (d, $J = 5.8$ Hz, 2H); ^{13}C NMR (100 MHz, $CDCl_3$) δ 192.0, 162.7, 159.9, 155.5, 135.6, 134.6, 129.4, 128.6, 127.7, 127.6, 127.0, 123.8, 118.9, 113.8, 97.0, 51.3; HRMS (ESI-TOF) (m/z) calculated $C_{17}H_{14}NO_3^+$:

280.0968; found 280.0971 $[M+H]^+$.

(Z)-4-(Benzylamino)-3-((benzylimino)methyl)-2H-chromen-2-one (54a''): Yellow solid;



yield: 150 mg (85%); mp: 168–170 °C; ^1H NMR (400 MHz, CDCl_3) δ 13.21 (s, 1H), 8.95 (s, 1H), 8.03 (dd, $J = 8.3, 1.2$ Hz, 1H), 7.56 – 7.50 (m, 1H), 7.37 – 7.32 (m, 6H), 7.28 – 7.19 (m, 4H), 7.09 – 7.01 (m, 2H), 5.02 (d, $J = 3.7$ Hz, 2H), 4.62 (s, 2H); ^{13}C NMR (100 MHz, CDCl_3) δ 163.0,

161.9, 156.8, 154.3, 139.6, 136.8, 132.6, 129.1, 128.5, 128.1, 127.7, 127.6, 126.8, 126.7, 123.3, 118.4, 115.1, 93.2, 64.7, 51.4; HRMS (ESI-TOF) (m/z) calculated $\text{C}_{24}\text{H}_{21}\text{N}_2\text{O}_2^+$: 369.1580; found 369.1598 $[\text{M}+\text{H}]^+$.

3.4 X-ray Crystallography Studies of 54a

Crystals of **54a** were screened under a microscope for mounting in a nylon loop attached to a goniometer head. Initial crystal evaluation and data collection were performed on a Kappa APEX II diffractometer equipped with a CCD detector (with the crystal-to-detector distance fixed at 60 mm) and sealed-tube monochromated MoK radiation using the program APEX2.⁶⁸ By using the program SAINT⁶⁸ for the integration of the data, reflection profiles were fitted, and values of F^{69} and (F^2) for each reflection were obtained. Data were also corrected for Lorentz and polarization effects. The subroutine XPREP⁶⁹ was used for the processing of data that included determination of space group, application of an absorption correction (SADABS)⁶⁹, merging of data, and generation of files necessary for solution and refinement. The crystal structure was solved and refined using SHELX 97.⁷⁰ In each case, the space group was chosen based on systematic absences and confirmed by the successful refinement of the structure. Positions of most of the non-hydrogen atoms were obtained from a direct methods solution. Several full-matrix least-squares/difference Fourier cycles were performed, locating the remainder of the non-hydrogen atoms. All non-hydrogen atoms were refined with anisotropic displacement parameters. All hydrogen atoms were placed in ideal positions and refined as riding atoms with individual isotropic displacement parameters. All figures were drawn using MERCURY V 3.0⁷¹ and Platon.⁷²

Crystal data for 54a (CCDC No. 1575437): $\text{C}_{24}\text{H}_{18}\text{N}_2\text{O}_2$, Mr = 366.40 g/mol, monoclinic, space group $C2/c$, $a = 21.348(4)$ Å, $b = 9.871(2)$ Å, $c = 17.745(4)$ Å, $\alpha = 90^\circ$, $\beta = 92.423(5)^\circ$, $\gamma = 90^\circ$, $V = 3736(1)$ Å³, $Z = 8$, $T = 296(2)$ K, $D_{\text{calcd}} = 1.303$ g/cm³; Full matrix least-square on F^2 ; $R_1 = 0.046$, $wR_2 = 0.1064$ for 2274 observed reflections [$I > 2\sigma(I)$] and $R_1 = 0.073$, $wR_2 = 0.1199$ for all 3294 reflections; GOF = 1.024. CCDC No. 1575437.

3.5 References

- (1) Li, C. J. *Accounts of Chemical Research* **2008**, *42*, 335-344.
- (2) Sun, C. L.; Li, B. J.; Shi, Z. J. *Chemical Reviews* **2010**, *111*, 1293-1314.
- (3) Gini, A.; Brandhofer, T.; Mancheno, O. G. *Organic & Biomolecular Chemistry* **2017**, *15*, 1294-1312.
- (4) Li, B. J.; Shi, Z. J. *Chemical Society Reviews* **2012**, *41*, 5588-5598.
- (5) Alberico, D.; Scott, M. E.; Lautens, M. *Chemical Reviews* **2007**, *107*, 174-238.
- (6) Miao, J.; Ge, H. *European Journal of Organic Chemistry* **2015**, *2015*, 7859-7868.
- (7) Wendlandt, A. E.; Suess, A. M.; Stahl, S. S. *Angewandte Chemie International Edition* **2011**, *50*, 11062-11087.
- (8) Jia, X.; Peng, F.; Qing, C.; Huo, C.; Wang, X. *Organic Letters* **2012**, *14*, 4030-4033.
- (9) Lyons, T. W.; Sanford, M. S. *Chemical Reviews* **2010**, *110*, 1147-1169.
- (10) Shang, R.; Ilies, L.; Nakamura, E. *Chemical Reviews* **2017**, *117*, 9086-9139.
- (11) Xie, J.; Pan, C.; Abdukader, A.; Zhu, C. *Chemical Society Reviews* **2014**, *43*, 5245-5256.
- (12) Yang, Y.; Lan, J.; You, J. *Chemical Reviews* **2017**, *117*, 8787-8863.
- (13) Bergmann, L.; Zink, D. M.; Brase, S.; Baumann, T.; Volz, D. In *Photoluminescent Materials and Electroluminescent Devices*; Springer: **2017**, p 201-239.
- (14) Rao, W. H.; Shi, B. F. *Organic Chemistry Frontiers* **2016**, *3*, 1028-1047.
- (15) Fonseca Guerra, C.; Sanz Miguel, P. J.; Cebollada, A.; Bickelhaupt, F. M.; Lippert, B. *Chemistry—A European Journal* **2014**, *20*, 9494-9499.
- (16) Guo, X. X.; Gu, D. W.; Wu, Z.; Zhang, W. *Chemical Reviews* **2014**, *115*, 1622-1651.
- (17) Hirano, K.; Miura, M. *Chemical Communications* **2012**, *48*, 10704-10714.
- (18) Liu, J.; Chen, G.; Tan, Z. *Advanced Synthesis & Catalysis* **2016**, *358*, 1174-1194.
- (19) King, A. E.; Huffman, L. M.; Casitas, A.; Costas, M.; Ribas, X.; Stahl, S. S. *Journal of the American Chemical Society* **2010**, *132*, 12068-12073.
- (20) Allen, S. E.; Walvoord, R. R.; Padilla Salinas, R.; Kozlowski, M. C. *Chemical Reviews* **2013**, *113*, 6234-6458.
- (21) Cavani, F.; Teles, J. H. *ChemSusChem: Chemistry & Sustainability Energy & Materials* **2009**, *2*, 508-534.
- (22) He, J.; Wasa, M.; Chan, K. S.; Shao, Q.; Yu, J. Q. *Chemical Reviews* **2016**, *117*, 8754-8786.

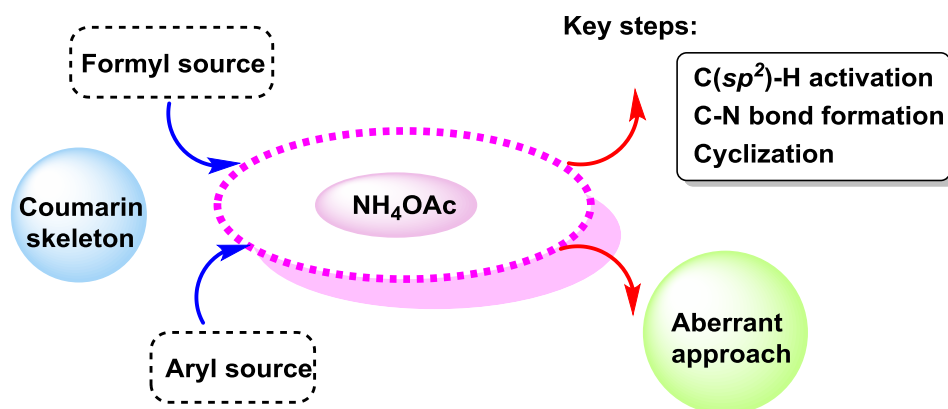
- (23) Wang, B.; Qiu, D.; Zhang, Y.; Wang, J. *Beilstein Journal of Organic Chemistry* **2016**, *12*, 796-804.
- (24) Xie, J.; Zhu, C. *Sustainable C (sp³)-H Bond Functionalization*; Springer, **2016**.
- (25) Zhang, F. L.; Hong, K.; Li, T. J.; Park, H.; Yu, J. Q. *Science* **2016**, *351*, 252-256.
- (26) Zhang, C.; Tang, C.; Jiao, N. *Chemical Society Reviews* **2012**, *41*, 3464-3484.
- (27) Zhao, B.; Du, H.; Shi, Y. *Journal of the American Chemical Society* **2008**, *130*, 7220-7221.
- (28) Li, J.; Neuville, L. *Organic Letters* **2013**, *15*, 1752-1755.
- (29) Chen, H.; Chiba, S. *Organic & Biomolecular Chemistry* **2014**, *12*, 42-46.
- (30) Takemura, N.; Kuninobu, Y.; Kanai, M. *Organic & Biomolecular Chemistry* **2014**, *12*, 2528-2532.
- (31) Li, Y.; Li, Z.; Xiong, T.; Zhang, Q.; Zhang, X. *Organic Letters* **2012**, *14*, 3522-3525.
- (32) Tian, H.; Qiao, H.; Zhu, C.; Fu, H. *RSC Advances* **2014**, *4*, 2694-2704.
- (33) Wang, Z.; Ni, J.; Kuninobu, Y.; Kanai, M. *Angewandte Chemie* **2014**, *126*, 3564-3567.
- (34) Huang, P. C.; Gandeepan, P.; Cheng, C. H. *Chemical Communications* **2013**, *49*, 8540-8542.
- (35) Gholap, A. V.; Maity, S.; Schulzke, C.; Maiti, D.; Kapdi, A. R. *Organic & Biomolecular Chemistry* **2017**, *15*, 7140-7146.
- (36) Modak, A.; Dutta, U.; Kancherla, R.; Maity, S.; Bhadra, M.; Mobin, S. M.; Maiti, D. *Organic Letters* **2014**, *16*, 2602-2605.
- (37) Cai, Z. J.; Wang, S. Y.; Ji, S. J. *Organic Letters* **2012**, *14*, 6068-6071.
- (38) Wang, X.; Qiu, X.; Wei, J.; Liu, J.; Song, S.; Wang, W.; Jiao, N. *Organic Letters* **2018**, *20*, 2632-2636.
- (39) Zhang, J.; Yu, C.; Wang, S.; Wan, C.; Wang, Z. *Chemical Communications* **2010**, *46*, 5244-5246.
- (40) Wan, C.; Zhang, J.; Wang, S.; Fan, J.; Wang, Z. *Organic Letters* **2010**, *12*, 2338-2341.
- (41) Sang, P.; Xie, Y.; Zou, J.; Zhang, Y. *Organic Letters* **2012**, *14*, 3894-3897.
- (42) Scherlach, K.; Nützmann, H. W.; Schroeckh, V.; Dahse, H. M.; Brakhage, A. A.; Hertweck, C. *Angewandte Chemie International Edition* **2011**, *50*, 9843-9847.
- (43) Cheng, C.; Chen, W.-W.; Xu, B.; Xu, M.-H. *Organic Chemistry Frontiers* **2016**, *3*, 1111-1115.

- (44) Kshirsagar, U. A.; Parnes, R.; Goldshtein, H.; Ofir, R.; Zarivach, R.; Pappo, D. *Chemistry—A European Journal* **2013**, *19*, 13575-13583.
- (45) Adityachaudhury, N.; Gupta, P. *Phytochemistry* **1973**, *12*, 425-428.
- (46) Ambre, P. K.; Pissurlenkar, R. R.; Wavhale, R. D.; Shaikh, M. S.; Khedkar, V. M.; Wan, B.; Franzblau, S. G.; Coutinho, E. C. *Medicinal Chemistry Research* **2014**, *23*, 2564-2575.
- (47) Sashidhara, K. V.; Palnati, G. R.; Singh, L. R.; Upadhyay, A.; Avula, S. R.; Kumar, A.; Kant, R. *Green Chemistry* **2015**, *17*, 3766-3770.
- (48) Zhou, Z.; Liu, H.; Li, Y.; Liu, J.; Li, Y.; Liu, J.; Yao, J.; Wang, C. *ACS Combinatorial Science* **2013**, *15*, 363-369.
- (49) Chen, J.; Liu, W.; Zhou, B.; Niu, G.; Zhang, H.; Wu, J.; Wang, Y.; Ju, W.; Wang, P. *The Journal of Organic Chemistry* **2013**, *78*, 6121-6130.
- (50) Cao, X.; Lin, W.; Yu, Q.; Wang, J. *Organic Letters* **2011**, *13*, 6098-6101.
- (51) Sheng, J.; Xu, T.; Zhang, E.; Zhang, X.; Wei, W.; Zou, Y. *Journal of Natural Products* **2016**, *79*, 2749-2753.
- (52) Belal, M.; Khan, A. T. *RSC Advances* **2016**, *6*, 18891-18894.
- (53) Mackey, K.; Pardo, L. M.; Prendergast, A. M.; Nolan, M. T.; Bateman, L. M.; McGlacken, G. P. *Organic Letters* **2016**, *18*, 2540-2543.
- (54) Cheng, C.; Chen, W.-W.; Xu, B.; Xu, M.-H. *The Journal of Organic Chemistry* **2016**, *81*, 11501-11507.
- (55) Dey, A.; Ali, M. A.; Jana, S.; Samanta, S.; Hajra, A. *Tetrahedron Letters* **2017**, *58*, 313-316.
- (56) Peng, S.; Gao, T.; Sun, S.; Peng, Y.; Wu, M.; Guo, H.; Wang, J. *Advanced Synthesis & Catalysis* **2014**, *356*, 319-324.
- (57) Lin, C.-H.; Yang, D.-Y. *Organic Letters* **2013**, *15*, 2802-2805.
- (58) Scherlach, K.; Nutzmann, H. W.; Schroeckh, V.; Dahse, H. M.; Brakhage, A. A.; Hertweck, C. *Angewandte Chemie International Edition* **2011**, *50*, 9843-9847.
- (59) Selles, P.; Mueller, U. *Organic Letters* **2004**, *6*, 277-279.
- (60) Beccalli, E. M.; Contini, A.; Trimarco, P. *Tetrahedron* **2005**, *61*, 4957-4964.
- (61) Vadagaonkar, K. S.; Kalmode, H. P.; Prakash, S.; Chaskar, A. C. *New Journal of Chemistry* **2015**, *39*, 3639-3645.

- (62) Jalli, V. P.; Jaggavarapu, S. R.; Kamalakaran, A. S.; Gangisetty, S. K.; Nanubolu, J. B.; Gaddamanugu, G. *Tetrahedron Letters* **2013**, *54*, 1491-1494.
- (63) Yang, F.; Li, J.; Xie, J.; Huang, Z. Z. *Organic Letters* **2010**, *12*, 5214-5217.
- (64) Xie, P.; Xie, Y.; Qian, B.; Zhou, H.; Xia, C.; Huang, H. *Journal of the American Chemical Society* **2012**, *134*, 9902-9905.
- (65) Xie, P.; Xia, C.; Huang, H. *Organic Letters* **2013**, *15*, 3370-3373.
- (66) Rout, S. K.; Guin, S.; Banerjee, A.; Khatun, N.; Gogoi, A.; Patel, B. K. *Organic Letters* **2013**, *15*, 4106-4109.
- (67) Itazaki, M.; Nakazawa, H. In *Iron Catalysis II*; Springer: **2015**, p 47-81.
- (68) Singh, S. K.; Chandna, N.; Jain, N. *Organic Letters* **2017**, *19*, 1322-1325.
- (69) Bruker, A.; SAINT, A. *Acta Crystallogr., Sect. A: Fundam. Crystallogr* **2008**, *64*, 112.
- (70) Scheldrick, G. *Acta Crystallogr A* **2008**, *64*, 112-122.
- (71) Macrae, C. F.; Bruno, I. J.; Chisholm, J. A.; Edgington, P. R.; McCabe, P.; Pidcock, E.; Rodriguez-Monge, L.; Taylor, R.; Streek, J. v. d.; Wood, P. A. *Journal of Applied Crystallography* **2008**, *41*, 466-470.
- (72) Spek, A. *University of Utrecht* **1999**.

Chapter 4

NH₄OAc-promoted C(sp²)-H Bond Activation and C-N Bond Formation: An Aberrant Cascade Synthesis of Coumarin-fused Quinolinones



4.1 Introduction

With the increasing voice of sustainable chemistry, cascade reactions have been exemplified as a subject of prime attention due to cost-effectiveness, atom-economical and environmentally-benign protocols. The undeniable benefits of the cascade reactions have sparked the zeal of organic chemists for synthesizing polycyclic skeletons from simpler molecular assemblies under this banner.¹⁻³ In this context, various transition-metal-catalyzed cascade reactions have been applied for different organic transformations. However, due to the allied challenges and intuitive drawbacks associated with transition-metal-catalyzed strategies such as, usage of expensive and moisture sensitive catalysts, requirement of supporting ligands and additives, a continuous buzz has been created for developing methodologies under transition-metal-free conditions.⁴⁻⁹ Thus, metal-free cascade reactions have developed a significant repute leading to construction of synthetic bioactive and natural products.

Quinoline scaffold is highly noticed and privileged pharmacophore present in several natural products, and complex bioactive entities.

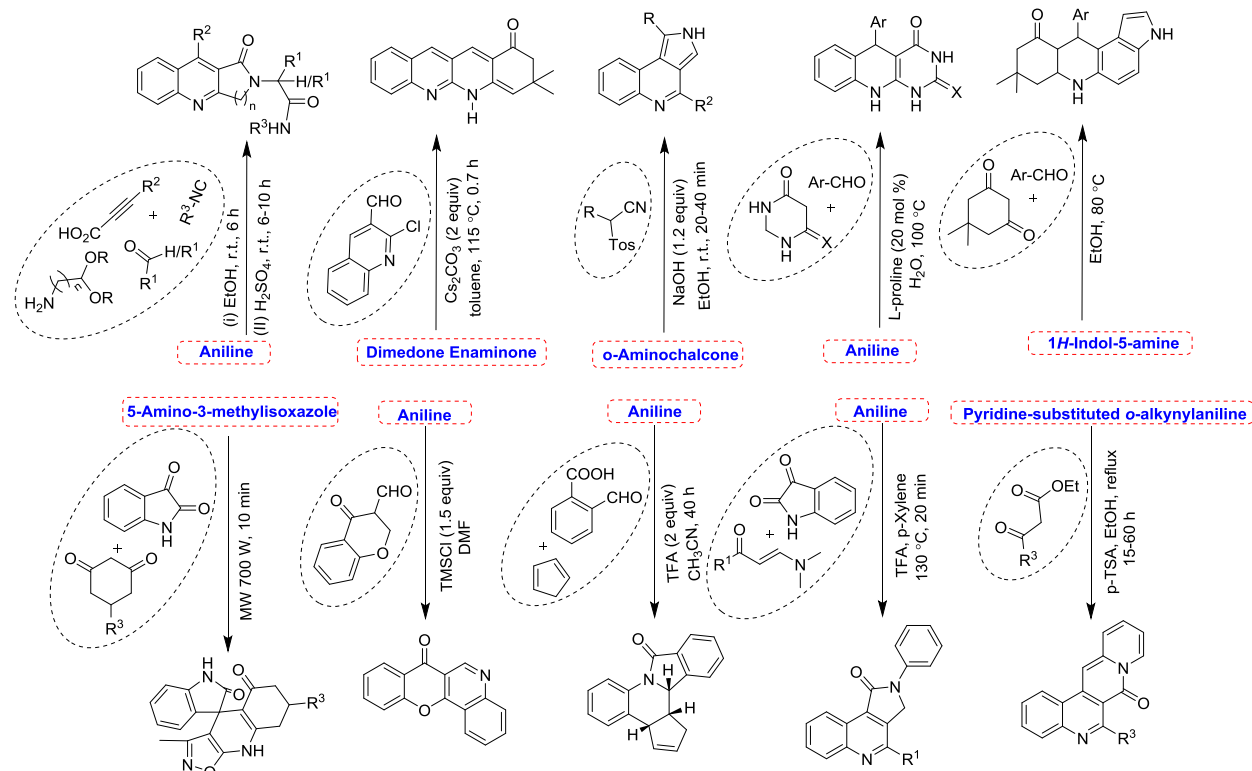
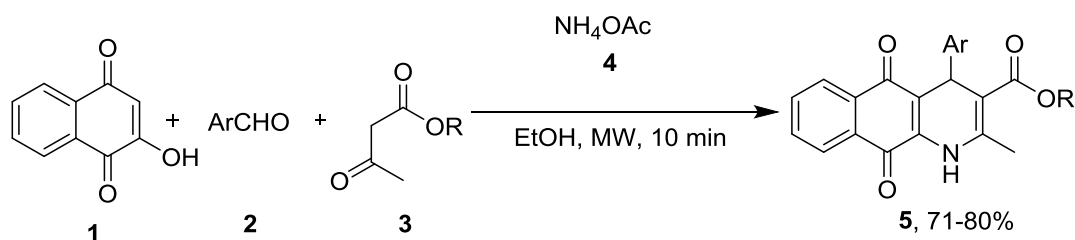


Figure 4.1.1: Overview of metal-free strategies reported for the synthesis of quinoline-fused heterocycles

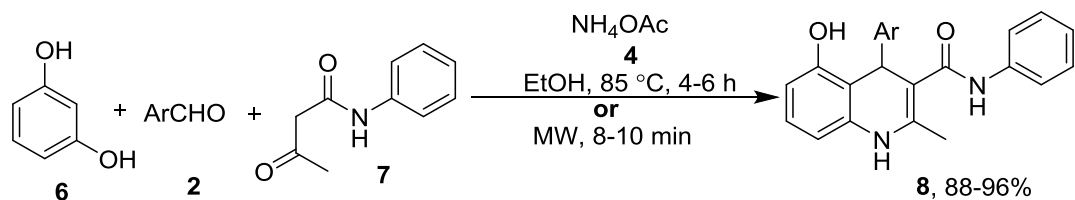
Quinoline-fused heterocycles have displayed a wide range of biological activities including, antimalarial,¹⁰ antidepressant,¹¹ antiviral,¹² antipsychotic,¹³ and anticancer.¹⁴ Noticeable efforts have been made towards the construction of different quinoline-fused heterocycles under metal-free reaction conditions, some of which are summarized in Figure 4.1.1.¹⁵⁻²⁴

In this context, the use of ammonium acetate (NH_4OAc) as an inexpensive nitrogen source has been exemplified in various C-C/C-X bond forming/breaking transformations.²⁵⁻³⁰ Particularly, ammonium acetate has been used as a nitrogen source for the construction of 1,4-dihydroquinolines and other quinoline-fused heterocycles under metal-free conditions. For example, Bala *et al.* reported a domino reaction between 2-hydroxy-1,4-naphthaquinone (**1**), aromatic aldehydes (**2**), methyl/ethyl acetoacetate (**3**) and ammonium acetate (**4**) in ethanol under microwave irradiation to afford a series of tetrahydrobenzo[g]quinoline-5,10-diones (**5**) in fairly good yields (Scheme 4.1.1).³¹



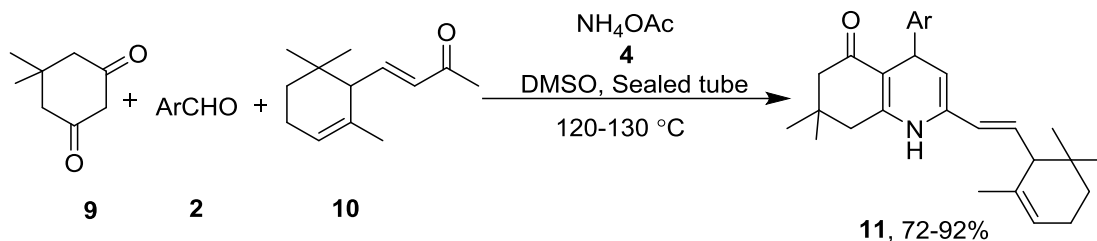
Scheme 4.1.1: NH_4OAc -mediated domino synthesis of tetrahydrobenzo[g]quinoline-5,10-diones (**5**)

Chidurala *et al.* reported one-pot multicomponent reaction between resorcinol (**6**), aromatic aldehydes (**2**), acetoacetanilide (**7**) and ammonium acetate (**4**) under both conventional and microwave irradiation conditions to afford substituted 1,4-dihydroquinolines (**8**) in decent yields (Scheme 4.1.2).³²



Scheme 4.1.2: NH_4OAc -mediated synthesis of substituted 1,4-dihydroquinolines (**8**)

Findik *et al.* reported a one-pot protocol for the synthesis of 7,8-dihydroquinolin-5-(1*H*,4*H*,6*H*)-ones (**11**) by reacting dimedone (**9**), α -ionone (**10**), ammonium acetate (**4**) and arylaldehydes (**2**) in DMSO under reflux conditions (Scheme 4.1.3).³³



Scheme 4.1.3: NH_4OAc -mediated synthesis of substituted 7,8-dihydroquinolin-5-ones (**11**)

Strikingly, coumarin derivatives play a significant role in designing a number of fascinating fluorescent heterocyclic architectures that have exhibited profound applications in medicinal and material chemistry.³⁴⁻³⁹ Accordingly, tremendous efforts have been devoted in the past towards the construction of coumarin-fused polycyclic heterocycles *via* conventional or modern flourishing chemistry.⁴⁰⁻⁴³ In this realm, chromene-fused quinolines form an integral part of several natural products including santiagonamine,⁴⁴ and have been identified as potential antibacterial⁴⁵ and anticancer agents,⁴⁶ fluorescent sensors,⁴⁷ dyes⁴⁸ for mitochondrial imaging,⁴⁹ estrogen receptor β -selective ligands,⁵⁰ selective non-steroidal progesterone receptor modulators,⁵¹ and glucocorticoid modulators⁵² (Figure 4.1.2).

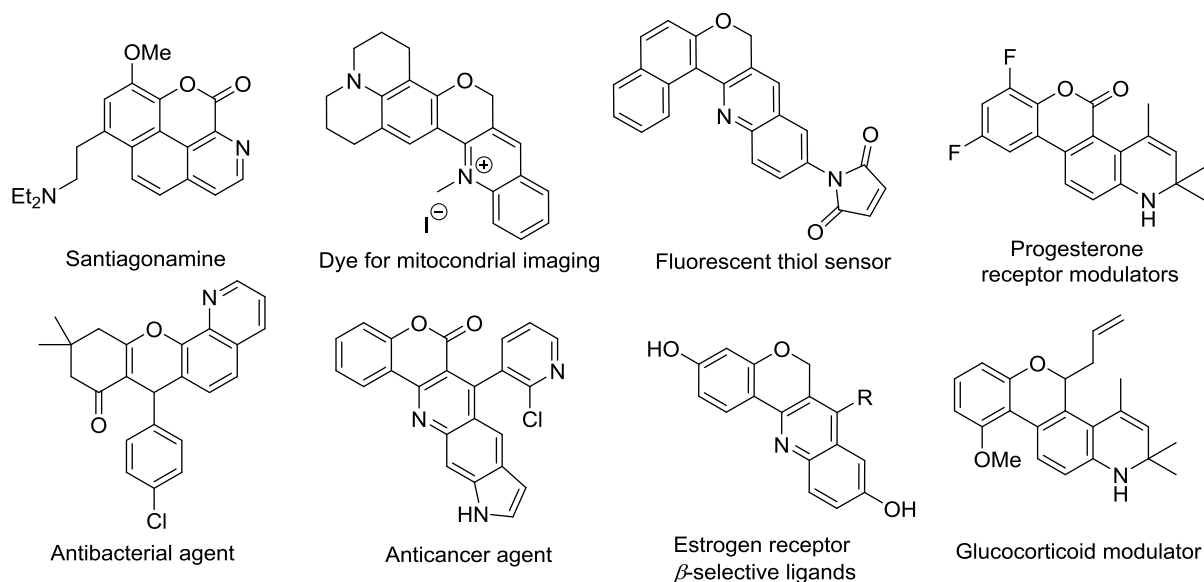
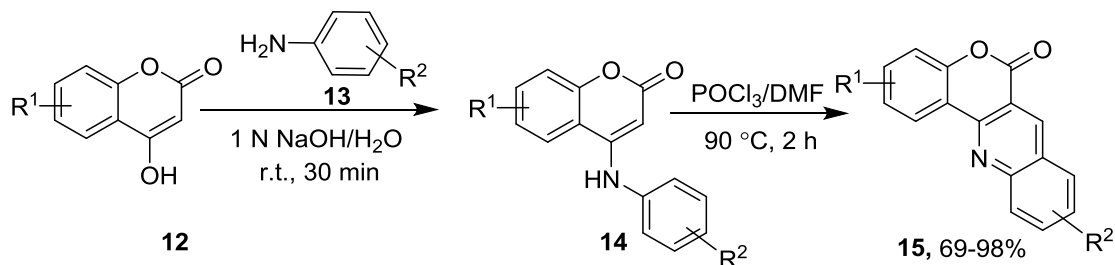


Figure 4.1.2: Selective examples of reported chromene-fused quinolines

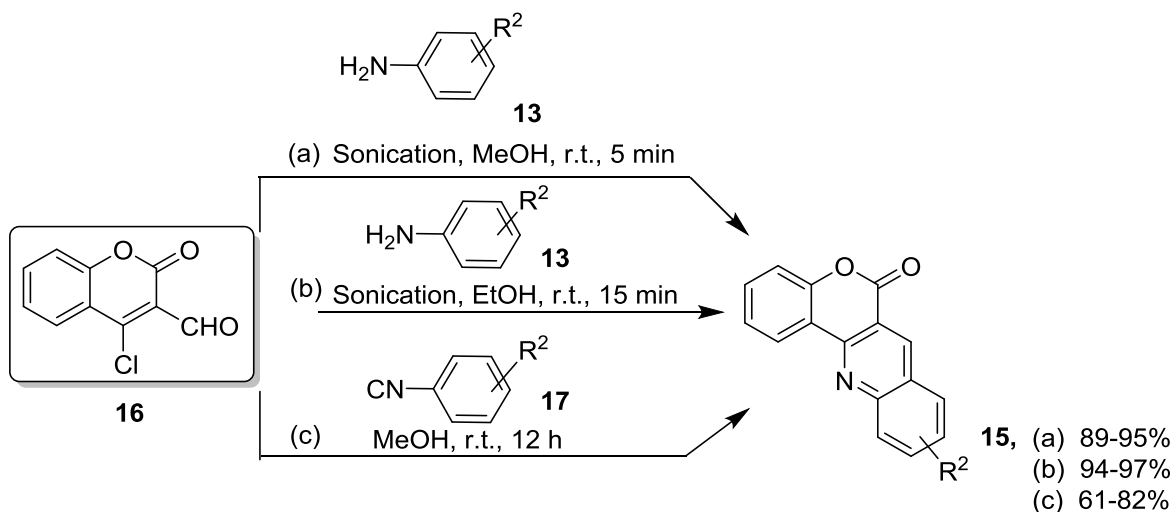
In particular, the applicative value of substituted 6*H*-chromeno[4,3-*b*]quinolin-6-ones has stimulated considerable attention of organic chemists towards their construction in the past decade. A number of traditional strategies have been developed for its synthesis under Vilsmeier-Haack conditions. In 1987, Tabakovic *et al.* documented the synthesis of 6*H*-chromeno[4,3-*b*]quinolin-6-ones (**15**) *via* amination of 4-hydroxycoumarin (**12**) with aromatic amines (**13**), and

subsequent intramolecular cyclization under Vilsmeier-Haack conditions (DMF/ POCl_3) (Scheme 4.1.4).⁵³



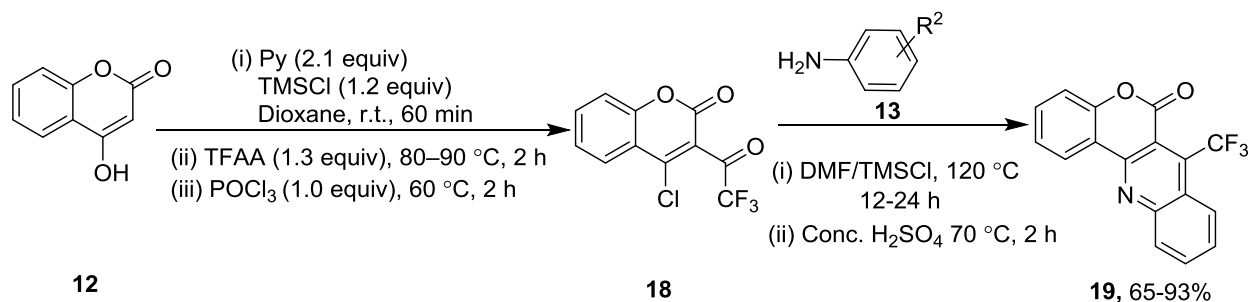
Scheme 4.1.4: Synthesis of 6H-chromeno[4,3-b]quinolin-6-ones under Vilsmeier-Haack conditions (15)

Subsequently, scientists such as Pal,⁵⁴ Prasad⁵⁵ and Wu⁵⁶ developed traditional approaches for the synthesis of 6H-chromeno[4,3-b]quinolin-6-ones (15) from 4-chloro-3-formylcoumarin (16) under appropriate conditions. For example, Pal *et al.* documented a catalyst-free direct cyclization protocol by reacting 4-chloro-3-formylcoumarin (16) with different aromatic amines (13) in MeOH using sonication to afford 15 in 89-95% yields (Scheme 4.1.5a).⁵⁴ Interestingly, compound 15 was found to possess remarkable anticancer activities. Similarly, Prasad *et al.* also prepared compound 15 by direct cyclization of 4-chloro-3-formylcoumarin (16) with aromatic amines (13) in EtOH using sonication (Scheme 4.1.5b).⁵⁵ Wu *et al.* used aryl isocyanides (17) as coupling partner for the effective cyclization with 4-chloro-3-formylcoumarin (16) in MeOH at room temperature to afford 15 in 61-82% yields (Scheme 4.1.5c).⁵⁶



Scheme 4.1.5: Traditional strategies for the synthesis of 6H-chromeno[4,3-b]quinolin-6-ones (15) from 4-chloro-3-formylcoumarin (16)

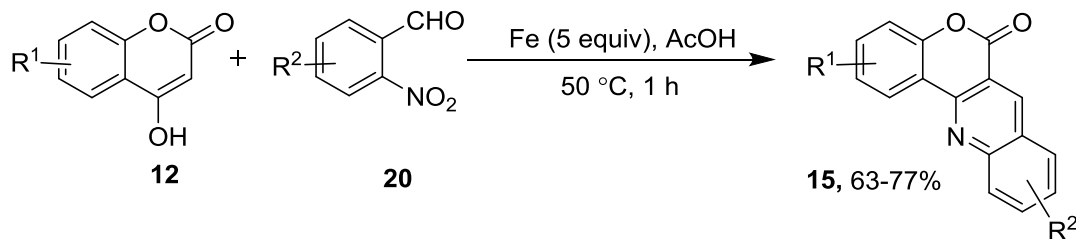
Iaroshenko group prepared 7-(trifluoromethyl)-6*H*-chromeno[4,3-*b*]quinolin-6-ones (**19**) from 4-hydroxycoumarin (**12**) in two steps. The first step involves the synthesis of 4-chloro-3-(trifluoroacetyl)-2*H*-chromen-2-one (**18**) by direct TMSCl-mediated acylation of 4-hydroxy-2*H*-chromen-2-one (**12**) with TFAA, followed by the treatment with POCl₃. Thereafter, the reaction of **18** with aromatic amines (**13**) using DMF/TMSCl, followed by cyclization in concentrated sulfuric acid afforded **19** in decent yields (Scheme 4.1.6).⁵⁷



Scheme 4.1.6: Multistep synthesis of 7-(trifluoromethyl)-6*H*-chromeno[4,3-*b*]quinolin-6-ones (**19**)

Despite reasonable advancements, the allied drawback of traditional Vilsmeier–Haack formylation has led to the discovery of new strategies involving the use of aldehydes as methine source substrate, for preparing 6*H*-chromeno[4,3-*b*]quinolin-6-one.

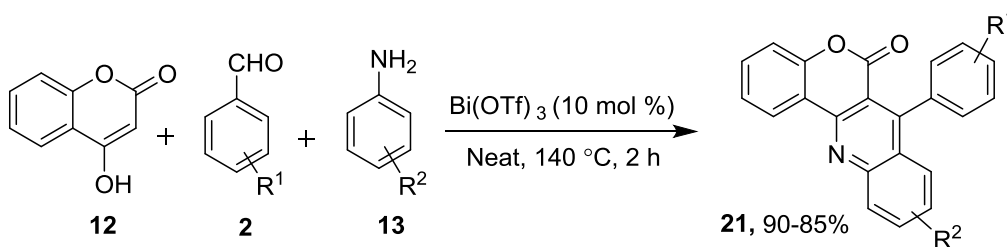
In conjunction to this ideology, Rajawinslin *et al.* implemented a one-pot strategy for the reductive cyclization of 2-nitrobenzaldehydes (**20**) and 4-hydroxycoumarin (**12**) using an excess of Fe powder in AcOH at 50 °C (Scheme 4.1.7). The standard protocol was also amenable for the synthesis of dibenzonaphthyridinones in 81% yield.⁵⁸



Scheme 4.1.7: Fe-mediated synthesis of 6*H*-chromeno[4,3-*b*]quinolin-6-ones (**15**)

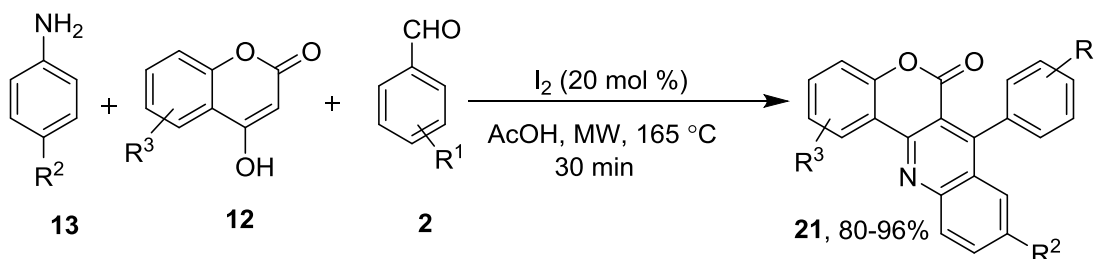
In 2014, Khan *et al.* disclosed a bismuth triflate-catalyzed two-step strategy for the synthesis of 7-aryl-6*H*-chromeno[4,3-*b*]quinolin-6-ones (**21**) *via* multicomponent reaction between 4-hydroxycoumarin (**12**), aldehydes (**2**) and aromatic amines (**13**) under neat condition (Scheme

4.1.8). Interestingly, photophysical studies of the products were determined and promising quantum yields were obtained.⁵⁹



Scheme 4.1.8: $\text{Bi}(\text{OTf})_3$ -catalyzed synthesis of 7-aryl-6H-chromeno[4,3-b]quinolin-6-ones (**21**)

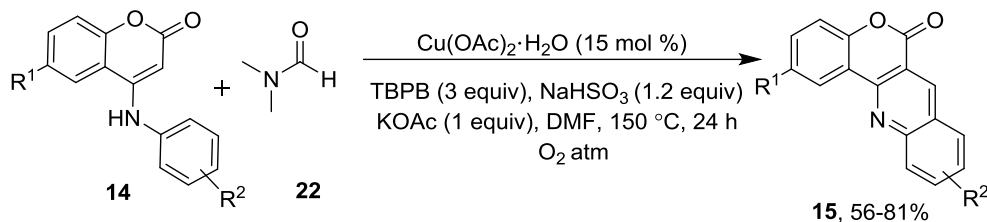
In 2015, Sashidhara *et al.* improved the synthetic methodology by employing iodine as a catalyst for coupling aromatic amines (**13**), aromatic aldehydes (**2**) and substituted 4-hydroxycoumarin (**12**) in acetic acid to afford the 7-aryl-6H-chromeno[4,3-b]quinolin-6-ones (**21**) in good-to-excellent yields under microwave-assisted condition (Scheme 4.1.9).⁵¹



Scheme 4.1.9: I_2 -catalyzed synthesis of 7-aryl-6H-chromeno[4,3-b]quinolin-6-ones (**21**)

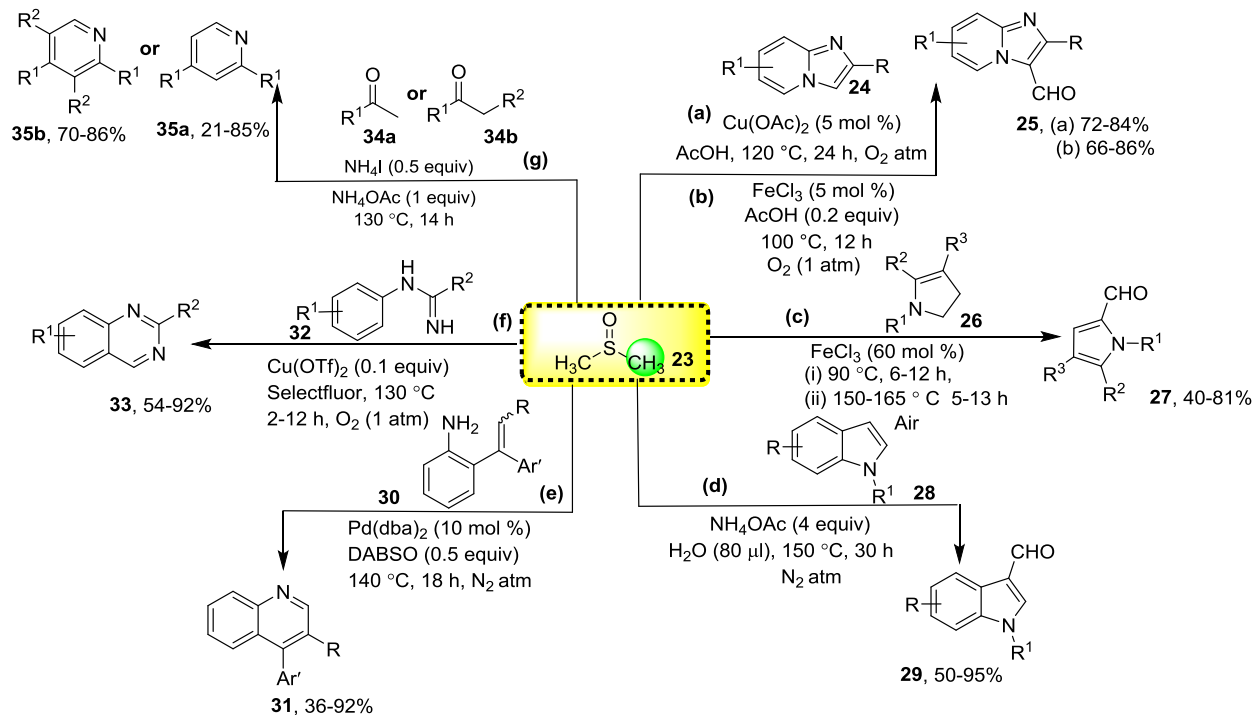
Furthermore, the direct introduction of the carbonyl group in a heterocyclic system is highly desirable due to its prevalent presence in various natural products, commercialized drugs, and synthetic materials. With this advent interest in developing smart $\text{C}(\text{sp}^2)\text{-H}$ formylation protocols *via* C-H activation, much efforts have been devoted by various research groups using different amines (*N*-methylaniline, *N,N*-dimethylaniline, TMEDA and HMTA) and various solvents (MeOH, DMSO and DMF) as formylation precursors under metal-catalyzed and metal-free conditions.

In this regard, Weng *et al.* reported a noticeable Cu-catalyzed cyclization protocol in an oxygen atmosphere to afford functionalized 6H-chromeno[4,3-b]quinolin-6-ones (**15**) from 4-(phenylamino)-2H-chromen-2-ones (**14**), employing DMF (**22**) as a methine source and TBPB as an oxidant (Scheme 4.1.10).⁶⁰



Scheme 4.1.10: Cu-catalyzed synthesis of 6H-chromeno[4,3-b]quinolin-6-ones (**15**) using DMF as methine source

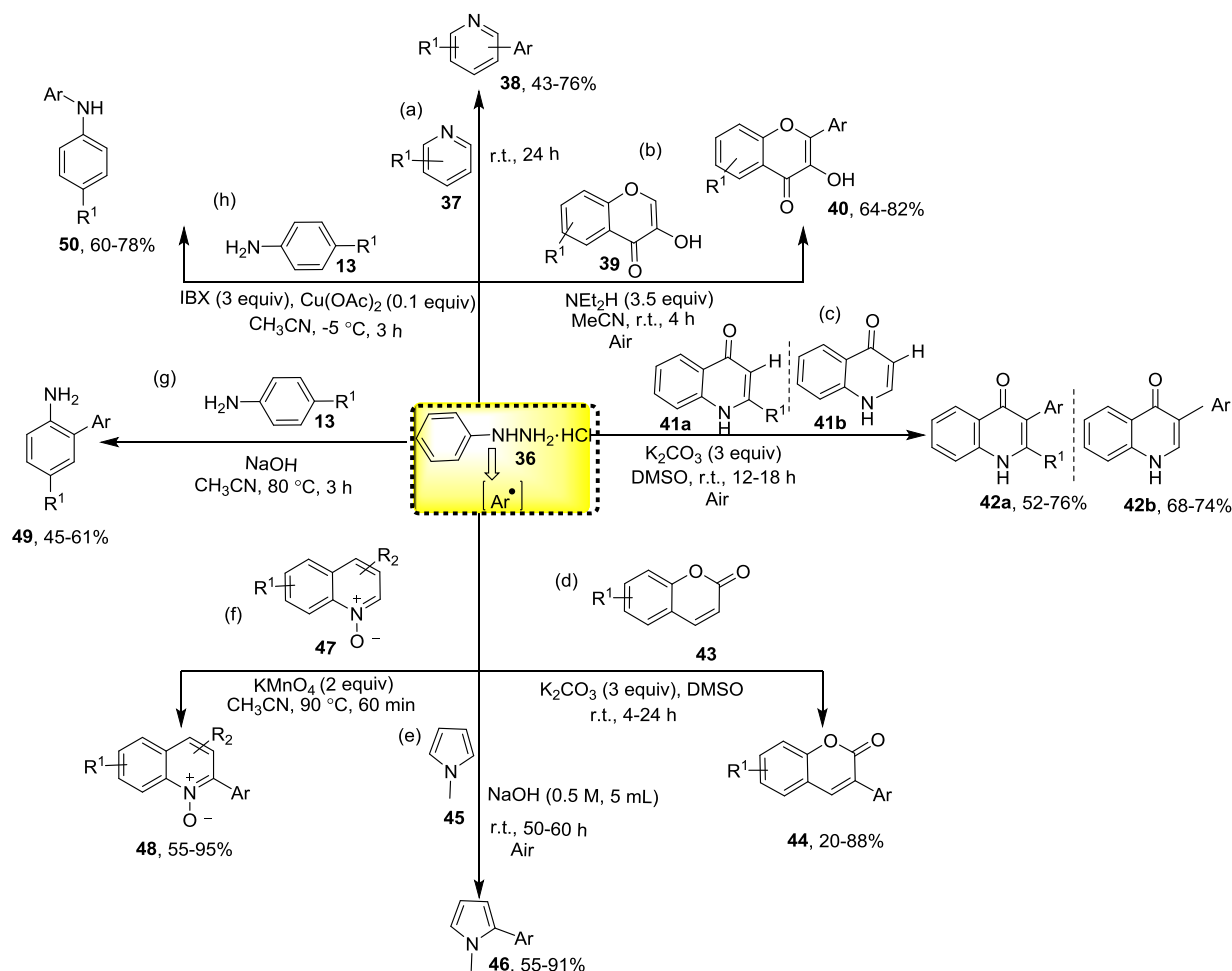
Recently, Dimethyl sulfoxide (DMSO) (**23**) has been exemplified as a formyl source in numerous organic transformations. For example, Cao *et al.* reported a Cu-catalyzed protocol for C-3 formylation of imidazo[1,2-*a*]pyridines (**24**) using dimethyl sulfoxide (**23**) to afford **25**, utilizing molecular oxygen as the oxidant (Scheme 4.1.11a).⁶¹ The reaction was described to proceed *via* single electron transfer (SET) radical pathway. Afterward, Xiang *et al.* prepared the same C-3 formylated products (**25**) under Fe(III)-catalyzed conditions using dimethyl sulfoxide (**23**) as the formyl source. A similar single electron transfer oxidation process involvement was proposed with the assistance of ferric chloride and molecular oxygen (Scheme 4.1.11b).⁶² Zang *et al.* reported Fe-catalyzed tandem oxidation/formylation reaction from readily available 2,3-dihydro-1*H*-pyrroles (**26**) with DMSO (**23**) in air atmosphere to afford the desired products **27** in moderate-to-good yields (Scheme 4.1.11c).⁶³ Similarly, Fei *et al.* reported a metal-free protocol for NH_4OAc -promoted C-3 formylation of indoles (**28**) with DMSO (**23**) under nitrogen atmosphere to afford 3-formyl indoles (**29**) in good-to-excellent yields (Scheme 4.1.11d).⁶⁴ Furthermore, incorporation of “-CH-” group using DMSO in a cascade process has led to the construction of interesting heterocyclic architectures. For example, Yuan *et al.* documented Pd-catalyzed annulation of *ortho*-vinyl anilines (**30**) with DMSO (**23**), which served as a “-CH-” fragment in this transformation to afford 4-arylquinolines (**31**) (Scheme 4.1.11e).⁶⁵ Lv *et al.* presented an intermolecular annulation protocol for the synthesis of quinazolines (**33**) *via* C-N bond formation between N-H bond of amidines (**32**) and the $\text{C}(\text{sp}^3)\text{-H}$ bond of DMSO **23** (Scheme 4.1.11f).⁶⁶ In relevance to the above work, Pan *et al.* reported a convenient and efficient method for the synthesis of symmetrical and unsymmetrical pyridines (**35a** & **35b**) *via* ammonium iodide-promoted cyclization of ketones (**34a** & **34b**) with DMSO (**23**) and ammonium acetate (**4**) (Scheme 4.1.11g). In this reaction system, DMSO was used not only as an effective reaction medium but also as the source of C-4 or C-6 for the formation of pyridines.⁶⁷



Scheme 4.1.11: Metal-free and metal-catalyzed strategies for formylation or methine insertion using DMSO (**23**)

In striking contrast, arylhydrazines (**36**) are valuable coupling partners in organic synthesis, capable of generating aromatic amines,⁶⁸ and aryl radicals⁶⁹⁻⁷⁶ under appropriate reaction conditions. Direct arylation from arylhydrazines under metal-free conditions *via* SET mechanism has been efficiently explored in the construction of numerous aryl/(hetero)aryl C-C bonds. In this realm, Li *et al.* documented a metal-free approach for the direct arylation of substituted pyridines (**37**) with arylhydrazines (**36**) at room temperature to afford C-3 and C-2 arylated products **38** in moderate-to-good yields (Scheme 4.1.12a).⁶⁹ Paul *et al.* documented metal-free hydroxyl group directed C-2 arylation of substituted 3-hydroxychromone (**39**) with arylhydrazines (**36**) in acetonitrile to afford good yields of arylated products **40** (Scheme 4.1.12b).⁷⁰ Ravi *et al.* used arylhydrazines (**36**) as coupling partner to afford **42a** & **42b** by direct arylation of substituted quinolin-4-ones (**41a** & **41b**) using K_2CO_3 in DMSO (Scheme 4.1.12c).⁷¹ In another report, the authors synthesized C-3 arylated coumarin (**44**) by reacting coumarins (**43**) with arylhydrazines (**36**) using K_2CO_3 in DMSO (Scheme 4.1.12d).⁷² Kocaoğlu *et al.* successfully achieved C-2 arylation of *N*-methylpyrrole (**45**) using arylhydrazines (**36**) as an aryl radical source in presence of NaOH under oxygen at room temperature to furnish C-2 arylated pyrroles (**46**) (Scheme 4.1.12e).⁷³ Yuan *et al.* reported metal-free protocol for C-2 arylation of substituted quinoline *N*-

oxides (**47**) using arylhydrazines (**36**) in presence of KMnO_4 , affording **48** in 55-95% yields (Scheme 4.1.12f).⁷⁴ Jiang *et al.* synthesized 2-aminobiaryls (**49**) by coupling substituted amines (**13**) and arylhydrazines (**36**) under metal-free conditions using NaOH as a base (Scheme 4.1.12g).⁷⁵ Interestingly, IBX was effectively utilized by Jadhav *et al.* for the *N*-arylation of aromatic amines (**13**) to afford **50**, *via* generation of aryl free radicals from arylhydrazines (**36**) (Scheme 4.1.12h).⁷⁶

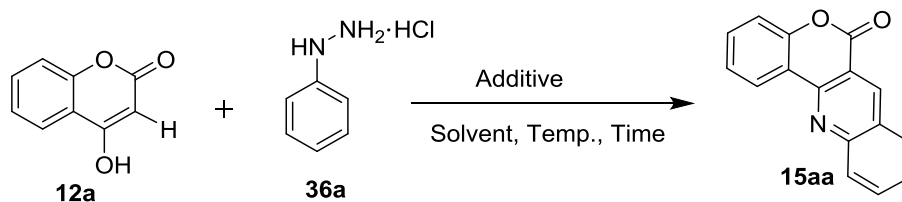


Scheme 4.1.12: Selective examples of metal-free arylation strategies from arylhydrazines (**36**)

To the best of our knowledge, the employment of arylhydrazines remains unexplored for the synthesis of chromene-fused quinolinones. Thus, we envisioned the dual purpose of NH_4OAc to promote Pummerer reaction for C-3 formylation of 4-hydroxycoumarin using DMSO, and simultaneously act as a nitrogen source for trapping aryl radical that is expected to be generated from arylhydrazone, to afford 6*H*-chromeno[4,3-*b*]quinolin-6-ones in a tandem fashion.

4.2 Results and Discussion

From the outset of the proposed work, we began investigating the model reaction between 4-hydroxycoumarin (**12a**) (1 equiv), and phenylhydrazine hydrochloride (**36a**) (1.2 equiv) under ammonium-promoted conditions (Table 1). Gratifyingly, we witnessed the formation of a product in 35% yield after heating **12a** and **36a** using NH₄OAc (1 equiv) at 130 °C in DMSO for 5 h under ambient conditions (Table, 4.2.1 entry 1). Purification and characterization of the product using ¹H NMR, ¹³C NMR, HRMS unequivocally confirmed it to be 6*H*-chromeno[4,3-*b*]quinolin-6-one (**15aa**). This unprecedented formation of a chromene-fused quinolinone from phenylhydrazine hydrochloride (**36a**) as an aryl source propel us to further optimize this tandem protocol with respect to concering time, solvent, and reactant/reagent concentrations. Time optimization studies revealed that heating the model reaction up to 6 h produces an increment in the yield of **15aa** to 42%, however no further noticeable amelioration in its yield was observed by further increasing the reaction time (Table 4.2.1, entries 2-3). Delightfully, a step-wise change in the equivalents of NH₄OAc from 1 to 3 aids an augmentation in the yield of **15aa** to 70%, albeit the use of 4 equivalents of NH₄OAc produced no further noticeable change (Table 4.2.1, entries 4-6). Also, no enrichment in the yield of **15aa** was noticed by increasing the concentration of **36a** to 1.5 equivalents (Table 4.2.1, entry 7). Next, solvent screening studies were performed which suggested DMF and DMA to be poor solvents for the desired transformation, yielding <10% of **15aa**, while MeOH and 1,4-dioxane to be completely unsuitable as expected (Table 4.2.1, entries 8-11). The use of external oxidants were next examined; the results of which inferred that no product was formed in presence of TBHP, H₂O₂, K₂S₂O₈ under nitrogen atmosphere, while the use of molecular O₂ furnished **15aa** in 73% yield (Table 4.2.1, entries 12-15). Finally, the use of other amine sources, including (NH₄)₂CO₃, NH₄Cl, NH₂NH₂ and NH₃ were explored; these amine sources produced lower yields of **15aa** under similar reaction conditions (Table 4.2.1, entries 16-19). Based on the screening results, the use of NH₄OAc (3 equiv) in DMSO at 130 °C was chosen as the optimal reaction condition.

Table 4.2.1: Selected optimization of reaction conditions^a for the synthesis of **15aa**

Entry	Additive (equiv)	Reaction Conditions			Oxidant	Yield ^b (%)
		Solvent	T (°C)	Time (h)		
1.	NH ₄ OAc (1)	DMSO	130	5	Air	35
2.	NH ₄ OAc (1)	DMSO	130	6	Air	42
3.	NH ₄ OAc (1)	DMSO	130	8	Air	43
4.	NH ₄ OAc (2)	DMSO	130	6	Air	50
5.	NH₄OAc (3)	DMSO	130	6	Air	70
6.	NH ₄ OAc (4)	DMSO	130	6	Air	71
7. ^c	NH ₄ OAc (3)	DMSO	130	6	Air	70
8.	NH ₄ OAc (3)	DMF	130	6	Air	<10
9.	NH ₄ OAc (3)	DMA	130	6	Air	<10
10.	NH ₄ OAc (3)	MeOH	70	6	Air	-
11.	NH ₄ OAc (3)	1,4-dioxane	115	6	Air	-
12. ^d	NH ₄ OAc (3)	DMSO	130	6	TBHP	0
13. ^d	NH ₄ OAc (3)	DMSO	130	6	H ₂ O ₂	0
14. ^d	NH ₄ OAc (3)	DMSO	130	6	K ₂ S ₂ O ₈	0
15.	NH ₄ OAc (3)	DMSO	130	6	O ₂	73
16.	(NH ₄) ₂ CO ₃ (3)	DMSO	130	6	Air	50
17.	NH ₄ Cl (3)	DMSO	130	6	Air	30
18.	NH ₂ NH ₂ (3)	DMSO	130	6	Air	20
19.	Aq. NH ₃	DMSO	130	6	Air	30

^aReaction conditions: **12a** (0.30 mmol), **36a** (0.36 mmol), additive (as specified), oxidant (3 equiv in case of an external oxidant), solvent (3 mL), under air; ^bIsolated yield; ^c**12a** (0.30 mmol), **36a** (0.45 mmol); ^dNitrogen atmosphere.

The ^1H and ^{13}C NMR spectra of **15aa** are depicted in Figure 4.2.1 and Figure 4.2.2, respectively.

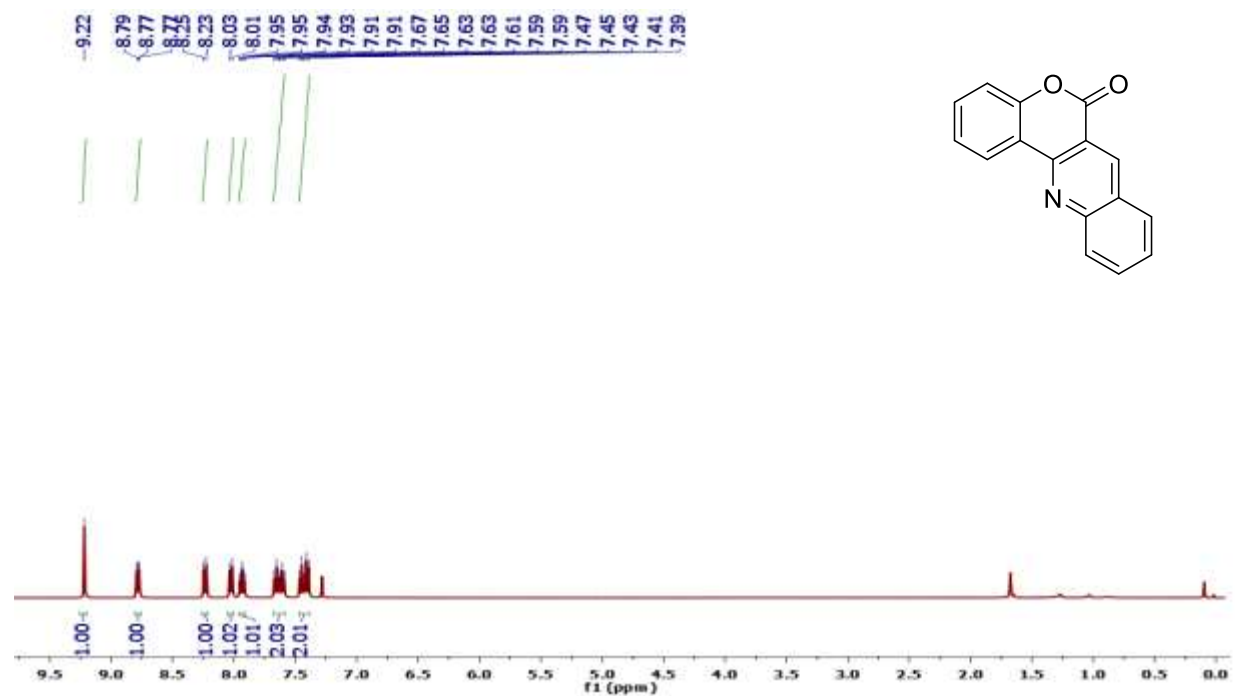


Figure 4.2.1: ^1H NMR spectrum of **15aa** in CDCl_3

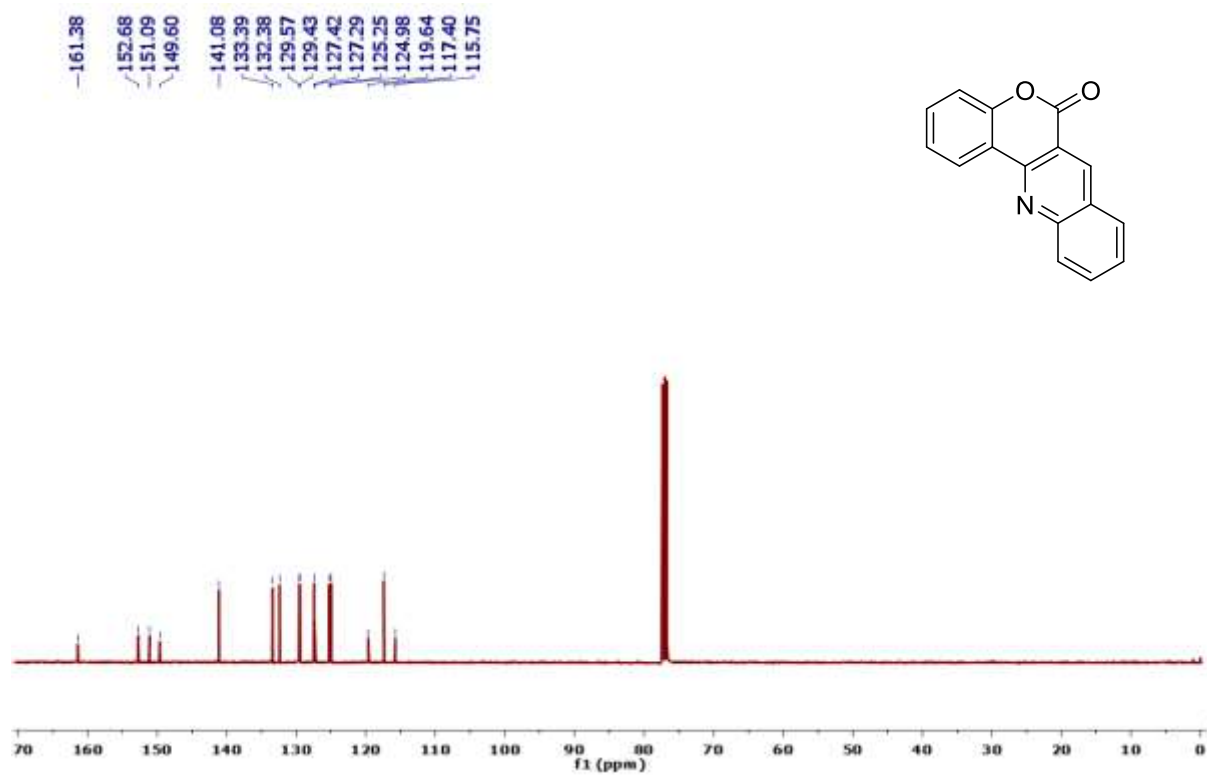
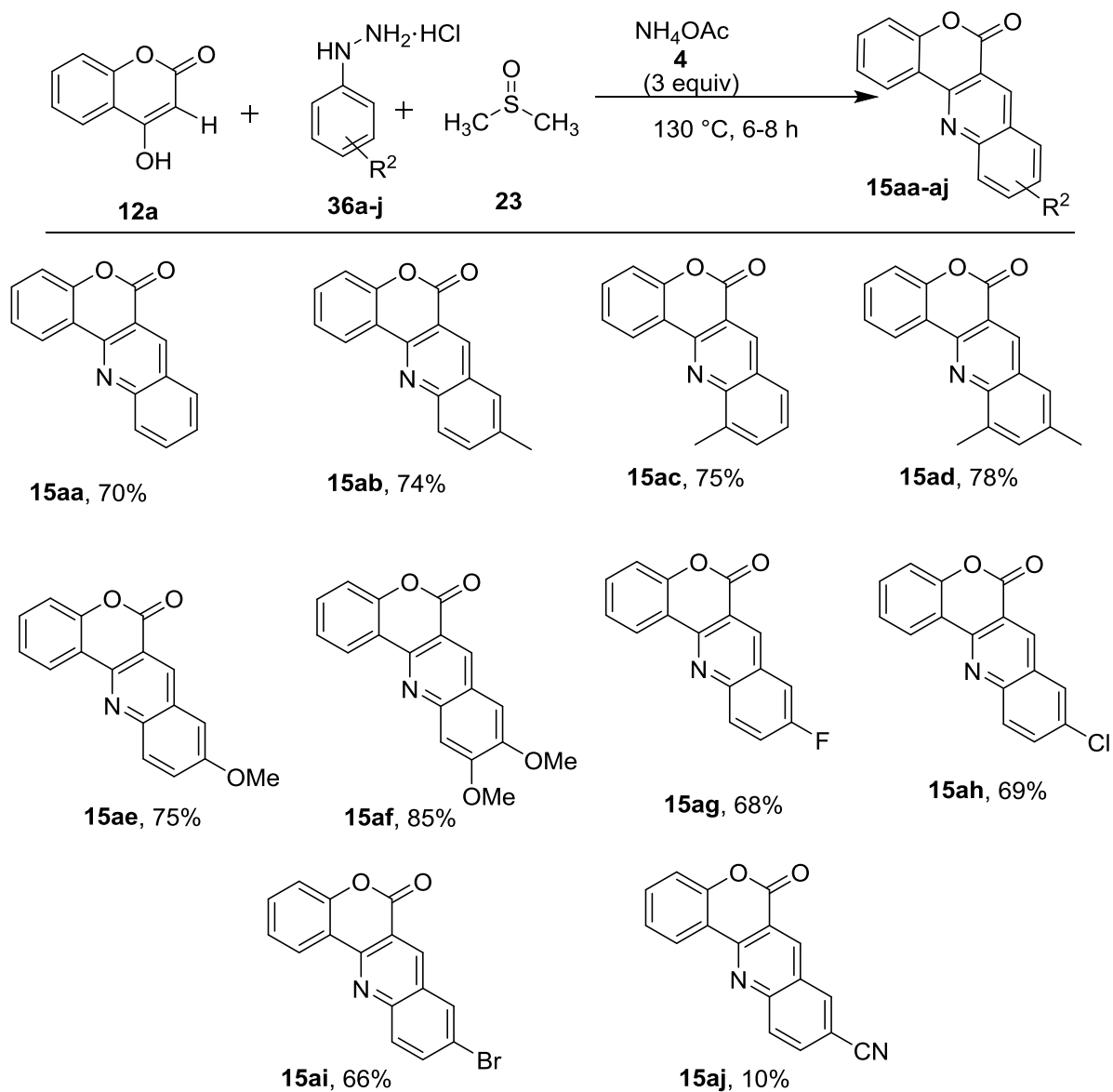


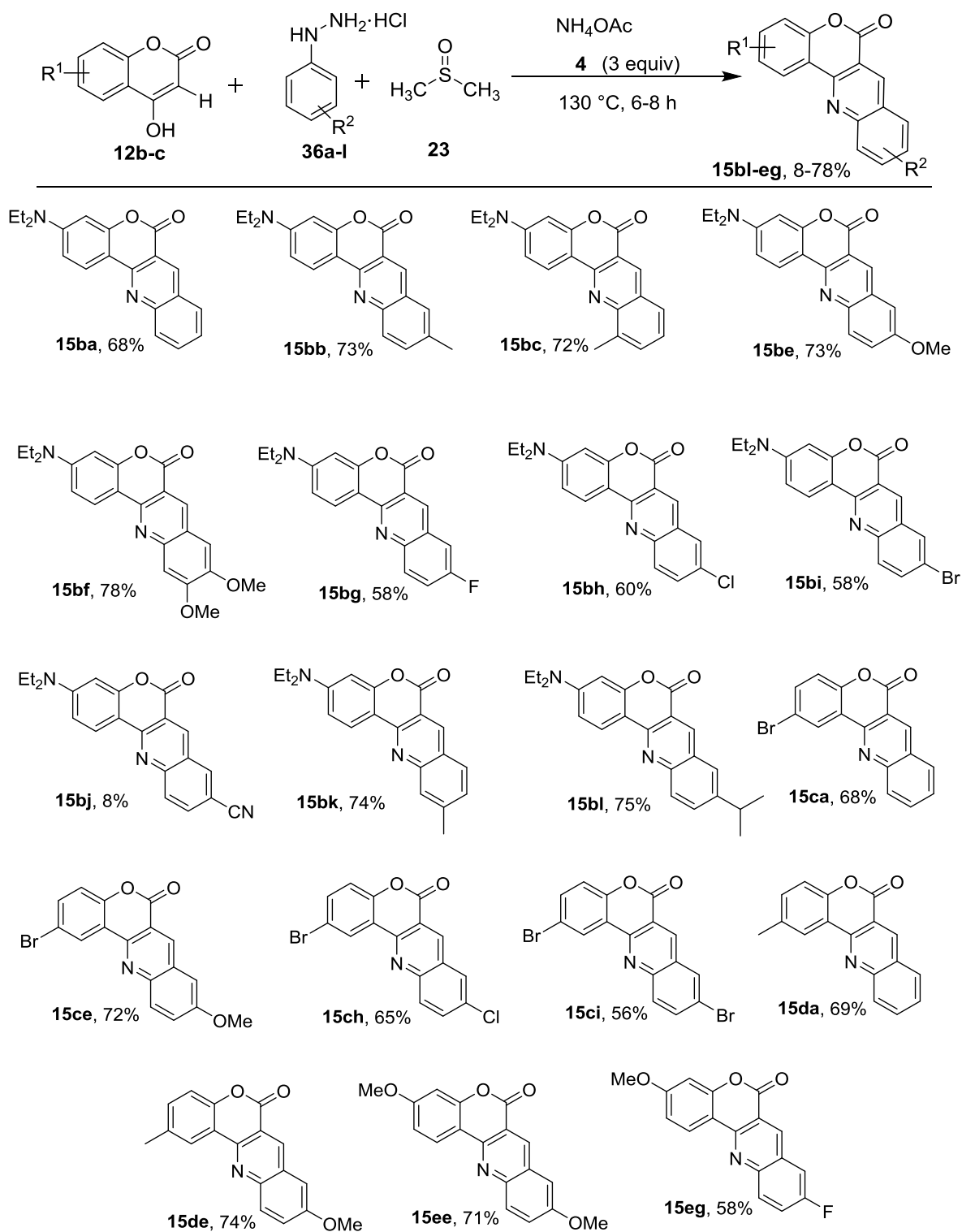
Figure 4.2.2: ^{13}C NMR spectrum of **15aa** in CDCl_3

Having optimized reaction conditions in hand, we next investigated the generality of this cascade protocol by using a wide range of arylhydrazine hydrochlorides (**36a-j**) as coupling partners with 4-hydroxycoumarin (**12a**) (Scheme 4.2.1). Arylhydrazine hydrochlorides possessing electron-donating and electron-withdrawing groups were well tolerated under optimized conditions to deliver the corresponding substituted 6*H*-chromeno[4,3-*b*]quinolin-6-ones (**15aa-ai**) in 66-85% yields. Overall, some variations in the electronic environment of arylhydrazine hydrochlorides have shown noticeable results. The presence of electron-donating groups (**36b-f**: R² = 4-Me, 2-Me, 4-OMe, 2,4-diMe, 3,4-diOMe) on phenyl group of arylhydrazine hydrochlorides exhibited good reactivity, offering chromene-fused quinolinones (**15ab-af**) in 74-85% yields, while moderate electronically-deficient arylhydrazine hydrochlorides (**36g-i**: R² = F, Cl, Br) afforded the fused products **15ag-ai** in comparatively lower yields (66-69%). Unfortunately, the use of 4-cyanophenylhydrazine hydrochloride (**36j**) yielded only 10% of the cyano functionalized 6*H*-chromeno[4,3-*b*]quinolin-6-one (**15aj**).

With our advent interest in synthesizing highly fluorescent heterocycles, we next explored the performance of 7-(*N,N*-diethylamino)-4-hydroxycoumarin (**12b**) with a variety of arylhydrazine hydrochlorides (**36a-c**, **36e-i**, **36k-l**) under optimized conditions. Pleasingly, **12b** reacted quite well with electron-rich and electron-deficient arylhydrazine hydrochlorides (**36a-c**, **36e-i**, **36k-l**), affording the expected fluorescent chromene-fused quinolinones (**15ba-bc**, **15be-bi**, **15bk-bl**) in 58-78% yields (Scheme 4.2.2). In this case, the only exception was the reaction of 4-cyanophenylhydrazine hydrochloride (**36j**) with **12b** that afforded cyano functionalized 7-(diethylamino)-6*H*-chromeno[4,3-*b*]quinolin-6-one (**15bj**) in only 8% yield. Here again, electronically-rich arylhydrazine hydrochlorides exhibited better reactivity over the electron-deficient ones. In addition, electron-deficient 6-bromo-4-hydroxycoumarin (**12c**) showcased moderate reactivity for a number of arylhydrazine hydrochlorides (**36a**, **36e**, **36h** & **36i**), affording their corresponding chromene-fused quinolinones **15ca**, **15ce**, **15ch** & **15ci** in 56-72% yields (Scheme 4.2.2). On the other hand, methyl and methoxy substituted 4-hydroxycoumarins (**12d** & **12e**) displayed slightly better reactivity towards different arylhydrazine hydrochlorides (**36a**, **36e**, **36g**) to furnished their corresponding chromene-fused quinolinones (**15da**, **15de**, **15ee** & **15eg**) in 58-74% yields (Scheme 4.2.2). All the synthesized compounds were isolated by column chromatography, and characterized by detailed spectroscopic analysis.

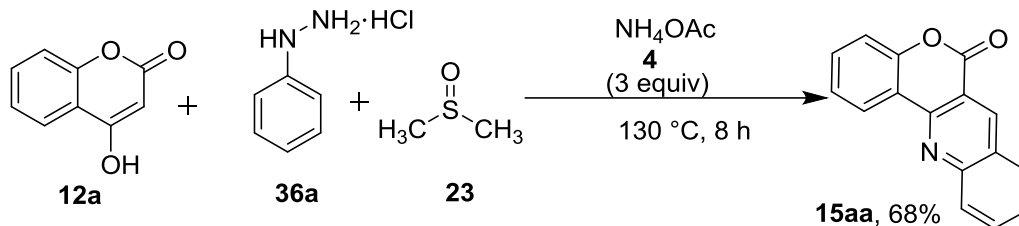


Scheme 4.2.1: Substrate Scope of arylhydrazine hydrochlorides (**36a-j**) and 4-hydroxy coumarin for the synthesis of chromene-fused quinolinones (**15aa-aj**)



Scheme 4.2.2: Substrate Scope of arylhydrazine hydrochlorides (**36a-l**) and 4-hydroxy coumarins for the synthesis of chromene-fused quinolinones (**15ba-eg**)

To assess the scalability of this metal-free tandem protocol, a gram-scale reaction was performed between **12a** and **36a** under optimized conditions to afford the desired **15aa** in 68% (1.017 g) yield, which is almost closer in yield as obtained on a small scale (Scheme 4.2.3).



Scheme 4.2.3: Gram-scale synthesis of **15aa**

To further confirm the proposed structure, as a representative example, single crystals of **15ba** were grown from a mixture of ethyl acetate and hexanes for X-ray diffraction (XRD) studies. Compound **15ba** crystallizes in the $R\bar{3}$ (No. 148) group. An ORTEP diagram of the **15ba** (CCDC No. 1862858) is shown in Figure 4.2.3.

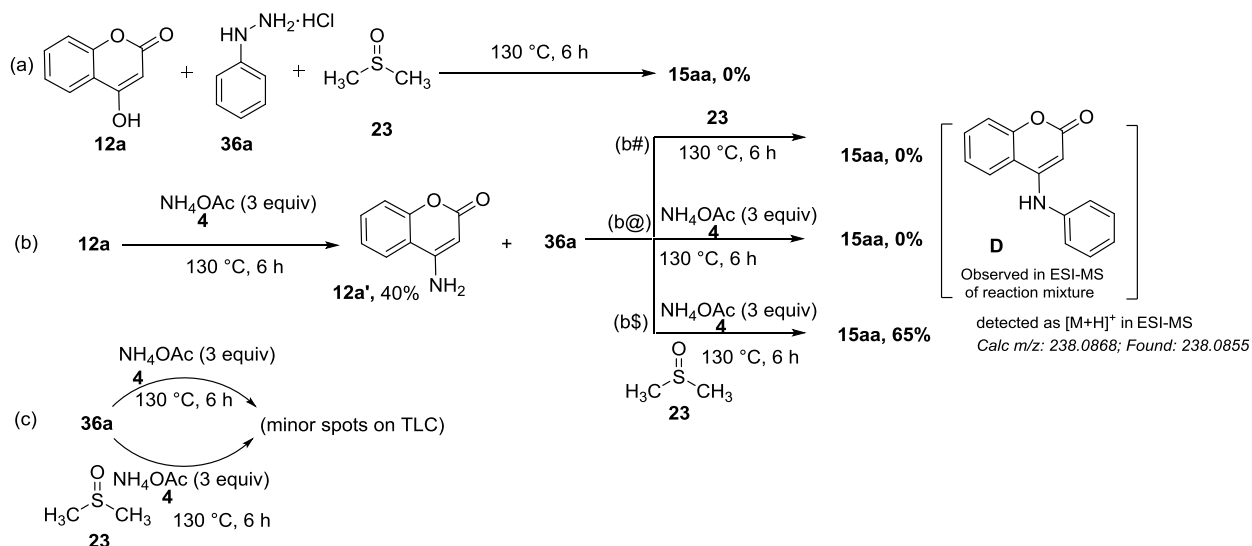


Figure 4.2.3: ORTEP diagram of **15ba**

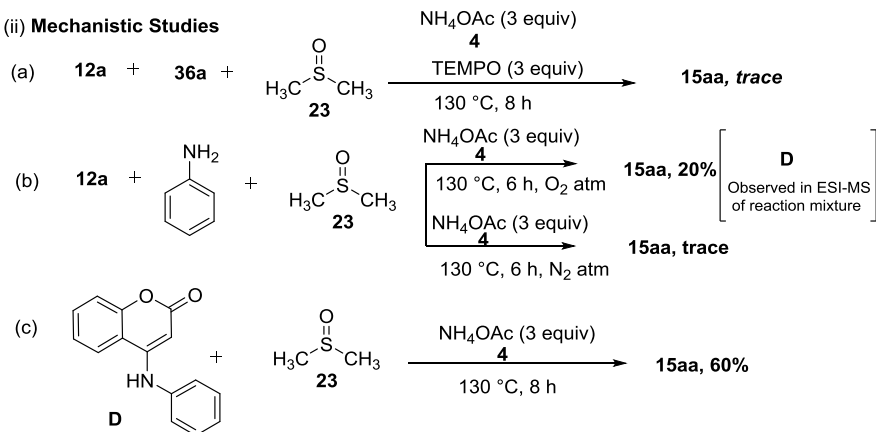
To gain insights into the mechanistic pathway, a series of preliminary experiments were performed. The reaction of 4-hydroxycoumarin (**12a**) and phenylhydrazine hydrochloride (**36a**) in DMSO at 130 °C produced no product at all, thereby indicating a crucial participation of NH_4OAc in this cascade process (Scheme 4.2.4ia). Reaction of **12a** with NH_4OAc (3 equiv) under neat conditions at 130 °C for 6 h furnished 4-aminocoumarin (**12a'**) in 40% yield, which on further reaction with **36a** in DMSO (without NH_4OAc , Scheme 4.2.4ib#) or using NH_4OAc (in absence of DMSO, Scheme 4.2.4ib@) did not yield **15aa** at all. It is worth mentioning that 4-aminophenyl coumarin (**D**) was observed in ESI-MS of their respective reaction mixtures. On the other hand, the reaction of 4-aminocoumarin (**12a'**) with **36a** using NH_4OAc in DMSO under optimized conditions afforded **15aa** in 65% yield (Scheme 4.2.4ib\$). No prominent product was isolated by reacting **36a** with NH_4OAc , in presence or absence of DMSO under described reaction conditions (Scheme 4.2.4ic). Notably, the failure of the model reaction to proceed in the

presence of radical scavenger TEMPO (3 equiv) advocates about the involvement of radical species during the course of reaction mechanism (Scheme 4.2.4iia). The reaction of aniline instead of phenylhydrazine hydrochloride with **12a** under optimized conditions yielded the product **15aa**, albeit in only 20% after 6 h under ambient conditions, whereas trace amount of **15aa** was observed (on TLC) in a nitrogen atmosphere (Scheme 4.2.4iib). This indicates a crucial role of atmospheric oxygen in the reaction pathway. To further confirm the formation of 4-(phenylamino)-2*H*-chromen-2-one (**D**) as one of the intermediates in the reaction between **12a** and **36a**, **D** was synthesized by standard procedure.⁶⁰ Pleasingly, **D** on further heating in DMSO using ammonium acetate (3 equiv) yielded the desired product **15aa** in 60% yield after 8 h, thereby indicating that its formation could be involved in the reaction mechanism (Scheme 4.2.4iic). Contentedly, the formation of **15aa'** in the presence of deuterated DMSO-*d*₆ (**23a'**) affirmed DMSO as a methine source in the disclosed transformation (Scheme 4.2.4iii). Unfortunately, no other intermediate was isolated in pure form, even on repeated attempts. Thus, we planned to monitor the model reaction *via* analyzing its mass spectra (Scheme 4.2.4iv). To our delight, ESI-HRMS of the reaction mixture recorded after 1 h detected the presence of the peaks at *m/z* 238.0897, 268.0933 and 266.0744, corresponding to the molecular formula C₁₅H₁₂NO₂ [M+H]⁺, C₁₆H₁₄NO₃ [M+H]⁺ and C₁₆H₁₂NO₃ [M+H]⁺, respectively, which indicated the possible formation of intermediates **D**, **H**, and **I** during the course of the reaction. The ESI-MS of reaction mixture is shown in Figure 4.2.4.

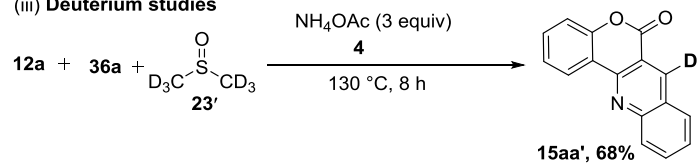
(i) Control Experiment:



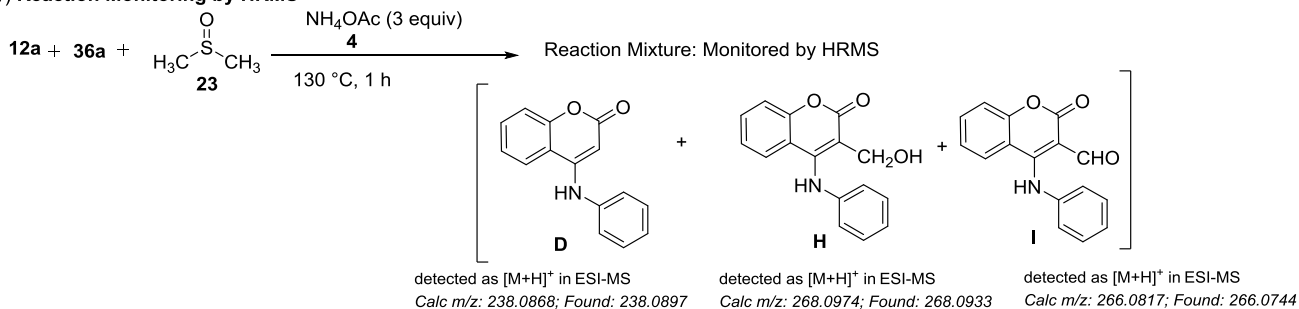
(ii) Mechanistic Studies



(iii) Deuterium studies



(iv) Reaction Monitoring by HRMS



Scheme 4.2.4: Preliminary experiments for investigating the reaction mechanism

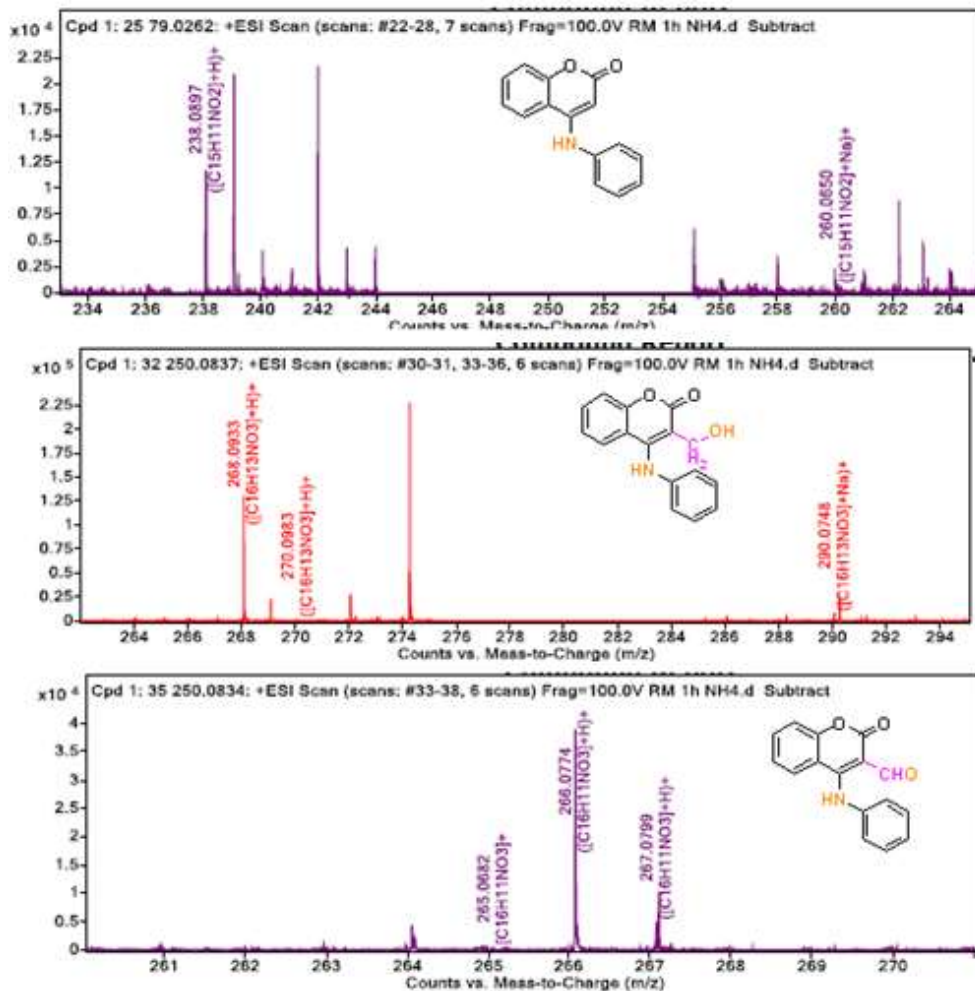
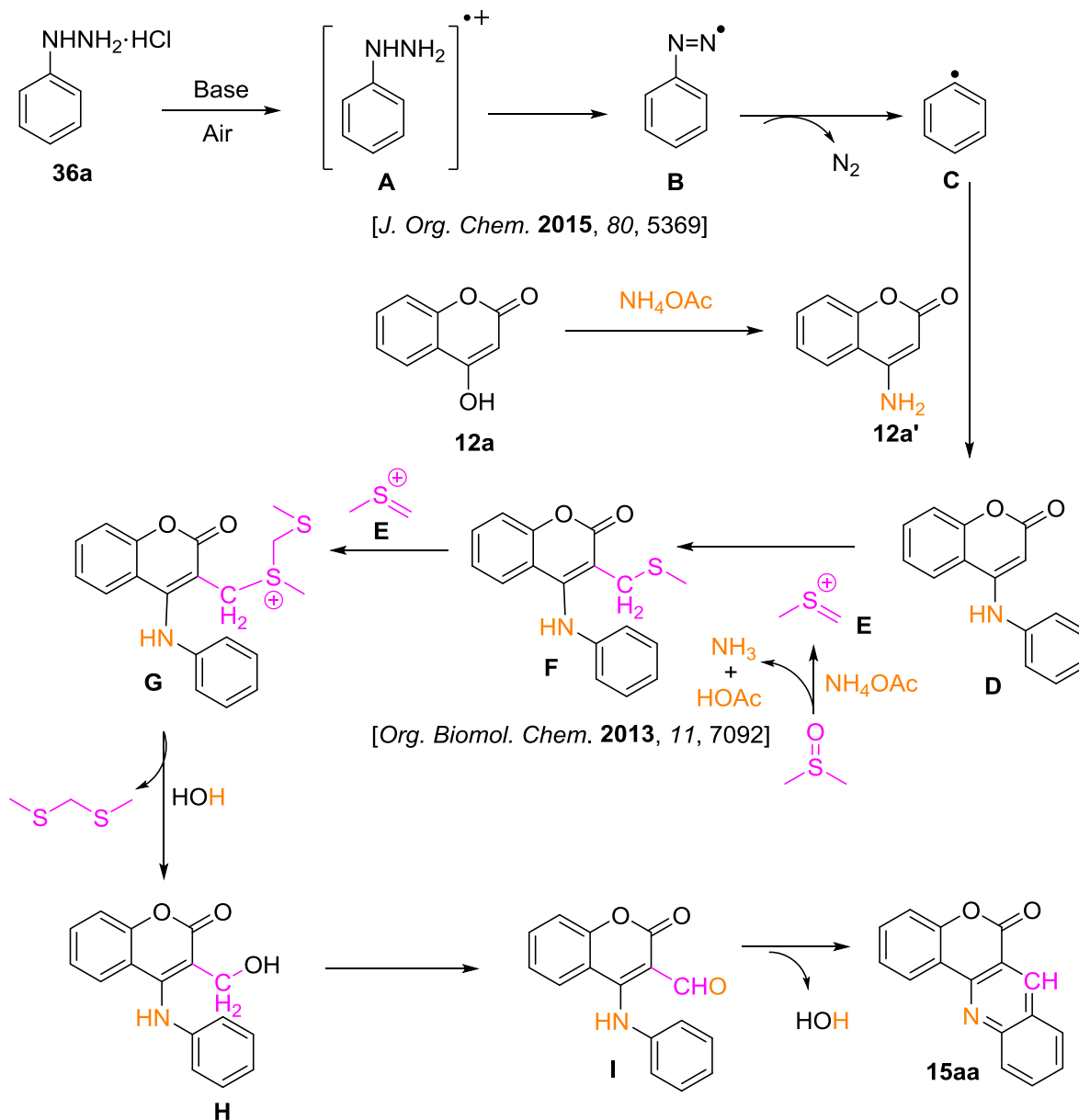


Figure 4.2.4: ESI-HRMS of the crude reaction mixture (**15aa**) after 1 h

Based upon the above studies and literature reports,^{61-64,71} a postulated mechanism is illustrated in scheme 4.2.5. The overall process consists of two main steps that could be assumed to proceed either simultaneously or consecutively. The first step of the reaction is believed to be initiated by the decomposition of phenylhydrazine hydrochloride (**36a**) to a phenyl radical (**C**) *via* formation of **A** and diazonium radical (**B**) *via* single electron transfer (SET) mechanism.⁷¹ Subsequently, amination of 4-hydroxycoumarin (**12a**) with ammonium acetate, followed by arylation by phenyl radical (**C**) furnishes 4-(phenylamino)-2*H*-chromen-2-one (**D**). Thereafter, the second step involves the activation of DMSO by ammonium acetate to produce thionium ion (**E**), which undergoes a nucleophilic attack by **D** to produce **F** *via* Pummerer-type reaction, as established by Cheng.⁶⁴ The sulfur atom in **F** attacks another molecule of thionium ion (**E**) to generate intermediate **G**, which upon nucleophilic attack by water affords C-3 hydroxymethyl intermediate (**H**). Subsequently, oxidation of **H** takes place to produce 4-(phenylamino)-2*H*-

chromen-2-one-3-carbaldehyde (**I**). Finally, aldol-type intramolecular nucleophilic addition in **I**, followed by dehydration affords the desired product **15aa**. However, there is still one question that remains to be addressed, *i.e.* the source of water (as nucleophile) in the proposed mechanism. We anticipated that the hygroscopic behavior of ammonium acetate under ambient conditions could be a possible source of water in the reaction mixture.



Scheme 4.2.5: Plausible mechanism

Interestingly, compounds **15aa-15aj** & **15ca**, **15ce**, **15ch** & **15ci** showed blue fluorescence, whereas **15ba-bc**, **15be-bj**, **15bk-bl** showed intense green fluorescence in the solution phase (or solid state) at room temperature under a UV lamp (Figure 4.2.5; a,-f). The fluorescence emission maxima (λ_{Em}) of all the compounds (**15aa-ci**) were recorded in THF, and their quantum yields were calculated (Figure 4.2.5, Table 4.2.2).

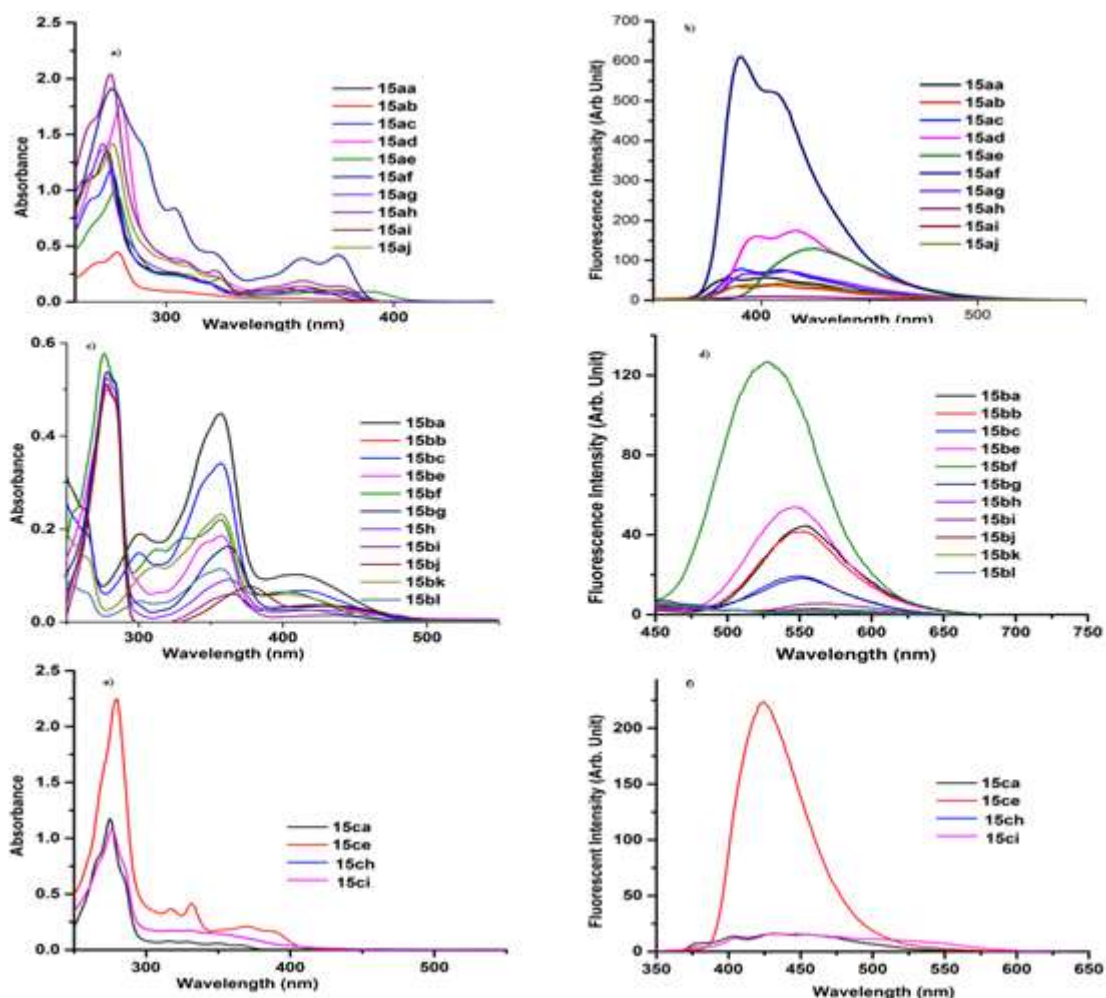


Figure 4.2.5: UV absorption spectra of **15aa-15aj** (a), **15ba-bl** (c) and **15ca**, **15ce**, **15ch** & **15ci** (d), and emission spectra of **15aa-15aj** (b), **15ba-bl** (d) and **15ca**, **15ce**, **15ch** & **15ci** (f) in THF (5×10^{-5} M) & (8×10^{-6} M) at 25 °C

Table 4.2.2: Absorption and fluorescence data of coumarin-fused quinolinones (**15aa-ci**)^a

Compound	λ_{Abs} (nm)	λ_{Em} ^b (nm)	Quantum Yield (Φ) ^d
15aa	366, 353, 274	390 ^b	0.0110
15ab	367, 354, 279	389 ^b	0.0230
15ac	358, 353, 276	390 ^b	0.0200
15ad	361, 347, 280	398 ^b	0.0310
15ae	372, 323, 278	364 ^b	0.0430
15af	376, 317, 276	390 ^b	0.0560
15ag	373, 316, 272	394 ^b	0.0100
15ah	373, 322, 276	395 ^b	0.0098
15ai	377, 322, 277	395 ^b	0.0090
15aj	377, 321, 274	395 ^b	0.0089
15ba	413, 357, 263	553 ^c	0.0120
15bb	414, 358, 265	553 ^c	0.0115
15bc	414, 358, 265	553 ^c	0.0111
15be	416, 358, 278	552 ^c	0.053
15bf	406, 357, 276	526 ^c	0.060
15bg	417, 363, 278	554 ^c	0.0011
15bh	417, 362, 278	555 ^c	0.010
15bi	418, 366, 277	552 ^c	0.0098
15bj	417, 378, 278	552 ^c	0.0096
15bk	414, 357, 266	554 ^c	0.0110
15bl	411, 357, 266	553 ^c	0.0100
15ca	316, 275	431 ^b	0.0099
15ci	317, 279	425 ^b	0.018
15ch	316, 276	431 ^b	0.0096
15ci	316, 279	431 ^b	0.0086

^aMeasured in THF (5×10^{-5} M) & (8×10^{-6} M) at 25 °C; ^bExcited at 340 nm; ^cExcited at 370 nm;

^dMeasured with quinine sulfate in 0.1 N H₂SO₄ as standard.

In summary, we have developed an efficient, atom-economical and metal-free cascade protocol for the synthesis of chromene-fused quinolinones; wherein DMSO, NH₄OAc and arylhydrazine served as formyl, nitrogen and aryl sources, respectively. The deuterium study confirmed DMSO to be a methine source. The strategy exhibited the use of inexpensive and economical reagents, easy availability of the substrates, and moderate functional group tolerability. This protocol opens a new avenue for the green synthesis of chromeno-quinoline derivatives.

4.3 Experimental Section

General materials and methods

All reagents and chemicals were purchased from commercial source and used as received. All reactions were performed under air atmosphere unless otherwise noted. ^1H NMR spectra were recorded on 400 MHz spectrometer, and chemical shifts are reported in δ units, parts per million (ppm), and referred to the internal standard TMS set as 0.00 ppm, relative to residual chloroform (7.26 ppm) and DMSO (2.5 ppm) in the deuterated solvent. Data are reported as follows: the following abbreviations were used to describe peak splitting patterns : s = singlet, d = doublet, t = triplet, dd = doublet of doublet and m = multiplet. Coupling constants J were reported in Hz. The ^{13}C NMR spectra were reported in ppm relative to deuteriochloroform (77.0 ppm) and [d_6] DMSO (39.5 ppm). Melting points were determined on a capillary point apparatus equipped with a digital thermometer and are uncorrected. High resolution mass spectra were recorded with a TOF analyzer spectrometer by using electrospray mode. Flash column chromatography was performed on silica gel, 100–200 mesh. Analytical and preparative thin-layer chromatography was carried out on silica gel 60 F-254 plates. Products were visualized using UV and shown blue colour and yellow colour under uv light. Absorption spectra were recorded using dual beam Thermo Evolution 201 UV/Vis/NIR spectrophotometer and fluorescence spectra were recorded using a Shimadzu RF-5301PC spectrofluorometer. The data were analyzed using related software. The concentration of compounds **15aa-15aj** & **15ca, 15ce, 15ch** & **15ci** was 5×10^{-5} M and **15ba-bc, 15be-bj, 15bk-bl** was 8×10^{-6} M in all the solutions. Fluorescence quantum yield (ϕ) values were obtained by the following equation. The fluorescence quantum yields were calculated by comparing the total fluorescence intensity (F) under the whole spectrum range by taking standard compound quinine sulfate (prepared as 0.1 N H_2SO_4 solution, $\phi_s = 0.55$).

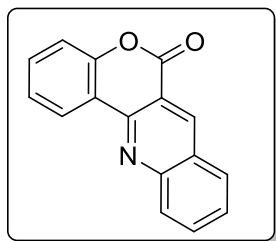
$$\phi_i = \phi_s \frac{F_i Ab_s \eta_s^2}{F_s Ab_i \eta_i^2}$$

Where, Ab : absorbance at a particular wavelength; F: fluorescence spectrum area; and η : refraction index. The subscripts in the symbols refer to the standard (s) and to the sample (i).

General procedure for the synthesis of coumarin-fused quinolinones

A mixture of 4-hydroxycoumarin (**12**, 0.30 mmol, 1.0 equiv), arylhydrazine hydrochloride (**36**, 0.36 mmol, 1.2 equiv), NH_4OAc (0.90 mmol, 3.0 equiv) were heated in DMSO (3.0 mL) at 130 °C under ambient conditions for 6-8 h. On completion of the reaction as indicated by TLC, the reaction mixture was cooled to room temperature, and diluted with ice-water. The mixture was extracted with ethyl acetate (3 × 20 mL), and the organic layer was separated and dried over Na_2SO_4 . The organic layer was concentrated and the crude product was subjected to silica gel column chromatography [SiO_2 (100-200 mesh), with (hexanes/EtOAc, 19:1) as the eluent to afford pure 6*H*-chromeno[4,3-*b*]quinolin-6-ones (**15**).

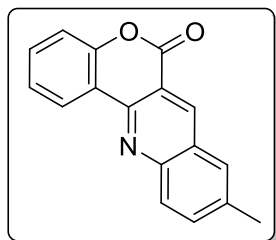
6*H*-Chromeno[4,3-*b*]quinolin-6-one (15aa**):** White solid; yield: 52.3 mg (70%); mp: 223–224



°C (lit.⁶⁰ 221.9–223.1 °C); ^1H NMR (400 MHz, CDCl_3) δ 9.22 (s, 1H), 8.78 (dd, $J = 7.9, 1.5$ Hz, 1H), 8.24 (d, $J = 8.6$ Hz, 1H), 8.02 (d, $J = 8.2$ Hz, 1H), 7.96 – 7.91 (m, 1H), 7.68 – 7.59 (m, 2H), 7.47 – 7.39 (m, 2H); ^{13}C NMR (100 MHz, CDCl_3) δ 161.4, 152.7, 151.1, 149.6, 141.1, 133.4, 132.4, 129.6, 129.4, 127.4, 127.3, 125.3, 125.0, 119.6, 117.4, 115.8;

HRMS (ESI-TOF) (m/z) calculated $\text{C}_{16}\text{H}_{10}\text{NO}_2^+$: 248.0706; found 248.0707 [$\text{M}+\text{H}$] $^+$.

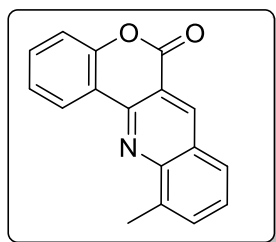
9-Methyl-6*H*-chromeno[4,3-*b*]quinolin-6-one (15ab**):** White solid; yield: 58.5 mg (74%); mp:



211–213 °C (lit.⁶⁰ 234.4–235.1 °C); ^1H NMR (400 MHz, CDCl_3) δ 9.12 (s, 1H), 8.77 (dd, $J = 7.8, 1.0$ Hz, 1H), 8.14 (d, $J = 9.2$ Hz, 1H), 7.76 (d, $J = 6.8$ Hz, 2H), 7.64 – 7.57 (m, 1H), 7.47 – 7.38 (m, 2H), 2.61 (s, 3H); ^{13}C NMR (100 MHz, CDCl_3) δ 161.5, 152.5, 149.8, 148.8, 140.1, 137.6, 135.9, 132.1, 129.2, 127.9, 127.3, 125.1, 124.9, 119.7, 117.3, 115.7,

21.7; HRMS (ESI-TOF) (m/z) calculated $\text{C}_{17}\text{H}_{12}\text{NO}_2^+$: 262.0863; found 262.0862 [$\text{M}+\text{H}$] $^+$.

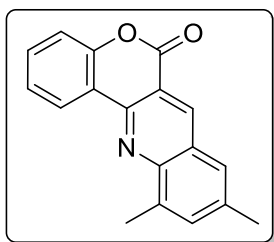
11-Methyl-6*H*-chromeno[4,3-*b*]quinolin-6-one (15ac**):** Off-white solid; yield: 59.3 mg (75%);



mp: 221–223 °C (lit.⁶⁰ 209.6–211.7 °C); ^1H NMR (400 MHz, CDCl_3) δ 9.23 (s, 1H), 8.93 – 8.83 (m, 1H), 7.90 (d, $J = 8.1$ Hz, 1H), 7.83 – 7.77 (m, 1H), 7.65 – 7.60 (m, 1H), 7.60 – 7.54 (m, 1H), 7.50 – 7.47 (m, 1H), 7.46 – 7.42 (m, 1H), 2.98 (s, 3H); ^{13}C NMR (100 MHz, CDCl_3) δ 161.5, 152.6, 149.9, 148.2, 140.9, 137.7, 133.1, 132.1, 127.2, 127.2, 127.2,

125.2, 124.8, 120.0, 117.3, 115.3, 17.9; HRMS (ESI-TOF) (m/z) calculated $\text{C}_{17}\text{H}_{12}\text{NO}_2^+$: 262.0863; found 262.0859 [$\text{M}+\text{H}$] $^+$.

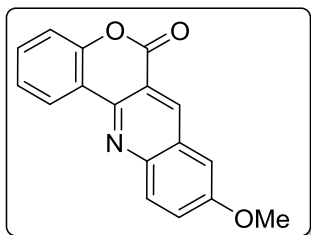
9,11-Dimethyl-6*H*-chromeno[4,3-*b*]quinolin-6-one (15ad): White solid; yield: 65.0 mg (78%);



mp: 228–230 °C (lit.⁶⁰ 219.8–220.5 °C); ¹H NMR (400 MHz, CDCl₃) δ 9.07 (s, 1H), 8.81 (dd, *J* = 7.9, 1.6 Hz, 1H), 7.62 – 7.57 (m, 3H), 7.47 – 7.39 (m, 2H), 2.91 (s, 3H), 2.56 (s, 3H); ¹³C NMR (100 MHz, CDCl₃) δ 161.7, 152.5, 148.8, 147.6, 140.1, 137.3, 137.3, 135.8, 131.8, 127.5, 125.8, 125.1, 124.8, 120.2, 117.3, 115.4, 21.7, 17.8; HRMS (ESI-TOF)

(*m/z*) calculated C₁₈H₁₄NO₂⁺: 276.1019; found 276.1003 [M+H]⁺.

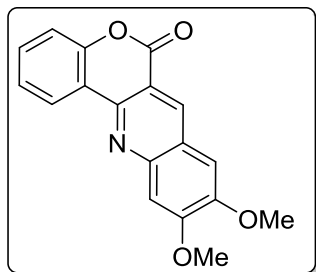
9-Methoxy-6*H*-chromeno[4,3-*b*]quinolin-6-one (15ae): White solid; yield: 62.9 mg (75%);



mp: 234–236 °C (lit.⁶⁰ 233.5–235.0 °C); ¹H NMR (400 MHz, CDCl₃) δ 9.14 (s, 1H), 8.78 (dd, *J* = 7.9, 1.6 Hz, 1H), 8.18 (d, *J* = 9.3 Hz, 1H), 7.64 – 7.58 (m, 2H), 7.48 – 7.41 (m, 2H), 7.26 (d, *J* = 2.8 Hz, 1H), 4.02 (s, 3H); ¹³C NMR (100 MHz, CDCl₃) δ 161.6, 158.4, 152.3, 147.7, 147.5, 139.0, 131.8, 131.0, 128.5, 127.1, 124.9, 124.9, 119.9,

117.3, 115.9, 105.6, 55.8; HRMS (ESI-TOF) (*m/z*) calculated C₁₇H₁₂NO₃⁺: 278.0812; found 278.0800 [M+H]⁺.

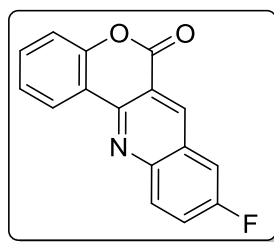
9,10-Dimethoxy-6*H*-chromeno[4,3-*b*]quinolin-6-one (15af): White solid; yield: 79.0 mg



(85%); mp: 280–282 °C; ¹H NMR (400 MHz, CDCl₃) δ 9.04 (s, 1H), 8.75 (dd, *J* = 7.8, 1.4 Hz, 1H), 7.62 – 7.57 (m, 1H), 7.56 (s, 1H), 7.49 – 7.39 (m, 2H), 7.22 (s, 1H), 4.16 (s, 3H), 4.10 (s, 3H); ¹³C NMR (100 MHz, CDCl₃) δ 161.8, 156.0, 152.4, 150.8, 149.3, 148.1, 137.9, 131.7, 124.8, 124.7, 123.6, 119.9, 117.4, 114.0, 107.6, 105.8, 56.5, 56.3; HRMS (ESI-TOF) (*m/z*) calculated C₁₈H₁₄NO₄⁺: 308.0917;

found 308.0913 [M+H]⁺.

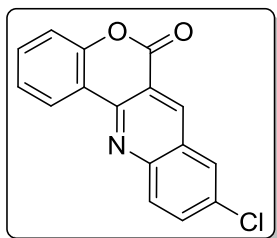
9-Fluoro-6*H*-chromeno[4,3-*b*]quinolin-6-one (15ag): White solid; yield: 54.6 mg (68%); mp:



244–245 °C (lit.⁶⁰ 242.3–243.0 °C); ¹H NMR (400 MHz, CDCl₃) δ 9.18 (s, 1H), 8.76 (dd, *J* = 7.9, 1.6 Hz, 1H), 8.26 (dd, *J* = 9.3, 5.2 Hz, 1H), 7.68 – 7.64 (m, 1H), 7.67 – 7.60 (m, 2H), 7.48 – 7.40 (m, 2H); ¹³C NMR (100 MHz, CDCl₃) δ 161.5 (*J*_{C-F} = 85.3 Hz), 159.4, 152.6, 149.0 (*J*_{C-F} = 2.7 Hz), 148.3, 140.2 (*J*_{C-F} = 6.1 Hz), 132.4, 132.2 (*J*_{C-F} = 8.9 Hz), 127.9,

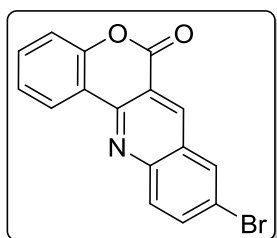
127.8, 125.1 (*J*_{C-F} = 3.3 Hz), 124.0 (*J*_{C-F} = 26.2 Hz), 119.4, 117.4, 116.4, 112.0 (*J*_{C-F} = 21.8 Hz); HRMS (ESI-TOF) (*m/z*) calculated C₁₆H₉FO₂⁺: 266.0612; found 266.0603 [M+H]⁺.

9-Chloro-6H-chromeno[4,3-b]quinolin-6-one (15ah): White solid; yield: 58.7 mg (69%); mp:



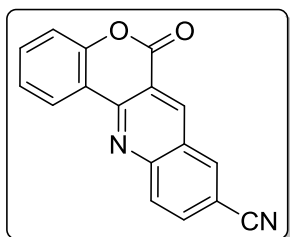
240–242 °C (lit.⁶⁰ 245.7–246.4 °C); ¹H NMR (400 MHz, CDCl₃) δ 9.13 (s, 1H), 8.75 (d, *J* = 6.9 Hz, 1H), 8.18 (d, *J* = 9.0 Hz, 1H), 8.00 (d, *J* = 1.5 Hz, 1H), 7.85 (dd, *J* = 9.0, 1.9 Hz, 1H), 7.63 (t, *J* = 7.0 Hz, 1H), 7.49 – 7.37 (m, 2H); ¹³C NMR (100 MHz, CDCl₃) δ 161.0, 152.7, 149.8, 149.4, 140.0, 134.3, 133.4, 132.7, 131.1, 127.8, 127.7, 125.2, 125.1, 119.3, 117.5, 116.5; HRMS (ESI-TOF) (*m/z*) calculated C₁₆H₉ClNO₂⁺ : 282.0316; found 282.0314 [M+H]⁺.

9-Bromo-6H-chromeno[4,3-b]quinolin-6-one (15ai): White solid; yield: 65.9 mg (66%); mp:



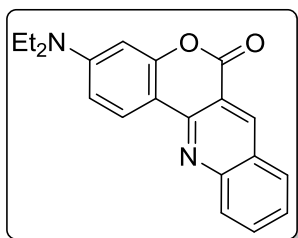
232–234 °C (lit.⁶⁰ 230.0–231.0 °C); ¹H NMR (400 MHz, CDCl₃) δ 9.09 (s, 1H), 8.72 (d, *J* = 7.9 Hz, 1H), 8.14 (d, *J* = 1.7 Hz, 1H), 8.08 (d, *J* = 9.0 Hz, 1H), 7.96 (dd, *J* = 9.1, 2.0 Hz, 1H), 7.66 – 7.59 (m, 1H), 7.47 – 7.36 (m, 2H); ¹³C NMR (100 MHz, CDCl₃) δ 160.9, 152.7, 149.9, 149.6, 139.9, 136.8, 132.7, 131.2, 131.1, 128.2, 125.2, 125.1, 121.5, 119.3, 117.5, 116.4; HRMS (ESI-TOF) (*m/z*) calculated C₁₆H₉BrNO₂⁺ : 325.9811; found 325.9809 [M+H]⁺.

6-Oxo-6H-chromeno[4,3-b]quinoline-9-carbonitrile (15aj): White solid; yield: 8.24 mg



(10%); mp: 229–231 °C; ¹H NMR (400 MHz, CDCl₃) δ 9.32 (s, 1H), 8.81 (d, *J* = 2.4 Hz, 1H), 8.46 (d, *J* = 1.6 Hz, 1H), 8.38 – 8.34 (m, 1H), 8.06 (dd, *J* = 8.9, 1.8 Hz, 1H), 7.72 – 7.67 (m, 1H), 7.52 – 7.44 (m, 2H); ¹³C NMR (100 MHz, CDCl₃) δ 160.4, 153.2, 152.3, 151.7, 141.7, 135.5, 133.6, 133.4, 131.1, 126.5, 125.7, 125.3, 119.0, 117.8, 117.6, 117.3, 111.2; HRMS (ESI-TOF) (*m/z*) calculated C₁₇H₉N₂O₂⁺ : 273.0659; found 273.0620 [M+H]⁺.

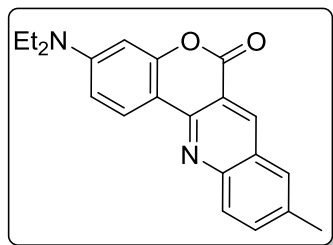
3-(Diethylamino)-6H-chromeno[4,3-b]quinolin-6-one (15ba): Yellow solid; yield: 46.4 mg



(68%); mp: 170–172 °C; ¹H NMR (400 MHz, CDCl₃) δ 9.07 (s, 1H), 8.47 (d, *J* = 9.0 Hz, 1H), 8.11 (d, *J* = 8.5 Hz, 1H), 7.91 (d, *J* = 8.0 Hz, 1H), 7.86 – 7.80 (m, 1H), 7.55 – 7.48 (m, 1H), 6.71 (dd, *J* = 9.0, 2.5 Hz, 1H), 6.52 (d, *J* = 2.5 Hz, 1H), 3.46 (q, *J* = 7.1 Hz, 4H), 1.26 (t, *J* = 7.1 Hz, 6H); ¹³C NMR (100 MHz, CDCl₃) δ 162.3, 154.7, 151.5,

151.1, 150.6, 140.9, 133.0, 129.4, 128.9, 126.3, 126.2, 126.0, 114.7, 109.1, 107.3, 97.9, 44.8, 12.6; HRMS (ESI-TOF) (m/z) calculated $C_{20}H_{19}N_2O_2^+$: 319.1441; found 319.1459 $[M+H]^+$.

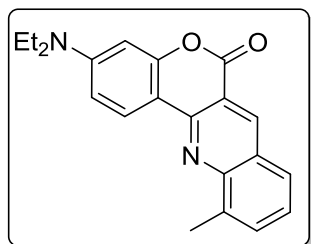
3-(Diethylamino)-9-methyl-6H-chromeno[4,3-b]quinolin-6-one (15bb): Yellow solid; yield:



52.0 mg (73%); mp: 179–181 °C; 1H NMR (400 MHz, $CDCl_3$) δ 8.99 (s, 1H), 8.47 (d, $J = 9.0$ Hz, 1H), 8.02 (d, $J = 9.2$ Hz, 1H), 7.67 (d, $J = 4.5$ Hz, 2H), 6.72 (dd, $J = 9.0, 2.3$ Hz, 1H), 6.54 (d, $J = 2.2$ Hz, 1H), 3.47 (q, $J = 7.1$ Hz, 4H), 2.56 (s, 3H), 1.26 (t, $J = 7.1$ Hz, 6H); ^{13}C NMR (100 MHz, $CDCl_3$) δ 162.5, 154.5, 150.9, 150.2,

149.9, 140.1, 136.0, 135.5, 128.6, 128.0, 126.4, 126.1, 114.6, 109.1, 107.5, 97.9, 44.8, 21.5, 12.6; HRMS (ESI-TOF) (m/z) calculated $C_{21}H_{21}N_2O_2^+$: 333.1598; found 333.1598 $[M+H]^+$.

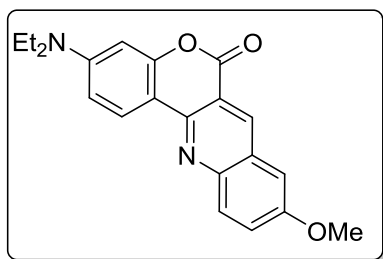
3-(Diethylamino)-11-methyl-6H-chromeno[4,3-b]quinolin-6-one (15bc): Yellow solid; yield:



51.2 mg (72%); mp: 175–177 °C; 1H NMR (400 MHz, $CDCl_3$) δ 9.22 (s, 1H), 8.19 – 8.16 (m, 1H), 7.93 (d, $J = 8.5$ Hz, 1H), 7.74 – 7.70 (m, 1H), 7.50 – 7.46 (m, 1H), 6.78 – 6.69 (m, 2H), 3.52 (q, $J = 7.1$ Hz, 4H), 2.87 (s, 3H), 1.31 (d, $J = 7.1$ Hz, 6H); ^{13}C NMR (100 MHz, $CDCl_3$) δ 160.0, 154.0, 150.6, 149.6, 147.7, 139.3, 136.0, 135.9,

132.6, 129.4, 128.6, 127.4, 125.6, 109.4, 100.0, 97.1, 45.1, 18.3, 12.5; HRMS (ESI-TOF) (m/z) calculated $C_{21}H_{21}N_2O_2^+$: 333.1598; found 333.1554 $[M+H]^+$.

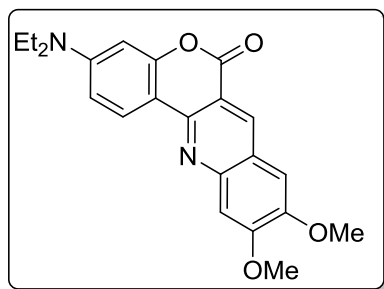
3-(Diethylamino)-9-methoxy-6H-chromeno[4,3-b]quinolin-6-one (15be): Red solid; yield:



54.4 mg (73%); mp: 183–185 °C; 1H NMR (400 MHz, $CDCl_3$) δ 9.11 (s, 1H), 8.60 (d, $J = 8.9$ Hz, 1H), 8.18 (d, $J = 9.3$ Hz, 1H), 7.65 (dd, $J = 9.2, 2.6$ Hz, 1H), 7.29 (d, $J = 2.4$ Hz, 1H), 6.88 (dd, $J = 8.9, 2.1$ Hz, 1H), 6.70 (d, $J = 2.0$ Hz, 1H), 4.12 (s, 3H), 3.63 (q, $J = 7.0$ Hz, 4H), 1.43 (t, $J = 7.0$ Hz, 6H); ^{13}C NMR (100

MHz, $CDCl_3$) δ 162.4, 157.3, 154.3, 150.6, 148.6, 147.9, 138.9, 130.3, 127.2, 126.4, 125.8, 114.7, 109.0, 107.5, 105.8, 97.9, 55.6, 44.7, 12.6; HRMS (ESI-TOF) (m/z) calculated $C_{21}H_{21}N_2O_3^+$: 349.1547; found 349.1542 $[M+H]^+$.

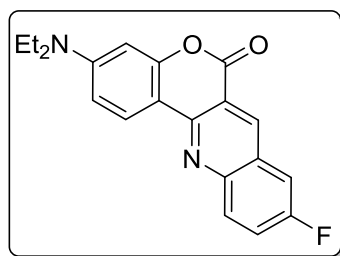
3-(Diethylamino)-9,10-dimethoxy-6*H*-chromeno[4,3-*b*]quinolin-6-one (15bf): Red solid;



yield: 62.9 mg (78%); mp: 192–194 °C; ^1H NMR (400 MHz, CDCl_3) δ 8.90 (s, 1H), 8.44 (d, $J = 9.0$ Hz, 1H), 7.45 (s, 1H), 7.13 (s, 1H), 6.75 – 6.72 (m, 1H), 6.57 (d, $J = 2.5$ Hz, 1H), 4.13 (s, 3H), 4.06 (s, 3H), 3.46 (t, $J = 7.1$ Hz, 4H), 1.26 (t, $J = 7.1$ Hz, 6H); ^{13}C NMR (100 MHz, CDCl_3) δ 162.61, 155.7, 154.4, 150.7, 149.7, 138.0, 125.6, 122.2, 112.7, 109.0, 107.6, 107.3, 106.4,

106.0, 100.7, 98.0, 56.4, 56.2, 44.8, 12.6; HRMS (ESI-TOF) (m/z) calculated $\text{C}_{22}\text{H}_{23}\text{N}_2\text{O}_4^+$: 379.1652; found 379.1653 $[\text{M}+\text{H}]^+$.

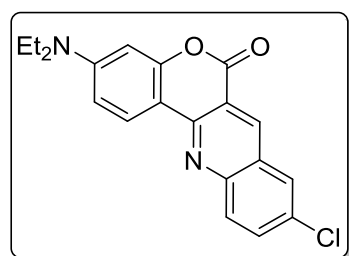
3-(Diethylamino)-9-fluoro-6*H*-chromeno[4,3-*b*]quinolin-6-one (15bg): Yellow solid; yield:



41.8 mg (58%); mp: 188–190 °C; ^1H NMR (400 MHz, CDCl_3) δ 9.01 (s, 1H), 8.43 (d, $J = 9.0$ Hz, 1H), 8.11 (dd, $J = 9.3, 5.2$ Hz, 1H), 7.64 – 7.58 (m, 1H), 7.52 (dd, $J = 8.4, 2.8$ Hz, 1H), 6.71 (dd, $J = 9.0, 2.5$ Hz, 1H), 6.52 (d, $J = 2.5$ Hz, 1H), 3.47 (q, $J = 7.1$ Hz, 4H), 1.27 (t, $J = 7.1$ Hz, 6H); ^{13}C NMR (100 MHz, CDCl_3) δ 161.5 ($J_{\text{C-F}} = 88.3$ Hz), 158.6, 154.6, 151.1, 150.1 ($J_{\text{C-F}} = 2.3$ Hz), 148.6, 140.0 ($J_{\text{C-F}} = 5.8$ Hz), 131.4 ($J_{\text{C-F}} = 8.8$ Hz), 126.6 ($J_{\text{C-F}} = 10.0$ Hz), 126.1, 123.3 ($J_{\text{C-F}} = 25.9$ Hz), 115.3, 112.0 ($J_{\text{C-F}} = 21.6$ Hz), 109.1, 107.1, 97.9, 44.8, 12.5; HRMS (ESI-TOF) (m/z) calculated $\text{C}_{20}\text{H}_{18}\text{FN}_2\text{O}_2^+$: 337.1347;

found 337.1331 $[\text{M}+\text{H}]^+$.

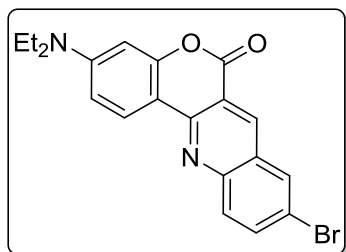
9-Chloro-3-(diethylamino)-6*H*-chromeno[4,3-*b*]quinolin-6-one (15bh): Yellow solid; yield:



45.2 mg (60%); mp: 185–187 °C; ^1H NMR (400 MHz, CDCl_3) δ 9.00 (s, 1H), 8.46 (d, $J = 9.0$ Hz, 1H), 8.06 (d, $J = 9.1$ Hz, 1H), 7.90 (d, $J = 2.3$ Hz, 1H), 7.76 (dd, $J = 9.1, 2.4$ Hz, 1H), 6.73 (dd, $J = 9.0, 2.5$ Hz, 1H), 6.54 (d, $J = 2.5$ Hz, 1H), 3.48 (q, $J = 7.1$ Hz, 4H), 1.27 (t, $J = 7.1$ Hz, 6H); ^{13}C NMR (100 MHz, CDCl_3) δ 161.9,

154.7, 151.3, 150.9, 149.9, 139.9, 133.8, 131.6, 130.5, 127.7, 126.7, 126.2, 115.4, 109.2, 107.0, 97.9, 44.8, 12.5; HRMS (ESI-TOF) (m/z) calculated $\text{C}_{20}\text{H}_{18}\text{ClN}_2\text{O}_2^+$: 353.1051; found 353.1065 $[\text{M}+\text{H}]^+$.

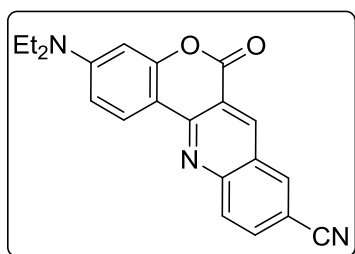
9-Bromo-3-(diethylamino)-6*H*-chromeno[4,3-*b*]quinolin-6-one (15bi): Yellow solid; yield:



49.2 mg (58%); mp: 184–186 °C; ^1H NMR (400 MHz, CDCl_3) δ 8.95 (s, 1H), 8.42 (d, $J = 9.0$ Hz, 1H), 8.04 (d, $J = 2.2$ Hz, 1H), 7.96 (d, $J = 9.1$ Hz, 1H), 7.86 (dd, $J = 9.1, 2.2$ Hz, 1H), 6.71 (dd, $J = 9.0, 2.5$ Hz, 1H), 6.51 (d, $J = 2.5$ Hz, 1H), 3.47 (q, $J = 7.1$ Hz, 4H), 1.27 (t, $J = 7.1$ Hz, 6H); ^{13}C NMR (100 MHz, CDCl_3) δ 161.8,

154.7, 151.3, 150.9, 150.0, 139.7, 136.2, 131.1, 130.5, 127.2, 126.3, 119.5, 115.3, 109.2, 106.9, 97.9, 44.8, 12.6; HRMS (ESI-TOF) (m/z) calculated $\text{C}_{20}\text{H}_{18}\text{BrN}_2\text{O}_2^+$: 397.0546; found 397.0538 $[\text{M}+\text{H}]^+$.

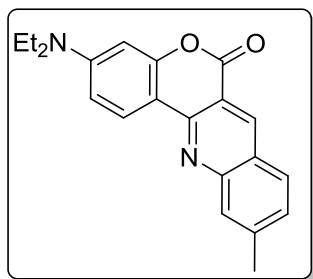
3-(Diethylamino)-6-oxo-6*H*-chromeno[4,3-*b*]quinoline-9-carbonitrile (15bj): Yellow solid;



yield: 5.88 mg (8%); mp: 191–193 °C; ^1H NMR (400 MHz, CDCl_3) δ 9.10 (s, 1H), 8.48 (d, $J = 9.0$ Hz, 1H), 8.31 (d, $J = 1.8$ Hz, 1H), 8.16 (d, $J = 8.9$ Hz, 1H), 7.93 (dd, $J = 8.9, 1.9$ Hz, 1H), 6.75 (dd, $J = 9.1, 2.5$ Hz, 1H), 6.55 (d, $J = 2.5$ Hz, 1H), 3.50 (q, $J = 7.1$ Hz, 4H), 1.29 (t, $J = 7.1$ Hz, 6H); ^{13}C NMR (100 MHz, CDCl_3) δ 161.3, 155.2, 153.0, 152.3, 152.0, 141.3, 135.5, 133.0, 130.2, 126.8, 125.4, 118.4,

116.1, 109.4, 109.2, 106.6, 97.8, 44.9, 12.5; HRMS (ESI-TOF) (m/z) calculated $\text{C}_{21}\text{H}_{18}\text{N}_3\text{O}_2^+$: 344.1394; found 344.1387 $[\text{M}+\text{H}]^+$.

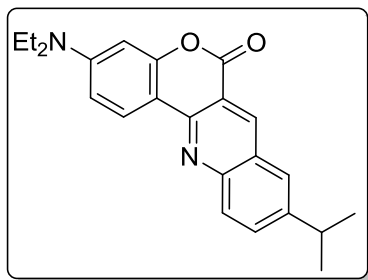
3-(Diethylamino)-10-methyl-6*H*-chromeno[4,3-*b*]quinolin-6-one (15bk): Yellow solid; yield:



52.7 mg (74%); mp: 182–184 °C; ^1H NMR (400 MHz, CDCl_3) δ 9.02 (s, 1H), 8.47 (d, $J = 9.0$ Hz, 1H), 7.92 – 7.87 (m, 1H), 7.80 (d, $J = 8.3$ Hz, 1H), 7.35 (dd, $J = 8.4, 1.5$ Hz, 1H), 6.72 (dd, $J = 9.0, 2.5$ Hz, 1H), 6.54 (d, $J = 2.5$ Hz, 1H), 3.46 (q, $J = 7.1$ Hz, 4H), 2.60 (s, 3H), 1.26 (t, $J = 7.1$ Hz, 6H); ^{13}C NMR (100 MHz, CDCl_3) δ 162.4, 154.7, 151.6, 151.0, 150.7, 144.1, 140.5, 129.0, 128.4, 127.8, 126.2, 124.5, 113.9,

109.0, 107.4, 97.9, 44.8, 22.3, 12.6; HRMS (ESI-TOF) (m/z) calculated $\text{C}_{21}\text{H}_{21}\text{N}_2\text{O}_2^+$: 333.1598; found 333.1605 $[\text{M}+\text{H}]^+$.

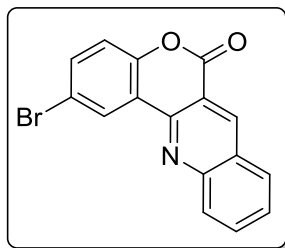
3-(Diethylamino)-9-isopropyl-6H-chromeno[4,3-b]quinolin-6-one (15bl): Red solid; yield:



57.9 mg (75%); mp: 180–182 °C; ^1H NMR (400 MHz, CDCl_3) δ 9.05 (s, 1H), 8.48 (d, $J = 9.0$ Hz, 1H), 8.06 (d, $J = 8.8$ Hz, 1H), 7.79 – 7.70 (m, 2H), 6.72 (dd, $J = 9.0, 2.5$ Hz, 1H), 6.55 (d, $J = 2.5$ Hz, 1H), 3.47 (q, $J = 7.1$ Hz, 4H), 1.39 (s, 3H), 1.38 (s, 3H), 1.28 (brs, 1H), 1.26 (t, $J = 6.1$ Hz, 6H); ^{13}C NMR (100 MHz, CDCl_3) δ 162.4, 154.6, 150.9, 150.5, 150.0, 146.7, 140.4, 133.2,

128.7, 126.4, 126.1, 125.3, 114.6, 109.0, 107.5, 97.9, 44.8, 34.0, 29.7, 23.7, 12.6; HRMS (ESI-TOF) (m/z) calculated $\text{C}_{23}\text{H}_{25}\text{N}_2\text{O}_2^+$: 361.1911; found 361.1908 $[\text{M}+\text{H}]^+$.

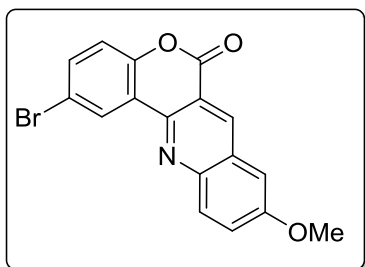
2-Bromo-6H-chromeno[4,3-b]quinolin-6-one (15ca): White solid; yield: 46.0 mg (68%); mp:



218–220 °C; ^1H NMR (400 MHz, $\text{DMSO}-d_6$) δ 9.39 (s, 1H), 8.73 (brs, 1H), 8.35 (d, $J = 8.2$ Hz, 1H), 8.24 (d, $J = 9.5$ Hz, 1H), 8.10 – 8.04 (m, 1H), 7.89 – 7.83 (m, 1H), 7.82 – 7.77 (m, 1H), 7.47 (d, $J = 8.4$ Hz, 1H); ^{13}C NMR (100 MHz, $\text{DMSO}-d_6$) δ 160.5, 152.0, 150.3, 148.3, 141.5, 135.4, 134.5, 130.4, 129.3, 128.4, 127.8, 127.0, 121.8, 120.2, 117.3,

116.5; HRMS (ESI-TOF) (m/z) calculated $\text{C}_{16}\text{H}_9\text{BrNO}_2^+$: 325.9811; found 325.9810 $[\text{M}+\text{H}]^+$.

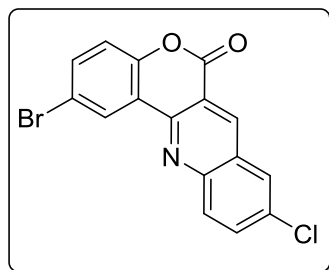
2-Bromo-9-methoxy-6H-chromeno[4,3-b]quinolin-6-one (15ce): White solid; yield: 53.3 mg



(72%); mp: 220–224 °C; ^1H NMR (400 MHz, CDCl_3) δ 9.10 (s, 1H), 8.88 (d, $J = 2.4$ Hz, 1H), 8.17 (brs, 1H), 7.66 (dd, $J = 8.7, 2.5$ Hz, 1H), 7.61 (dd, $J = 9.3, 2.8$ Hz, 1H), 7.30 (s, 1H), 7.25 (d, $J = 2.8$ Hz, 1H), 4.01 (s, 3H); ^{13}C NMR (100 MHz, CDCl_3) δ 161.0, 158.7, 151.2, 147.6, 146.2, 139.0, 134.4, 131.0, 128.8, 127.5, 127.4, 121.5, 119.1, 118.0, 115.7, 105.6, 55.8; HRMS

(ESI-TOF) (m/z) calculated $\text{C}_{17}\text{H}_{11}\text{BrNO}_3^+$: 355.9917; found 355.9911 $[\text{M}+\text{H}]^+$.

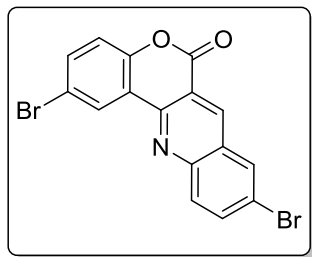
2-Bromo-9-chloro-6H-chromeno[4,3-b]quinolin-6-one (15ch): White solid; yield: 48.9 mg



(65%); mp: 221–223 °C; ^1H NMR (400 MHz, CDCl_3) δ 9.15 (s, 1H), 8.89 (d, $J = 2.4$ Hz, 1H), 8.21 (d, $J = 9.1$ Hz, 1H), 8.04 (d, $J = 2.3$ Hz, 1H), 7.90 (dd, $J = 9.1, 2.3$ Hz, 1H), 7.71 (dd, $J = 8.7, 2.5$ Hz, 1H), 7.31 (d, $J = 8.7$ Hz, 1H); ^{13}C NMR (100 MHz, CDCl_3) δ 160.4, 151.5, 149.4, 148.6, 140.2, 135.4, 134.7, 133.9, 131.2, 128.0, 127.9, 127.8, 121.0, 119.3, 118.2, 116.3; HRMS (ESI-TOF) (m/z)

calculated $C_{16}H_8BrClNO_2^+$: 361.9400; found 361.9316 $[M+H]^+$.

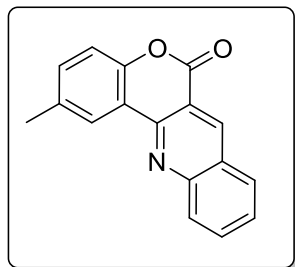
2,9-Dibromo-6H-chromeno[4,3-b]quinolin-6-one (15ci): White solid; yield: 47.0 mg (56%);



mp: 232–234 °C; 1H NMR (400 MHz, $CDCl_3$) δ 9.17 (s, 1H), 8.92 (brs, 1H), 8.23 (d, $J = 2.2$ Hz, 1H), 8.16 (d, $J = 9.1$ Hz, 1H), 8.03 (dd, $J = 9.1, 2.2$ Hz, 1H), 7.73 (dd, $J = 8.7, 2.4$ Hz, 1H), 7.32 (d, $J = 8.7$ Hz, 1H); ^{13}C NMR (100 MHz, $CDCl_3$) δ 160.9, 151.6, 149.6, 148.7, 142.3, 140.1, 137.1, 135.4, 131.2, 131.2, 128.5, 128.0, 122.0, 121.0,

119.3, 118.2, 116.3; HRMS (ESI-TOF) (m/z) calculated $C_{16}H_8Br_2NO_2^+$: 403.8916; found 403.8906 $[M+H]^+$.

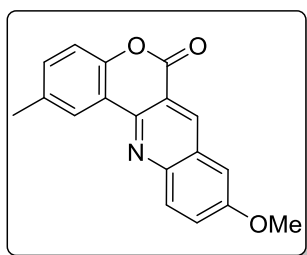
2-Methyl-6H-chromeno[4,3-b]quinolin-6-one (15da): White solid; yield: 51.5 mg (69%); mp:



231–233 °C; 1H NMR (400 MHz, $CDCl_3$) δ 9.26 (s, 1H), 8.61 (s, 1H), 8.28 (d, $J = 8.6$ Hz, 1H), 8.06 (d, $J = 8.2$ Hz, 1H), 7.96 – 7.93 (m, 1H), 7.70 – 7.66 (m, 1H), 7.44 – 7.41 (m, 1H), 7.32 (d, $J = 8.4$ Hz, 1H), 2.55 (s, 3H); ^{13}C NMR (100 MHz, $CDCl_3$) δ 161.5, 151.1, 150.9, 149.8, 141.2, 134.8, 133.4, 129.5, 129.5, 127.4, 127.3, 125.0, 119.2, 117.2, 115.9, 21.0; HRMS (ESI-TOF) (m/z) calculated $C_{17}H_{12}NO_2^+$:

262.0863; found 262.0843 $[M+H]^+$.

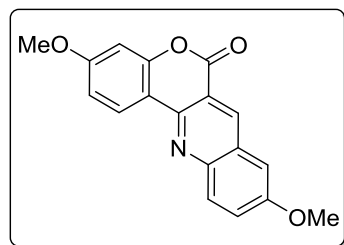
9-Methoxy-2-methyl-6H-chromeno[4,3-b]quinolin-6-one (15de): White solid; yield: 61.1 mg



(74%); mp: 237–239 °C; 1H NMR (400 MHz, $CDCl_3$) δ 9.07 (s, 1H), 8.54 – 8.48 (m, 1H), 8.13 (d, $J = 9.3$ Hz, 1H), 7.58 (dd, $J = 9.3, 2.8$ Hz, 1H), 7.37 (dd, $J = 8.3, 1.8$ Hz, 1H), 7.29 – 7.26 (m, 1H), 7.21 (d, $J = 2.8$ Hz, 1H), 4.00 (s, 3H), 2.52 (s, 3H); ^{13}C NMR (100 MHz, $CDCl_3$) δ 161.7, 158.3, 150.4, 147.6, 147.5, 139.0, 134.6, 132.7, 130.8, 128.4, 127.0, 124.6, 119.3, 117.1, 116.0, 105.6, 55.8, 21.0;

HRMS (ESI-TOF) (m/z) calculated $C_{18}H_{14}NO_3^+$: 292.0968; found 292.0948 $[M+H]^+$.

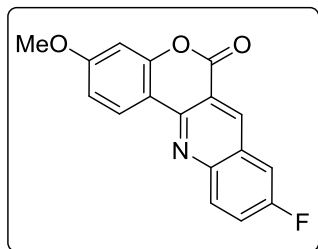
3,9-Dimethoxy-6H-chromeno[4,3-b]quinolin-6-one (15ee): White solid; yield: 56.6 mg (71%);



mp: 235–237 °C; 1H NMR (400 MHz, $CDCl_3$) δ 9.08 (s, 1H), 8.65 (d, $J = 8.8$ Hz, 1H), 8.13 (d, $J = 9.3$ Hz, 1H), 7.58 (dd, $J = 9.3, 2.8$ Hz, 1H), 7.22 (d, $J = 2.8$ Hz, 1H), 7.01 (dd, $J = 8.8, 2.5$ Hz, 1H), 6.90 (d, $J = 2.4$ Hz, 1H), 4.00 (s, 3H), 3.94 (s, 3H); ^{13}C NMR (100 MHz, $CDCl_3$) δ 162.8, 158.0, 153.7, 147.7, 147.6, 139.2, 130.6,

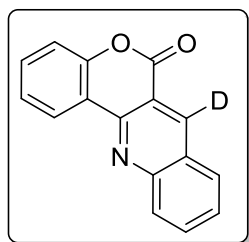
128.0, 127.1, 126.0, 115.1, 112.8, 105.7, 101.4, 55.8, 55.8; HRMS (ESI-TOF) (m/z) calculated $C_{18}H_{14}NO_4^+$: 308.0917; found 308.0893 $[M+H]^+$.

9-Fluoro-3-methoxy-6H-chromeno[4,3-b]quinolin-6-one (15eg): White solid; yield: 44.5 mg



(58%); mp: 239–241 °C; 1H NMR (400 MHz, $CDCl_3$) δ 9.14 (s, 1H), 8.65 (d, $J = 8.8$ Hz, 1H), 8.22 (dd, $J = 9.3, 5.2$ Hz, 1H), 7.71 – 7.66 (m, 1H), 7.62 (dd, $J = 8.3, 2.8$ Hz, 1H), 7.02 (dd, $J = 8.8, 2.5$ Hz, 1H), 6.90 (d, $J = 2.4$ Hz, 1H), 3.95 (s, 3H); ^{13}C NMR (100 MHz, $CDCl_3$) δ 163.3, 161.5 ($J_{C-F} = 28.7$ Hz), 159.1, 154.0, 149.3 ($J_{C-F} = 2.5$ Hz), 148.4, 140.3 ($J_{C-F} = 6.1$ Hz), 131.8 ($J_{C-F} = 8.9$ Hz), 127.3 ($J_{C-F} = 10.2$ Hz), 126.28, 123.9 ($J_{C-F} = 26.1$ Hz), 115.6, 112.9, 112.5, 112.0 ($J_{C-F} = 21.1$ Hz), 101.5, 55.8; HRMS (ESI-TOF) (m/z) calculated $C_{17}H_{11}FNO_3^+$: 296.0717; found 296.0690 $[M+H]^+$.

6H-chromeno[4,3-b]quinolin-6-one-7-d (15aa’): White solid; yield: 51.1 mg (68%); mp: 210–



212 °C; 1H NMR (400 MHz, $CDCl_3$) δ 8.84 (dd, $J = 7.9, 1.6$ Hz, 1H), 8.29 (d, $J = 8.6$ Hz, 1H), 8.07 (d, $J = 8.1$ Hz, 1H), 8.09 – 8.04 (m, 1H), 7.71 – 7.61 (m, 2H), 7.50 – 7.42 (m, 2H); ^{13}C NMR (100 MHz, $CDCl_3$) δ 161.4, 152.8, 151.2, 149.7, 133.4, 132.4, 129.6, 129.4, 127.4, 127.3, 125.3, 125.0, 119.7, 117.4, 115.8; HRMS (ESI-TOF) (m/z) calculated $C_{16}H_9DNO_2^+$: 249.0769; found 249.0735 $[M+H]^+$.

4.4 X-ray Crystallography Studies of 15ba

A suitable crystal was mounted in a nylon loop attached to a goniometer head for initial crystal evaluation. Data were collected on a Kappa APEX II diffractometer equipped with a CCD detector (with the crystal-to-detector distance fixed at 60 mm) and sealed-tube monochromated Mo K α radiation using the program APEX2.⁷⁷ Using the program SAINT⁷⁷ data was integrated, reflection profiles were fitted, and values of F^2 and $\sigma(F^2)$ for each reflection were obtained. Lorentz and polarization effects were applied to the data. The subroutine XPREP⁷⁷ was used for the determination of space group, application of an absorption correction (SADABS),⁷⁷ merging of data, and generation of files necessary for solution and refinement. Using Olex2,⁷⁸ the structure was solved with the ShelXT⁷⁹ structure solution program using Intrinsic Phasing and refined with the ShelXL⁷⁹ refinement package using least squares minimisation. Several full-matrix least-squares/difference Fourier cycles were performed for the convergence of refinement. All non-hydrogen atoms were refined with anisotropic displacement parameters. The

lattice water molecule was highly disordered. Therefore, the Olex2⁷⁸ masking program was used to remove those peaks. All hydrogen atoms were placed in ideal positions and refined as riding atoms with individual isotropic displacement parameters. All figures were drawn using MERCURY V 3.10.2.⁸⁰

Crystal data for 15ba (CCDC No. 1862858): C₂₀H₁₈N₂O₂, Mr = 318.36, a = 23.7547(17) Å, b = 23.7547(17) Å, c = 15.1366(16) Å, $\alpha = 90^\circ$, $\beta = 90^\circ$, $\gamma = 120^\circ$, V = 7397.0(13) Å³, Z = 18, trigonal, space group $R\bar{3}$ (No. 148), D_{calc} = 1.286 g/cm³, T = 100(2) K; Full matrix least-square on F²; R₁ = 0.0636, wR₂ = 0.1669 for 2285 observed reflections [I > 2σ(I)] and R₁ = 0.0766, wR₂ = 0.1737 for all 2914 reflections; GOF = 1.040. CCDC # 1862858.

4.5 References

- (1) Nicolaou, K.; Chen, J. S. *Chemical Society Reviews* **2009**, 38, 2993-3009.
- (2) Schuster, M.; Blechert, S. *Angewandte Chemie International Edition in English* **1997**, 36, 2036-2056.
- (3) Tietze, L. F.; Beifuss, U. *Angewandte Chemie International Edition in English* **1993**, 32, 131-163.
- (4) Sun, C. L.; Shi, Z. J. *Chemical Reviews* **2014**, 114, 9219-9280.
- (5) Xie, J.; Jiang, H.; Cheng, Y.; Zhu, C. *Chemical Communications* **2012**, 48, 979-981.
- (6) Matcha, K.; Narayan, R.; Antonchick, A. P. *Angewandte Chemie International Edition* **2013**, 52, 7985-7989.
- (7) Cheng, G.; Zeng, X.; Shen, J.; Wang, X.; Cui, X. *Angewandte Chemie International Edition* **2013**, 52, 13265-13268.
- (8) Zhang, H.; Pan, C.; Jin, N.; Gu, Z.; Hu, H.; Zhu, C. *Chemical Communications* **2015**, 51, 1320-1322.
- (9) Mousseau, J. J.; Charette, A. B. *Accounts of Chemical Research* **2012**, 46, 412-424.
- (10) Foley, M.; Tilley, L. *Pharmacology & Therapeutics* **1998**, 79, 55-87.
- (11) Sun, X. Y.; He, X. J.; Pan, C. Y.; Liu, Y. P.; Zou, Y. P. *Medicinal Chemistry Research* **2012**, 21, 3692-3698.
- (12) Zemtsova, M.; Zimichev, A.; Trakhtenberg, P.; Klimochkin, Y. N.; Leonova, M.; Balakhnin, S.; Bormotov, N.; Serova, O.; Belanov, E. *Pharmaceutical Chemistry Journal* **2011**, 45, 267.

- (13) Ramamoorthy, P. S.; Mcdevitt, R. E.; Google Patents: United States patent US 7,071,185. 2006 Jul 4., **2006**.
- (14) Afzal, O.; Kumar, S.; Haider, M. R.; Ali, M. R.; Kumar, R.; Jaggi, M.; Bawa, S. *European Journal of Medicinal Chemistry* **2015**, *97*, 871-910.
- (15) Shah, A. A.; Chenard, L. K.; Tucker, J. W.; Helal, C. J. *ACS Combinatorial Science* **2017**, *19*, 675-680.
- (16) Fu, L.; Feng, X.; Wang, J. J.; Xun, Z.; Hu, J. D.; Zhang, J. J.; Zhao, Y. W.; Huang, Z. B.; Shi, D. Q. *ACS Combinatorial Science* **2014**, *17*, 24-31.
- (17) Hu, Z.; Li, Y.; Pan, L.; Xu, X. *Advanced Synthesis & Catalysis* **2014**, *356*, 2974-2978.
- (18) Khalafi Nezhad, A.; Sarikhani, S.; Shahidzadeh, E. S.; Panahi, F. *Green Chemistry* **2012**, *14*, 2876-2884.
- (19) Zhou, Y. J.; Chen, D. S.; Li, Y. L.; Liu, Y.; Wang, X. S. *ACS Combinatorial Science* **2013**, *15*, 498-502.
- (20) Yuvaraj, P.; Manivannan, K.; Reddy, B. S. *Tetrahedron Letters* **2015**, *56*, 78-81.
- (21) Plaskon, A. S.; Ryabukhin, S. V.; Volochnyuk, D. M.; Gavrilenko, K. S.; Shivanyuk, A. N.; Tolmachev, A. A. *The Journal of Organic Chemistry* **2008**, *73*, 6010-6013.
- (22) Khadem, S.; Udachin, K. A.; Enright, G. D.; Prakesch, M.; Arya, P. *Tetrahedron Letters* **2009**, *50*, 6661-6664.
- (23) Yu, F. C.; Zhou, B.; Xu, H.; Li, Y. M.; Lin, J.; Yan, S. J.; Shen, Y. *Tetrahedron* **2015**, *71*, 1036-1044.
- (24) Peng, L.; Wang, H.; Peng, C.; Ding, K.; Zhu, Q. *Synthesis* **2011**, *2011*, 1723-1732.
- (25) Sim, Y. K.; Lee, H.; Park, J. W.; Kim, D. S.; Jun, C. H. *Chemical Communications* **2012**, *48*, 11787-11789.
- (26) Yan, R.; Zhou, X.; Li, M.; Li, X.; Kang, X.; Liu, X.; Huo, X.; Huang, G. *RSC Advances* **2014**, *4*, 50369-50372.
- (27) Kanakaraju, S.; Prasanna, B.; Basavoju, S.; Chandramouli, G. *Arabian Journal of Chemistry* **2017**, *10*, S2705-S2713.
- (28) Thomas, J.; Jana, S.; Liekens, S.; Dehaen, W. *Chemical Communications* **2016**, *52*, 9236-9239.
- (29) Yi, Y.; Lee, H.; Jun, C. H. *Chemical Communications* **2016**, *52*, 10171-10174.
- (30) Chang, M. Y.; Wu, M. H.; Tai, H. Y. *Organic Letters* **2012**, *14*, 3936-3939.

- (31) Bala, B. D.; Balamurugan, K.; Perumal, S. *Tetrahedron Letters* **2011**, *52*, 4562-4566.
- (32) Chidurala, P.; Jetti, V.; Pagadala, R.; Meshram, J. S.; Jonnalagadda, S. B. *Journal of Heterocyclic Chemistry* **2015**, *52*, 1302-1307.
- (33) Findik, E.; Ceylan, M.; Elmastas, M. *Journal of Heterocyclic Chemistry* **2012**, *49*, 253-260.
- (34) Jung, H.; Lee, H.; Kang, S.; Shin, D.-H.; Kay, K.-Y.; Park, J. *Molecular Crystals and Liquid Crystals* **2017**, *654*, 90-95.
- (35) Sun, H.; Fan, H.; Peng, X. *The Journal of Organic Chemistry* **2014**, *79*, 11359-11369.
- (36) Khan, R. I.; Pitchumani, K. *RSC Advances* **2016**, *6*, 20269-20275.
- (37) Czarna, M.; Kaminska, I.; Ortyl, J. *Technical Issues* **2015**, *2015*, 3-10.
- (38) Myung, N.; Connelly, S.; Kim, B.; Park, S. J.; Wilson, I. A.; Kelly, J. W.; Choi, S. *Chemical Communications* **2013**, *49*, 9188-9190.
- (39) Sun, H.; Peng, X. *Bioconjugate Chemistry* **2013**, *24*, 1226-1234.
- (40) Martinez, R.; Cortes, E.; Toscano, R. A.; Alfaro, L. J. *Journal of Heterocyclic Chemistry* **1990**, *27*, 1273-1276.
- (41) Chen, Z.; Bi, J.; Su, W. *Chinese Journal of Chemistry* **2013**, *31*, 507-514.
- (42) Goswami, L.; Gogoi, S.; Gogoi, J.; Boruah, R. K.; Boruah, R. C.; Gogoi, P. *ACS Combinatorial Science* **2016**, *18*, 253-261.
- (43) Harvey, R. G.; Cortez, C.; Ananthanarayan, T. P.; Schmolka, S. *The Journal of Organic Chemistry* **1988**, *53*, 3936-3943.
- (44) Markey, M. D.; Fu, Y.; Kelly, T. R. *Organic Letters* **2007**, *9*, 3255-3257.
- (45) Vasamsetty, S.; Medidi, S.; Ampolu, S.; Majji, R. K.; Kotupalli, M. R.; Satyanarayana, C. C.; Nowduri, A.; Sanasi, P. D. *Green and Sustainable Chemistry* **2017**, *7*, 141.
- (46) Thigulla, Y.; Kumar, T. U.; Trivedi, P.; Ghosh, B.; Bhattacharya, A. *ChemistrySelect* **2017**, *2*, 2718-2721.
- (47) Kand, D.; Kalle, A. M.; Talukdar, P. *Organic & Biomolecular Chemistry* **2013**, *11*, 1691-1701.
- (48) Wu, X.; Zhang, Y.; Takle, K.; Bilsel, O.; Li, Z.; Lee, H.; Zhang, Z.; Li, D.; Fan, W.; Duan, C. *Acs Nano* **2016**, *10*, 1060-1066.
- (49) Liu, X.; Li, Y.; Ren, X.; Yang, Q.; Su, Y.; He, L.; Song, X. *Chemical Communications* **2018**, *54*, 1509-1512.

- (50) Vu, A. T.; Campbell, A. N.; Harris, H. A.; Unwalla, R. J.; Manas, E. S.; Mewshaw, R. E. *Bioorganic & Medicinal Chemistry Letters* **2007**, *17*, 4053-4056.
- (51) Sashidhara, K. V.; Palnati, G. R.; Singh, L. R.; Upadhyay, A.; Avula, S. R.; Kumar, A.; Kant, R. *Green Chemistry* **2015**, *17*, 3766-3770.
- (52) Sundahl, N.; Bridelance, J.; Libert, C.; De Bosscher, K.; Beck, I. M. *Pharmacology & Therapeutics* **2015**, *152*, 28-41.
- (53) Tabaković, K.; Tabaković, I.; Ajdini, N.; Leci, O. *Synthesis* **1987**, *1987*, 308-310.
- (54) Mulakayala, N.; Rambabu, D.; Raja, M. R.; Chaitanya, M.; Kumar, C. S.; Kalle, A. M.; Krishna, G. R.; Reddy, C. M.; Rao, M. B.; Pal, M. *Bioorganic & Medicinal Chemistry* **2012**, *20*, 759-768.
- (55) Prasad, J. V.; Reddy, J. S.; Kumar, N. R.; Solomon, K. A.; Gopikrishna, G. *Journal of Chemical Sciences* **2011**, *123*, 673-679.
- (56) Wu, J.; Wang, X. *Organic & Biomolecular Chemistry* **2006**, *4*, 1348-1351.
- (57) Iaroshenko, V. O.; Ali, S.; Babar, T. M.; Dudkin, S.; Mkrtchyan, S.; Rama, N. H.; Villinger, A.; Langer, P. *Tetrahedron Letters* **2011**, *52*, 373-376.
- (58) Rajawinslin, R.; Gawande, S. D.; Kavala, V.; Huang, Y. H.; Kuo, C. W.; Kuo, T. S.; Chen, M. L.; He, C. H.; Yao, C. F. *RSC Advances* **2014**, *4*, 37806-37811.
- (59) Khan, M. N.; Pal, S.; Karamthulla, S.; Choudhury, L. H. *New Journal of Chemistry* **2014**, *38*, 4722-4729.
- (60) Weng, Y.; Zhou, H.; Sun, C.; Xie, Y.; Su, W. *The Journal of Organic Chemistry* **2017**, *82*, 9047-9053.
- (61) Cao, H.; Lei, S.; Li, N.; Chen, L.; Liu, J.; Cai, H.; Qiu, S.; Tan, J. *Chemical Communications* **2015**, *51*, 1823-1825.
- (62) Xiang, S.; Chen, H.; Liu, Q. *Tetrahedron Letters* **2016**, *57*, 3870-3872.
- (63) Zhang, Z.; Tian, Q.; Qian, J.; Liu, Q.; Liu, T.; Shi, L.; Zhang, G. *The Journal of Organic Chemistry* **2014**, *79*, 8182-8188.
- (64) Fei, H.; Yu, J.; Jiang, Y.; Guo, H.; Cheng, J. *Organic & Biomolecular Chemistry* **2013**, *11*, 7092-7095.
- (65) Yuan, J.; Yu, J. T.; Jiang, Y.; Cheng, J. *Organic & Biomolecular Chemistry* **2017**, *15*, 1334-1337.

- (66) Lv, Y.; Li, Y.; Xiong, T.; Pu, W.; Zhang, H.; Sun, K.; Liu, Q.; Zhang, Q. *Chemical Communications* **2013**, *49*, 6439-6441.
- (67) Pan, X.; Liu, Q.; Chang, L.; Yuan, G. *RSC Advances* **2015**, *5*, 51183-51187.
- (68) Zhang, Y.; Tang, Q.; Luo, M. *Organic & Biomolecular Chemistry* **2011**, *9*, 4977-4982.
- (69) Li, Y.; Liu, W.; Kuang, C. *Chemical Communications* **2014**, *50*, 7124-7127.
- (70) Paul, S.; Bhattacharya, A. K. *Organic & Biomolecular Chemistry* **2018**, *16*, 444-451.
- (71) Ravi, M.; Chauhan, P.; Kant, R.; Shukla, S. K.; Yadav, P. P. *The Journal of Organic Chemistry* **2015**, *80*, 5369-5376.
- (72) Chauhan, P.; Ravi, M.; Singh, S.; Prajapati, P.; Yadav, P. P. *RSC Advances* **2016**, *6*, 109-118.
- (73) Kocaoglu, E.; Karaman, M. A.; Tokgoz, H.; Talaz, O. *ACS Omega* **2017**, *2*, 5000-5004.
- (74) Yuan, J. W.; Li, W. J.; Xiao, Y. M. *Tetrahedron* **2017**, *73*, 179-186.
- (75) Jiang, T.; Chen, S. Y.; Zhuang, H.; Zeng, R. S.; Zou, J. P. *Tetrahedron Letters* **2014**, *55*, 4549-4552.
- (76) Jadhav, R. R.; Huddar, S. N.; Akamanchi, K. G. *European Journal of Organic Chemistry* **2013**, *2013*, 6779-6783.
- (77) APEX, S. *SAINT; Bruker AXS inc: Madison, WI, USA*, **2008**.
- (78) Dolomanov, O. V.; Bourhis, L. J.; Gildea, R. J.; Howard, J. A.; Puschmann, H. *Journal of Applied Crystallography* **2009**, *42*, 339-341.
- (79) Sheldrick, G. M. *Acta Crystallographica Section A: Foundations and Advances* **2015**, *71*, 3-8.
- (80) Macrae, C. F.; Bruno, I. J.; Chisholm, J. A.; Edgington, P. R.; McCabe, P.; Pidcock, E.; Rodriguez Monge, L.; Taylor, R.; Streek, J. v. d.; Wood, P. A. *Journal of Applied Crystallography* **2008**, *41*, 466-470.

Chapter 5

Conclusions of the Thesis

5.1 General conclusions

Coumarin-appended and coumarin-fused heterocycles are considered as valuable targets in synthetic chemistry because of their broad range of applications in the field of material and medicinal chemistry. Coequally, coumaryl-labelled/tagged amino acids have received special interest due to their sensitivity to pH and solvent polarity that makes them excellent fluorescent molecules to investigate numerous biological processes in living organisms. Thus, synthesis of these heterocyclic architectures in minimum number of steps from readily available precursors *via* conventional or modern flourishing chemistry is a highly appealing area of research. Consecutively, tandem modification concept has also become a powerful approach for the diversity-oriented synthesis without the necessity of pre-activation of substrates. The ongoing periodical documentation on fluorescent molecules allude our interest in synthesizing coumarin-appended amino acids and azaheterocycles, and study their photophysical properties and related applications. The work disclosed in the present thesis entitled “**Coumarin-appended Amino Acids and Azaheterocycles: Design, Synthesis, Photophysical Studies and Sensing Applications of Selected Compounds**” was successfully executed in due diligence of sustainable chemistry, and the thesis has been divided into five chapters (Figure 5.1.1).

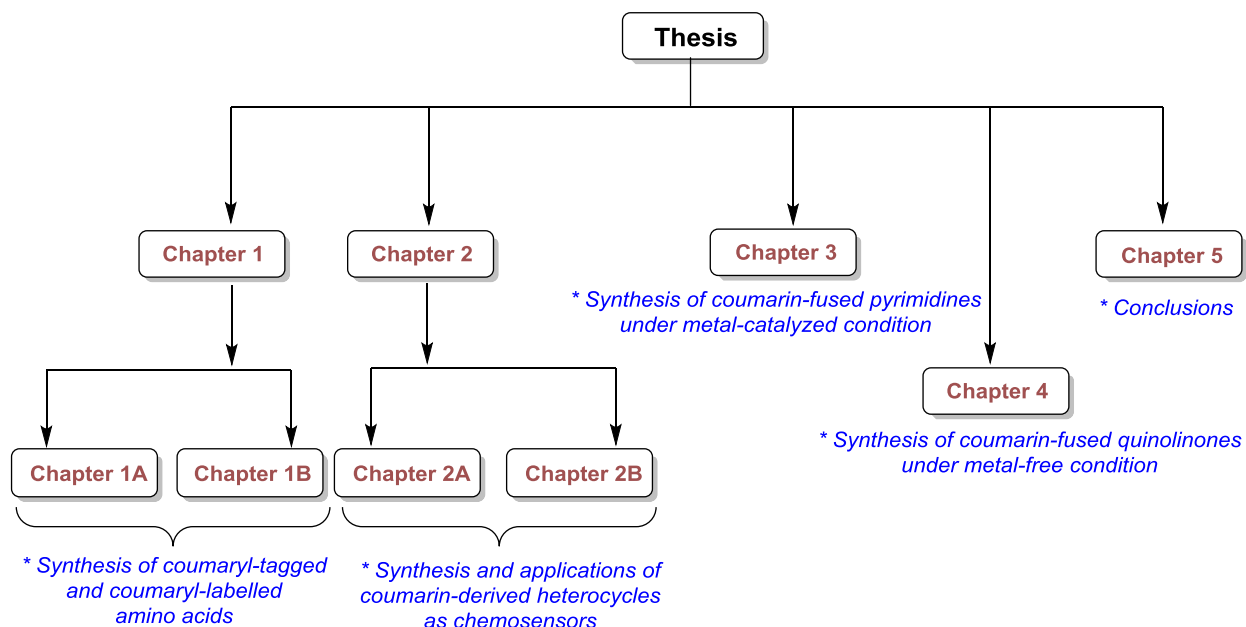


Figure 5.1.1: A diagram describing the systematic division of the thesis

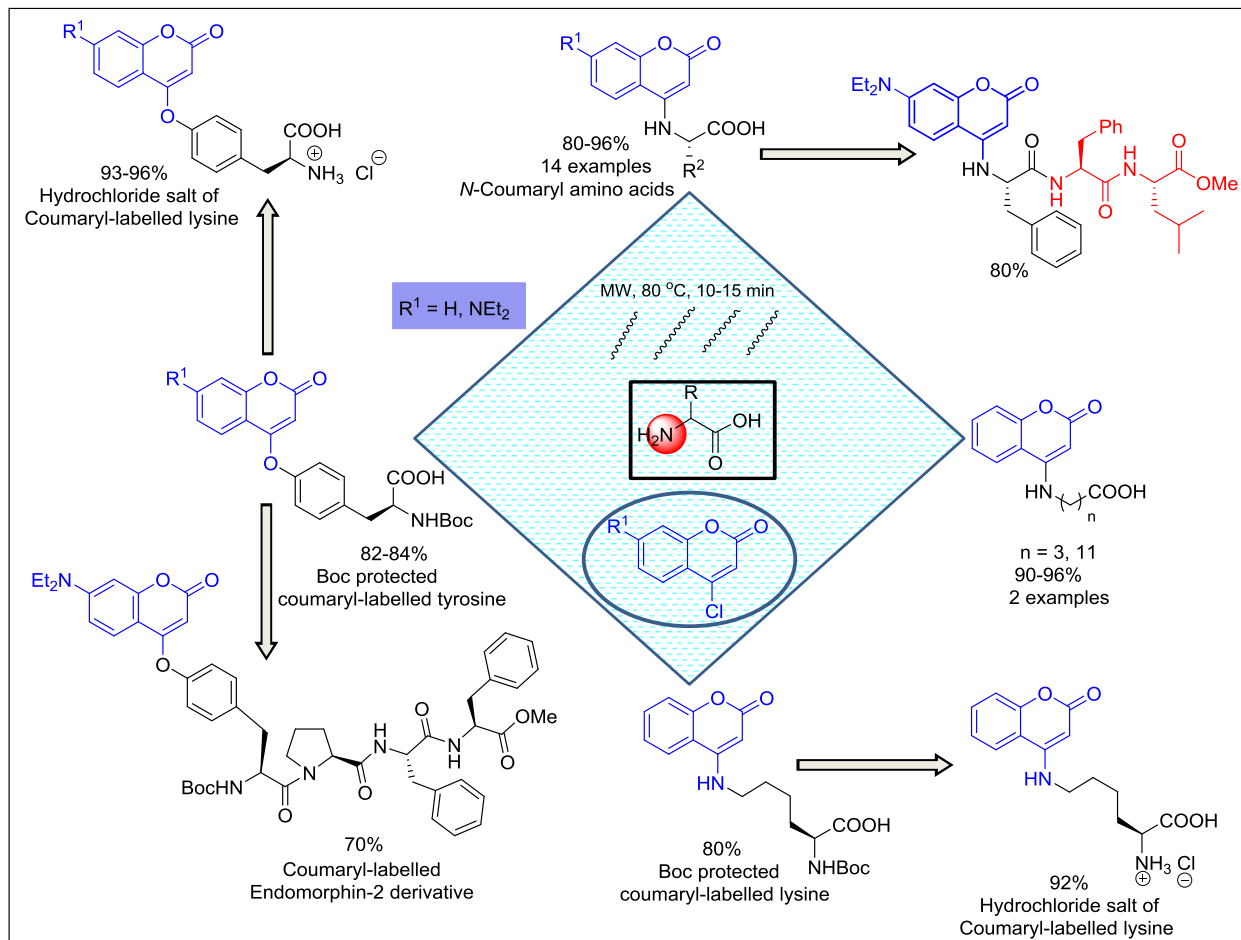
A chapter-wise summary is presented below:

5.2 Specific conclusions

The **first chapter** of thesis is divided into two parts:

Chapter 1A: Copper-catalyzed C-N/C-O Coupling in Water: A Facile Access to Coumaryl-tagged and Coumaryl-labelled Amino Acids

Chapter 1A first describes the vital importance of coumaryl-tagged and coumaryl-labelled amino acids/peptides, and the existing strategies known for their synthesis in order to provide a background on the work conducted in the past. Taking a lead from the drawbacks associated with the existing synthetic strategies, we developed a straightforward Cu-catalyzed microwave-assisted protocol for the synthesis of *N*-coumaryl amino acids by coupling 4-chlorocoumarin and α -L-amino acids in water. Interestingly, various α -amino acids possessing polar and non-polar side chains such as L-Ala, L-Val, L-Ile, L-Met, L-Trp, L-Ser, L-Phe and L-Tyr showcased good reactivity, affording their corresponding *N*-coumaryl amino acids in 80-96% yields. The developed strategy was also employed for coupling unnatural amino acids, γ -aminobutyric acid (GABA) and 12-aminolauric acid to the coumarin moiety. All the products were well characterized by their detailed spectral analysis (^1H NMR, ^{13}C NMR, and high-resolution mass spectrometry). Absorption and fluorescence spectra of all synthesized compounds were recorded, and quantum yields were computed. The chemical applicability of the synthesized *N*-coumaryl amino acids as a fluorescent probe was illustrated by coupling a representative *N*-coumaryl amino acid with a *N*-terminus dipeptide under coupling conditions to afford *N*-coumaryl tripeptide in high yield. Since the inclusion of a fluorescent labelled amino acid at definite site in proteins is an important strategy for understanding the mechanism of biologically relevant processes, the methodology was extended to synthesize coumaryl-labelled lysine and tyrosine motifs by coupling 4-chlorocoumarin with Boc-protected α -*N*-lysine and α -*N*-tyrosine, respectively under Cu-catalyzed microwave-assisted conditions in water. Finally, to illustrate a practical application of coumaryl-labelled amino acids as potential fluorescent label, a coumaryl-labelled synthetic derivative of opioid tetrapeptide, Endomorphin-2 was synthesized by peptide bond coupling between *C*-terminus coumaryl-labelled tyrosine with *N*-terminus tripeptide, $\text{HCl}\cdot\text{NH}_2\text{-L-Pro-L-Phe-L-Phe-OMe}$.

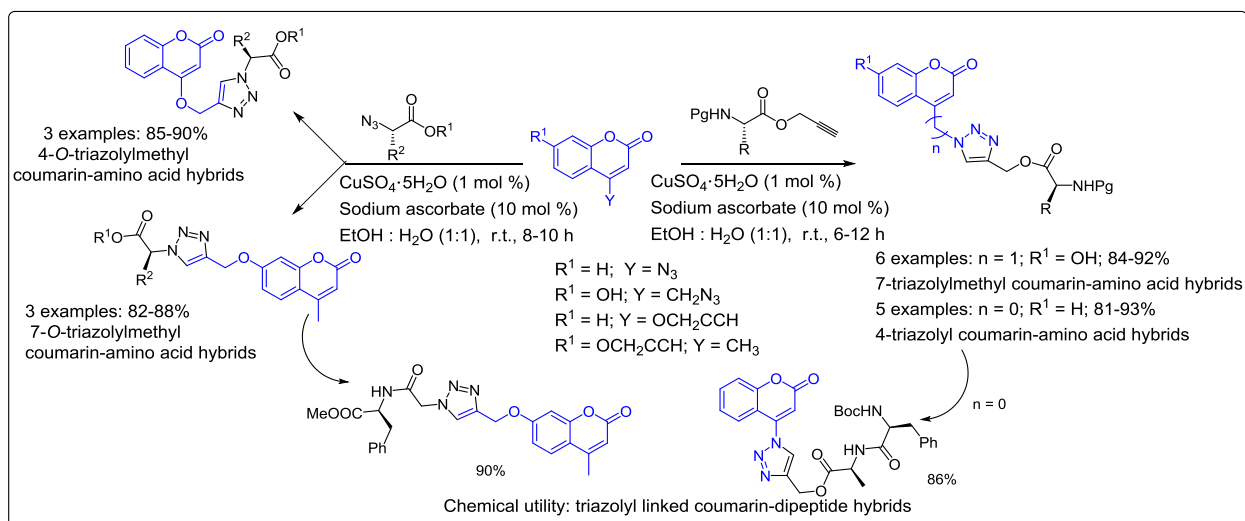


Scheme 5.2.1: Synthesis of *N*-coumarin amino acids and coumarin-labelled lysine and tyrosine motifs

Chapter 1B: Copper-catalyzed [3+2] Cycloaddition: A Facile Access to Triazolyl Linked Coumarin-amino acid Hybrids

Chapter 1B first describes the importance of triazole-modified peptidomimetics, and summarizes the synthetic strategies known for different triazolyl linked coumarin-appended bioconjugates. Inspired from the existing reports, we successfully explored the application of click chemistry for synthesizing triazolyl linked coumarin-amino acid/peptide hybrids using two strategies. Following first strategy, Cu-catalyzed azide-alkyne cycloaddition (CuAAC) reaction between clickable protected amino acyl *O*-propargyl esters and 4-azido-2*H*-chromen-2-one (or 7-hydroxy-4-azidomethyl-2*H*-chromen-2-one) comfortably afforded 4-triazolyl (or 4-triazolylmethyl) linked coumarin-amino acid/peptide hybrids in good-to-excellent yields. While following the second strategy, Cu-catalyzed [3+2] cycloaddition reaction between clickable 4-methyl-7-(prop-2-ynyloxy)-2*H*-chromen-2-one (or 4-(prop-2-ynyloxy)-2*H*-chromen-2-one) and

α -azido esters furnished two series of 7-*O*-triazolylmethyl and 4-*O*-triazolylmethyl coumarin-amino acid hybrids in 82–90% yields. All the products were completely characterized by their detailed spectral analysis (^1H NMR, ^{13}C NMR, and high-resolution mass spectrometry). The synthesized compounds exhibited good fluorescence properties, as evident from their detailed absorption and emission studies. In addition, the chemical applicability of the synthesized triazolyl linked coumarin-amino acid hybrids as fluorescent labels was successfully exemplified by coupling them with appropriate *C*- or *N*-terminus amino acids, furnishing corresponding triazolyl linked coumarin-peptide hybrids in high yields.



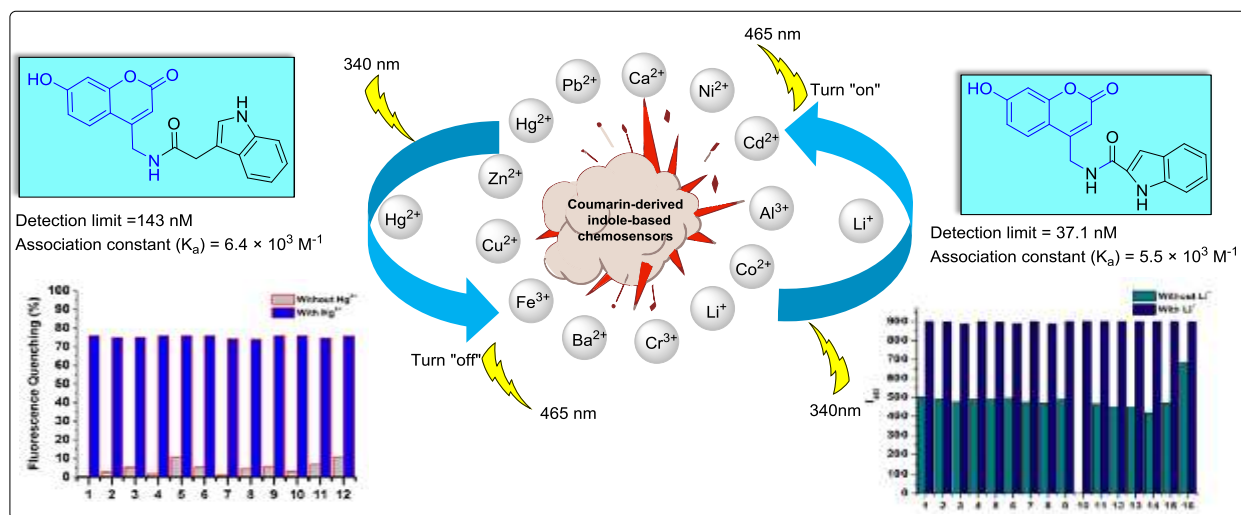
Scheme 5.2.2: Synthesis of triazolyl linked coumarin-amino acid/peptide hybrids

The **second chapter** of the thesis is also divided into two parts:

Chapter 2A: Coumarin-derived Selective Hg^{2+} & Li^+ Chemosensors: Synthesis, Experimental and Theoretical Investigations

Chapter 2A presents a brief description on fluorescence sensing, and the reported examples of coumarin-derived chemosensors known for metal ion detection, with special emphasis on Hg^{2+} and Li^+ ions. Due to the limitations associated with the existing Hg^{2+} and Li^+ ion chemosensors, two coumarin-derived indole-based probes were synthesized and identified as efficient sensors for selective detection of Hg^{2+} and Li^+ in organo-aqueous media. The indole-based probes were synthesized in high yields by coupling 7-hydroxy-4-(aminomethyl)coumarin with indole-3-acetic acid and indole-2-carboxylic acid, respectively at room temperature. Among these, *N*-((7-hydroxy-2-oxo-2*H*-chromen-4-yl)methyl)-2-(1*H*-indol-3-yl)acetamide displayed remarkable selectivity towards Hg^{2+}

sensing in H₂O-DMF mixture as a turn-off fluorescence response, with a detection limit of 143 nM and association constant (K_a) of $6.4 \times 10^3 \text{ M}^{-1}$ between the probe and Hg²⁺. While *N*-((7-hydroxy-2-oxo-2*H*-chromen-4-yl)methyl)-1*H*-indole-2-carboxamide showed remarkable selectivity towards Li⁺ ion sensing in H₂O-CH₃CN as a turn-on fluorescence response, with a detection limit of 37.1 nM and association constant (K_a) of $5.5 \times 10^3 \text{ M}^{-1}$ between the probe and Li⁺. The most probable binding site of complexing Hg²⁺ and Li⁺ to the respective probes was explained on the basis of detailed UV-Vis spectroscopic studies, Benesi-Hildebrand plots, ¹H NMR titrations and DFT calculations.

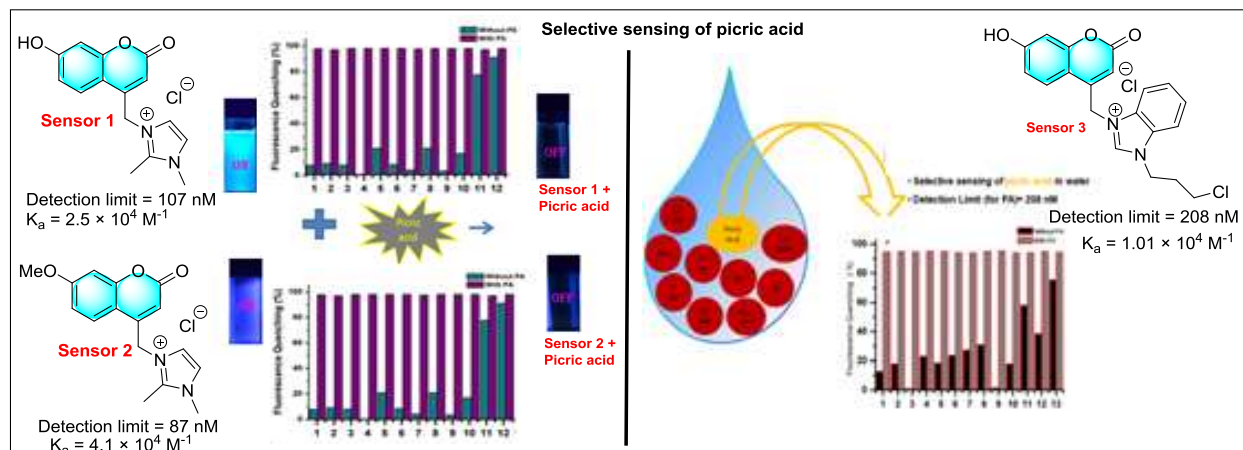


Scheme 5.2.3: Synthesis and application of coumarin-derived indole-based probes towards Hg²⁺ and Li⁺ ions sensing

Chapter 2B: Coumarin-derived Sensors for Picric Acid Detection: Synthesis, Experimental and Theoretical Investigations

Chapter 2B presents an overview on the existing chemosensors known for picric acid detection, and their associated drawbacks. Later, in a zeal to develop water-soluble probes capable of detecting picric acid at very low concentrations in aqueous medium, two coumarin-derived imidazolium salts and one benzimidazolium salt was synthesized in excellent yields, by coupling substituted 4-(chloromethyl)-7-hydroxy-2*H*-chromen-2-ones with 1,2-dimethylimidazole and 1-(3-chloropropyl)benzimidazole, respectively. The probes displayed remarkable efficiency towards selective sensing of picric acid in aqueous medium in presence of other aromatic/non-aromatics analytes. The Stern–Volmer quenching constant (K_{SV}) for sensors were found to be $2.2 \times 10^4 \text{ M}^{-1}$, $5 \times 10^4 \text{ M}^{-1}$ and $1.58 \times 10^4 \text{ M}^{-1}$, while the detection limits for picric acid were

calculated to be 107 nM, 87 nM and 208 nM, respectively. Based on the UV–Visible studies, and time resolved fluorescence results, the formation of ground-state charge-transfer complex formation appears to be predominant mechanism in solution, which also got support from DFT calculations.

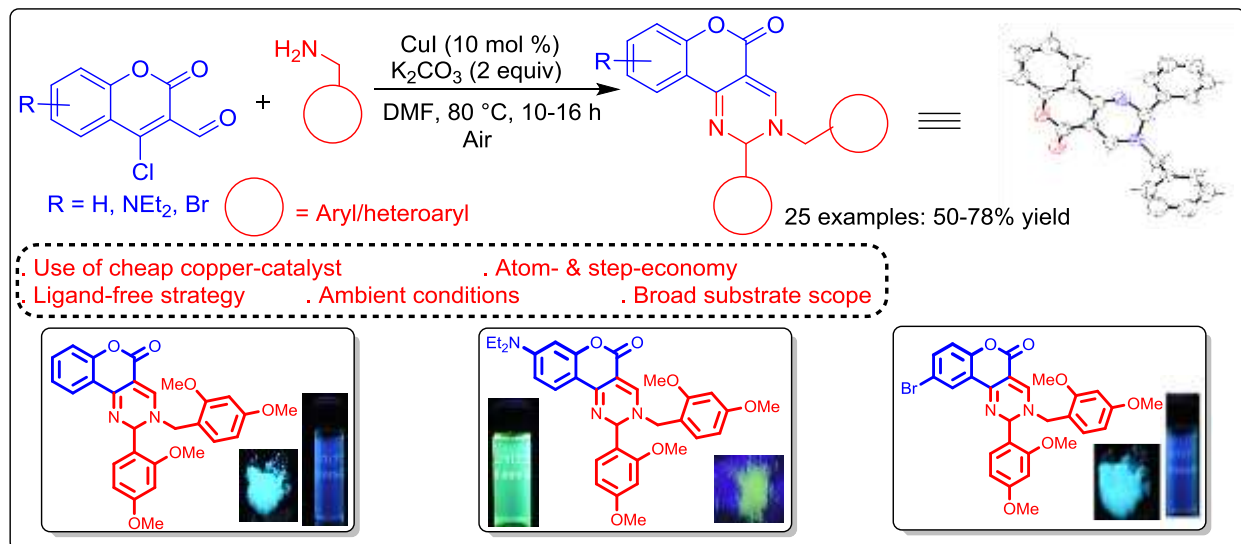


Scheme 5.2.4: Synthesis and application of coumarin-derived imidazolium and benzimidazolium salts towards picric acid sensing

Chapter 3: Copper-catalyzed Cross-Dehydrogenative $C(sp^3)$ –N Bond Coupling: An Unprecedented Tandem Synthesis of Coumarin-fused Pyrimidines

Chapter 3 of the thesis commences with a brief introduction on Cu-catalyzed C–C/C–X (X = O, P, N, S) bond forming reactions *via* CDC approach, particularly intramolecular $C(sp^3)$ –C or $C(sp^3)$ –N bond forming reactions, leading to the development of different heterocyclic frameworks. In addition, the importance of coumarin-fused pyrimidines, and the gaps in the existing strategies known for their synthesis is summarized. Later, an efficient, one-pot Cu-catalyzed tandem synthesis of fluorescent 3-benzyl-2-phenyl-2,3-dihydro-5H-chromeno[4,3-*d*]pyrimidin-5-ones from 4-chloro-3-formylcoumarin and benzylamines by *in situ* intramolecular cross-dehydrogenative $C(sp^3)$ –N bond formation under ligand-free ambient conditions. This synthesis was easily scalable, and an array of benzylamines delivered coumarin-fused pyrimidine in moderate-to-good yields. All the synthesized compounds were purified by column chromatography, and characterized by detailed spectroscopic analysis. Detailed investigations were performed to propose the mechanism of this unprecedented reaction. These coumarin-fused pyrimidines exhibited interesting photophysical properties and high quantum yields, and would

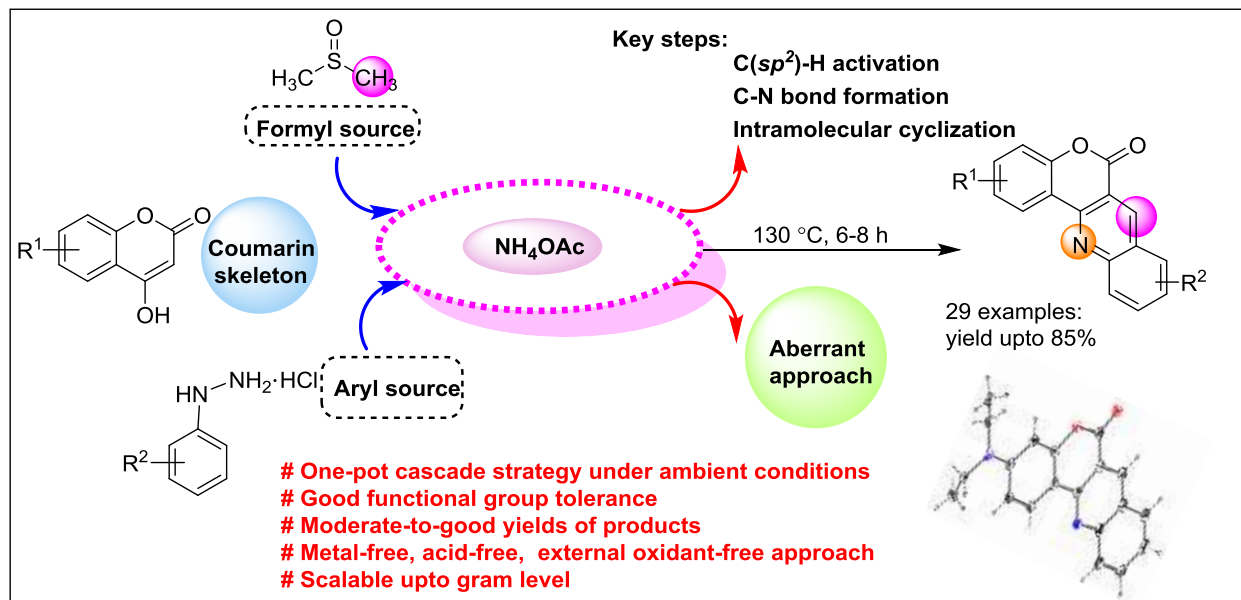
be potential candidates for facilitating suitable studies in medicinal chemistry and material science.



Scheme 5.2.5: Cu-catalyzed synthesis of coumarin-fused pyrimidines *via* $\text{C}(sp^3)\text{-N}$ bond formation

Chapter 4: NH_4OAc -promoted $\text{C}(sp^2)\text{-H}$ Bond Activation and C-N Bond Formation: An Aberrant Cascade Synthesis of Coumarin-fused Quinolinones

Chapter 4 of the thesis initially describes the importance and the existing reports on metal-free cascade strategies with emphasis on the use of DMSO as a formyl source, ammonium acetate as a nitrogen source and arylhydrazine as an aryl source. In addition, the importance of coumarin-fused quinolinones and the drawbacks in the existing conventional and metal-catalyzed strategies known for their synthesis is summarized. Later, a concise cascade strategy for the synthesis of 6*H*-chromeno[4,3-*b*]quinolin-6-ones was developed from 4-hydroxycoumarins and arylhydrazine hydrochlorides in DMSO. The synthetic strategy relies on dual role of ammonium acetate in generating 4-(aminophenyl)coumarin from 4-hydroxycoumarin and arylhydrazine *via* aryl radical formation, and $\text{C}(sp^2)\text{-H}$ formylation of coumarin using DMSO as a methine source. The strategy was scalable, and an array of arylhydrazine hydrochlorides delivered chromene-fused quinolinones in good-to-excellent yields. All the synthesized compounds were purified by column chromatography, and characterized by detailed spectroscopic analysis. A detailed mechanistic investigation was performed to understand the mechanism of this unique process. All the synthesized coumarin-fused quinolinones exhibited interesting photophysical properties.



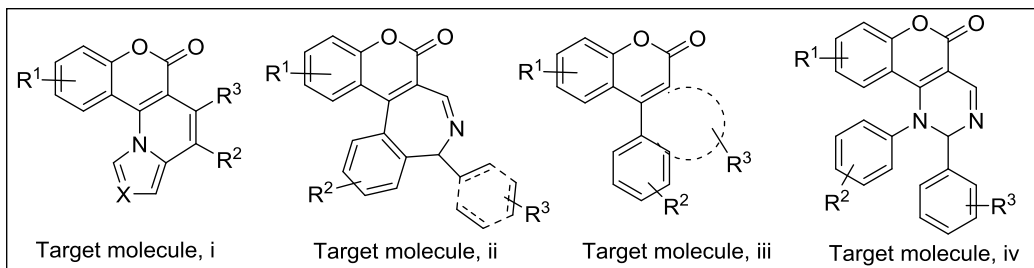
Scheme 5.2.6: Metal-free cascade synthesis of coumarin-fused quinolinones

5.3 Future scope of the research work

The current thesis reflects the development of new strategies for the synthesis of coumaryl-tagged/labelled amino acids, and coumarin-appended and fused heterocycles under the metal-catalyzed and metal-free conditions. In addition, preliminary photophysical properties of the synthesized products were studied. Based on the work conducted, the following signifies the future scope:

1. The methodologies developed for preparing coumaryl-tagged/labelled amino acids could be directly applied for site specific tagging/labelling of amino acids in peptide/proteins.
2. Coumaryl-labelled lysine and tyrosine motifs could themselves be used for preparing specific lysine and tyrosine containing fluorescent peptides/proteins for understanding their action *via* bioimaging and other related techniques.
3. The newly developed coumarin-fused pyrimidines and coumarin-fused quinolinones scaffolds could be appropriately functionalized, and sensing applications can thereafter be explored on the resultant probes.
4. The metal-catalyzed and metal-free strategies developed could be explored on other heterocyclic moieties that are structurally/electronically similar to coumarin, to furnish their corresponding fused pyrimidines and quinolinones.

5. New metal-catalyzed and metal-free strategies could be developed to synthesize other related coumarin-fused heterocycles (i-iv).



1. S. Kumari, S. M. A. Shakoor, D. Markad, S. K. Mandal, R. Sakhuja “NH₄OAc-promoted cascade approach towards aberrant synthesis of chromene-fused quinolinones” *European Journal of Organic Chemistry* **2019**, 2019, 705–714.
2. S. Kumari, S. M. A. Shakoor, S. Khullar, S. K. Mandal, R. Sakhuja “An unprecedented tandem synthesis of fluorescent coumarin-fused pyrimidines via copper-catalyzed cross-dehydrogenative C(sp³)-N bond coupling” *Organic & Biomolecular Chemistry* **2018**, 16, 3220–3228.
3. S. Kumari, S. M. A. Shakoor, K. Bajaj, S. H. Nanjgowda, P. Mall, R. Sakhuja “Copper-catalysed C-N/C-O coupling in water: a facile access to *N*-coumaryl amino acids and fluorescent tyrosine & lysine labels” *Tetrahedron Letters* **2016**, 57, 2732-2736.
4. S. Kumari, S. Joshi, A. Sarmah, D. D. Pant, Rajeev Sakhuja “Highly selective sensing of li⁺ in H₂O/CH₃CN via fluorescence 'turn-on' response of a coumarin-indole linked dyad: an experimental and theoretical study” *Journal of Fluorescence* **2016**, 26, 2177–2185.
5. S. Kumari, S. Joshi, T. C. Cordova-Sintjago, D. D. Pant, R. Sakhuja “Highly sensitive fluorescent imidazolium-based sensors for nanomolar detection of explosive picric acid in aqueous medium” *Sensors and Actuators B: Chemical* **2016**, 229, 599–608.
6. S. Kumari, S. Joshi, S. M. A. Shakoor, D. S. Agarwal, S. S. Panda, D. D. Pant, R. Sakhuja “Synthesis, absorption, and fluorescence studies of coumaryl-labelled amino acids and dipeptides linked via triazole ring” *Australian Journal of Chemistry* **2015**, 68, 1415-1426.
7. S. Joshi, S. Kumari, A. Sarmah, D. D. Pant, R. Sakhuja, “Detection of Hg²⁺ ions in aqueous medium using an indole-based fluorescent probe: experimental and theoretical investigations” *Journal of Molecular Liquids* **2017**, 248, 668–677.
8. S. Joshi, S. Kumari, E. Chamorro, D. D. Pant, R. Sakhuja “Fluorescence quenching of a benzimidazolium-based probe for selective detection of picric acid in aqueous medium” *ChemistrySelect* **2016**, 1, 1756–1762.
9. S. Joshi, S. Kumari, A. Sarmah, R. Sakhuja, D. D. Pant. “Solvatochromic shift and estimation of dipole moment of synthesized coumarin derivative: Application as

sensor for fluorogenic recognition of Fe³⁺ and Cu²⁺ ions in aqueous solution” *Journal of Molecular Liquids* **2016**, 222, 253–262.

10. S. Joshi, S. Kumari, R. Bhattacharjee, A. Sarmah, R. Sakhuja, D. D. Pant “Experimental and theoretical study: determination of dipole moment of synthesized coumarin–triazole derivatives and application as turn off fluorescence sensor: High sensitivity for iron(III) ions” *Sensors and Actuators B: Chemical* **2015**, 220, 1266–1278.
11. S. Joshi, S. Kumari, R. Bhattacharjee, R. Sakhuja, D. D. Pant, “Estimation of ground and excited-state dipole moments of synthesized coumarin derivative, (S)-(1-((7-hydroxy-2-oxo-2*H*-chromen-4-yl) methyl)-1*H*-1,2,3-triazol-4-yl)methyl 2-(((9*H*-fluoren-9-yl)methoxy) carbonylamino)-3-phenylpropanoate from a solvatochromic shift and theoretical methods” *Journal of Molecular Liquids* **2015**, 209, 219–223.
12. S. Joshi, S. Kumari, R. Bhattacharjee, R. Sakhuja, D. D. Pant “Estimation of ground and excited state dipole moments of synthesized coumarin derivative [*N*-(2-oxo-2*H*-chromen-4-yl)imino]triphenyl-phosphorane” *Journal of Molecular Liquids* **2014**, 200, 115–119.

Poster:

1. **S. Kumari**, S. Joshi, A. Sarmah, D. D. Pant, R. Sakhuja “Detection of Hg²⁺ ions in Aqueous Medium Using an Indole-Based Fluorescent Probe: Experimental and Theoretical Investigations” at 24th ISCBC 2018, Department of chemistry, Manipal University Jaipur, Rajasthan, January 11-13th 2018.
2. **S. Kumari**, S. Joshi, A. Sarmah, D. D. Pant, R. Sakhuja “Detection of Hg²⁺ ions in Aqueous Medium Using an Indole-Based Fluorescent Probe: Experimental and Theoretical Investigations” at NFM 2017, Department of chemistry, Birla Institute of Technology and Science Pilani, Pilani Campus, Rajasthan, November 16-18th 2017.
3. **S. Kumari**, R. Sakhuja “Enantioselective copper-catalyzed direct C-N/C-O coupling in water: A facile access to fluorescent labelled amino acids and Leu-enkephalin” at 22nd ISCBC-2016, Department of chemistry, organized by Uka Tarsadia University, Surat, India, during February 6-8th, 2016.
4. **S. Kumari**, S. Joshi, R. Sakhuja “Imidazolium and Benzimidazolium Appended Fluorescent Probes for Highly Selective Sensing of Picric Acid in Aqueous Medium” at OCSD-2016, Department of Chemistry, Birla Institute of Technology and Science Pilani, Pilani Campus, Rajasthan, August 29-30th, 2016.
5. **S. Kumari**, S. Joshi, D. D. Pant, R. Sakhuja “Highly Sensitive Fluorescent Imidazolium Based Sensors for Nanomolar Detection of Explosive Picric Acid in Aqueous Medium” at CCDDR-2015, Department of chemistry, Malaviya National Institute of Technology Jaipur, Rajasthan, November 23-25th, 2015.
6. **S. Kumari**, S. M. A. Shakoor, R. Sakhuja “Enantioselective copper-catalyzed direct C-N/C-O coupling in water: A facile access to fluorescent labelled amino acids and *leu-enkephalin*” at NDCS-2015, Department of chemistry, Birla Institute of Technology and Science Pilani, Pilani Campus, Rajasthan, October 16-18th, 2015.
7. **S. Kumari**, S. Joshi, R. Sakhuja “Estimation of ground and excited state dipole moments of synthesized coumarin-triazole derivatives and application as turn off fluorescence sensor: high sensitivity for iron (III) ions: Experimental and theoretical studies” at FCASI-2015, Department of Chemistry, University of Rajasthan, Jaipur, Rajasthan, march 13-14th, 2015.

8. **S. Kumari**, S. M. A. Shakoor, D. S. Agarwal, R. Sakhuja “Amino Acid/peptides based Fluorescent Labels : Synthesis and Photo-physical studies” at NFM 2014, Department of chemistry, Birla Institute of Technology and Science Pilani, Pilani Campus, Rajasthan, November 07-08th 2014.
9. **S. Kumari**, S. M. A. Shakoor, D. S. Agarwal, R. Sakhuja “Fluorescent Labeling of Amino Acids *via* Click Chemistry” at 20th ISCBC-2016, Department of chemistry, University of Delhi, New Delhi, March 1-4th 2014.

SANTOSH KUMARI obtained her master's degree in Organic Chemistry from Rajasthan University, Jaipur, India in 2010. In December 2011, she cleared the Joint UGC-NET JRF conducted by CSIR, New Delhi with 85th rank in India. She also cleared GATE-2011 conducted by IIT Madras. She is the recipient of Gargi Award-2003 and 2004 from Government of Rajasthan for her best academic achievements in class X examination. She joined Department of Chemistry, BITS Pilani, Pilani Campus for Ph.D. program in January 2013 under the guidance of Dr. Rajeev Sakhuja. During the tenure of Ph.D. programme, she was actively involved in the synthesis of coumaryl-appended amino acid and coumarin-fused heterocycles. In addition, she has also developed novel coumarin-derived heterocycles that were found to be selective for the metal ions and explosive analytes. She has published twelve research articles in peer-reviewed international journals, and presented papers in six national and three international conferences.

Her main research attention lies in the development of new methods towards the formation of organic materials using novel cascade strategies under metal-free conditions, and explore their sensing abilities.

Brief Bibliography of the Supervisor

[A-4]

Dr. Rajeev Sakhuja obtained his M.Phil. and Ph.D. degrees from Department of Chemistry, University of Delhi, New Delhi in the area of heterocyclic chemistry. Following this, he pursued his postdoctoral research with Prof. Alan R. Katritzky at the Center of Heterocyclic Compounds, University of Florida, Gainesville, and after that with Prof. Raymond Booth at Department of Medicinal Chemistry, the University of Florida from 2009-2012. After returning, he joined the Department of Chemistry, BITS Pilani, Pilani Campus as an Assistant Professor in March 2012. Following Ph.D., he has eleven years of post-PhD research experience in the broad field of organic synthesis. Dr. Sakhuja is presently an Associate Professor in Department of Chemistry, leading an independent research group at Birla Institute of Technology & Science, Pilani where his current area of research interest lies in the development of metal-catalyzed and metal-free strategies for the functionalization of heterocycles, synthesis of biologically important heterocyclic scaffolds, along with the development of organic materials with sensing and gelation abilities. His active contribution in these areas has fetched him forty eight research articles, 4 reviews in peer-reviewed journals of international repute. He was successfully completed four sponsored projects funded by government agencies (DST & UGC), and private organization (BITS seed grant & additional research grant) in the past five years.